APPROVED FOR RELEASE: 2007/02/09: CIA-RDP82-00850R000500020034-7



JPRS L/10265

20 January 1982

# USSR Report

## ELECTRONICS AND ELECTRICAL ENGINEERING

(FOUO 1/82)

FBIS FOREIGN BROADCAST INFORMATION SERVICE



APPROVED FOR RELEASE: 2007/02/09: CIA-RDP82-00850R000500020034-7

APPROVED FOR RELEASE: 2007/02/09: CIA-RDP82-00850R000500020034-7

NOTE

JPRS publications contain information primarily from foreign newspapers, periodicals and books, but also from news agency transmissions and broadcasts. Materials from foreign-language sources are translated; those from English-language sources are transcribed or reprinted, with the original phrasing and other characteristics retained.

Headlines, editorial reports, and material enclosed in brackets [] are supplied by JPRS. Processing indicators such as [Text] or [Excerpt] in the first line of each item, or following the last line of a brief, indicate how the original information was processed. Where no processing indicator is given, the information was summarized or extracted.

Unfamiliar names rendered phonetically or transliterated are enclosed in parentheses. Words or names preceded by a question mark and enclosed in parentheses were not clear in the original but have been supplied as appropriate in context. Other unattributed parenthetical notes within the body of an item originate with the source. Times within items are as given by source.

The contents of this publication in no way represent the policies, views or attitudes of the U.S. Government.

COPYRIGHT LAWS AND REGULATIONS GOVERNING OWNERSHIP OF MATERIALS REPRODUCED HEREIN REQUIRE THAT DISSEMINATION OF THIS PUBLICATION BE RESTRICTED FOR OFFICIAL USE ONLY.

APPROVED FOR RELEASE: 2007/02/09: CIA-RDP82-00850R000500020034-7

APPROVED FOR RELEASE: 2007/02/09: CIA-RDP82-00850R000500020034-7



JPRS L/10265

20 January 1982

# USSR REPORT

# ELECTRONICS AND ELECTRICAL ENGINEERING

(FOUO 1/82)

## CONTENTS

AMPLIFIERS

Noise in Ferroprobes and Magnetic Amplifiers..... 1

Amplifier for KMP201UPI Automatic Switch..... 41

ANTENNAS

Antennas and Feeder Lines..... 42

Antenna Device With Electrical Beam Oscillation in Two Planes..... 75

CERTAIN ASPECTS OF COMPUTER HARD AND SOFT WARE: CONTROL, AUTOMATION, TELEMECHANICS, TELEMETERING, MACHINE DESIGNING AND PLANNING

Magnetic Bubble Data Storage and Processing Devices..... 77

Device for Taking Median Value..... 120

Microprocessor Psychodiagnostic Device Patent..... 123

CERTAIN ASPECTS OF PHOTOGRAPHY, MOTION PICTURES AND TELEVISION

TV Contour Detector..... 124

Parameter Selection of Optical Systems for Scanning Reproducing Devices With Kinescopes..... 134

Multimicroprocessor System for Processing Audio Signal in Frequency Region..... 141

Automatic Restoration of Movie Films by Computer..... 150



APPROVED FOR RELEASE: 2007/02/09: CIA-RDP82-00850R000500020034-7

APPROVED FOR RELEASE: 2007/02/09: CIA-RDP82-00850R000500020034-7



COMMUNICATIONS, COMMUNICATION EQUIPMENT, RECEIVERS AND TRANSMITTERS, NETWORKS, RADIO PHYSICS, DATA TRANSMISSION AND PROCESSING, INFORMATION THEORY

Microwave Delay Line..... 156

Methods for Finding Breaks in Optical Cables..... 158

Control System for Arc Discharger Switching Using Field Distortion Technique..... 166

Wideband Photoelectronic Receiver..... 170

Device for Controlling PIN-Diode Attenuator..... 176

Silicon Radio-Frequency p-i-n Diodes for Communications Equipment..... 179

Principles of the Design of Nonlinear Pulse-Frequency Signal Selectors..... 184

Device for Addition of Powers..... 204

Radio Receiver Patent..... 207

CONVERTERS, INVERTERS, TRANSDUCERS

Waveguide Reflecting Phase Inverter..... 208

Solid-State Phase Inverter Control Device..... 212

INSTRUMENTS, MEASURING DEVICES AND TESTERS, METHODS OF MEASURING, GENERAL EXPERIMENTAL TECHNIQUES

Precision Digital Infrared Phase Meter With Frequency Conversion of Laser Radiation..... 216

Panoramic Measuring Device for Complex Parameters of Microwave Devices..... 221

Wideband Integrated Circuit Digital Power Meter for Laser Radiation..... 225

Subnanosecond Pyroelectric Infrared Radiation Detector..... 229

Integrated Temperature Sensor Using Silicon Diode Matrices..... 233



APPROVED FOR RELEASE: 2007/02/09: CIA-RDP82-00850R000500020034-7

APPROVED FOR RELEASE: 2007/02/09: CIA-RDP82-00850R000500020034-7



MICROELECTRONICS

Prospects of Using Media With Higher Dielectric Constant in Microwave GIS Technology..... 236

Problems of Modeling Elements of Large-Scale Integrated Circuits With Submicronic Dimensions..... 244

Selected Abstracts of Articles From Journal 'MICROELECTRONICS', September-October 1981..... 269

OSCILLATORS, MODULATORS, GENERATORS

Technological AMTs 1550 Crystal Oscillator..... 273

PUBLICATIONS, INCLUDING COLLECTIONS OF ABSTRACTS

Abstracts From Journal 'METROLOGY', September 1981..... 275

Acoustical Distance Measurement and Control Methods..... 278

Cascade Generators..... 283

Classification of Thyristors..... 286

Control Systems for Thyristor Frequency Converters..... 289

Digital Encoding of Television Images..... 292

Electrical and Optical Properties of Semiconductors..... 296

Electronic Microwave Devices..... 299

Industrial Telephone Communication, Electrical Signaling and Installation of Electric Clocks..... 307

Measurement Elements in Power System Emergency Automatic Equipment..... 310

Mechanical Section Design for Overhead Superhigh Voltage Lines.... 313

Modeling and Testing of Radio Equipment..... 317

Modern Methods and Devices for Data Display..... 321

Pulse Radar Circuits..... 328

Problems of Optimal Detection and Localization of Malfunctions in Radioelectronic Equipment..... 332



APPROVED FOR RELEASE: 2007/02/09: CIA-RDP82-00850R000500020034-7

APPROVED FOR RELEASE: 2007/02/09: CIA-RDP82-00850R000500020034-7



Methods of Optimization in Controlling Electrical Power Systems..... 335

Prospects for Development for Maritime Electrical Engineering..... 338

Radar Data Processing Against Interference Background..... 342

Radio Measurements.. ..... 351

Superconducting Accelerating Microwave Structures..... 355



APPROVED FOR RELEASE: 2007/02/09: CIA-RDP82-00850R000500020034-7

APPROVED FOR RELEASE: 2007/02/09: CIA-RDP82-00850R000500020034-7



AMPLIFIERS

UDC 620.179.143:621.375.3

# NOISE IN FERROPROBES AND MAGNETIC AMPLIFIERS

Moscow IZMERENIYA, KONTROL', AVTOMATIZATSIYA in Russian No 4 (38), 1981 pp 37-53

[Article by Yu.V. Afanas'yev and V.N. Gorobey, engineers]

[Text] Introduction

Ferroprobes (FZ's) and magnetic amplifiers (MU's) have received extensive application in measuring equipment and automation [1-4]. FZ's and MU's are distinguished by high reliability and long life, noise immunity and the ability to operate over a wide temperature range, low power requirement and low cost. The high sensitivity characteristic of FZ's and MU's has been responsible for their use for detecting and measuring very low values of a magnetic field or current.

The maximum capabilities of FZ's and MU's are limited by the level of their intrinsic noise. This concept usually includes noise from induction from the power circuit, the noise of cores, detectable during cyclic reversal of magnetization, and the thermal noise of windings. Noise in cores, which has begun to be called magnetic noise, has the highest value.

The nature of magnetic noise has been studied already for more than 30 years. However, in spite of the successes achieved, many aspects of this phenomenon, which is interesting from the viewpoint of physics and important from that of practical application, have continued to remain unclear.

In 1971 N.N. Kolachevskiy's monograph was published, which summarized the results of theoretical and experimental studies of the nature of magnetic noise during the preceding period. New experimental data requiring analysis have been gained since then [5].

In this article an attempt is made to discuss these data, and also to turn attention to certain experimentally established facts making it possible to lower the level of magnetic noise in ferroprobes and magnetic amplifiers by one to two orders of magnitude.

Transformation Ratios of Ferroprobes and Magnetic Amplifiers

Ferroprobes and magnetic amplifiers are active inductive transformers, i.e., additional energy is induced in them (by means of an excitation winding supplied





APPROVED FOR RELEASE: 2007/02/09: CIA-RDP82-00850R000500020034-7

APPROVED FOR RELEASE: 2007/02/09: CIA-RDP82-00850R000500020034-7



with alternating current), because of which transformation itself is rendered possible.

The e.m.f. in the output winding (called the measuring winding below) is determined by the equation:

$$e_\Sigma = -sw\vec{\xi}\vec{i}^{\circ}_{u}\frac{d}{dt}\vec{B}_\Sigma(\vec{H}_\Sigma), \tag{1}$$

where $s$ is the total cross-sectional area of the cores covered by the measuring winding; $w$ is the number of turns of the winding; $\vec{i}^{\circ}_{u}$ is the magnetic axis (normal to the plane of the winding's turns); $\xi < 1$ is the design factor [2]; $\vec{B}_\Sigma$ is the vector of total magnetic induction; $\vec{H}_\Sigma = \vec{H}_1 + \vec{H}_0$ is the vector of the total field strength; $\vec{H}_1$ is the vector of the strength of the excitation field; and $\vec{H}_0$ is the vector of the strength of the measured field.

For magnetic amplifiers the relationship between the field strength and input current, $i_{vkh}$, is determined by the expression

$$H_0 = w_{vx}i_{vx}/l,$$

where $w_{vkh}$ is the number of turns of the input winding and $l$ is the length of the center line of a ring core.

Experience has shown that components $e_\Sigma(t)$, multiples of the frequency of the excitation field, because of the nonlinearity of the characteristics of cores of ferroprobes and magnetic amplifiers, prove to be functions not only of $\vec{H}_1$, but also of $\vec{H}_0$, and even when $\vec{H}_0 = \text{const}$.

Let us expand nonlinear dependence $\vec{B}_\Sigma(\vec{H}_\Sigma)$ into a Taylor series, being limited for sufficiently low values of $H_0$ to two terms of the series [6]:

$$\vec{B}_\Sigma(\vec{H}_\Sigma) = \mu_0[\mu^*\vec{H}_1 + \hat{\mu}^*\vec{H}_0], \tag{2}$$

where $\hat{\mu}^*$ is the tensor of the relative magnetic permeability of the core, $\mu^*$ is the normal relative permeability of the core and $\mu_0$ is the magnetic constant.

Tensor $\hat{\mu}^*$ takes into account the anisotropic properties of the core acquired by it in superposition of field $\vec{H}_1$, whereby the material of the core is assumed to be isotropic. Adjusted for the principal axis (the axis of symmetry of the core, x, y and z; $\vec{x}^{0} \| \vec{H}_1$), tensor $\hat{\mu}^*$ becomes diagonal and is defined by three components, whereby one of them, $\mu^*_{xx}$, is the same as the differential permeability, $\mu^*_{xx} = \mu^*_d = (1/\mu_0)/(dB/dH)$, and the other two, $\mu^*_{yy}$ and $\mu^*_{zz}$, as the normal permeability, $\mu^* = (1/\mu_0)/(B/H)$. In all cases the asterisk indicates the necessity of taking into account the demagnetization coefficient of the core (in a ferroprobe) in the respective directions.

Substituting (2) in (1), we find



APPROVED FOR RELEASE: 2007/02/09: CIA-RDP82-00850R000500020034-7

APPROVED FOR RELEASE: 2007/02/09: CIA-RDP82-00850R000500020034-7



$$e_{\Sigma} = -s\omega\xi\mu_0\left(\varepsilon\begin{vmatrix}\mu_д^{\cdot} & -H\frac{d\cos\beta}{dt}\\ \mu^{*} & \frac{dH_1}{dt}\cos\beta\end{vmatrix} + \frac{d}{dt}H_0\begin{vmatrix}\mu_д^{\cdot} & -\sin\alpha\sin\beta\\ \mu^{*} & \cos\alpha\cos\beta\end{vmatrix}\right), \tag{3}$$

where $\varepsilon <<$ is the so-called imbalance coefficient, taking into account the non-ideal isolation of the measuring circuit from the excitation circuit, and angles $\alpha$ and $\beta$ equal: $\alpha = \vec{H}_0 \hat{;} \vec{H}_1$ and $\beta = \vec{I}_m^{o} \hat{;} \vec{H}_1$.

The expression obtained makes it possible to study transformation processes in ferroprobes and magnetic amplifiers with any relative orientation of vectors $\vec{H}_0$, $\vec{H}_1$ and $\vec{I}_m^{o}$, in particular, with a longitudinal ($\alpha = 0$), transverse ($\alpha = \pi/2$) and rotating ($\alpha = \omega t$) excitation field, as well as with various spectral compositions of the excitation field.

Having become widespread is the operating mode of a ferroprobe and magnetic amplifier utilizing the central symmetry of the major hysteresis loop of the cores. In this mode the cores are excited by means of a strong variable field whose spectrum contains only the fundamental wave and odd harmonics. Then the spectrum of permeability $\mu_d^{*}$ and $\mu^{*}$ will contain a constant component and even harmonics:

$$\mu_д^{\cdot}(t) = \mu_{д0}^{\cdot} + \sum_{n=1}^{\infty}\mu_{д2n}^{\cdot}\cos(2n\omega t + \varphi_{2n}),$$
$$\mu^{*}(t) = \mu_0^{\cdot} + \sum_{n=1}^{\infty}\mu_{2n}^{\cdot}\cos(2n\omega t + \varphi_{2n}), \tag{4}$$

where $\mu_{д2n}^{*}$ and $\mu_{2n}^{*}$ are the amplitudes of even harmonics or Fourier coefficients computed in a certain manner from analytical dependences $\mu_d^{*}[H_1(t)]$, $\mu^{*}[H_1(t)]$; $n = 1, 2, 3, \ldots$; $\omega$ is the angular frequency of the fundamental wave of the excitation field, $H_1(t)$; and $\phi_{2n}$ represents initial phases depending on the value of the coercive force of the dynamic hysteresis loop.

Substituting (4) in (3) we find that the imbalance e.m.f., associated with the first determinant of expression (3), will have an odd-harmonic spectrum, since the net e.m.f., proportional to the value of $H_0$ and associated with the second determinant, will have an even-harmonic spectrum. Therefore ferroprobes and magnetic amplifiers operating in this mode are often called even-harmonic.





APPROVED FOR RELEASE: 2007/02/09: CIA-RDP82-00850R000500020034-7

APPROVED FOR RELEASE: 2007/02/09: CIA-RDP82-00850R000500020034-7



Since any even harmonic in the spectrum of the output e.m.f. (usually called the second harmonic) can be easily filtered from odd harmonics of noise, then the threshold sensitivity of ferroprobes and magnetic amplifiers operating in the mode indicated is determined not by the peak value of components of the imbalance e.m.f., but by the level of the magnetic noise in cores near the even harmonic used. It is not difficult also to demonstrate that within the framework of the assumptions made fluctuations in harmonics of the excitation field, $H_1(t)$, in harmonics of permeability $\mu_d^*(t)$ and $\mu^*(t)$ and the imbalance coefficient, $\varepsilon$, can result in broadening of the lines of only odd noninformative harmonics of spectrum $e_\Sigma(t)$. This is the main advantage of the ferroprobe and magnetic amplifier operating mode discussed.

Taking into account expressions (3) and (4) it is not difficult to obtain expressions for the transformation ratios of a ferroprobe and magnetic amplifier. For example, for a ferroprobe and magnetic amplifier with longitudinal excitation with a piecewise linear approximation of curve B(H) of the cores and sinusoidal, triangular and square-pulse forms of the excitation field wave, we get the following transformation ratios for the second harmonic:

$$\left.\begin{aligned} G_{\text{эсин}} &= \frac{dE_2}{dB_0} = \frac{8}{\pi}\,\omega\, ws\,\xi\,\mu^*_{\text{д max}}\frac{H_s}{H_m}\sqrt{1-\left(\frac{H_s}{H_m}\right)^2}, \\ G_{\text{этр}} &= \frac{dE_2}{dB_0} = \frac{4}{\pi}\,\omega\, ws\,\xi\,\mu^*_{\text{д max}}\sin\left(\pi\frac{H_s}{H_{\max}}\right), \\ G_{\text{энр}} &= \left.\frac{dE_2}{dB_0}\right|_{H_{\max} > H_s} = \frac{4}{\pi}\,\omega\, ws\,\xi\,\mu^*_{\text{д max}}\sin(\pi-\tau), \end{aligned}\right\} \tag{5}$$

where $B_0 = \mu_0 H_0$ is the induction of the measured field; $E_2$ is the peak value of the e.m.f. of the second harmonic; $H_s$ is the strength of the saturation field of the cores; $H_m$ or $H_{max}$ is the peak or maximum value of the excitation field; and $\tau$ is the duration of a pulse.

The dependence of the transformation ratios of a ferroprobe and magnetic amplifier on the degree of relative overexcitation of their cores is illustrated in fig 1.

Calculations performed according to equations (5) have demonstrated that in practice ferroprobe and magnetic amplifier transformation ratios of dozens of microvolts per nanotesla (μV/nT) are completely achievable. Since the noise level of electronic amplifiers connected to the output of a ferroprobe and magnetic amplifier is estimated in tenths and hundredths of a microvolt (at frequencies above $10^3$ Hz in the 1 Hz band), then these numerical values of the transformation ratios of ferroprobes and magnetic amplifiers are totally sufficient in order to detect and measure by their means magnetic fields at the level of single numbers of picoteslas. However, the magnetic noise of ferroprobes and magnetic amplifiers interferes with this.



APPROVED FOR RELEASE: 2007/02/09: CIA-RDP82-00850R000500020034-7

APPROVED FOR RELEASE: 2007/02/09: CIA-RDP82-00850R000500020034-7



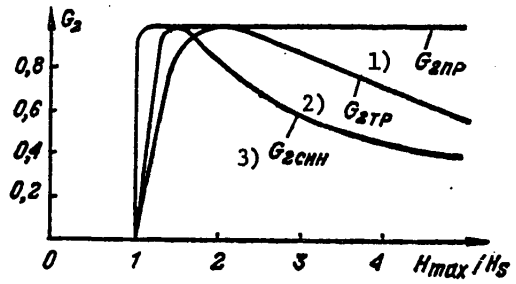


Figure 1. Dependence of Transformation Ratios of a Ferroprobe and Magnetic Amplifier on Degree of Relative Overexcitation of Cores

Key:
1. Square-pulse
2. Triangular
3. Sine-wave

Magnetic Noise Spectrum; Relationship Between Noise Level and Threshold Sensitivity of Ferroprobes and Magnetic Amplifiers

Cyclic magnetic reversal of the cores of ferroprobes and magnetic amplifiers is accompanied by Barkhausen abrupt changes whose parameters--intensity, duration and initial phase--fluctuate, varying from cycle to cycle, which results in the origin of magnetic noise.

It has been established experimentally that the spectrum of magnetic noise is periodic. In it it is possible to isolate relatively uniform and sufficiently extended sections situated between discrete lines--harmonics of the frequency of magnetic reversal (excitation) of the core, as well as distinctly uniform and considerably less extended sections directly abutting the discrete lines and characterized by a rise in spectral density.

The manifestation of noise in sections of the first type can be described by means of the so-called "shot model" [5, 7, 8].

The appearance of noise in sections of the second type does not follow from any kind of theoretical structure, as the result of which noise in these sections has begun to be called excess. Excess noise was detected experimentally [5, 9]. Later it was established by many authors that the rise in spectral density of excess noise obeys the rule $1/f^{\gamma}$, where $f$ is the frequency of tuning out from a line (for a demodulated ferroprobe and magnetic amplifier signal, the excitation frequency) and $\gamma$ is an indicator which varies over a range of 0.5 to 1.8. Observance of this rule has provided an occasion for making certain analogies, in connection with which excess noise has begun to be called also flicker noise [5].



APPROVED FOR RELEASE: 2007/02/09: CIA-RDP82-00850R000500020034-7

APPROVED FOR RELEASE: 2007/02/09: CIA-RDP82-00850R000500020034-7



It must be emphasized that in many practical cases (when measuring constant and slowly varying magnetic fields and electric current) it is precisely excess noise with its characteristic rise in keeping with the 1/f rule which determines the threshold sensitivity of ferroprobes and magnetic amplifiers. Therefore, studying the nature of excess noise and finding methods of effectively suppressing it have become of first-rate importance for practical applications.

Let us now dwell on the relationship between the noise level and the threshold sensitivity of ferroprobes and magnetic amplifiers.

If the noise process is stationary and ergodic (this assumption agrees with the experimental data), the root-mean-square value of the noise's e.m.f. equals

$$\sigma_E = \sqrt{\int_{f_1}^{f_2} g_f(f)\,df},$$

where $g_f$ is the spectral power density of the noise process in $V^2/Hz$ and $f_1$ and $f_2$ are the lower and upper limits of the frequency band selected.

Let us call the output noise level of a ferroprobe and magnetic amplifier the value of $\overline{E}_{sh} = \kappa\sigma_E$, where $\kappa$ is a coefficient depending on the law of distribution of magnetic noise and the prescribed confidence level of the estimate [4]. As illustrated in [10], the noise of a ferroprobe and magnetic amplifier is distributed according to a normal law; therefore, with $\kappa = 3$ the value of the estimate of $\overline{E}_{sh}$ equals the maximum (with a probability of 0.997) peak value of the noise's e.m.f., which makes it possible to relate $\overline{E}_{sh}$ to the frequently encountered estimates "for the width of the noise track" or "from peak to peak," equal to $2\overline{E}_{sh}$.

As was demonstrated in the first section, the output e.m.f. of a ferroprobe and magnetic amplifier depends on a whole series of factors; therefore it is more convenient to use not the value of $\overline{E}_{sh}$, but the value of $\overline{B}_{sh}$, determined from the equation

$$\overline{B}_m = \frac{\overline{E}_m}{G} = \frac{\kappa\sqrt{\int_{f_1}^{f_2} g_f(f)\,df}}{G}, \tag{6}$$

where G is the transformation ratio of a ferroprobe and magnetic amplifier (when these devices operate at the second harmonic of the output e.m.f., $G = G_2$).

We call the value of $\overline{B}_{sh}$ also the threshold sensitivity of a ferroprobe and magnetic amplifier [4].



APPROVED FOR RELEASE: 2007/02/09: CIA-RDP82-00850R000500020034-7

APPROVED FOR RELEASE: 2007/02/09: CIA-RDP82-00850R000500020034-7



The noise level is often also related to the value of $b_f = \sqrt{g_1}/G$ $(T/Hz^{1/2})$. The value of $b_f$ can be called the spectral density of peak values of magnetic noise. The relationship between $b_f$ and $\overline{B}_{sh}$ is determined by the expression

$$\overline{B}_{ш} = \varkappa \sqrt{\int_{f_1}^{f_2} g_f^*(f)\, df}.$$

Let us note that the increase in values of $\overline{B}_{sh}$ and $b_f$ when nearing the discrete lines (excess noise) is considerably smoother than in the value of $g_f$. This is because of the fact that both quantities $\overline{B}_{sh}$ and $b_f$ are proportional to $\sqrt{g_f}$.

Let us make the following calculation. Let us represent the spectral density curve, $g_f(f)$, of the demodulated signal of a ferroprobe and magnetic amplifier in the form of uniform ($f > f_2$) and nonuniform ($f < f_2$) sections, where $f_2$ is the upper-limit frequency of excess noise, corresponding to the bend in the curve (fig 2). For the uniform section, $g_f(f) = g_c = \text{const}$ ; for the nonuniform $g_f(f) = g_c/f^{\gamma}$. Let $\gamma = 1$ and $f_2 = 1$ Hz (with strong overexcitation of the cores of a ferroprobe and magnetic amplifier these values are close to real). Then for the nonuniform section of the spectrum it is possible to write

$$\sigma_E = \sqrt{\int_{f_1}^{f_2} \frac{g_c}{f}\, df} = \sqrt{g_c \ln \frac{f_2}{f_1}}.$$

Taking into account the respective values of $f_1$ and $f_2$ and keeping in mind that according to (6) $\overline{B}_{sh} \simeq \sigma_E$, we find that for $f_1 = 10^{-3}$ Hz, $B_{sh} \simeq 2.6\sqrt{g_c}$ and for $f_1 = 10^{-7}$ Hz, $B_{sh} \simeq 4\sqrt{g_c}$.

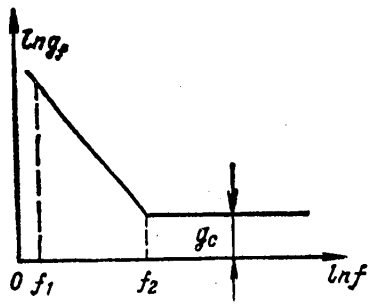


Figure 2. Spectral Power Density of Magnetic Noise of a Demodulated Signal of a Ferroprobe and Magnetic Amplifier





APPROVED FOR RELEASE: 2007/02/09: CIA-RDP82-00850R000500020034-7

APPROVED FOR RELEASE: 2007/02/09: CIA-RDP82-00850R000500020034-7



It is obvious from this calculation that increasing the time for observing the noise process from dozens of minutes to several months does not result in any substantial increase in the level of excess noise over the level of ordinary magnetic noise. For the same frequency band with a width of 1 Hz this excess is 2.6- to fourfold (these values correspond to the experimental data in [11]), which makes it possible to estimate the threshold sensitivity of a ferroprobe and magnetic amplifier from recordings of noise obtained in relatively brief realizations.

Let us also note that at frequencies below $10^{-3}$ Hz it is difficult to distinguish the recorded noise of a ferroprobe and magnetic amplifier from zero fluctuations and drift whose origin can also not be related to processes taking place in cores. This zero drift and fluctuations on one hand hamper obtainment of the spectral distribution of excess noise at ultralow frequencies and on the other explain the often encountered inconsistency between calculation and experimental data on the noise level at these frequencies.

Prerequisites for the Origin of Excess Noise Near the Second Harmonic

As was already mentioned, the appearance of excess noise does not follow from any theoretical constructions. This relates especially to excess noise near the second harmonic of the magnetic reversal frequency. Therefore, attempts have been made from the very beginning and continue to be made to find some independent sources of fluctuations causing the origin of excess noise.

The idea that the excess noise of ferroprobes and magnetic amplifiers operating at the second harmonic is of a different physical nature than ordinary magnetic noise was first expressed by R. Ya. Berkamn [9], but he did not suggest any physical or formal mathematical model explaining the origin of excess noise.

M. Vayner [12] attempted to explain the appearance of a false signal for the second harmonic and the rise in noise near it on account of the magnetostriction phenomenon. He correctly established that magnetostrictive lengthening of the cores of a ferroprobe results in the movement of lines of force intersecting the turns of the measuring winding twice per cycle; however, he did not study the change in direction of these lines from half-cycle to half-cycle, as the result of which the original equation presented by him proved to be invalid. A critique of Vayner's model is given in [13]. In spite of the erroneousness of Vayner's model, the fact itself of a correlation between the level of excess noise and the magnetostriction coefficients of the ferromagnetic materials used is interesting and has been established by other authors and, as will be demonstrated below, finds an explanation within the framework of the dislocation model of noise.

N.N. Kolachevskiy and coworkers [5, 14] suggested that excess noise in ferromagnetics magnetically reversed cyclically can be associated with fluctuations in magnetic permeability, similarly to how flicker noise in granulated resistors observed during the passing of electric current through them is related to fluctuations in the value of resistances. However, as already indicated above, fluctuations in the magnetic permeability of cores, on the assumption of central symmetry of the hysteresis loop and the absence of a constant component and even harmonics in the excitation current, cannot result in the origin of excess noise near even induction or e.m.f. harmonics, i.e., this assumption taken by itself



APPROVED FOR RELEASE: 2007/02/09: CIA-RDP82-00850R000500020034-7

APPROVED FOR RELEASE: 2007/02/09: CIA-RDP82-00850R000500020034-7



cannot serve as the basis of the mechanism for the origin of excess noise near even induction and e.m.f. harmonics.

Actually, let us assume that the differential permeability of the cores, $\mu_d^*$, fluctuates. Then instead of series (4) it is possible to write

$$\mu_д^*(t) = \mu_{д0}^* + \sum_{n=1}^{\infty} \mu_{д2n}^* \cos(2n\omega t + \varphi_{2n}) +$$

$$+ \Delta\mu_{д0}^*(t) + \sum_{n=1}^{\infty} \Delta\mu_{д2n}^*(t) \cos(2n\omega t + \varphi_{2n}), \tag{7}$$

where $\mu_{d0}^*$ and $\mu_{d2n}^*$ are the mean values of the parameters and $\Delta\mu_{d0}^*$ and $\Delta\mu_{d2n}^*$ are increments in the parameters (their fluctuation values).

By definition $\Delta\mu_{d0}^*(t) = 0$ and $\Delta\mu_{d2n}^*(t) = 0$. It is possible to assume also that the fluctuation spectrum is concentrated near zero frequency and even harmonic lines. Substituting (7) in (3) with $H_0 = 0$ and $H_1 = H_m \sin \omega t$, and assuming that the fluctuation processes in different cores are mutually not correlated, we find the output e.m.f. of a ferroprobe and magnetic amplifier with longitudinal excitation ($\alpha = \beta = 0$):

$$e(t) = -\bar{\omega} s w \xi \mu_0 H_m \cos\omega t \{ \varepsilon [\mu_{д0}^* + \sum_{n=1}^{\infty} \mu_{д2n}^* \cos(2n\omega t + \varphi_{2n})] + k^{-1/2} [\Delta\mu_{д0}^*(t) + \sum_{n=1}^{\infty} \Delta\mu_{д2n}^*(t) \cos(2n\omega t + \varphi_{2n})] \}, \tag{8}$$

where $k$ is the number of cores. It is obvious from the expression obtained that the output e.m.f. spectrum contains only diffused lines of the fundamental frequency and odd harmonics.

Some investigators perceive the common physical nature of both ordinary and excess noise. The periodicity of the spectrum of $g(\omega)$ with its characteristic rises near even and odd harmonics of the magnetic reversal frequency is explained by them by the correlation of Barkhausen abrupt changes originating in different magnetic reversal cycles [15].

Let us note that the correlation approach was used earlier, too, for explaining the periodicity of the $g(\omega)$ spectrum. For example, F.V. Bunkin, based on fulfillment of the obligatory condition $g(0) = 0$, demonstrated that correlation of the peak values of Barkhausen abrupt changes separated by a whole number of magnetic reversal half-cycles must result in rises in spectral density near odd and in dips near even harmonics. This conclusion was used for a long time in order to prove the impossibility of describing rises in noise near even harmonics by means of the correlation approach. However, as N.N. Kolachevskiy correctly observed,



APPROVED FOR RELEASE: 2007/02/09: CIA-RDP82-00850R000500020034-7

APPROVED FOR RELEASE: 2007/02/09: CIA-RDP82-00850R000500020034-7



the result obtained by F.V. Bunkin is only one consequence of the assumption of preservation of the strict symmetry of the hysteresis loop during cyclic magnetic reversal.

P.Ye. Kotlyar [16], based on the opposite assumption (first expressed by K.A. Goronina) demonstrated that the correlation approach is totally suitable also for describing rises in noise near even and odd harmonics. He obtained an equation from which it followed that the level of noise near even harmonics is higher the more significant the asymmetry of the loop and the longer the correlation time for Barkhausen abrupt changes.

The assumption of the asymmetry of the hysteresis loop as the major prerequisite for the origin of excess noise near even harmonics was also used in studies by the authors of the present article [4, 17]. We believe that this assumption does not contradict the law regarding the minimum free energy in a ferromagnetic. This law lies at the basis of the extremely great symmetry of the major dynamic loops of ferromagnetics but its statistical nature is revealed with an increase in the sensitivity and accuracy of measurements. The law begins to be fulfilled only "on average," in a stretch of a great number of magnetic reversal cycles, which at the same time indicates the fluctuation nature of the appearance of asymmetry of the loop.

Formally, within the framework of the transformation mechanism which we discussed in the first section, the appearance of excess noise near even induction and e.m.f. harmonics must be related to the presence of odd harmonics of the permeability of ferroprobe or magnetic amplifier cores. Actually, with violation of the symmetry of the loop we must write, instead of (4),

$$\mu_{д}^{\bullet}(t) = \mu_{д0}^{\bullet} + \sum_{n=1}^{\infty} \mu_{д2n}^{\bullet} \cos(2n\omega t + \varphi_{2n} + \Delta\varphi) + \\ + \sum_{n=1}^{\infty} \nu_{2n-1}(t)\, \mu_{д(2n-1)}^{\bullet} \sin\left[(2n-1)\omega t + \right. \\ \left. + \varphi_{2n-1} + \Delta\varphi\right], \tag{9}$$

where $\Delta\phi$ is the phase increment caused by asymmetry of the loop and $\nu_{n2-1}(t)$ represents random weighting functions with a mathematical expectation of zero ($\overline{\nu_{2n-1}(t)} = 0$).

Substituting (9) in (3) and limiting ourselves to a discussion of noise only near even e.m.f. harmonics, we find by analogy with (8) and under the same conditions that:



APPROVED FOR RELEASE: 2007/02/09: CIA-RDP82-00850R000500020034-7

APPROVED FOR RELEASE: 2007/02/09: CIA-RDP82-00850R000500020034-7



$$e(t) = -\omega k^{-1/s} sw \xi \mu_0 H_m \cos \omega t \sum_{n=1}^{\infty} \nu_{2n-1}(t) \times$$

$$\times \mu_{\Delta(2n-1)}^{\bullet} \sin [(2n-1)\omega t + \varphi_{2n} + \Delta\varphi] =$$

$$= -\omega k^{-1/s} sw \xi \sum_{n=1}^{\infty} \nu_{2n-1}(t) B_{2n} \sin (2n\omega t + \varphi_{2n}^{1}) , \quad (10)$$

where $B_{2n}$ represents coefficients of the series (the constant component and peak values of even induction harmonics);

$$\varphi_{2n}^{'} = F(\varphi_{2n-1} , \Delta\varphi) .$$

It is obvious from expression (10) that the spectral distribution of excess noise near the zero frequency and even harmonics depends on the spectrum of weighting functions $\nu_{2n-1}(t)$ . If the energy spectrum of functions $\nu_{2n-1}(t)$ varies according to the 1/f rule, then the energy spectrum of excess noise will also vary according to the same law.

In fig 3, in which a schematic representation is given of asymmetric hysteresis loops corresponding to an individual cycle or some sequence of magnetic reversal cycles, it is obvious that the asymmetry of the loop can be related to a difference in positive and negative coercive forces (fig 3a), to a difference in residual induction (fig 3b), to the different slope of loop back edges (fig 3c) or to their bending (fig 3d), to different squareness ratios of the loop or different values of maximum induction (fig 3e). A constant component and even induction and e.m.f. harmonics are evidenced in all these cases.

M.V. Bukharov [18] directly related excess noise near zero frequency and even induction harmonics to fluctuations in coercive forces and residual induction of the loop, considering these fluctuations statistically independent. He demonstrated that relative deviations in these values of by $10^{-3}$ to $10^{-4}$ are completely sufficient to cause excess noise at the level observed in practice and he established a quantitative relationship between noise levels at zero frequency and in even harmonics. From the expressions obtained by him it also follows that the spectral distribution of excess noise obeys the law of the spectral distribution of fluctuations in these parameters of the loop.

Thus, fluctuations in parameters of the dynamic loop of a ferromagnetic, resulting if only in short-duration asymmetry of it, as well as the presence of a correlation in Barkhausen abrupt changes, explaining rises in spectral density of the noise, are basic, if not the major, prerequisites for the origin of excess noise near even induction and e.m.f. harmonics.



APPROVED FOR RELEASE: 2007/02/09: CIA-RDP82-00850R000500020034-7

APPROVED FOR RELEASE: 2007/02/09: CIA-RDP82-00850R000500020034-7



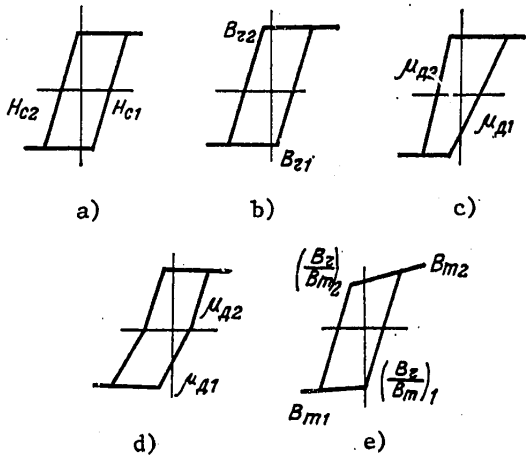


Figure 3. Asymmetric Hysteresis Loops

Let us investigate the physical essence of these prerequisites.

"Dislocation" Model of Noise; Role of Magnetostriction

Barkhausen abrupt changes originate primarily as the result of elastic interaction between moving domain boundaries and defects in the crystal lattice. Dislocations are the largest defects in ferromagnetics [19, 20].

The interaction of a boundary with a dislocation is described by the Peach-Keller equation [19]:

$$\vec{p} = -\int d\vec{l}\,(\hat{\sigma}^{M}\vec{b}), \tag{11}$$

where $\vec{p}$ is the force of interaction; $d\vec{l}$ is an element of the length of the dislocation line, $l$; $\hat{\sigma}^{M}$ is the tensor of magnetostriction internal stresses caused by the change in the direction of magnetization at the boundary; $\vec{b}$ is the Burgers vector.

G. Rider made a calculation of internal stresses for the most important plane boundaries encountered in iron, nickel and cobalt. It was demonstrated that with the proper choice of the system of coordinates (axis $z$ is oriented along the normal line to the boundary) it is possible to utilize only three components of tensor $\hat{\sigma}^{M}$. For a straight-line dislocation situated parallel to the plane of the boundary, from (11) it follows that



APPROVED FOR RELEASE: 2007/02/09: CIA-RDP82-00850R000500020034-7

APPROVED FOR RELEASE: 2007/02/09: CIA-RDP82-00850R000500020034-7



$$p_z = \hat{\sigma}^M_{11} l_y b_x - \hat{\sigma}^M_{22} l_x b_y + \hat{\sigma}^M_{12} (l_y b_y - l_x b_x), \tag{12}$$

where $l_i$ and $b_i$ are components of vectors $\vec{l}$ and $\vec{b}$.

Let us find the conditions under which force $p_z$ is minimized and, consequently, the intensity of Barkhausen abrupt changes and the noise level associated with them are diminished.

It is obvious from (12) that force $p_z$ becomes equal to zero if vector $\vec{l}$ or $\vec{b}$ are perpendicular to the plane of the boundary. These orientations are permissible and possible for single cases of interaction between boundaries and dislocations. However, it is not known how to render so favorable orientations possible if not for all but if only for a sufficiently great number of these types of interaction. Therefore, for practical purposes another method of minimizing force $p_z$ is obviously more effective--reducing the absolute values of components $\sigma^M_{11}$, $\sigma^M_{22}$ and $\sigma^M_{12}$ of the tensor of internal stresses, $\hat{\sigma}^M$.

As Rider demonstrated [19, 20], components $\sigma^M_{11}$, $\sigma^M_{22}$ and $\sigma^M_{12}$ are proportional to magnetostriction coefficients $\lambda_{100}$ and $\lambda_{111}$ of the ferromagnetic material or alloy. In turn, coefficients $\lambda_{100}$ and $\lambda_{111}$ depend on the percentage content of nickel in the alloy [21]. Both coefficients pass through zero with a nickel content of 80 to 83 percent. Consequently, according to expression (12), alloys with this nickel content must possess minimum intensity of Barkhausen abrupt changes and the lowest noise level.

This conclusion agrees totally with experimental estimates of noise levels found earlier (for a wide range of alloys) [2, 12, 16, 22].

Elaboration of the conditions for minimizing force $p_z$ for alloys with values of coefficients $\lambda_{100}$ and $\lambda_{111}$ close to zero is of interest. The point is that in the nickel content range indicated (80 to 83 percent) coefficients $\lambda_{100}$ and $\lambda_{111}$ become equal to zero not simultaneously (cf. table 1) [23]. Therefore, in minimizing force $p_z$ it is necessary to take into account both the absolute values and signs of these coefficients, and a relationship with which both coefficients (the positive, $\lambda_{100}$, and the negative, $\lambda_{111}$) will differ from zero can prove to be optimum.

Experiments and calculations [24, 25] which we have made have confirmed this assumption.

Curves, plotted from our experimental data, characterizing the relationship between the noise level and the saturation magnetostriction, $\lambda_s$, of alloys used for various types of ferroprobes are presented in fig 4. (The parameters of the ferroprobes are presented below in the note to table 2.) It is obvious from fig 4 that the noise minimum is shifted into the region of negative values of $\lambda_s$. The values found in the experiment, $\lambda_s = -(0.5 \text{ to } 2.0) \cdot 10^{-6}$, are achieved only when coefficients $\lambda_{100}$ and $\lambda_{111}$ have different signs and coefficient $\lambda_{111}$ is negative.



APPROVED FOR RELEASE: 2007/02/09: CIA-RDP82-00850R000500020034-7

APPROVED FOR RELEASE: 2007/02/09: CIA-RDP82-00850R000500020034-7



Table 1. Dependence of Magnetostriction Coefficients $\lambda_{100}$ and $\lambda_{111}$ on Percentage Content of Nickel in Ni-Mo-Fe Alloys

| Процентное содержание 1) | | $\lambda_{100} \times 10^{-6}$ | $\lambda_{111} \times 10^{-6}$ |
|---|---|---|---|
| Ni | Mo | | |
| 80,36 | 4,26 | 2,11 | 0,22 |
| 81,0 | 3,50 | 1,12 | —0,89 |
| 82,0 | 5,0 | 0,63 | —0,45 |
| 84,0 | 2,69 | —2,12 | —2,34 |

Key:
1. Percentage content

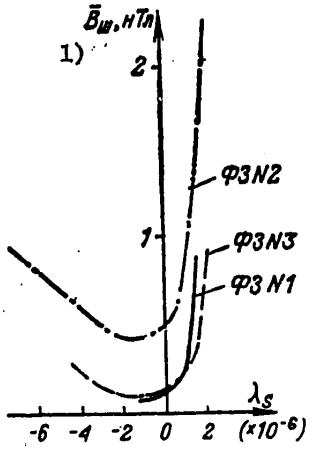


Figure 4. Relationship Between Noise Level, $\bar{B}_{sh}$, and Saturation Magnetostriction, $\lambda_s$, of Nickel-Iron Alloys for Various Types of Ferroprobes

Key:
1. $\bar{B}_{sh}$, nT

The experimental data do not agree completely with the calculated, since expression (12) was obtained with certain assumptions and, in addition, was extended by us to polycrystalline specimens of alloys. However, the results obtained testify to the advantage of the "dislocation" model of noise developed here and indicate a



APPROVED FOR RELEASE: 2007/02/09: CIA-RDP82-00850R000500020034-7

APPROVED FOR RELEASE: 2007/02/09: CIA-RDP82-00850R000500020034-7



different, as compared with that suggested earlier [12, 16], role of magnetostriction in the mechanism of the origin of noise.

Because of magnetostriction interaction is established between elements of the domain and dislocation structures of the ferromagnetic. Therefore, its role reduces to regulating these forms of interaction. Since the noise is determined by the intensity of these forms of interaction, the pattern described above is observed: With strong interaction the noise level correlates with the value of $|\lambda_s|$ ; with slight interaction, when it is necessary to take into account the signs of coefficients $\lambda_{100}$ and $\lambda_{111}$ , the noise minimum shifts to the region of negative values of $\lambda_s$ .

The relationships found relate to an equal degree both to ordinary and to excess noise.

Let us now explain on the basis of the "dislocation" model the excess noise phenomenon itself.

Since action equals counteraction, then from (11) it follows that not only does a dislocation act on a boundary with a force of p , preventing its motion, but the boundary acts on the dislocation with the same force, but with the opposite sign. But the reaction of a dislocation to this effect is considerably slower than the opposite. This is due to kinetic restructuring of the dislocation's structure, obeying the laws of plasticity [19]. A dislocation has low mobility. Rates of their motion (under low stresses) equal $10^{-9}$ m/s and less. Domain boundaries, on the other hand, are exceptionally mobile. Therefore, "repeatability" of events of interaction between boundaries and dislocations for the duration of hundreds and thousands of magnetic reversal cycles is precisely the physical prerequisite for the establishment of the correlation of Barkhausen abrupt changes and, consequently, the appearance of excess noise near discrete lines--harmonics of the magnetic reversal frequency.

Let us now discuss aspects of the interaction of magnetization with dislocations resulting in asymmetry of the hysteresis loop and fluctuations in it.

In [16] attention was turned to the presence in ferromagnetics of asymmetric microhysteresis loops. It was noted that in spite of considerable averaging, taking place with the superposition of these loops in the bulk of the ferromagnetic, the resulting or macrohysteresis loop can remain asymmetric. Here two questions remain unclear: What causes the asymmetry of microresistive loops and why averaging does not result in strict symmetry of the resulting loop. The answer to the first question is given in [20]. The authors discovered a "gate effect," consisting in the fact that when a domain boundary passes through a dislocation in a number of instances a new domain originates, and the very fact of its origin depends on the direction of motion of the boundary. If a domain originates in forward motion of the boundary, then its reverse motion "erases" the domain. This fact also causes asymmetry of microresistive loops. The answer to the second question must be found in the kinetics of the restructuring of domain and dislocation structures. In spite of the fact that a domain structure rather quickly "adapts" to a dislocation structure, the very fact of the restructuring of the latter creates situations in which the overall gate effect in the ascending portion of



APPROVED FOR RELEASE: 2007/02/09: CIA-RDP82-00850R000500020034-7

APPROVED FOR RELEASE: 2007/02/09: CIA-RDP82-00850R000500020034-7



the loop can predominate over that in the descending portion and vice-versa. This predominance is evidenced in a difference in the coercive forces of the loop (cf. fig 3).

Stresses created by dislocations influence not only displacement processes but also processes of rotation and center formation. Inducing anisotropy, these stresses prevent synchronous (i.e., with the frequency of the excitation field) magnetic reversal of "inflexible" regions and fix for a certain time centers for the origin of regions of opposite magnetization. The characteristic delay times here are also determined by the kinetics of restructuring of the dislocation structure, which results in if only a short-duration difference in the residual and maximum induction of the loop, as well as in a difference in its squareness ratio (cf. fig 3b and 3).

As mentioned in the preceding section, fluctuations resulting in asymmetry of the loop are completely sufficient for the origin of excess noise near even harmonics of the magnetic reversal frequency.

Thus, within the framework of the "dislocation" theory it is possible to find conditions under which minimization of the magnetic noise of ferromagnetics subjected to magnetic reversal cyclically is achieved, which is of great practical significance. In addition, it is possible to explain the role of magnetostriction in the mechanism of the origin of noise (which previously appeared puzzling), to understand the nature of the correlation of Barkhausen abrupt changes separated by a great number of cycles and the nature of fluctuations of the parameters of the resulting hysteresis loop and, at the same time, to explain the origin of excess noise near discrete lines--harmonics of the magnetic reversal frequency--including near even harmonics.

Factors Influencing the Noise Level in Ferroprobes and Magnetic Amplifiers

The difficulties in studying the basic mechanisms and in constructing an appropriate theory of magnetic noise lie primarily in the multifactor nature of this phenomenon. Noise depends not only on the properties and parameters of the ferromagnetic material or alloy used, but also on the volume and form of cores, their fabrication technology, heat treatment features, parameters of the excitation field, external mechanical stresses and the temperature gradient in the bulk of cores.

Let us discuss the influence of these factors on the noise level in ferroprobes and magnetic amplifiers.

Composition of the Alloy

As was already indicated above, the cores of low-threshold ferroprobes and magnetic amplifiers must be made of alloys containing 80 to 83 percent nickel. The fact of a correlation between noise level and the percentage content of nickel in the alloy was noted in [2, 22]. An experimental alloy containing 81.2 percent Ni, 2.5 percent Mo and 16.3 percent Fe was recommended in [16] as a low-noise alloy, and in [26] an alloy containing 81.5 percent Ni and 6 percent Mo.



APPROVED FOR RELEASE: 2007/02/09: CIA-RDP82-00850R000500020034-7

APPROVED FOR RELEASE: 2007/02/09: CIA-RDP82-00850R000500020034-7



In connection with the development of new nickel-iron alloys, we made studies of the noise properties of new alloys and ones previously used with a percentage content of nickel close to that indicated [17, 24].* The results of these studies are given in table 2, in which the noise levels measured are compared not only with the values of saturation magnetostriction, $\lambda_s$, but also with other parameters of alloys.

Table 2. Relationship Between Noise Level in Ferroprobes and Parameters of Nickel-Iron Alloys

| Марка сплава 1) | 2) Параметры сплавов | | | | 3) Уровень шума ФЗ[1] $B_ш$, нТл (в полосе частот 0.001...1.0 Гц) для четырех различных образцов (№ 1—№ 4) | | | |
|---|---|---|---|---|---|---|---|---|
| | $\lambda_s \times 10^{-6}$ | $H_c$, А/м | $\mu_a \times 10^3$ | 4) $B_s$, Тл | № 1 | № 2 | № 3 | № 4 |
| 79НЗМ | 2,0 | 3,2 | 14 | 0,85 | 0,28 | — | — | — |
| 79НМ | 2,0 | 2,4 | 20 | 0,73 | 0,22 | 0,82 | 0,17 | — |
| 80НХС | — | 2,4 | 22 | 0,63 | 0,14 | — | — | — |
| 83НФ | 0,5 | 1,6 | 58 | 0,60 | 0,065 | 0,40 | 0,12 | 0,028 |
| 81НМА[2] | 0,5 | 0,88 | 66 | 0,70 | 0,060 | 0,34 | 0,065 | 0,015 |
| 82НМП | —1,5 | 1,35 | 64 | 0,67 | 0,050 | 0,27 | 0,04 | 0,012 |
| 84Н | —14 | — | — | — | — | 2,0 | — | — |

Key:
1. Type of alloy
2. Parameters of alloys
3. Noise level in ferroprobe, $B_{sh}$, nT (in the 0.001 to 1.0 Hz frequency band) for four different samples (Nos 1 to 4)[1]
4. T

[1]Parameters of ferroprobes: No 1--core dimensions 130 X 2.8 X 0.1 mm, frequency $f_v$ = 1 kHz ; No 2--core dimensions 10 X 1.2 X 0.05 mm, frequency $f_v$ = 25 kHz ; No 3--core dimensions, loop (20 X 6) - (18 X 4) X 0.05 mm, frequency $f_v$ = 25 kHz; No 4--ring (diameter 13.2 mm, width 1.5 mm, thickness 0.12 mm), $f_v$ = 12.5 kHz .

[2]Annealing was performed at 800 °C, holding for 3 h, cooling at a rate of 200 °C/h to 600 °C, then at a rate of 400 °C/h.

*The alloys were developed by the TsNIIChermet [Central Scientific Research Institute of Ferrous Metallurgy] imeni I.P. Bardin Institute of Precision Alloys. The parameters and characteristics of the new alloys (except alloy 82NMP) are regulated by GOST [All-Union State Standard] 10160-75, "Alloys, Precision, Magnetically Soft."



APPROVED FOR RELEASE: 2007/02/09: CIA-RDP82-00850R000500020034-7

APPROVED FOR RELEASE: 2007/02/09: CIA-RDP82-00850R000500020034-7



From table 2 it is obvious that new alloys 81NMA, 83NF and 82NMP have a lower noise level than alloy 79NM and 80NKhS used in ferroprobes and magnetic amplifiers previously. Furthermore, alloys 81NMA and 83NF are characterized by a lower value of saturation magnetostriction, $\lambda_s = 0.5 \cdot 10^{-6}$. Alloy 82NMP (82NMP-VI), characterized by a negative value of $\lambda_s = -(0.5 \text{ to } 1.5) \cdot 10^{-6}$, has the lowest noise level.*

Shifting of the noise minimum into the region of negative values of $\lambda_s$ is in agreement with the "dislocation" model of noise and the theoretical postulates discussed in the preceding section.

Magnetic Properties of the Alloy

The magnetic properties of alloys and the parameters characterizing them are divided into structure-sensitive and structure-insensitive. Under the heading of structure-sensitive parameters come the coercive force, $H_c$, permeability, $\mu$, and hysteresis losses, W; under structure-insensitive come saturation induction, $B_s$, and other parameters. Within the framework of the "dislocation" theory of noise developed by us it is to be expected that it is precisely the structure-sensitive parameters of alloys which will correlate with the noise level observed.

It is also obvious from table 2 that for the group of alloys with positive magnetostriction ($\lambda_s > 0$) the noise level measured actually correlates both with the coercive force, $H_c$, and with a value which is the inverse of the initial magnetic permeability, $\mu_a$. These data do not contradict those obtained earlier in [22, 27].

If the main contribution to noise power is actually made by the halting of domain boundaries in dislocations, then the spectral density of the noise's e.m.f., $g_\varepsilon$, must be proportional to the volume density of dislocations, $\rho$, and, consequently, according to what was said in the second section, the following proportionality must also be observed:

$$\bar{B}_m \sim \rho^{1/2}.$$

On the other hand, from applications of the theory of the ductility of materials to ferromagnetics it follows that [19]:

$$H_c \sim \mu_a^{-1} \sim \rho^{1/2}.$$

Therefore, within the framework of the "dislocation" model a relationship between the noise level, $\bar{B}_{sh}$, and quantities $H_c$ and $\mu_a^{-1}$ is completely natural. The curve reflecting this relationship is shown in fig 5 [17].

In [14] on the basis of certain experimental data and assumptions regarding the capacity for the fulfillment of an inverse proportion relationship between the

*The parameters and properties of alloy 82NMP are presented in the catalogue "Novyye pretsizionnyye splavy" [New Precision Alloys], Moscow, Chermetinformatsiya. 1979.



APPROVED FOR RELEASE: 2007/02/09: CIA-RDP82-00850R000500020034-7

APPROVED FOR RELEASE: 2007/02/09: CIA-RDP82-00850R000500020034-7



coercive force, $H_c$, and maximum permeability, $\mu_{max}$, the conclusion is drawn that for the purpose of improving the signal-to-noise ratio it is necessary to strive to increase the ratio $\mu_{max}/|\lambda_s|$. In this connection it is necessary to make the following comments. First, with an increase in $\mu_{max}$ not only the legitimate signal can increase, but also the noise, especially when the increase in $\mu_{max}$ is caused by formation of the alloy's texture. Therefore it is hardly possible to achieve considerable improvement of the signal-to-noise ratio only by increasing the value of $\mu_{max}$. Second, a distinct inverse proportion relationship has been established up to now only for quantities $H_c$ and $\mu_a$ [17, 19], but not for quantities $H_c$ and $\mu_{max}$. Third, as was already explained in detail, it is not possible to utilize the absolute value $|\lambda_s|$, since the noise minimum is shifted into the region of negative values.

Let us discuss the relationship between noise and hysteresis losses. Hysteresis losses, W, are proportional to product $H_c B_s$; therefore the spectral density of the noise must be proportional to this quantity. However, since the structure-sensitive parameter of an alloy is all the same the coercive force, $H_c$, and not the saturation induction, $B_s$, then the noise correlates more strongly with quantity $H_c$ than with $B_s$ (cf. table 2).

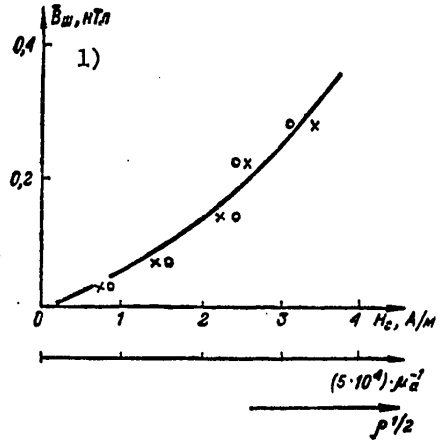


Figure 5. Dependence of Noise Level, $\bar{B}_{sh}$, on Coercive Force, O, and the Inverse Value of the Original Magnetic Permeability, X, with a Coupling Constant of $5\cdot10^4$

Key:
1. $\bar{B}_{sh}$, nT



APPROVED FOR RELEASE: 2007/02/09: CIA-RDP82-00850R000500020034-7

APPROVED FOR RELEASE: 2007/02/09: CIA-RDP82-00850R000500020034-7



The squareness of the hysteresis loop also influences the noise level. Already with the data of [1] it was possible to conclude that the noise increases with an increase in squareness of the loop. New data [14, 28] confirm this. It was noted in [14] that in alloys with a square loop the noise increases on account of the consolidation of individual regions magnetically reversed simultaneously. It is also noted that the consolidation of these regions and, consequently, the reduction of their number, must result chiefly in an increase in excess noise. In our opinion the increase in both excess and ordinary noise in alloys with a square loop is associated primarily with the presence of a texture preventing the magnetic reversal of "inflexible" regions. This question will be discussed below.

Volume and Form of Cores; Their Fabrication Technology

It was demonstrated above that the spectral noise density, $g_f$, is proportional to the volume density of dislocations, $\rho$. From this the conclusion can be drawn that with a given $\rho$ the spectral noise density must be proportional also to the volume of the core, i.e., $g_f \sim \rho$.

However, since with a change in the volume of cores, v, not only quantity $g_f$ changes, but also quantity G --the transformation ratio of ferroprobes and magnetic amplifiers--and both these quantities enter into expression (6) for the threshold sensitivity, $\overline{B}_{sh}$, then dependence $\overline{B}_{sh}(v)$ will be more complex. Let us discuss some particular cases.

Let there be a ferroprobe with relatively short cores. The maximum differential permeability of these cores is determined by the expression [1, 2]:

$$\mu^{\bullet}_{\text{д max}}\Big|_{m \,<\, \mu_{\text{д max}}} \cong m = A\frac{l^2}{s}, \tag{15}$$

where $\mu_{d\,max}$ is the maximum differential permeability of the material; m is the permeability of the form; and $A = A(l, s)$ is a function depending slightly on $l$ and $s$.

Substituting expression (15) in (5) and disregarding dependence $A(l, s)$, we get $G \sim l^2$, i.e., the transformation ratio of a ferroprobe with short cores does not depend on the area, s, of their cross section. Therefore, with one and the same internal maximum strength of the excitation field, disregarding the influence of the demagnetization factor on processes of the origin of Barkhausen abrupt changes and their space correlation [5], we get from (6):

$$\overline{B}_{\text{ш ФЗ}}\Big|_{\substack{m \,<\, \mu_{\text{д max}};\\ s = \text{const} \neq 0}} \sim v^{-2/3}. \tag{16}$$

It is obvious from expression (16) that in ferroprobes it is feasible to increase the volume of cores only on account of increasing their length. When the volume of cores is increased on account of increasing their cross-sectional area with



APPROVED FOR RELEASE: 2007/02/09: CIA-RDP82-00850R000500020034-7

APPROVED FOR RELEASE: 2007/02/09: CIA-RDP82-00850R000500020034-7



an assigned length, as the experimental data in [1, 19] demonstrate, the reduction in the noise level, $\overline{B}_{sh}$, is exceedingly slight. Moreover, as will be demonstrated below, with an assigned length ferroprobe cores have an optimum cross-sectional area (with regard to the noise minimum).

The situation is otherwise with magnetic amplifiers. In closed cores of magnetic amplifiers a demagnetization factor for the circular field measured is lacking, as the result of which the transformation ratios prove to be proportional to the cross-sectional area of the cores, i.e., $G \sim s$. Therefore, with the same assumptions we get from (6):

$$\overline{B}_{\text{ш MУ}}\Big|_{l=\text{const}\neq 0} \sim v^{-1/4}. \tag{17}$$

From this it is obvious that, unlike ferroprobes, in magnetic amplifiers it is feasible to increase their volume precisely by increasing their cross-sectional area.

It must be emphasized that the transformation ratio of a magnetic amplifier, because of the absence of a demagnetization factor in its cores, is always higher than the transformation ratio of a ferroprobe. Therefore, in spite of the higher exponent for $v$ in expression (16) the noise level, $\overline{B}_{sh}$, is higher in a ferroprobe than in a magnetic amplifier [1]. With a great increase in the length of ferroprobe cores condition $m \ll \mu_{d\,max}$ is violated and expression (16) becomes invalid. At the limit, when the influence of the demagnetization factor in ferroprobe cores can be disregarded, dependence $\overline{B}_{sh}(v)$ will be described by expression (16).

Expression (17) agrees well with the experimental data in [1, 10] (as noted in [2], this agreement with the experimental data indicates the absence of substantial transverse correlation of noise in cores) and reflects rather graphically the fact that the spectral density of noise power is actually proportional to the volume of the cores, $g_f \sim v$. On the basis of this, in [10] it is suggested that the noise properties of materials and alloys be characterized by parameter $C_B$ (let us use our symbols--cf. the second section):

$$C_B = g_f v^{1/4} = \frac{\sqrt{g_f v}}{G_{MУ}},$$

which does not depend on the volume of cores, since $g_f v \sim v^2$ and $G_{MU}$ [magnetic amplifier] $\sim v$ (with $l$ = const).

The cores of ferroprobes and magnetic amplifiers are usually made of a rolled narrow strip 0.02 to 0.1 mm thick. Thinner strips are not used because of worsening of their magnetic properties (reduction of initial and maximum permeability



APPROVED FOR RELEASE: 2007/02/09: CIA-RDP82-00850R000500020034-7

APPROVED FOR RELEASE: 2007/02/09: CIA-RDP82-00850R000500020034-7



and increase in coercive force [29]), and thicker ones because of the spin effect and losses associated with it [1, 29].

Cores are made by the method of die forging or winding onto a supporting frame (a spool). In the latter instance a strip of the prescribed width is cut by means of precision roller shears. After the stock is cut out and cut burrs are removed and their surface is chemically or electrically polished. These operations reduce the density of defects (dislocations) originating in large quantity in the vicinity of the cutout line or cutoff line.

A further reduction in the density of defects is achieved by heat treating the cores.

Heat Treatment of Cores

The great influence of this factor is explained by the fact that in the heat treating process certain types of defects are partly eliminated and internal stresses are reduced [19, 21].

The mode of heat treatment of cores is characterized by the maximum annealing temperature, the medium in which annealing takes place and the rate of cooling of cores.

The dependence of the noise level on the maximum annealing temperature for cores was studied in [24, 30]. It was established that the minimum noise level for cores made of alloy 81NMA is achieved at annealing temperatures lower than those recommended, and precisely at 800 °C. According to the data of [30], at the same annealing temperature a noise minimum is observed also in cores made of alloys 79NM and 83NF, and for alloy 79NM this effect occurs if the alloy is produced by the electron beam remelting method, but not by open induction melting. In [24] the effect of a reduction in noise level with a reduction in the maximum annealing temperature for cores is related to an increase in the hardness of the alloy, and in [30] to the formation of its fine-grained structure. These explanations are contradictory and the effect itself requires further study.

The dependence of the noise level on the medium in which annealing of cores takes place was noted in [26, 30]. Annealing in a hydrogen atmosphere as compared with annealing under vacuum results in an approximately 1.5-fold reduction in noise level.

The dependence of the noise level on the cooling rate of cores has been discussed in a number of studies. In [22] the following general rule was established for a considerable number of binary nickel-iron alloys: The noise is reduced with rapid cooling of cores. Unfortunately, in this study data are not given on the procedure and rate for cooling cores and an explanation is not given of the pattern observed itself. It is necessary to judge regarding this from the data of other studies. For example, in [21, 31] it is noted that with the rapid cooling of cores the alloy becomes less ordered and more magnetically soft than with slow cooling. Rapid cooling is conducive to a reduction of magnetic anisotropy [21] and, consequently, to the probability of the existence of "inflexible" regions which



APPROVED FOR RELEASE: 2007/02/09: CIA-RDP82-00850R000500020034-7

APPROVED FOR RELEASE: 2007/02/09: CIA-RDP82-00850R000500020034-7



result in asymmetry of the loop and is one of the reasons for the appearance of noise near even harmonics of the output e.m.f. of a ferroprobe and magnetic amplifier.

The question regarding the magnetic texture of the material acquired in the process of cooling of cores deserves attention. The permeability of the form of ferroprobe cores varies over a range of $(1 \text{ to } 20) \cdot 10^3$. Therefore, even in the magnetic field of the earth induction in cores can have values on the order of 0.1 T and result in the formation of a magnetic texture. The appearance of a texture will also be conducive to the securing of "inflexible" regions.

In [24, 30] a study was made of the influence of the rate of cooling of ferroprobe cores at 100 and 1500 °C/h over a temperature range of 700 to 350 °C. A noticeable difference was not observed in the minimum achievable noise levels corresponding to these rates. However, it was found in [30] that two- to threefold lower values of the excitation current correspond to a faster rate of cooling (1500 °C/h) for cores made of alloy 79NM, whereby the same noise minimum is achieved. These studies are of undisputed interest since they make it possible to obtain information on the mechanisms for the origin of noise at the stage of rotation processes and therefore should be continued.

Excitation Field Parameters

These include peak value, degree of inhomogeneity, direction and frequency.

A curve characterizing the dependence of the noise level, $\overline{B}_{sh}$, on the peak value of the excitation field, $H_m$, for ferroprobes and magnetic amplifiers with longitudinal excitation and output at the second harmonic is shown in fig 6.

It is possibe to explain this shape of the $\overline{B}_{sh}(H_m)$ curve if this curve is represented as the resultant of two other curves, also shown in fig 6. The first characterizes the growth in volume density of the interaction of domain boundaries with defects (dislocations) or, which is the same thing, the increase in the number of Barkhausen abrupt changes; the second characterizes the drop or reduction in fluctuations of the parameters of abrupt changes and consequently parameters of the hysteresis loop as the maximum magnetic reversal cycle is approached.

With very low peak values of the excitation field, interaction of domain boundaries with dislocations is reversible (the Rayleigh region), Barkhausen abrupt changes still do not originate here and noise in the ordinary sense of this word (i.e., as some random process) is absent. However, strong displacements (on the order of $10^{-8}$ to $10^{-6}$ T) are observed in magnetic amplifiers and ferroprobes. These displacements are the result of a great number of "inflexible" regions not partaking in the magnetic reversal process, and can be regarded as a "frozen" fluctuation of a specific parameter of the hysteresis loop.

As the peak value of the excitation field increases, the interaction of boundaries with dislocations becomes irreversible, Barkhausen abrupt changes originate and individual "inflexible" regions begin to be magnetically reversed (although not in step). The "brittle springs" model [32] gives a clear idea of these processes.



APPROVED FOR RELEASE: 2007/02/09: CIA-RDP82-00850R000500020034-7

APPROVED FOR RELEASE: 2007/02/09: CIA-RDP82-00850R000500020034-7



The sudden rise in noise in this section is directly related to the increase in the volume density of these forms of interaction. Finally, with a specific peak value of the excitation field the growth in noise ceases. In spite of a continued increase in the number of Barkhausen abrupt changes the mechanism for the suppression of fluctuations of the parameters of abrupt changes and for stabilization of the parameters of the hysteresis loop goes into effect. The balance of increases in these two trends also determines the point of the maximum on the $\overline{B}_{sh}(H_m)$ curve. The noise level is reduced, first rather quickly and then more slowly, with a further increase in the peak value of the excitation field.

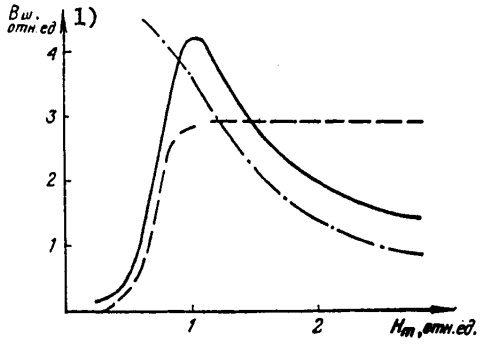


Figure 6. Dependence of Noise Level, $\overline{B}_{sh}$, (Normal Component) on Peak Value of the Excitation Field, $H_m$ $(H_{max})$ : --- curve characterizing intensity of Barkhausen abrupt changes; -·- curve characterizing number of "inflexible" regions and level of fluctuations caused by them

Key:

1. $B_{sh}$, relative units

A similar dependence for $\overline{B}_{sh}(H_m)$ is observed in testing various designs of ferroprobes and magnetic amplifiers [1, 2, 9, 10, 16, 33]. Furthermore, as emphasized in [10], the drop in noise is associated precisely with the peak or maximum value of the excitation field and not with the form of its wave. At the same time, since the value of $B_{sh}$ is inversely proportional to the transformation ratio, G, (cf. expression (6)), which in many cases diminishes with an increase in the excitation field, effective lowering of the noise level on account of an increase in the maximum value of the field is made possible with a square-pulse wave form (cf. fig 2). A close to square-pulse wave form is achieved, for example, in the ferroresonance mode of exciting magnetic amplifiers and ring ferroprobes [34].



APPROVED FOR RELEASE: 2007/02/09: CIA-RDP82-00850R000500020034-7

APPROVED FOR RELEASE: 2007/02/09: CIA-RDP82-00850R000500020034-7



Experience has demonstrated that with an increase in the peak value of the excitation field both ordinary and excess noise are reduced. Furthermore, excess noise is "retained against," as it were, discrete lines--harmonics of the magnetic reversal frequency [11]. This behavior of excess noise can be related to the ever more complete and synchronous (i.e., with the frequency of the excitation field) magnetic reversal of "inflexible" regions, as well as to symmetrization of the hysteresis loop, which was talked about in the third and fourth sections.

The fairly slow drop in noise in strong fields is associated with the existence of crystallographic and induced anisotropy. It is precisely anisotropy which prevents the synchronous magnetic reversal of "inflexible" regions. Therefore, for the purpose of the effective suppression of noise on account of an overexcited operating mode for ferroprobes and magnetic amplifiers it is necessary to use materials possessing not only low values of saturation magnetostriction, but also low values of crystallographic anisotropy constants, as well as slightly textured materials. Under the heading of these materials come the already discussed nickel-iron alloys, in which the effectiveness of noise suppression on account of overexcitation increases with an increase in the rate of cooling of cores after they are annealed [22, 30, 31]. The strong influence of the rate of cooling of an alloy on the noise level leads to the conclusion that not only these alloys but also the amorphous materials under intense development [35] can prove to be promising for use in ferroprobes and magnetic amplifiers. The fabrication of amorphous materials involves the exceedingly rapid cooling of a melt put into a rotating drum. The cooling rate can reach $16^6$ °C/s. As a result a magnetically soft material is produced with a homogeneous structure and lacking magnetocrystalline anisotropy. Data on magnetic noise in these materials is presented in the section "Ring Ferroprobe with Low Threshold Sensitivity."

It has also been demonstrated in an experiment that the effectiveness of the suppression of noise by increasing the peak value of the excitation field depends on the degree of inhomogeneity of this field. In the majority of studies [1, 2, 27] devoted to studying the nature of excess noise, this dependence is directly related to the existence of "inflexible" regions and the hysteresis memory of cores, determined from the level of the residual signal of a ferroprobe or magnetic amplifier after the short-duration influence on its cores of a strong steady magnetic field. It is known that the noise is reduced if, other conditions being equal, arrow-shaped or ring cores are used, making possible high uniformity of induction along their length. The external constant field (the measured or compensating) must also be homogeneous. It has been noted also that inhomogeneity of the external field results in asymmetry of the hysteresis loop [36].

An attempt at a "model" interpretation of the phenomena discussed here was made in [4]. Based on a model of "reversible ellipsoids of striction" various experimental facts were compared and again the role of crystallographic and induced anisotropy in suppressing noise by means of changing the parameters of the excitation field was emphasized. It was demonstrated that the elongated (sheetlike) shape of "inflexible" regions in the direction of the excitation field prevents their magnetic reversal and is one of the main reasons for the origin of excess noise, hysteresis memory and asymmetry of the magnetic reversal loop of ferroprobe and magnetic amplifier cores.



APPROVED FOR RELEASE: 2007/02/09: CIA-RDP82-00850R000500020034-7

APPROVED FOR RELEASE: 2007/02/09: CIA-RDP82-00850R000500020034-7



The model of "reversible ellipsoids of striction" makes it possible to understand also the dependence of noise level not only on a change in peak value, but also on a change in direction of the excitation field. In particular, the fact of a reduction in noise in ferroprobes with transverse excitation with the application of an added longitudinal variable field to cores [37], in a Schonstedt ferroprobe with "skew magnetic reversal" of cores [38], and in a Langvagen ferroprobe with the excitation of cores by means of a rotating field [39] becomes totally explainable. From the same model it is not difficult to draw the conclusion that the methods of excitation enumerated will be effective only with the presence of anisotropy. If the anisotropy is eliminated, the noise must depend slightly on the change in direction of the excitation field, which has been observed experimentally.

With the excitation of ferroprobe and magnetic amplifier cores by means of a rotating field with a sufficiently high "peak value," displacement processes and, consequently, events of the interaction of domain boundaries with dislocations resulting in Barkhausen abrupt changes are practically eliminated from the magnetic reversal cycle. This means that, at least, the level of ordinary magnetic noise in a ferroprobe and magnetic amplifier with a rotating excitation field must be considerably lower than in ferroprobes and magnetic amplifiers with longitudinal excitation. A rotating field acts effectively on excess noise and hysteresis memory only with the presence of crystallographic and induced anisotropy. The spectral distribution of noise in ferroprobes and magnetic amplifiers with a rotating excitation field requires additional study. The promise of these ferroprobes and magnetic amplifiers for measuring the parameters of weak and ultraweak magnetic fields is undisputed.

Let us now discuss the dependence of the noise level on the frequency of the excitation field. It is obvious that with an increase in the frequency of the excitation field the number of interactions of domain boundaries with dislocations per unit of time also increases. By analogy with what was said above we conclude that the spectral density of noise, $g_f$, (cf. the third section) must be proportional to the frequency, $f_b = \omega/2\pi$, of the excitation field, i.e., $g_f \sim f_b$. However, the noise level, $\overline{B}_{sh}$, depends not only on $g_f$, but also on the transformation ratio of the ferroprobe and magnetic amplifier. Since according to (5) $G \sim f_b$, for $\overline{B}_{sh}$ we have [1,2]:

$$\overline{B}_{sh} \sim f_v^{-1/2} \tag{18}$$

It is obvious from (18) that the noise is reduced with an increase in the frequency of the excitation field. However, at least two factors prevent an unlimited increase in the frequency of the excitation field: an increase in magnetic reversal losses and ever greater manifestation of the spin effect; and approaching subharmonics or the fundamental frequency of the magnetostrictive resonance of cores. Both factors result in an increase in noise [1, 2, 16]. Let us dwell in greater detail on the second factor. It was experimentally established in [16] that both ordinary and excess noise increase abruptly as magnetostrictive resonance is approached. In [16] this rise in noise is associated with fluctuations in the parameters of defects (dislocations) and with their possible migration. Within the framework of the model of "reversible ellipsoids of striction" the rise in noise



APPROVED FOR RELEASE: 2007/02/09: CIA-RDP82-00850R000500020034-7

APPROVED FOR RELEASE: 2007/02/09: CIA-RDP82-00850R000500020034-7



can be associated also with induced (on account of mechanical vibrations of the core) macroscopic and microscopic anisotropy [4, 35]. It is possible to avoid these undesirable phenomena if the length of a ferroprobe and magnetic amplifier rod core and the diameter of a ring core, with an assigned frequency, $f_h$, of the excitation field, do not equal the forbidden values, determined by equations (19):

$$l_{\text{забр}} = \frac{k}{4nf_h}\sqrt{\frac{E}{\rho}},$$
$$d_{\text{забр}} = \frac{1}{2\pi nf_h}\sqrt{\frac{E}{\rho}}\sqrt{1+(1-k)^2}, \tag{19}$$

where $n = 1, 2, 3, \ldots$ represents the order of perturbing vibrations (taking into account the parity of the magnetostriction effect); $k = 1, 2, 3, \ldots$ is the order of mechanical vibrations of the cores during resonance; $E$ is the elastic modulus; and $\rho$ is the density of the core material.

External Mechanical Stresses

As we know [21], external unidirectional mechanical stresses resulting in the extension or compression of cores alter substantially the shape of magnetization curves. Here the effects observed depend on the sign of saturation magnetostriction, $\lambda_s$. If $\lambda_s > 0$, then extension of a sample results in a sudden increase in maximum magnetic permeability and a reduction in initial permeability. With $\lambda_s < 0$ the opposite picture is observed. Already from these facts, taking into account what was said above, it would be possible to conclude that the noise should increase with the extension of cores made of alloys with $\lambda_s > 0$ and decrease for those made of alloys with $\lambda_s < 0$.

The results of direct measurements are presented in [40]. The author relates to the induction of magnetic anisotropy the rise in noise in samples with $\lambda_s > 0$ with the presence of a tensile load. Tension results in an increase in domains the direction of magnetization in which is close to the direction of tension. This direction also becomes an easy axis. If the external field is directed along this axis then on average Barkhausen abrupt changes should increase. In samples with $\lambda_s < 0$ the easy axis is perpendicular to the direction of tension. Therefore, when a field is applied in the direction of tension the intensity of Barkhausen abrupt changes will be reduced. With this samples become less anisotropic than before the beginning of tension.

The model of "reversible ellipsoids of striction" [4] gives a clear idea of the mechanisms described here.

It is hardly feasible to utilize these mechanisms for the purpose of suppressing noise. However, they should be recalled in all cases when cores are subjected to external stresses because of working conditions, e.g., when they are rigidly fastened to a base and the transformers themselves--the ferroprobe and magnetic amplifier--are designed for operation over a broad temperature range.



APPROVED FOR RELEASE: 2007/02/09: CIA-RDP82-00850R000500020034-7

APPROVED FOR RELEASE: 2007/02/09: CIA-RDP82-00850R000500020034-7



Temperature Changes

Let us dwell first of all on the dependence of the noise level, $\bar{B}_{sh}$, on the change in the mean temperature of cores. Direct measurements of the spectral density of magnetic noise in various ferromagnetics over a wide temperature range--from helium temperatures to Curie points--made by N.N. Kolachevskiy [5] have demonstrated that the noise level remains unchanged for nickel-iron alloys in the 100 to 300 °K temperature range.

Invariability of the noise level in the range indicated for the variation of mean temperatures of the samples studied can be associated first with the relative constancy both of saturation magnetostriction and of magnetic anisotropy [21] and second with the relative constancy of magnetic characteristics, i.e., the coercive force and initial permeability, which bear information regarding the volume density of dislocations [19].

With an increase in temperature to values close to the Curie point, saturation magnetostriction and magnetic anisotropy begin to diminish suddenly (more rapidly than saturation induction), the coercive force is reduced and initial permeability is increased, which, taking into account relationships (11), (13) and (14), as well as what was said above, should result in a reduction in Barkhausen abrupt changes and noise level. The dependence of the noise level on the change in temperature as the Curie point is approached for alloy 72NMDKh with a low Curie point was analyzed in detail in [41]. In fig 7 these dependences, $\bar{B}_{sh}(T)$, are compared with dependences $B_s(T)$ and $\mu_a(T)$ for the same alloy, taken by us from [29]. It is obvious from the dependences presented that a maximum on the $\mu_a$ curve corresponds to the noise minimum, which agrees with equations (13) and (14).

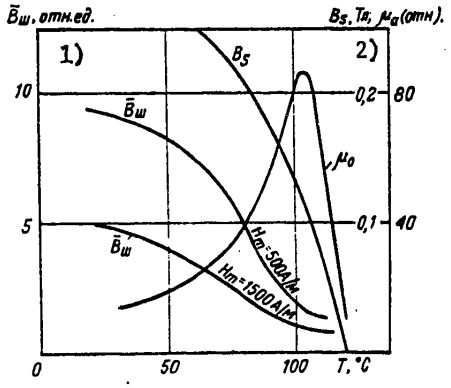


Figure 7. Dependence of $\bar{B}_{sh}$, $B_s$ and $\mu_a$ on Temperature as the Curie Point Is Approached for Alloy 72NMDKh

Key:
1. $\bar{B}_{sh}$, relative units
2. $B_s$, T; $\mu_a$ (relative)





APPROVED FOR RELEASE: 2007/02/09: CIA-RDP82-00850R000500020034-7

APPROVED FOR RELEASE: 2007/02/09: CIA-RDP82-00850R000500020034-7



In the region of low temperatures (less than 100 °K) magnetic anisotropy begins to increase [21], which according to the model of "reversible ellipsoids of striction" and what was said above should result in an increase at least in excess noise [4]. An increase in noise in a ferroprobe at low temperatures was described in [42]. The ferroprobe was placed in a superconducting shield and cooled from room temperature to the temperature of liquid helium. At room temperature (300 °K) the noise level equals 0.3 nT, at the temperature of liquid nitrogen (77 °K) 0.9 nT and at the temperature of liquid helium 3.0 nT, i.e., an order higher than at room temperature.* The ferroprobe was also heated to 423 °K. Within the range of 300 to 423 °K a noticeable change in noise level in the ferroprobe was not detected (the ferroprobe cores were made of alloy 79NM with a Curie point of $\Theta$ = 723 °K).

Let us now proceed to a discussion of the question of the influence of time and space changes in temperature on the noise level.

In [5] a brief survey of publications is given in which a study was made of the relationship between the nonrecurrence of Barkhausen abrupt changes and temperature changes. Referring to [43], in which a strong dependence of the noise level in nickel-iron alloys on the rate of change in temperature was observed, the author expressed the hypothesis that this dependence is caused by the "settling" of energy states and by a change in the magnetic structure of the ferromagnetic.

Another interpretation of this dependence is also possible. With a sudden change in the temperature of the environment, because of the slower propagation of heat in the core, described by the heat conduction equation, a temperature gradient originates in its depth. Both fluctuations in the parameters of Barkhausen abrupt changes and fluctuations in thermoelectric current [44], which add their contribution to excess noise, can be associated with the origin of a gradient and its subsequent elimination on account of equalization of the temperature in the core.

A direct relationship between the noise level and the temperature gradient component for the length of ferroprobe cores was established in [45]. Cores of uniform cross section were used, the magnetic induction in which, as we know [1, 2], is nonuniform even with a homogeneous external field: Induction is maximum at the center of the core and diminishes toward the ends according to a parabolic law. The temperature was measured along the length of cores when the latter were retained against bases made of AG-4S or DSV molding material with low heat conductivity and it was established that the shape of the $T(x)$ curve, where $x$ is the distance from the center of the core, in general features agrees with the shape of the $B(x)$ curve. Furthermore, the noise level in the ferroprobe was measured. Then the same cores were placed on bases made of VT1-0 titanium, the thermal conductivity of which is two orders of magnitude higher than that of bases made of

*This experiment was partly repeated at the All-Union Scientific Research Institute of Metrology imeni D.I. Mendeleyev Scientific Production Association in 1978 by V.I. Sheremet and V.N. Gorobey with a ferroprobe of a different design. At the temperature of liquid nitrogen the noise level proved to be three- to fourfold higher than at room temperature.



APPROVED FOR RELEASE: 2007/02/09: CIA-RDP82-00850R000500020034-7

APPROVED FOR RELEASE: 2007/02/09: CIA-RDP82-00850R000500020034-7



molding materials. The measurements demonstrated that with the presence of titanium bases the temperature along the length of the cores is equalized, and the noise (chiefly its excess component) is reduced two- to 2,5-fold.

Later the authors of this article made a similar experiment (without plotting the T(x) curve) with arrow-shaped cores making possible sufficient homogeneity of magnetic induction along their length. Replacement of the bases did not result in such a considerable change in the noise level in the ferroprobe.

From these experiments it follows that, first, the noise level is actually associated with the temperature gradient in cores and, second, the temperature gradient itself in many cases is caused by the inhomogeneity of magnetic induction in cores, appearing either on account of their shape or on account of the inhomogeneity of the excitation field. Both these facts must be taken into account in designing a low-threshold ferroprobe and magnetic amplifier.

In our opinion studies of temperature influences on the noise level, especially in the area of explaining the physical pattern of these influences, should be continued.

Other Factors

Let us dwell briefly on some other factors the mechanism of the influence of which however still requires its own interpretation.

It has been observed that the noise is reduced when ferroprobe and magnetic amplifier cores are placed in a viscous medium or fluid, e.g., glycerine. The core of a ring ferroprobe was placed in GKZh-94 fluid, and a three- to fourfold reduction in noise was observed.* This effect is apparently associated with a reduction in the intensity of magnetostriction vibrations of the core on account of suppression of the reflected acoustic wave [46].

A dependence of the noise level on the diameter of the turns of an excitation coil has been observed. It has been established that with the same excitation current a threefold reduction in the diameter of the turns of an excitation winding results in a two- to 2.5-fold reduction in noise level. We observe this effect both for rod and for ring ferroprobes.

A dependence of the noise level of a ferroprobe on the diameter of the turns of the measuring winding was observed even earlier [33] and again confirmed by our experiments. It was established that the greater the diameter of the turns the lower the noise level. In our experiments a twofold increase in the diameter of the measuring coil resulted in a 1.5- to twofold reduction in noise (with a simultaneous and quite considerable reduction in imbalance e.m.f.). One

*The experiment was prepared by L.Ya. Bushuyev and was conducted in a superconducting shield by V.I. Sheremet, Yu.N. Bobkov and V.N. Gorobey.



APPROVED FOR RELEASE: 2007/02/09: CIA-RDP82-00850R000500020034-7

APPROVED FOR RELEASE: 2007/02/09: CIA-RDP82-00850R000500020034-7



noncontradictory explanation of the noise reduction effect is given in [33] and other explanations can be given on the basis of taking into account features of the space correlation of the e.m.f. of the noise in the vicinity of ferroprobe and magnetic amplifier cores [16].

Ring Ferroprobe with Low Threshold Sensitivity

Taking into account the ideas developed in this article regarding the nature of magnetic noise and earlier established and newly discovered experimental factors resulting in a reduction in noise, we developed a ring ferroprobe with low threshold sensitivity.

The advantage of a ring ferroprobe over a rod type is first of all the high homogeneity of the excitation field, which eliminates a number of sources of noise indicated in the preceding section.

Actually the ring ferroprobe was invented by Ashenbrenner and Goubou. Considerably later improved designs of ring ferroprobes were suggested by Geiger and, independently of him, R.Ya. Berkman [2]. Gordon [13, 26] substantially improved the parameters of ring ferroprobes on account of using a new nickel-iron alloy (close in chemical composition to domestic alloy 82NMP) and using a metallic supporting loop onto which a strip of this alloy was wound and was annealed together with it. As a material for the supporting loop Gordon used the alloy Inconel X-750, with negligibly low magnetic susceptibility and a temperature coefficient of linear expansion close to that for permalloy. Structurally the ferroprobe is designed so that the ring core, fastened to the supporting loop and surrounded by the excitation winding, can turn in relation to a fixed measuring coil rigidly fastened to the ferroprobe's case. Because of rotation balancing of the ferroprobe was achieved, making possible minimum imbalance e.m.f.* This ferroprobe was used with success in making magnetic measurements in outer space.

The ring ferroprobe described here imitates Gordon's design in its general features, but domestic materials were used for the supporting loop and core and other dimensions were selected for the core.

In keeping with the considerations discussed above, a strip 0.02 mm thick and 1.5 mm wide of a nickel-iron alloy--permalloy 82NMP--was used for the core. Ohmic-resistance alloys, in particular, alloy NM23KhYu [29], were selected as materials for the supporting loop. After fabricating and pickling the supporting loop, the turns of the permalloy strip are laid into its groove and the last turn of the strip is fastened to the one preceding it by spot welding. After this the core together with the supporting loop is heat treated.

*Of course, the balancing of rod-type ferroprobes is accomplished by matching cores in pairs.



APPROVED FOR RELEASE: 2007/02/09: CIA-RDP82-00850R000500020034-7

APPROVED FOR RELEASE: 2007/02/09: CIA-RDP82-00850R000500020034-7



The dimensions of the core were selected out of design considerations and from the assigned frequency of the excitation field--12.5 kHz. The diameter of the core, $d_{opt} = 13.2$ mm, was calculated by taking into account equation (19). The thickness of the permalloy strip ($\Delta = 0.02$ mm) was selected from the relationship in [1, 2]:

$$\Delta \leqslant \Delta_{max} = 4 f_\delta^{-1/2}.$$

As we know, a ring core possesses the property of demagnetization in relation to the external measured field. Therefore, as well as taking into account the complex nature of the dependence of the noise level in a ferroprobe on the area of the core's cross section, we experimentally found the number of turns of the strip in the core with which the noise is minimal; this number proved to equal six.

The permeability of the shape of the ring core was calculated from the equation in [4]:

$$m = \frac{1.28\pi d}{4\delta h(\ln \frac{3.6d}{\delta + h} - 1)} = 419,$$

where $d$, $\delta$ and $h$ are the diameter, width and thickness of the core ($\delta = 1.5$ mm, $h = 6$ and $\Delta = 0.12$ mm).

On top of the loop with the core is wound a single-layer toroidal excitation winding whose number of turns equals 130. At the moment of the core's saturation a current of 0.6 A flows through the winding, which creates a circular field strength of $H_{max} = 1700$ A/m (approximately equals 20 Oe).

The loop with the core and excitation winding is placed inside the measuring coil, designed as two sections and wound in order to make possible identical capacitive coupling between its output terminals and the excitation circuit. The number of coil turns equals 500. The maximum achievable transformation ratio under no-load conditions is calculated by taking into account equations (5) and (15) by the equation

$$G_{2\,max}\Big|_{\substack{B \to 0;\\ m < \mu_{\Delta\,max}}} = 16 f_\delta \delta h w_2 \xi m.$$

With $f_\delta = 12.5$ kHz, $\delta h = 0.18$ mm$^2$, $w_2 = 500$, $\xi = 0.6$ [2] and $m = 419$, $G_{2max} = 4.5$ μV/nT. The computed value of $G_{2max}$ agrees well with that determined experimentally (approximately 5 μV/nT).

On top of the measuring coil on a special loop are wound a compensation winding, feedback winding and other windings.



APPROVED FOR RELEASE: 2007/02/09: CIA-RDP82-00850R000500020034-7

APPROVED FOR RELEASE: 2007/02/09: CIA-RDP82-00850R000500020034-7



The circuit of the measuring apparatus by means of which the noise level in the ferroprobe developed was estimated is presented in fig 8. It includes the elements of a standard magnetometer, a recorder, a spectrum analyzer and a shield (superconducting or ferromagnetic) inside of which the ferroprobe is placed in the measuring process.*

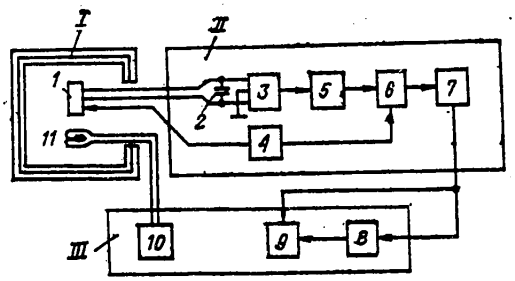


Figure 8. Diagram of Measuring Apparatus for Estimating the Noise Level in a Ferroprobe: I--ferromagnetic and/or superconducting shield; II--electronics of magnetometer; III--testing and recording devices; 1--ferroprobe; 2--input circuit capacitor; 3--differential amplifier; 4--driver; 5--selective amplifier; 6--synchronous detector; 7--d.c. amplifier; 8--spectrum analyzer; 9--recorder; 10--calibrator; 11--calibration coil

Voltage of triangular form with a fundamental frequency of 12.5 kHz produced by a precision oscillator (a 100-kHz quartz self-excited oscillator, an 8:1-countdown frequency divider and an integrator) is supplied to the ferroprobe's excitation winding. The level of even harmonics in the oscillator's output voltage does not exceed 0.01 percent, which in combination with effective balancing of the ferroprobe (suppression at a frequency of $2f_b$ = 25 kHz is not less than 50) guarantees minimum zero drift. As already mentioned, the current at the moment of saturation of the ferroprobe's core equals 0.6 A.

The ferroprobe's measuring coil is tuned by means of a capacitor in resonance to a frequency of $2f_b$ = 25 kHz . With this the ferroprobe's transformation ratio with the maximum excitation current indicated increases to 40 μV/nT. The loop thus formed is connected to the input of a wideband differential amplifier. Then the ferroprobe's signal sequentially enters a selective amplifier with a gyrator filter, a synchronous detector and d.c. amplifier. The real band of the measuring channel in terms of the demodulated signal is 0 to 100 Hz.

*The circuit diagram of the magnetometer was developed by Yu.N. Bobkov.



APPROVED FOR RELEASE: 2007/02/09: CIA-RDP82-00850R000500020034-7

APPROVED FOR RELEASE: 2007/02/09: CIA-RDP82-00850R000500020034-7



The channel's output is connected to a type N-327 recorder and type S4-54 spectrum analyzer.

The measuring procedure reduces to the following. The ferroprobe being tested is placed in the working space of the ferromagnetic or superconducting shield and is fastened to a special turning table by means of which the ferroprobe is turned around its center 180 degrees. As the result of this turning, the ferroprobe's steady zero drift is revealed in the shield's residual field. Then the position of the ferroprobe is fixed and the noise is recorded. The duration of the recording (realization) is determined by the lower limit of the section of the spectrum analyzed and by the conditions of the experiment: In a ferromagnetic shield whose residual field is subject to changes, short, e.g., 30-minute realizations, are recorded (which corresponds to a lower-limit frequency of 0.001 Hz); in a superconducting shield whose residual field is stable over time [42], extended, e.g., 24-hour realizations are recorded. The noise recording scale (the transformation ratio of the measuring channel) is tested periodically by supplying the required current value to the ferroprobe's calibration winding or to a standard coil put onto it.

A fragment of a recording of noise (10-minute realization) and of the excess component of noise for eight hours of the operation of a ferroprobe in a superconducting shield is presented in fig 9.

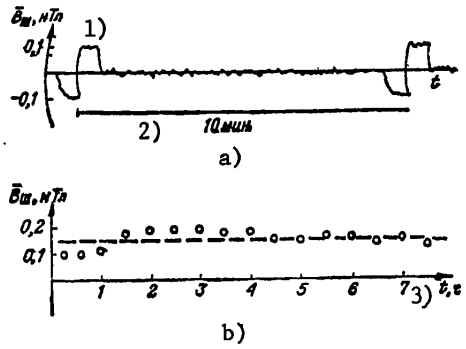


Figure 9. Results of Tests of a Ring Ferroprobe: a--fragment of recording of noise; b--excess component of noise

Key:
1. $\overline{B}_{sh}$, nT
2. Minutes
3. Hours



APPROVED FOR RELEASE: 2007/02/09: CIA-RDP82-00850R000500020034-7

APPROVED FOR RELEASE: 2007/02/09: CIA-RDP82-00850R000500020034-7



The processing of experimental data (in the infralow frequency region of the spectrum processing can be performed both manually and automatically [47]), obtained for no less than five samples of the ferroprobe developed, showed that with the excitation conditions selected the spectral distribution of noise actually has the form presented in fig 2. In the 1 to 100 Hz section the noise is uniform and, adjusted for the 1 Hz band, equals $B_{sh} \sim 0.005$ nT ; in the 0.001 to 1 Hz section $B_{sh} \sim 0.01$ to 0.015 nT; and finally the zero drift after 8 h of observation does not exceed 0.1 nT. As mentioned earlier, at the present time it is still difficult to say whether the zero drifts observed are a reflection of noise processes in the ferroprobe's core or are the result of the existence of coherent noise in the channel's electronics. We consider only the zero values measured in the 0.001 to 100 Hz frequency band reliable.

The data presented testify to the fact that in the ring ferroprobe developed the noise level adjusted for a unit of volume of the core is an order of magnitude lower than the adjusted noise level obtained earlier [9], which was achieved mainly on account of using new nickel-iron alloys with a low value of $\lambda_s$ and primarily alloy 82NMP, as well as on account of taking into account other factors enumerated above. The noise level reached, of course, is not the limit. In our opinion in the immediate future ferroprobes and magnetic amplifiers will be developed with a noise level on the order of 0.001 nT (1 pT). Information is already available to the effect that on the basis of using new alloys the noise level in a magnetic amplifier has been brought to the level of the thermal noise of the input winding.*

In conclusion let us note that in addition to alloys 82NMP, 81NMA and 83NF (cf. table 2) amorphous alloy 84KSP-A was also tested in the ferroprobe developed. A strip 0.04 mm thick and 1.5 mm wide was used, which, just as the permalloy, was wound and fastened to a supporting loop. The core was not annealed. Under the ferroprobe excitation conditions and with the measuring procedure indicated earlier in the 0.001 to 1 Hz frequency band a noise level of $B_{sh} \sim 0.1$ nT was achieved. And although this is an order lower than that achieved when using alloy 82NMP, the result all the same must be considered quite encouraging since amorphous materials are being studied and developed intensively. In addition, in a number of cases the requirement of ensuring the maximum low threshold sensitivity is not imposed on ferroprobes and magnetic amplifiers. Therefore, amorphous materials can be used already now in ferroprobes and magnetic amplifiers. The advantages of these materials are obvious. In particular, cores made of them do not have to be heat treated and are not very sensitive to mechanical stresses.

Conclusion

The picture of the origin of magnetic noise which we have discussed is obviously not complete and lacking internal contradictions. It will of course be refined as the result of further theoretical and experimental research. This relates

*R.Ya. Berkman's report at the third interdepartmental "Magnetic Noise in Ferroprobes and Magnetic Amplifiers" conference, Moscow, MFTI [Moscow Physicotechnical Institute], October 1979.



APPROVED FOR RELEASE: 2007/02/09: CIA-RDP82-00850R000500020034-7

APPROVED FOR RELEASE: 2007/02/09: CIA-RDP82-00850R000500020034-7



especially to precisely defining the role of magnetic anisotropy. But what has already been established testifies to considerable potential possibilities for suppressing magnetic noise, primarily by the intelligent and purposeful choice of ferromagnetic materials. At the present moment we have available a group of new nickel-iron alloys (81NMA, 83NF and 82NMP) which make it possible, other conditions being equal, to reduce the noise level by an order of magnitude as compared with alloys 79NM and 80NKhS, used previously in low-threshold ferroprobes and magnetic amplifiers. There is no doubt that the development and study of new alloys, including amorphous, will lead to further progress in the area of reducing the level of magnetic noise.

The establishment of a correlation between the level of magnetic noise and individual parameters of the ferromagnetic materials used will make it possible to use the "noise" method for controlling the quality of the materials themselves. Agreeing with the authors of [48], who have developed this trend and stress its promise, we wish once more to emphasize the multifactor nature of the phenomenon studied.

In our opinion further efforts in the area of studying the nature of magnetic noise, constructing a quantitative theory of the phenomenon and developing low-threshold ferroprobes and magnetic amplifiers, as well as of using the "noise" method in nondestructive testing of ferromagnetic materials should be directed toward isolation of all the many factors and determination of the influence of each factor individually. Of course, painstaking analytical work is required here and the creation of unique apparatus with ferromagnetic and superconducting shields and the formulation of sufficiently detailed and polished experiments.

The need for the coordination of efforts is also obvious.

Bibliography

1. Rozenblat, M.A. "Magnitnyye elementy avtomatiki i vychislitel'noy tekhniki" [Magnetic Elements of Automation and Computer Technology], Moscow, Nauka, 1966, 768 pages.

2. Afanas'yev, Yu.V. "Ferrozondy" [Ferroprobes], Leningrad, Energiya, 1969, 168 pages.

3. Razin, G.I. and Shchelkin, A.P. "Beskontaktnoye izmereniye elektricheskikh tokov" [Noncontact Measurement of Electric Current], Moscow, Atomizdat, 1974, 160 pages.

4. Afanas'yev, Yu.V., Studentsov, N.V., Khorev, V.N., Chechurina, Ye.N. and Shchelkin, A.P. "Sredstva izmereniy parametrov magnitnogo polya" [Equipment for Measuring Parameters of a Magnetic Field], Leningrad, Energiya, 1979, 320 pages.

5. Kolachevskiy, N.N. "Magnitnyye shumy" [Magnetic Noise], Moscow, Nauka, 1971, 136 pages.



APPROVED FOR RELEASE: 2007/02/09: CIA-RDP82-00850R000500020034-7

APPROVED FOR RELEASE: 2007/02/09: CIA-RDP82-00850R000500020034-7



6. Langvagen, Ye.N. "Methods of Experimental Determination of Differential Magnetic Permeability of Ferromagnetics with Complex Magnetization," IZVESTIYA VUZOV, ELEKTROMEKHANIKA, No 3, 1970, pp 250-256.

7. Bunkin, F.V. "On the Question of the Statistical Nature of the Magnetic Reversal of Ferromagnetics," ZHTF, Vol 26, No 8, 1956, pp 1782-1789.

8. Grachev, A.A. "On the Continuous Spectrum of the E.M.F. of Cyclic Magnetic Reversal," IZVESTIYA VUZOV, RADIOFIZIKA, Vol 1, No 2, 1958, pp 71-76.

9. Berkman, R.Ya. "Intrinsic Noise of Ferroprobes and Procedure for Studying It," GEOFIZICHESKOYE PRIBOROSTROYENIYE, No 7, 1960, pp 25-43.

10. Afanasenko, M.P. and Berkman, R.Ya. "Intrinsic Noise of Magnetic Modulators" in "Otbor i peredacha informatsii" [Information Screening and Transfer], No 42, 1974, pp 53-60.

11. Afanasenko, M.P. and Berkman, R.Ya. "Influence of Design and Electrical Parameters on Level of Intrinsic Noise of Magnetic Modulators" in "Otbor i peredacha informatsii," No 42, 1974, pp 61-65.

12. Weiner, M.M. "Magnetostrictive Offset and Noise in Flux Gate Magnetometers," IEEE TRANS. ON MAGN., Vol 5, No 2, 1969, pp 98-105.

13. Gordon, D.I., Lundsten, R.H. and Scarzello, J.F. "Offset and Noise in Fluxgate Magnetometers," IEEE TRANS. ON MAGN., Vol 6, No 4, 1970, p 818.

14. Kolachevskaya, V.V., Kolachevskiy, N.N., Rozhdestvenskiy, V.V. and Strygin, L.V. "Spectral Distribution of Magnetic Noise Near Harmonics of the Magnetic Reversal Frequency," RADIOTEKHNIKA I ELEKTRONIKA, Vol 16, No 7, 1971, pp 1211-1215.

15. Mari, Zh. "Nizkochastotnyye parametricheskiye usiliteli s ortogonal'nym magnitnym upravleniyem" [Low-Frequency Parametric Amplifiers with Orthogonal Magnetic Control], Moscow, Mir, 1967, 231 pages.

16. Kotlyar, P.Ye. "Issledovaniye magnitnykh shumov v ferrozondakh" [Investigation of Magnetic Noise in Ferroprobes], author's abstract of candidate's dissertation, Novosibirsk, USSR Academy of Sciences Siberian Division Institute of Automation and Electrometry, 1971, 17 pages.

17. Afanas'yev, Yu.V., Gorobey, V.N. and Trukats, V.A. "Some Results of the Investigation of Magnetic Noise in Ferroprobes," TRUDY METROLOGICHESKIKH INSTITUTOV SSSR, No 215 (275), 1978, pp 47-52.

18. Bukharov, M.V. "Influence of Fluctuations of Hysteresis Loop Parameters on Level of Excess Magnetic Noise in Magnetomodulation Transformers" in "Fizika magnitnykh materialov" [Physics of Magnetic Materials], Kalinin, KGU, 1979, pp 13-19.



APPROVED FOR RELEASE: 2007/02/09: CIA-RDP82-00850R000500020034-7

APPROVED FOR RELEASE: 2007/02/09: CIA-RDP82-00850R000500020034-7



19. Berner, R. and Kronmyuller, G. "Plasticheskaya deformatsiya monokristallov" [Plastic Deformation of Single Crystals], edited by A.N. Orlov, Moscow, Mir, 1969, 272 pages.

20. Vlasko-Vlasov, V.K., Dedukh, L.M. and Nikitenko, V.I. "Polarization-Optical Investigation of Processes of Magnetization Around Individual Dislocations in Single Crystals of Yttrium-Iron Garnet," ZHURNAL EKSPERIMENTAL'NOY I TEORETICHESKOY FIZIKI, Vol 65, No 1, 1973, pp 377-395.

21. Vonsovskiy, S.V. and Shur, Ya.S. "Ferromagnetizm," Moscow and Leningrad, Gosudarstvennoye izdatel'stvo tekhniko-teoreticheskoy literatury, 1948, 816 pages.

22. Gordon, D.I. "An Experimental Study of Barkhausen Noise in Nickel-Iron Alloys," REVIEWS OF MODERN PHYSICS, Vol 25, No 1, 1953, pp 56-57.

23. Puzey, I.M. and Molotilov, B.V. "Magnetostriction of Nickel-Iron-Molybdenum Alloys," IZVESTIYA AN SSSR, SERIYA FIZIKA, Vol 22, No 10, 1958, pp 1244-1250.

24. Afanas'yev, Yu.V., Gorobey, V.N., Mart'yanova, K.D., Pluchek, B.Ya., Sosnin, V.V. and Sherbakova, T.I. "Low-Noise Nickel-Iron Alloys for Cores of Ferroprobes and Magnetic Modulators," IZMERITEL'NAYA TEKHNIKA, No 10, 1977, pp 63-65.

25. Afanas'yev, Yu.V. and Gorobey, V.N. "Role of Magnetostriction in the Mechanism of the Origin of Noise in Ferroprobes and Magnetic Modulators," METROLOGIYA, No 4, 1980, pp 47-54.

26. Gordon, D.I., Lundsten, R.H., Chiarodo, R.A. and Helms, H.H. "A Fluxgate Sensor of High Stability for Low Field Magnetometry," IEEE TRANS. ON MAGN., Vol 4, No 3, 1968, pp 397-401.

27. Yanus, R.I., Drozhzhina, V.I., Fridman, L.A. and Vedenev, V.A. "Influence of Coercive Force of Ferroprobe Cores on Stability of the Zero Signal," GEOFIZICHESKOYE PRIBOROSTROYENIYE, No 7, 1960, pp 5-16.

28. Lavrent'yev, A.G. and Ponomarev, Yu.F. "On the Question of the Relationship Between Magnetic Noise and Amount of Magnetostriction," FIZIKA METALLOV I METALLOVEDENIYE, Vol 41, No 6, 1976, pp 1182-1187.

29. Molotilov, B.V., editor. "Pretsizionnyye splavy. Spravochnik" [Precision Alloys, a Handbook], Moscow, Metallurgiya, 1974, 848 pages.

30. Yefremov, V.F., Kadinskaya, L.G., Yur'yeva, Ye.K., Shcherbakova, T.I. and Sosnin, V.V. "Materials for Ferroprobes with a Low Level of Magnetic Noise," GEOFIZICHESKAYA APPARATURA, No 65, 1978, pp 23-31.

31. Bozort, R.M. "The Permalloy Problem," REVIEWS OF MODERN PHYSICS, Vol 25, No 1, 1953, pp 42-48.



APPROVED FOR RELEASE: 2007/02/09: CIA-RDP82-00850R000500020034-7

APPROVED FOR RELEASE: 2007/02/09: CIA-RDP82-00850R000500020034-7



32. Baldwin, Y.A. and Milstein, F. "Barkhausen Noise Power Versus Size of a Minor Hysteresis Loop," J. APPL. PHYS., Vol 44, No 10, 1973, pp 4739-4742.

33. Scouten, D.C. "Sensor Noise in Low-Level Fluxgate Magnetometers," IEEE TRANS. ON MAGN., Vol 8, No 2, 1972, pp 223-231.

34. Acuna, M.H. "Fluxgate Magnetometers for Outer Planets Exploration," IEEE TRANS. ON MAGN., Vol 10, No 3, 1974, pp 519-523.

35. Masumoto, T., Hashimoto, K. and Fujimori, H. "Recent Development of Research on Amorphous Metals," TOHOKU UNIVERSITY RESEARCH INSTITUTE SCIENCE REPORTS, SERIES A, Vol 25, No 6, 1975, pp 232-244.

36. Berkman, R.Ya., Mikhaylovskiy, V.N., Martynyuk-Lototskiy, R.Ye. and Spektor, Yu.I. "Quadrature Component of the E.M.F. of Magnetomodulation Sensors in Measurements in Inhomogeneous Magnetic Fields" in "Magnitnyye elementy avtomatiki, telemekhaniki, izmeritel'noy i vychislitel'noy tekhniki" [Magnetic Elements in Automation, Telemechanics and Measuring and Computing Equipment], Kiev, Izdatel'stvo AN USSR, 1964, pp 183-189.

37. Afanas'yev, Yu.V. "Status and Prospects of the Development of Ferroprobe Magnetometry," GEOFIZICHESKAYA APPARATURA, No 60, 1977, pp 17-35.

38. Ness, N.F. "Magnetometers for Space Research," SPACE SCIENT. REV., Vol 11, 1970, pp 459-554.

39. Langvagen, Ye.N. "Ferroprobes with Excitation by Means of a Rotating Field," GEOFIZICHESKAYA APPARATURA, No 57, 1975, pp 31-37.

40. Kolachevskiy, N.N. "Experimental Study of the Influence of Elastic Stresses, Heat Treating and Crystalline Structure of a Ferromagnetic Sample on Intensity of Magnetic Noise," FIZIKA METALLOV I METALLOVEDENIYE, Vol 11, No 2, 1961, pp 211-214.

41. Afanasenko, M.P. and Berkman, R.Ya. "Reduction of Intrinsic Noise of Magnetic Modulators When the Core Operates Near the Curie Point," OTBOR I PEREDACHA INFORMATSII, No 48, 1976, pp 83-86.

42. Bondarenko, S.I., Sheremet, V.I., Vinogradov, S.S. and Ryabovol, V.V. "Multilayer Superconducting Shield for Producing a Deep Magnetic Vacuum," ZHURNAL TEKHNICHESKOY FIZIKI, Vol 45, No 1, 1975, pp 124-129.

43. Lütgemeier, H. "Magnetization Processes in a Bulk Nonmagnetic State Which Occur as the Result of a Change in Temperature," ZS. ANGEW. PHYS., Vol 16, No 3, 1963, p 167.

44. Samoylovich, A.G. and Korenblit, L.L. "Thermionic Eddy Currents in an Anisotropic Medium, FIZIKA TVERDOGO TELA, Vol 3, No 7, 1961, pp 2054-2059.



APPROVED FOR RELEASE: 2007/02/09: CIA-RDP82-00850R000500020034-7

APPROVED FOR RELEASE: 2007/02/09: CIA-RDP82-00850R000500020034-7



45. Zaytsev, A.V. and Gorobey, V.N. "Influence of Temperature Gradient of Cores on Noise Level in Ferroprobes," METROLOGIYA, No 4, 1980, pp 43-47.

46. Mayer, V.V. "Prostyye opyty s ul'trazvukom" [Simple Experiments with Ultrasound], Moscow, Nauka, 1978, 160 pages.

47. Afanas'yev, Yu.V., Gorobey, V.N. and Makeyev, V.I. "Automated Analysis of Magnetic Noise in the Infralow Frequency Band" in "Tezisy dokladov. Vsesoyuznaya nauchno-tekhnicheskaya konferentsiya 'Povysheniye effektivnosti proizvodstva i kachestva produktsii na osnove standartizatsii' (g. Gor'kiy, may, 1977)" [Theses of Papers; All-Union Scientific and Technical Conference "Improvement of Production Efficiency and Product Quality on the Basis of Standardization" (Gor'kiy, May, 1977)], Moscow, Standarty, 1977, pp 327-329.

48. "Magnetic Noise Method in Nondestructive Testing" (papers relating to this section) in "Tezisy dokladov nauchno-tekhnicheskogo soveshchaniya 'Effekt Barkgauzena i yego ispol'zovaniye v tekhnike'" [Theses of Papers at the "Barkhausen Effect and Its Employment in Engineering" Scientific and Technical Conference], Izhevsk, 1977, pp 127-179.

COPYRIGHT: Tsentral'nyy nauchno-issledovatel'skiy institut informatsii i tekhniko-ekonomicheskikh issledovaniy priborostroyeniya, sredstv avtomatizatsii i sistem upravleniya (TsNIITEIpriborostroyeniya), 1981

8831
CSO: 1860/59



APPROVED FOR RELEASE: 2007/02/09: CIA-RDP82-00850R000500020034-7

APPROVED FOR RELEASE: 2007/02/09: CIA-RDP82-00850R000500020034-7



UDC 621.375

AMPLIFIER FOR KMP201UPI AUTOMATIC SWITCH

Moscow PRIBORY I SISTEMY UPRAVLENIYA in Russian No 9, Sep 81 p 23

[Article by engineer V. I. Shamenko]

[Text] The amplifier for the KMP201UPI automatic switch is designed for use in a set with a polarized relay without self-reset for the protection of combined electrical measurement devices from electrical overloads. The minimum operating voltage at minimum voltage supply is not greater than 0.6 volts. The leakage current at the input is not greater than 0.02 microamperes. The bandpass is not smaller than 0-20,000 Hz. The output current is not smaller than 20 milliamperes. The consumption current is 100 microamperes. The maximum allowable input voltage is 1000 volts. The operating conditions are as follows: temperature range -- -10 to+ 50°C; relative air humidity at 25°C -- up to 98%; air pressure -- 86 to 106 kPa.

The amplifier is manufactured by the "Mikroprovod" NPO [Scientific Production Association] (Kishenev).

COPYRIGHT: Izdatel'stvo "Mashinostroyeniye", "Pribory i sistemy upravleniya", 1981

2291
CSO: 1860/75



APPROVED FOR RELEASE: 2007/02/09: CIA-RDP82-00850R000500020034-7

APPROVED FOR RELEASE: 2007/02/09: CIA-RDP82-00850R000500020034-7



# ANTENNAS

UDC 621.396.67(075.8)

ANTENNAS AND FEEDER LINES

Moscow ANTENNO-FIDERNYYE USTROYSTVA in Russian 1981 (signed to press 8 Dec 80) pp 2-4, 238-265, 278-280

[Annotation, excerpted foreword, chapter 13, appendix 1 and table of contents from book "Antennas and Feeder Lines", by Georgiy Nikolayevich Kocherzhevskiy, Third Edition, revised and supplemented, authorized by the USSR Ministry of Higher and Intermediate Special Education as a Textbook for Students of Higher Educational Institutes Studying in the Speciality "Radio Communications and Radio Broadcasting", Izdatel'stvo "Radio i svyaz'", 20,000 copies, 280 pages]

[Text] The major topics of radio wave transmission and reception theory and the operational principles of the main types of antennas are treated. Methods of designing antennas with specified properties are analyzed, for example, broadband, frequency independent, etc. The types of antennas and feed lines for radio communications and broadcasting, television, space communications, etc. are treated. As compared to the publication which came out in 1972, the material has been substantially revised, and chapters have been added where the parameters which characterize the directional properties of antennas are treated, as well as a section on the influence of metal bodies on the radiation of antennas, etc.

The book is intended for students at electrical engineering communications institutes. The book was reviewed by Ye. N. Vasil'yev.

Foreword

The book consists of two parts. The fundamentals of antenna theory are printed in Part I (Chapters 1-7). The major types of antennas used for various frequency bands are treated in Part II (Chapters 8-13). Considerable attention is devoted to the specific features of antennas for line-of-sight radio relay links, passive repeaters, space radio communications, television, etc.

General questions of electromagnetic wave transmission through feed lines (the types of feeders and their components, matching techniques, etc.) are set forth in the course on engineering electrodynamics, and for this reason, only the specific features of antenna feed lines for various wavelengths are treated in this course.



APPROVED FOR RELEASE: 2007/02/09: CIA-RDP82-00850R000500020034-7

APPROVED FOR RELEASE: 2007/02/09: CIA-RDP82-00850R000500020034-7



Attention is devoted to a number of questions in the book which are of considerable practical interest. These include: the application of the results of solving the integral equation of antennas (the method of point matching) to the calculation of the input impedance of a symmetrical dipole and the current distribution in coupled dipoles; accounting for the influence of metal bodies on antenna radiation; the design of antennas with a modulated phase velocity; optimum feed radiators for single reflectors and dual reflector antennas; some new types of dual reflector antennas and antennas for radio broadcasting at medium wavelengths; feed lines for delivering high power to shortwave antennas; self-complementary antenna arrays; ring directors; methods of antenna miniaturization; a procedure for calculating (using a computer) currents in multielement antennas with a series feed (traveling wave antennas with coupling elements, log periodic antennas), etc.

The author would like to express his gratitude to the head of the department of antennas and engineering electrodynamics of the Moscow Electrical Engineering Institute for Communications, honored scientist and engineer, doctor of the engineering sciences and professor G.Z. Ayzenberg for assisting in the work on the manuscript and for considerable valuable advice.

The author is grateful to the reviewers, the head of the department of antennas and radio wave propagation of Moscow Electrical Engineering Institute and doctor of the engineering sciences, professor Ye.N. Vasil'yev and senior instructors V.N. Volovskiy and V.V. Belostotskiy, who made a number of valuable comments which assisted in improving the contents of the manuscript; he is also extremely grateful to candidates of the engineering sciences and lecturers G.A. Yerokhin, M.E. Zhurbenko and V.A. Sokolov, who courteously allowed the use of several of the results of their work.

## CHAPTER 13. ANTENNAS FOR RADIO COMMUNICATIONS AND BROADCASTING AT MYRIAMETER (VERY LONG), KILOMETER (LONG) AND HECTOMETER (MEDIUM) WAVELENGTHS

### 13.1. Problems in the Design of VLF, LF and MF Antennas

*Specific features of VLF, LF and MF band antennas.* Very low frequency (VLF), $\lambda$ = 10 - 100 km and low frequency (LF), $\lambda$ = 1 - 10 km, waves propagate in two ways: directly at the surface of the earth (a ground wave) and by means of reflection from the lower boundary of the ionosphere (a space wave). Ground waves are comparatively poorly absorbed in the soil and bend (diffract) well about the spherical surface of the earth. At distances of up to 2,000 to 3,000 km, communications is accomplished using ground waves, while at greater distances, by virtue of space waves.

Medium frequency wavelengths (MF) of $\lambda$ = 100 to 1,000 m are absorbed much more strongly in the soil than LF and VLF waves, and bend more poorly about the spherical surface of the earth. For this reason, the propagation range of ground waves is limited to a distance of 500 to 700 km and falls off with decreasing wavelength. Medium waves can propagate over great distances during nighttime hours in the form of space waves (there is the D layer on the propagation path during the day which is an extremely strong absorber of medium wavelengths).



APPROVED FOR RELEASE: 2007/02/09: CIA-RDP82-00850R000500020034-7

APPROVED FOR RELEASE: 2007/02/09: CIA-RDP82-00850R000500020034-7



Communication at medium wavelengths is stable only in the absence of interference between ground and space waves, which occurs at a distance of approximately 50 to 200 km from the transmitter (the reliable reception zone). The near fading zone is located further out, where the field of the ground and space waves are commensurate. As a consequence of the continuous change of the space wave field phase, reception in this zone is unstable. The near field fading is of a selective nature: waves corresponding to the different modulating frequencies interfere in different ways. As a consequence of this, there are nonlinear distortions during reception. With a further increase in the distance from the transmitter, the space wave field begins to predominate.

Reception in the space wave field zone is possible only during nighttime hours. Reception here is also unstable, since waves which are reflected once or twice from the ionosphere (the phenomenon of far field fading) as well as waves with a changed polarization plane, can arrive here at considerable distances from the transmitter.

The positive properties of VLF and LF frequencies are the stable field intensity at the reception site and the fact that the intensity is not dependent on the season of the year, day, meteorological conditions, state of the ionosphere, etc. This also applies to medium waves which propagate in the form of ground waves.

Drawbacks to VLF, LF and MF communications are: the considerable absorption of electromagnetic energy in the soil (which increases with decreasing wavelength), the comparatively high level of atmospheric interference, and the impossibility of using antennas with a significant directional gain. Because of this, a field intensity level sufficient for reception can be assured only by means of high power transmitters. One of the drawbacks to medium and long wave lengths is also the impossibility of transmitting wide bandwidths.

At the present time, LF and VLF are primarily used for radio telegraph service, in particular, for radio communications with submarines, for radio navigation, etc. The shortwave portion of the long wave band (1,050 - 2,000 m) is used for radio broadcasting. Medium wavelengths are employed for radio broadcasting (the 200 - 550 m portion of the band), for communications with mobile radio stations, in aviation radio service, etc.

Because of the specific features of VLF, LF and MF propagation, the radiation maximum of antennas for these bands should be directed along the surface of the earth. Unbalanced vertical dipoles (see §5.3) have the appropriate directional patterns and produce a vertically polarized field. The use of horizontal antennas which create a horizontally polarized field is not expedient, since they radiate poorly along the surface of the earth. Such antennas are used only for reception (see §13.3).

The height of antenna supports is governed by engineering and economic considerations (the cost of a support increases approximately in proportion to the cube of the height). An acceptable height for supports at VLF and LF frequencies is usually 150 to 250 m. Some medium wave antennas have a height of up to 350 and even



APPROVED FOR RELEASE: 2007/02/09: CIA-RDP82-00850R000500020034-7

APPROVED FOR RELEASE: 2007/02/09: CIA-RDP82-00850R000500020034-7



up to 500 m. Because of the low relative height of VLF and LF antennas, their directional pattern in the vertical plane is essentially no different from the directional pattern of an elementary dipole. In the medium wave band, the antenna height can be commensurate with the wavelength and is usually equal to $0.16\lambda$ - $0.63\lambda$. For this reason, MF antennas have greater directional properties in the vertical plane, which is especially important to eliminate radiation at large angles to the horizontal, increase the zone of reliable reception and place the near field fading zone far away from the transmitter.

Antennas used for radio broadcasting in predominantly some definite direction or for radio service between two points should have unidirectional properties in the horizontal plane, something which is achieved by using two or more radiators (coupled dipoles).

Because of the small relative length (height) of VLF and LF antennas, their radiation resistance is low (tenths or units of ohms); it can be commensurate with the loss resistance, and in a number of cases, is considerably less than the latter, because of which the efficiency of an antenna, without taking special steps, proves to be extremely low. For such antennas to radiate a high power, the currents in them should be large, something which leads to large energy losses in the ground, the tuning elements, the insulators, etc.

The reactive component of the input impedance of a short antenna is extremely large (it can achieve several thousands of ohms) and is of a capacitive nature. For this reason, the voltage at the feed points of the antenna is also high: $U_0 = I_0\sqrt{R_{in}^2 + X_{in}^2}$, where $R_{in} = R_{\Sigma 0} + R_{loss}$; $R_{loss}$ is the loss resistance referenced to the current at the feed points of the antenna. Since $X_{in} >> R_{in}$, then one can approximately set $U_0 = I_0 X_{in}$.

To avoid electrical flashover of insulators, flare leakage (the "corona" phenomenon), etc., the voltage at the antenna terminals, as well as the voltage between its various points and ground should not exceed the permissible level. This limits the power which can be delivered to the antenna.

A large reactive power is stored in the antenna because of its large reactance and large current. The Q of the antenna is quite high, because of which, such an antenna has a very narrow bandwidth, which can sometimes prove to be inadequate even for the slow transmission of telegraph signals. The major tasks of VLF and LF antenna design are outlined from what has been said: increasing the power in the transmiting antenna; reducing the voltages in the antenna; extending the passband of antenna frequencies; increasing antenna efficiency.

These problems can be solved by increasing the radiation resistance, reducing the loss resistance and the reactance of the antenna.

In the case of MF antennas, the solution of the problems posed above is simplified significantly, since these antennas have a comparatively long relative length and their radiation resistance amounts to tens of ohms. However, an additional problem arises in the design of MF antennas, which consists in designing an antenna which has antifading properties, the use of which increase the reliable reception area.



APPROVED FOR RELEASE: 2007/02/09: CIA-RDP82-00850R000500020034-7

APPROVED FOR RELEASE: 2007/02/09: CIA-RDP82-00850R000500020034-7



*Methods calculating the major parameters of VLF, LF and MF antennas.* To increase the radiation resistance without increasing antenna height (see §5.3), as well as reduce the potentials in the antenna and expand its bandwidth, VLF and LF antennas are made in the form of T, Γ-shaped or umbrella radiators with extremely extensive horizontal and vertical members (consisting of several parallel wires). In this case, the horizontal portion is intended only for increasing the antenna capacitance and almost plays no part in the radiation, since the field generated by it is cancelled out by its mirror image field. The antenna curtain usually contains from 2 to 16 conductors. The spacing between the conductors is 1 to 3 meters. Copper or bronze stranded cable with a diameter of 6 to 10 mm is usually employed for the conductors. The ends of the conductors of a horizontal curtain are secured to antenna spreaders (Figure 13.1a). The support towers (steel or wood) are held in the vertical position by means of several levels of guys. The guys are broken up into short sections to reduce the currents induced in them by the antenna field. The length of a horizontal section can run to 250 m and more. One of the generator terminals is connected to a system of conductors buried in the ground - the grounding system (Figure 13.1b).

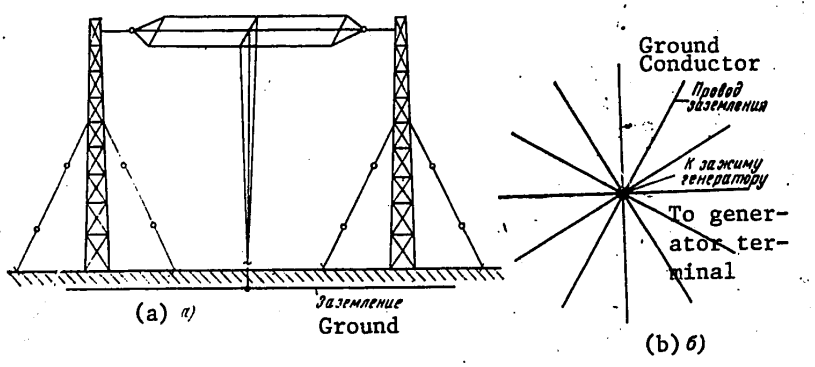


Figure 13.1.

The characteristic impedance of an antenna with very extensive horizontal and vertical sections can amount to about 150 to 200 ohms. However, even with this low characteristic impedance, the antenna bandwidth proves to be extremely narrow because of the low radiation resistance.

Since there is no need at medium wavelengths for an antenna with an extensive horizontal section, medium wave broadcasting antennas are usually made in the form of antenna masts (Figure 13.2a) or antenna towers (Figure 13.2b). The base of the antenna tower is secured to the ground by means of insulators; no guys are needed to secure this antenna. Antenna masts are held in the vertical position by a small number of guys. In these antennas, the generator is connected to the lower end of the steel masts or tower, and the radiator is the mast or tower itself. In a number of cases, to increase the effective height, the antenna masts or towers are equipped with a capacitive load at the top. This load takes the form of either a metal (solid or wire) disk, or a portion of the upper level of guys. Adding a capacitive





APPROVED FOR RELEASE: 2007/02/09: CIA-RDP82-00850R000500020034-7

APPROVED FOR RELEASE: 2007/02/09: CIA-RDP82-00850R000500020034-7



load at the top makes it possible to reduce the antenna height by 20 to 30 percent. The height of antenna towers usually runs to 60 to 200 meters, and that of antenna masts from 60 to 350 meters. The positive properties of these antennas as compared to wire ones are: the presence of just one mast or tower (in the case of wire antennas, a minimum of two masts is required), something which saves antenna field space; less distortion of the directional pattern because of the absence of a large number of guys, suspension cables, etc.; and the greater mechanical strength.

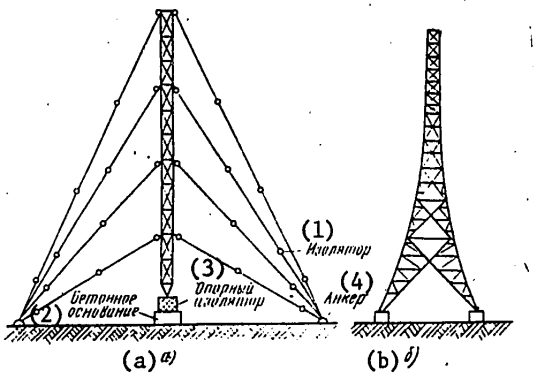


Figure 13.2.

Key: 1. Insulator;
2. Concrete foundation;
3. Base support insulator;
4. Anchor.

The radiation resistance of very long wave and long wave antennas is computed from (5.8). In the case of a short vertical antenna ($l/\lambda < 0.1$), without its horizontal section the effective height $l_d = l/2$ (see §5.3). Where there is an extremely extensive horizontal portion [see (5.12)], $l_d \approx l$, i.e., it almost doubles. Thus, in the sense of boosting the radiation resistance, an extensive horizontal section of an antenna is equivalent to approximately doubling the height of an antenna. It is enormously simpler and less expensive to make even an extremely extensive horizontal section than to increase the height of an antenna, for example, from 200 to 400 m.

The radiation resistance of a medium wave, unloaded antenna, referenced to the current antinode, if $l/\lambda > 0.2$, is computed from (3.21); in this case, the constant factor is chosen equal to 30. The graph of Figure 3.6 can be used for this same purpose. The more complex formula of [7] is used to calculate $R_{\Sigma\pi}$ of a medium wave loaded antenna.





APPROVED FOR RELEASE: 2007/02/09: CIA-RDP82-00850R000500020034-7

APPROVED FOR RELEASE: 2007/02/09: CIA-RDP82-00850R000500020034-7



If the inequality $l_э < 0.35$ ($l_э$ is the equivalent antenna length), then the radiation resistance referenced to the current at the feed points is:

$$R_{\Sigma 0} = R_{\Sigma n}/\sin^2 kl_э.$$

If $l_э/\lambda > 0.35$, then the law governing the current distribution along a vertical antenna is close to a hyperbolic sine and the radiation resistance referenced to the current at the feed points can be determined from the approximate formula [7]:

$$R_{\Sigma 0} = \frac{R_{\Sigma n}}{(R_{\Sigma n}/W_в)^2 + \sin^2 kl_э}.$$

where $W_B$ is the characteristic impedance of the vertical section of the antenna.

Another way of increasing $R_\Sigma$ consists in using complex antennas of several vertical coupled dipoles (antennas with several downleads). Such antennas are employed for high power very long wave and long wave radio stations. A schematic of a complex antenna is shown in Figure 13.3, which in essence consists of three T-antennas contiguous with each other. The feed from the transmitter is delivered to the central downlead. All of the downleads are tuned by means of the variable inductances L so that the currents in them prove to be in phase and approximately equal. The radiation resistance of each vertical conductor is the sum of the inherent resistance of the given conductor and the resistances induced in it by the other vertical conductors. The induced resistances can be calculated using the induced e.m.f. technique (see §4.2), and the internal radiation resistances of the downleads are calculated using (5.8). Because of the fact that the currents in all of the downleads are in phase and approximately equal in magnitude, and the spacings between the downleads are small as compared to the wavelength (the spacings between the downleads amount to a few hundred meters), the induced resistances prove to be close in magnitude to the internal resistances. For this reason, the overall radiation resistance of one downlead is $R_{\Sigma 1} \approx nR_{\Sigma 11}$, where $R_{\Sigma 11}$ is the internal radiation resistance of the downlead; n is the number of downleads. The total radiation resistance of the entire antenna is $R_\Sigma = R_{\Sigma 1} + R_{\Sigma 2} + \ldots + R_{\Sigma n} \approx n^2 R_{\Sigma 11}$.

Thus, the radiation resistance of an antenna with several (n) downleads increases approximately as $n^2$ as compared to the radiation resistance of one vertical antenna of the same length.

Such a large rise in the radiation resistance is achieved at the cost of a considerable increase in the complexity and expense of the antenna. It should be kept in mind that the radiation resistance of complex very long wave and long wave antennas, consisting of several downleads, is nonetheless low and usually amounts to units of ohms. Since the radiation resistance of an antenna with several downleads increases as compared to a single antenna by a factor of $n^2$ times, while the loss resistance increases approximately n times, the efficiency of a complex antenna is increased.

Efforts are made in the design of VLF, LF and MF antennas to reduce the electromagnetic energy losses and increase antenna efficiency. The losses in the surface



APPROVED FOR RELEASE: 2007/02/09: CIA-RDP82-00850R000500020034-7

APPROVED FOR RELEASE: 2007/02/09: CIA-RDP82-00850R000500020034-7



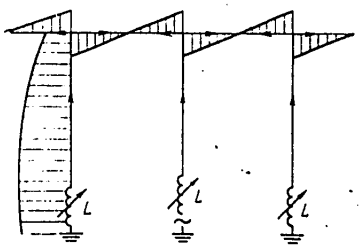


Figure 13.3.

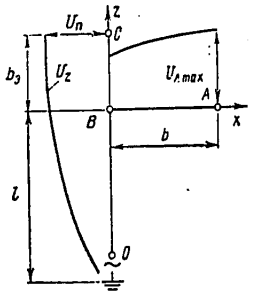


Figure 13.4.

of the ground which is incorporated directly in the antenna current circuit, and in the tuning elements (especially the loading coils) play a major role. The losses in the coils are reduced by means of an efficient structural design and the use of wires with a low impedance at high frequencies. To reduce losses in the ground, a grounding system or a counterpoise is set up, the underlying concept of which consists in reducing the currents flowing directly in the upper layer of the soil. A ground can be made in the form of a system of radial conductors buried a small depth in the ground (down to about 0.5 m), which are joined together at the center and connected to a terminal of the generator (see Figure 13.1b). Since the specific resistance of the ground conductors is considerably less than the soil resistance, the majority of the currents shorted to ground flow to the generator terminal via these conductors, because of which, losses in the ground are reduced.

A counterpoise is made in the form of a grid of wires suspended below the antenna at a slight height above the ground. All of the conductors are joined together and connected to one of the generator terminals. In this case, the majority of the displacement currents branching off to ground from the antenna is intercepted by the counterpoise conductors and routed in the form of conductance currents to the generator terminal. Thus, it is as if the counterpoise shields the antenna from the ground; approximately 60 to 70 percent of the antenna current is shorted through it and 30 to 40 percent through the ground. Counterpoises are usually employed at medium wavelengths in the case of soil which is poorly suited for grounding devices (hard or poorly conducting soil), as well as at short wavelengths for mobile radio stations with asymmetrical vertical antennas.

A ground or counterpoise should encompass the area on which the bulk of the near field is concentrated. The number of radial ground conductors is usually 80 to 120. Vertical antennas without a horizontal section or umbrella antennas have all of the radial wires of the same length, exceeding 10 to 20 percent of the antenna height. In the case of T or Γ-shaped antennas, the length of the ground (counterpoise) conductors increases as the projection of the horizontal portion of the antenna onto the ground is approached and should exceed the amount of this projection by approximately the mast height. Complex (sectionalized) grounds are sometimes used in high power LF and VLF transmitters. Antenna efficiencies close to 90 percent



APPROVED FOR RELEASE: 2007/02/09: CIA-RDP82-00850R000500020034-7

APPROVED FOR RELEASE: 2007/02/09: CIA-RDP82-00850R000500020034-7



have been successfully achieved at VLF frequencies using such grounds, as well as by means of special measures to reduce losses in tuning elements. To calculate the losses in the ground and grounding systems, it is necessary to know the current density distribution in the near field of the antenna. S.I. Nadenenko [59] and B.V. Braude [60] have made a substantial contribution to the development of design methods for grounds.

The permissible power in an antenna is governed by the value of the electrical field intensity components, $E_n$, normal to the conductor, at which electrical breakdown of the insulators can occur or the ionization of air close to the antenna begins (the "corona" phenomenon), as well as by the current level at which the conductors begin to heat up. The cross-section of the antenna conductors should be chosen so that the current density in them does not exceed 5 amp/mm$^2$ (the effective value).

Porcelain antenna insulators sustain a voltage of approximately 1 kilovolt. In the case of comparatively low power transmitters (tens of kilowatts and less), insulator strings sustain a voltage of up 50 KV are used for the antenna. In the case of high power transmitters (hundreds of kilowatts), special insulators are used which sustain voltages above 100 KV.

The permissible field intensity at the conductors should be less than the critical value (see §12.2). The amplitude of $E_{cr}$ at VLF and LF frequencies in the case of moist air amounts to about 14 KV/cm [60]. In the case of a vertical antenna with a horizontal portion (Figure 13.4), the voltage at any section of the equivalent vertical antenna, $U_z = U_\pi \cos k(l + b_э - z)$, where $U_\pi$ is the voltage amplitude at the voltage antinode (point C).

The voltage between the end of the vertical section of the real antenna (point B) and ground is:

$$U_B = U_\pi \cos kb_э \qquad (13.1)$$

It is known from the theory of long lines that the voltage and current in the corresponding antinodes are related by the expression:

$$U_\pi = I_\pi W_v \qquad (13.2)$$

where $W_v$ is the characteristic impedance of the vertical part of the antenna;

$$I_\pi = I_0 / \sin kl_э \qquad (13.3)$$

By replacing $U_\pi$ in (13.1) with expression (13.2) and substituting expression (13.3) in place of $I_\pi$, we obtain:

$$U_B = I_0 W_в \cos kb_э / \sin kl_э \qquad (13.4)$$





APPROVED FOR RELEASE: 2007/02/09: CIA-RDP82-00850R000500020034-7

APPROVED FOR RELEASE: 2007/02/09: CIA-RDP82-00850R000500020034-7



The voltage in a real antenna is maximum at the end of the horizontal part (point A). Since the voltage distribution is $U_x = U_{A\,max}\cos k(b - x)$ along the horizontal section AB, where x is the present coordinate read out from point B, then the voltage at the end of the vertical portion of the antenna (point B), and the maximum voltage at point A are related by the expression:

$$U_B = U_{A\,max}\cos kb. \tag{13.5}$$

Equating (13.4) and (13.5), we find:

$$U_{A\,max} = \frac{I_0 W_в \cos kb_э}{\cos kb \sin kl_э}. \tag{13.6}$$

It can be seen from the given expression that to reduce the voltage in the antenna it is necessary that: for a specified input power, the current $I_0$ be reduced (i.e., increase the antenna radiation resistance); the characteristic impedance of the vertical pa t of the antenna be reduced, i.e., increase the downlead capacitance; the equivalent length increase $b_э$ be increased, for which the ratio $W_{hor}/W_v$ should be reduced, as can be seen from (5.9), i.e., increase the capacitance of the horizontal portion of the antenna as compared to the vertical ($C_{1hor} > C_{1ver}$).

We will note that expression (13.6) is also justified for T-shaped and umbrella antennas. In all cases, b is to be understood as the length of one arm (beam).

The voltage $U_A$ max should notexceed the permissible level, i.e., $U_{A\,max} \leq U_{доп}[U_{per}]$. The power delivered to the antenna is $P_0 = I_0^2 R_{in}/2$. Substituting its expression from (14.6) here in place of $I_0$, we obtain the formula for calculating the permissible level of power delivered to the antenna:

$$P_{0\,per} = P_{0\,доп} = \frac{R_{вх}}{2}\left(\frac{U_{A\,доп}\cos kb \sin kl_э}{W_в \cos kb_э}\right)^2. \tag{13.7}$$

For an antenna without a horizontal section (b = 0), expression (13.7) assumes the form:

$$P_{0\,доп} = \frac{R_{вх}}{2}\left(\frac{U_{A\,доп}}{W_в}\sin kl\right)^2.$$

Keeping expression (12.5) in mind and replacing $W_A$ in it with $W_г$ [$W_{hor}$], expression (13.7) can be written in the form:

$$P_{0\,доп} = \frac{R_{вх}}{2}\left(\frac{E_{п\,доп}\, na\, W_г \cos kb \sin kl_э}{60 W_в \cos kb_э}\right)^2, \tag{13.8}$$

where a is the conductor radius; n is the number of conductors in the horizontal part.



APPROVED FOR RELEASE: 2007/02/09: CIA-RDP82-00850R000500020034-7

APPROVED FOR RELEASE: 2007/02/09: CIA-RDP82-00850R000500020034-7



In those cases where $l/\lambda \geq 0.35$, the current in the antenna should be considered as having a hyperbolic sine distribution. In this case, if the antenna does not have a horizontal part, the permissible power can be computed from (12.9), keeping in mind the fact that $W_A = W_B$ [= $W_{ver}$].

To calculate the permissible power, the permissible value of $E_n$ as well as other quantities, it is necessary to know the characteristic impedances of the vertical and horizontal parts of the antenna. The characteristic impedances are calculated by any approximation technique, for example, Hou's method [6, 50].

The characteristic impedance of an antenna mast or antenna tower can be approximated with the formula $W_A = 60(\ln[l/\rho_э] - 1)$, where $\rho_э$ is the equivalent radius of the tower. If the antenna mast or tower has a triangular or square cross-section, then $\rho_э$ represents the radius of a circle inscribed in the cross-section.

In the case of a large number of conductors in an antenna curtain, B.V. Braude [60] proposed the substitution of solid metal surfaces for the wire curtains in the calculations, where these surfaces have the size and shape of the corresponding wire sections of the antenna.

The passband of VLF, LF and MF antennas is governed by the dependence of the input impedance of the antenna on frequency (the directional properties of the antenna change little with a change in frequency). With small changes in frequency as compared to the resonant frequency, the antenna behaves as a conventional resonant circuit. The antenna bandwidth is defined on analogy with such a circuit as the frequency passband, at the edges of which the current amplitude in the antenna with a constant voltage at its input drops off by a factor no more than $\sqrt{2}$ as compared to the current amplitude at resonance. The current phase within the bounds of the passband should change linearily with a change in frequency and be symmetrical relative to the resonant frequency.

We shall consider an antenna operating in a heavily loaded mode ($\lambda_p >> \lambda_0$ or $l_э << \lambda_p$, where $\lambda_0$ is the resonant wavelength of the antenna; $\lambda_p$ is the working wavelength), representing it in the form of a series resonant circuit, consisting of an input reactance $X_{in} = -iW_v \cot kl_э$, having a capacitive nature in this case, a loading coil inductance $L_y$ (Figure 13.5a) and the resistances $R_{in} = R_{\Sigma 0} + R_{loss}$. The relative passband of such a circuit when operating close to resonance is $2\Delta f_p Q_A$, where $Q_A$ is the quality factor of the antenna circuit, as is well known, equal to $Q_A = X_{in.r}/R_{in}$; $f_p$ is the resonant (working) frequency of the antenna circuit; $X_{in.r}$ is the reactive component of the input impedance of the antenna when $f = f_p$.

Since in this case:

Consequently, $Q_A \approx W_v/k_p l_э R_{in}$ and the relative passband is $2\Delta f/f_p = R_{in} k_p (l + b_э)/W_v$. Thus, to increase the antenna bandwidth, $R_{in}$ must be increased (by virtue of increasing the radiation resistance), the characteristic impedance of the antenna must be reduced and its equivalent length increased.

The bandwidth of antennas operating in lightly loaded or shortened modes can be calculated from the formulas available in [6], 62].



APPROVED FOR RELEASE: 2007/02/09: CIA-RDP82-00850R000500020034-7

APPROVED FOR RELEASE: 2007/02/09: CIA-RDP82-00850R000500020034-7



*Antenna feed.* The feed for wire antennas is usually accomplished by means of transmitting the electromagnetic energy from the output circuit of the generator using special coupling elements to the antenna downlead. In this case, the antenna downlead is brought directly to the radio station building. Antenna masts and antenna towers are fed using coaxial feed lines. Sometimes, coaxial lines are made in the form of a number of conductors, wound along the generatrix of a cylinder. In the first case, the load on the generator is the input impedance of the antenna. To transmit the maximum power from the generator to the antenna, this load should be purely resistive and have a magnitude determined by the operating conditions of the generator. In the second case, for the same purpose, the feeder should be loaded into a resistance equal to its characteristic impedance W, i.e., it should operate in a traveling wave mode. The generator in this case is loaded into a resistance equal to the characteristic impedance of the feeder.

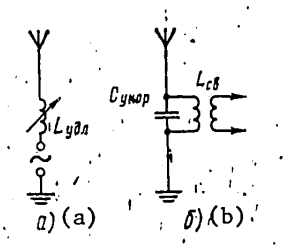


Figure 13.5.

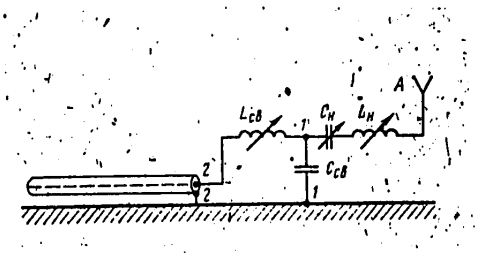


Figure 13.6.

The task of matching the antenna to the generator or to the feed line can be broken down into two parts: tuning the antenna to resonance by means of compensating for the reactive component of its input impedance and transforming the input resistance of the antenna to the requisite value. Matching is accomplished by means of lumped reactive tuning and coupling elements. To illustrate the design procedure for coupling elements [50], we shall consider a capacitively coupled matching circuit (Figure 13.6). If the antenna is tuned to resonance by means of tuning elements $L_H$ [Lload] and $C_H$ [Cload], then the impedance at points 1-1 is:

$$\underline{Z}_{1-1}=\frac{R_{вх}/i\omega C_{св}}{R_{вх}+1/i\omega C_{св}}=R_{вх}/(1+i\omega C_{св}R_{вх});$$

or, by eliminating the imaginary component in the denominator,

$$\underline{Z}_{1-1}=R_{вх}/(1+\omega^2 C_{св}^2 R_{вх}^2)-i\omega C_{св}R_{вх}^2/(1+\omega^2 C_{св}^2 R_{вх}^2);$$

So that the cable operate in a traveling wave mode, the impedance at points 2-2 should be purely resistive and equal to the characteristic impedance of the cable. This will be the case when the following conditions are met:

$$R_{вх}/(1+\omega^2 C_{св}^2 R_{вх}^2)=W;\ \omega L_{св}-(\omega C_{св}R_{вх}^2)/(1+\omega^2 C_{св}^2 R_{вх}^2)=0,$$





APPROVED FOR RELEASE: 2007/02/09: CIA-RDP82-00850R000500020034-7

APPROVED FOR RELEASE: 2007/02/09: CIA-RDP82-00850R000500020034-7



where $L_{CB}$ [$L_{coupling}$] is the inductance inserted to compensate for the reactive component of the impedance $Z_{1-1}$.

The unknowns $C_{CB}$ and $L_{CB}$ can be determined from these equations:

$$C_{coupl.} = C_{CB} = \frac{1}{\omega R_{BX}} \sqrt{\frac{R_{BX}}{W} - 1}; \quad L_{CB} = \frac{W}{\omega} \sqrt{\frac{R_{BX}}{W} - 1} \qquad (13.9); \ (13.10)$$

As can be seen from the formulas cited here, this circuit can operate only when $R_{in}/W > 1$, i.e., it is a step-down configuration.

13.2. Medium Wave Broadcasting Antennas

Guide antenna masts are used primarily for radio broadcasting at medium wavelengths. In antenna masts with an insulated base (see Figure 13.2), the insulator not only provides electrical isolation of the antenna from ground, but is also the mast support. This insulator should have good electrical and mechanical strength, since the weight of the tower resting on the insulator can 100 to 200 tons.

Because of the nonuniform pressure distribution over the cross-section of the insulator for other reasons, mechanical damage to support base insulators is possible, something which can lead to a serious accident. The use of support insulators increases the antenna cost and reduces its operational reliability. For this reason, antenna masts with a grounded base which do not require support insulators are of considerable interest, where these towers are mounted on metal foot bearings, fastened to a firm reinforced concrete foundation.

Also interesting is the possibility of transforming already finished and existing towers and masts at radio centers which were constructed for other purposes (television towers, etc.) into a radiator. There are two types of antenna masts with a grounded base: shunt fed and top fed antennas, proposed by G.Z. Ayzenberg [63]. In the case of the shunt fed antenna (Figure 13.7), the radio frequency voltage is fed to a certain point a, located at a distance $l_2$ from the lower end of the tower, by means of an inclined conductor, which is the continuation of the center lead of the coaxial line.

If the length (height) of the mast, $l_1 + l_2 = l$, amounts to $\lambda/4$, then the reactances of the segments $l_1$ and $l_2$ cancel each other out. The input impedance of the antenna is purely resistive in this case. By selecting the feed connection point a, it can be made equal to the value W of the feed line and matched so that the antenna and the feed line have no additional matching devices. If the input impedance of the antenna is complex, then its reactance is compensated by a variable reactance inserted in the sloping line. Since the sloping line, the lower part of the tower and ground form a loop antenna, the radiation of which is superimposed on the radiation of the antenna tower, the directional pattern of the latter is slightly distorted.





APPROVED FOR RELEASE: 2007/02/09: CIA-RDP82-00850R000500020034-7

APPROVED FOR RELEASE: 2007/02/09: CIA-RDP82-00850R000500020034-7



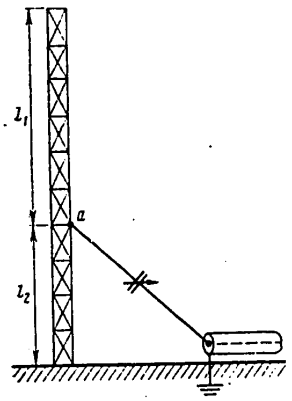


Figure 13.7

To explain the operational principle of a top fed antenna tower, we shall represent it in the form of a circular metal cylinder with a grounded base, inside which the vertical conductor is fastened to insulators (Figure 13.8a). A metal disk which represents a capacitive load, is connected to the upper end of this conductor, which extends out beyond the cylinder. In structural terms, this load is usually a portion of the upper level of guys, while the cylinder is a conventional type tower. The feed from the generator to the antenna uses a coaxial line, the shield of which is connected to the body of the tower, while the inner conductor is connected to the inner conductor of the tower. Thus, the cylinder (the tower) and its internal conductor represent a coaxial line with a large cross-section. Because of the fact that the inner conductor extends out beyond the limits of the cylinder and has a load at the top end, the current flowing along the internal surface of the cylinder also continues to its outer surface. The currents flowing through the outer surface of the tower (the cylinder) radiates the electromagnetic field. For this reason, from a radiation viewpoint, it is as if the generator is inserted between points a and b, i.e., is located at the top of the tower (Figure 13.8b). At the grounded base of the tower (point 0) there is always a current antinode (using the method of mirror images, it is easy to show that the point 0 is the short circuit point). The antenna is tuned to resonance and matched to the feed line by means of a special circuit. Top fed antenna towers are widespread among the radio broadcasting centers of the Soviet Union.

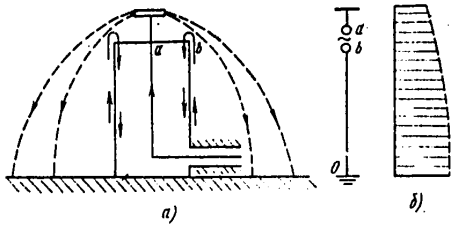


Figure 13.8.

To increase the reliable reception area, the antenna radiation at angles greater than 45° to the horizontal should be reduced, so that the angles of arrival of the space waves in the near fading field amount to 45 - 85°. Antennas which have directional patterns in the vertical plane which provide for maximum radiation along the surface of the earth and little radiation at comparatively high angles (starting at 40 to 50°) are called *antifading*. It is conventionally assumed that an antenna has satisfactory antifading properties if the field intensity at elevation angles exceeding 50° amounts to no more than 10 to 15 percent of the field intensity in a horizontal direction. The best directional pattern, from the viewpoint of antifading properties, is had by an antenna with a relative length of $l/\lambda = 0.53$ ($kl = 190°$) (Figure 13.9a). It is well known that an antenna with a relative length of $l/\lambda = 0.63$ has the maximum gain in the horizontal direction. However, there is a sidelobe in the directional pattern of such an antenna which produces marked radiation at angles of 40 to 60° to the horizontal.





APPROVED FOR RELEASE: 2007/02/09: CIA-RDP82-00850R000500020034-7

APPROVED FOR RELEASE: 2007/02/09: CIA-RDP82-00850R000500020034-7



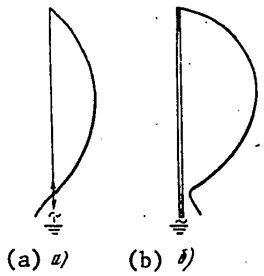


Figure 13.9.

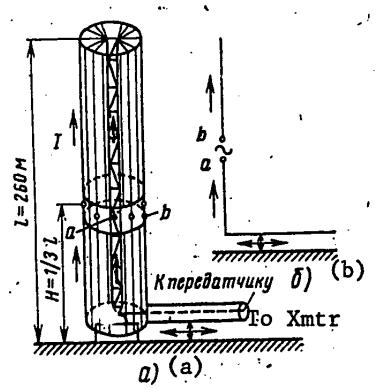


Figure 13.10.

The use of antifading antennas makes it possible to increase the reliable reception area by a factor of 2 to 2.5 times as compared to a short antenna. It should be kept in mind that the thinner antenna (the greater its characteristic impedance), the better its antifading properties will manifest. With an increase in antenna thickness, the current at the node increases (Figure 13.9b), the sidelobe widens and radiation is found at angles which are the most dangerous from the viewpoint of near field fading. A large characteristic impedance leads to a rise in the potentials in the antenna (a reduction in the permissible power) and to a decrease in the bandwidth. For this reason, the characteristic impedance is to be chosen taking into account obtaining sufficiently good antifading properties, the requisite bandwidth and the specified power.

Both antenna masts with an insulated base and antenna masts with a grounded base can be used as antifading antennas.

Wire antennas and antenna masts with grounded or insulated bases cannot operate throughout the entire radio broadcasting band (200 to 2,000 m). The working band on the long wave side is limited by the reduction in the radiation resistance and the corresponding decrease in the efficiency; on the short wave side it is limited by the sharp reduction in radiation along the surface of the earth, if $l/\lambda > 0.7$. The broadband antenna with a variable current distribution (ARRT) proposed by G.Z. Ayzenberg, can operate throughout the entire broadcast range at wavelengths of 200 to 600 and 600 to 2,000 m. In this case, this antenna has antifading properties in the 200 to 600 m band [64].

One of the variants of an ARRT antenna [65, 66] takes the form of an antenna mast 260 m high, insulated at the base (Figure 13.10a). The lower portion of the mast, H, which amounts to one-third of its height $l$, is surrounded by a cylindrical shield with a diameter of about 10 m, consisting of 9 to 12 wires. The lower ends of these wires are connected to the shield of the wire coaxial line, coming from the generator. In a first approximation, the wires of the shield can be treated as a solid cylinder and the entire lower portion of the antenna enveloped by this cylinder can be treated as a coaxial line.



APPROVED FOR RELEASE: 2007/02/09: CIA-RDP82-00850R000500020034-7

APPROVED FOR RELEASE: 2007/02/09: CIA-RDP82-00850R000500020034-7



To reduce the characteristic impedance of the antenna (down to 170 to 100 ohms), widen the passband correspondingly and increase the maximum transmitter power (more than 150 KW), the upper portion of the tower is surrounded by a wire cylinder, which is insulated from the lower cylinder. The lower and upper ends of the wire of the upper cylinder are connected to the start of the upper portion of the tower and to its top end respectively.

The points a and b (the upper ends of the lower portion of the tower and the lower cylinder) can be considered the generator connection points. The radiation is produced by currents flowing through the wires of the lower and upper cylinders (Figure 13.10b). We will note that the current exiting at point b to the exterior surface of the lower cylinder coincides in phase with the current flowing through the upper portion of the antenna. The current distribution can be adjusted by a variable reactance $X_H$ inserted between ground and the lower end of the wire shield. It is made in the form of a short circuited loop, for which the external shield of the feed line is used. The quantity $X_H$ is adjusted by moving the short circuiting device. The current antinode is located at the short circuit point and is moved when the short circuiting device is moved. The antenna operates without current distribution adjustment in a range of 600 to 2,000 m. It has an elevated radiation resistance in this mode.

An antenna was subsequently designed having two feed points 44, 66]. With the appropriate alignment and a tower height of 300 m, this antenna has a greater gain (up to four).

A specific feature of ARRT antennas is the extremely slight dependence of the directional pattern on the characteristic impedance of the antenna. This is explained by the fact that the power is delivered to the antenna at its base, but at a height of $H = 0.3\lambda$ to $0.5\lambda$, because of which, the nature of the current distribution depends slightly on $W_A$ and is close to sinusoidal. For this reason, even for a low value of $W_A$ (100 to 170 ohms), the antifading properties remain good.

In a number of cases, it is desirable for medium wave radio broadcasting to use antennas which are directional in the horizontal plane. This makes it possible to distribute the radiated power in specific directions, as well as to reduce crosstalk interference of radio stations.

To provide broadcast coverage for a territory having the shape of a sector, an antenna system has been designed which consists of four shunt fed antennas, located at the corners of a square [67]. Two of them are fed from the transmitter, while the other two play the part of a passive reflector. One can obtain four coverage sectors by combining the dipoles which operate as the antennas and reflectors in various ways by means of an appropriate switching system.

To provide broadcast coverage for territories which are considerable distances away, a medium wave antenna system has been developed which consists of eight shunt fed antenna towers, arranged in two rows [68]. Four towers, arranged in one row, are fed from a transmitter; the other four play the part of a tuned passive reflector. The spacing between the rows is 75 m. The antenna has a controlled directional pattern in a sector of $\pm 30°$. The gain of the antenna system in a range of



APPROVED FOR RELEASE: 2007/02/09: CIA-RDP82-00850R000500020034-7

APPROVED FOR RELEASE: 2007/02/09: CIA-RDP82-00850R000500020034-7



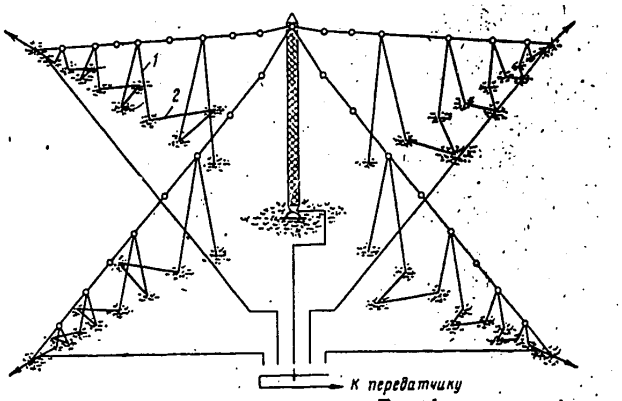


Рис. 13.11 To the transmitter

Figure 13.11.

185 to 575 m varies from 28 to 5. Shunt fed antenna towers with a reduced characteristic impedance ($W_A \approx$ Ohm) were chosen as the radiator. The reduction in $W_A$ is achieved by means of suspending a wire cylinder with a diameter of 15 m around the trunk of the tower, where the cylinder is made from 15 to 16 wires with a diameter of 16 mm. The wires of the cylinder at the top of the tower and at a height of 0.5 H are connected to the grounded trunk of the tower. The height of the antenna tower is H = 110 m.

The antennas considered here require an extremely complex tuning and switching system. Moreover, when the wavelength changes, the directional pattern in the vertical and horizontal planes change substantially.

When the vertical antennas are replaced by four logperiodic antennas, suspended on one common support (Figure 13.11), each antenna, with the appropriate choice of the configuration and number of elements, makes it possible to obtain a directional pattern with a width of 70 to 100° in the horizontal plane and a satisfactory directional pattern in the vertical plane (from the viewpoint of antifading properties) [69]. Changing the irradiation sector is accomplished by switching the transmitter to the corresponding antenna. The directional properties of the antenna practically do not change in a wavelength range of 200 to 600 m. The traveling wave ratio in the feeder in this range does not drop below 0.5.

The development of strong polymer film technology created the conditions for the design of new antenna structures. G.Z. Ayzenberg and V.N. Uryadko in the USSR developed a pneumatic antenna mast made of solid polymer material. It takes the form of a truncated cone 60 meters high (Figure 13.12)[not reproduced] made of high strength polymer, maintained under an excess air pressure (the pressure in the balloon is somewhat higher than atmospheric pressure). Either metal guys intended at the same time for also supporting the antenna in a vertical position or a system of wires tightly fitting the cylinder are used as the radiators. The advantage



APPROVED FOR RELEASE: 2007/02/09: CIA-RDP82-00850R000500020034-7

APPROVED FOR RELEASE: 2007/02/09: CIA-RDP82-00850R000500020034-7



of such antennas consists in the set-up speed, the possibilities for adjusting the height, etc.

When placing several antenna towers on a site of limited size, it is necessary to take steps to reduce the electromagnetic coupling between them (to increase the isolation), which leads to the distortion of the directional patterns of the antennas, i.e., improve the electromagnetic compatibility of the antennas. Work which has been done in this area indicates that it is essential to provide for special tuning of the antennas by means of inserting tuning impedances in them in conjunction with filter circuits, the value of which depends on the spacing between the antennas and their height.

## 13.3. Long Wave and Medium Wave Receiving Antennas

*The major types of receiving antennas.* VLF, LF and MF receiving antennas differ significantly from transmitting antennas both in terms of the structural design and types. The problems related to delivering large powers to the antenna and the appearance of large potentials in it are absent in receiving antennas. The efficiency of these antennas down to a certain minimum is likewise of no great importance. In the wavelength ranges considered here, atmospheric and industrial interference, as well as interference from other radio stations have a high level, and to increase the signal/noise ratio it is necessary to use antennas which have a more or less directional pattern. However, the use of such antennas, because of their large dimensions, is possible only in the case of professional radio reception, and even then not always.

The main types of receiving antennas are: loop antennas of various types, traveling wave antennas, ominidirectional vertical unbalanced antennas. The latter differ from transmitting antennas only in the small dimensions and structural design.

*Loop antennas.* A loop antenna takes the form of one or more series connected turns of a conductor. In this case, the loops can have different shapes (circular, rectangular, triangular, etc.). The planes of the loops are arranged perpendicular to the surface of the earth (a vertical loop). Loop antennas are used as the receiving antennas for radio communications, radio broadcasting and various special purposes. The dimensions of loop antennas vary in a wide range: from very small (tens of centimeters) multiturn loops with magnetic dielectric cores, housed inside the receivers, to external loops installed in a loop antenna field, the linear dimensions of which can exceed 100 m. The size of all loop antennas (even the largest) used in the VLF, LF and MF bands are small as compared to the wavelength. For this reason, these loops can be considered elementary (see §1.2).

If a plane vertically polarized wave impinges on a single turn rectangular loop (Figure 13.13a), the sides of which, ab and ce are perpendicular to the horizontal plane, where the direction of arrival of the wave makes an angle $\phi$ with the plane of the loop (Figure 13.13b), then the electrical field intensity at the point a is $\dot{E}_1 = E_0 e^{\frac{-ikd}{2}\cos\varphi}$, where $E_0$ is the field intensity in the center of the loop.





APPROVED FOR RELEASE: 2007/02/09: CIA-RDP82-00850R000500020034-7

APPROVED FOR RELEASE: 2007/02/09: CIA-RDP82-00850R000500020034-7



Correspondingly, the field intensity at point c is $\dot{E}_2 = E_0 e^{(ikd/2)\cos\phi}$. Since the loop is an elementary one, the e.m.f.'s induced in conductors 1 and 2 of the loop are determined by the expressions:

$$\dot{\mathcal{E}}_1 = E_0 h e^{-\frac{ikd}{2}\cos\varphi}; \quad \dot{\mathcal{E}}_2 = E_0 h e^{+\frac{ikd}{2}\cos\varphi}.$$

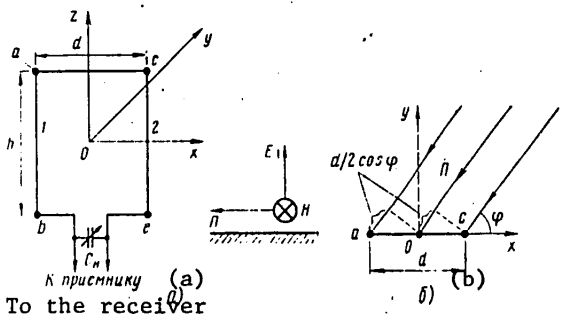


Figure 13.13.

These e.m.f.'s are identical in value, but shifted in phase because of the difference in the path of the rays and act counter to each other. The resulting e.m.f. across the terminal of the loop is equal to their difference:

$$\dot{\mathcal{E}}_p = \dot{\mathcal{E}}_2 - \dot{\mathcal{E}}_1 = i\,2E_0 h \sin(kd\cos\varphi/2).$$

Since the loop dimensions are small and $d/\lambda << 1$, the sine can be replaced by its argument. Then:

$$\dot{\mathcal{E}}_p = i E_0 kdh \cos\varphi. \qquad (13.11)$$

As follows from the given formula, the directional pattern of a loop takes the form of a regular number eight. This has already been established in §1.2 from the analogy between an elementary loop and an elementary magnetic dipole. The phase of the e.m.f. changes to the opposite sign when the direction of wave arrival changes by 180°. If a wave arrives from a direction perpendicular to the plane of the loop ($\phi = 90°$), then the e.m.f.'s $\mathcal{E}_1$ and $\mathcal{E}_2$ induced in conductors 1 and 2 have identical phases (the difference in the travel of the rays is zero) and tne resulting e.m.f. is equal to zero. In this case, there is no current in the loop and the voltage across the terminals is zero: there is no reception. The reception maximum is obtained in the case where the direction of wave arrival coincides with the plane of the loop ($\phi = 0$).



APPROVED FOR RELEASE: 2007/02/09: CIA-RDP82-00850R000500020034-7

APPROVED FOR RELEASE: 2007/02/09: CIA-RDP82-00850R000500020034-7



By employing the concept of effective length to a loop antenna, based on (6.12), we obtain:

$$l_д = \mathcal{E}_р / E_0 = \frac{2\pi}{\lambda} S,$$

where S = hd is the area encompassed by the loop.

Since the effective length of a loop is extremely small, the radiation resistance is also low (even for large outdoor loops, it amounts to only tenths of an ohm). The radiation resistance of a loop antenna is significanly less than the loss resistance and the antenna efficiency is very poor. For this reason, loop antennas are not usually employed as transmitting ones (radio beacons are an exception). To increase the effective height of a loop antenna, multiple turns loops are employed, i.e., loops made of a number of series connected turns.

The reactive component of the input impedance of a loop is usually of an inductive nature (a short circuited line of short length), and a capacitor is inserted to compensate for it (tune the loop to resonance). When tuning the resonant circuit of the loop--capacitor, the voltage across the receiver terminal increases by a factor of Q times, where Q is the quality factor of the loop circuit. The effective length of a tuned loop also increases by a factor of Q. The quality factor of a loop circuit can reach values of 200 to 300.

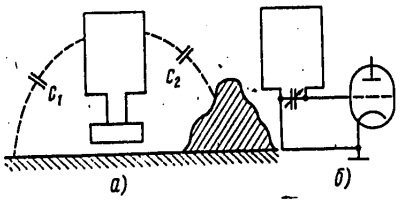


Figure 13.14.

To increase the signal/noise ratio, the directional pattern of a loop must be turned so that the direction of arrival of the interference coincides with the perpendicular to the plane of the loop. Of primary importance for reception quality is the depth of the directional pattern minima of the loop. Minima in the directional pattern are equal to zero only in the case of a completely electrically symmetrical loop; this symmetry is disrupted if conductors 1 and 2 of the loop have different impedances for the current flowing in them (for example, if the sides of the loop have different capacitances to ground because of their unequal positioning with respect to it or any other objects) (Figure 13.14) as well as in the case where the loop is connected to the unbalanced input of a receiver.

If the impedances of the vertical sides of the loop are not equal, then with a wave incoming from a direction perpendicular to the loop plane, the identical e.m.f.'s induced in them generate unequal but constant currents over the length of each side of the loop, $I_1$ and $I_2$. Because of this, a certain resultant current $I_p = I_1 - I_2$ is established in the loop, and a potential difference appears across the loop terminals, i.e., the reception takes place. This phenomenon is called the antenna effect of a loop. As a result of the antenna effect, the directional pattern is distorted, the null (reception) directions disappear and instead of them there are shallow minima. Where the antenna effect of a loop is present, the ability to tune



APPROVED FOR RELEASE: 2007/02/09: CIA-RDP82-00850R000500020034-7

APPROVED FOR RELEASE: 2007/02/09: CIA-RDP82-00850R000500020034-7



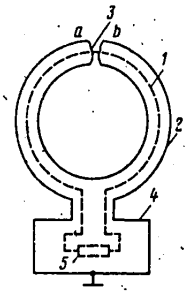


Figure 13.15.

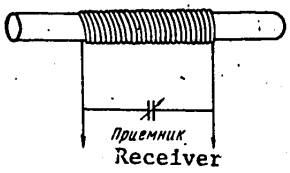


Figure 13.16.

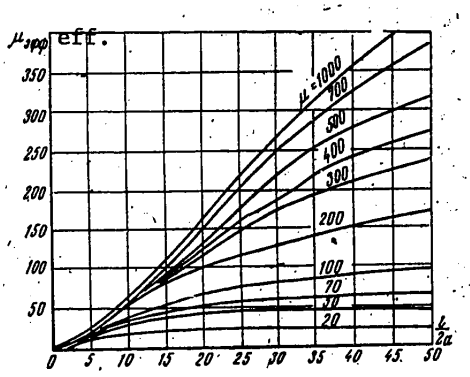


Figure 13.17.

out interference incoming from a particular direction is degraded. If the loop is used for direction finding, the antenna effect leads to errors in determing the location of the target.

To eliminate the antenna effect, the signs of the loop and the conductors of the feed lines should be completely symmetrical relative to ground and surrounding objects. Moreover, the input circuitry of the receiver front end should also be symmetrical. However, such a circuit is used rather rarely, since in this case the design is complicated and the cost of the receiver is increased. Considerably more widespread is the connection of the loop to the asymmetrical input of a receiver using any kind of balancing device.

To combat the antenna effect, it is most effective to use shielded loop antennas (Figure 13.15), where the receiver is housed in a common shield with the loop. A shielded loop antenna takes the form of a single turn or multiple turn loop 1, enclosed in a metal tube (shield) 2. There is a cutout 3 at the top of the tube, which is usually covered with a dielectric sleeve. The lower part of the tube makes a transition to metal housing 4, in which receiver 5 is housed. An incoming wave induces an e.m.f. in the outer surface of the shield, because of which, at points a and b of the gap there proves to be an applied potential difference, which generates a current in the inside surface of the shield. The outer surface of the shield and the conductors of the loop represent a coaxial line. For this reason, a current appears in the conductors of the loop which is equal in magnitude but opposite in direction to the current flowing in the inner surface of the shield, and a voltage is generated across the terminals of the receiver. The most important fact is that the potential difference applied to the gap, which generates the current in the loop, is governed exclusively by the currents in the outer surface of the shield and does not depend on any imbalance in the arms of the loop, in the input circuits of the receiver, etc. The sides of the shield (more precisely, their exterior surfaces) are usually symmetrical with respect to ground, and when a wave arrives perpendicularly to the plane of the loop, the e.m.f.'s occurring in the



APPROVED FOR RELEASE: 2007/02/09: CIA-RDP82-00850R000500020034-7

APPROVED FOR RELEASE: 2007/02/09: CIA-RDP82-00850R000500020034-7



exterior surfaces of the two sides of the shield prove to be equal in magnitude and phase, because of which the potential difference applied to the gap is zero and no current appears in the conductors of the loop. Thus, a shielded loop proves to be free of the antenna effect.

Magnetic dielectric cores are used to increase the effective length of a loop (Figure 13.16). The e.m.f. induced in a loop with a magnetic core can be determined from the formula [7]:

$$\mathcal{E}_p = -i\frac{2\pi}{\lambda}\mu nSE_0\cos\varphi. \qquad (13.12)$$

It can be seen from a comparison of (13.12) and (13.11) that inserting a core in the loop which is made of a material having magnetic properties increases the effective length of the loop by a factor of $\mu$ times.

Magnetic dielectrics are used the cores, i.e., materials having a high magnetic permeability and a low conductivity (ferrites, and Alsifer, etc.).

The effective loop length and the e.m.f. increase by a factor only in the case of a rod of infinite length. In actual cases, the increase in the effective loop length amounts to $\mu_{eff}$ times, where $\mu_{eff} < \mu$ because of the end effect (the demagnetization of the ends of the core). Thus,

$$l_d = (2\pi/\lambda)\mu_{eff}nS. \qquad l_\mu = \frac{2\pi}{\lambda}\mu_{э\phi\phi}nS.$$

The quantity $\mu_{eff}$ depends on the relative magnetic permeability of the core material and its shape. The demagnetizing effect of the ends of the rod, and consequently, the reduction in $\mu_{eff}$ as compared to $\mu$, is greater, the smaller the ratio of the rod length $l$ is to its cross-section (Figure 13.17). The effective length of a loop antenna is proportional to the area of the loop, however, it is not advantageous to increase the loop area, since in this case, $\mu_{eff}$ decreases. The number of turns in the loop cannot be chosen too great: in this case, the internal capacitance of the coil (the loop) rises and it becomes difficult to tune the loop with a capacitor. Loops with magnetic dielectric cores (magnetic antennas) are widely used broadcast receiver antennas; the small overall dimensions of such antennas make it possible to place them directly inside the receiver. The use of magnetic antennas is not limited to the LF and MF bands. The range of applications for these antennas extends in the direction of shorter wavelengths in step with the improving parameters of magnetic dielectrics, and reaches the VHF band.

The effective length of a loop antenna is proportional to the loop area; therefore, for professional radio broadcast reception (radio repeaters) or for other types of professional reception, large stationary loop antennas are used, which are set up in an antenna field using towers. The major advantage of loop antennas over vertical asymmetrical antennas is the presence of reception nulls in the horizontal plane, which make it possible to tune out interfering signals, while in the case





APPROVED FOR RELEASE: 2007/02/09: CIA-RDP82-00850R000500020034-7

APPROVED FOR RELEASE: 2007/02/09: CIA-RDP82-00850R000500020034-7



of small loop antennas used for individual reception, the directional patterns are controlled by simply rotating the loop or the entire receiver, complex and expensive structures are required to rotate large loops.

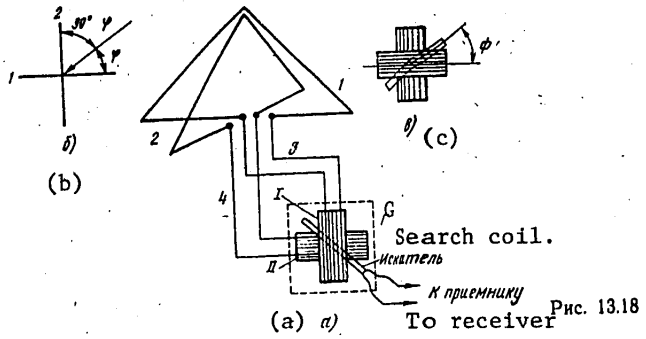


Рис. 13.18

Figure 13.18.

The directional pattern of large stationary loop antennas can be controlled by means of an extremely simple (goniometric) device. A goniometric antenna system (Figure 13.18a) consists of three main parts: an antenna of two mutually perpendicular loops 1 and 2, two balanced feed lines 3 and 4 and the goniometer G. The goniometer consists of three small coils: two stationary (stator) 1 and 2, positioned in mutually perpendicular planes, and one moving (rotor) so-called search coil. The stator coil 1 is inserted in the circuit of the first loop, while stator coil 2 is inserted in the circuit of the second loop. The rotor coil rotates about an axis passing through the center of the stator coils. It is connected to the receiver. Tuning elements are inserted in the circuit of the search coil and the circuit formed in this fashion is tuned to resonance with the station being received. The goniometer is set up a considerable distance away from the antenna in the receiving station room.

We shall consider the operational principle of a goniometric antenna. The normalized directional characteristics of loops 1 and 2 are determined by the expressions:

$$F_1(\varphi) = \cos\varphi\,;\; F_2(\varphi) = \sin\varphi,$$

where $\phi$ is the angle between the direction to the station being received and the plane of the first loop (Figure 13.18b).

With the action of the e.m.f.'s induced in the loops, currents appear in the stationary coils inserted in these loops. The current flowing through the coil connected to loop 1 is $I_1 = I_0\cos\phi$, where $I_0$ is the current in the coil when the direction of the incoming wave coincides with the plane of the loop.

The current flowing through the coil inserted in loop 2 is $I_2 = I_0\sin\phi$. In both formulas, the current $I_0$ is the same, since both loops and the coils inserted in



APPROVED FOR RELEASE: 2007/02/09: CIA-RDP82-00850R000500020034-7

APPROVED FOR RELEASE: 2007/02/09: CIA-RDP82-00850R000500020034-7



them are completely identical. The coefficient of mutual induction between the stationary coil 1 and the search coil is $M_1 = M_0\cos\Phi$, where $\Phi$ is the angle between coil 1 and the search coil (Figure 13.19c); $M_0$ is the coefficient of mutual induction when the planes of the stationary and moving coils coincide. The coefficient of mutual induction between coil 2 and the search coil is $M_2 = M_0\sin\Phi$.

The electromotive forces induced by the stationary coils 1 and 2 in the search coil are equal to the following respectively:

$$\mathcal{E}_1 = I_0\omega M_0\cos\varphi\cos\Phi;\ \mathcal{E}_2 = I_0\omega M_0\sin\varphi\sin\Phi.$$

The resulting e.m.f. in the search coil is equal to the sum of the e.m.f.'s induced by the stationary coils: $\mathcal{E}_p = \mathcal{E}_1 + \mathcal{E}_2 = I_0\omega M_0(\cos\phi\cos\Phi + \sin\phi\sin\Phi)$. This formula can be transformed: $\mathcal{E}_p = I_0\omega M_0\cos(\phi - \Phi)$. Thus, the normalized directional pattern of the goniometric antenna is:

$$F(\varphi) = \cos(\varphi - \Phi). \qquad 13.13$$

This directional pattern is no way different from the directional pattern of a conventional loop antenna. As can be seen from (13.13), by changing the position of the search coil (the angle $\Phi$), one can control the directional pattern of the antenna. The maximum reception direction is obtained when $\phi = \Phi$; there is a reception null when $\phi - \Phi = \pm 90°$. Thus, the rotation of the search coil yields the same effect as the rotation of the loop antenna.

A goniometric antenna makes it possible to tune out interfering stations by means of setting the null of the directional pattern on the interfering station. This antenna also allows for reducing the level of directional atmospheric interference.

Each outside loop of the goniometer is usually made in the form of an isosceles triangle, for which the base is approximately four times the height. Only one tower is needed to string such an antenna. The lower conductor is suspended at a height of 2.5 m. At LF wavelengths, the height of the loop runs up to 70 to 100 m and at MF wavelengths, up to 10 m and more. Antennas are being developed in which small ferrite antennas are used instead of the large outside loops.

If a vertical unbalanced antenna is added to a loop or goniometric antenna, positioning the vertical antenna, for example, in the center of the loop (Figure 13.19a), then unidirectional reception (a cardioid directional pattern) can be obtained by means of a special phasing device. This is easily illustrated if the loop antenna is replaced by the magnetic dipole equivalent to it. Then the loop antenna and the electrical dipole can be treated as two mutually perpendicular dipoles: an electrical and a magnetic one (Figure 13.19b). It is well known (see §1.4) that the directional pattern of such an antenna (see Figure 1.8) is defined by the formula $(F(\phi) = 1 + \cos\phi$. A unidirectional cardioid type pattern (Figure 13.19c) has advantages over the bidirectional pattern of a loop or goniometer, since it permits a significant reduction in the level of an interfering signal incoming from



APPROVED FOR RELEASE: 2007/02/09: CIA-RDP82-00850R000500020034-7

APPROVED FOR RELEASE: 2007/02/09: CIA-RDP82-00850R000500020034-7



directions in a range of angles of 90 to 270° without markedly reducing the useful signal level. Moreover, such a directional pattern makes it possible to unambiguously determine the direction to the station being received. Detailed data on loop antennas can found in [70].

*The single wire traveling wave antenna (OB).* Radio broadcast reception quality at radio repeaters can be improved by using an atenna with considerable directional properties. Such antennas include the single conductor traveling wave antenna (OB). This antenna takes the form of a horizontal conductor (Figure 13.20a) with a length (L) of from a half-wave to several wavelengths, strung at a height of 2.5 to 4.5 m above the ground. One end of the conductor is connected to the receiver, while the other is connected a resistance $R_H$, equal to the characteristic impedance of the conductor. The other end of the load resistance is connected to a ground lead. Althought the antenna is positioned horizontally above the surface of the earth, it is designed for receiving the vertically polarized field of a ground wave. Because of the finite conductance of the soil, the Poynting vector of a vertically polarized ground wave, radiated by a transmitting radio station, is not parallel to the surface of the earth, but makes a certain angle $\Delta_\varepsilon$ with it. Because of the

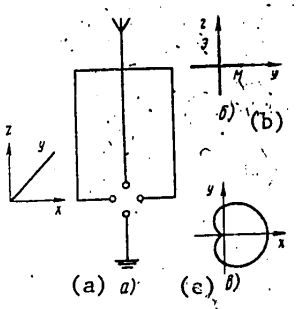


Figure 13.19.

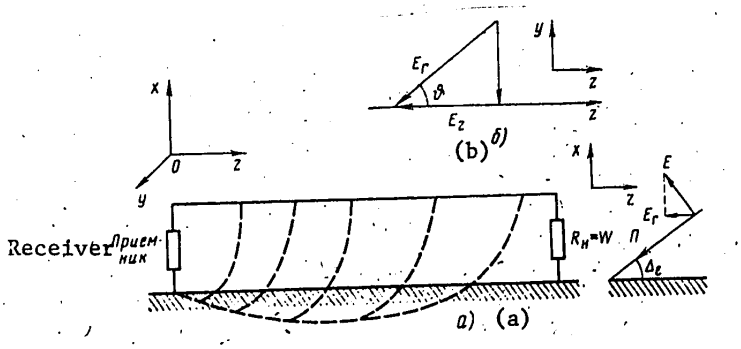


Figure 13.20.

slope of the Poynting vector, a horizontal component of the vector E appears ($E_h$ = E sin $\Delta_\varepsilon$) of the incoming field, which induces an e.m.f. in the conductor. With the action of the e.m.f. in the conductor, a current appears, the second conductor for which is the ground. Although the antenna is used as a receiving one, it is more convenient to analyze its operation in a transmit mode. Since the conductor is loaded into a resistance equal to its characteristic impedance, a traveling current wave is established in the conductor. Because of the fact that the spacing between the conductor and ground is small and the conductivity is not infinitely high, the currents penetrate a certain depth into the earth. The soil has a substantial influence on the parameters of the conductor. Because of the fact that dielectric permittivity of the soil is greater than the dielectric permittivity of air, the phase velocity of the wave in the conductor proves to be less than the speed of light.

The electromotive force induced in an element of the conductor is proportional to the value of the $E_z$ field intensity component parallel to the axis of the



APPROVED FOR RELEASE: 2007/02/09: CIA-RDP82-00850R000500020034-7

APPROVED FOR RELEASE: 2007/02/09: CIA-RDP82-00850R000500020034-7



conductor (Figure 13.20b). This component is $E_z = E_h\cos\theta$, where $\theta$ is the angle between the $E_h$ component and the axis of the conductor.

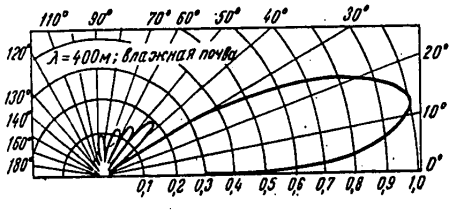


Figure 13.21.
Wavelength = 400 m; moist soil.

The maximum e.m.f. is induced in an element of the conductor by the wave incoming from a direction which coincides with the axis of the conductor. Based on what has been said, as well as keeping (7.36) in mind, the directional pattern of the single wire traveling wave antenna in the horizontal plane, if the current attenuation in the conductor is not taken into account, can be represented in the form:

$$f(\vartheta) = \frac{\cos\vartheta}{c/v - \cos\vartheta} \sin\left[\frac{kL}{2}(c/v - \cos\vartheta)\right]. \qquad (13.14)$$

The directional pattern of a 2,000/2.5 single wire traveling wave antenna (the numerator in the fraction is the antenna length; the denominator is the antenna height; both dimensions are in meters) in the vertical plane of the antenna is shown in Figure 13.21. In the case of moist soil, the antenna has a directional pattern which is pressed closer to the earth and a lower sidelobe level than in the case of dry soil. The efficiency and directional gain of the single wire traveling wave antenna, because of the high energy losses in the soil and in the absorbing resistance, are quite small, because of which this antenna is not, as a rule, used as a transmitting antenna.

The gain of the antenna can be increased by making it from two or more conductors, spaced a certain distance apart [71].





APPROVED FOR RELEASE: 2007/02/09: CIA-RDP82-00850R000500020034-7

APPROVED FOR RELEASE: 2007/02/09: CIA-RDP82-00850R000500020034-7



APPENDIX 1

Questions of Antenna Miniaturization

*The use of active radiators.* As was indicated in §7.7, the realization of the phenomenon of antenna ultradirectionality (the possibility of an unlimited increase in the directional gain of an antenna with finite dimensions) is extremely difficult. The narrowing of an antenna directional pattern and increasing directional gain in practice entail increasing its dimensions.

The problem of reducing antenna size basically reduces to decreasing the dimensions of poorly directional antennas, forming complex highly directional antenna systems. It is well-known that the directional gain of a poorly directional antenna of sufficiently small dimensions almost does not decrease with a further reduction in its size (the directional gain of a symmetrical dipole with a reduction of an arm from $l/\lambda = 0.25$ to nearly 0 changes from 1.64 to 1.5). However, with a reduction in the length of a conventional dipole, the resistive component decreases (by virtue of radiation) and the reactive component of its input impedance increases, which leads to a narrowing of the bandwidth of the antenna and to a reduction in its efficiency. Such a dipole begins to behave like an ultradirectional antenna. The attempt to match such an antenna to a feed line or to the input circuits of a receiver by means of a passive four-pole network made of reactive components does not yield the requisite results, even in an extremely narrow passband.

The application of radiators with active semiconductor devices inserted in them (active radiators, see §11.5) is promising in the sense of designing poorly directional, extremely short electrical or miniature magnetic dipoles. Such radiators with low noise sensitive amplifiers built into them are the elements of a complex antenna array operating in the short wave or meter wavelength bands, and can find independent applications as receiving antennas. The application of an active element with a high gain and considerable sensitivity directly in an antenna increases the sensitivity of the receiver, facilitates the matching and makes it possible to achieve considerable band coverage of the device with small overall dimensions.

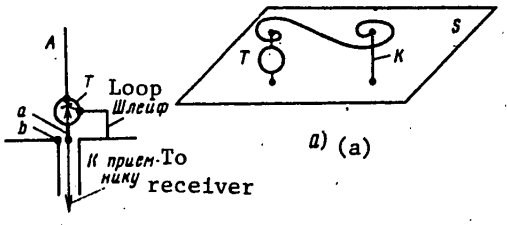


Figure A1.1.

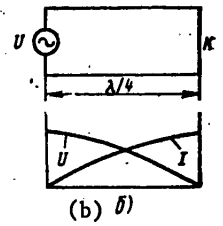


Figure A1.2.



APPROVED FOR RELEASE: 2007/02/09: CIA-RDP82-00850R000500020034-7

APPROVED FOR RELEASE: 2007/02/09: CIA-RDP82-00850R000500020034-7



Active miniature dipole antennas, used as independent receiving antennas installed in fixed and mobile facilities are called ultraminiature integrated circuit antennas (SIA).

By way of example, a dipole A of very short length is depicted in Figure A1.1, where the active element, transistor T, is inserted in a cutout in the dipole, and the transistor is intended both for amplifying the received antenna signal and for matching it to the coaxial cable coming to the receiver (points ab) [6, 72]. The short conductor, Sh (loop), which is connected to one of the transistor leads, where the other end of the loop is shorted to ground, has an inductive reactance, which is transformed by the transistors so that the capacitive reactance of the antenna is compensated at points ab. The extremely low resistive component of the antenna input impedance is also made equal to the characteristic impedance at points ab by means of the transistor. Transistor matching proves to be extremely broadband. Thus, for the circuit of Figure A1.1. the voltage at the receiver input in a frequency range of 2 to 50 MHz changes by a factor of approximately 1.5 times.

If there is no broadband requirement, then one can use the device, the operational principle of which is explained in Figure A1.2a. The active element T is connected to one end of a quarter-wave line, made in the form of a loop or helix and arranged above metal plate S. The other end of the loop is connected to the plate by means of the short circuiting device K, which plays the part of the radiator. An equivalent circuit of the device is shown in Figure A1.2b. This device has the following parameters: the height of the short circuiting link is $K\lambda/50$; the transverse dimensions of the plate are $\lambda/20$; the efficiency is $\eta$ = 80 percent; and the passband is 1 percent. Such an antenna is housed in the helmets of astronauts and serves for communications with the spacecraft.

*Stripline antenna array designs. Inflatable and pneumatic antennas. Other trends in the reduction of antenna size.* Imparting a flat shape to dipoles and reducing the antenna wave is achieved by using multiple dipole antennas in a stripline printed circuit board design. The feed system is simplified in such antennas and fabrication while observing the requisite precision is facilitated. This makes it possible to use printed circuit multiple dipole antennas in the decimeter and centimeter bands. Dipoles and other elements of antenna arrays (segments of coupling feed lines, phasing elements) are made in the form of conducting lines (strips) on dielectric plates (or polymerfilms), which in turn are placed on metallic substrates (shields). A shield can take the form of a thin metal film applied to a polymer film. Such a technique can be used to make, for example, in-phase multiple dipole antennas, director antennas, surface wave antennas, etc.

Stripline antenna arrays can be used in inflatable antennas. Such an antenna takes the form of an air balloon made of soft polymer film. Two flat film partitions are placed inside the balloon sphere at a distance of approximately $\lambda/4$ from each other, where the stripline antenna array is applied to one of the partitions using printed circuit technology, while the other is coated with a continuous metal film (an aperiodic reflector).

If a portion of the sphere is coated with a solid metal film and it is given the shape of a paraboloid, then one can make an inflatable parabolic antenna. When not operating, inflatable antennas occupy very little space.



APPROVED FOR RELEASE: 2007/02/09: CIA-RDP82-00850R000500020034-7

APPROVED FOR RELEASE: 2007/02/09: CIA-RDP82-00850R000500020034-7



Pneumatic antenna masts can be used in the short wave and medium wave bands (see §13.2, Figure 13.12 [not reproduced]), the positive qualities of which are fast set-up and take-down, transportation simplicity, the possibility for adjusting the height, etc.

Radio electronics hardware makes it possible to increase the effective surface of mobile receiving antennas by many times through the use of artificial (synthesized) apertures (see §11.5).

Multibeam antennas can be included among the techniques of reducing antenna size. In this case, several antennas which provide for communications in different directions are replaced by one antenna.

Nearly flush mounted dielectric or ribbed surface wave antennas yield a savings in overall dimensions (see §9.3).

*Miniaturization of waveguide channel components.* It is known that a reduction in waveguide size is accompanied by an increase in losses and a reduction in the ultimate power. However, it is expedient in a number of cases to use miniature channel components. When a waveguide is filled with a dielectric, the transverse dimensions are reduced by a factor of $\sqrt{\varepsilon_r}$ times. The attenuation factor in metal as compared to the attenuation factor in a conventional waveguide increases by approximately $\sqrt{\varepsilon_r}$ times. The attenuation factor in a waveguide, which is governed by the losses in the dielectric, is proportional to $\tan\delta\sqrt{\varepsilon}$ ($\tan\delta$ is the tangent of the loss angle). High quality dielectrics are frequently used to reduce the attenuation in the dielectric (sapphire, ruby, polycor, sitall, etc.), for which $\varepsilon_r$ = = 7 to 10 and $\tan\delta = (1\text{--}4) \cdot 10^{-4}$.

A further reduction in the cross-section is possible by means of using striplines. A stripline can be produced by applying metallic strips with a thickness of a few microns and a width of a few millimeters to a dielectric.

Dielectric filled waveguides, and striplines make it possible to design miniature resonators, and consequently, miniature filters for various purposes. Small cross-section lines can also be used to produce miniature directional couplers, circulators and other components of a waveguide channel. The composition of ferrite elements and volumetric resonators makes it possible to reduce the system of isolation filters used on radio relay links.

Interest has been manifest recently in the use of subcritical waveguides, i.e., waveguides which operate at frequencies below the critical, as various components of microwave channels [73]. If subcritical waveguides are used in the waveguide components installed in satellites and other flight vehicles, this will make it possible to reduce the overall size of a number of microwave assemblies by a factor of 5 to 10.

A subcritical waveguide section in conjunction with an inhomogeneity introduced into it (stops, pins), makes it possible in principle to design microwave assemblies for various purposes. Such waveguides are used as resonators, stopband and bandpass filters, etc.



APPROVED FOR RELEASE: 2007/02/09: CIA-RDP82-00850R000500020034-7

APPROVED FOR RELEASE: 2007/02/09: CIA-RDP82-00850R000500020034-7



Also interesting is the possibility of utilizing subcritical waveguides as the radiating elements of a phased antenna array. Such an element takes the form of an extremely short waveguide section with a small cross-section (at a wavelength of $\lambda \approx 10$ cm, the length of an element is about 2.5 cm and its cross-section dimensions are approximately 1.9 by 0.875 cm), which is driven with a coaxial line. With a large scanning angle of the phased antenna array, the spacing between adjacent elements is $\lambda/2$. The cost and weight of such a phased antenna array is considerably lower than for an antenna with conventional waveguide elements.

Table of Contents


| | |
|---|---|
| Foreword | 3 |
| List of Main Symbols Used | 4 |
| Introduction | 6 |
| Part I. Fundamentls of Antenna Theory | 9 |
| Chapter 1. Elementary Radiators | 9 |
| 1.1. The radiation of an elementary electrical dipole | 9 |
| 1.2. The radiation of an elementary magnetic dipole | 11 |
| 1.3. An elementary radiating slot | 12 |
| 1.4. The radiation of a Huygens source | 15 |
| Chpater 2. Parameters Characterizing the Directional and Polarization Properties of Antennas | 16 |
| 2.1. General remarks. The directional characteristic (pattern) of an antenna | 16 |
| 2.2. The directional gain (KND) and gain (KU) of an antenna | 20 |
| 2.3. The polarization parameters of an antenna. The tourniquet radiator | 22 |
| 2.4. On the problem of electromagnetic compatability (EMS) of antennas | 26 |
| Chpater 3. The Symmetrical Electrical Dipole in Free Space | 27 |
| 3.1. The problem of the radiation of a thin electrical dipole | 27 |
| 3.2. The directional properties of a symmetrical dipole | 32 |
| 3.3. The radiation power and radiation resistance of a symmetrical diplole | 36 |
| 3.4. The input impedance of a symmetrical dipole | 37 |
| 3.5. The directional gain of a symmetrical dipole. The effective length of an antenna | 39 |
| 3.6. The symmetrical slot dipole | 40 |
| Chapter 4. The Mutual Coupling of Dipoles | 43 |
| 4.1. The directional properties of a system of two coupled dipoles | 43 |
| 4.2. Calculating the radiation resistance of coupled dipoles using the technique of induced e.m.f.'s | 47 |
| 4.3. Calculating the current in passive dipoles | 51 |
| 4.4. The problem of current distribution in coupled dipoles in a rigorous formulation | 52 |




APPROVED FOR RELEASE: 2007/02/09: CIA-RDP82-00850R000500020034-7

APPROVED FOR RELEASE: 2007/02/09: CIA-RDP82-00850R000500020034-7



Chapter 5. The Influence of Ground and Metallic Bodies on the Radiation of Antennas Located Close to Them 54

5.1. The solution of the problem of the radiation of a dipole located above the surface of the earth using the method of mirror images 54
5.2. The radiation of symmetrical dipoles positioned above the surface of the earth 57
5.3. Asymmetrical vertical grounded dipole 61
5.4. The influence of metallic bodies on the radiation of dipoles located close to them 65

Chapter 6. Some Questions of Receiving Antenna Theory 68

6.1. The application of the reciprocity principle to the study of receiving antennas 68
6.2. The power dissipated in the load of a receiving antenna 72
6.3. Polarization matching of receiving and transmitting antennas 74
6.4. The equivalent noise temperature of an antenna 76

Chapter 7. Methods of Obtaining Narrow Directional Patterns 79

7.1. Radiator arrays. The uniform linear antenna array 79
7.2. The in-phase antenna array 82
7.3. Controlling the directional pattern of a uniform linear array 85
7.4. End-fire antenna arrays (traveling wave antennas) 87
7.5. The radiation of excited surfaces. The directional pattern and directional gain of a radiating aperture 94
The influence of phase distortions on the directional properties of a radiating surface 102
7.6. Planar (two-dimensional) antenna arrays 105
7.7. The problem of antenna design. Optimal directional patterns 107

Part II. Types of Antennas 110

Chapter 8. Dipole and Slot VHF Antennas 110

8.1. Simple dipole antennas 110
8.2. Methods of increasing the working bandwidth of dipole antennas 113
8.3. Frequency independent antennas 115
8.4. Log periodic antennas (LPA's) 118
8.5. Feed for simple dipole antennas 123
8.6. Slot antennas 127
The radiation of a slot cut in a flat shield of limited dimensions or in the wall of a waveguide (127). Multiple slot waveguide antennas (131)
8.7. Television antennas 134
The antennas of television transmitting centers (134). Receiving television antennas. Community TV reception systems (138).



APPROVED FOR RELEASE: 2007/02/09: CIA-RDP82-00850R000500020034-7

APPROVED FOR RELEASE: 2007/02/09: CIA-RDP82-00850R000500020034-7



Chapter 9. End-Fire VHF Band Antennas 140

9.1. Director antennas 140
9.2. Helical antennas 143
9.3. Surface wave antennas (APV) 149
General remarks (149). Dielectric rod antennas (150). Impedance antennas (152). Phase velocity modulated antennas (155). Fast wave antennas (157).

Chapter 10. Aperture Antennas 158

10.1. Horn antennas 158
Operational principle and majo- properties (158). Horns with a circularly polarized field (164)
10.2. Lens antennas 165
10.3. Reflector (parabolic) antennas 170
The operational principle of a parabolic antenna and its directional pattern (170). The directional gain of a parabolic antenna (176). Parabolic antenna subdishes (180). The influence of the fabrication precision of a reflector antenna on its directional properties (185). A reflector antenna in the form of a parabolic cylinder (189).
10.4. The parabolic horn antenna (RPA). Dual reflector antennas. Periscope antennas 191
10.5. Passive repeater antennas for radio relay links 200

Chapter 11. Multi-Element Antenna Arrays with a Controllable Directional Pattern 203

11.1. General information 203
11.2. The maximum permissible spacing between the elements of a phased antenna array. Mutual coupling of array elements 204
11.3. Methods of electrical control of the directional pattern of a phased antenna array. Methods of controlling phase shifters 207
11.4. Arrays of active radiators. Multibeam and repeater arrays 211
11.5. The concept of antenna arrays with signal processing 213

Chapter 12. Shortwave Antennas for Radic Communications and Broadcasting 213

12.1. Specific features of shortwave antennas 213
12.2. Some general questions of feeding shortwave antennas 215
12.3. Simple shortwave antennas 219
12.4. The in-phase horizontal broadband antenna (SGD antenna) 221
12.5. The rhombic antenna 226
12.6. The traveling wave antenna with coupling elements 231
12.7. The log periodic antenna 235

Chapter 13. Antennas for Radio Communications and Broadcasting at Myriameter (Very Long), Kilometer (Long) and Hectometer (Medium) Wavelengths 238

13.1. Questions of very long, long and medium wavelength antenna design 238



APPROVED FOR RELEASE: 2007/02/09: CIA-RDP82-00850R000500020034-7

APPROVED FOR RELEASE: 2007/02/09: CIA-RDP82-00850R000500020034-7



Specific features of VLF, LF and MF band antennas. Methods of calculating the main parameters of VLF, LF and MF antennas. Antenna feed. 247
13.2. Medium wave broadcasting antennas 249
13.3. Long wave and medium wave receiving antennas 254
The major types of receiving antennas. Loop antennas. Single wire traveling wave antenna (OB) 261

Appendix 1. Questions of Antenna Miniaturization 262
The use of active radiators. Stripline antenna arrays. Inflatable and pneumatic antennas. Other trends in antenna size reduction. The miniaturization of waveguide channel components.

Appendix 2. The Solution of Hallen's Integral Equation by the Technique of Point Matching 265

Appendix 3. Calculating the Currents in Dipoles Fed with a Series Balanced Feed Line (Traveling Wave Antennas with Coupling Elements; Log Periodic Antennas) 267

Appendix 4. Calculating the Directional Pattern of an Antenna in the Form of a Paraboloid of Rotation 270

Appendix 5. Calculating the Directional Pattern of a Parabolic Cylinder 272

Bibliography 275

COPYRIGHT: Izdatel'stvo "Radio i svyaz'", 1981

8225
CSO: 1860/41



APPROVED FOR RELEASE: 2007/02/09: CIA-RDP82-00850R000500020034-7

APPROVED FOR RELEASE: 2007/02/09: CIA-RDP82-00850R000500020034-7



UDC 621.396.6 (088.8)

# ANTENNA DEVICE WITH ELECTRICAL BEAM OSCILLATION IN TWO PLANES

Moscow OPISANIYE IZOBRETENIYA 586769 in Russian 23 Feb 81

[Description of USSR Patent No. 586769 by V.M. Ginzburg and I.N. Belova, filed 8 Mar 60, published 23 Feb 81, class H p1 Q 21/00]

[Text] This invention is in the area of antenna technology and can be used in radar.

There exists an antenna device with electrical rocking of the beam in two planes which consists of a reflector, radiator and lens.

However, the existing antenna device cannot transmit high power levels and does not eliminate aberrations when the beam rocks through a wide scanning sector.

The purpose of the present invention is to increase the transmitted power level while improving efficiency and reducing abberations.

In order to do this, a lens is inserted between the reflector and its focus, displaced from the focus along the axis of the reflector, the coefficient of refraction of which is varied electrically under program control. The lens consists of a matrix of waveguides containing electrically controlled phase inverters.

The drawing shows a schematic representation of the proposed antenna device.

The antenna device with electrical beam rocking in two planes consists of reflector 1, radiator 2, and lens 3. Lens 3 is located between reflector 1 and its focus, and is displaced from the focus along the axis of reflector 1.

The lens consists of waveguides 4, which form a matrix. The waveguides contain electrically controlled phase inverters.

The proposed antenna device operates as follows.

Let reflector 1 be parabolic with focus at point F. At a certain moment in time $t_1$, lens 3 converts the planar wavefront incident upon it to a spherical front with center at point F, i.e., the beam of the antenna device will be directed along the reflector axis 9'F. At the next moment in time $t_2$, lens 3 must convert the incident planar wave to a certain different spherical front whose center is moved away from the focus to point B (shown by dotted lines). Then the beam of the antenna



APPROVED FOR RELEASE: 2007/02/09: CIA-RDP82-00850R000500020034-7

APPROVED FOR RELEASE: 2007/02/09: CIA-RDP82-00850R000500020034-7



device is tilted with respect to the axis of the reflector by a certain angle in accordance with the shift of the new center of radiation from the focus.

The beam can thus be rocked within the required solid angle by electrically changing the parameters of lens 3, comprised of matrix of waveguides 4, and with the help of the electrically controlled phase inverters in the waveguides.

Since only a small portion of the energy strikes each electrically controlled phase inverter because of the relatively large number of elements and the substantial distance between lens 3 and primary radiator 5, the proposed antenna device can transmit and receive high power levels. Furthremore, parallel feed ensures high efficiency even with relatively high losses in the phase inverters.

This system makes it possible to compensate for beam distortion during rocking. l. order to accomplish this, instead of simply turning the wavefront at the output of the lens, it is necessary to introduce additional changes in the phase along its aperture which would create distributions at its output such as to compensate for phase front distortions caused by aberrations.

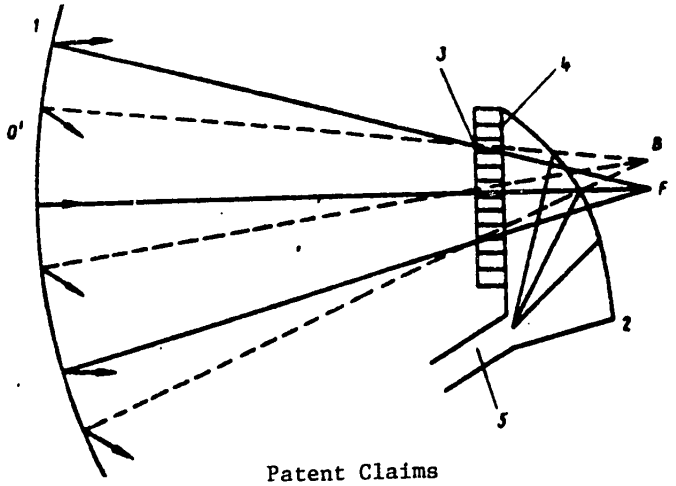


Patent Claims

1. An antenna device with electrical rocking of the beam in two planes comprised of a spherical reflector, radiator and lens, distinguished by the fact that in order to increase the transmitted power level with improved efficiency and reduced aberration distortions, a lens is placed between the reflector and its focus and shifted out of focus along the axis of the reflector, the coefficient of refraction of which is varied electrically under program control.

2. A device per paragraph 1 above, distinguished by the fact that the lens used consists of a matrix of waveguides containing electrically controlled phase inverters.

6900
CSO: 8144/0218-B



APPROVED FOR RELEASE: 2007/02/09: CIA-RDP82-00850R000500020034-7

APPROVED FOR RELEASE: 2007/02/09: CIA-RDP82-00850R000500020034-7



CERTAIN ASPECTS OF COMPUTER HARD AND SOFT WARE: CONTROL, AUTOMATION, TELEMECHANICS, TELEMETERING, MACHINE DESIGNING AND PLANNING

UDC 681.3.016:669

# MAGNETIC BUBBLE DATA STORAGE AND PROCESSING DEVICES

Moscow IZMERENIYA, KONTROL', AVTOMATIZATSIYA in Russian No 4 (38), 1981 pp 18-36

[Article by M.A. Rozenblat, doctor of technical sciences]

[Text] Introduction

In 1960-1970 a new class of magnetic materials was discovered and created which possess special properties not characteristic of magnetic materials. The most important of these properties consist in the fact that in thin wafers (films) made of these materials and magnetized in a direction perpendicular to the plane of the wafer cylindrical magnetic domains [magnetic bubbles] can form, bounded by the upper and lower surfaces of the wafer (fig 1).* The region surrounding a bubble is magnetized in the opposite direction. These bubbles have high mobility, moving at a relatively high speed under the effect of an external (controlling) magnetic field directed in a certain manner. In this respect the behavior of bubbles is similar to the behavior of cylindrical permanent magnets floating on the surface of a fluid: If a thin magnetically soft wafer is presented to such a magnet then it will be attracted to the end of the wafer, magnetizing it. Under the influence of another permanent magnet or electromagnet a floating cylindrical permanent magnet will either be attracted to it or be repelled by it with a force, F , depending on whether they face one another with unlike or like poles. Mobile bubbles behave in precisely the same manner with the only difference that their motion is associated not with mass transfer, but with a change in the direction of magnetization of adjacent regions, which also explains the ability to produce high rates of motion for bubbles. The mutual repulsion of two closely positioned bubbles can be used for the purpose of implementing logic functions in bubble devices.

On the basis of mobile bubbles integrated large-capacity memories have been constructed in which the presence of a bubble corresponds to a binary 1 and its absence to a binary 0. In these memories, executed in the form of shift registers, the following basic operations with bubbles are usually implemented: entry of

*A magnetic domain is a region of spontaneous magnetization in a magnetic material distinguished by the fact that the magnetic moments of all atoms in this region are directed parallel to one another and behave as a single team. Each domain is magnetized to saturation in some direction [1].



APPROVED FOR RELEASE: 2007/02/09: CIA-RDP82-00850R000500020034-7

APPROVED FOR RELEASE: 2007/02/09: CIA-RDP82-00850R000500020034-7



data by the generation of a bubble; moving bubbles certain strictly fixed distances under the influence of a control (propagating) signal; retention of bubbles at certain strictly fixed positions when the power is cut off or propagating pulses cease; erasure of information by the annihilation of bubbles; formation of an electrical signal depending on the presence or absence of a bubble in a given position; switching the direction of motion of bubbles (switching the direction of information transfer); and splitting of a single bubble (branching of information).

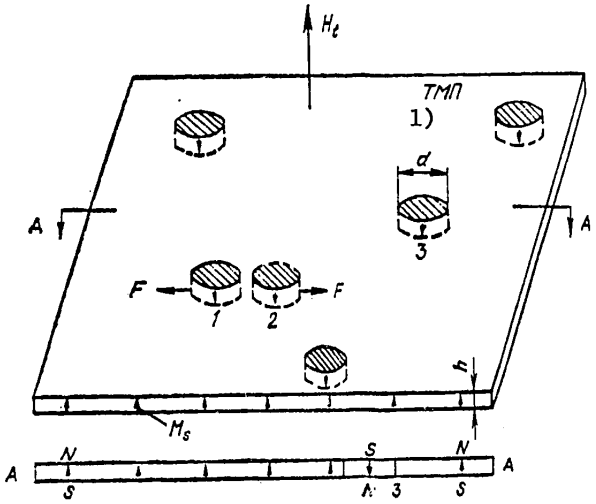


Figure 1. Magnetic Bubbles in Thin Magnetic Films with Uniaxial Anisotropy: TMP--thin magnetic film; h--thickness of TMP; $H_e$--external magnetic field; M--saturation magnetization of TMP; 1, 2, 3--magnetic bubbles; d--diameter of bubble

Key:
1. TMP

Developments under way in the area of bubble memories have been occasioned by the possibility of creating on the basis of mobile bubbles compact reliable and relatively inexpensive memories, necessary both for filling the gap with regard to access time which exists between modern semiconductor memories with random access (access time of 0.1 to 0.6 μs) and disk memories (access time of 10 to 100 ms) used in computers with a large memory capacity, and as a relatively inexpensive external (bulk) storage in microcomputers and microprocessor systems, installed on the same printed circuit board as the microprocessor and retaining information when the power is cut off (the power independence of bubble memories).

The main advantages of bubble memories as compared with semiconductor memories with random access (ZUPV's) is their lower unit cost (the cost per unit of information stored) and power independence, and as compared with disk storages--short



APPROVED FOR RELEASE: 2007/02/09: CIA-RDP82-00850R000500020034-7

APPROVED FOR RELEASE: 2007/02/09: CIA-RDP82-00850R000500020034-7



access time, compactness and high reliability. These advantages of bubble memories are caused both by the fact that their operating principle makes it possible to create simple small-sized memory cells and by the fact that the main component of a memory--the storage, formed by memory cells together with the bubble readin, switching, branching and readout elements--is fabricated by the same integrated technology as are semiconductor ZUPV's, but with a much smaller number and greater simplicity of technological operations (table 1). As a result, greater information capacity can be obtained for a bubble storage, reaching approximately $10^6$ to $10^7$ bits/cm$^2$. These advantages of bubble memories make their application especially promising in computing, data processing, testing and measuring and control systems where high reliability and low cost and small size and low power requirement are of first-rate importance.

Table 1. Comparison of Technology for Semiconductor and Bubble Integrated Circuits

| Characteristics of technology and parameters of integrated circuits | Type of integrated circuit | | |
|---|---|---|---|
| | Semiconductor | | Bubble |
| | Using bipolar transistors | Using MIS transistors | |
| Total number of technological operations | 130 | 38 | 8 |
| Number of basic technological operations | 32 | 22 | 4 |
| Number of high-temperature operations | 10 | 2 | None |
| Number of masking operations | 6 | 5 | 2(1) |
| Number of diffusion operations | 4 | 2-3 | None |
| Number of intracircuit connections | 6-10 | 2-10 | None |
| Memory capacity achieved, kbits | 4 | 64 | 1024 |

The major development work at the present time is aimed at constructing large-capacity memories on a single chip. However, on the basis of bubble logic circuits it is possible to create memories with distributed internal logic, associative memories, single-chip microprocessor systems based on bubbles, etc. The possibility of designing mini- and microcomputers in which all necessary processing, storage and data transfer functions are implemented with bubbles is discussed in [2, 3].

Bubble magnetic media materials possess good magnetooptical properties: a low coefficient of light absorption in the visible region of the spectrum and a strongly pronounced magnetooptic Faraday effect (rotation of the polarization plane of linearly polarized light when it passes through a magnetized body). These properties are possessed to a greater extent by orthoferrite wafers and bismuth-containing ferrite garnet films, for which the magnetooptic Faraday coefficient equals approximately $10^4$ deg/cm [4]. These properties of bubble materials make it possible to construct on their basis magnetooptic devices for the preparation of data, displays, light modulators, changeable transparencies for holographic recording, magnetically controlled diffraction gratings and two-dimensional light-deflecting devices. On the basis of bubble materials it is



APPROVED FOR RELEASE: 2007/02/09: CIA-RDP82-00850R000500020034-7

APPROVED FOR RELEASE: 2007/02/09: CIA-RDP82-00850R000500020034-7



also possible to create integrated heads for multichannel recording on magnetic tape with enhanced density and other devices in which the external fields of bubbles create an appropriate control effect.

The application of magnetic bubbles represents a new rapidly developing and promising field. The purpose of this study is a systematized presentation of the physical fundamentals and design principles of bubble devices (basically memories) and a discussion of their properties, development prospects and application.

Conditions for the Existence and Properties of Mobile Magnetic Bubbles

In any magnetic body, including in a thin magnetic film (TMP), a domain structure is established which is in conformity with the minimum value of its total free magnetic energy, $W$ . One condition for the existence of mobile bubbles in a TMP (and in wafers) is the presence in them of a single direction, common to the entire film, of easy magnetization, perpendicular to its surface and characterized by a sufficiently high value of the internal field of uniaxial anisotropy, $H_a$ . Under the influence of this field, even with the existence of external fields, whose strength should be much lower than $H_a$ , a TMP is magnetized only perpendicularly to its surface, i.e., along the axis (direction) of easy magnetization (OLN), which corresponds to a zero value of the energy of magnetic anisotropy, $W_a$ . The strength of $H_a$ is numerically equal to the value of the strength of the field which must be applied perpendicularly to the OLN of the film in order to turn the direction of magnetization 90 degrees. In a film evenly magnetized along the OLN there is an internal demagnetizing field, $H_r = -M_s$ , where $M_s$ is the film's saturation magnetization. The condition $H_a > (H_r)$ [as published] must be fulfilled for bubble devices, since otherwise self-generation of a bubble is possible under the influence of field $H_r$ . The ratio $Q = H_a/|H_r| = H_a/M_s$ is called the figure of merit of a bubble medium material. It is desirable that $Q \geq 2$ . For orthoferrites $Q \gg 1$ and not infrequently is greater than 100, and for ferrite garnet films usually $Q = 2$ to $5$ .

In the absence of an external magnetic field, strip domains, illustrated in fig 2, where the black and white strips correspond to opposite directions of magnetization, form in a bubble medium material under the influence of the internal demagnetizing field. Here the mean magnetization of the wafer practically equals zero. In view of the fact that the diameter, $d$ , of a bubble depends on the strength, $H_e$ , of the external (homogeneous) magnetic field, a bubble medium material is often characterized by the width, $b_p$ , of strip domains with $H_e = 0$ .

Each domain is bounded in the body of the wafer by a cylindrical boundary (wall) having a finite width of $\Delta \approx 0.1$ to $0.5$ $\mu$ . Within the limits of a domain boundary a gradual transition is made from one direction of magnetization to another, corresponding to the next domain. This transition can be of various natures, which substantially influences the dynamic properties of bubbles. So-called Néel boundaries exist in which the direction of magnetization rotates around the axis perpendicular to the plane of the wafer, and Bloch boundaries in which the change in magnetization between neighboring domains takes place by means of gradual rotation of the direction of magnetization around an axis situated parallel to the surface of the wafer and perpendicular to the walls of the boundary. Some combination of Néel and Bloch boundaries is often observed in bubbles.



APPROVED FOR RELEASE: 2007/02/09: CIA-RDP82-00850R000500020034-7

APPROVED FOR RELEASE: 2007/02/09: CIA-RDP82-00850R000500020034-7



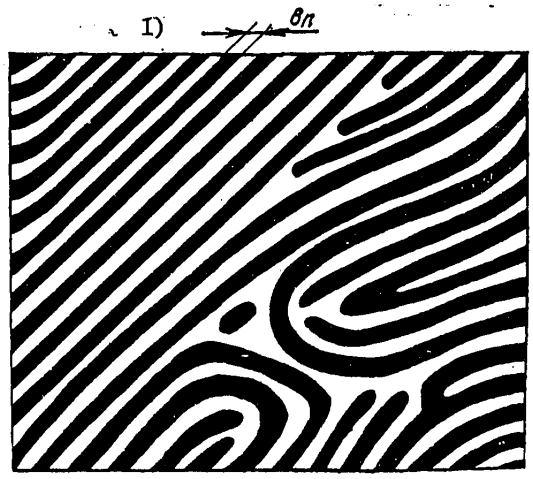


Figure 2. Strip Domains in the Absence of an External Magnetic Field

Key:

1. $b_p$

Assuming that $W_a = 0$ (magnetization of the bubble is parallel to the axis of easy magnetization (OLN)), for the free energy of an isolated bubble under the influence of field $H_e$ directed along the OLN counter to the magnetization of the bubble, we get $W = W_{st} + W_{gr} + W_e$, where $W_{st}$ is the energy caused by the internal field of the bubble, $W_{gr}$ is the energy of a domain boundary and $W_e$ is the energy of the bubble in external field $H_e$. Energy $W_{st}$ tends to expand the bubble and $W_{gr}$ and $W_e$ to compress it. In a certain range of values of $H_e$ an equilibrium state is established ($\partial W/\partial d = 0$), characterized by a certain value of the diameter of the bubble, $d = f(H_e)$. The value of $d$ also depends on the thickness, $h$, of the bubble medium material and on its physical properties [4, 5, 6, 7, 8, 9], which can be characterized by parameter $\ell_0$, called the characteristic length of the material:

$$\ell_0 = \sigma_{gr}/\mu_0 M_s^2,$$

where $\sigma_{gr}$ is the specific energy of the domain boundary in $J/m^2$ and $\mu_0 = 4\pi \cdot 10^{-7}$ H/m is the magnetic constant.

For bubble materials $h$ is usually chosen to equal (5 to 10)$\ell_0$, whereby the mean diameter of the bubble equals $d_{sr} = 0.5(d_k + d_p) \approx 10\ell_0$, where $d_k$ is the minimum diameter of a stable bubble with $H_e = H_{max}$ and $d_p$ is the maximum diameter of a stable bubble with $H_e = H_{min}$ ($d_p < b_p$). With $H_e > H_{max}$ annihilation of the bubble takes place, and with $H_e < H_{min}$ the bubble is transformed





APPROVED FOR RELEASE: 2007/02/09: CIA-RDP82-00850R000500020034-7

APPROVED FOR RELEASE: 2007/02/09: CIA-RDP82-00850R000500020034-7



into a strip domain (fig 3). Therefore, the condition for stable operation of a bubble device is $H_{min} < H_e < H_{max}$. Ratios $d_p/d_k$ and $H_{max}/H_{min}$ depend on the ratio $h/\ell_0$. With $h/\ell_0 \leq 5$, $d_p/d_k = 3.5$ and $H_{max}/H_{min} \approx 1.6$. The required value of $d_{sr}$, determined by the prescribed information storage density, is achieved by selectin materials with values of $\sigma_{gr}$ and $M_s$ making it possible to obtain $\ell_0 \approx 0.1 d_{sr}$, whereby $\sigma_{gr}$ depends on the type of domain boundary.

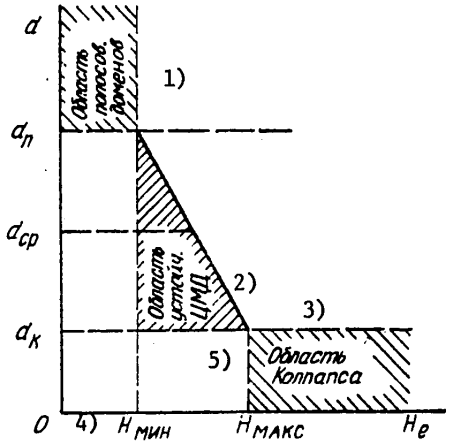


Figure 3. Dependence of Diameter of a Bubble on Strength of the External Magnetic Field

Key:
1. Strip domain region
2. Stable bubble region
3. Collapse region
4. $H_{min}$
5. $H_{max}$

The following equation is true:

$$d = (d_p H_{max} - d_k H_{min})/(H_{max} - H_{min}) - (d_p - d_k)H_e/(H_{max} - H_{min}),$$

$H_{min} < H_e < H_{max}$. With $H_e = 0.5\,(H_{min} + H_{max}) = H_{sr}$ [mean], $d = d_{sr}$.

Let $x$ equal the coordinate of the center of the bubble along a certain direction in the plane of the bubble medium material. If the components of energy $W$ of the bubble are functions of $x$, then the bubble is influenced by the force

$$F_x + \frac{dW}{dx} = \frac{dW_{en}}{dx} + \frac{dW_{ep}}{dx} + \frac{dW_e}{dx},$$



APPROVED FOR RELEASE: 2007/02/09: CIA-RDP82-00850R000500020034-7

APPROVED FOR RELEASE: 2007/02/09: CIA-RDP82-00850R000500020034-7



which causes displacement of the bubble if it exceeds a certain threshold value of $F_0$, corresponding to the coercive force, $H_c$, of the bubble medium material (it is assumed that the values of individual derivatives are constant within the limits of the area occupied by the bubble). Then from this expression it is possible to find the velocity, V, of the bubble along direction x [10]:

$$V = \frac{\mu_{rp}}{2}(a_1 \Delta h - a_2 \Delta H_e + a_3 \Delta M_s - a_4 \times$$
$$\times \Delta\sigma_{rp} - \frac{8}{\pi} H_c \operatorname{sign} V),$$

where $\mu_{gr}$ is the mobility of the domain boundary; $\Delta h$, $\Delta H_e$, $\Delta M_s$ and $\Delta\sigma_{gr}$ represent changes in the respective quantities along a distance of one bubble diameter in direction x; and $a_1$, $a_2$, $a_3$ and $a_4$ are positive coefficients.

$$\Delta h = d\frac{\partial h}{\partial x} = d \operatorname{grad} h(x),$$
$$\Delta H_e = d \operatorname{grad} H_e(x), \text{ etc.}$$

It is obvious from this expression that motion of the bubble can be accomplished by creating a gradient in the thickness of the wafer, external field, magnetization or domain boundary energy in the required direction. By the creation of a specific distribution of the thickness, magnetization or external field gradient it is possible to produce preferred motion "paths" or steady positions of the bubble, which makes it possible, in particular, to reduce the influence of random fields (interference). Other conditions being equal, the bubble will move in the direction of the thicker section of the TMP (wafer), of the section with the higher value of $M_s$, in the direction of the lower value of $H_e$ ($\Delta H_e < 0$), etc. By utilizing, for example, the dependence of $M_s$ on temperature, it is possible to control the motion of a bubble by means of a laser beam which causes local heating of the wafer. In particular, if $M_s$ increases with the temperature ($\Delta M_s > 0$) and it is possible to disregard the influence of a change in $\sigma_{gr}$, then the bubble will follow the motion of the laser beam.

In the majority of bubble devices control of the bubble's motion is accomplished by means of local changes in $H_e$ with h = const, $M_s$ = const and $\sigma_{gr}$ = const. In this case the absolute value of the velocity of the bubble equals

$$V = \frac{\mu_{rp}}{2}(\Delta H - \frac{8}{\pi} H_c) = \mu(\Delta H - H_0), \quad \Delta H > H_0,$$

where $\mu$ is the mobility of the bubble, $\Delta H$ is the absolute value of the difference of components, normal to the surface of the film, of the strength of the external (local) magnetic field at the front and rear boundaries of the bubble, determined in relation to the direction of its motion, and $H_0$ is the threshold field caused by the coercivity, $H_c$, of the bubble medium material. Equations $\mu = \mu_{gr}/2$ and $H_0 = 8H_c/\pi$ are of an approximate nature.



APPROVED FOR RELEASE: 2007/02/09: CIA-RDP82-00850R000500020034-7

APPROVED FOR RELEASE: 2007/02/09: CIA-RDP82-00850R000500020034-7



A specific relationship exists between the dynamic and static parameters of bubble materials [5, 6, 7, 8, 9]:

$$\mu_{rp} = \frac{4\gamma^2 A}{\lambda} \frac{M_s}{\sigma_{rp}},$$

where $\gamma$ is the gyromagnetic ratio, equal to $2.22 \cdot 10^5$ (M/K) for electron spins; $\lambda$ is the Landau-Lifshits damping parameter, characterizing the influence of viscous drag and having dimensionality of the frequency; and $A = \sigma_{gr}^2 / 8 H_a M_s$ is a constant characterizing the exchange energy of the material.

Obviously,

$$\mu_{rp} = \frac{\gamma^2 \sigma_{rp}}{2\lambda H_a} = \frac{\gamma^2}{\lambda} \left( \frac{A}{2\pi Q} \right)^{1/2},$$

i.e., other conditions being equal, an increase in the figure of merit, Q , of a bubble material results in a reduction in $\mu_{gr}$ and, consequently, in $\mu$ . An effective method of increasing $\mu$ (the speed of response of bubble devices) is the creation of materials with heightened values of $\gamma$ and/or low values of $\lambda$ .

With an increase in $\Delta H$ there is a reduction in $\mu$ . In addition, the velocity of a bubble is limited at the higher end by the maximum value of $V_{pr}$ . The value of $\mu$ also depends on the structure of a bubble boundary. Generally, the boundary of a bubble consists of sections with a Bloch boundary structure separated by sections with a Néel structure and called vertical Bloch lines (VBL's). The number, n , of Néel sections or VBL's is always even and can be positive or negative. In the particular case when the structure of a bubble boundary conforms everywhere to a Bloch boundary, $n = 0$ . The value of n is positive in those cases when in moving along the direction of magnetization of Bloch sections of the boundaries of a bubble Néel sections are encountered in which the direction of magnetization corresponds to the general direction of the transfer of magnetic flux from the bubble into the surrounding region. Otherwise $n < 0$ . The state of a bubble boundary is characterized by parameter $S = 1 + n/2$ .

The expression presented above for velocity V corresponds to $S = 0$ . It is important that with $S = 0$ the direction of motion of the bubble coincides with the direction of the maximum value of grad $H_e$ . With an increase in the absolute value of S , $\mu$ is reduced and angle $\phi$ (angle of drift) increases, composed of the direction of motion of the bubble and the direction of grad $H_e$ [9]:

$$\varphi = \arcsin \frac{8 S V}{\gamma d \Delta H_a}.$$

The static properties of the bubble change simultaneously: $H_{max}$ is increased and $d_k$ is reduced. The absolute value of S increases in the process of motion of



APPROVED FOR RELEASE: 2007/02/09: CIA-RDP82-00850R000500020034-7

APPROVED FOR RELEASE: 2007/02/09: CIA-RDP82-00850R000500020034-7



the bubble and dynamic restructuring of the domain boundary takes place. Bubbles with high absolute values of $S$ are called hard or inflexible.

Among the methods eliminating the formation of hard bubbles, the most widespread is the method of forming on the surface of the bubble medium material a thin (less than one micron) layer with anisotropy of the "easy plane" type. This method is distinguished by the fact that any direction in the plane of this layer is a direction of easy magnetization. As a result, the boundary of the bubble can receive only a definite structure corresponding to $S = 0$ or $S = 1$. In bubble media fabricated in the form of thin ferrite garnet wafers with a negative magnetostriction coefficient, an "easy plane" is most often formed by the method of ion introduction (ion implantation), e.g., by the implantation of hydrogen or neon ions, which causes compression of the surface layer.

With $S = 1$, the change in mobility of a bubble as compared with the mobility of a bubble with $S = 0$ is inconsiderable, although the angle of drift, $\phi$, can be quite noticeable. This phenomenon is utilized in certain bubble memories which have been developed for increasing the density of the storage of information, which is written in the form of a definite structure for bubble boundaries, e.g., a structure with $S = 0$ corresponds to a binary 1 and a structure with $S = 1$ to binary 0 [9, 11].

Bubble Medium Materials

Orthoferrites, representing antiferromagnetics with a chemical composition of $RFeO_3$, where $R$ is any rare earth element or yttrium or a combination of two elements ($R = R'_x R''_{1-x}$), were first used as bubble media [4, 6]. Orthoferrites have high values of their figure of merit, $Q$, bubble mobility and the magneto-optic Faraday coefficient. However, the mean diameter of bubbles in them is relatively great and for materials with a single rare earth component it equals 80 to 100 $\mu$. Only for mixed orthoferrites is it possible to obtain $d_{sr} = 20$ to 25 $\mu$, but with considerable worsening of the temperature stability of the material's parameters. Therefore, orthoferrites are used primarily in various magnetooptic devices where a small diameter of bubbles is not required.

Of other materials in which stable mobile bubbles can exist, in bubble memories, only ferrite garnet thin films are widely used, grown on a nonmagnetic garnet substrate (usually of gadolinium gallium garnet, $Gd_3Ga_5O_{15}$) by the liquid-phase epitaxy method [4, 9, 12, 13, 14, 15, 16, 17]. At the present time many compositions of epitaxial ferrite garnet films have found an application, having the formula $(R_1R_2...)_3(FeM)_5O_{12}$, where $R$ is a rare earth element or yttrium, $M$ is a metal (usually aluminum or gallium, sometimes Ge, Si or Mn, partly replacing Fe). By changing the composition of the film it is possible to change over a wide range the values of $M_s$, $H_a$, $Q$, $\ell_0$ ($d_{sr}$), $\mu$ and their dependence on the temperature. Uniaxial anisotropy with the OLN perpendicular to the surface of the film in ferrite garnet films is usually the result of great magnetocrystalline or exchange anisotropy induced in the process of growing the film. In certain cases it can also be the result of mismatching of the lattice constants of the substrate and film, which causes great elastic stresses in the film and results because of magnetostriction in the formation of the required $H_a$ field.



APPROVED FOR RELEASE: 2007/02/09: CIA-RDP82-00850R000500020034-7

APPROVED FOR RELEASE: 2007/02/09: CIA-RDP82-00850R000500020034-7



The key parameters of certain ferrite garnet epitaxial films making it possible to obtain values of $d_{sr}$ of 0.5 to 10 μ are given in table 2 [13, 14, 15, 16, 17]. The parameters of a number of other films and their temperature characteristics, which are of first-rate importance, are also presented in [4, 9, 12].

Table 2. Key Parameters of Some Ferrite Garnet Thin Magnetic Films

| Состав пленки 1) | $l_0$, мкм 2) | h, мкм | Q | $H_a$, А/см | $H_{макс}$, А/см 3) | μ, см²/А·с 4) | $V_{макс}$, м/с 5) |
|---|---|---|---|---|---|---|---|
| $Gd_{2,2}\ Lu_{0,8}\ Fe_{4,3}\ Mn_{0,4}\ Al_{0,3}\ O_{12}$ | 0,92 | 2,32 | 25 | 3370 | 28,5 | 1880 | 450 |
| $Eu_{2,7}\ Lu_{0,3}\ Fe_{4,3}\ Al_{0,7}\ O_{12}$ | 0,62 | 2,54 | 12 | 2380 | 66 | 440 | 300 |
| $Eu_{2,7}\ Lu_{0,3}\ Fe_{4,2}\ Mn_{0,1}\ Al_{0,7}\ O_{12}$ | 0,32 | 2,66 | 22 | 4400 | 95 | 350 | 100 |
| $Eu_{1,45}\ Y_{0,45}\ Ca_{1,1}\ Fe_{3,9}\ Si_{0,6}\ Ge_{0,5}\ O_{12}$ | 0,6 | 4 | 7,5 | 1200 | 65 | 875 | 300 |
| $Y_{1,2}\ Lu_{0,5}\ Sm_{0,4}\ Ca_{0,9}\ Fe_{4,1}\ Ge_{0,9}\ O_{12}$ | 0,35 | — | 5,3 | 1390 | — | 325 | — |
| $Y_1\ Lu_{0,7}\ Sm_{0,5}\ Ca_{0,8}\ Fe_{4,2}\ Ge_{0,8}\ O_{12}$ | 0,19 | — | 3,5 | 1400 | 200 | 377 | — |
| $La_{0,6}\ Lu_{2,1}\ Sm_{0,3}\ Fe_{4,1}\ Ga_{0,9}\ O_{12}$ | 0,14 | — | 2,6 | 1040 | 175 | 630 | — |
| $La_{0,2}\ Lu_{1,6}\ Sm_{0,6}\ Ca_{0,6}\ Fe_{4,4}\ Ge_{0,6}\ O_{12}$ | 0,12 | — | 2,9 | 1800 | 320 | 380 | — |
| $Eu_1\ Tm_2\ Fe_{4,3}\ Ga_{0,7}\ O_{12}$ | 0,2 | 1,66 | 10 | 3500 | — | 230 | — |
| $Eu_{0,8}\ Tm_{2,2}\ Fe_{4,5}\ Ga_{0,5}\ O_{12}$ | 0,[illegible]3 | 1,0 | 3 | 1690 | — | 1250 | — |
| $Eu_{1,7}\ Yb_{1,3}\ Fe_5\ O_{12}$ | 0,[illegible] | 2,8 | 2,1 | 2440 | — | 500 | — |

Key:
1. Composition of film
2. h, μ
3. $H_{max}$, A/cm
4. μ, $cm^2/A \cdot s$
5. $V_{max}$, m/s

Studies are being conducted on the use in bubble devices of two-layer and even three-layer films with layers differing in chemical composition and physical properties [4, 9]. Two-layer films can be used for eliminating the formation of hard bubbles, for producing stable bubbles without an external field, $H_e$, or for constructing bubble devices based on the use of interaction of the domains of two different layers.

Basic Elements of Magnetic Bubble Integrated Circuits (IC's)

To the basic elements of integrated circuits employing magnetic bubbles belong elements making possible the generation of bubbles, the propagation of bubbles along shift registers, fixing of the position of bubbles in the information storage mode (without propagation), changing the direction of motion of bubbles, the exchange of bubbles between two shift registers, the multiplication (splitting) of bubbles, the readout of information, the erasure of bubbles and logic operations. The major portion of the area of integrated circuits employing magnetic bubbles is occupied by propagation elements, forming shift registers. Since all functional elements must be fabricated in a single technological process with a minimum number of lithographing and registration operations, the choice of design principle and



APPROVED FOR RELEASE: 2007/02/09: CIA-RDP82-00850R000500020034-7

APPROVED FOR RELEASE: 2007/02/09: CIA-RDP82-00850R000500020034-7



type of propagation elements to a considerable extent determines the choice of all remaining functional elements of integrated circuits utilizing magnetic bubbles, which must match propagation elements in the technological respect and with respect to regions of stable operation (OUR's).

Two main classes of bubble device shift registers exist. The first includes integrated circuits in which local changes of the magnetic fields causing the shifting of bubbles are accomplished by an external magnetic field which is alternating in terms of direction and is common to all integrated circuits; under the influence of this field magnetization of thin magnetically soft (permalloy) elements located on the surface of the bubble film or of structures implanted in the surface layer of the film with anisotropy of the "easy plane" type takes place. A characteristic feature of integrated circuits of this class, which we will call bubble integrated circuits with common field control, is the absence of conduction lines in the integrated circuits, used for propagating the bubbles. To the second class belong magnetic bubble integrated circuits with local current control, in which local changes of the propagating magnetic field are accomplished by means of electric current flowing through conductors arranged in a certain manner on the surface of the bubble film. Bubble integrated circuits of the first class with permalloy control elements have been preferred for use at the present time.

A circuit for controlling the motion of bubbles by means of magnetizing a permalloy core is presented in fig 4. The bubble medium, 1, is covered with a dielectric, 2 (usually $SiO_2$ with a thickness, $h_n$, of 0.4 to 0.5 μ), on top of which is placed a rectangular core, 3, made of a permalloy thin magnetic film (core thickness of 0.3 to 0.5 μ). An external magnetic field, $H_e$, makes possible the existence of stable bubbles (cf. fig 3). Possible initial positions of bubbles are designated by the numbers 4, 5 and 6. The external control field, $H_{upr}$, directed along the longitudinal axis of the core, 3, from right to left, is turned on the instant the bubble is at position 4 (fig 4b). The core is magnetized and at its left end is formed a north pole, which attracts the bubble, causing it to move from position 4 to position 7, corresponding to the minimum free energy of the bubble in the total external field. If the bubble is at position 5, then it is repelled by the right south pole of the core and also goes to position 7. A bubble at position 6 is repelled by the core and moves to the right.

The force acting on the bubble and its stable position (UP) under the permalloy core are determined by the distribution of component $H_z$, normal to the surface of the film, of the core's external field, averaged for the thickness, h, of the bubble medium film. The distribution of this component along the longitudinal axis (x) for a value of $y = 0$ is shown in fig 4c for the case when it is possible to disregard the influence of the bubble on magnetization of the core. The bubble's stable position (UP) corresponds to the region of minimum values of $H_z$; this region is usually called a magnetostatic well (MSYa). The problem of enabling a specific path of movement of the bubble reduces essentially to enabling the corresponding law of displacement of the MSYa, which carries along the bubble in it.

With $H_{upr} = 0$, the permalloy core can be magnetized, although to a lesser degree, under the influence of a bubble located near it. Here for a bubble at position 4 or 7 with $H_{upr} = 0$, position 7 is stable as previously, corresponding to the minimum of free energy. For a bubble at position 5 or 6, the nearest stable



APPROVED FOR RELEASE: 2007/02/09: CIA-RDP82-00850R000500020034-7

APPROVED FOR RELEASE: 2007/02/09: CIA-RDP82-00850R000500020034-7



position is the right edge, 8, of the core (the center of the bubble is set beneath this edge). Thus, the same permalloy elements can be used not only for controlling the motion of bubbles, but also for fixing the position of bubbles when the power is cut off ($H_{upr} = 0$).

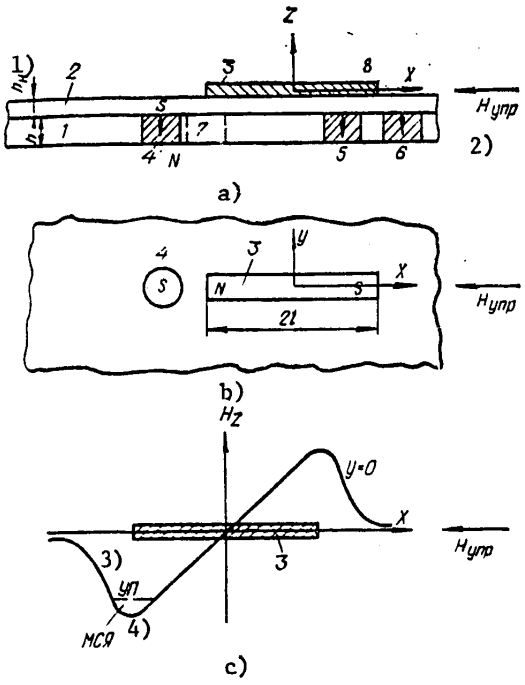


Figure 4. Diagram for Controlling the Motion of a Bubble by Means of Magnetizing a Permalloy Core

Key:
1. $h_n$
2. $H_{upr}$ [control]
3. UP [stable position]
4. MSYa [magnetostatic well]

Field $H_z$, acting on a bubble and the magnetostatic well, is directed counter to $H_e$ and results in an increase in the diameter of the bubble. Therefore, in bubble devices with permalloy control elements $H_e$ is selected to be greater than $H_{sr\ [mean]}$ (cf, fig 3) for the purpose of enabling a broad region of stable operation (OUR). As a consequence, the annihilation of bubbles is sometimes observed when $H_{upr}$ is cut off and there is a corresponding reduction in the depth of the magnetostatic well. This is often eliminated by orienting the permanent magnets creating field $H_e$ so that a small field component is formed in the plane of the thin magnetic film of the bubble medium. This component, magnetizing permalloy cores with $H_{upr} = 0$, creates magnetostatic wells which reliably retain bubbles at specific positions.





APPROVED FOR RELEASE: 2007/02/09: CIA-RDP82-00850R000500020034-7

APPROVED FOR RELEASE: 2007/02/09: CIA-RDP82-00850R000500020034-7



Let us discuss the principles of the design of bubble shift registers (SR's) based on permalloy control elements having the form of a T and I (fig 5). Here four directions are distinguished (1, 2, 3, 4), of the control field, $H_{upr}$, clockwise, and on the permalloy elements by these same numbers are indicated positions at which with these directions of $H_{upr}$ positive poles are formed. With the first position of $H_{upr}$ let a bubble be at position 1 of an element I. When $H_{upr}$ is turned 90 degrees (to direction 2) a north pole forms in position 2 of this element and the bubble goes into this position. One more turn of $H_{upr}$ by 90 degrees moves the bubble to position 3 of element I. With the next turn of $H_{upr}$ by 90 degrees (direction 4) a north pole forms at lower end 4 of core A and the bubble goes into this position. When $H_{upr}$ is turned 360 degrees the bubble occupies position 1 under element II, i.e., is shifted by a single cycle by a linear extent of $\lambda$. T-shaped elements I, II, III, V, VI and VII and cores A and b located between them serve the purpose of shifting the bubble linearly along the SR and elements 0 and IV of changing the direction of motion of the bubble. With a change in the direction of rotation of $H_{upr}$ the direction of motion of the bubble is changed to the opposite, which is the result of the symmetry of the shifting elements.

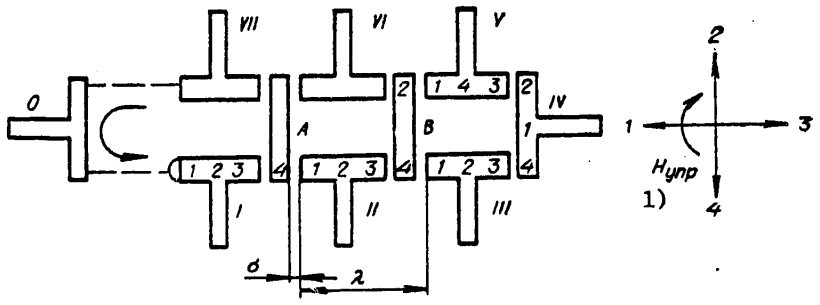


Figure 5. Magnetic Bubble Shift Register Utilizing T-I Permalloy Elements

Key:
1. $H_{upr}$

In recent times preference has been given to shifting elements with a single gap with a shift cycle of $\lambda$, which are less critical with regard to the width of the gap, $\delta$, between neighboring elements and make it possible to increase the ratio $\delta/d_{sr}$ and to reduce the ratio $\lambda/d_{sr}$ and the mutual influence of bubbles moving along adjacent tracks (SD's) and to expand the integrated circuit's OUR. The use of these elements increases the information density of bubble integrated circuits without increasing the resolution of the photolithography equipment used. Some of the most widespread single-gap permalloy shifting elements, which have many modifications, are presented in fig 6 (a and b--asymmetric chevrons; c and d--asymmetric subdisks; e--a "tapir"; f and g--symmetric chevrons; and h--a symmetric Y element) [18, 19, 20, 21, 22, 23]. In the first five types of elements bubbles can be moved only from left to right with rotation of the control field, $H_{upr}$, clockwise (fig 6i) and in the last three in any direction depending on the



APPROVED FOR RELEASE: 2007/02/09: CIA-RDP82-00850R000500020034-7

APPROVED FOR RELEASE: 2007/02/09: CIA-RDP82-00850R000500020034-7



direction of rotation of $H_{upr}$ (fig 6j). The wider OUR in asymmetric elements (a to e) is caused by the fact that the increased mass (area) of the permalloy at the end of the element "receiving" the bubble facilitates the bubble's crossing the gap between two neighboring elements. Symmetric elements g and h have a wider OUR than simplest chevron f, which is used primarily in bubble expanders included in magnetoresistive readout devices, passive magnetic bubble splitters and some logic elements.

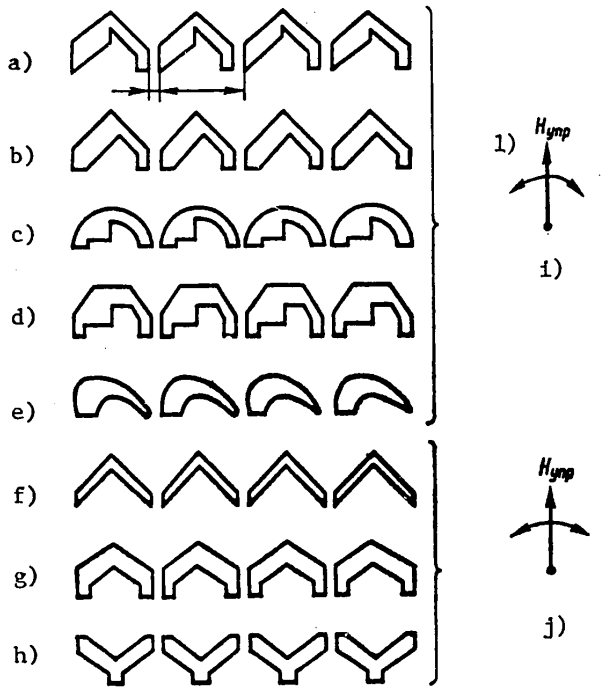


Figure 6. Single-Gap Permalloy Shifting Elements

Key:
1. $H_{upr}$

Displacement field $H_e$ is usually created by two flat permanent magnets (1 and 2 in fig 7a) and field $H_{upr}$ by current $i_x$ and $i_y$ flowing through two orthogonally positioned coils X and Y, inside of which there are one or more magnetic bubble integrated circuits. The coils with the integrated circuits and the permanent magnets are placed in a single case, which serves simultaneously as a magnetic shield protecting the bubble module from the influence of external magnetic fields with strength up to 4000 A/m [24]. With identical permanent coils X and Y current $i_x = I_m \sin \omega t$ and $i_y = I_m \cos \omega t$ flowing through them create field $H_{upr}$, which rotates in the plane of the bubble integrated circuit with an



APPROVED FOR RELEASE: 2007/02/09: CIA-RDP82-00850R000500020034-7

APPROVED FOR RELEASE: 2007/02/09: CIA-RDP82-00850R000500020034-7



angular velocity of $\omega$ and a constant amplitude. However, the amplitude of $H_{upr}$ can also not be constant. Therefore, control current $i_x$ and $i_y$ of triangular form (fig 7b) are widely used, which are more simple to form, especially when a bubble memory operates in the start-stop mode [25]. In this case the vector of $H_{upr}$ in a polar system of coordinates describes a rectangle with corners situated on axes x and y (fig 7c), where axis x is in line with the direction of motion of the bubble. The change from the bubble shift mode to the storage mode is carried out at moment $\omega t = 2n\pi$ ($n = 1, 2, \ldots$), where $i_y = 0$, by changing current $i_x$ from $-I_m$ to zero (current $i_y$ thereby must remain equal to zero). Motion of the bubble is restored by changing $i_x$ from zero to its maximum negative value with $i_y = 0$ and by subsequently changing $i_x$ and $i_y$ according to fig 7b.

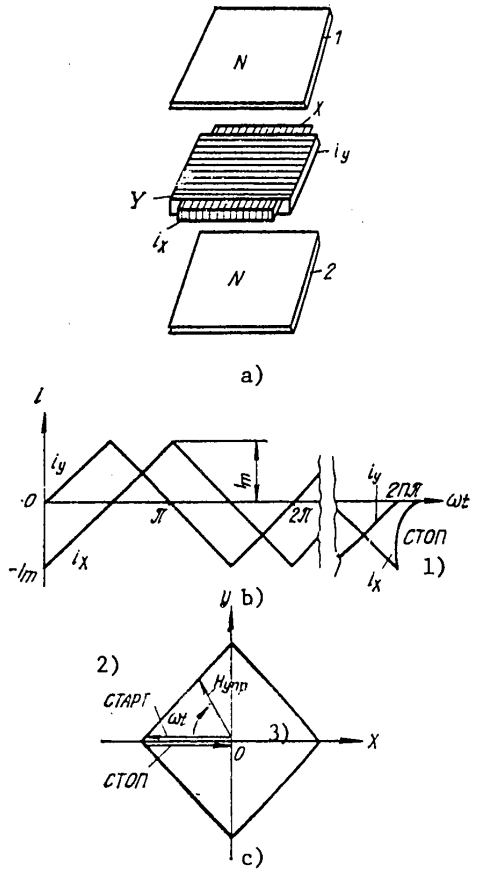


Figure 7. Diagram of Formation of Displacement and Control Fields for a Magnetic Bubble Module

[Key on following page]



APPROVED FOR RELEASE: 2007/02/09: CIA-RDP82-00850R000500020034-7

APPROVED FOR RELEASE: 2007/02/09: CIA-RDP82-00850R000500020034-7



Key:
1. Stop
2. Start
3. $H_{upr}$

Three main principles are known for designing magnetic bubble generators (G's): by means of a current loop, creating a local magnetic field directed counter to $H_e$ and sufficient for the origin of a bubble (fig 8a and b); by means of division by means of a current pulse, $i_g$, of a bubble self-originating beneath a massive permalloy element with a large leakage field (fig 8c); by using a massive permalloy element as the units generator (G1) and erasing by means of current $i_A$ the bubble formed, if it is required to write a 0 (fig 8d).

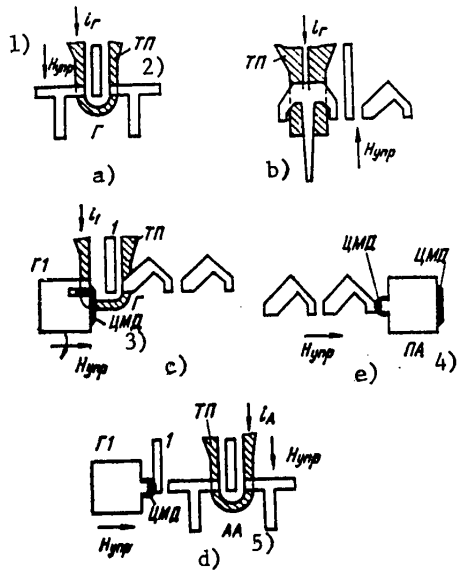


Figure 8. Diagram of Functional Elements of Bubble Integrated Circuits

Key:
1. $H_{upr}$
2. TP [current loop]
3. Bubble
4. PA [passive annihilator]
5. AA [active annihilator]

The erasure device, also called an annihilator, can be designed similarly to the current generator (fig 8a), but with the reverse direction of current $i_A$ for the purpose of creating a total field greater than the collapse field, $H_{max}$. In addition to such an "active" annihilator (AA), passive annihilators (PA's) are used, designed similarly to passive "1" generators (fig 8d). Bubbles approaching a "massive" permalloy element are captured by it and are not transmitted further. Current loops are formed by thin-film lines usually made of an Al-Cu alloy. Bubble generators for other shifting elements are designed similarly (cf. fig 6).



APPROVED FOR RELEASE: 2007/02/09: CIA-RDP82-00850R000500020034-7

APPROVED FOR RELEASE: 2007/02/09: CIA-RDP82-00850R000500020034-7



Current pulses $i_g$ and $i_A$ must be phased in a specific manner in relation to $H_{upr}$, as is conventionally illustrated in fig 8, for the purpose of enabling the proper operation of G's and AA's. In a generator (fig 8c) the distance between element 1 and G1 is such that with $i_g = 0$ element 1 cannot capture a domain formed on the right face of G1 with the corresponding direction of $H_{upr}$. In the circuit given (fig 8d) such capture does take place and with the rotation of $H_{upr}$ a domain is stretched and then split, forming two magnetic bubbles, one of which continues moving around generator G1, and the other is directed toward the AA.

In essence generator G in fig 8c forms an active splitter or replicator (AR), and in the circuit in fig 8d, a passive bubble splitter (PR). These bubble splitters (replicators) are used in bubble integrated circuits for branching information for the purpose of readout without removing the bubble from the shift register (SR), which serves the purpose of the prolonged storage of information. Many variants of AR's exist, one of which is presented in fig 9 [22, 23, 26]. Here the AR serves the purpose of transferring information from SR-1 to SR-2 while storing the transferred information for the purpose of readout without removing the bubble. SR-1 is designed in such a manner that with a certain direction of $H_{upr}$ the bubble, traveling beneath it, is stretched along the entire element. If at this moment current pulse $i_r$ is supplied to the current loop (TP), then the bubble is divided into two parts which are mutually repelled. One of them continues to move through SR-1, and the second goes to SR-2. If current pulse $i_p$ is supplied to the point of stretching of the bubble along element 1, the bubble arriving at this element is conveyed to SR-2 without splitting. In this case we get a one-way switch (OP) for the direction of motion of the bubble (only from SR-1 to SR-2). Two-way switches (DP's) exist, making it possible to transfer a bubble both from SR-1 to SR-2 and from SR-2 to SR-1. The function performed is determined by the phase shift between the switching current, $i_p$, and the control field. With $i_p = 0$, bubbles are moved in step independently of one another through SR-1 and SR-2. In addition to these elements, according to the same principle are designed switches (KO's) for swapping bubbles between two shift registers and universal switches (KO-R's) which implement either the function of swapping bubbles or the function of splitting bubbles depending on the instant of the supply of and phase of the control current [22, 23, 26].

In fig 10 is presented a diagram of a passive bubble splitter (PR) designed with permalloy elements of the symmetric chevron type. Moving from left to right along element 1, the bubble is captured by elements 2 and 3, is stretched and is divided into two bubbles, which continue to move through channels I and II. If the direction of rotation of $H_{upr}$ is changed, then the bubbles will be moved through channels I and II from right to left. In this case elements 1, 2 and 3 form an OR circuit implementing a logical OR function with the entry of a bubble through one of the channels (the simultaneous entry of two bubbles can cause failure because of their mutual repulsion).

The readout of information, represented by the presence or absence of a bubble, can be accomplished by any circuits reacting to the magnetic field of a bubble or its alteration and based on utilization of the electromagnetic induction phenomenon, the magnetooptic effect, the magnetoresistive effect, the Hall effect, etc. Only the magnetoresistive effect has received practical application in modern bubble memories in view of the technological advantages: execution of the



APPROVED FOR RELEASE: 2007/02/09: CIA-RDP82-00850R000500020034-7

APPROVED FOR RELEASE: 2007/02/09: CIA-RDP82-00850R000500020034-7



magnetoresistive bubble sensor (detector) from the same permalloy thin magnetic film as the other functional elements of the integrated circuit in a single technological process. The level of the output signal of the sensor is $U_{sch} = I_d \Delta R_d = I_d k R_d$, where $I_d$ is the current of the sensor and $\Delta R_d$ is the change in the initial resistance of the sensor, $R_d$, under the effect of the magnetic field of the bubble read. The value of $I_d$ is limited to a value on the order of 5 to 10 mA, and coefficient $k$ is low (0.02 to 0.03). Therefore, for the purpose of raising $U_{sch}$ to the level required for reliable readout against a background of interference, increasing $R_d$ by increasing the length of the sensor is resorted to, whereby it is necessary at the same time to stretch the bubble read in order for the sensor to be completely under the influence of its field. The simplest variant of a readout unit (SU) consisting of a chevron domain expander (RD) and a sensor (MD) formed by a chain of series-connected permalloy elements is illustrated in fig 11. Behind the sensor usually comes a circuit which reduces the domain to normal dimensions, after which the bubble can be directed to any SR or annihilator (PA), if erasure is required after reading. Often a second compensating sensor is provided, positioned directly behind the first and connected together with it in a bridge circuit for the purpose of reducing noise caused by the field of $H_{upr}$. Not infrequently in RD's asymmetric chevrons of a special shape are used for the purpose of expanding its OUR, as well as other methods of connecting MD elements for the purpose of raising the level of the output signal [20, 22, 23]. In bubble devices with a nominal domain diameter of 2 to 3 μ the number of chevrons in the MD reaches 300 to 500, which makes it possible to produce a strip domain 1.5 mm long. This stretching of the bubble read is usually achieved in 15 to 30 cycles of the shifting field.

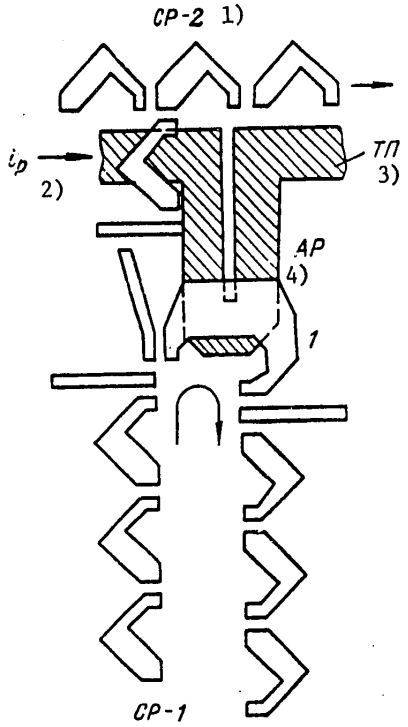


Figure 9. Diagram of Active Bubble Splitter

Key:
1. SR-2
2. $i_r$
3. Current loop
4. Active splitter





APPROVED FOR RELEASE: 2007/02/09: CIA-RDP82-00850R000500020034-7

APPROVED FOR RELEASE: 2007/02/09: CIA-RDP82-00850R000500020034-7



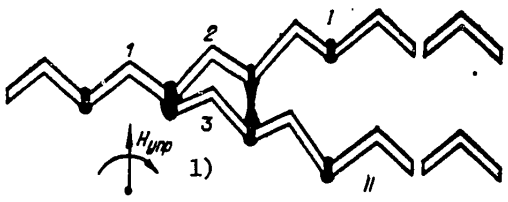


Figure 10. Diagram of Passive Bubble Splitter

Key:
1. $H_{upr}$

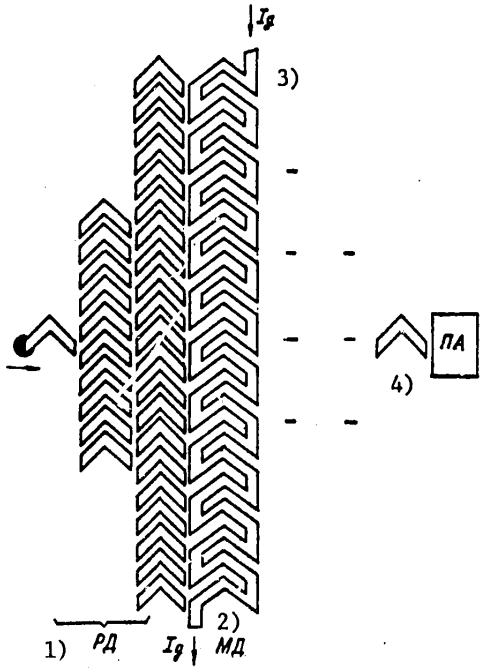


Figure 11. Diagram of Bubble Integrated Circuit Readout Unit

Key:
1. RD [domain expander]
2. MD [sensor]
3. $I_d$
4. PA [passive annihilator]



APPROVED FOR RELEASE: 2007/02/09: CIA-RDP82-00850R000500020034-7

APPROVED FOR RELEASE: 2007/02/09: CIA-RDP82-00850R000500020034-7



Structure of a Magnetic Module (Integrated Circuit) for a Bubble Memory

A bubble memory magnetic module is a functionally and structurally complete item consisting of one or more magnetic bubble integrated circuits and elements creating magnetic displacement and control fields (cf. fig 7a) and placed in a shared shielding case with the necessary electric terminals. The structure of a magnetic module is determined by the structure of the bubble integrated circuit, which depends on the purpose of the memory and on the principle used for controlling the magnetic bubble.

Two main classes of bubble memories exist. In memories of the first class the sequential single-channel and/or multichannel readin and readout of binary information are accomplished the same as when recording on moving magnetic tape. To the second class belong memories in which information is written and read in pages or blocks according to an address assigned for each page. The writing or reading of information (words) takes place sequentially within the limits of a page. The addresses of pages can be assigned in an arbitrary manner. Bubble memories of the second type make it possible to reduce substantially the time for accessing information, the minimization of which is one of the main objectives when using bubble memories as part of a computer.

A typical structural diagram of one memory bubble integrated circuit of the first class is presented in fig 12. The circuit works in the following manner. During readin, current pulses, $i_{zp\ [readin]}$, phased with current creating a rotating $H_{upr}$ field, enter the controlled bubble generator, G, so that when a 1 is written a bubble appears in the output of the G and does not when a 0 is written. The bubbles generated are moved under the influence of $H_{upr}$ in the direction of the merger point, S, and enter the shift register, SR. If N is the capacity of the SR and $n_{GS}$ is the number of cycles between G and point S, then $N + n_{GS}$ shift periods (rotations of $H_{upr}$) after the beginning of the entry the free SR is filled. Here the entry occurs only during the first N periods, and during the entry period the current in the active annihilator, AA, equals $i_A = 0$. The last written bit will be at point S, and part of the written information in register section SV. Often the entire capacity of the SR, N, is not used, but only the capacity, $N_r$, of the section of the SR from point S to the active splitter (replicator), AR. In this case after the completion of an entry (after $N_r + N_{GS}$ periods) the first bit entered will be found opposite the splitter, AR, and can proceed to be read out immediately, by supplying current pulses, $i_r$, to the AR in step with the shifting current. The bubble in the AR is split: One part is sent to the readout unit, Sch, and then to the passive annihilator, PA, and the second to point S for further storage in the SR. After kN periods, where k is a whole number, the information written in the SR assumes its initial arrangement. If it is necessary to erase or to replace information entered earlier, then when the bubble arrives at the position of AA an erase pulse, $i_A$, is supplied. It is possible to enter new information simultaneously, since the distance (number of cycles) from G and from AA to the merger point, S, is made identical.

The readout (access) time for the first bit, $t_1$, and the average time for reading out a random bit, $t_{sr}$, after the entry of $n_r$ bits equals:



APPROVED FOR RELEASE: 2007/02/09: CIA-RDP82-00850R000500020034-7

APPROVED FOR RELEASE: 2007/02/09: CIA-RDP82-00850R000500020034-7



$$t_1 = \frac{n_{p.cч}}{f}\ ;\ t_{cp} = \frac{2n_{p.cч} + N_p}{2f}\ .$$

where $n_{r.sch}$ is the number of cycles between the AR and detector, MD, of the readout unit (cf. fig 11) and $f$ is the operating frequency of the rotating field.

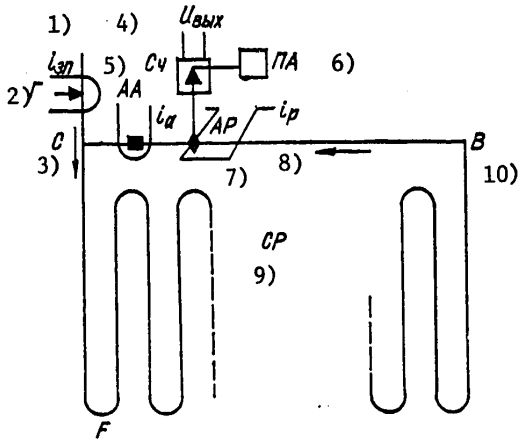


Figure 12. Structural Diagram of Bubble Integrated Circuit with One Shift Register

Key:

1. $i_{zp}$ [readin]
2. G
3. S
4. Output
5. Readout unit
6. Passive annihilator
7. Active splitter
8. $i_r$
9. Shift register
10. V

The number of electric terminals for a single integrated circuit equals $\ell_e = 8$ when using a single magnetoresistive sensor in the readout unit. When two MD's [magnetoresistive sensors] are used, $\ell_e = 9$ . The total number of terminals of a bubble module with a single integrated circuit, taking into account the terminals of the coils creating the control field, equals $L_e = \ell_e + 4$ . Up to eight integrated circuits are often placed in a single module for the purpose of reducing the cost of a memory. If recording and readout take place in them in parallel, as in a multitrack tape recorder, then the lines controlling the operation of the AA and R's can be connected in series, and one of the ends of all write and read lines can be connected to a common point. Then the minimum number of module terminals equals $L_{e.min} = 2n_{IC} + 9$ , where $n_{IC}$ is the number of integrated circuits in the module. But if independent writing or reading are required, then all AA's and AR's must have individual terminals, and then $L_{e.min} = 4n_{IC} + 5$ . The value of $L_{e.min}$ limits the maximum number of integrated circuits in a single module.



APPROVED FOR RELEASE: 2007/02/09: CIA-RDP82-00850R000500020034-7

APPROVED FOR RELEASE: 2007/02/09: CIA-RDP82-00850R000500020034-7



There is another limitation in the fact that all integrated circuits of a given module must have identical OUR's [regions of stable operation]. Otherwise the OUR of the module will be smaller than the OUR of an individual integrated circuit.

The key parameters of some magnetic modules designed on the basis of single-register integrated circuits are presented in table 3 [27, 28, 29].

Table 3. Key Parameters of Some Bubble Memory Modules with Single-Register Integrated Circuits

| Type of module, firm, country | Module parameters | | | | | | |
|---|---|---|---|---|---|---|---|
| | Mean domain diameter, $d_{sr}$, $\mu_m$ | Module capacity, $n_{IC}N_r$, kbits | Operating frequency, f, kHz | Mean access time, $t_{sr}$, s | Temperature range, °C | | Maximum power requirement, P, V·A |
| | | | | | Operating | Information storage | |
| 29A, Western Electric, USA | 3 | 4X68 | 48 | 0.71 | 0;+50 | -40;+80 | 4 |
| FBM31DA, Fujitsu, Japan | 3 | 4X74 | 125 | 0.29 | -20;+70 | -40;+90 | 2 |
| POS-8, Rockwell International, USA | 4 | 8X103 | 160 | 0.32 | -10;+60 | -40;+85 | 6.2 |

In single-register bubble integrated circuits usually $N \sim 100$ kbits, since any defect in a sequential register puts the entire integrated circuit out of order and increasing $N_r$ increases the probability of the occurrence of defects. The optimum value of $N_r$ increases in proportion to improvement of the technology for producing bubble integrated circuits.

Typical examples of the application of first-class bubble memories are airborne high-reliability sequential information recording and readout systems, equipment for the digital recording and repeated reproduction of voice messages, systems for the numerical program control of machine tools and the like.

Second-class bubble memories have been developed and used most widely. Numerous variants of the structure of bubble integrated circuits exist for these memories [20-23, 26, 30-34]. One of the first structural diagrams which received practical application is presented in fig 13. The integrated circuit contains one distributing register, RR, also called an input/output register, and m storage registers, NR's, serving the purpose of storing information. The distance between adjacent NR's equals two cycles. Each NR is connected to the RR via its own exchange switch, KO. All KO's are ordinarily controlled in step by a single shared current, $i_{obm\,[exchange]}$, for the purpose of reducing the number of integrated circuit terminals, $\ell_e$. However, the use of several independently controlled groups of





APPROVED FOR RELEASE: 2007/02/09: CIA-RDP82-00850R000500020034-7

APPROVED FOR RELEASE: 2007/02/09: CIA-RDP82-00850R000500020034-7



KO's increases considerably the flexibility of an integrated circuit and often makes it possible to speed considerably the accessing of information.

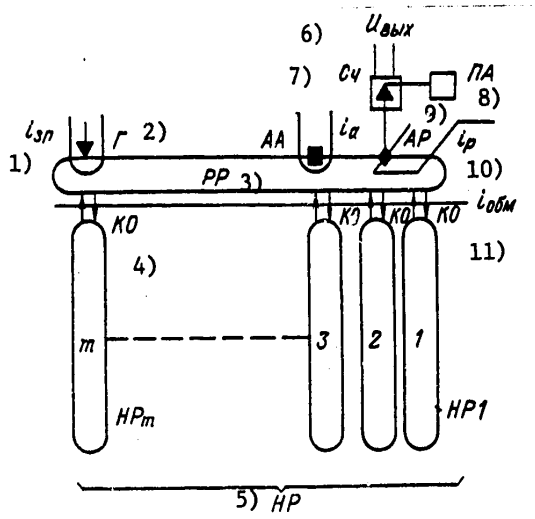


Figure 13. Structural Diagram of Bubble Integrated Circuit with Many Storages and a Single Distributing Register

Key:

1. $i_{zp}$ [readin]
2. G
3. Distributing register
4. Exchange switch
5. Storage registers
6. Output
7. Readout unit
8. PA [passive annihilator]
9. Active splitter
10. $i_r$
11. $i_{obm}$ [exchange]

With $i_{obm} = 0$, the RR and NR's are not interconnected and bubbles move through all registers independently of one another. During a write operation, a block of information, usually in the form of like bits of m words forming a single page, is entered into the RR by means of the generator, G. When the first word (bit) is opposite $NR_1$ and the last opposite $NR_m$, a current pulse, $I_{obm}$, transfers the entire page from the RR to the NR's. If other information was previously entered in the individual locations of the NR's, then by means of the $I_{obm}$ pulse it is first removed to the RR (the bubbles removed are placed between the bubbles of the new page to be entered), after which the new information is transferred from the RR into the NR's. The page removed can be read out, just as in the circuit in fig 12, and then erased by means of the AA and PA. It is also possible to erase without reading out, if $i_r$ is set equal to zero. For the purpose of reading out without erasing, the bubbles removed from the storage registers to the input/output register, $M_{NR} = M_{RR} + 1$ periods after the removal, passing the AR, AA and point S, again arrive at their KO's and are transferred by current $I_{obm}$ back to the storage registers. Here $M_{NR}$ and $M_{RR}$ are the capacities of the storage





APPROVED FOR RELEASE: 2007/02/09: CIA-RDP82-00850R000500020034-7

APPROVED FOR RELEASE: 2007/02/09: CIA-RDP82-00850R000500020034-7



and input/output registers, respectively. They differ by one, since when information is removed from the NR's to the RR this information is delayed by a single cycle.

The circuit in fig 13 has two shortcomings: The speed of the input and output of information is twofold less than the speed of motion of bubbles through storage registers, since there should be a distance of two cycles between adjacent words entered into the input/output register during a write operation, and the same distance is obtained in the removal of information from the storage register to the input/output register for readout; the time of a complete accessing cycle during readout, made up of the access time and the regeneration time (input back into the storage register), is relatively long. A number or methods have been suggested for eliminating these shortcomings [23, 26, 30-33], the implementation of one of which is illustrated in fig 14. In the circuit presented in this figure, at one end of all storage registers there is an input/output register, RR-1, connected to the storage registers by means of exchange switches (KO's), and at the other end an output register, RR-2, for the readout unit, Sch, connected to the storage registers by means of active bubble splitters, AR's. The input and output of information with the speed of its movement through the storage registers are made possible by dividing the storage registers into two groups: odd and even. Bubble generator G1 operates at odd cycles of the shifting field and G2 at even, i.e., the write operation is carried out in each cycle. When new information is entered the old information removed through the exchange switches is erased in the passive annihilator. Information is always read out without removing it from storage registers. The two information flows removed from the odd and even storage registers through the AR to the individual RR-2 registers merge at point S into a single flow, which enters the readout unit and PA.

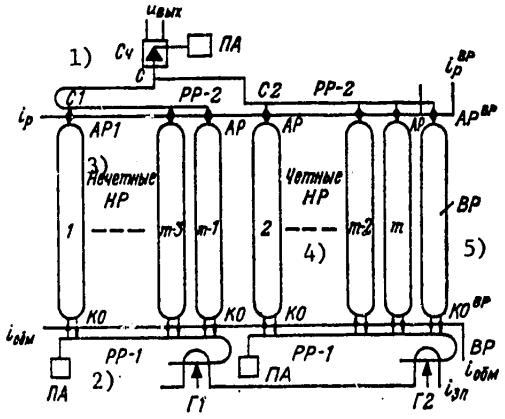


Figure 14. Structural Diagram of Bubble Integrated Circuit with Reduced Access Time and Increased Data Transfer Rate

Key:

1. S [merger point]
2. RR-1
3. Odd storage registers
4. Even storage registers
5. VR [auxiliary storage register]

[Cf. figs 12 and 13 for remaining symbols]





APPROVED FOR RELEASE: 2007/02/09: CIA-RDP82-00850R000500020034-7

APPROVED FOR RELEASE: 2007/02/09: CIA-RDP82-00850R000500020034-7



The mean time, $t_{sr}$, for producing a word (bit) of a random page in the circuit in fig 14 during readout equals:

$$t_{ср} = \frac{1}{f}\left(\frac{M_{нр}}{2} + \frac{m}{2} + l_{сч}\right),$$

where $l_{sch} \sim m/2$ is the number of cycles between $AR_1$ and Sch [readout unit]. The minimum value of $t_{sr}$ approximately equals $\sqrt{2N}/f$ and is achieved with $M_{NR} \sim 2m$, where $N = mM_{NR}$ is the information capacity of the integrated circuit. The mean time, $t_1$, for accessing the first word of a random page equals:

$$t_1 = \frac{1}{f}\left(\frac{M_{нр}}{2} + l_{сч}\right).$$

The mean time, $t_{zam}$, for replacing a random page after its preliminary readout equals:

$$t_{зам} = t_{ср} + \frac{M_{нр}}{2f}.$$

With an assigned value of the capacity, N, of the integrated circuit, the choice of ratio $M_{NR}/m$ is determined not only on the condition of minimizing the access time in a specific operating mode of the memory (readout, write, replacement of information after readout), but also by the required size of pages (usually $m = 2^k$, where k is a whole number) and by the permissible power dissipated by the KO's and AR (the dissipated power increases in proportion to m), and by the feasibility, for technological reasons, of using bubble media chips having a shape close to square, which for the circuit in fig 14 is consistent with $M_{NR} \sim 4m$.

If in the circuit in fig 14 symmetric (reversible) shifting elements (cf. fig 6) are used and a page to be read out is moved to the terminals of the AR into RR-2 through the shortest route, then with $M_{NR} \sim 4m$ we get a minimum value of $t_{sr} \sim f^{-1}\sqrt{N}$.

The speed of the input and output of information is also brought to the speed of its movement in storage registers by increasing twofold the length of shift elements in the input/output register as compared with shift elements in storage registers. In this case a bubble travels the distance between two neighboring storage registers through the input/output register in only one cycle of the rotating field and the necessity of dividing storage registers into odd and even disappears (cf. fig 14). Bubble integrated circuits have been designed on this principle (fig 15), possessing the same properties as integrated circuits designed according to the circuit in fig 14, but simpler in the technological respect [23, 34].



APPROVED FOR RELEASE: 2007/02/09: CIA-RDP82-00850R000500020034-7

APPROVED FOR RELEASE: 2007/02/09: CIA-RDP82-00850R000500020034-7



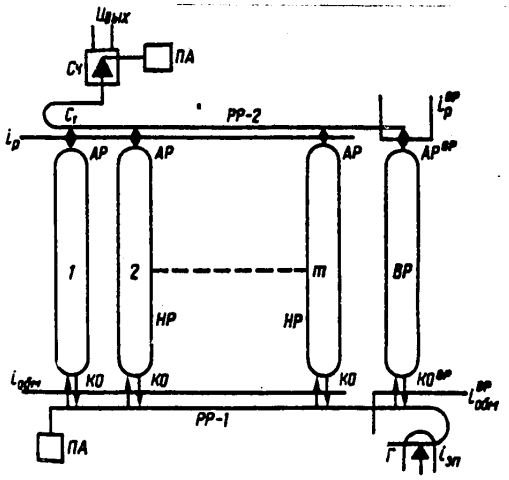


Figure 15. Variant of Structural Diagram of a Bubble Integrated Circuit with Short Access Time
[Cf. figs 12, 13 and 14 for key]

Since storage registers (NR's) occupy the major portion of an integrated circuit, defects in a chip or permalloy element most often cause malfunctioning of only one or several NR's of the class of memories discussed (cf. figs 13, 14 and 15). Therefore, an excess number, $m_{izb}$, of storage registers is usually provided in them, which makes it possible to increase considerably the percentage of the yield of suitable circuits under conditions of series production. The relative value of $m_{izb}/m$ is determined by economic considerations and depends on the production technology level reached. The addresses of malfunctioning or unused NR's can be stored either in an auxiliary NR (VR in the circuits in figs 14 and 15), which has individually controlled exchange switches ($KO^{VR}$'s) and replicators ($AR^{VR}$'s) connecting this VR to RR-1 and RR-2, or in a read-only (programmable) storage (PPZU). When a VR is used it also serves the purpose of storing tags (a code) for the starting position of all NR's, which is necessary for synchronizing the operation of a bubble memory when it changes from the storage mode to write or read modes. Otherwise information on the current position of information in the NR's must be stored permanently in an external semiconductor counter with a scaling factor of $M_{NR}$, including when the controlling magnetic field is switched off.

In addition to redundant storage registers (NR's) which serve the purpose of increasing the yield of suitable integrated circuits, $m_k$ additional NR's are often provided, employed for using codes which detect and correct errors. There are four different kinds of errors. They are "mild" errors originating only during readout (they cannot appear in repeated readout); "serious" errors originating as the result of the disappearance or appearance of a superfluous bubble in the NR; errors appearing in catastrophic failure of an NR, KO or of the AR connecting NR's with the RR; and errors resulting from failure of the generator, RR or readout unit, i.e., complete failure of the integrated circuit. The probabilities, $P_i$,



APPROVED FOR RELEASE: 2007/02/09: CIA-RDP82-00850R000500020034-7

APPROVED FOR RELEASE: 2007/02/09: CIA-RDP82-00850R000500020034-7



of the appearance of errors of each kind are interrelated as follows: $P4 << << P3 << P2 << P1$ . Therefore, even the detection of errors and repeated readout in the majority of cases are sufficient for the elimination of errors. The redundant codes used correct the first three kinds of errors. When errors of the third kind are detected (catastrophic failure of NR's, KO's or the AR) in modern bubble integrated circuits a transfer is provided by means of software from the malfunctioning NR to one of the redundant. Redundant bubble integrated circuits or magnetic modules are used in the most important cases for eliminating the influence of total failure of the integrated circuit.

The key parameters of some series-produced bubble modules with an RR-NR structure are presented in table 4 [21, 23, 31-37]. The temperature ranges for normal operation and the storage of information without losses are approximately the same as indicated in table 3 and, for example, for a module of the RBM 256 type equal -10 to +65 °C and -50 to +100 °C, respectively. Unlike bubble modules of the first class of memories (table 3) a single second-class memory module (table 4) includes as a rule only one integrated circuit, which is explained by the great number of terminals and great complexity of these circuits and the need to limit the total power dissipated in the KO's and AR and to provide a sufficiently wide region of stable operation (OUR). The use of one high-capacity integrated circuit per module makes possible the high flexibility of bubble memories and is economically feasible. The mean access time, $t_{sr} = \sqrt{N}$ , increases with an increase in the capacity, N , of integrated circuits. Therefore, for the purpose of reducing $t_{sr}$ and increasing the data transfer rate, integrated circuits are used which contain several (C) RR-NR groups operating in parallel, each of which has its independent generator and readout. For example, in a module of the Texas Instruments (USA) TIB1000 type, $C = 2$ and in a Nippon Electric (USA) module on which there are data available only for experimental models $C = 4$ [21]. Its distinctive feature is the fact that because of the use of symmetric shifting elements (cf. fig 6h) and the two-way motion of bubbles in NR's a low value of $t_{sr}$ is achieved.

With $m = 2^k$ , by selecting the page length, $Q = 2^q < m$ $(q = 0, 1, \ldots, K-1)$ , during a single operating cycle of KO switches or the AR the simultaneous input into NR's or output into RR-2 of $R = m/Q = 2^{k-q} \geq 2$ pages of information are possible. And if the number of cycles between G and KO1 and between KO1 or AR1 and the readout unit in the circuits in figs 14, 15 and 16 does not have a common divisor differing from one, then in these circuits it is possible to accomplish the continuous readin or readout of several (s) blocks of information, i.e., it is possible to obtain a page capacity of $Q = sm \leq N$ , $s = 2, 3, \ldots, N/m$ . Thus, by the appropriate choice of the parameters of the integrated circuit and by programming the memory's operating mode it is possible to obtain any page size regardless of the value of $m$ chosen.

The effectiveness of using error combating coding for increasing the reliability of bubble modules can be characterized by the data presented in table 5 as applied to modules of the Texas Instruments (USA) TIB1000 and TIB500 types (cf. table 4), for which $m = 256$ and $m_k = 18$ [34]. The probability of the appearance of a page with an undetected and uncorrected error (table 5) corresponds to the rate of the appearance of undetected and uncorrected errors, $\lambda = 1.5 \cdot 10^{-5}$/bit . Hence, the mean time between failures for a bubble memory with a capacity of 100 Mbits and a data transfer rate of 5 Mbits/s, prior to the appearance of an undetected and uncorrected error, equals 4 years with continuous round-the-clock



APPROVED FOR RELEASE: 2007/02/09: CIA-RDP82-00850R000500020034-7

APPROVED FOR RELEASE: 2007/02/09: CIA-RDP82-00850R000500020034-7



operation. Therefore, the appearance of errors of the first or second kind, not associated with catastrophic failure, is the most probable. Based on magnetic modules of the POS-8 type (cf. table 3) an airborne bubble memory has been designed with a capacity of 100 Mbits with a mean time between failures of not less than 41,000 h [38].

Table 4. Some Parameters of Bubble Memory Modules with an RR-NR [Input/Output Register - Storage Register] Structure

| 1) Тип модуля, фирма, страна | 2) Средний диаметр $d_{ср}$, мкм | 3) Полезная емкость $N^*$, Мбит | Емкость накопительных регистров $m \times M_{нр}$, 4) кбит | 5) Число избыточных регистров, $m_{изб} + m_к$ | Рабочая частота $f$, кГц 6) | Скорость передачи информации $f_{ц}^{**}$, 7) кбит/с | 8) Среднее время считывания $t_{ср}$, мс | 9) Потребляемая мощность $P$, В·А | 10) Хранение информации о дефектных НР |
|---|---|---|---|---|---|---|---|---|---|
| TIB0203, Texas Instruments, США 11) | 3 | 0,092 | 144×641 | 13 | 100 | 46 | 4 | 0,7 | 13) ППЗУ или ВР |
| TIB1000, Texas Instruments, США | 2 | 2,024 | 2×256××2049 | 2×44 | 100—200 | 171—342 | 11,2—5,6 | 1,2 | ВР |
| TIB0500, Texas Instruments, США | 2 | 0,512 | 256×2049 | 44 | 100—200 | 85—171 | 11,2—5,6 | 1,2 | ВР |
| TIB0250, Texas Instruments, США | 2 | 0,256 | 256×1025 | 44 | 100—200 | 85—175 | 5,6—2,8 | 1,2 | ВР |
| RBM256, Rockwell International, США | 3,2 | 0,256 | 256×1025 | 26 | 150 | 136 | 4 | 0,82 | ППЗУ |
| RBM411, Rockwell International, США | 2 | 1,024 | 512×2052 | 60 | 150 | 135 | 88 | 1,4 | ППЗУ |
| FBM43DA, Fujitsu, Япония 12) | 3 | 0,267 | 256×1033 | 8 | 100 | 97 | 6 | 0,67 | ППЗУ или ВР |
| Модуль фирмы Nippon Electric, Япония | 3 | 0,075 | 4×67××280 | — | 300 | 1200 | 0,34 | — | — |
| IM7110, Intel, США | 2,7 | 1,024 | 256×4096 | 64 | 62,5—125 | 85—170 | 25—50 | 1,9 | ВР |
| NBM2256, National Semiconductor, США | 2,7 | 0,256 | 256×1024 | 26 | 100 | 91 | 7 | 0,75 | ВР |

Key:

1. Type of module, firm, country
2. Mean diameter, $d_{sr}$, μ
3. Useful capacity, N*, Mbits
4. Capacity of storage registers, m X $M_{NR}$, kbits
5. Number of redundant registers, $m_{izb} + m_k$
6. Operating frequency, f, kHz
7. Data transfer rate, $f_{ts}$**, kbits/s
8. Mean readout time, $t_{sr}$, ms
9. Power requirement, P, V·A
10. Storage of information on defective NR's
11. USA
12. Japan
13. Programmable ROM or VR [auxiliary register]

*Determined by the number, m, of working NR's without taking into account $m_{izb}$ and $m_k$.

**Determined by the operating frequency, f, the number of parallel write and read channels, the number of redundant NR's ($m_{izb}$ and $m_k$) and VR's.



APPROVED FOR RELEASE: 2007/02/09: CIA-RDP82-00850R000500020034-7

APPROVED FOR RELEASE: 2007/02/09: CIA-RDP82-00850R000500020034-7



Table 5. Improvement of Reliability of Bubble Memories with Error Combating Coding

| Kind of errors in 256-bit page of data | Probability of appearance of a page with an error | Corrected errors, % | Detected errors, % |
|---|---|---|---|
| Isolated random error | $3 \cdot 10^{-4}$ | 100 | - |
| Isolated constant error | $3 \cdot 10^{-6}$ | 100 | - |
| Random pair of random errors | $3 \cdot 10^{-8}$ | 50 | 100 |
| Package of two random errors | $3 \cdot 10^{-9}$ | 100 | - |
| Package of two constant errors | $3 \cdot 10^{-11}$ | 100 | - |
| Package of three or four random errors | $3 \cdot 10^{-11}$ | - | 100 |
| Random pair of constant errors | $3 \cdot 10^{-12}$ | 50 | 100 |
| Package of five random errors | $3 \cdot 10^{-12}$ | - | 100 |
| Any three random errors | $3 \cdot 10^{-12}$ | - | 87 |
| One random and package of two random errors | $8 \cdot 10^{-13}$ | - | 100 |
| Undetected and uncorrected errors | $4 \cdot 10^{-13}$ | - | - |

Bubble Memory Control and Interface Circuits

Bubble memories, in addition to magnetic modules, contain two groups of electronic circuits. The first serves the purpose of directly controlling bubble modules and performs the following functions: the formation of current $i_x$ and $i_y$ creating the controlling magnetic field; formation of readin current, $i_{zp}$, exchange current, $i_{obm}$, splitting current, $i_r$, and information erasure current, $i_A$; and the amplification and formation of output signals, $U_{vykh}$, during readout. These functions are usually performed individually for each bubble module, but with the presence in a module of several integrated circuits or integrated circuits with several independent RR-NR groups, a readin current generator and a readout amplifier are provided for each of them. In individual instances for bubble modules operating in parallel shared current generators are used for $i_x$, $i_y$, $i_r$ and $i_A$ (in the circuit described in [33] these currents are shared by four modules operating in parallel).

The second group of electronic circuits, forming the so-called controller, serves the purpose of linking the bubble memory with a central processor (TsP) (or a microprocessor (MP)), an on-line memory in the form of a random-access memory (ZUPV) and/or other units, as well as for performing a number of operations making it possible to improve the reliability and speed of response of the bubble memory. A controller's functions usually include the following: conversion of a parallel flow of data arriving from the central processor or random-access memory through a k-wire data line (usually $k = 8$, 16 or 32 ) into one or more (according to the



APPROVED FOR RELEASE: 2007/02/09: CIA-RDP82-00850R000500020034-7

APPROVED FOR RELEASE: 2007/02/09: CIA-RDP82-00850R000500020034-7



number of bubble modules operating in parallel) sequential flows of data for entry into the bubble memory and reverse serial-parallel conversion during readout; matching rates of transfer of data between the central processor, random-access memory and bubble modules by means of a buffer storage operating at a variable speed; selection of bubble modules in keeping with instructions arriving from the central processor (or microprocessor) and control of readin, readout and/or the erasure of specific pages; control of the start and stop of motion of bubbles and ensurance of the preservation of information and of its position in bubble modules with a sudden cutoff of power; storage of information on the current position of pages or the restoration of this information after the memory is turned on; ensurance of a specific page size; ordering the sequence of readin signals and of signals readout taking into account the presence of malfunctioning NR's; coding and decoding of information for the purpose of detecting and correcting errors; repeated readout with the detection of uncorrected errors; checking the working order of the memory and protecting it from improper influences; output of information on the state of the controller and memory; enabling the memory to operate in the interrupt mode; implementation of the optimum procedure for satisfying requests for access to the bubble memory according to the criterion of the minimum mean operating time; and enabling the possibility of increasing the capacity of the memory by adding new bubble modules; etc. [33, 34, 35, 39].

The implementation of these functions is achieved by a combination of hardware and software. The controller is a control unit with microprogram control. Programs are stored in the programmable ROM of the controller and can be changed within certain limits with a change in the structure of bubble modules and the method of controlling the memory (e.g., for the purpose of enabling its operation in parallel or multiplex modes, the direct-access mode, in a mode minimizing the mean access time, etc.). Bubble memory controllers are usually designed as special-purpose semiconductor large-scale integrated circuits (LSIC's), but can be designed also on the basis of standard microprocessor elements and integrated circuits. The structure of controllers can be modified over a wide range depending on the structure of bubble modules and of the entire memory, the set of functions to be implemented, etc, [32, 33, 34, 35].

One or more bubble modules together with the common control circuits form a memory unit. A structural diagram of the simplest memory unit with one bubble module (of the type illustrated in fig 14 or 15) is presented in fig 16. In this circuit the current generators and readout amplifier represent actuating units performing instructions arriving from the controller through the instruction line (ShK). Data to be entered or read out arrive through the data line (ShD). Individual control elements are often designed as a single integrated circuit which can serve several bubble modules included in a single memory unit. Since the greatest power is dissipated in continuously operating coil current generators, they are usually designed on the basis of transistor and diode microassemblies. A typical circuit for a current generator for one coil (Y) and the control voltages of transistors are illustrated in fig 17. With $nT \leq t \leq (n + 0.25)T$, where $n = 0, 1, 2, \ldots$ and $T$ is the cycle of the control field, voltages U1 and U3 render transistors T1 and T3 conducting and current $i_y$ rises exponentially with a time constant determined by the coil's inductance and the circuit's resistance. With $t = (n + 0.25)T$ transistors T1 and T3 are cut off and current $i_y$, closed via Schottky diodes D1 and D3, diminishes exponentially. With $t = (n + 0.25)T$





APPROVED FOR RELEASE: 2007/02/09: CIA-RDP82-00850R000500020034-7

APPROVED FOR RELEASE: 2007/02/09: CIA-RDP82-00850R000500020034-7



transistors T2 and T4 are opened for a quarter cycle, forming a negative half-cycle for current $i_y$. Current $i_y$ produced in this manner has a form close to triangular (cf. fig 7b). Control voltages U1, U3 and U2, U4 for the $i_x$ current generator are shifted in phase one quarter cycle relative to the like voltages of the generator for current $i_y$. Transition to the information storage mode is accomplished by stopping the supply of control voltages to both generators with $t = n(T)$. The level of voltage U1 is greater than U3 and U2 is greater than U4, since voltages U1 and U2 must make possible the saturation of transistors T1 and T2 at the appropriate intervals. Control voltages can enter the coil current generators from the controller or be formed by means of logic elements and voltage level bias circuits included in the coil current generators themselves. In the latter instance the number of lines linking the controller with the memory unit is reduced and changeover from the shift mode to the storage mode or vice-versa can be accomplished under the influence of a single control signal ("start-stop") arriving from the controller to the coil current generators.

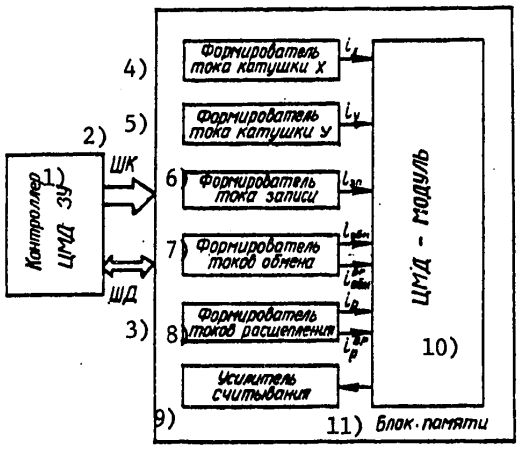


Figure 16. Structure of Memory Unit with Bubble Modules

Key:

1. Bubble memory controller
2. Instruction line
3. Data line
4. Current generator for coil X
5. Current generator for coil Y
6. Readin current generator
7. Exchange current generator
8. Splitting current generator
9. Readout amplifier
10. Bubble module
11. Memory unit

A diagram of a second-class bubble memory controller (an integrated circuit with an RR-NR-RR structure) is presented in fig 18. The data register makes it possible to convert the parallel k-bit code into a serial code during readin and to change it back after the readout of information from bubble modules. The addresses of NR's unused and, if this is required, microprograms for controlling the control



APPROVED FOR RELEASE: 2007/02/09: CIA-RDP82-00850R000500020034-7

APPROVED FOR RELEASE: 2007/02/09: CIA-RDP82-00850R000500020034-7



Instruction generator (FKU) are stored in the programmable ROM (PPZU). A page counter with a scaling factor equal to the capacity of the NR serves the purpose of storing the current address of pages. The binary code in its output corresponds to the number of the page found opposite the exchange switches (KO's). When this number agrees with the address of the page to which access is required, the address comparator included in the FKU operates and the FKU issues an exchange instruction to the memory unit selected. A replication instruction during readout is formed similarly, for a specific address, taking into account the fact that the AR's in the circuits in figs 14 and 15 are shifted $M_{NR}/2$ cycles relative to the KO's. Ordering of data is accomplished in the following manner. During readin signals from the address decoder and word counter enter the PPZU, in which information on malfunctioning NR's is stored, and if the NR for the address in question is malfunctioning, a 0 appears in the PPZU's output and the word to be entered is transferred for entry with a delay of one cycle. During readout, a word (bit) arriving from an unused NR is omitted, i.e., does not enter the data register. These functions are easily implemented by means of a shift register, for example, designed with D-V flip-flops, which can also be included in the error correction circuit.

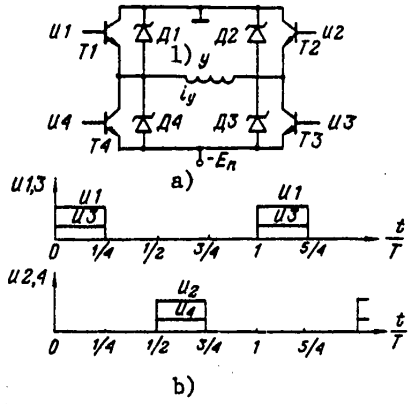


Figure 17. Circuit for Generating Control Coil Current

Key:
1. Diode

For the precise synchronization and phasing of signals controlling bubble modules there is a stable synchronization pulse generator whose frequency is 50- to 100-fold higher than the frequency of the bubble module's control field. The beginning, end and intermediate changes in control signals are formed by timer-counters included in the FKU.

The presence in the controller of one or more buffer data registers operating at variable speed makes it possible to accomplish the exchange of data between the bubble memory controller and central processor or random-access memory with high speed (up to 5 to 10 Mbits per single buffer register). The controller can control



APPROVED FOR RELEASE: 2007/02/09: CIA-RDP82-00850R000500020034-7

APPROVED FOR RELEASE: 2007/02/09: CIA-RDP82-00850R000500020034-7



the operation of a great number of memory units in the multiplex mode, whereby individual memory units are connected by turns to common address and data lines, and the ordering of data and the detection and correction of errors are performed for each block [34]. For the purpose of improving the efficiency of the bubble memory the controller can organize its operation in such a manner that part of the memory units accomplish the exchange of information with the central processor or random-access memory and part with peripheral units, and then they change places, etc. A typical structural diagram of a microcomputer is presented in fig 19, which includes a random-access memory, programmable ROM, ROM and bubble memory and the possibility is provided of directly linking the input/output unit (UVV) both with the microprocessor (MP) and with the bubble memory.

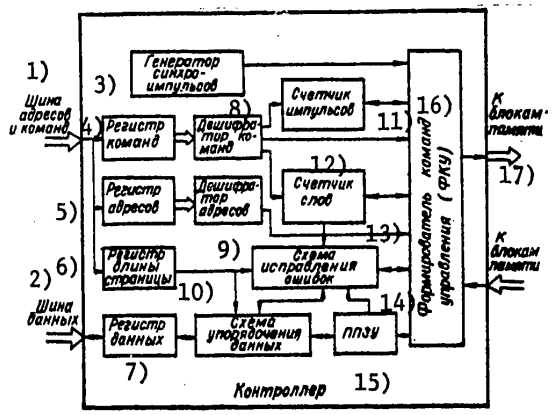


Figure 18. Structural Diagram of Bubble Memory Controller

Key:

1. Address and instruction line
2. Data line
3. Synchronization pulse generator
4. Instruction register
5. Address register
6. Page length register
7. Data register
8. Instruction decoder
9. Address decoder
10. Data ordering circuit
11. Pulse counter
12. Word counter
13. Error correction circuit
14. PPZU [programmable ROM]
15. Controller
16. Control instruction generator (FKU)
17. To memory units

Trends in Further Development of Bubble Memories

Major trends in further development of bubble memories reflect the aspiration of lowering the unit cost, of improving the speed of response and reliability and of expanding the functional characteristics of these memories. Reduction of the unit cost of a bubble memory (cost in terms of memory capacity) can be achieved by increasing the information storage density, j , or capacity of a single integrated circuit upon the condition that the capacity of the integrated circuit increases



APPROVED FOR RELEASE: 2007/02/09: CIA-RDP82-00850R000500020034-7

APPROVED FOR RELEASE: 2007/02/09: CIA-RDP82-00850R000500020034-7



more rapidly than the cost of production. Hitherto an increase in the information density, $j$, of bubble integrated circuits has been achieved by reducing the mean (nominal) diameter, $d_{sr}$, of the bubble and the spacing of the shifting structure, $\lambda = ad_{sr}$. With this $j \sim \lambda^{-2}$.

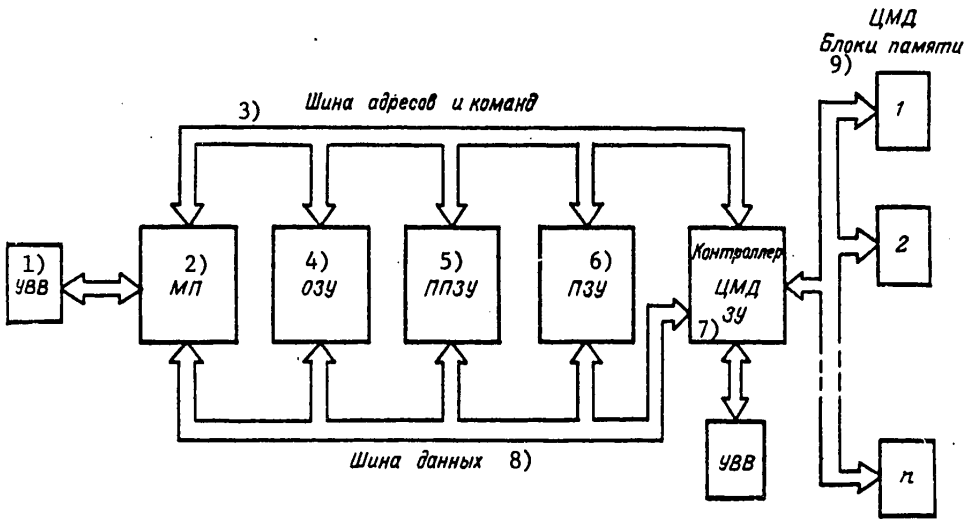


Figure 19. Structural Diagram of Microcomputer Containing a Bubble Memory

Key:

1. Input/output unit
2. Microprocessor
3. Address and instruction line
4. RAM
5. Programmable ROM
6. ROM
7. Bubble memory controller
8. Data line
9. Bubble memory unit

The minimum value of $a$, limited by the mutual influence of neighboring bubbles when using single-gap shifting elements (cf. fig 6), equals 4. The minimum value of $d_{sr}$ for bubble integrated circuits with the familiar types of permalloy shifting elements (cf. fig 6) is limited by the resolution of the lithographing equipment used and by substantial worsening of the effectiveness of the use of permalloy elements for controlling the motion of bubbles with a reduction in their linear dimensions in keeping with $d_{sr}$ with a simultaneous increase in the required value of $H_{upr\ [control]}$ [40]. At the present time integrated circuits are being produced with a bubble diameter of $d_{sr} = 1.8$ to 2 $\mu$m ($\lambda = 7.5$ to 8 $\mu$). It is assumed that the minimum values of $d_{sr}$ and $\lambda$ for integrated circuits with permalloy shifting elements equal respectively 1 and 4 $\mu$m, which makes it possible to obtain an information density, $j$, on the order of 6 Mbits/cm$^2$.



APPROVED FOR RELEASE: 2007/02/09: CIA-RDP82-00850R000500020034-7

APPROVED FOR RELEASE: 2007/02/09: CIA-RDP82-00850R000500020034-7



Among bubble integrated circuits with shared field control the most widespread have become integrated circuits with ion-implanted shifting structures [41, 42]. In these, upon rotation of the external control field, $H_{upr}$, bubbles move along a chain of abutting nonimplanted disks (ND's in fig 20a) or rectangles (NP's in fig 20b). Nonimplanted chains are formed by coating by the method of photolithography individual regions of a ferrite garnet film with a protective layer which does not admit ions implanted in the surrounding region. In the implanted regions (IO's) an "easy" surface is formed, magnetized in the direction of the influence of field $H_{upr}$. At the interface of implanted and nonimplanted regions magnetic holes form, which exert a corresponding influence on the bubbles, which can be moved simultaneously along both directions of the chain of abutting disks (rectangles), e.g., clockwise. The chain of abutting nonimplanted disks thus forms a closed bubble shift register. Elements have been developed which implement in ion-implanted bubble integrated circuits the functions required for constructing a memory (bubble generation, switching, readout, etc.) [42].

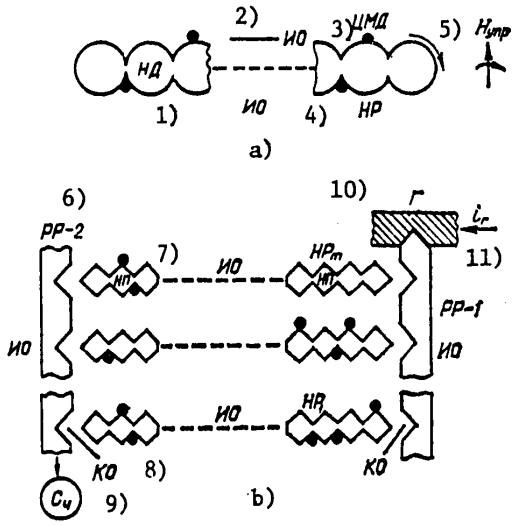


Figure 20. Ion-Implanted Bubble Shifting Structures

Key:

1. Nonimplanted disk
2. Implanted region
3. Bubble
4. Storage register
5. $H_{upr}$
6. Input/output unit No 2
7. Nonimplanted rectangle
8. Exchange switch
9. Readout unit
10. Generator
11. Generator current

Ion-implanted shifting structures have two important advantages as compared with the permalloy discussed earlier: less strict requirements for lithographic resolution because of the absence of gaps which are critical in terms of their size between neighboring elements (approximately eightfold lower resolution is required





APPROVED FOR RELEASE: 2007/02/09: CIA-RDP82-00850R000500020034-7

APPROVED FOR RELEASE: 2007/02/09: CIA-RDP82-00850R000500020034-7



for producing the same $d_{sr}$ and $\lambda$ in these structures), and the lack of the need to increase $H_{upr}$ in proportion to a reduction in $d_{sr}$ and $\lambda$ [40]. These structures, because of the absence of nontransparent permalloy elements on the surface of the ferrite garnet film, can be used in various magnetooptic domain devices (displays, changeable transparencies, etc.).

Another method of creating local changes in the magnetic properties of ferrite garnet films for controlling the motion of bubbles is the selective annealing of individual sections of a film by means of a focused laser beam. For example, by this method are produced parallel annealed channels with enhanced magnetization, $M_s$, along which bubbles are propagated under the influence of an appropriate control field [43].

The minimum distance, $\lambda$, between neighboring bubbles in integrated circuits can be reduced twofold (from $4d_{sr}$ to $2d_{sr}$) if the active section of the integrated circuit (the storage) is completely filled with bubbles. In this case a so-called domain array is formed in which the interaction of neighboring bubbles is of a constant nature, which makes it possible to reduce $a$ and $\lambda = ad_{sr}$. Here information (a 0 or 1) must be represented not in the form of the absence or presence of a bubble, but in the form of a certain state of its boundary, characterized by the value of $S$ (cf. the section "Conditions for the Existence and Properties of Mobile Bubbles"). With a given value of $d_{sr}$ the utilization of domain arrays makes it possible to increase fourfold the surface density of information, $j$. The propagation of bubbles in the array, in particular, can be accomplished by means of permalloy elements with large gaps of noncritical size [11].

A quite promising method of lowering the cost of a bubble module is the creation of functional elements making it possible to fabricate bubble integrated circuits with permalloy or ion-implanted elements with the use of only one lithography stage. In the first group of circuits for this it is necessary to form permalloy conductors simultaneously with propagating elements [20, 44, 45, 46]. A bubble module can be simplified by employing two-layer ferrite garnet films as bubble media not requiring a permanent bias field [47].

A disadvantage of a bubble module with a shared control field is the relatively high, primarily reactive, power which must be supplied to the coils creating the rotating controlling magnetic field, $H_{upr}$. This power is proportional to the space in which the field is created and which is much greater than the volume of the ferrite garnet film with control elements. The required power grows somewhat more rapidly than the operating frequency, $f$, since with an increase in frequency it is necessary to increase $H_{upr}$. It is precisely the permissible value of the power required for the coils which limits the maximum operating frequency of a bubble integrated circuit with field control to values of approximately 300 kHz, which is far below the maximum operating frequency determined by the mobility or maximum speed of bubbles. One way of substantially reducing the power requirement and accordingly increasing the maximum operating frequency of bubble devices is to change from shared field control to local current control. In the latter instance local magnetic fields accomplishing the propagation of bubbles are created by the current flowing through conductors located on the surface of the ferrite garnet film. At the same time there is a drastic reduction in the space occupied by the controlling magnetic field and the reactive power necessary for creating it.



APPROVED FOR RELEASE: 2007/02/09: CIA-RDP82-00850R000500020034-7

APPROVED FOR RELEASE: 2007/02/09: CIA-RDP82-00850R000500020034-7



A number of designs of bubble integrated circuits with local current control have been suggested [45, 48]. An operating frequency of 4 to 5 MHz has been obtained for some experimental bubble propagation circuits and this is not the limit. Quite promising is the accomplishment of local current control (without permalloy elements) by means of two perforated conducting layers applied to the surface of a ferrite garnet film with an intermediate insulating layer [48]. The current flowing around a hole (perforation) creates a local magnetic field which influences a bubble near the hole. By the appropriate distribution of holes in two conducting layers and by alternating the current flowing through these layers it is possible to provide the required propagation of bubbles, as well as to perform the functions of generating, stretching and changing the direction of motion of bubbles. It has been predicted that on the basis of this local current control bubble integrated circuits will be created with an information density of $j \approx 10^7$ bits/cm$^2$ and with an operating frequency reaching 4 to 20 MHz.

One more important trend in the development of bubble integrated circuits is the creation of new types of functional elements (coders, decoders, logic elements, arithmetic units, etc.) compatible in the technological respect and in terms of region of stable operation with propagation elements [49, 50, 51]. The creation of these elements will make it possible to increase considerably the effectiveness of the application of bubble memories in computing systems (to reduce access time and the amount and cost of external electronics and to improve the reliability and expand the functional capabilities of memories).

Substantial improvement of the characteristics of bubble memories can be achieved by structural and software methods: by dynamic ordering of information in the memory, by organizing a memory with minimum access time, by accomplishing content accessing, etc. [32, 51, 52, 53, 54]. Let us limit ourselves to discussing only one possible bubble integrated circuit structure making it possible to improve considerably the speed of response of a memory. We divide a bubble integrated circuit into four groups of individually controlled registers: input register RR-1, input register RR-2, a group of buffer registers (BR's) and a group of storage registers (NR's) (fig 21). It is assumed that by means of control current $i_1$, $i_2$, $i_{BR}$ and $i_{NR}$ it is possible to enable the operation of any group either in the bubble motion mode or in the stationary bubble storage mode, regardless of the state of the other groups of registers. A bubble integrated circuit with local current control [48] affords this possibility. The BR's and NR's are interconnected by means of exchange switches (KO's) and with RR-1 and RR-2 by means of universal switches (UK's) which implement, depending on the phase for supplying the control current, either an exchange function or a switching function. The storage in short buffer arrays of pages which are required before others considerably reduces access time in readout. Consequently, it is advisable to enter directly into the BR by means of generator G2 pages which in the immediate future must be removed to the central processor or random-access memory. Otherwise, if all buffer registers are filled, it is possible to use G1, as in the circuits in figs 14 and 15. If the required page is in storage registers, then it can first be transferred to buffer registers and then to RR-2 for readout. Furthermore, the mean access time for these pages is not longer than in bubble integrated circuits with the ordinary structure (cf. fig 14 and 15), since the BR's and NR's operate in the independent start-stop mode, which makes it possible to coordinate their operation. The addition of an added readout unit for RR-2 makes it possible to



APPROVED FOR RELEASE: 2007/02/09: CIA-RDP82-00850R000500020034-7

APPROVED FOR RELEASE: 2007/02/09: CIA-RDP82-00850R000500020034-7



reduce the mean time for access from NR's. The structure of this circuit (fig 21) possesses important advantages even without G2 and Sch2 [readout unit No 2]. The ordering of information in NR's and BR's is accomplished easily in it. The page to be reordered is removed from the NR to RR-1, where it is stored without movement and the information in the NR is shifted the required number of steps, after which the page previously removed is put back into the NR, etc. Similarly, by means of RR-2, information in BR's can be ordered, too. In connection with the increase in the capacity of the bubble integrated circuit the implementation of two memory levels (BR's and NR's) in a single integrated circuit can serve as a quite effective means of reducing the access time which, of course, necessitates complication of the controller.

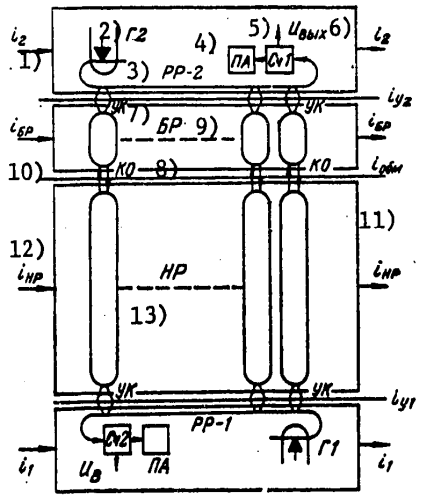


Figure 21. Use of Buffer Registers in a Bubble Integrated Circuit for Reducing Access Time

Key:

1. Generator current
2. Generator No 2
3. Input unit No 2
4. Passive annihilator
5. Readout unit No 1
6. Output voltage
7. Universal switch
8. Exchange switch
9. Buffer registers
10. Buffer register current
11. Exchange current
12. Storage register current
13. Storage registers

Conclusion

The above reflects the results of only the first stage in the development of bubble integrated circuits and memories based on them. Already now the feasibility is clearly obvious of extensively using bubble memories in instrument making, control systems and computer equipment, especially taking into account the real



APPROVED FOR RELEASE: 2007/02/09: CIA-RDP82-00850R000500020034-7

APPROVED FOR RELEASE: 2007/02/09: CIA-RDP82-00850R000500020034-7



prospects for reducing the unit cost, improving the speed of response and reliability and expanding the functional capabilities of bubble memories.

The highest technical and economic result from the use of bubble memories can be achieved only if the potential capabilities and distinctive features of these memories are taken into account as early as the stage of designing a new instrument, unit, computer or system.

At the present time the most promising areas of application of bubble memories are the following: the bulk storage of microcomputers and microprocessor systems; a relatively high-speed computer buffer storage between the random-access memory and main external storage; the bulk storage of dispersed computing, control and data processing systems, e.g., a terminal storage; reliable and compact storage of modified control programs, e.g., in systems for the numerical program control of machine tools; and measuring and testing instruments with mathematical processing of measurement results.

In the next few years must be expected the appearance of bubble devices which accomplish not only the storage but also the processing of information, including for performing the functions indicated in the introduction.

Bibliography

1. Vonsovskiy, S.V. "Magnetizm" [Magnetism], Moscow, Nauka, 1971, p 1031.

2. Minnick, R.C. et al. "Magnetic Bubble Computer Systems," AFIPS PROC., Vol 41, pp 1279-1298.

3. Naden, R.A. "One-Chip Stored-Program Magnetic Bubble Processor" in "Proc. IEEE National Aerospace and Electronic Conf.," 1974, p 42.

4. Balbashov, A.M. and Chervonenkis, A.Ya. "Magnitnyye materialy dlya mikroelektroniki" [Magnetic Materials for Microelectronics], Moscow, Energiya, 1979, p 216.

5. Boyarchenkov, M.A., Prokhorov, N.L., Rayev, V.K. and Rozental', Yu.D. "Magnitnyye domennyye logischekiye i zapominayushchiye ustroystva" [Magnetic Domain Logic and Memory Units], Moscow, Energiya, 1974, p 176.

6. Bobek, E. and Della Torre, E. "Tsilindricheskiye magnitnyye domeny" [Magnetic Bubbles], Moscow, Energiya, 1977, p 192.

7. O'Dell, T. "Magnitnyye domeny vysokoy podvizhnosti" [High-Mobility Magnetic Domains], Moscow, Mir, 1978, p 200.

8. Bar'yakhtar, V.G. "Magnetic Bubbles," USPEKHI FIZICHESKIKH NAUK, Vol 121, No 4, 1977, pp 593-628.

9. Lisovskiy, F.V. "Fizika tsilindricheskikh magnitnyye domenov" [Physics of Magnetic Bubbles], Moscow, Sovetskoye Radio, 1979, p 192.



APPROVED FOR RELEASE: 2007/02/09: CIA-RDP82-00850R000500020034-7

APPROVED FOR RELEASE: 2007/02/09: CIA-RDP82-00850R000500020034-7



10. Thiele, A.A. et al. "The Energy and General Translation Force of Cylindrical Magnetic Domains," BSTJ, Vol 50, No 3, 1971, pp 711-724.

11. Brown, B.R. et al. "High-Density Devices Using Permalloy Propagation of Wall-Coded Bubbles," IEEE TRANS. ON MAGNETICS, Vol 15, No 6, 1979, pp 1501-1506.

12. Dudorov, V.N., Randoshkin, V.V. and Telesnin, R.V. "Synthesis and Physical Properties of Single-Crystal Films of Rare Earth Ferrite Garnets," USPEKHI FIZICHESKIKH NAUK, Vol 122, No 8, 1977, pp 253-293.

13. Doyle, W.D. et al. "A Comparison of Frequency Limited Bubble Device Performance and Material Characteristics," IEEE TRANS. ON MAGNETICS, Vol 14, 1978, pp 303-305.

14. Breed, D.J. et al. "New Bubble Materials with High Peak Velocity," IEEE TRANS. ON MAGNETICS, Vol 13, No 5, 1977, pp 1087-1094.

15. Makino, H. and Hibya, T. "Comparison of Eight Mixed Garnet Systems for 7 μm Period Bubble Devices," J. APPL. PHYS., Vol 50, No 11, 1979, pp 7815-7817.

16. Kestigian, M. et al. "Past, Present and Future Small Bubble Diameter Magnetic Memory Materials," J. APPL. PHYS., Vol 50, No 3, 1979, pp 2161-2166.

17. Blank, S.L. et al. "Design and Development of Single-Layer Ionimplantable Small Bubble Materials for Magnetic Bubble Devices," J. APPL. PHYS., Vol 50, No 3, 1979, pp 2155-2160.

18. Dimyan, M.Y. and Hubbell, W.C. "Comparison Between the Propagation Margins of Asymmetrical Chevron and Half-Disk Circuits at 100 kHz," J. APPL. PHYS., Vol 49, No 3, 1978, pp 1900-1907.

19. Il'yashenko, E.I. et al. "Optoelectrical Study of Bubble Propagation in Field Access Devices," IEEE TRANS. MAGNETICS, Vol 15, No 3, 1978, pp 1120-1123.

20. Lomov, L.S., Parinov, Ye.P. and Chirkin, G.K. "Magnetic Bubble Integrated Circuits," ELEKTRONNAYA PROMYSHLENNOST', No 6 (60), 1977, pp 65-75.

21. Yoshimi, K. et al. "Design and Characterization of 3 μm Bubble Memory Chips Using Patterns," J. APPL. PHYS., Vol 49, No 3, 1978, pp 1918-1923.

22. Orihara, S. et al. "An 8 μm Period Bubble Memory Device with Relaxed Function Designs," IEEE TRANS. MAGNETICS, Vol 15, No 6, 1979, pp 1692-1696.

23. Bullock, D.C. et al. "Design and Fabrication of Large Capacity Bubble Memory Devices," IEEE TRANS. MAGNETICS, Vol 15, No 6, 1979, pp 1697-1702.

24. Hayes, D.J. "Single-Chip Bubble Memory Packaging," IEEE TRANS. MAGNETICS, Vol 15, No 6, 1979, pp 1901-1903.



APPROVED FOR RELEASE: 2007/02/09: CIA-RDP82-00850R000500020034-7

APPROVED FOR RELEASE: 2007/02/09: CIA-RDP82-00850R000500020034-7



25. Yamigishi, K. et al. "A New Proposal on Field-Access Bubble Drives," IEEE TRANS. MAGNETICS, Vol 11, No 1, 1975, pp 16-20.

26. Bonyhard, P.I. "A Novel Major/Minor Loop Memory Chip Organization for High Performance Without Block Replication," J. APPL. PHYS., Vol 50, No 3, 1979, pp 2213-2215.

27. Williams, J.E. "Magnetic Bubble Memory in Telephone Systems" in "Proc. Conf. 'Electro'," 1977, pp 12-13.

28. Yamagishi, K. "The Progress of Magnetic Bubble Development in Japan" in "Proc. 3rd USA-Japan Computer Conf.," 1978.

29. Becker, F.J. et al. "An 8 X $10^5$ Bit Bubble Memory Cell for Spacecraft Applications" in "Digests 1980 Intermag. Conf., N.Y.," 1980, pp 12-2 [as published].

30. Ypma, J.E., Gergis, I.S. and Archer, J.L. "64K Fast Access Chip Design," PROC. AIP, Vol 29, 1976, pp 51-53.

31. "Single-Chip Magnetic Bubble Memories with a 250-kBit Capacity," ELEKTRONIKA, No 17, 1978, pp 3-5.

32. Dzhordzh, P.K. and Reyling, Dzh. "Magnetic Bubble Memories--State of the Art and Development Prospects," ELEKTRONIKA, No 16, 1979, pp 23-26.

33. Meviti, U.K. "Use of Bubble Memories in a Bulk Storage," ELEKTRONIKA, No 7, 1979, pp 36-43.

34. Koks, Dzh. "Series of Three Bubble Memories with High Packaging Density and a Complete Set of Interface Integrated Circuits," ELEKTRONIKA, No 23, 1979, pp 41-49.

35. Brayson, D. et al. "Set of Large-Scale Integrated Circuits for Joint Use with Bubble Memories," ELEKTRONIKA, No 9, 1979, pp 23-32.

36. "Fujitsu Bubble Memory" (firm's catalogue), 1979.

37. Chester, M. "Magnetic Bubble Memory Update," COMPUTER DESIGN, No 5, 1980, pp 232-236.

38. Stermer, R.L. "Bubble Memories for Spacecraft Data Recorders" in "Digests Intermag Conf.," Cal., 1977.

39. Kartsev, M.A. "Arkhitektura tsifrovykh vychislitel'nykh mashin" [Architecture of Digital Computers], Moscow, Nauka, 1978, p 296.

40. Kryder, M.N. "Magnetic Bubble Device Scaling and Density Limits," IEEE TRANS. MAGNETICS, Vol 15, No 3, 1979, pp 1009-1016.



APPROVED FOR RELEASE: 2007/02/09: CIA-RDP82-00850R000500020034-7

APPROVED FOR RELEASE: 2007/02/09: CIA-RDP82-00850R000500020034-7



41. Milchev, Yu.K. and Chirkin, G.K. "Ion-Implanted Structure for Propagation of Cylindrical Magnetic Domains," ZARUBEZHNAYA RADIOELEKTRONIKA, No 12, 1978, pp 68-69.

42. Nelson, T.J. et al. "Design of Bubble Device Elements Employing Ion-Implanted Propagation Patterns," BELL SYSTEM TECHN. J., Vol 59, No 2, 1980, pp 229-257.

43. Argyle, B.E. and De Luca, J.C. "Bubble Automotion Channels by Laser Annealing" in "Digests Intermag Conf., N.Y.," 1980, p 27-2.

44. Ahn, K.Y. et al. "Fabrication of SLM Conductor-First 2 μm Bubble Devices," IEEE TRANS. MAGNETICS, Vol 15, No 5, 1979, pp 1333-1335.

45. Dekker, E.H.L.G. et al. "Conductor and Transfer-Gate Performance of Single-Mask Field-Current Access Magnetic-Bubble Devices," J. APPL. PHYS., Vol 49, No 3, 1978, pp 1927-1929.

46. Ahn, K.Y. and Kane, S.M. "Toward a Single-Mask Processing of Ionimplanted Bubble Devices," IEEE TRANS. MAGNETICS, Vol 15, No 6, 1979, pp 1648-1650.

47. Zebrowski, J.J. and Humpherey, F.B. "Dynamic Behavior of Domain Walls in Double Layer Self-Biasing Garnet Films," IEEE TRANS. MAGNETICS, Vol 15, No 6, 1979, pp 1915-1921.

48. Bobeck, A.H. et al. "Current-Access Magnetic Bubble Circuits," BELL SYSTEM TECH. J., Vol 58, No 6, 1979, pp 1453-1540.

49. Boyarchenkov, M.A., Vasil'yeva, N.P. and Rozental', Yu.D. "Logicheskiye ustroystva na magnitnykh sredakh s upravlyayemym dvizheniyem domenov" [Logic Devices Employing Magnetic Media with Controlled Motion of Domains], Moscow, Energiya, 1978, p 160.

50. Teyerman, V.A. and Titov, G.V. "Circuits with Selective Accessing of Information for Magnetic Bubble Memories," ZARUBEZHNAYA ELEKTRONNAYA TEKHNIKA, No 16, 1979, pp 3-45.

51. Chang, H. "Major Activity in Magnetic Bubble Technology," COMPUTER DESIGN, No 11, 1979, pp 117-125.

52. Lee. S.Y. and Chang, H. "Associative-Search Bubble Devices for Content-Addressible Memory and Array Logic," IEEE TRANS. COMPUTERS, Vol 28, No 9, 1979, pp 627-637.

53. Bongiovanni, G.C. and Luccio, F. "Permutation of Data Blocks in a Bubble Memory," COMMUN. ACM, Vol 22, No 1, 1979, pp 21-25.



APPROVED FOR RELEASE: 2007/02/09: CIA-RDP82-00850R000500020034-7

APPROVED FOR RELEASE: 2007/02/09: CIA-RDP82-00850R000500020034-7



54. Lin, W.S. and Jino, M. "Intelligent Magnetic Bubble Memories and Their Applications in Data Base Management Systems," IEEE TRANS. COMPUTERS, Vol 28, No 12, 1979, pp 888-906.

COPYRIGHT: Tsentral'nyy nauchno-issledovatel'skiy institut informatsii i tekhniko-ekonomicheskikh issledovaniy priborostroyeniya, sredstv avtomatizatsii i sistem upravleniya (TsNIITEIpriborostroyeniya), 1981

8831
CSO: 1860/59



APPROVED FOR RELEASE: 2007/02/09: CIA-RDP82-00850R000500020034-7

APPROVED FOR RELEASE: 2007/02/09: CIA-RDP82-00850R000500020034-7



UDC 681.355 (088.8)

# DEVICE FOR TAKING MEDIAN VALUE

Moscow OPISANIYE IZOBRETENIYA 702381 in Russian 7 Dec 79

[Description of USSR Patent No 702381 by F.I. Kerbnikov, N.E. Mengazetdinov and M.A. Rozenblat, filed 6 Jun 78, published 7 Dec 79, class G 06 G 7/12]

[Text] This invention is in the area of automation, computing and measurement technology and can be used in high reliability, high precision systems for measuring and transmitting analog signals.

There exist devices which take the median value [1] which extract the median from an ordered sequence of input signals. These devices contain an odd number of channels operating in parallel whose outputs are combined and connected to a common load.

The closest known median-extracting device to the proposed invention is that described in [2], which has in each nonlinear conversion channel an amplifier which is connected through a current limiter to the load and which has common negative feedback.

In this device, the amplifier in each channel can be in the linear region under the condition

$$|(U_{in_i}-U_{out})K_i| < \varepsilon_0, \tag{1}$$

where $U_{in_i}$ -- voltage at input of ith channel;

$$U_{out}=\text{med}[(U_{in_1}-U_{out})K_1, \ldots, (U_{in_i}-U_{out})K_i, \ldots, (U_{in_{2n+1}}-U_{out})K_{2n+1}] \tag{2}$$

$U_{out}$ - device output voltage;
$K_i$ - gain of shorted amplifier of ith channel;
$\varepsilon_0$ - size of linear zone of current limiter;
$2n+1$ - number of channels operating in parallel.

When condition (1) is not met, the amplifiers in the nonlinear conversion channels are saturated. In practice, when $K \gg 1$, only one channel is



APPROVED FOR RELEASE: 2007/02/09: CIA-RDP82-00850R000500020034-7

APPROVED FOR RELEASE: 2007/02/09: CIA-RDP82-00850R000500020034-7



operating in the linear region, while the amplifiers in the other channels are saturated. The saturated condition of the amplifiers has no effect when dc signals are being converted, since there is always at least one amplifier in the linear state.

When processing time-varying input signals (especially if the signals are close to one another), condition (1) is necessarily violated for the channel in the linear condition due to changes in frequency and level of input signal and variation in K from amplifier to amplifier. This causes the channels to be switched abruptly. When this happens, the amplifier which had been in the linear region is saturated, and an amplifier in another channel for which condition (1) is met must be switched to the linear condition. However, there is a delay involved in the latter amplifier exiting the saturated condition. The time difference between the entry of the amplifier into the saturated condition and its exit from that condition causes excursions of the voltage at the output of the reproducing device, the presence of which constricts significantly the frequency response of undistorted signal transmission.

The purpose of the present invention is to increase the speed of the device and expand the operating frequency band.

This goal is achieved by adding a smoothing capacitor in parallel with the current limiter to the median-extraction device, which contains $2n + 1$ channels, each of which consists of a series-connected input scaling resistor, amplifier and current limiter, the output of which is connected to the output of the device and also to the input of the amplifier through a scaling feedback register.

The drawing shows the functional diagram of the device for extracting the median value.

Each channel of the device contains input scaling resistor 1, amplifier 2, current limiter 3, scaling feedback resister 4 and smoothing capacitor 5.

Amplifier 2 in each channel is connected to the common load through a parallel network (capacitor 5 - current limiter 3).

The device operates as follows.

When channels are switched, the change in the voltage at the output of the amplifier which had been in the linear region passes through smoothing capacitor 5 and resister 4 to the input of that amplifier, thus causing it to take longer for the amplifier to become saturated. When the times required for the amplifier to reach the saturated state and to exit that state are the same (which is easily achieved by selecting the value of capacitor 5), the distortions at the output of the device are fully eliminated, and the operating frequency band is increased to the bandwidth of a single amplifier used in its channels.



APPROVED FOR RELEASE: 2007/02/09: CIA-RDP82-00850R000500020034-7

APPROVED FOR RELEASE: 2007/02/09: CIA-RDP82-00850R000500020034-7



The use of the capacitor makes it possible to expand the operating frequency band maximally (up to the bandwidth of the amplifiers used) at minimum cost (one additional element per channel), while the operating frequency band of the prototype is narrower than the bandwidths of the amplifiers used in it by a factor of 2-4.

## Patent Claims

A device for extracting a median value, consisting of 2n + 1 parallel channels, each of which consists of series-connected input scaling resister, amplifier and current limiter, the output of which is connected to the output of the device and also through feedback scaling resistor to the input of the amplifier, distinguished by the fact that in order to increase speed and expand operating bandwidth, each channel contains a smoothing capacitor connected in parallel to the current limiter.

## Information Sources Used in Evaluation

1. Gil'bo, Ye.P., Chelpakov, I.B. "Obrabotka signalov na osnove uporyadochennogo vybora" [Signal Processing Based on Ordered Selection]. Moscow, Sovetskoye radio, 1975.

2. UK Patent No 1362378, class NKI G 4 G, published 1974 (prototype).

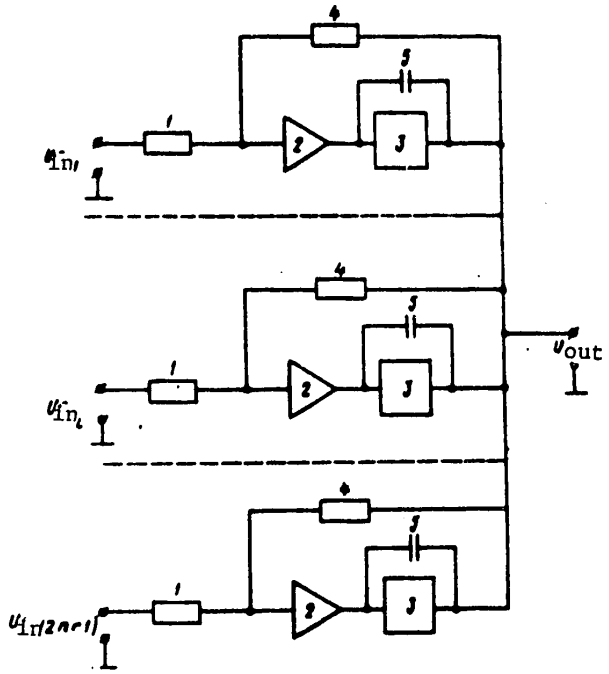


6900
CSO: 8144/0218-B



APPROVED FOR RELEASE: 2007/02/09: CIA-RDP82-00850R000500020034-7

APPROVED FOR RELEASE: 2007/02/09: CIA-RDP82-00850R000500020034-7



MICROPROCESSOR PSYCHODIAGNOSTIC DEVICE PATENT

Moscow OTKRYTIYA, IZOBRETENIYA, PROMYSHLENNYYE OBRAZTSY, TOVARNYYE ZNAKI in Russian No 29, 1981 (signed to press 10 Jul 81) p 296

[Text] Patent No 11032

Claim No 20122
Class 24-02

Microprocessor Psychodiagnostic Device

Authors: F. I. Romanov, N. V. Danilin, N. N. Zubov, P. K. Malyutin, V. A. Merkulov, A. V. Starshikov and M. A. Khadzhiakhmetov

Priority as of 1 August 1979

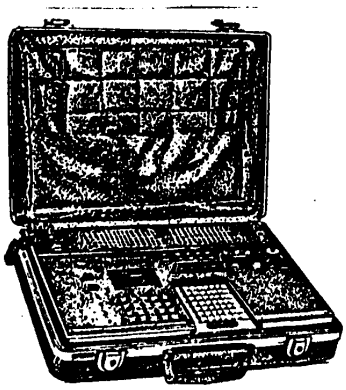

COPYRIGHT: VNIIPI, 1981

CSO: 1860/80-P



APPROVED FOR RELEASE: 2007/02/09: CIA-RDP82-00850R000500020034-7

APPROVED FOR RELEASE: 2007/02/09: CIA-RDP82-00850R000500020034-7



CERTAIN ASPECTS OF PHOTOGRAPHY, MOTION PICTURES AND TELEVISION

UDC 621.397.2

# TV CONTOUR DETECTOR

Moscow TEKHNIKA KINO I TELEVIDENIYA in Russian No 9, Sep 81 pp 40-43

[Article by A. V. Anan'in, T. S. Gryaznova and M. N. Stinov, Institute of Electrical Engineering of Communications, Novosibirsk]

[Text] One way of increasing the transit capacity of TV communications channels is to use adaptive TV systems capable, (depending upon the subject of the transmitted picture, dimensions of picture parts, the presence or absence of movements etc.), of controlling the TV channel parameters automatically. This makes it possible to eliminate redundancy in the transmitted data and multiplex the communications channel with additional data. Contour and motion detectors may serve as picture analyzers of such adaptive systems. The first are used to evaluate the contour dimensions of the picture parts and their complexity (presence of bends, sharp angles) and, therefore, the necessary width of the transmission band of the TV channel; the second are used to evaluate the speed of movement of the picture elements and, therefore, the possibility of such multiplexing in time at which there will be a hardly noticeable or no stroboscopic effect in the reproduced picture.

This paper considers one possible variation of the TV contour detector, in which the principle of electronic-optical filtration (EOF) is used. This method is the simplest from the technical implementation viewpoint and makes possible its wide use of standard TV equipment in the device.

As is well known, the statistical distribution of contour elements of real pictures have maxima in the vertical and horizontal directions; therefore, the problem of separating full contours can be considered solved to a great degree of authenticity if the problem of separating the vertical and horizontal boundaries of the contours is solved. The proposed device uses the filtration properties of the electron beam of an electron beam tube which has a certain aperture [1,2,3]. As shown in [4], the simplest filter capable of solving the problem of separating contour boundaries is electron-optical shading (shading focus).

The spectral function of energy distribution in the shading aperture of the beam for a normal law may be described by expression [4]



APPROVED FOR RELEASE: 2007/02/09: CIA-RDP82-00850R000500020034-7

APPROVED FOR RELEASE: 2007/02/09: CIA-RDP82-00850R000500020034-7



$$\tilde{\rho}(x, y) = \frac{1}{2\pi} \exp\left\{-\left(\frac{\omega_x^2}{4\beta_1^2} + \frac{\omega_y^2}{4\beta_2^2}\right)\right\}, \qquad (1)$$

where $\beta_1$ and $\beta_2$ are respectively horizontal and vertical dimensions of the shading.

As follows from (1), depending upon the orientation of the shading with respect to the scanning direction, it may fulfill the function of the lower $(\beta_2 > \beta_1)$, as well as the upper spatial frequencies $(\beta_1 \geq \beta_2)$. The EOF implementation process is shown in Fig. 1.

The shading aperture of the electron beam of receiving electron-beam tube can be formed by a single or double quadrupole magnetic lens[5], placed in the neck of the tube where there is no deflecting field.

The orientation of the shading from frame to frame is determined by the direction of the current in the coils of the quadrupole lens. If, in the first frame, the shading is oriented normally to the scanning direction and the horizontal boundaries of the contours are separated, then in the second frame, with a horizontal orientation of the shading, the vertical boundaries of the contours are separated.

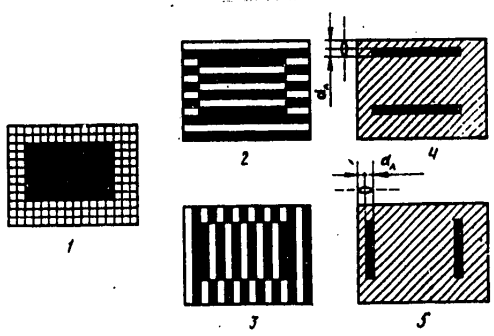


Fig. 1. Implementation of electron-optical filtration in the TV receiving tube. 1 -- initial picture; 2, 3 -- for polarity inversion of adjacent lines and elements and undistorted beam aperture; 4, 5 -- at EOF output of lower and upper boundaries.



APPROVED FOR RELEASE: 2007/02/09: CIA-RDP82-00850R000500020034-7

APPROVED FOR RELEASE: 2007/02/09: CIA-RDP82-00850R000500020034-7



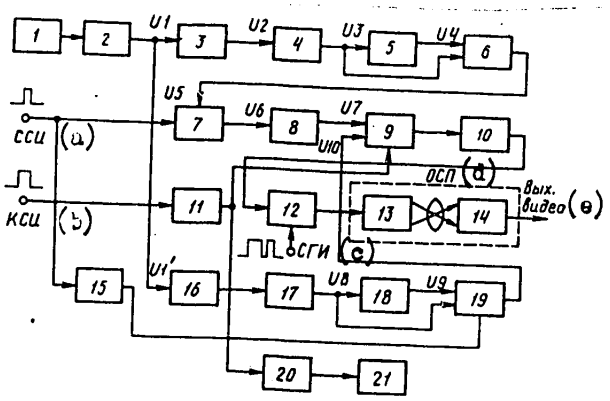


Fig. 2. Structural arrangement of a device for separating contours of optical objects.

a. SSI
b. KSI
c. SGI
d. OSP
e. Video output

A two-gradation operating mode is used in the device in which the output signal can assume only two values: "1" (white level) and "0" (black level). Reducing the signal to two grades (limiting the video signal output of the camera) improves the signal/noise ratio and eliminates the nonuniformity of the video signal. Moreover, processing the video signal in the digital form is simplified considerably. The block diagram of the device is shown in Fig. 2, and Fig. 3 shows the signal time diagrams at corresponding points of Fig. 2.

Video monitoring device 13 and TV transmitting tube camera form an optically coupled pair (OSP).

The vertical boundary signal is formed as follows.

The output signal from TV camera 1 is sent to video signal processing unit 2 in which the level of black is established. From the processing unit the signal is sent to amplifier-limiter 3 which reduces it to the two-gradation form. To improve the transition boundaries from black to white and back, the output signal of the amplifier-limiter is sent to forming device 4. To make possible the transition from black to white and back, it is necessary to have direct, as well as inverse video signals for which purpose inverter 5 is introduced in the circuit. Video signals are sent from the forming device to the strobing pulse former 6 that forms the pulses into decomposition elements $t_{эл}$ long, with the start of these pulses coinciding with the boundaries of changes in the brightness of the picture.



APPROVED FOR RELEASE: 2007/02/09: CIA-RDP82-00850R000500020034-7

APPROVED FOR RELEASE: 2007/02/09: CIA-RDP82-00850R000500020034-7



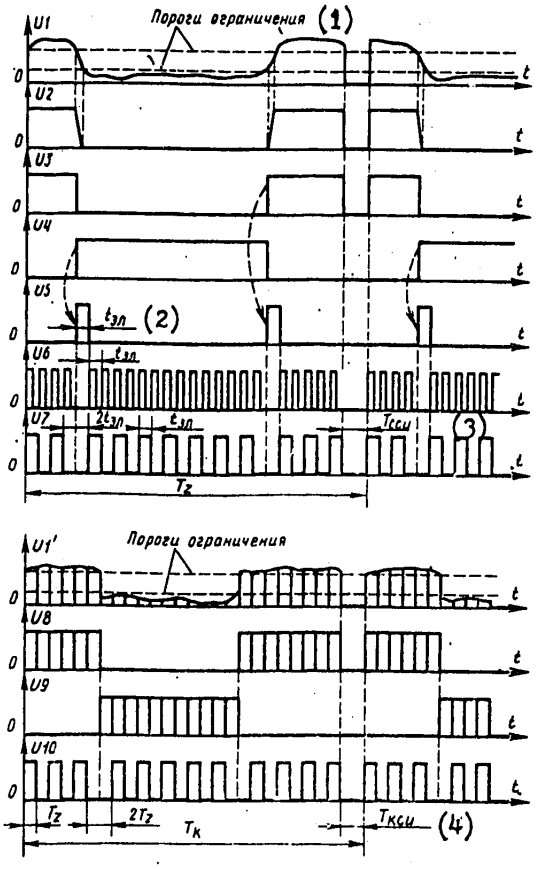


Fig. 3. Time diagrams of the separation process of vertical $U_p$ and horizontal $U'_p$ contour boundaries

1. Threshold boundaries
2. $t_{эл}$
3. $T_{ssc}$
4. $T_{ksi}$



APPROVED FOR RELEASE: 2007/02/09: CIA-RDP82-00850R000500020034-7

APPROVED FOR RELEASE: 2007/02/09: CIA-RDP82-00850R000500020034-7



To obtain element-by-element switching, an impact excitation oscillator 7 is introduced in the circuit which is synchronized by horizontal sync pulses (SSI). The oscillation period of the oscillator is equal to the time of decomposition element $t_{эл}$. From the impact excitation oscillator the signal is sent to trigger 8 and we have symmetrical pulses at the trigger output with a period equal to two decomposition elements $2t_{эл}$, i.e., an element-by-element switching is practically implemented.

If the initial picture contains the vertical boundary of the brightness drop, then a signal appears at the output of strobing pulse former 6 that disconnects impact excitation oscillator 7 for the duration of the decomposition element. In this case, at the trigger 8 output, two adjacent elements of the horizontal line have the same polarity at the moment the strobing pulse arrives. If the initial picture does not contain the vertical boundary of brightness drop, then there is no strobing signal, the oscillation mode of the impact excitation oscillator does not change and this means that the signals of all adjacent elements of each horizontal line have different polarities.

The formation of the horizontal boundary signal occurs as follows. The video signal from processing unit 2 is sent to amplifier-limiter 16 which changes it to the two-gradation form. Then the signal passes through forming device 17 and inverter 18. The direct and inverse video signals proceed to electronic switch 19 controlled by a symmetrical pulse with period $2t_z$ from trigger 15, initiated by horizontal sync pulse (SSI). As a result, direct and inverse signals in turn appear at the output of the electronic switch. If the initial picture contains a horizontal boundary brightness drop, the signal polarities of two adjacent lines coincide where the drops occur. When there is no horizontal boundary of brightness drop in the initial picture, the video signal polarities of adjacent lines are different.

As noted previously, the information on the full contour may be obtained by separating from the video signal one information frame about the vertical boundaries and another one about the horizontal boundaries. For this purpose, the output signals from element-by-element switching trigger 8 and line electronic switch 19 are sent to line electronic switch 9 controlled by symmetrical pulses with period $2T_k$ from trigger 11. The switch output signal is amplified by preamplifier 10 and is then sent to nonlinear adder 12 where quenching pulses SGI are mixed into it. The video signal formed in this manner is sent to video monitoring device 13 which is a component part of the coupled pair (OSP). The OSP in this case fulfills two basic functions: first, it provides for the output of information on the contours in the form of electrical signals, and secondly, due to the inertia of the transmitting tube of OSP camera 14, the alternation of information on the horizontal and vertical boundaries of the contours from frame to frame are transformed into continouous information.

The current direction in the quadrupole magnetic lens 21 coils, placed in the neck of the VKU [Video monitoring device] OSP kinescope, must change from frame to frame. This is achieved by a device for controlling quadrupole lens 20, done by



APPROVED FOR RELEASE: 2007/02/09: CIA-RDP82-00850R000500020034-7

APPROVED FOR RELEASE: 2007/02/09: CIA-RDP82-00850R000500020034-7



voltage-current converter [6] controlled by symmetrical pulses with a period of $2T_k$ produced by trigger 11.

A characteristic feature of the device is that, depending upon the spatial disposition of the initial picture elements, the contour boundaries observed on the VKU OSP screen may be dark or light with respect to background brightness.

The instantaneous brightness of the background $B_{cp}$ (averaging the brightness of two adjacent lines or elements when scanned by the shading aperture) and of the vertical $B_B$ and horizontal $B_г$ boundaries for double scanning of the phosphorus elements with a high afterflow time $\tau_{Л}$ is evaluated by expressions:

$$B_{\Phi}=0{,}5\,B_m\,\exp(-t/\tau_{Л}),\quad B_B\simeq B_г\simeq B_m\exp(-t/\tau_{Л}),$$

where $\tau_{Л}$ is the time constant of the phosphorus glow of the VKU kinescope; therefore, the brightness of light boundaries is found to be twice that of the background, while the brightness of the dark boundaries is equal to zero ($B_T=0$), when the modulation characteristic of the kinescope is fully utilized. In this case, the output signal of camers OSP is found to have three gradations ($m_{вых}=3$).

One of the basic parameters of the device is the contrast sensitivity which may be evaluated by the minimum signal/noise ratio that provides for a reliable separation of the optical object contours. For a small number of gradations, the following expression [7] is true:

$$\frac{\psi_{вых}}{k_m}=\sqrt{m_{вых}(m_{вых}+1)}, \qquad (2)$$

here $k_m$= coefficient that takes into account the reliability of detecting the boundary signal.

Although (2) is true for linear systems in which there are no gradation distortions ($\gamma=1$), it may be used to some approximation at the given case because $\gamma_{OSP}\simeq 1$. Value $k_m$ takes into account the presence of noises depending, as well as not depending, on the signal; therefore [7]:

$$\frac{1k}{\sqrt{2}}\leqslant k_m\leqslant\sqrt{2}\,k,$$

where lower boundary $k_m$ is set for systems in which there are no noises related directly to the signal (only external noises are present), while upper boundary k is for systems in which the noises are related directly to the signal. For estimating calculations, it may be assumed that $k_m=k$.



APPROVED FOR RELEASE: 2007/02/09: CIA-RDP82-00850R000500020034-7

APPROVED FOR RELEASE: 2007/02/09: CIA-RDP82-00850R000500020034-7



Coefficient k determines the probability of detecting the signal of boundary $p_c$ in a given interval of the OSP output signal. When relating k and $p_c$, determined by the probability interval, assuming $p_c=1-10^{-5}$ (error probability of $10^{-5}$ is entirely acceptable for machine data processing of contours) we will find $k \approx 4.42$. According to (2), in this case $\overline{\psi_{вых}} \approx 15$.

The obtained value $\overline{\psi_{вых}}$ must be fulfilled for the highest frequency components of the boundary signal, in this case for the signal of vertical boundaries that have frequencies of $f_B=6.5$ megaHz of the standard TV channel. If a vidicon transmitting camera is used in the OSP, the basic factors influencing the $\overline{\psi_{вых}}$ will be the noises of the output preamplifier stage (vidicon noises are insignificant and may be neglected), as well as aperture distortions of the vidicon. The first determine the value of the equivalent noise current at the preamplifier input and the second -- the reduction in the value of the signal current due to the aperture-frequency characteristic of the vidicon.

By using a simple antinoise correction and a field effect transistor at the input stage, the value of the equivalent noise current at the preamplifier input can be obtained by expression [8]:

$$i_ш^2 = \frac{4kT}{R} f + \int_0^f \left[ i_{шп}^2 + e_{шп}^2 \frac{1+(\omega RC)^2}{R^2} \right] df, \qquad (3)$$

where $i_{шп}$ -- equivalent quadratic mean of noise current of the field effect transistor; $1_{шп}$ -- equivalent quadratic means of noise emf of the field effect transistor; R -- resistance of vidicon load; C -- capacitance at amplifier input which includes the capacitance of the wiring, the input capacitance of the field effect transistor and the capacitance of the vidicon target with respect to the transistor source.

In accordance with (3), the aperture-frequency characteristic of the vidicon for Gaussian distribution of energy in the electron beam

$$\Phi(a_1; \xi) = \exp\left\{ -\left( \frac{\pi a_1 \xi}{2} \right)^2 \right\}, \qquad (4)$$

where $a_1=2r_1/\delta$ -- relative transverse dimension of the electron beam; $r_1$ -- its radius; $\delta = h/z$ -- scanning pitch; $\xi = m/z = f/f_B$ -- relative scanning frequency.

Using (3) and (4), the following expression can be used for the signal/noise ratio:



APPROVED FOR RELEASE: 2007/02/09: CIA-RDP82-00850R000500020034-7

APPROVED FOR RELEASE: 2007/02/09: CIA-RDP82-00850R000500020034-7



$$\psi = \frac{i_c \exp -\left(\frac{\pi a_1 \xi}{2}\right)^2}{\sqrt{\left[\frac{4kT}{R} + i_{шп}^2 + \frac{e_{шп}^2}{R^2}\right] f + \frac{4}{3}\pi^2 C^2 i_{шп}^2 f^3}}. \quad (5)$$

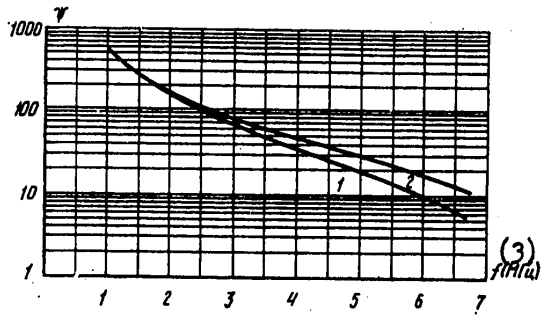


Fig. 4. Relationship between the signal/noise ratio of high frequency components of the contour boundary signal and transmission bandwidth of the device.

1. Vidicon LI415
2. Vidicon LI418
3. f(megaHz)

Fig. 4 shows the relationship between the signal/noise ratio of high frequency components of the contour boundary signal and the transmission band of the device designed on the basis of formula (5). In calculating curves in Fig. 4, the following parameter values were used: $i_c$=0.2 microamps; C=20 picofarads; R=1 megohm; the field effect transistor was

$$\text{KP303V}\left(i_{шп} \simeq 0.5\times10^{-16}\ \frac{\text{A}}{\sqrt{\text{Hz}}};\quad e_{шп} \simeq 5\times10^{-9}\ \frac{\text{B}}{\sqrt{\text{Hz}}}\right).$$

In the operating mode, taking into account the effect of reading the front edge of the beam and for standard raster dimensions $a_1 \simeq 0.8$ for LI415 and $a_1 \simeq 0.6$ for LI418.

It may be seen from Fig. 4 that for $f_B$=6.5 megaHz values $\psi$ =7 and $\psi$ =14 do not reach the necessary value of $\psi$ =15. However, if the transmission band is



APPROVED FOR RELEASE: 2007/02/09: CIA-RDP82-00850R000500020034-7

APPROVED FOR RELEASE: 2007/02/09: CIA-RDP82-00850R000500020034-7



reduced to 6.2 megaHz (quality indicators of the device will be practically preserved), it is possible to reach the required values of $\gamma_{вых}$ for the OSP camera using the LI418 vidicon. It follows from what was stated above that when using a device for separating contours in adaptive TV communications channels, higher resolution vidicons should be used in the OSP camera.

An experimental model of a device for separating contours made with an arrangement as per Fig. 2 had the following characteristics.

Swing of the output signal boundaries with load $\rho$ =150 ohms, not less than 0.5 volts.

Signal/noise ratio for vertical boundary of contour not less than 18 (vidicon LI418 used in the OSP camers).

Swings of control signals not less than 1.5 volts.

The investigations made confirmed the possibility of using the methods of electron-optical filtration in detectors of full contours of optical objects, which make it possible to create them on the basis of adaptive TV communications channels.

In conclusion, it must be noted that the method described for separating contours by the electron-optic filtration method may be implemented by two arrangements. In the first, electron-optical filtration is used directly in the TV transmitting tube as considered above. In the second case, it is necessary to have a spatial coupling between the basic TV camera and the camera for contour separation.

BIBLIOGRAPHY

1. Markovich, M. G.; Ol'khovitskiy, L. A.; Tsukkerman, I. I." Electron-Optical Filtration contours." TEKHNIKA KINO I TELEVIDENIYA. 1965, No 7, pp 41-44.

2. Baykin, I. A. "Spatial Filtration of Pictures by Simultaneous Scanning with Apertures of Different Dimensions and Shapes." Problems of Radioelectronics, series "Tekhnika televideniya." 1960, No 4.

3. Mezhov, F. D,; Noshchenko, V. S.; Seredinskiy, A. V. "Two-Dimensional Filter for Suppressing Interferences in TV Pictures." Problems on Radioelectronics, series "Tekhnika televideniya." 1968, No 1.

4. Gorelik, S. L.; Katz, B. M. "Electron Beam Tubes in Data Processing Systems." Moscow, "Energiya," 1977.

5. Markovich, M. G. "Short Double, Four-, Six-, Eight-Pole Lenses as Aberration Correctors When Deflecting Electron Beams." ZhTF [Journal of Technical Physics], 1972, No 1, pp 42-47.

6. Katayev, S. I.; Uvarov, N. B. "Voltage to Current Conversion for ELT [Electron Beam Tube]. TEKHNIKA KINO I TELEVIDENIYA, 1974, No 3, pp 55-57.



APPROVED FOR RELEASE: 2007/02/09: CIA-RDP82-00850R000500020034-7

APPROVED FOR RELEASE: 2007/02/09: CIA-RDP82-00850R000500020034-7



7. Gurevich, S. B. "Efficiency and Sensitivity of TV Systems." Leningrad, "Energiya," 1964.

8. Gershberg, A. Ye. "Transmitting TV Tubes with Internal Photoeffect." Leningrad, "Energiya," 1973.

9. Ryftin, Ya. A. "TV System," Moscow, "Sov, radio," 1967.

COPYRIGHT: "Tekhnika kino i televideniya", 1981

2291
CSO: 1860/77



APPROVED FOR RELEASE: 2007/02/09: CIA-RDP82-00850R000500020034-7

APPROVED FOR RELEASE: 2007/02/09: CIA-RDP82-00850R000500020034-7



UDC 621.397.13

# PARAMETER SELECTION OF OPTICAL SYSTEMS FOR SCANNING REPRODUCING DEVICES WITH KINESCOPES

Moscow TEKHNIKA KINO I TELEVIDENIYA in Russian No 9, Sep 81 pp 37-39

[Article by V. S. Babenko and A. I. Kravets, Institute of Civil Aviation Engineers, Kiev]

[Text] Scanning systems (TVS) include systems with comparatively large scanning angles along the horizontal (100° and greater). The scanning zone is increased and the efficiency of spatial perception is raised in scanning TVS which is especially important in several TV applications. In developing scanning TV systems it is necessary to solve a number of complicated problems related to the development of the general principles of scanning TV and the creation of scanning transmitting cameras, a communications channel and reproducing scanning devices (PVU).

In spite of the abundance of various projects, the closest to realization are scanning TV systems of the multichannel type. Multichannel PVU are used in such systems for the reproduction of pictures. The general visual field in such PVU is divided optically in three parts and is transmitted over three parallel channels. The scanned picture is reproduced either on a cylindrical screen by means of three TV projectors, or by several kinescopes. The basic shortcomings of projection PVU are awkwardness, complexity and high cost. The shortcoming of PVU using kinescopes is the relatively short observation distance and the presence of visible seams in the picture at the junction zone of the screens. Multichannel PVU with collimation system kinescopes are free from such shortcomings. Such systems, acting as magnifiers, make it possible to separate the pictures from the kinescope screens and transfer them comparatively long distances. In this case, parameters of the system may be selected so that there are no seams at the boundaries of the partial pictures. This improves the reproduction characteristics of space sharply and increases the scanning effect of the PVU.

We will consider the basic relationships for the optical part of this type of PVU and will determine the conditions that its parameters must satisfy. We consider the dimensions and other parameters of partial pictures in the kinescopes and the collimation systems equal, while the observation angles of the partial pictures are considered comparatively small.



APPROVED FOR RELEASE: 2007/02/09: CIA-RDP82-00850R000500020034-7

APPROVED FOR RELEASE: 2007/02/09: CIA-RDP82-00850R000500020034-7



The basic arrangement of the three-channel projection system (top view) of the PVU, satisfying these conditions is shown in Fig. 1.

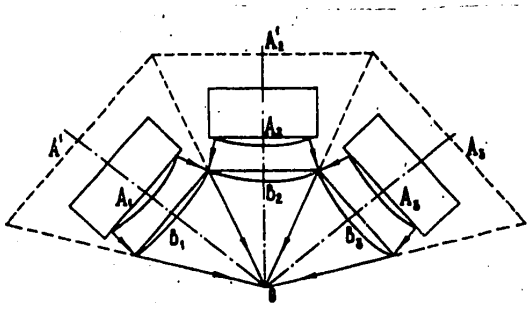

Fig. 1. Basic projection system (top view) for a three-channel PVU.

Partial pictures are formed on kinescope screens $A_1$, $A_2$ and $A_3$. These pictures are viewed by the observer from point 0 through lenses $L_1$, $L_2$ and $L_3$. The virtual images $A_1$, $A_2$ and $A_3$ viewed by the observer are amplified and carried a comparatively large distance. With a correct choice of the parameters of the projection system, the partial virtual pictures are found to be joined.

The course of beams in the channel for forming one partial picture is shown in Fig. 2. In calculating the dimensions of the projection system, it is necessary to take into account the conditions for joining the pictures on the kinescope screens and the virtual pictures; the virtual partial pictures along the horizontal; and the collimation lenses along the horizontal. The basic formulas relating to the optical parameters of an n-channelPVU are shown in the Table.

Depending upon the value of $b_{\text{п}}$ /f' the following cases are possible:

$l_{\text{п}}/f' > 1$, i.e., the eye of the observer is at a distance from the lens that exceeds the focal distance, and $b/b_{\text{п}} < 1$;

$l_{\text{п}}/f' = 1$, i.e., the eye of the observer is located at the focus of the lens and $b/b_{\text{п}} = 1$;

$l_{\text{п}}/f' < 1$, i.e., the eye of the observer is located a smaller than focal distance from the lens and $b/b_{\text{п}} > 1$.



APPROVED FOR RELEASE: 2007/02/09: CIA-RDP82-00850R000500020034-7

APPROVED FOR RELEASE: 2007/02/09: CIA-RDP82-00850R000500020034-7



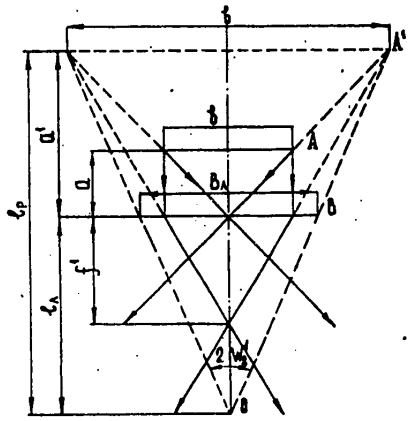

Fig. 2. Course of beams and basic values that determine the projection arrangement of the partial picture.

The analysis of the cited expressions indicates that the smallest optical distortions and the greatest boundaries for possible location of the observer's eye with respect to the lens corresponds to the case where the observer is removed from the lens by a distance that exceeds the focal distance. However, in this case, the angles of the viewed partial pictures are comparatively small ($2W'_r$ =10 to 20°); therefore, a fairly large number of kinescopes must be used in the PVU. The fact that the film should be wider than the picture on the kinescope screen should also be considered a drawback. Of interest is the case where the observer is located in the focal plane of the lens since conditions for joining the elements of the optical system in this variation do not depend on amplification. But such a system may be realized only when the lens parameters satisfy relationship

$$b_n/2f' = \operatorname{tg} W_r.$$

In the third case (distance between observer and lens is less than the focal distance), large viewing angles $2W'_r$ may be obtained with a small number of kinescopes. But under such conditions, various kinds of optical picture distortions are more prominent and the boundaries of possible spatial location of the observer's eye are minimal.

In calculating the PVU projection system, horizontal $2W_r$ and vertical $2W_B$ angles of the pictures viewed are initial. The remaining values are partially given and partially determined. The following variations of dimensional calculation are



APPROVED FOR RELEASE: 2007/02/09: CIA-RDP82-00850R000500020034-7

APPROVED FOR RELEASE: 2007/02/09: CIA-RDP82-00850R000500020034-7



Table

| Parameters | Formulas* |
|---|---|
| Primary partial pictures: | |
| width | $b = [b_л + 2f'(V-1)\operatorname{tg} W'_г]/V$ |
| height | $h = [h_Л + 2f'(V-1)\operatorname{tg} W_в]/V$ |
| distance between centers of adjacent kinescope screens | $d = 2(l_Л + a)\sin W'_г$ |
| Lenses | |
| focal distance | $f' = l_л[V(b/b_Л) - 1]/(1-V)$ |
| width | $b_Л = 2l_л \operatorname{tg} W'_г$ |
| height | $h_л = 2l_л \operatorname{tg} W'_в$ |
| Projection system | |
| distance from lens to kinescope screen | $a = f'(V-1)/V$ |
| distance from lens to observer | $l = l_р - a' = b_л/2\operatorname{tg} W'_г$ |
| system amplification | $V = \left(\frac{h'}{h}\right) = \left(\frac{b'}{b}\right) = b_Л(l_л + f')/(L_в b - b_Л f')$ |
| Virtual image | |
| width | $b' = bV = 2l_р \operatorname{tg} W'_г$ |
| height | $h' = hV = 2l_р \operatorname{tg} W_г$ |
| distance from lens | $a' = (b - 2l\operatorname{tg} W'_г)/(2\operatorname{tg} W'_г - b/f')$ |
| Observations | |
| general horizontal viewing angle | $2W_г = 2nW'_г$ |
| horizontal angle of partial picture viewing | $2W'_г + 2\operatorname{arctg}(b/2l_р)$ |
| vertical viewing angle | $2W_в = 2\operatorname{arctg}(h/2l_р)$ |
| viewing distance | $L_р = l_л + a = b'/2\operatorname{tg} W'_г$ |

*Values in formulas explained in Fig. 2.

typical for the considered problems. According to the given dimension of the picture on the kinescope screen and the dimensions of the resulting picture, it is possible to determine the parameters of the lens and the mutual location of the elements of the projection system. When the dimensions of the picture on the kinescope screen and the parameters of the lens are given it is possible to calculate the values that determine the mutual position of the elements of the projection system. Another variation of the calculation is possible if the dimensions of the resulting picture and of the parameters of the lens are given. In this



APPROVED FOR RELEASE: 2007/02/09: CIA-RDP82-00850R000500020034-7

APPROVED FOR RELEASE: 2007/02/09: CIA-RDP82-00850R000500020034-7



case, the position of the elements of the projection system and the dimensions of the pictures on the kinescope screens are determined

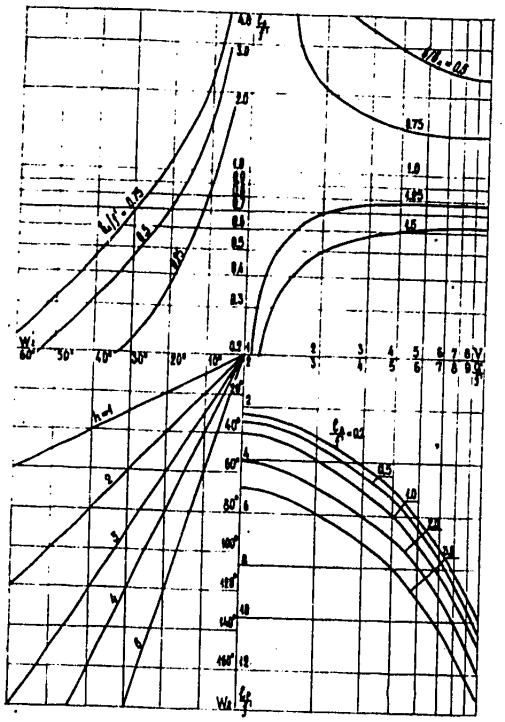

Fig. 3. Nomogram for calculating the basic PVU parameters.

To illustrate the nature of the relationships and to evaluate the realizability regions, a nomogram is shown in Fig. 3 that interconnects the basic parameters of the projection system. This nomogram eases the PVU calculations greatly. When calculating the dimensions of the PVU projection system, it is necessary to proceed from the minimum number of channels (the number of kinescopes and lenses respectively).

When using standard kinescopes and complete filling of their screen with pictures, ratio b/h is 1.25 to 1.33 for horizontal and 0.75 to 0.8 for the vertical position of the width of the kinescope screen. The problem of selecting the number of kinescopes may be simplified by using the nomogram in Fig. 4 that shows the relationship between viewing angles $W_r$ /$W_B$ and the number of kinescopes for various



APPROVED FOR RELEASE: 2007/02/09: CIA-RDP82-00850R000500020034-7

APPROVED FOR RELEASE: 2007/02/09: CIA-RDP82-00850R000500020034-7



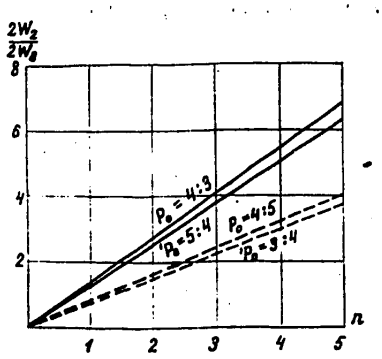


Fig. 4. Nomogram interconnecting the relationship between viewing angles $W_г / W_в$ and the number of kinescopes at various orientations of kinescope screens:

———— - horizontal orientation kinescope screens;

— — — — - vertical orientation.

orientations (horizontal and vertical) of their screens. It should be taken into account that the number n should be only discrete. If ratio $W_г / W_в$ produces fractional n, then its values must be rounded out to the nearest whole number and a smaller value of n will mean a less full utilization of the height of the screen while a greater value -- a less full utilization of the width of the screen. The utilization of the vertical position of the kinescope screens for a given $W_г / W_в$ ratio is related to an increase in the number of kinescopes and lenses, but makes it possible to increase the dimensions of the resulting picture. Utilizing kinescopes with large screens makes it possible to obtain large pictures with moderate amplifications, but is related to the necessity of using larger diameter lenses.

Single lenses produce geometrical and chromatic distortions, especially noticeable at the edges of the field of the picture. These distortions are greater the greater the system amplification and the greater the deviation of the observer's eyes from the central position. Practically, the amplification should not be greater than 3 to 5, while the spatial position of the observer's eyes when viewing the pictures should not change essentially. Geometrical and chromatic distortions may be reduced by introducing correcting elements into the optical system whose parameters are determined as a result of corresponding calculations. The distortions may be reduced considerably in a two-lens system, although the system complexity is increased while the coefficient of the optical transmission is reduced.



APPROVED FOR RELEASE: 2007/02/09: CIA-RDP82-00850R000500020034-7

APPROVED FOR RELEASE: 2007/02/09: CIA-RDP82-00850R000500020034-7



The necessity of using lenses of fairly large dimensions causes serious difficulties. The use of plastic Fresnel lenses may be considered a compromise solution. However, the use of such lenses leads to noise caused by beats between the TV picture and the lens rasters. PVU of the mirror type are free from many shortcomings of the lens systems, since their basic optical elements are spheric mirrors. For spatial spacing between kinescopes and the observer, additional semitransparent mirrors are used in mirror PVU that complicate the system and, what is very essential, reduce the optical transmission coefficient. The calculation of mirror PVU dimensions has, of course, specific features although the basic principles are the same as for lens PVU.

To obtain high quality pictures, special measures must be taken on the mechanical, optical and electrical matching of components and projection system parameters of partial pictures. Single type kinescopes with matched characteristics (color, brightness and contrast) must be used in the channels. Distortions caused by noncorrespondence in position, dimensions, linearity and partial pictures (especially along the vertical) etc. should be reduced to a minimum.

In conclusion, we will note that the principles considered above may be used to calculate the dimensions not only of scanning, but also of wide-angle VU [Reproducing devices] of the mosaic type whose picture field is composed of kinescope screens set up on both the horizontal and vertical directions.

COPYRIGHT: "Tekhnika kino i televideniya", 1981

2291
CSO: 1860/77



APPROVED FOR RELEASE: 2007/02/09: CIA-RDP82-00850R000500020034-7

APPROVED FOR RELEASE: 2007/02/09: CIA-RDP82-00850R000500020034-7



UDC 681.84: 621.3.037.372

# MULTIMICROPROCESSOR SYSTEM FOR PROCESSING AUDIO SIGNAL IN FREQUENCY REGION

Moscow TEKHNIKA KINO I TELEVIDENIYA in Russian No 9, Sep 81 pp 24-28

[Article by Ye. I. Grinberg and M. I. Peregud, All-Union Scientific Research Motion Picture Institute]

[Text] The process for producing phonograms for cinema films is related to a large number of conversions implemented on the initial audio signals. In the development of equipment and methods for the digital processing of audio signals it is possible to separate a number of stages, each of which is typical in its level of treatment of computer facilities.

In the first stage, at the beginning of the seventies, investigations of basic types of signal conversions on universal computers began. The most important result of the work at this stage was the understanding of the necessity to create specialized devices to process signals in real time and use Fourier transformations for the implementation of almost all kinds of filtration of the audio signal [3].

In the second stage, work was done on creating specialized digital devices with low and medium degrees of integration. Due to the high cost of implementing computer operations on the given component base, digital delay lines, reverberators and other devices using the delay line principle became the first to be used widely in audio recording equipment [1, 4].

At present, considerable experience has accumulated in our country and abroad on simulating the digital conversion processes of audio signals, and creating specialized devices to implement individual functions.

The realization of the majority of electroacoustic conversions (adaptive noise reduction, adaptive interference compensation, frequency correction) is related to the calculation of a signal packet with a pulse characteristic of a converter.

Inasmuch as the most efficient method is calculating packets in the frequency region, a multimicroprocessor system for processing audio signals was created as a basis, using equipment to transform initial Fourier signals.



APPROVED FOR RELEASE: 2007/02/09: CIA-RDP82-00850R000500020034-7

APPROVED FOR RELEASE: 2007/02/09: CIA-RDP82-00850R000500020034-7



The parameters of the system were selected on the basis of work carried out in the electroacoustic laboratory of the NIKFI [All-Union Scientific Research Motion Picture Institute] [3].

According to the results of the indicated work, the system should be able to do the following:

1. Implement audio signal conversion in the frequency region for discretization frequencies of up to 40 kHz in real time, process the spectrum and restore the signal in the time domain.

2. Implement audio signal conversion into a 16-bit binary code with a total error not exceeding 3 to 4 low-order bits (the number of spectral components up to 1024 complex numbers).

3. Provide the possibility of being increased to provide for processing in real time signals with higher discretization frequency.

4. Provide the possibility of simultaneous conversion of several audio signals with a joint processing of the spectral characteristics.

5. Be inexpensive, small and light, highly efficient and have a single type of universal system to carry out investigations, as well as to produce specialized devices on its basis.

6. Have a design anticipating the connection of new data sources and users without changing the equipment part of the system center.

7. Have a low level of internal audio noises, required for operation in specialized places.

The purpose of this paper is to describe the design of the system and its component parts for processing signals with the greatest discretization frequency. In appropriate comments, possibilities will be indicated for reducing the system when the discretization frequency and the number of initial signals are lowered.

The basic problem in creating the system is the implementation of direct and inverse Fourier transformations of the high speed initial signal.

The realization of the Fourier processor using low and medium degrees of integration circuits leads to very substantial expenditures for microcircuits and current consumption and, as a result, to a high cost of equipment, large size, low reliability etc.

In recent years, the appearance of domestic microprocessors made it possible to design economical Fourier processors. The series K589 microprocessor set was selected as the basic one.

The given set has the highest speed of operation among the microprocessors being manufactured.



APPROVED FOR RELEASE: 2007/02/09: CIA-RDP82-00850R000500020034-7

APPROVED FOR RELEASE: 2007/02/09: CIA-RDP82-00850R000500020034-7



The microprogram organization makes it possible to control, by expanded arithmetic, external circuits simultaneously with the operation implementation in the processor. The indicated advantages determine practically a one-to-one choice of series K589 series microprocessors for the Fourier analysis of the audio signals.

The general structure of the system is shown in Fig. 1. Four basic parts may be separated in the system: specialized processors with an expanded arithmetic on the K589 microprocessor series, analog-digital and digital-analog converters for communications with sources and users of audio data, a control device with the 580 series of microprocessors and service equipment.

The initial audio signals are converted by analog-digital converters from the analog to the digital form and are stored in a buffer memory. As it becomes freed, the first specialized processor reads the stored data. Having implemented a given number of algorithm "layers" on the obtained data, the specialized processor, in the course of implementing its last own algorithm "layer," transfers the intermediate results to the next specialized processor and introduces the next in turn input readings. All specialized processors included in the system operate the same. Thus, all specialized processors operate in parallel which makes it possible to provide for processing signals in various ranges of frequency discretization by changing the number of specialized processors. When increasing the discretization frequency, the number of layers in the algorithm being implemented in one processor is reduced, while the number of processors is increased, insuring the required transit capacity of the system.

For comparatively low discretization frequencies (in the case of processing speech signals, in the digital adaptive interference compensator etc.) the number of algorithm "layers" implemented in one processor is increased, while the total number of processors in the system is reduced. This general principle for designing systems for processing rapidly flowing signals, which provides for the implementation of the above-cited basic requirements, was laid at the basis of creating a multimicroprocessor system to process audio signals in the frequency region.

The last specialized processor processes the obtained spectrum (for example, multiplication by the weighting function, smoothing etc.) and transfers the processed values to the first processor for implementating the inverse Fourier transformation.

After completing the algorithm of the inverse Fourier transformation, the data from the last specialized processor are entered into the buffer memory (or into the required external device), which implements the equalization of the period of output readings ahead of the digital-analog converter.

The calculation of the weighting functions for processing the spectrum, the required constants, the loading of data into the last specialized processor and the system control are implemented by the control unit made of series K580 microprocessors. The use of the microprocessors is determined by the requirements of the relative simplicity of programing and the comparatively low speed in receiving the data. The system controller is used basically only in the investigating complex, since the required data is already calculated and stored in the permanent memory of the last specialized processor.



APPROVED FOR RELEASE: 2007/02/09: CIA-RDP82-00850R000500020034-7

APPROVED FOR RELEASE: 2007/02/09: CIA-RDP82-00850R000500020034-7



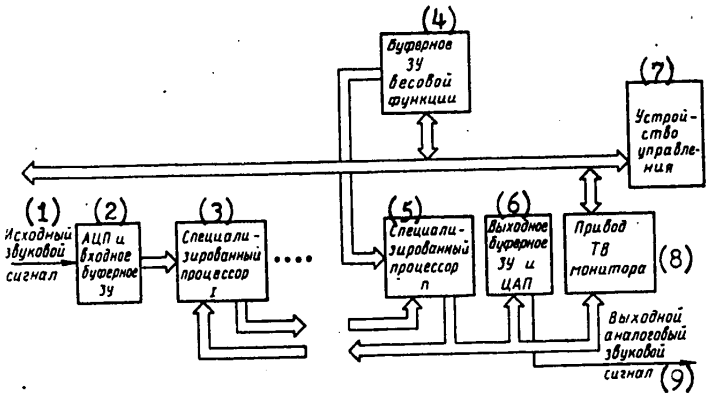


Fig. 1. Structure of a multiprocessor system for processing audio signals in the frequency regions.

1. Initial audio signal
2. Analog-digital converter [ATsP] and input buffer memory
3. Specialized processor 1
4. Buffer memory of the weighted function
5. Specialized processor n
6. Output buffer memory and analog-digital converter
7. Control unit
8. Drive of TV monitor
9. Output analog audio signal

Service devices make it possible to represent the spectral characteristics obtained on the TV monitor and assign the required amplitude-frequency characteristics by means of a "light pen."

The specialized processor consists of the following: the 16-bit processor proper, a parallel 16x8 bit multiplier, a permanent memory (PZU) of trigonometric functions and output registers.

It is well known [1, 2] that conversion done on each reading in each "layer" of the rapid Fourier transformation (BPF) algorithm consists of four multiplier operations and several adding operations where one of the multipliers is a sine or cosine of the given argument. Since the multiplication operation and, especially, the calculation of the trigonometric functions made in the processor require large expenditures of time, a multiplier and a permanent memory of trigonometric constants are introduced into the specialized processor as external devices.



APPROVED FOR RELEASE: 2007/02/09: CIA-RDP82-00850R000500020034-7

APPROVED FOR RELEASE: 2007/02/09: CIA-RDP82-00850R000500020034-7



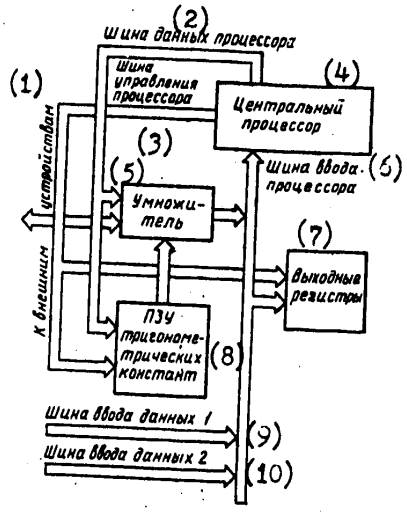


Fig. 2. Structural arrangement of the specialized processor

1. To external devices
2. Processor data bus
3. Processor control bus
4. Central processor
5. Multiplier
6. Processor input bus
7. Output registers
8. Permanent memory for trigonometric functions
9. Data input bus 1
10. Data input bus 2

The processor itself (Fig. 3) consists of eight microcircuits of the K589IK02 central process unit [TsPE], a K589IK03 accelerated transfer circuit, a K589IK01 microprogram control unit (BMU), a microprogramed permanent memory made of K556RT5 components and a main memory made of K541RU1 microcircuits.

In the reprogramable permanent memory (PPZU) there are recorded microprograms for implementing those concrete "layers" of the algorithm done by the given processor, set in a concrete position in the system's structure.



APPROVED FOR RELEASE: 2007/02/09: CIA-RDP82-00850R000500020034-7

APPROVED FOR RELEASE: 2007/02/09: CIA-RDP82-00850R000500020034-7



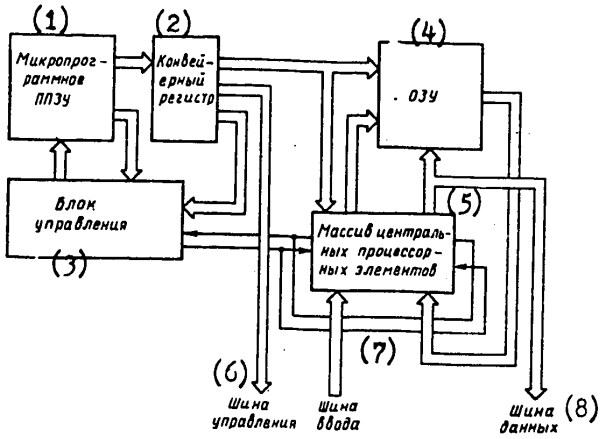


Fig. 3. Structure of the central processor

1. Reprogramed permanent memory (PPZU)
2. Conveyor register
3. Control unit
4. Main memory
5. Data file of the central processor components
6. Control bus
7. Input bus
8. Data bus

Besides the microprogram of the given part of the total algorithm of the system, service microprograms for cleaning out the main memory (OZU), the initial setting of all processor registers and expanded arithmetic, as well as monitoring the efficiency of the processor are recorded in the PPZU.

Each microinstruction along with standard control fields BMU and TsPE, includes nonstandard control fields of recording and readout processes of all external circuits connected to the processor and the OZU. Additional registers are introduced into the processor circuit to increase the operating speed of the processor and span the operations conveyor registers in time which are installed at the outputs of microprogram PPZU and make it possible to reduce the synchronous signal period of the processor. Input registers of data and OZU addresses make it possible for the central processor units to do the conversions without waiting for the end of the access cycle to the OZU.

The OZU has a capacity of 4K 16-bit words. Half the memory is used for storing the intermediate results of direct conversion, while the second half -- for storing the intermediate results of the inverse Fourier transformations (the result of the calculations -- up to 1024 absolute values of the spectrum and up to 1024 phase points).



APPROVED FOR RELEASE: 2007/02/09: CIA-RDP82-00850R000500020034-7

APPROVED FOR RELEASE: 2007/02/09: CIA-RDP82-00850R000500020034-7



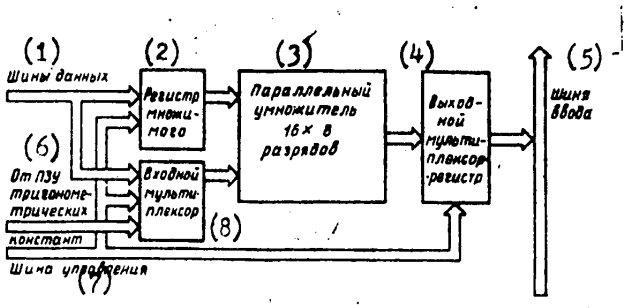


Fig. 4. Structural arrangement of the multiplier

1. Data bus
2. Multiplicand register
3. Parallel 16x8 bit multiplier
4. Output multiplexer register
5. Input bus
6. From permanent memory of trigonometric functions constants
7. Control bus
8. Input multiplexer

The basic processor functions are:

1. Form addresses, data and control signals for microprogram PPZU, OZU and PZU trigonometric constants.

2. Do arithmetic operations of adding and subtracting taking into account the signs of the values.

3. Control loading and reading of multiplier data.

4. Control data recording into output registers and data reading from ATsP or previous specialized processors. Also control the weighting function and required OZU functions.

In choosing the structural arrangement of the multiplier, it is necessary to establish a compromise between expenditures for equipment and speed of operation taking into account the possibilities of the remaining parts of the specialized processor. The structural arrangement of the multiplier is shown in Fig. 4. Its operational part is a parallel 16x8-bit multiplier.

The multiplicand value is stored in a 16-bit register. Data to the multiplicand register inputs is entered from the data buses of the central processor. The



APPROVED FOR RELEASE: 2007/02/09: CIA-RDP82-00850R000500020034-7

APPROVED FOR RELEASE: 2007/02/09: CIA-RDP82-00850R000500020034-7



control of recording in the multiplicand register is implemented by a separate microinstruction field.

An 8-bit number is entered into the multiplier inputs from the multiplexer outputs. In accordance with the address sent to the multiplexer input from the separate microinstruction field, the multiplier may use the high-order byte in the PZU of trigonometric constants, the low-order byte of the same PZU, the high-order byte on the data processor buses or the low-order byte on the data processor buses.

The output multiplier multiplexer sends either 16 high-order bits of the result or 8 high-order bits of the results to the input processor buses.

To reduce the size and power consumption of the multiplicand register, the input and output multiplexers are made with K555 series microcircuits. Such a connection of the multiplier to the processor makes possible rapid implementation of operations on the number in the process of calculating the direct and inverse Fourier transformations, as well as in processing the obtained spectral characteristics.

Besides the multiplier, two data sources that have a controlled tristable output (for example,, the ATsP and the preceding specialized output) may be connected to the buses of the input/output processor.

Permission for the passage of data from the ATsP or preceding specialized processor is given by separate microinstruction fields. The specialized processors are coupled by means of an output register made of K555IR16 microcircuits.

The absolute value and phase are calculated in the last specialized processor in accordance with the obtained 1024 complex readings of the spectrum. Each point of the absolute value may be multiplied by the corresponding value of the weighting function (or processed according to the given algorithm) after which the results obtained are sent to the first specialized processor for the start of the inverse process of the Fourier transformation. Reading the weighting function values and the required constants in processing the spectrum is implemented over the second external bus (instead of over the ATsP output).

To provide for the possibility of a flexible change in the system of the number of specialized processors, a complex of microprograms is being developed that takes into account the distribution of the number of "layers" in the BPF algorithm in each specialized processor.

Conclusions

The analysis which was carried out indicated that in using three specialized processors (each mounted on three KAMAK plates), it is possible to convert, process and restore audio signals with discretization frequencies of 40 kHz in real time.

Connecting 10 specialized processors makes it possible to expand the frequency range of the processed signals to discretization speeds of 100-125 kHz.

If, in the investigation process, it is required to obtain spectra without restoration of signals in the time domain, then for the same number of special processors the discretization frequency may be doubled.



APPROVED FOR RELEASE: 2007/02/09: CIA-RDP82-00850R000500020034-7

APPROVED FOR RELEASE: 2007/02/09: CIA-RDP82-00850R000500020034-7



At present, only schematic diagrams have been developed. The design documentation for the system is being developed.

BIBLIOGRAPHY

1. Rabiner, P.; Gould, B. "Theory and Application of Digital Processing of Signals." Moscow, "Mir," 1978.

2. Gold, B.; Reyder, Ch. "Digital Processing of Signals." Moscow, "Sov. Radio," 1973.

3. Belkin, B. G. "Development of a Digital System for Recording-Reproducing Sound in Motion Pictures. "Tekhnika kino i televideniya," 1978, No 11, pp 3-12

4. Belkin, B. G.; Baryshnenkov, Yu. N.; Gordon, M. G.; Neverovskiy, K. V.; Raver, L. Yu.; Tsygankov, M. V. "Digital Devices for Processing Audio Signals in Real Time." Teletekhnika-80" exhibition. Scientific-Technical reports. 1980.

COPYRIGHT: "Tekhnika kino i televideniya", 1981

2291
CSO: 1860/77



APPROVED FOR RELEASE: 2007/02/09: CIA-RDP82-00850R000500020034-7

APPROVED FOR RELEASE: 2007/02/09: CIA-RDP82-00850R000500020034-7



UDC 791.44.025: 681.322

# AUTOMATIC RESTORATION OF MOVIE FILMS BY COMPUTER

Moscow TEKHNIKA KINO I TELEVIDENYA in Russian No 9, Sep 81 pp 32-36

[Article by B. L. Borilin and V. V. Pospelov, USSR Scientific-Research Center of Technical Documentation]

[Excerpts] In recent years, automated methods for processing pictures based on using the computer are being used widely [7-16]. These methods are used to solve problems of various natures; automatic analysis of pictures, recognition of visual images, improvement of picture quality, easing of their visual interpretation etc. The processing of pictures with computers consists of three basic stages:

conversion of the picture into digital form and its introduction into the computer;

mathematical processing of the digital data in the computer;

withdrawal of the processed digital data from the computer and its reverse conversion into a picture.

Picture processing in digital form may be done in two modes: automatically in accordance with given programs, and in a dialogue mode with the computer, a process in which the operator watching the picture on a TV screen of a special display can intervene in the processing, selecting necessary programs and their parameters.

The automated methods used to solve the problem of eliminating defects and raising the quality of the picture make it possible to do the following:

eliminate a large number of picture defects (correction of various distortions and filtration of various kinds of interferences);

process the entire picture, as well as its individual parts up to its smallest elements with dimensions of $10^{-2}$ to $10^{-3}$ mm;

carry out the processing with high flexibility due to the dialogue selection of programs and parameters;

obtain high reproducibility of processing results due to the ability of the computer to repeat many times and convert the picture to a given accuracy;



APPROVED FOR RELEASE: 2007/02/09: CIA-RDP82-00850R000500020034-7

APPROVED FOR RELEASE: 2007/02/09: CIA-RDP82-00850R000500020034-7



preserve the original picture fully since only its "digital image" is subjected to the conversions;

reduce the number of manual operations to a minimum.

Due to its advantages, methods for processing pictures by computers are used widely for improving the quality of space, astronomic, medical and other pictures which is confirmed by many publications [12-14, 17-20]. This article describes briefly the results of the theoretical and experimental investigation of the automated method of restoring photographic documents, and discusses the possibilities and prospects for automated restoration of films at the NITsTD SSSR.

Any black and white photograph and photographic document can be represented mathematically by a function of two variables $U(x, y)$ that describes the optical density distribution in the photographic material plane. The defective photographic document may be described by another function $V(x, y)$ obtained from $U(x,y)$ by several conversions

$$V=A(U) \qquad (1)$$

The difficulty in the problem of restoring the initial picture $U(x,y)$ is that, as a rule, the exact form of operator A is unknown.

Therefore, hypotheses are proposed with respect to the kind of conversion of A, on the basis of the analysis of the distorted document, after which the parameters of this conversion are chosen in the process of solving equation (1) on the computer. The correctness criterion of the proposed hypothesis and of the parameters selected is an expert evaluation of the quality of the restored picture $\tilde{U}(x,y)$.

As a result of investigating defects of archival photographic documents [21], it was proposed to divide them into seven groups: frequency-contrast, gradation, cracks, structural, spots, scratches, and other defects (not included in the basic groups).

Mathematical models of the most typical defects of photographic documents of the six basic groups are now available and theoretical and experimental investigations of methods for their elimination by means of a computer were carried out [22]. It was established that the most efficient are dialogue (interactive) methods for the restoration processing of photographic documents which allow the operator flexibility in controlling the restoration process by watching the picture and selecting the necessary programs and parameters to process it.

The investigations done made it possible to formulate basic requirements for the automated system for processing pictures (ASOIZ) intended for the restoration of photographic documents.

The ASOIZ was created on the basis of the LSI-2 minicomputer, apparatus for input-output of photographs of the American firm "Optronics" and the Pericolor" (France) display processor [23]. At present, system software is being developed and production work is being done (so far on a small scale) on digital restoration and recording in digital form of unique and especially valuable photographic documents of the USSR State Archives Fund.



APPROVED FOR RELEASE: 2007/02/09: CIA-RDP82-00850R000500020034-7

APPROVED FOR RELEASE: 2007/02/09: CIA-RDP82-00850R000500020034-7



We will consider the possibilities and prospects of the automated restoration of movie films. The black-and-white movie film is described mathematically by a function of three variables U(x,y,t) where t is time; a color movie film is a vector function {R(x,y,t), G(x,y,t), B(s,y,t)} where R, G, B are respectively the red, green and flue components of the optical density of the color movie film. If each frame of the black-and-white movie film in the digital form represents a two-dimensional data file of 1.5 million eight-bit binary digits, then the volume of digital data containing the information about the entire movie film will be tens of billions of bytes. Processing such large data files, even with modern powerful computers, is impossible at present. However, the rapid development of computer equipment makes it possible to hope that digital restoration of movie films may be done in the near future. In our opinion, promising ways to solve this problem are:

using matrix processors that make it possible to process in parallel thousands of picture elements (by using such a processor, a rapid Fourier transformation of a data file of a thousand numbers may be made in 0.01 seconds [25]);

creating programs controlled digital devices that do various operations on processing pictures in real time (with the speed of the video signal passing through them).

In this case, the ASOIZ could play the role of a system that would develop algorithms for the elimination of typical defects in movie films. Then specialized devices, created on the basis of these algorithms, would make it possible to process hundreds of movie film frames at a high speed.

As already mentioned before, from the mathematical standpoint, a movie film may be considered as a function of three variables. An important feature of this function is the presence of two groups of variables essentially different in nature: these are spatial variables x, y and time variable t. For such functions a very promising interference filtration method is an expansion of this function into a bilinear series [24]:

$$U(x,y,t)=U_1(x,y)\ \varphi_1(t)\quad U_2(x,y)\ \varphi_2 t\quad \ldots \qquad (2)$$

Obviously, in restoring movie films, it is advisable to subdivide them into parts (plans) containing uniform frames averaging 2 to 3 seconds in length.

The general principles of designing a system of digital processing of movie films were formulated by L. F. Artyushin [26]. Automated systems for restoring movie films must consist of a specialized ASOIZ containing three basic subsystems: converting movie films into digital forms and back; processing and storing data files of digital data; visual representation of digitalized movie films.

Requirements of these three subsystems are greater than the corresponding ASOIZ subsystems intended for restoration of movie films. The subsystem for converting movie films into digital form and back may be created on the basis of high speed TV or laser scanning devices (for example, electronic copying equipment for



APPROVED FOR RELEASE: 2007/02/09: CIA-RDP82-00850R000500020034-7

APPROVED FOR RELEASE: 2007/02/09: CIA-RDP82-00850R000500020034-7



element-by-element printing of movie film pictures [27]). The subsystem for processing and storing digital data files must contain a high speed computer operating in the time sharing mode (or a complex of several computers), a matrix processor, specialized program control digital devices for processing pictures and high capacity (about $10^8$ bytes) magnetic disc memories.

The subsystem for visual representation of the digitalized movie films must be an interactive display processor (one or several), equipped with a main memory, a high speed processor and flexible dialogue facilities for processing the pictures (light pen, courser, trackball etc.)

The processes for the input-output of movie film pictures and the transfer of digital data files between subsystems must be controlled by micro or minicomputers without the loss of time by the central system processor.

The development of an automated system for restoring movie film pictures is a complicated but realistic problem, substantiated by an already created electronic multiplication system and by obtaining combined movie film pictures by computers [28, 29]. In the future, when automated systems for processing movie film pictures are introduced in practice, it will become possible to use digital methods to create movie films. Their realization will open up great prospects for the restoration of movie films, as well as for the development and improvement of technical and creative cinematography processes.

BIBLIOGRAPHY

1. "Manual for Recognizing and Eliminating Defects in Movie Films and Microfilms." All-Union Scientific Research Institute of Document Management and Archives. Moscow, 1973.

2. Fridman, I. M.; Petrov, A. I. "Storing Lenin's Movie Films." TEKHNIKA KINO I TELEVIDENIYA, 1970, No 4, pp 19-26; 1980, No 4, pp 3-7.

3. Volkman, H. "Thesen zur Dauerkonservierung und Restaurierung Audiovisueller Informationstrager." Berlin, 1975.

4. "Storage and Restorational-Conservational Processing of Movie Films and Microfilms." Interrepublic Technical Conditions (for Document Standardization) 55-4-69. Moscow, 1969.

5. "Movie Films. Additional (Restoration-Preventive) Processing of Initial Film Materials at Cinema Studios and Movie Film Copying Factories. "RTM [Guiding Technical Materials] 19-6-71. Moscow, 1971.

6. "Restoration of Faded Photographs. Review of Domestic and Foreign Literature on Motion Picture Equipment." Moscow, 1973, No 1 (5).

7. Rozenfeld', A. "Recognizing and Processing Pictures by Digital Computers." Moscow, "Mir," 1972.



APPROVED FOR RELEASE: 2007/02/09: CIA-RDP82-00850R000500020034-7

APPROVED FOR RELEASE: 2007/02/09: CIA-RDP82-00850R000500020034-7



8. Grishin, M. P.; Kurbanov, Sh. M; Markelov, V. P. "Automatic Input and Processing Photographs by Computers." Moscow, "Energiya," 1976.

9. Khant, B. R. "Digital Processing of Pictures." in book "The Use of Digital Processing of Signals." Moscow, "Mir," 1980 pp 192-267.

10. "Processing of Pictures and Digital Filtration." T. Khuang, editor. Moscow, "Mir," 1979.

11. Endryus, G. "Use of Digital Computers for Processing Pictures." Moscow, "Energiya," 1977.

12. "Iconics. Spatial Filtration of Pictures. Photographic Systems." Symposium of articles, D. S. Lebedev, editor. Moscow, "Nauka," 1970.

13. "Iconics. Digital Holography. Processing of Pictures." Symposium of articles, D. S. Lebedev, editor. Moscow "Nauka," 1975.

14. "Iconics. Digital Processing and Filtration of Pictures" D. S. Lebedev, editor. "Problems of Cybernetics." No 38, Moscow, VINITI [All-Union Institute of Technical Information], 1978.

15. "Processing Pictures by Digital Computers." Symposium of articles, G. Endryus and L. Inlo, editors. Moscow, "Mir," 1973.

16. Yaroslavskiy, L. P. "Introduction to Digital Processing of Pictures." Moscow, "Sov. Radio," 1979.

17. Belikova, T. P.; Kronrod, M. A.; Chochia, P. A.; Yaroslavskiy, L. P. "Digital Processing of Pictures of the Mars Surface transmitted by "Mars-3" and "Mars-4" AMS [Automatic Mars Station]. "Space Investigations," 1975, 13, No 6, pp 898-906.

18. "Space Investigations of the Earth. Methods of Processing Video Data by Computers." Moscow, "Nauka," 1978.

19. Klimenko, V. L. "Digital Processing of Pictures." "Radioelectronics Abroad" 1975, No 4 pp 13-32.

20. Digital Processing of Signals and its Application." Symposium of articles, L. P. Yaroslavskiy, editor. Moscow, "Nauka," 1981.

21. Borilin, B. L. "Qualimetric Evaluation of Archive Document Defects. "SOVETSKIYE ARKHIVY, 1981, No 3 pp 37-40.

22. Borilin, B. L.; Chochia, P. A. "Restoration of Photographs by Computers." SOVETSKIYE ARKHIVY, 1980, No 3 pp 45-48.

23. Borilin, B. L.; Pospelov, V. V. "Restoration and Conservation of Photographs by Computers." Express information. VNII Documentation and Archive Management, Series "Norms and Specifications for Storing Documents." 1980, No 2 (11), pp 1-7.



APPROVED FOR RELEASE: 2007/02/09: CIA-RDP82-00850R000500020034-7

APPROVED FOR RELEASE: 2007/02/09: CIA-RDP82-00850R000500020034-7



24. Pospelov, V. V. "Approximation of Functions of Several Variables by Products of Functions of One Variable." Preprint IPM [Institute of Applied Mathematics] 1978, No 32.

25. Integral Array Processor for Eclipse S/250. Prospectus of Data General Co., United States.

26. Artyushin, L. F. "Prospects of Using Electronic and Computer Equipment in Technological Processes of Cinematography." TEKHNIKA KINO I TELEVIDENIYA, 1979 No 11, pp 7-17.

27. Artyushin, L. F.; Ioshin, O. I.; Ovilko, O. G.; Muchiyev, S. G. "Kinotelevision System of Printing and Recording Color Pictures by a Laser Beam on a Movie Film from Film Materials and Video Tapes. "TEKHNIKA KINO I TELEVIDENIYA," 1977, No 7, pp 3-11.

28. Tel'nov, N. I. "Processing Pictures by Computers and Electronic Multiplication." TEKHNIKA KINO I TELEVIDENIYA," 1978, No 7, pp 70-81.

29. Holt, W. The New Electronic Composite Photography and Image Modification system. American Cinematographer, 1975, 5, No 4, pp 421-425, 438, 474.

COPYRIGHT: "Tekhnika kino i televideniya", 1981

2291
CSO: 1860/77



APPROVED FOR RELEASE: 2007/02/09: CIA-RDP82-00850R000500020034-7

APPROVED FOR RELEASE: 2007/02/09: CIA-RDP82-00850R000500020034-7



COMMUNICATIONS, COMMUNICATION EQUIPMENT, RECEIVERS AND TRANSMITTERS, NETWORKS, RADIO PHYSICS, DATA TRANSMISSION AND PROCESSING, INFORMATION THEORY

UDC 621.372 (088.8)

# MICROWAVE DELAY LINE

Moscow OPISANIYE IZOBRETENIYA 637900 in Russian 15 Dec 78

[Description of USSR Patent No 637900 by A.V. Vashkovskiy, V.I. Zubkov, V.N. Kil'dishev and B.A. Murmuzhev, filed 9 Dec 76, published 15 Dec 78, class H 01 1 P 9/00]

[Text] This invention is in the area of radio engineering and can be used in antenna feeder systems to delay microwave signals.

A microwave delay line exists which contains a rectangular magnetized ferrite plate and input and output coaxial antennas installed at opposite ends of the ferrite plate [1].

However, this device has a small delay; furthermore, parasitic resonances are excited in it.

The purpose of the present invention is to increase the delay time and eliminate parasitic resonances.

In order to accomplish this, the ferrite plate in the microwave delay line contains an additional flat metal spiral with width and spacing which are multiples of half the length of the surface magnetostatic wave; furthermoer, the beginning and end of the metal spiral are located directly at the coaxial antennas, which are installed at opposite corners of the plate; the portion of the ends of the ferrite plate on which the metal spiral is wrapped is rounded.

The drawing presents a diagram of the proposed microwave delay line.

The microwave delay line consists of rectangular magnetized ferrite plate 1 and input and output coaxial antennas 2 and 3; ferrite plate 1 is furthermore magnetized by permanent magnet 4, and metal spiral 6 is wrapped around its rounded ends 5; in addition, input and output coaxial antennas 2 and 3 are fastened to opposite ends 7 of ferrite plate 1.

The microwave delay line operates as follows.

Input coaxial antenna 2 in the vicinity of face 7 of ferrite plate 1 excites a surface magnetostatic wave signal which propagates along the waveguide region



APPROVED FOR RELEASE: 2007/02/09: CIA-RDP82-00850R000500020034-7

APPROVED FOR RELEASE: 2007/02/09: CIA-RDP82-00850R000500020034-7



formed by flat metal spiral 6 and the adjacent upper surface of ferrite plate 1. The surface magnetostatic wave signal follows rounded phase 5 to the bottom of ferrite plate 1 and propagates to the poposite side along the second turn of flat metal spiral 6.

Thus, the surface magnetostatic wave signal moves from the top of ferrite plate 1 to its bottom n times (where n is the number of turns of flat metal spiral 6), each time propagating over a different turn of flat metal spiral 6 to output coaxial antenna 3, where the surface magnetostatic wave signal is converted to a delayed electromagnetic signal.

25

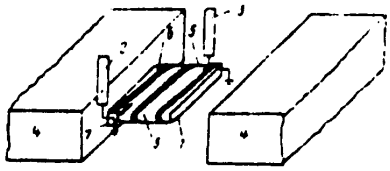

Patent Claims

1. A microwave delay line containing a rectangular magnetized ferrite plate and input and output coaxial antennas fastened to opposite faces of a ferrite plate, distinguished by the fact that in order to increase delay time and eliminate parasitic resonances, an additional flat metal spiral is wound on the ferrite plate with width and spacing multiples of half the length of the surface magnetostatic wave; furthermore, the metal spiral begins and ends directly at the coaxial antennas, which are fastened to opposite diagonals of the plate.

2. A microwave delay line as described in paragraph 1, distinguished by the fact that the portion of the faces of the ferrite plate around which the metal spiral is wound.

Information Sources
Used in Evaluation

1. L.H. Brundte, N.J. Freedmann 1, "Electron. Lett" 1968, ¶4, 7, p. 132.

6900
CSO: 8144/0218-B



APPROVED FOR RELEASE: 2007/02/09: CIA-RDP82-00850R000500020034-7

APPROVED FOR RELEASE: 2007/02/09: CIA-RDP82-00850R000500020034-7



UDC 621.372.8:535

# METHODS FOR FINDING BREAKS IN OPTICAL CABLES

Moscow ELEKTROSVYAZ' in Russian No 9, Sep 81 (manuscript received 4 Aug 80) pp 25-28

[Article by S.M. Vernik and A.M. Kuznetsov]

[Text] Successful operation of communication links is determined to a significant extent by the capability for finding breaks with sufficient accuracy. The solution to this problem usually involves major difficulties both in developing measurement methodology and in creating measurement instrumentation. For optical cable communication links (OCCL), especially long links with attenuation on the order of 30-40 dB, solving this problem involves additional difficulties arising from the complexity of the propagation and reflection of light signals in optical fibers (OF).
We shall examine possible methods for finding breaks in OF and OC as a whole, primarily methods suitable for use on long links.

It is known that not all actual breaks in an optical fiber (OF) result in complete cessation of signal propagation. For example, a break in an OF with vertical spalling and 2-5 μm separation of the OF in the cable causes only an insignificant increase in signal attenuation. Therefore, we shall consider an OF break to be damage which causes the propagation of light energy to crease completely. There are three basic methods for locating OF breaks.

The method of measuring the light energy emitted into the environment is used for quality control of initial semifinished items, or "bars", from which optical fibers are drawn, and for finding OF breaks and large (of the order of 2-3%) imperfections. Quality control of bars is done by irradiating them with a visible-spectrum gas laser ($\lambda$ = 0.62 μm). When this is done, the spots at which the OF imperfections are located glow. The quality of the bar can be judged by the intensity of the glowing and the number of glowing spots. By processing the visual observations statistically, a correlation can be established between bar quality and OF imperfections.

The spots in which large OF imperfections are located emit part of the light signal energy into the environment. The measurement signal input to the OF consists of powerful light transmissions (on the order of 1-3 W) transmitted at a frequency



APPROVED FOR RELEASE: 2007/02/09: CIA-RDP82-00850R000500020034-7

APPROVED FOR RELEASE: 2007/02/09: CIA-RDP82-00850R000500020034-7



of 1-5 KHz. The light signals emitted into the environment are captured by the photodetector in the receiver and converted to current (voltage) pulses, which are then amplified in a high-gain narrowband amplifier which is tuned to the repetition frequency of the light pulses.

During the measurement process, the OF is moved with respect to the photodetector and the radiation intensity is recorded, with the power distribution of the emitted signals along the OF characterizing the distribution of the imperfections. The location of a break in the OF usually corresponds to high amplitude of the emitted signal. Preliminary findings indicate that this method can be implemented if the dynamic range of the receiver is between 110 and 140 dB.

The method of measuring the intensity of Rayleigh backscatter is widely used in measuring the distribution of imperfections along OCCL and the internal attenuation of OF and OC.

Figure 1 shows a functional diagram of a measuring device which implements this method. The measured OCCL 5 is pulsed with short (2-5 ns) high-power light pulses (1-2 W), which are input to the optical cable through differential device 4. The reflected backward scattered flux reaches receiver 6; the screen of CRT 7 (or other display) displays the intensity of the backward scattered flux as a function of the length of the line (or signal propagation time), as well as the location of imperfections in the optical fiber. A break in the OF is characterized by a sharp drop in scattered power.

The basic shortcoming of this method is the low level of the backward scattered flux, which prevents this method from being used to find breaks in long OCCL because of the insufficient sensitivity of the receiver. In addition, when there are relatively large imperfections (which occurs at the existing level of OF and OC fabrication technology) the power of the oncoming light pulse flux may be significantly higher than the power of the Rayleigh scattering flux. This circumstance results in distortion of the measurement findings.

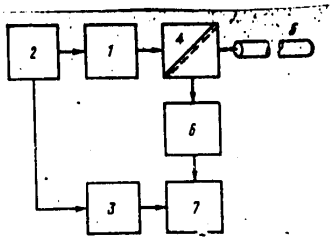


Figure 1

The location method for finding breaks in optical fibers is identical to the impulse method of measuring imperfection distribution on cable communication links.

The functional diagram of the instrument used in the location method is analogous



APPROVED FOR RELEASE: 2007/02/09: CIA-RDP82-00850R000500020034-7

APPROVED FOR RELEASE: 2007/02/09: CIA-RDP82-00850R000500020034-7



to figure 1. Generator 1, which outputs light pulses 5-10 ns long is triggered by electronic master oscillator 2, which simultaneously triggers CRT sweep generator 3 with a slight delay ($\tau_z$). The outgoing pulse is passed through differential system 4 into the measured optical fiber 5. Part of the energy reflected from imperfections in the OF creates a backward light flux which reaches photodetector 6 and is converted to voltage pulses. After amplification in amplifier 7, these are applied to the vertical plates of the CRT, causing the electron beam to be deflected up or down from the middle of the y axis. The arrival time of the reflected pulses is registered in the scale of the sweep time s(t), which is easily converted to the distance in kilometers to the break (figure 2):

$$x = 0.5\ s(t)\ v \tag{1}$$

where v is the propagation speed of light energy.

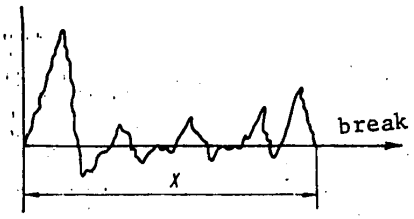


Figure 2

The location of the break is determined by the distance x, beyond which no reflected pulses reach the receiver.

The main difference between the parameters of the scheme in figure 1, which is used to measure the location of breaks and distribution of imperfections using the location method, and the parameters of analogous schemes used to measure the intensity of the backward scattered flux, is that the receiver used in the location method has a narrower operating bandwidth. This makes it possible to implement a receiver amplifier with a dynamic range of 50-60 dB. Furthermore, as was indicated above, the signals reflected from imperfections and breaks usually exceed the intensity of the backward scattered flux by several orders of magnitude. This method thus makes it possible to make measurements on long OCCL.

It is apparent from examining the functional diagram in figure 1 and the description of its operation that it is analogous to the well known circuits used in type R5 or UIP devices [3], which are intended for investigating the distribution of imperfections and finding breaks in cable conductors as a large imperfection in which the coefficient of reflection is equal or close to unity. This circumstance is of great significance, since it makes it fairly simple to implement a device to determine a location of optical fiber breaks in the



APPROVED FOR RELEASE: 2007/02/09: CIA-RDP82-00850R000500020034-7

APPROVED FOR RELEASE: 2007/02/09: CIA-RDP82-00850R000500020034-7



form of an attachment to the type R5 devices which are in quantity production. However, when measuring optical cables it is necessary to allow for the singularities of optical signal propagation and reflection of optical flux in optical fibers, which lead to the appearance of additional errors.

Error of location method. During transmission over optical fibers, optical signals are attenuated due to losses in the OF, which causes the energy of the outgoing light pulse $W_0$ at the end of an optical cable with length L to drop to

$$W_L = W_0 e^{-0.23\alpha L} \tag{2}$$

where $\alpha$ is the OF attenuation factor, dB.

The energy of a pulse fully reflected from the end of the line as measured at the beginning of the line

$$W_{ref} = W_0 e^{-0.46\alpha L} \tag{3}$$

Knowing the amount of attenuation of an OCCL repeater section $a_{rep}$, we can determine the minimum dynamic range of the instrument $a_{min} = 2a_{rep}$. In order to determine the dynamic range of the instrument, we must add to $a_{min}$ the attenuation $a_{iref}$ which characterizes the energy loss during reflection at a point located at a distance of $L_i$ from the beginning of the OCCL. These losses are random, and comprise the function $\psi_i$ of the set of random quantities made up of the absolute value of the coefficient of reflection at the ith point $P_i$, the distribution of the angles at which light waves of various modes are reflected from the surface of the break in the optical fiber $\phi_i\mu$, where $\mu$ is the mode number of the light wave. Furthermore, $a_{iref}$ is a function of the OF aperture angle $\theta$ and the propagation conditions for individual modes in the OF. Thus,

$$a_{iref} = \psi_i (P_i, \phi_i, \theta) \tag{4}$$

is random as well.

Figure 3 shows some possible profiles of optical fiber breaks and the oscillograms of the reflected signals which correspond to them. The smallest losses occur if the surface of the break is perpendicular to the axis of the fiber (figure 3a), while the greatest losses are observed if the angle between the plane of the break and the axis of the fiber is 45° (figure 3b); when the surface of the break is complex (figure 3c), the amount of loss is random. In addition to losses due to reflection, losses in the differential section $a_{dif}$ of the measuring instrument must also be allowed for. Consequently,



APPROVED FOR RELEASE: 2007/02/09: CIA-RDP82-00850R000500020034-7

APPROVED FOR RELEASE: 2007/02/09: CIA-RDP82-00850R000500020034-7



$$a_{in} = 2a_{rep} + a_{ref} + a_{def} \quad (5)$$

If we limit ourselves to measuring the location of an optical fiber break from both sides of a repeater sector,

$$a_{in\ min} = a_{rep} + a_{ref} + a_{def} \quad (6)$$

The maximum value of $a_{in}$ which can be realized in practice is 80-90 dB with outgoing pulse power of the order of the 1-2 W. Losses in the differential device are usually 8-10 dB [1], while the attenuation of the repeater sector is 30-35 dB. It follows from this that $a_{ref}$ cannot be more than 0-10 dB when measuring from one end of a repeater sector; the value is 25-35 dB when measuring from both ends, which makes it possible to locate the OF break quite accurately.

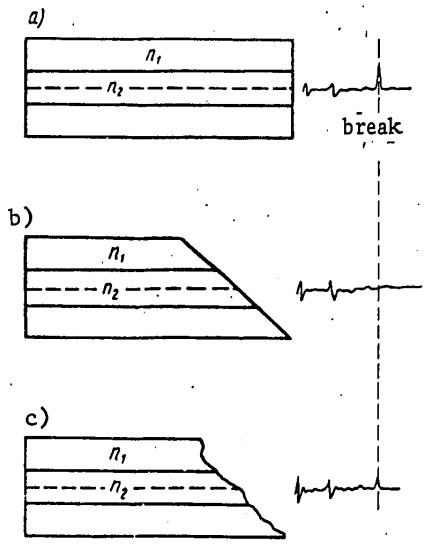


Figure 3

THe duration of the pulsing signal also has an effect on the error in determining the location of an OF break [2]. In determining this error, allowance must be made for pulse stretching in the line. Propagating through an optical fiber, a light pulse with duration $t_0$ at the beginning of the fiber stretches due to the dispersion of the OF material, the relationship between the group delay time and the mode number of the light waves, and the random dispersion of the group



APPROVED FOR RELEASE: 2007/02/09: CIA-RDP82-00850R000500020034-7

APPROVED FOR RELEASE: 2007/02/09: CIA-RDP82-00850R000500020034-7



delay time values in the optical fiber.

These distortions cause the outgoing pulses to become longer in proportion to their distance from the light source. As a result, the resolution of the method is uneven: it is greatest at the beginning of the line and least at the end. The amount by which a pulse is stretched depends upon the type of fiber and the characteristics of the radiation source.

For example, when an incoherent light pulse with duration $t_0$ is transmitted through a multimode fiber, it stretches to a length of [1]

$$t_1 = (t_0^2 + \Delta\tau_d^2 L^2 + \Delta\tau^2 L^2)^{\frac{1}{2}}, \tag{7}$$

by the end of a repeater sector with length L, where $\Delta\tau$ is the dispersion of the group delay time per unit of length in the multimode fiber caused by the presence of different modes; $\Delta\tau_d$ is the pulse expansion per unit of length due to dispersion in the material and the dispersion of the intrinsic waves.

When the intrinsic modes are mixed in fiber imperfections, the pulse at the end of the fiber expands to a value of [1]

$$t_1 = (t_0^2 + \Delta\tau_d^2 L^2 + \Delta\tau^2 L_c L)^{\frac{1}{2}}, \tag{8}$$

where $L_c$ is the average length of the optical fiber within which there is a complete exchange of energy between modes.

In practice $L > L_c$; $\Delta\tau >> \Delta\tau_d$ and the amount of pulse widening $\Delta t$ is proportional to $\sqrt{L}$. For example, for $n/n = 0.01$ the dispersion $\Delta t$ of the group delay time is 48.4 ns/km, while it is 24.2 ns/km for a coherent light source. For a gradient fiber, we have 4.84 ns/km and 2.42 ns/km, respectively. Thus, with an outgoing pulse of $t_0$ = 10 ns, when the light source is incoherent the pulse stretches to 34.2 ns by the end of the first kilometer of the line. These data indicate that there is no point in making the outgoing pulses any shorter than 5-10 ns.

The maximum measurement error of the location of a break corresponds to the maximum value of $a_{ref}$, where no reflected pulse is observed on the screen of the instrument at the point of the break (cf. figure 3b). In this case, the operator usually assumes that the break is located at the fiber imperfection which is closest to the pulse generator (figure 4a), which has the appearance shown in figure 4b after the break. The measurement error here will be determined by the highly regular sector $l_{reg}$ of the optical fiber where no reflected pulses are observed.

As the quality of optical fibers improves, $l_{reg}$ will increase to the length of the optical cable lines, since junction reflections which are recorded by pulsed devices generally arise at the points at which cables are joined.



APPROVED FOR RELEASE: 2007/02/09: CIA-RDP82-00850R000500020034-7

APPROVED FOR RELEASE: 2007/02/09: CIA-RDP82-00850R000500020034-7



With the help of the location method, these reflections can be used to determine the structural length of the optical cable within which the break has occurred.

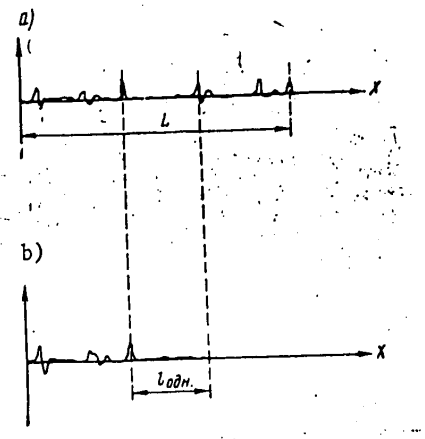


Figure 4

Conclusions. Analysis of the location method for finding optical fiber breaks shows that possible measurement errors are a strong function of a number of random factors which can lead to intolerably large error. In order to limit this error, it is seen as advisable during OCCL construction to measure the distribution of imperfections along the cable and include these characteristics in the OCCL documentation. Changes in these characteristics, as measured from both ends of a repeater sector and supplemented with factual data concerning the length of optical cable structural segments, the distribution of imperfections, the amounts of reflections at structural interfaces and the actual optical cable attenuation can be used to judge the steadiness of optical cable parameters by periodically measuring the distribution of imperfections, and to find optical fiber breaks more precisely. The characteristic of the distribution of imperfections obtained during these latter measurements can be used as a baseline for finding optical fiber breaks. Measuring the distribution of imperfections from both ends of a repeater section to the point of a break and beyond will promote a further improvement in the accuracy of locating fiber breaks.

Bibliography

1. Unger, G.G. "Opticheskaya svyaz'" [Optical communication]. Moscow, Izdatel'stvo svyaz'", 1979.



APPROVED FOR RELEASE: 2007/02/09: CIA-RDP82-00850R000500020034-7

APPROVED FOR RELEASE: 2007/02/09: CIA-RDP82-00850R000500020034-7



2. Grodnev, I.I., et. al., "Koaksial'nye kabeli svyazi" [Coaxial Communication Cables]. Moscow, Izdatel'stvo "svyaz'", 1970.

3. Kuchikyan, L.I. "Fizicheskaya optika volokonnykh svetovodov" [Physical Optics of Fiber Light Guides]. Moscow, Izdatel'stvo "Energiya", 1979.

4. Muradyan, A.G., Ginzburg, S.A., "Sistemy peredachi informatsii po opticheskomu kabelyu" [Systems for Transmitting Information Over Optical Cable]. Moscow, Izdatel'stvo "svyaz'", 1980.

5. Teumin, I.I., "Volnovody opticheskoy svyazi" [Optical Communication Waveguide]. Moscow, Izdatel'stvo "svyaz'", 1978.

6. Makhlin, R.Ye., Titov, I.V., "Measurement of Reduced Coefficient of Reflection From End of Fiber During Break in Cable of Fiber Optic Communication Link," Pis'ma v ZhTF", Vol. 1, No. 11, 1975.

7. Makhlin, R.Kh, Kuznetsov, A.A., Titov, I.V., "Observation of Optical Pulses Reflected From Distant End of Fiber", Radiotekhnika i elektronika, Vol. 20, No. 6, 1975.

8. Guttman, J., Krumpholz, O., "Location of Imperfections in Optical Glass-Fiber Waveguides," Electronics Letters, 1975, Vol. 11, No. 10

9. Veno Y. Motoh Shimizu. Optical Fiber Fault Location Method. Applied Optics. 1976, Vol. 15, No. 6.

10. Personik, C.D., Photon Probe - an Optical-Fiber Time Domain Reflectometer, PSTJ, 1977, Vol. 56, No. 3.

11. "Detection and Localization of Fiber Breaks in Optical Communication Cables", NTZ, Vol. 90, No. 11, 1977.

COPYRIGHT: IZDATEL'STVO "RADIO I SVYAZ'","ELEKTROSVYAZ'", 1981

6900
CSO:1860/61



APPROVED FOR RELEASE: 2007/02/09: CIA-RDP82-00850R000500020034-7

APPROVED FOR RELEASE: 2007/02/09: CIA-RDP82-00850R000500020034-7



UDC 621.373.43

# CONTROL SYSTEM FOR ARC DISCHARGER SWITCHING USING FIELD DISTORTION TECHNIQUE

Moscow PRIBORY I TEKHNIKA EKSPERIMENTA in Russian No 4, Jul-Aug 81 (manuscript received 30 Nov 79) pp 133-135

[Paper by A.I. Gerasimov and Ye.G. Dubinov]

[Text] A discharger-enhancer filled with a gas up to 1 MPa is inserted in breaks in 26 cable sections, charged up to an identical potential difference of 15 to 30 KV, each with its internal conductor connected to the control electrode of its own arc discharger. When all of the cables are shorted (impedance of 2 ohms) by a common switcher, the rise time of their discharge current wave, $T_1$ = 40 to 70 nsec, is reduced by the enhancer down to 3.8 nsec. The scatter in the instants of discharge enhancer is $\leq 0.1\ T_1$. The discharge is of a multichannel nature when the discharge enhancer is filled with nitrogen and has a gap of 1 to 2 mm between the electrodes.

In dischargers where the electrical field distribution is distorted, it is necessary to rapidly change the polarity of the control electrode voltage [1]. When synchronously switching a large number of dischargers, sections of coaxial cables are used, the inner conductors of which connect the control electrodes of the dischargers and the switcher which is common to all the cables [2-4]. The precision of the mutual actuation of the dischargers, as well as the uniformity of the development of the current channels in them and the current distribution over the channels depend substantially on the rise time of the cable discharge current [2, 3]. If the cables which are connected in parallel to the shorting switcher number several tens of cables, while their charging voltage $U_0$ is $\geq$ 20 KV, then the rise time of the current through the switcher is usually $\geq$ 10 nsec.

A system of 26 sections of RK-50-11-13 cables (overall impedance of $\rho$ = 2 ohms) connected in parallel, which makes it possible to generate a cable discharge current wave with a rise time of < 5 nsec when $U_0 \geq$ 15 KV, is described in this paper.

A schematic of the control system for the 26 dischargers being actuated, $P_1$--$P_{26}$, and the switcher for the capacitive store C or the individual storage devices driving the load, V, is shown in Figure 1. The innner conductor of a RK-50-11-13





APPROVED FOR RELEASE: 2007/02/09: CIA-RDP82-00850R000500020034-7

APPROVED FOR RELEASE: 2007/02/09: CIA-RDP82-00850R000500020034-7



cable section 10 m long is connected to each control electrode 1 of the dischargers. The high voltage electrodes 2 and the storage device C have a potential of U applied, while electrodes 1 and the center conductors of the cables have a potential $U_0$ of the same polarity applied; $U_0$ usually is 0.3U - 0.5U. A common gas filled discharge enhancer, RO, similar to that described in [5], is inserted in breaks in the inner conductors of the cables. The equalization of the potentials shared by the electrodes of the enhancer of the cables sections of the shaping line (FL) and peaking line (OL) is accomplished through inductance coil L and resistor $R_1$; the peaking line section can be connected to the charging source just as the shaping line section. The switch K serves to short the cable. The parameters of the discharge current pulses of the shaping and peaking line cable sections are measured across shunt resistors $R_2$ and $R_3$, consisting of 20 TVO-0.25 resistors connected in parallel which are positioned in breaks in the outer conductors, while the voltage pulses at electrode 3 and at control electrodes 1 are measured by capacitive dividers $D_1$ ($C_1$, $C_2$,) and $D_2$ ($C_3$, $C_4$) respectively.

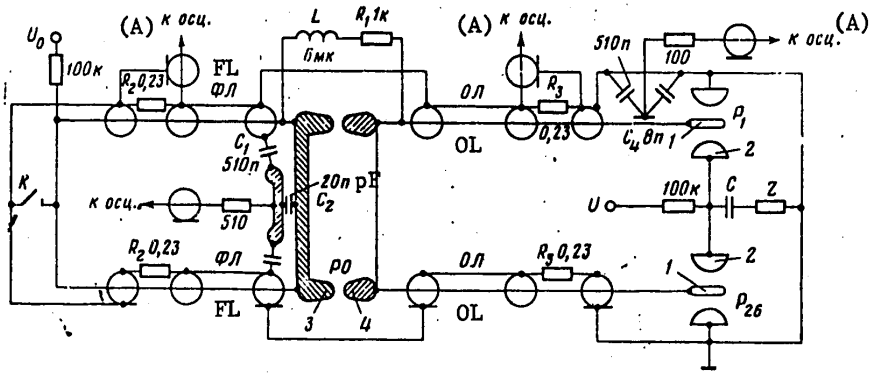


Figure 1. Schematic of the control system for the actuation of 26 dischargers, which switch the capacitive storage device C into the load. $C_1$ and $C_3$ are 10 capacitors of 51 pFd each.

Key: A. To the oscilloscope;

FL = shaping line;
OL = enhancement line.

Following the actuation of switch K, a discharge current wave is produced in the shaping line cables; it is reflected from the enhancer discharger as from a closed end with a change in the polarity of the electrode 3 voltage. When $Z_1 >> \rho$, where $Z_1$ is the impedance of L and $R_1$ in series, the maximum pulse potential difference between electrodes 3 and 4 is $2U_0$. By selecting the spacing $\delta$ between the electrodes, the pressure p and the kind of gas in the enhancer discharger, with a high overvoltage across the gap, one can obtain a multichannel discharge in the peaking discharger, which enhances the rise time of the discharge current pulse of the cables in the enhancement lines. The current wave reaching electrodes 1 has a leading edge shorter than the leading edge in the shaping lines, which stabilizes the actuation of dischargers $P_1$--$P_{26}$.





APPROVED FOR RELEASE: 2007/02/09: CIA-RDP82-00850R000500020034-7

APPROVED FOR RELEASE: 2007/02/09: CIA-RDP82-00850R000500020034-7



The system was studied for the case of $U_0$ = 15 to 30 KV, an enhancer discharger RO filled with $N_2$, an electron gas ($SF_6$) and mixtures of them [6], where an air discharger or a discharger with mechanically destroyed film insulation was used as the switcher K. The studies were conducted in sequences consisting of one-time actuations of the system with the subsequent polishing of the electrodes prior to each successive start. The inspection of the electrode surfaces of the peaking discharger showed that the number of erosion spots on the discharger electrodes with a diameter of 135 mm, filled with $N_2$, was greater than when filled with a mixture of $SF_6$ + $N_2$ and pure $SF_6$ and amounts to $\geq 3$; as a rule, a single discharge channel is produced in $SF_6$. The recording of the current pulses in two diametrically arranged enhancer line cables confirmed the multichannel of the discharge in $N_2$; the difference in the points in time when the wave reached resistors $R_3$ did not exceed the travel time for the speed of light around one-sixth of the peripheral length of the ring electrodes of the peaking discharger. Uniform spacing between electrodes 3 and 4 over the entire length of the periphery (a scatter of $\leq 0.05$ mm) is important for normal operation of the discharger. The calculated electromagnetic wave propagation time over half ofthe peripheral length of the electrodes amounts to about 0.7 nsec; in mixtures of gases and in $SF_6$, the indicated time difference was observed to run up to 0.6 nsec. The time scatter $\Delta T$ of the enhancer breakdown in $N_2$ was also less with the same gaps between the electrodes of the enhancer discharger. Taking these circumstances into account, results of measurements are given below for an enhancer discharger filled with $N_2$.

Typical oscilloscope traces of the discharge current pulse of the shaping line cables and the voltage changes across electrodes 1 of the dischargers corresponding to it when solid insulation of lavsan film [synthetic fiber similar to dacron] was used in the switch K, and the cables were charged at voltage of $U_0$ = 23 KV, the gap $\delta$ was 2 mm and the pressure p was 0.85 MPa $N_2$, are shown in Fig. 2 [not shown]. It is seen that with a switching current rise time of $T_1 \approx 40$ nsec, the voltage change time is $T_2 \approx 5$ nsec. When $\delta$ is reduced down to 1 mm, the time $T_2$ decreases down to $\approx 3.8$ nsec. For six values of $U_0$ and $\delta$, increasing the pressure p shifts the moment of enhancer discharge breakdown to the peak of the current pulse, however, $T_2$ changes little in this case. The scatter $\Delta T$ of the moments of enhancer discharger breakdown relative to the start of the current pulse in the shaping line, measured from the superimposition of 10 and more signals (Figure 2b), was $\leq 4$ nsec in a series of 100 actuations of the switch K. Under these same conditions, the scatter in $SF_6$ is greater by approximately a factor of two. Shortening the leading edge of the current pulse $T_1$ in the shaping line reduces the scatter in the time $\Delta T$; when an air gap discharger is used, $T_1$ increases up to 70 nsec and $\Delta T$ correspondingly increases up to 7 nsec. Splitting each cable in the enhancer line near the dischargers $P_1$--$P_{26}$ into conductors up to 2 m long which were matched to the characteristic impedance (100 ohms) did not degrade the speed of voltage polarity reversal at their ends, which made it possible to control the operation of 52 dischargers.

The enhancer discharger reliably operated throughout the entire range of variation in $U_0$, so that with static and pulsed charging after $\approx 100$ microseconds, no potential difference was produced between electrodes 3 and 4 of this discharger.



APPROVED FOR RELEASE: 2007/02/09: CIA-RDP82-00850R000500020034-7

APPROVED FOR RELEASE: 2007/02/09: CIA-RDP82-00850R000500020034-7



A similar system can be designed with a large number of cables. A further reduction in $T_2$ can be achieved by the sequential breakdown of several enhancement gaps [7].

BIBLIOGRAPHY

1. Barnes P.M., Gruber J.E., James T.E., J. SCIENT. INSTRUM., 1967, Vol 44, No 8, p 599.

2. Bosamykin V.S., Gerasimov A.I., Zenkov D.I. et al., "Gazorazryadnyye pribory (Trudy konferentsii po elektronnoy tekhnike" ["Gas Discharge Devices (Proceedings of the Conference on Electronics Engineering)"], Moscow, "Elektronika" All-Union Scientific Research Institute, 1970, No. 2 (18), p 94, 95.

3. Pavlovskiy A.I., Gerasimov A.I., Tananakin V.A., et al., PTE [EXPERIMENTAL ENGINEERING AND INSTRUMENTS], 1970, No 2, p 122.

4. Pavlovskiy A.I., Gerasimov A.I., Zenkov D.I., et al., ATOMNAYA ENERGIYA, 1970, Vol 28, No 5, p 432.

5. Pavlovskiy A.I. Kuleshov G.D., Gerasimov A.I., et al., PTE, 1976, No 6, p 134.

6. Gerasimov A.I., Saltykov V.B., PTE, 1979, No 4, p 265.

7. Vorob'yev P.A., Potalitsyn Yu.F., Collected Papers, "Elektrofizicheskaya apparatura i elektricheskaya izolyatsii" ["Electrophysical Equipment and Electrical Insulation"], Moscow, Energiya Publishers, 1970, p 140.

COPYRIGHT: Izdatel'stvo "Nauka", "Pribory i tekhnika eksperimenta", 1981

8225
CSO: 8144/0178



APPROVED FOR RELEASE: 2007/02/09: CIA-RDP82-00850R000500020034-7

APPROVED FOR RELEASE: 2007/02/09: CIA-RDP82-00850R000500020034-7



UDC 621.383.98

# WIDEBAND PHOTOELECTRONIC RECEIVER

Moscow PRIBORY I TEKHNIKA EKSPERIMENTA in Russian No 4, Jul-Aug 81 (manuscript received 3 Mar 80) pp 199-202

[Paper by R.R. Agishev, G.I. Il'in and A.N. Pikulev, Kazan' Aviation Institute imeni A.N. Tupolev]

[Text] The circuitry and operational principle of a photodector with a photomultiplier are described, which has a stepped amplitude response and makes it possible to receive optical signals in three modes: with manual setting of the gain, with timewise gain control and automatic gain control. The dynamic input range is 80 dB, the passband is 25 MHz and the maximum time for switching from channel to channel is 100 nsec.

The dynamic range of variation in optical signals fed to the input of a receiver can reach 80 to 100 dB, and without taking special steps to compress the dynamic range, this unavoidably leads to the overloading of the optical receiver and information losses. The most well-known methods of dyanamic range compresssion are the introduction of automatic and timewise gain control as well as the use of functional amplifiers; however, the precision of measurements of the output data in such optical receivers is poor.

One of the promising methods of dynamic range compression with high measurement precision and a large dynamic range of the signals being measured is the technique of stepped gain control. However, there are no sufficiently universal photodetectors at the present time which employ the given principle of analog signal compression. The circuit proposed in [1] for stepwise automatic gain control (a.g.c.) is convenient when working with sufficiently "smooth" signals, but cannot be satisfactory when recording rapidly changing signals. The use of delay lines [1, 2] to prevent information losses during switching leads to a narrowing of the passband of the entire device. Moreover, delay lines are inefficient in the case of repeated switching. A photodetector with timewise automatic gain control (t.a.g.c.) yields the best results [3], in which it is possible to select the requisite portion of the signal by setting a definite program. It is necessary in a number of other cases to analyze the entire signal at a fixed gain. Then it becomes expedient to manually control the photodetector operation: the signal is picked off of the selected dynode.



APPROVED FOR RELEASE: 2007/02/09: CIA-RDP82-00850R000500020034-7

APPROVED FOR RELEASE: 2007/02/09: CIA-RDP82-00850R000500020034-7



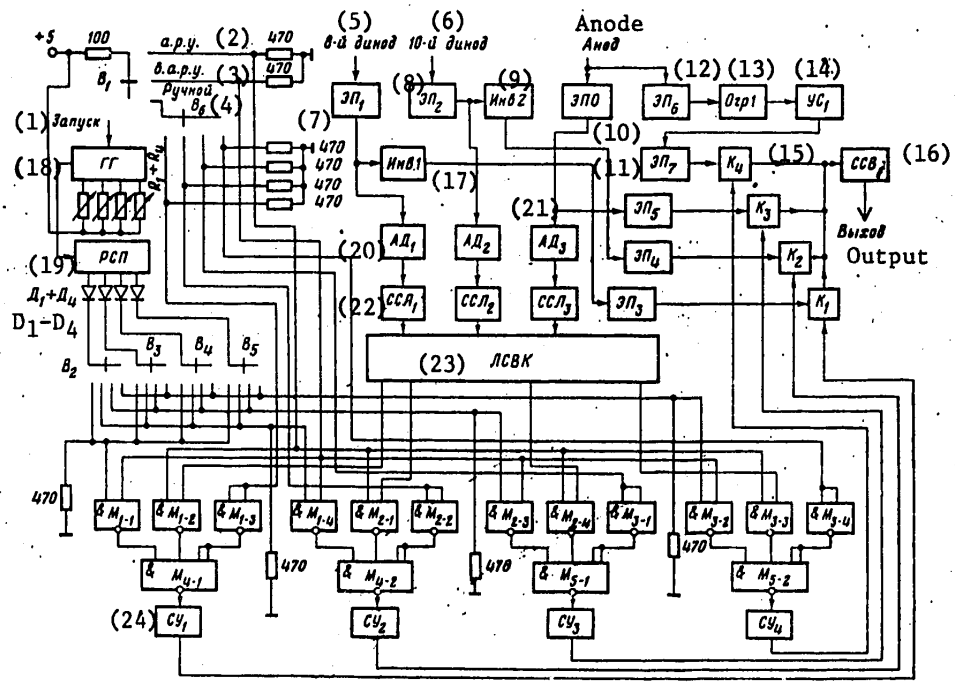


Figure 1. Functional block diagram of the wideband photoreceiver. $M_1$ - $M_3$ = 155LA3; $M_4$, $M_5$ = 155LA6; $D_1$ - $D_4$ = KD503.

Key:
1. Trigger;
2. Automatic gain control;
3. Time controlled automatic gain control;
4. Manual control;
5. 8th dynode;
6. 10th dynode;
7. $EP_1$ = emitter follower 1;
8. $EP_2$ = emitter follower 2;
9. Inv 2 = inverter 2;
10. EPO = emitter follower and limiter;
11. $EP_7$ = emitter follower 7;
12. $EP_6$;
13. Ogr1 = limiter 1;
14. $US_1$ = supplemental amplifier 1;
15. $K_4$ = switch 4;
16. SSV = output matching circuit;
17. Inv 1 = inverter 1;
18. GG = "Comb" generator;
19. RSP = voltage shift register;
20. $AD_1$ = amplifier discriminator 1;
21. $AD_3$ = amplifier discriminator 3;





APPROVED FOR RELEASE: 2007/02/09: CIA-RDP82-00850R000500020034-7

APPROVED FOR RELEASE: 2007/02/09: CIA-RDP82-00850R000500020034-7



[Key to Figure 1, continued:]

22. $SSL_1$ = logic level matching circuit 1;
23. LSVK = channel selection logic;
24. $SU_1$ = control circuit 1.

A photodetector is described in this paper which can operate in any of three modes: manual control, and with a.g.c. and t.a.g.c. The optical signal receiver is designed in accordance with the circuit described in [4]. The output signals are picked off of load resistors inserted in the dynode circuits of the photomultipliers. As studies have shown, to obtain a dynamic range of $10^4$, the output signals can be picked off of the 8th and 10th dynodes and the anode of the photomultiplier, and a supplemental amplifier with a gain of 10 can also be used for the signal from the anode. In this case, the relative error is $\leq$ 5 percent [5].

A functional block diagram of the receiver is shown in Figure 1. The signals from the 8th and 10th dynodes are fed to two identical channels. By way of example, we shall consider the passage of the signal from the 8th dynode. The signal is simultaneously fed to inverter Inv 1 and amplitude discriminator $AD_1$ through emitter follower $EP_1$. The negative polarity signal from Inv 1 is fed through emitter follower EP3 to switch $K_1$. The signal picked off of the photo multiplier anode is simultaneously fed to emitter follower and limiter EPO and emitter follower EP6. The voltage from the emitter follower and limiter is fed to discriminator AD3 and emitter follower EP5, and then to switch K3. The signal from the output of $EP_6$ is fed to the additional amplifier $US_1$ (to avoid overloading the amplifier by large signals, there is a limiter, Ogr 1 in the circuit) and goes through emitter follower $EP_7$ to switch 4. At each fixed point in time, only switch $K_i$ is unblocked, and the signal is fed from it through the SSV output matching circuit to the output of the device.

We shall treat the operation of the circuit in various modes. When the switch $B_1$ is in the "manual" position, a logic 1 voltage is fed to the sliding contact of the dynode switch $B_6$. The switch $B_6$ can feed the 1 voltage to logic gates $M_{1-3}$, $M_{2-2}$, $M_{3-1}$ and $M_{3-4}$. The voltage which appears in this case at the output of one of the four integrated circuit elements $M_4$ and $M_5$ unblocks the corresponding switch $K_i$ through the control circuits $SU_i$, and the signal is fed at the selected gain level to the output of the photodetector.

When operating in the time controlled a.g.c. mode, the switch $B_1$ unblocks gates $M_{1-1}$, $M_{1-4}$, $M_{2-3}$ and $M_{3-2}$ with a logic 1 voltage. A synchronizing pulse triggers the "comb" generator GG, which generates a series of four pulses. A voltage shift register (rsp) generates a train of query gating pulses from the "comb", which are fed through isolating diodes $D_1$ - $D_4$ to switches $B_2$ - $B_5$, which accomplish the requisite setting of the strobes. The interval between the comb generator pulses can be varied by means of potentiometers $R_1$ - $R_4$, and the channel interrogation time will change in this case. Thus, the requisite amplitude-time characteristic of the t.a.g.c. is generated. The strobe pulses in the selected sequence unblock the switches $K_i$ in interrogating the channels, through the unblocked t.a.g.c. gates, integrated circuits $M_4$ and $M_5$ and the $SU_i$ control circuits.



APPROVED FOR RELEASE: 2007/02/09: CIA-RDP82-00850R000500020034-7

APPROVED FOR RELEASE: 2007/02/09: CIA-RDP82-00850R000500020034-7



When operating in the a.g.c. mode, the logic 1 level incoming from switch $B_1$ unblocks gates $M_{1-2}$, $M_{2-1}$, $M_{2-4}$ and $M_{3-3}$. In this case, the control of the switches is transfered to the channel selection logic (LSVK). As has already been indicated, the input signals from emitter follower 1, emitter follower 2 and the emitter follower-limiter are fed to amplitude discriminators $AD_i$, designed around tunnel diodes. Then the logic 1 and 0 levels are fed to the channel selection logic through the logic level matching circuitry (SSL). Depending on whether the discrimination threshold was exceeded by the signals from the corresponding diodes, enable or inhibit signals are fed to the control inputs of the switches $K_i$ through a.g.c. gates $M_4$ and $M_5$, as well as through units $SU_i$, where each time the enable pulse is fed to only one switch.

In the initial state, the logic links between the channels are designed so that only one switch $K_4$ is open in this case. If the amplitude of the signal at the photomultiplier input is small, then the states of the discriminators $AD_i$ do not change, and a signal is fed through switch $K_4$ at maximum gain to the device output. If the signal rises so much that the discrimination threshold of $AD_3$ is exceeded, then a 1 signal is fed from the $SSL_3$ circuit, which provides for an inhibit logic function to switch $K_4$ and turns on $K_3$. The circuit operates in a similar fashion with other changes in the input optical signal.

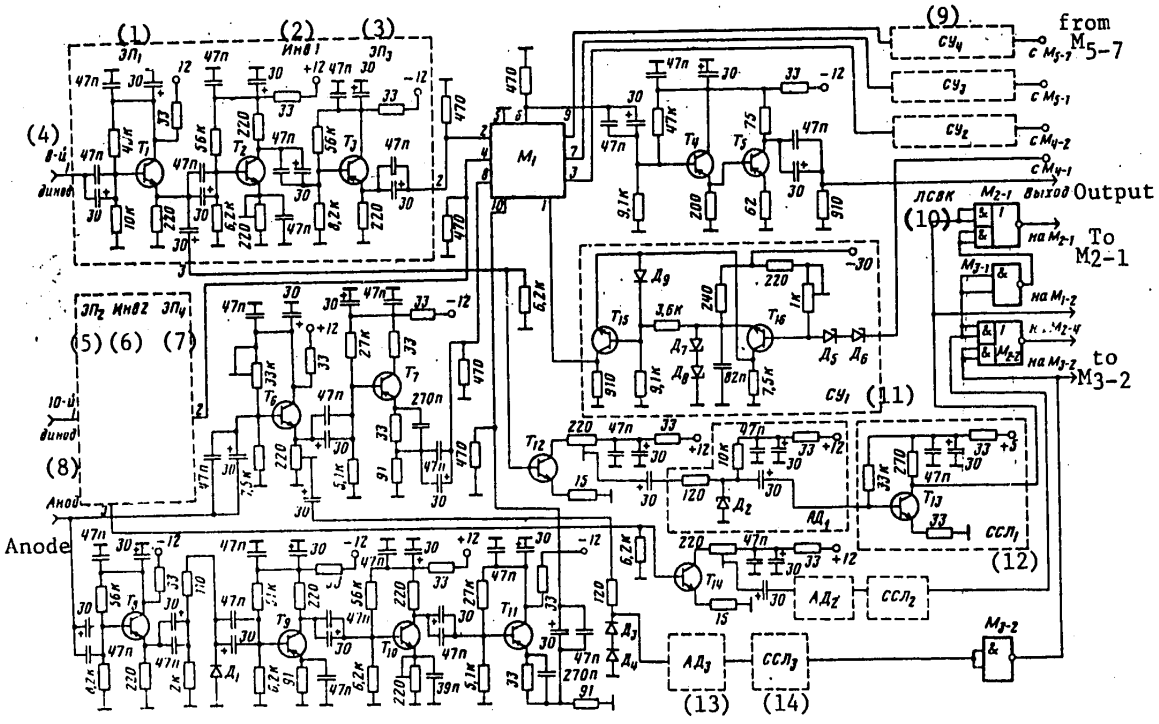


Figure 2. Basic schematic of the unit containing the analog processing and switching stages as well as the threshold gates and the channel selection logic.





APPROVED FOR RELEASE: 2007/02/09: CIA-RDP82-00850R000500020034-7

APPROVED FOR RELEASE: 2007/02/09: CIA-RDP82-00850R000500020034-7



[Caption and key to Figure 2, continued:]

$M_1$ = 190KT1; $M_2$ = 155LR1; $M_3$ = 155LA3; $T_1$, $T_6$, $T_{10}$ and $T_{13}$ = KT315A; $T_2$ = KT316A; $T_3$, $T_4$, $T_8$ and $T_9$ = KT326A; $T_5$, $T_7$ and $T_{11}$ = KT361A; $T_{15}$ and $T_{16}$ = KT339A; $T_{12}$ and $T_{14}$ = GT311B; $D_1$, $D_3$, $D_4$ and $D_9$ = KD503A; $D_2$ = GI304A; $D_5$ - $D_8$ = D814D.

Key: 1. $EP_1$ = emitter follower 1;
2. Inv 1 = inverter 1;
3. $EP_3$ = emitter follower 3;
4. 8th dynode;
5. Emitter follower 2;
6. Inverter 2;
7. Emitter follower 4;
8. 10th dynode;
9. $SU_4$ = control circuit 4;
10. LSVK = channel selection logic;
11. $SU_1$ = control circuit 1;
12. $SSL_1$ = logic level matching circuit 1;
13. $AD_3$ = amplitude discriminator 3;
14. $SSL_3$ = logic level matching circuit 3.

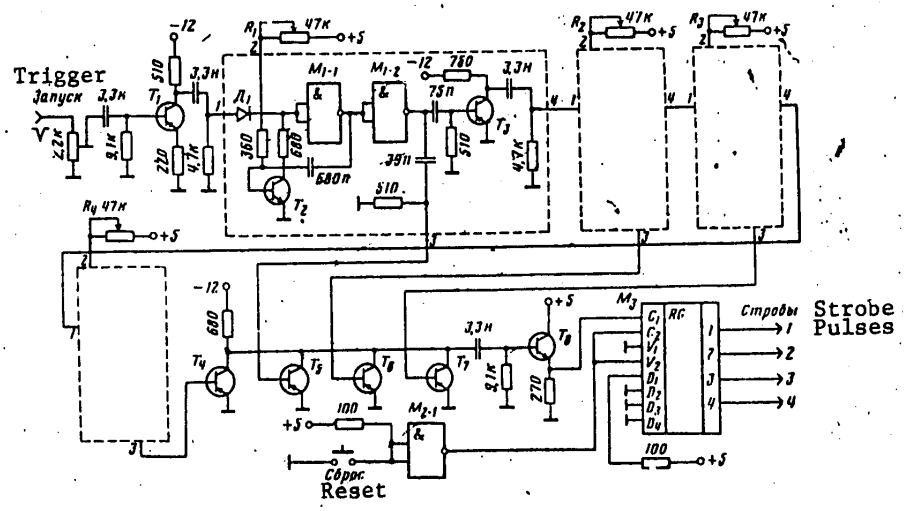


Figure 3. Basic shematic of the GG "comb" generator and the RSP voltage shift register. $M_1$ and $M_2$ = 155LA3; $M_3$ = 155IR1; $T_1$ and $T_3$ - $T_7$ = KT361A; $T_2$ and $T_8$ = KT315A; $D_1$ = KD503A.

A basic schematic of the unit in which the analog processor stages, the switching stages as well as the threshold gates and LSVK channel selection logic are





APPROVED FOR RELEASE: 2007/02/09: CIA-RDP82-00850R000500020034-7

APPROVED FOR RELEASE: 2007/02/09: CIA-RDP82-00850R000500020034-7



included is shown in Figure 2. A basic schematic of the GG "comb" generator and the RSP voltage shift register is shown in Figure 3.

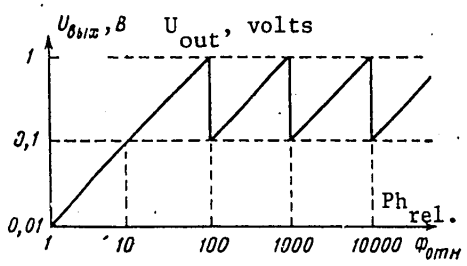


Figure 4. The amplitude-light response of the photo receiver when operating in the a.g.c. mode. $Ph_{rel.}$ is the normalized light flux at the photomultiplier input.

During testing of the photoreceiver in the a.g.c. mode, its amplitude-light response was recorded, which is shown in Figure 4. The characteristics were recorded with an FEU-84 [photomultiplier] in a monopulse mode. The light signal was generated in the form of a pulse 20 nsec to 1 μsec wide by a high power LED, to which a voltage was fed from a G5-56 generator. The output signal was monitored with a S8-12 oscilloscope.

The all-purpose photoreceiver makes it possible to register signals with a dynamic range of 80 dB and the passband of the devices is 25 MHz. The switching time from channel to channel is $\leq$ 100 nsec. When operating in the t.a.g.c. mode, the device makes it possible to produce an arbitrary amplitude-time characteristic with an operating time for each of the four channels of 0.5 to 5 μsec.

BIBLIOGRAPHY

1. Aver'yanov G.A., Safronov Yu.N., Savichev B.M., PTE, 1976, No. 4, p 162.

2. Brunov M.V., Golovkov V.P., Corbatyuk V.V., et al., PTE, 1975, No 6, p 137.

3. Il'in G.I., Pikulev A.N., Pol'skiy Yu.Ye., PTE, 1980, No 5, p 199.

4. Il'in G.I., Pikulev A.N., Pol'skiy Yu.Ye., Collected Papers, "IV Vsesoyuz. simposium po rasprostraneniyu lazernogo izlucheniya v atmosfere" ["Fourth All-Union Symposium on Laser Radiation Propagation in the Atmosphere"], Tomsk, Institute of Atmospheric Optics of the USSR Academy of Sciences Siberian Department, 1977, p 55.

5. Il'in G.I., Collected Papers, "Vsesoyuz. simpozium po lazernomu i akusticheskomy zondirovaniyu atmosfery" ["All-Union Symposium on Laser and Acoustic Sensing of the Atmosphere"], Tomsk, Institute of Atmospheric Optics of the USSR Academy of Sciences, Siberian Department, 1978, Part 4, p 138.

COPYRIGHT: Izdatel'stvo "Nauka", "Pribory i tekhnika eksperimenta", 1981

8225
CSO: 8144/0178



APPROVED FOR RELEASE: 2007/02/09: CIA-RDP82-00850R000500020034-7

APPROVED FOR RELEASE: 2007/02/09: CIA-RDP82-00850R000500020034-7



UDC 621.376.5 (088.8)

DEVICE FOR CONTROLLING PIN-DIODE ATTENUATOR

Moscow OPISANIYE IZOBRETENIYA 746784 in Russian 17 Jul 80

[Description of USSR Patent No 746784 by A.V. Andriyanov, A.V. Goryachev and G.B. Dzekhtser, filed 5 Jan 78, published 17 Jul 80, class H 01 P 1/22 H 01 P 1/40]

[Text] This invention is in the area of radio engineering and can be used to construct high-speed pin-diode attenuators in the microwave band.

There exists a device for controlling a pin-diode attenuator which contains series-connected master oscillator, delay element and first auxiliary oscillator, the output of which is connected to the control input of the pin-diode attenuator; between the other output of the first auxiliary oscillator and the control input of the pin-diode attenuator is connected an element with two stable states, and a second auxiliary oscillator is connected to the control input of the pin-diode attenuator [1].

However, this device is not fast enough.

The purpose of this invention is to reduce the duration of the leading edge of the attenuator output pulse.

In order to accomplish this, the device for controlling a pin-diode attenuator, consisting of series-connected master oscillator, delay element and first auxiliary oscillator with output connected to the control input of the pin-diode attenuator, has an element with two stable states connected between the other output of the first auxiliary oscillator and the control output of the pin-diode attenuator; a second auxiliary oscillator is connected to the control input of the pin-diode attenuator, the output of the master oscillator is connected to the other input of the element with two stable states, and an additional delay element is connected between the output of the master oscillator and the input of the second auxiliary oscillator.

Thd drawing shows the functional diagram of the proposed device.

The pin-diode attenuator controller contains pin-diode attenuator 1, master oscillator 2, element 3 with two stable states, first and second auxiliary oscillators 4 and 5, delay element 6 and additional delay element 7.



APPROVED FOR RELEASE: 2007/02/09: CIA-RDP82-00850R000500020034-7

APPROVED FOR RELEASE: 2007/02/09: CIA-RDP82-00850R000500020034-7



The device operates as follows.

When a pulse is output by master oscillator 2, element 3 with two stable states is in a state which allows the working current to pass through the pin-diodes, as a result of which there is practically no microwave signal at the output of diode attenuator 1. The leading edge of the pulse coming from master oscillator 2 triggers additional delay element 7, simultaneously switching element 3 with two stable states to a state which cuts off the working current to the control input of pin-diode attenuator 1 (a slight cut-off voltage is usually applied to the diodes in this case), as a result of which the charge begins to be dispersed from the base of the pin-diodes. Sometime later, additional delay element 7 triggers second auxiliary oscillator 5, which outputs a powerful enough pulse to the control input of pin-diode attenuator 1 to accelerate the dispersal of the accumulated charge from the base of the pin-diodes, as a result of which the output microwave power level rises rapidly to its maximum value. Additional delay element 7 is adjusted so that when the pulse is applied a significant portion of the accumulated charge is dispersed from the base of the pin-diodes, but the microwave power level at the output of pin-diode attenuator 1 does not exceed the value from which the counting of the length of the leading edge of the pulse begins (for example, 0.1 of the amplitude). As a result of this, the leading edge of the microwave power pulse is short, and the speed increases. The cutoff of the pulse from master oscillator 2 activates delay element 6, which, in turn, activates first auxiliary oscillator 4 somewhat later. A pulse is applied to the control input of pin-diode attenuator 1, providing rapid charge accumulation and, consequently, short cut off of the microwave power pulse.

Simultaneously, first auxiliary oscillator 4 acts upon element 3 with two stable states, resetting it to its initial state. Delay element 6 can thus also act as a pulse width regulating element.

The proposed device differs from the other existing device in that it is significantly faster, and has the capability of providing shorter microwave power pulses and, consequently, a wider range of modulating frequencies during pulse modulation. Furthermore, it also provides maximum suppression of the microwave signal during pauses.

## Patent Claims

A device for controlling a pin-diode attenuator containing series-connected master oscillator, delay element and first auxiliary oscillator, the output of which is connected to the control input of the pin-diode attenuator, with an element with two stable states connected between the other output of the first auxiliary oscillator and the control input of the pin-diode attenuator, and a second auxiliary oscillator connected to the control input of the pin-diode attenuator, distinguished by the fact that in order to decrease the duration of the leading edge of the attenuator output pulse the output of the master oscillator is connected to the other input of the element with two stable states, and an additional delay element is connected between the output of the master oscillator and the input of the second auxiliary oscillator.



APPROVED FOR RELEASE: 2007/02/09: CIA-RDP82-00850R000500020034-7

APPROVED FOR RELEASE: 2007/02/09: CIA-RDP82-00850R000500020034-7



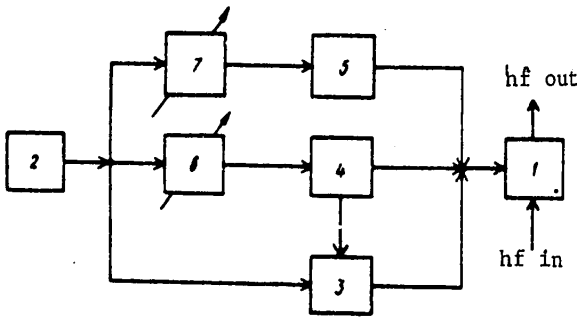


Information Sources
Used in Evaluation

1. Dzekhtser, G.B., et. al. "P-i-n=diody v shirokopolosnykh ustroystvakh SVCh" [Pin-diodes in Wideband Microwave Devices], Moscow, Sovetskoye radio, 1970, p 160, figure 4.19 (prototype).

6900
CSO: 8144/0218-B



APPROVED FOR RELEASE: 2007/02/09: CIA-RDP82-00850R000500020034-7

APPROVED FOR RELEASE: 2007/02/09: CIA-RDP82-00850R000500020034-7



UDC 621.389

# SILICON RADIO-FREQUENCY P-I-N DIODES FOR COMMUNICATIONS EQUIPMENT

Moscow ELEKTROSVYAZ' in Russian No 8, Aug 81 (manuscript received 15 Oct 79) pp 51-52

[Article by Yu. R. Nosov]

[Text] Silicon pin diodes are used widely in radio and wire communications. They are used in the SVCh [Super-high frequency] range as switches, modulators, attenuators and power limiters. Lately pin diodes are being widely used in the VCh (High-frequency) range in various ARU [Automatic gain control] circuits, variable rectifiers etc. In controlled attenuators, pin diodes are capable of providing ARU, both flat and sloped of up to 60-70 db with very high linearity and with a minimum of introduced noises. However, the development of such domestic devices was retarded by the lack of corresponding components. The proposed diode -- one of the first such types of domestic diodes has good electrical characteristics.

In recent year, the use of silicon switching and limiter diodes with a pin structure find wider and wider application. It was found that in the VCh range, such devices may be very useful in ARU and power limiter circuits etc.

Fig. 1 shows a KD413A, B diode: a -- exterior view; b -- the pin structure circuit; c -- the distribution of charge carriers in the switched-off state (solid line) and at various forward currents (broken lines); d -- equivalent circuit of the pin diode (1 -- $C_{dif}$; 2 -- $C_{tr}$; 3 -- $C_k$ are diffusion, junction and device capacitances respectively; $L_k$ -- inductance of the device), 4 -- $r_{dif}$ is the differential resistance of the diode, 5 -- $I_f$ is forward current.

The pin diode operates as follows: At forward current flowing through the diode, an intensive "pumping" of charge carriers into the base low conductivity region (i region) and their accumulation in it are implemented due to the effect of a double injection from the strongly alloyed $n^+$ and $p^+$ regions. First, at fairly high frequencies, the rectifying action of p-i and n-i junctions ceases (diffusion capacitance $C_{dif}$ in Fig. 1c is large) and the high frequency signal can pass through the diode without significant distortions. Secondly, the resistance of the base region becomes small and its value becomes dependent on forward current. Thus, in some frequency range, the pin diode is a current controlled resistive component.





APPROVED FOR RELEASE: 2007/02/09: CIA-RDP82-00850R000500020034-7

APPROVED FOR RELEASE: 2007/02/09: CIA-RDP82-00850R000500020034-7



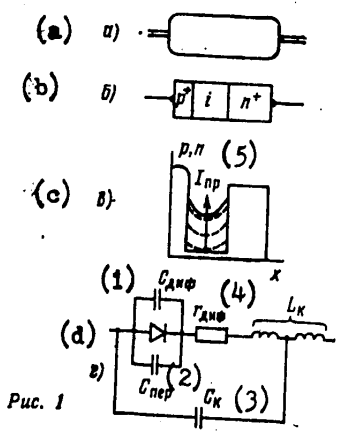


Рис. 1

Fig. 1

Table 1

Electrical parameters of KD413A, B devices

| Diode type | Constant forward voltage at $I_f$=20 ma, $U_f$, volts, not over | Diode Capacitance at $U_{rev}$=0, volts, $C_d$, pico-farads, not over | Differential resistance at $I_f$=2ma and f=50MHz, $r_{dif}$, ohms | | Switching charge at $I_f$=2ma, $U_{rev}$=10 volts, $Q_s$, nC, not less than |
|---|---|---|---|---|---|
| | | | not less than | not more than | |
| KD413A | 1 | 0.7 | 30 | 60 | 2 |
| KD413B | 1 | 0.7 | 40 | 80 | 2 |



APPROVED FOR RELEASE: 2007/02/09: CIA-RDP82-00850R000500020034-7

APPROVED FOR RELEASE: 2007/02/09: CIA-RDP82-00850R000500020034-7



The operating mechanism cited is achieved in type KD413A,B devices whose electrical parameters and maximum allowable operating modes are shown in Tables 1 and 2. The lower boundary of the working frequency range is determined fairly strictly by switching charge $Q_s$. Its value for the pin structure is related to the effective lifetime of charge carriers in the base $\tau_{eff}$ by a simple relationship

$$Q_s \approx I_f \tau_{eff}$$

Table 2

Operating modes of KD413A,B devices in the -60 to + 100°C temperature range

| Name of mode | Conventional designation | Allowable Value |
|---|---|---|
| Maximum allowable constant or average forward current | $I_f max$ | 20 ma |
| Maximum allowable constant reverse voltage | $U_{rev} max$ | 24 volts |
| Maximum allowable scattered power* | P max | 20 mw |

*The power liberated at the diode is calculated from approximate formula $P=IB_{-}I_f + I^2 x\ r_{dif}$, where $I_f$ -- forward bias current, I -- effective value of the high frequency current through the diode, $r_{dif}$ -- differential diode resistance at the selected value of $I_f$. Condition $P \leq P_{max}$ must be fulfilled.

The results of experimental investigations of the devices described are shown in Fig. 2.

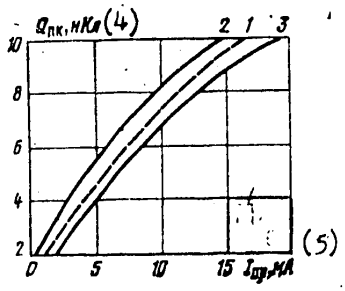


Fig. 2. 4 -- $Q_s$, nC; 5 -- $I_f$, ma



APPROVED FOR RELEASE: 2007/02/09: CIA-RDP82-00850R000500020034-7

APPROVED FOR RELEASE: 2007/02/09: CIA-RDP82-00850R000500020034-7



In a broad range of forward current changes, $\tau_{eff}$ may be considered constant and lying in the interval of 1 to 2 microseconds to a precision of up to 10-20%. The condition for determining the low value of the working frequency has the form:

$$\omega_{min} \quad \tau_{eff}=n >> 1,$$

where the value of n depends on the allowable level of signal distortion (incomplete disappearance of the rectifying action of the pin structure) and, in the majority of practical applications, may be assumed to be n=30...100. Thus, for the KD413A, B diodes we have

$$f_{min} \approx \frac{nI_f}{2\pi Q_s} \approx 3...10 \text{ megaHz}.$$

The upper boundary of the working range is determined by parasitic reactances (inductance, capacitance) of the design and of the pin structure itself and lies within 300...500 megaHz. A typical value of the full capacitance of the diode at fairly high reverse biases ( $\sim$ 10 volts) is close to 0.1...0.2 picofarads; the parasitic inductance of the structure is 2 nanohenries.

The basic parameter of the pin diode as a resistive component is its differential resistance at a given direct current measured at high frequencies (f=50 megaHz) and the form of relationship $r_{dif}=f(I_f)$.

To simplify the selection of the operating mode of the device with respect to the forward current, a two-sided limitation on the $r_{dif}$ parameter is introduced (Table 1); its actual spread is still smaller.

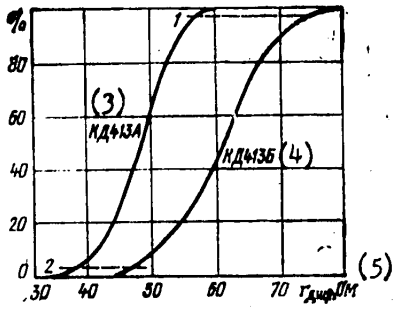


Fig. 3. 3 -- KD413A; 4 -- KD413B; 5 -- $r_{dif}$, ohms;



APPROVED FOR RELEASE: 2007/02/09: CIA-RDP82-00850R000500020034-7

APPROVED FOR RELEASE: 2007/02/09: CIA-RDP82-00850R000500020034-7



Fig. 3 shows the diode distribution function with respect to $r_{dif}$ values. 1, 2 are boundaries of a 95 percent spread. In the region of value change of $I_f$ by 3...4 orders of magnitude (from 5...10 microamperes to 10...20 milliamperes), the relationship between the differential resistance and the constant forward current is described to a high degree of accuracy by

$$r_{dif}=A/I_f$$

where A=70...110 millivolts for group A and A=90...140 millivolts for group B.

Structurally, the KD413A,B diodes are made in the form of miniature all-glass 1.2x2.8 mm cylinders with axial lead-outs and are suitable for wiring in hybrid microcircuits.

COPYRIGHT: Izdatel'stvo "Radio i svyaz'", "Elektrosvyaz'", 1981

2291
CSO: 1860/78



APPROVED FOR RELEASE: 2007/02/09: CIA-RDP82-00850R000500020034-7

APPROVED FOR RELEASE: 2007/02/09: CIA-RDP82-00850R000500020034-7



UDC 621.391:621.317.75

# PRINCIPLES OF THE DESIGN OF NONLINEAR PULSE-FREQUENCY SIGNAL SELECTORS

Moscow IZMERENIYA, KONTROL', AVTOMATIZATSIYA in Russian No 4 (38), 1981 pp 54-61

[Article by V.I. Korchun, engineer]

[Text] Devices possessing the properties of frequency selection are most often designed on the basis of classical analog structures (line filters) which, because of their simplicity and universality, are widely used in various fields of engineering. However, in recent times the attention of investigators and developers has been attracted by methods of designing nonlinear frequency-selective devices based on digital logic circuits [1]. In these devices the methods and principles of pulsed and digital equipment are used primarily; therefore, only digital circuits and components are required for implementing them. Interest in these methods can be explained by the following reasons:

The modern integrated technology for fabricating the components of electronic circuits is more compatible with engineering solutions based on employing the methods and principles of digital equipment, and not analog.

Frequency selection devices designed on the basis of digital logic elements make it possible to obtain specific values of a number of parameters and characteristics (speed of response, selectivity, stability of characteristics, simplicity of retuning, etc.) which are difficult or impossible to obtain by means of analog line circuits [2].

A great number of terms are required for designating nonlinear frequency-selective devices based on digital logic circuits, such as "nonlinear digital filter," "numerical filter," "discrete filter," "repetition rate pulse selector," "frequency detector," etc. Taking into account the fact that in designing these devices digital principles of isolating the frequency trait of pulsed signals are employed, below we will use the term "pulse frequency signal selector" (SChIS), limiting ourselves to the class of nonlinear devices.

SChIS's are used in various automation, computing and measuring equipment devices. They are used in particular for the precise fixing of the moment of time when a parameter, varying over time, of a process characterized by a frequency trait reaches a predetermined value. The basic functions of SChIS's are to analyze electrical signals belonging to a specific frequency region and fixing the moment of crossing specific threshold values.



APPROVED FOR RELEASE: 2007/02/09: CIA-RDP82-00850R000500020034-7

APPROVED FOR RELEASE: 2007/02/09: CIA-RDP82-00850R000500020034-7



Let us note that in spite of the common nature of problems solved by means of SChIS's and line filtering devices it is impossible to draw a parallel between these two classes of devices. Finding a mathematical equivalent of an SChIS in the categories customary for the theory of analog filters is quite a complex problem which still cannot be considered solved. Nevertheless, for the purpose of characterizing an SChIS it is possible to select parameters (cutoff frequency, transmission band, mean transmission frequency, equivalent figure of merit, etc.) which in the physical sense are sufficiently close to the corresponding parameters of line filters. This makes it possible to compare these devices to some extent.

A characteristic feature of nonlinear SChIS's is the absence of a distinctly pronounced transition region between the disappearance and appearance of the device's output signal. Therefore, by the cutoff frequency, $f_{gr}$, is understood the boundary value of the input signal's frequency with which the existence of a reaction in the SChIS's output is possible. The transmission band, $2\Delta f$, is defined as the difference between the high-frequency, $f_2$, and low-frequency, $f_1$, limits of the region of existence of the SChIS's output reaction, and the mean transmission frequency, $f_0$, of band selectors is found from the equation:

$$f_0 = \frac{f_1 + f_2}{2}.$$

The selective properties of an SChIS can be characterized by the percentage ratio of the transmission band to the mean frequency, or by the equivalent figure of merit, $Q_{ekv}$, determined by the expression

$$Q_{экв} = \frac{f_0}{2\Delta f} = \frac{f_1 + f_2}{2(f_2 - f_1)}. \quad (1)$$

The physical meaning of this parameter differs from the concept of the figure of merit of resonance systems; therefore, the term "equivalent figure of merit" is used.

The operating principle of an SChIS is based on comparing the time interval of the input pulse signal with the time parameter fixed. For the purpose of revealing the general properties and features of various SChIS structures, in this study the classification of selectors is based on the principles of the formation of the fixed time parameter and methods of implementing the comparison operation. It is possible to distinguish between the following groups of SChIS's according to this classification: SChIS's with a signal delay for a fixed time [3]; SChIS's which discriminate a time interval of specific duration [4]; SChIS's with direct comparison of the time interval of the input signal with the duration of a reference pulse [5]; and SChIS's which compare the measured and reference frequencies [6].

Depending on the required kind of output signal, the implementation of each of the design principles for SChIS's is accomplished by several methods, whereby special



APPROVED FOR RELEASE: 2007/02/09: CIA-RDP82-00850R000500020034-7

APPROVED FOR RELEASE: 2007/02/09: CIA-RDP82-00850R000500020034-7



attention is paid to improving the accuracy of fixing specific threshold values of the frequency [7] and also to improving the noise immunity of the device [8].

SChIS's with Delay of the Signal for a Fixed Time

A structural diagram and time diagrams of the operation of a selector making it possible to discriminate pulses repeating at a frequency of $f_0$ are shown in fig 1a and b. The controlled pulse train enters the input of a delay line, LZ, with a frequency of f (period $T = 1/f$) and one of the inputs of an AND gate. An input signal delayed for a time of $\tau_z = T_0$ enters the other input of the AND gate. If the repetition frequency, f, of input pulses equals $f_0$, where $f_0 = 1/T_0 = 1/\tau_z$, then the delayed pulses are synchronized with the following input pulses, $U_{vykh}$. Furthermore, a pulse signal, $U_{vykh}$, with a frequency of $f_0$ is formed in the output of the AND gate. It is easy to verify that the SChIS admits without hindrance also those pulses of multiple frequencies ($f = kf_0$; $k = 2, 3, 4, \ldots$) the distance between which equals $T_0$.

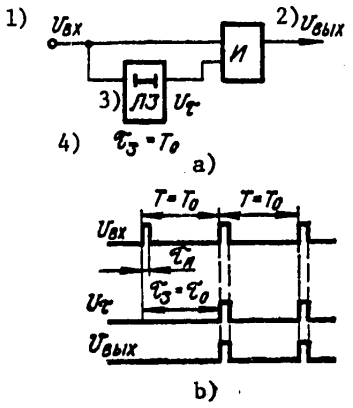


Figure 1. Circuit (a) and Time Diagrams of the Operation (b) of an SChIS with a Delay Line

Key:
1. $U_{vkh}$ [input]
2. $U_{vykh}$ [output]
3. LZ [delay line]
4. $\tau_z$

The transmission band of the selector at the mean frequency of $f_0$ depends on the duration, $\tau_i$, of input pulses:

$$2\Delta f = f_0 - f_1 = \frac{1}{T_0 - \tau_и} - \frac{1}{T_0 + \tau_и} \approx \frac{2\tau_и}{T_0^2}.$$

The equivalent figure of merit, $Q_{ekv}$, according to equation (1), also depends on the duration of input pulses:



APPROVED FOR RELEASE: 2007/02/09: CIA-RDP82-00850R000500020034-7

APPROVED FOR RELEASE: 2007/02/09: CIA-RDP82-00850R000500020034-7



$$Q_{\text{экв}} \approx \frac{T_0}{2\tau_{\text{и}}}.$$

Because of the influence of transient processes in the AND gate and delay line, LZ, as well as because of the effect of destabilizing factors causing instability of the delay time, $\tau_z$, the duration, $\tau_i$, of input pulses must not be less than a certain value. On the other hand, increasing the duration of input pulses results in a reduction in selectivity (selection accuracy). Therefore, it is necessary to select duration $\tau_i$ by taking into account these facts [9].

Since the SChIS (cf. fig 1) has an exceptionally high speed of response (the time for responding to the appearance of frequency $f = f_0$ does not exceed the period of the input signal), then the appearance of even a single noise pulse removed from the information pulse by a time of $T_0 \leq t < T_0 + \tau_i$ will result in the appearance of a spurious output pulse. For the purpose of improving the noise immunity of SChIS's of this type it is possible to increase the number of inputs of the AND gate to 3 to 10. With this signals with an increasing delay, $\tau_{z1} = T_0$, $\tau_{z2} = 2T_0$, $\tau_{z3} = 3T_0$, etc., are supplied to each successive input of the AND gate, for which purpose a sectional delay line is most often used [10]. Combination logic circuits (KLS's) containing AND gates, OR gates and flip-flops are often used instead of an AND gate [11].

With a high level of pulse noise and the presence of omissions of information pulses in pulse trains being discriminated, instead of a delay line controlled delay generators and gate generators synchronized with one another are used [12]. Selection is accomplished by gating the input signals with pulses of a set duration which follow at intervals of $T_0$. By repeated triggering of the delay generator and gate generator it is possible to check the first signal picked up repeatedly for truth. At the same time gate pulses can be generated also with individual omissions of information pulses (up to a certain predetermined number of information pulses omitted in succession), because of which the signal pickup time with fading of the pulse train--the SChIS's readiness time--is reduced to a minimum (on the order of the period of the input signal).

A general shortcoming of SChIS's with delay of the signal for a fixed time is the existence of a reaction at frequencies which are a multiple of the assigned. This shortcoming can be eliminated by means of the method of n-fold comparison per period [13], whose essence consists in the following. To a multi-input AND gate is fed an n-multiplet of additional pulses with intervals of $\tau$ whose formation is possible only upon condition of the arrival in succession of $n + 1$ pulses of the controlled train with a period of $T_0$. The method is implemented by means of a so-called delayed regeneration loop executed on the basis of a sectional delay line, registers and combination logic circuits. The time for the appearance of a pulse reaction in the output of an SChIS of this sort from the moment the input signal is supplied equals $nT_0$.



APPROVED FOR RELEASE: 2007/02/09: CIA-RDP82-00850R000500020034-7

APPROVED FOR RELEASE: 2007/02/09: CIA-RDP82-00850R000500020034-7



The lower limit of the frequency band of these SChIS'a is determined by the maximum achievable delay time, $\tau_z$, and the upper limit by the speed of response of logic elements and it can reach dozens of megahertz, which makes it possible to use the selectors in various radio engineering devices.

SChIS's with Discrimination of a Period of Specific Duration

Selectors of this type are designed on the basis of the principle of digital measurement of the period of the input signal. Passage of the input controlled pulse train to the device's output is permitted or inhibited depending on the result of the measurement. A structural diagram and operating diagrams of a an SChIS for narrowband selection are shown in fig 2a and b.

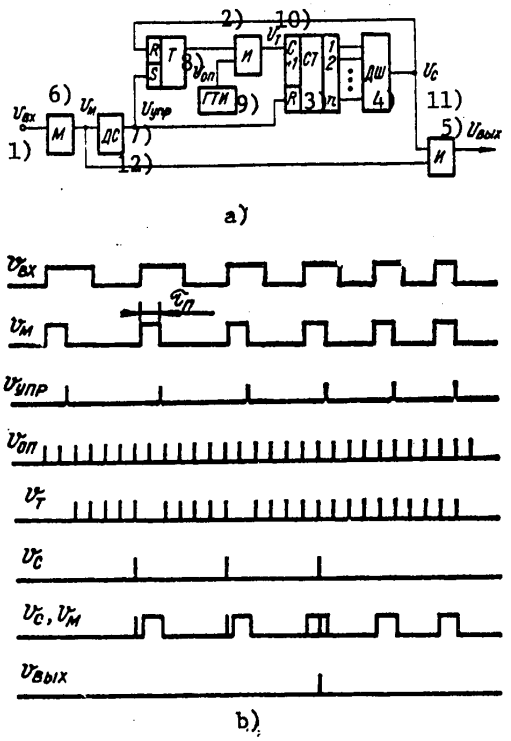


Figure 2. Circuit (a) and Time Diagrams of the Operation (b) of a Narrowband Digital SChIS

Key:

1. $U_{vykh\ [input]}$
2. AND gate
3. Counter
4. Decoder
5. $U_{vykh\ [output]}$
6. Base pulses
7. Control signals
8. Reference voltage
9. Timer
10. Clock pulses
11. Gating signal
12. Differentiation circuit





APPROVED FOR RELEASE: 2007/02/09: CIA-RDP82-00850R000500020034-7

APPROVED FOR RELEASE: 2007/02/09: CIA-RDP82-00850R000500020034-7



From voltage $U_{vkh}$ of the controlled train, by means of a one-shot multivibrator, M, base pulses, $U_m$, are formed, with a duration of $\tau_p$. In turn, the base pulses, $U_m$, are differentiated by means of differentiation circuit DS, in whose output are formed control signals, $U_{upr}$, of short duration, which coincide in time with the termination of the base pulses. Having received the next control signal, $U_{upr}$, the pulse counter, ST, is reset to the zero state and auxiliary flip-flop T by means of the same signal is set to the "one" state at the S input, thereby permitting the entry of clock pulses, $U_{op}$, from the output of the reference generator, GTI (with a frequency of $f_{op}$) through the AND gate into the counting input of the counter, ST. The decoder, DSh, analyzes the state of the n outputs of the counter and fixes the moment of the accumulation of the set number, N, of pulses (in this case N = 5), thereby forming the gating signal, $U_s$. With the arrival of signal $U_s$ flip-flop T is set to the zero state and closes the AND gate, at the same time inhibiting the entry of clock pulses, $U_t$, into the input of the counter, ST. When signals $U_s$ and $U_m$ are synchronized (for the purpose of clarity these signals are presented on the same diagram) the output AND gate forms a pulse reaction, $U_{vykh}$. The counting process begins from the start with the arrival of the next control signal, $U_{upr}$.

From the time diagrams (cf. fig 2b) it follows that with an assigned duration, $\tau_p$, of base pulses, $U_m$, a fixed value of the frequency, $f_{op}$, of the timer, GTI, and a set counter state decoding number, N, the synchronization of signals $U_s$ and $U_m$ and, accordingly, the appearance of signal $U_{vykh}$ in the SChIS's output are possible only in a limited region of input signal, $U_{vkh}$, frequencies [4].

The mean transmission frequency, the effective transmission band and the equivalent figure of merit of the SChIS are expressed, respectively, in the following manner:

$$f_0 = \frac{f_{on}}{2} \frac{2N - 1 + \tau_n f_{on}}{N(N - 1 + \tau_n f_{on})}; \tag{2}$$

$$2\Delta f = f_{on} \frac{\tau_n f_{on} - 1}{N(N - 1 + \tau_n f_{on})}; \tag{3}$$

$$Q_{экв} = \frac{2N - 1 + \tau_n f_{on}}{2(\tau_n f_{on} - 1)}. \tag{4}$$

This circuit for an SChIS, as is obvious from the equations given, with the appropriate choice of the values of N, $\tau_p$ and $f_{op}$, can make possible, generally speaking, as high indicators of selection parameters in the narrowband region as desired. As an example of the practical application of an SChIS of this sort can be cited the typical problem of producing frequency markers for a narrowband swept-signal source. In the 215 to 217 kHz band the selector makes it possible to produce markers with an error not greater than 2 Hz [2].

An analysis of equations (2) to (4) demonstrates that for the normal operation of the SChIS (fig 2) it is necessary to fulfill the conditions $f \ll f_{op}$ and $N \gg \gg \tau_p f_{op} > 1$. Since the value of the upper limit of frequency $f_{op}$ is determined by the speed of response of the digital element base and equals (for the most



APPROVED FOR RELEASE: 2007/02/09: CIA-RDP82-00850R000500020034-7

APPROVED FOR RELEASE: 2007/02/09: CIA-RDP82-00850R000500020034-7



widespread series of digital elements) 10 to 50 MHz, then it is feasible to implement according to this circuit an SChIS in the 100 to 500 kHz frequency band. This limit can be increased by one to two orders of magnitude in the immediate future [14].

In the transmission band the output signals of this SChIS can differ from the input in terms of the shape of pulses. In the majority of cases the following units of equipment are constructed on the basis of the direct use of the pulse reaction and additional conversion is not required. However, sometimes the problem is posed of discriminating pulse trains with a specified pulse repetition rate without their distortion [15].

In measuring equipment and in pattern recognition systems in signal processing the need often arises for the wideband selection of pulses, whereby the upper cutoff frequency is one to two orders of magnitude higher than the lower frequency. This type of selection can be accomplished by means of the SChIS whose structural diagram and operating diagrams are shown in fig 3a and b. Unlike the preceding circuit, here two different states of the pulse counter are decoded, characterized by the numbers $K$ and $N$, whereby $K \ll N$. Number $K$ is selected from the condition $f_2 = f_{op}/K$, where $f_{op}$ is the reference frequency and $f_2$ is the upper cutoff frequency and number $N$ is selected from the condition $f_1 = f_{op}/N$, where $f_1$ is the lower cutoff frequency.

The selector operates in the following manner. The circuit is set to the initial state by the trailing edge of the base pulse, $U_m$ (cf. fig 3b), after which the counter, ST, begins to be filled by pulses, $U_{op}$, from the reference generator, GTI. During the time corresponding to filling of counter $K$ with pulses, decoder DSh1 by means of its output signal, $U_1$, resets flip-flop T1 to the "one" state. If frequency $f$ of the input signal satisfies condition $f_1 < f < f_2$, then by the moment of the arrival of the next pulse of the input signal, $U_{vkh}$, "one" levels will be present in the direct output of flip-flop T1 and in the inverse output of flip-flop T2. The passage of input pulse $U_{vkh}$ through the AND gate to the output of the SChIS is permitted by "one" levels of signals $U_{t1}$ and $U_{t2}$. If $f > f_2$, then by the arrival of the next $U_{vkh}$ pulse counter ST is not able to number $K$ pulses and a "zero" level is maintained in the output of flip-flop T1, inhibiting passage of pulse $U_{vkh}$ through the AND gate.

If $f < f_1$, then counter ST is able to number $N$ pulses. By means of signal $U_{t2}$ from the output of decoder DSh2 flip-flop T2 is reset to the "one" state, and signal $U_{t2}$ (zero level) from the inverse output of the flip-flop inhibits the passage of the next input pulse, $U_{vkh}$, through the AND gate.

Thus, input pulses are transmitted to the output of the SChIS only upon the condition that $f_1 < f < f_2$. The selector makes possible the wideband selection of pulse signals with easily retunable values of threshold frequencies. Improvement of accuracy at the limits of the transmission band is achieved by increasing the reference frequency, $f_{op}$, and reducing the duration, $\tau_p$, of the base pulse, $U_m$ [16].

The time for the appearance of a pulse reaction in the output of an SChIS designed according to the principle of discriminating a period of specified duration is



APPROVED FOR RELEASE: 2007/02/09: CIA-RDP82-00850R000500020034-7

APPROVED FOR RELEASE: 2007/02/09: CIA-RDP82-00850R000500020034-7



not greater than the value of $T = 1/f$, where $f_1 < f < f_2$. Here splitting of the selected time interval between adjacent pulses, caused by the superposition of pulse noise, results in disabling of the SChIS and not only pulse noise but also the legitimate signal do not travel to its output. For the purpose of eliminating this shortcoming special measures for blocking spurious signals are used which complicate considerably the selector's circuit [17].

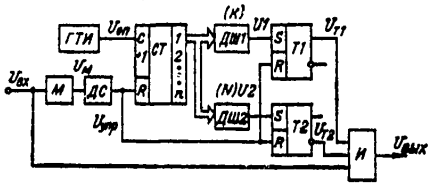


Figure 3. Diagram (a) and Time Diagrams of the Operation (b) of a Wideband Digital SChIS
[Cf. fig 2 for key]

SChIS with Direct Comparison of the Period of the Input Signal with the Duration of a Reference Pulse

The operation of these SChIS's is based on utilization of the phase relationships between pulses of the input signal and reference pulses [18]. The basic diagram of the selector and the time diagrams explaining its operation are presented in fig 4.



APPROVED FOR RELEASE: 2007/02/09: CIA-RDP82-00850R000500020034-7

APPROVED FOR RELEASE: 2007/02/09: CIA-RDP82-00850R000500020034-7



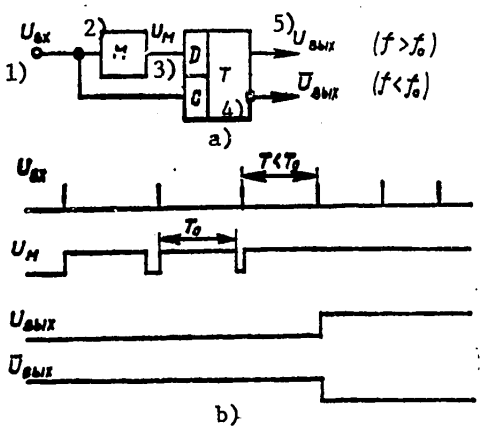


Figure 4. Circuit (a) and Time Diagrams of the Operation (b) of a Frequency Discriminator

Key:
1. Input signal
2. Multivibrator
3. Reference signal
4. Flip-flop
5. Output signal

The controlled pulse train, $U_{vkh}$, enters the input of a one-shot multivibrator, M, which generates a reference signal, $U_m$, of duration $T_0$, and the synchronization input of flip-flop T. The reference pulse, $U_m$, from the output of the multivibrator, M, is supplied to the information input (D) of this flip-flop. Since the leading edge of the SChIS's input signal in any case is in advance of the rise edge of pulse $U_m$ (because of the finite triggering time of the multivibrator), then the first pulse of train $U_{vkh}$ does not remove flip-flop T from the zero state. If the repetition rate of input pulses equals $T > T_0$, then by the moment of the arrival of the next pulse the multivibrator is able to return to the initial state. Thus, with $f < f_0$, where $f_0 = 1/T_0$, in the direct output of flip-flop T there is a steady zero level of $U_{vykh}$, and in the inverse output a steady "one" level of $\overline{U}_{vykh}$. And if the input pulse repetition rate is equal to or greater than $f_0$, then by the moment of the arrival of the next input pulse, $U_{vkh}$, the "one" level of the reference pulse, $U_m$, is retained in the information input of flip-flop T, as the result of which the flip-flop changes to the "one" state. Consequently, the state of the outputs of flip-flop T provides information on whether the frequency of input pulses exceeds the assigned threshold value of $f_0$ or not.

It is possible to use as a multivibrator any circuit which makes possible the sufficient stability of reference pulses. A one-shot multivibrator based on a D-flip-flop fabricated according to the CMOS technology (e.g., the domestic series K176) makes it possible to create an exceptionally economical pulse selector



APPROVED FOR RELEASE: 2007/02/09: CIA-RDP82-00850R000500020034-7

APPROVED FOR RELEASE: 2007/02/09: CIA-RDP82-00850R000500020034-7



circuit (fig 5). With an input pulse frequency of $f \geq f_0$, a single pulse is formed for each pair of input pulses in the circuit's output. With $f < f_0$ a pulse signal is absent. By changing the values of R and $C_1$, determining the duration, $T_0$, of the reference pulse of the multivibrator, assembled from flip-flop T1, it is possible to vary the selector's cutoff frequency from dozens of Hz to dozens of kHz, whereby $T_0 \approx 0.66 RC_1$. Diode V makes possible rapid restoration of the initial state of the multivibrator and capacitor $C_2$ serves the purpose of delaying the leading edges of the reference pulse in relation to input signal pulses. enabling stable operation of the selector [19].

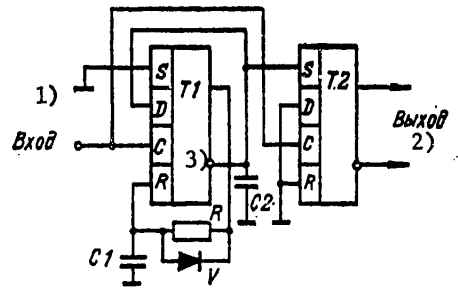


Figure 5. Circuit of Frequency Discriminator Employing CMOS Flip-Flops

Key:
1. Input
2. Output
3. T1 [flip-flop]

This circuit can be used in various automation devices. Since the permissible range of values of resistance R is sufficiently broad (20 kΩ to 10 MΩ), instead of a resistor it is possible to use also other resistive elements, e.g., thermistors or photoelectric cells. With a fixed repetition rate for input pulses (from a reference source) and varying resistance R, on the basis of this circuit it is possible to design an alarm signal sensor: When a specific temperature or illumination level is exceeded the selector begins to generate a train of output pulses. This signal can be used for automatically turning on or off various actuating mechanisms.

The employment of two frequency discriminators designed according to the circuit presented in fig 4 and an AND gate makes it possible to construct an SChIS by means of which it is possible to control not only the deviation of frequency from an assigned value but also the input signal frequency's lying in a specific range [20]. The values of the lower, $f_1$, and upper, $f_2$, cutoff frequencies of the SChIS are set independently of one another by the appropriate choice of the durations ($T_1$ and $T_2$) of one-shot multivibrators M1 and M2 (fig 6). This SChIS possesses an internal memory which can prove useful in certain measurements, e.g., with the disappearance of an input signal consisting of radio pulses the



APPROVED FOR RELEASE: 2007/02/09: CIA-RDP82-00850R000500020034-7

APPROVED FOR RELEASE: 2007/02/09: CIA-RDP82-00850R000500020034-7



flip-flops are not switched and all the output signals do not change before the appearance of an input signal.

The problem of the transmission of an input pulse train without distortion to the output of the SChIS is solved by adding an additional AND gate to one of whose inputs is supplied the input signal and to the other a control signal from an individual output of an SChIS designed according to the circuit presented in fig 6 [5, 7].

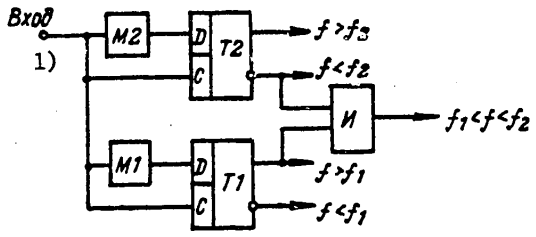


Figure 6. Circuit of General-Purpose SChIS

Key:
1. Input

If it is a problem of just narrowband selection then it is possible to do without flip-flops, using the circuit shown in fig 7. The input differentiating circuit, DS , makes possible independence of the SChIS's operation on the duration of input pulses. The duration of the output pulse of the one-shot multivibrator, M1 , determines the period of the assigned lower cutoff limit, $f_1$ , and the output pulse of one-shot multivibrator M2 sets the required upper-limit cutoff frequency, $f_2$ . A distinctive feature of this selector is that multivibrators M1 and M2 must have a paraphase output for producing the required logic levels of reference pulses $U_1$ and $U_2$ , and also possess the possibility of repeated triggering by the trailing edges of output pulses $U_d$ (fig 7b). The duration of output pulses in the transmission band corresponds to the duration of pulses $U_d$ [21].

The characteristics of an SChIS with direct comparison of the period of the input signal with the duration of the reference pulse are determined by the characteristics of the one-shot multivibrator (recovery time, temperature stability, simplicity of retuning duration of a pulse and the like); therefore, the choice of the multivibrator's circuit is basic in designing an SChIS of this type. For example, the use of the one-shot multivibrator discussed in [22], in addition to high stability indicators (e.g., relative variation of the duration of the output pulse with variation of the voltage of the power supply by one percent does not exceed 0.005 percent) also makes possible programmed setting of the value of the cutoff frequency.



APPROVED FOR RELEASE: 2007/02/09: CIA-RDP82-00850R000500020034-7

APPROVED FOR RELEASE: 2007/02/09: CIA-RDP82-00850R000500020034-7



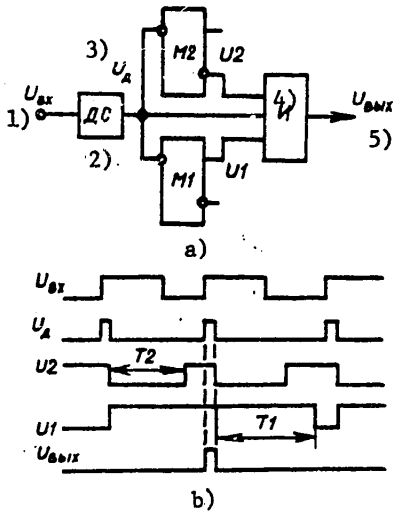


Figure 7. Circuit (a) and Time Diagrams of the Operation (b) of an SChIS with Separate Setting of the Limits of the Transmission Band (Parallel Connection of One-Shot Multivibrators)

Key:
1. Input
2. Differentiation circuit
3. Differentiation output
4. AND gate
5. Output signal

The stability of durations $T_1$ and $T_2$ fully determine the stability of the transmission limits of a band selector; therefore, in designing an SChIS with a narrow transmission band according to the circuit presented in fig 7 certain difficulties arise. With close values of $f_1$ and $f_2$, under the effect of destabilizing factors, superposition of the trailing edges of reference pulses is possible ($T_1 \approx T_2$), which results in disturbance of the circuit's normal operation. This disadvantage is eliminated in the circuit presented in fig 8. One-shot multivibrator M1 sets the upper cutoff frequency and multivibrator M2 the transmission bandwidth of the selector. In the circuits shown in figs 7 and 8 multivibrators with a paraphase output are used [21].

It is necessary to pay special attention to the noise immunity of the device when designing an SChIS employing a one-shot multivibrator. Since a multivibrator has high sensitivity to pulse noise it is necessary to take special measures to prevent false triggering. Multivibrators exist which possess high internal noise immunity, The circuit of one of them, a so-called digital monostable circuit, is shown in fig 9. With the presence of a high level in its output the multivibrator can be triggered only upon the arrival of a timing pulse (positive-going pulse).



APPROVED FOR RELEASE: 2007/02/09: CIA-RDP82-00850R000500020034-7

APPROVED FOR RELEASE: 2007/02/09: CIA-RDP82-00850R000500020034-7



By selecting the appropriate duration and frequency of timing pulses the noise immunity of the device can be increased by 60 to 80 dB [23].

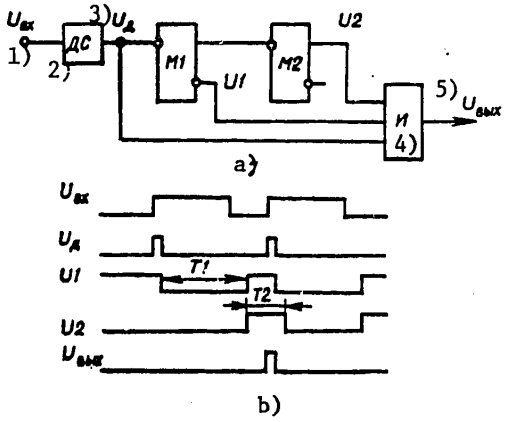


Figure 8. Circuit (a) and Time Diagrams of the Operation (b) of an SChIS with Series Connection of One-Shot Multivibrators

Key:
1. Input
2. Differentiation circuit
3. Differentiation output
4. AND gate
5. Output signal

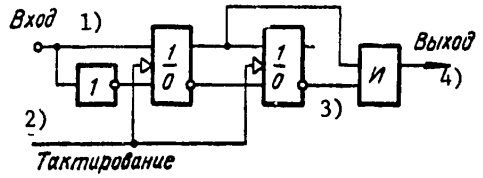


Figure 9. Diagram of Noise-Immune One-Shot Multivibrator

Key:
1. Input
2. Timing
3. AND gate
4. Output

The operating reliability of a narrowband SChIS in the selection of signals against a background of pulse noise can be increased also by integrating the isolated signal by means of a pulse counter. A reaction appears in the selector's output only if the number of pulses discriminated in the transmission band reaches a certain number [8].



APPROVED FOR RELEASE: 2007/02/09: CIA-RDP82-00850R000500020034-7

APPROVED FOR RELEASE: 2007/02/09: CIA-RDP82-00850R000500020034-7



SChIS with Comparison of the Measured and Reference Frequencies

The structural diagrams of these selectors differ from one another in the methods of implementing the comparison operation. The circuit of a selector is shown in fig 10 in which comparison of the controlled frequency, f , with the reference, $f_{op}$ , set by the timer, GTI , is accomplished by means of a combination logic circuit containing NAND gates (I4 and I5), flip-flops (T1 and T2) and a delay line, LZ . If frequencies f and $f_{op}$ are equal and the pulses of both trains are synchronized, then element I1 forms inhibit pulses equal in duration to the input pulses, the state of the outputs of elements I2 and I3 does not change and flip-flops T1 and T2 remain in the original (zero) state. Here a pulse reaction of the SChIS is absent in the outputs of elements I4 and I5 . With lack of synchronization or the partial synchronization of input pulses (and with equality of the frequencies) a reaction is also absent in the selector's output, since the flip-flops at the moment of arrival of each pair of input pulses are in states opposite one another, alternately inhibiting the passage to the selector's output of input pulses delayed by means of the delay line.

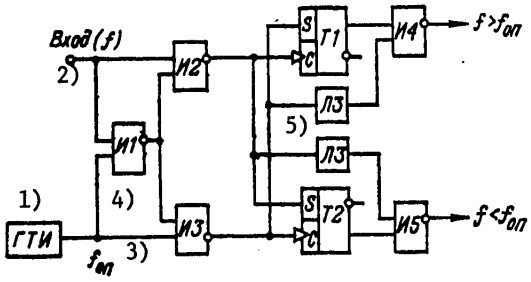


Figure 10. Circuit of SChIS with Simultaneous Comparison of the Input Frequency with the Reference Frequency

Key:
1. Clock
2. Input
3. Reference frequency
4. I1
5. Delay line

If frequencies f and $f_{op}$ differ from one another, then a pulse reaction forms in the appropriate output of the combination logic circuit; since flip-flops T1 and T2 will be in the inhibit (zero) state, [words missing] time segments equal in duration, periodically admitting (with division by two) input pulse flux through the elements of circuit I4 or I5 . In essence this circuit is the circuit of a frequency discriminator whose cutoff frequency, $f_{op}$ , is set by means of an external reference frequency generator, GTI [23].

A disadvantage of the comparison of frequencies by means of a combination logic circuit is that proper operation of the SChIS depends on the duration of input



APPROVED FOR RELEASE: 2007/02/09: CIA-RDP82-00850R000500020034-7

APPROVED FOR RELEASE: 2007/02/09: CIA-RDP82-00850R000500020034-7



pulse trains. Usually input signals must be preliminarily normalized in terms of pulse duration.

This disadvantage is eliminated in SChIS's whose operating principle is based on the integration of pulse trains by means of pulse counters and the comparison of accumulated values upon the expiration of a certain fixed time segment [24]. The selector contains (cf. fig 11) a reference frequency generator, GTI , two frequency dividers, DCh1 and DCh2 , a flip-flop, T , and a presetting unit, BU . If the controlled frequency, f , of the input signal is lower than the reference frequency, $f_{op}$ , then a carry pulse appears earlier in the output of divider DCh1 than in the output of divider DCh2 (the scaling factors, N , of the dividers are equal to one another). Here the output pulses of divider DCh1 retain flip-flop T in the zero state. Simultaneously with this a signal from the output of divider DCh1 "zeroes" divider DCh2 before the appearance of a carry pulse in its output. If $f > f_{op}$ , then a carry pulse appears earlier in the output of divider DCh2 , setting flip-flop T into the "one" state. By the same signal divider DCh1 is zeroed and, in addition, the presetting unit, BU , is triggered. The initial number, $N_1$ , is entered in counter-divider DCh2 by means of unit BU . Then flip-flop T is in the "one" state until the controlled frequency becomes less than $f_{op}(N - N_1)/N$ . Thus, the selector has hysteresis, which makes it possible to eliminate erroneous operation at the cutoff limit from phase noise. The value of the hysteresis is determined by initial number $N_1$ and can be varied over a wide range [25].

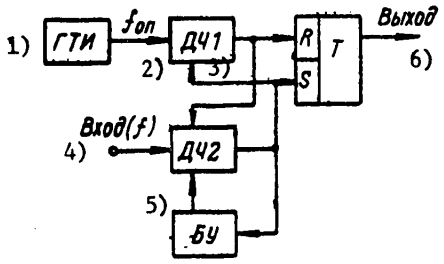


Figure 11. Diagram of SChIS with Frequency Dividers

Key:
1. Clock
2. Reference frequency
3. Frequency divider No 1
4. Input
5. Presetting unit
6. Output

The selector executed according to the circuit presented in fig 11 has a potential "one" output with $f > f_{op}$ and a "zero" with $f < f_{op}$ . When it is necessary to produce an undistorted $f_{op}$ or $f_{op}$ pulse train in the output, SChIS's are supplemented with switching circuits controlled by the outputs of the flip-flop [26]. The noise immunity of the selector increases with an increase in scaling factor N . However, it must be kept in mind that the speed of response of the device is



APPROVED FOR RELEASE: 2007/02/09: CIA-RDP82-00850R000500020034-7

APPROVED FOR RELEASE: 2007/02/09: CIA-RDP82-00850R000500020034-7



reduced since the time for the appearance of a reaction in the output of the circuit from the moment of the supply of the input signal equals $N/f$ .

This principle of designing SChIS's makes it possible to implement also devices for the band selection of pulses, which are designed on the basis of general-purpose binary counters operating in the frequency division mode [27]. The controlled pulse train with a frequency of $f$ (cf. fig 12) is supplied to the counting inputs of counter ST1 with a scaling factor of $M$ and of counter ST2 with a scaling factor of $N$, whereby $N > M$. Reference frequency pulses, $f_{op}$, differentiated by means of the DS block, are supplied from the output of auxiliary generator GTI to the setting inputs of counters ST1 and ST2. After the next setting to the zero state counters ST1 and ST2 begin to be filled with input signal pulses with a frequency of $f$ ($f \gg f_{op}$). After period of time $M/f$, a carry pulse appears in the output of counter ST1, which enters the counting input of counter ST3 (resultant pulse counter), whose reset input is connected to the output of counter ST2. The condition for formation of a carry pulse in the output of counter ST1, $M/f < 1/f_{op}$; and the condition for the absence of resetting of counter ST3 to zero by the carry pulse of counter ST2, $N/f > 1/f_{op}$, determine the condition for the accumulation of pulses in the resultant counter, $Mf_{op} < f < Nf_{op}$.

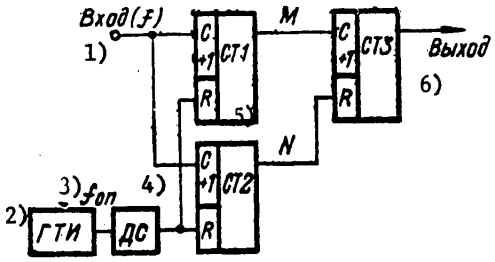


Figure 12. Diagram of Band SChIS Employing General-Purpose Binary Counters

Key:

1. Input
2. Clock
3. $f_{op}$
4. Differentiation circuit
5. Counter No 1
6. Output

The parameters of the SChIS are determined in the following manner:

Mean transmission frequency

$$f_0 = f_{on}\frac{M+N}{2}, \tag{5}$$





APPROVED FOR RELEASE: 2007/02/09: CIA-RDP82-00850R000500020034-7

APPROVED FOR RELEASE: 2007/02/09: CIA-RDP82-00850R000500020034-7



Transmission band

$$2\Delta f = f_{on}(N - M), \tag{6}$$

Equivalent figure of merit

$$Q_{экв} = \frac{M+N}{2(N-M)}. \tag{7}$$

As follows from expressions (5) to (7) the required parameters of the selector are made possible by selecting the appropriate values of M , N and $f_{op}$ . Thus, with M = 255 and N = 256 (two series-connected standard counters, e.g., series K155) the relative value of the transmission band equals less than 0.4 percent (an equivalent figure of merit of about 255). The disadvantage of this circuit is its low speed of response: The time for the appearance of a pulse reaction in the circuit's output equals $\tau_{ust} = K(M/f)$ , where K is the scaling factor of counter ST3 . The SChIS has a wide frequency band, determined by the choice of the value of the reference frequency and the speed of response of the counters [14].

Use of SChIS's for Processing Harmonic Signals

The design principles for an SChIS discussed call for the input signals being in the form of periodic pulse trains. For operation with signals whose shape differs from rectangular (e.g., harmonic signals of frequency-response communications and remote control systems), it is necessary first to convert the input signal, using special shapers (an amplifier-limiter, a Schmitt circuit, comparator and the like), which make possible the required curvature of the leading edges of the signal.

In many cases better results can be obtained when using digital methods of selecting frequency signals than when using line filters. For example, a nonlinear SChIS (fig 13) designed on the basis of two frequency discriminators is economical and has high selectivity and speed of response. It is based on the circuit discussed earlier in fig 6. A multivibrator assembled from comparators K1 and K2 (series K140 or K157 microcircuits) and flip-flops T1 and T2 makes possible the formation of two intercorrelated reference pulses of stable duration. Flip-flops T3 and T5 form a lower cutoff frequency discriminator and flip-flops T4 and T6 an upper cutoff frequency discriminator (all flip-flops are of series K176). The mean transmission frequency can be varied over a wide range from 200 Hz to 20 kHz by changing the values of R and C of the timing circuit. The circuit's selectivity is determined by ratio $R_1/R_2$ and does not depend on the mean transmission frequency. The typical value of $Q_{экв}$ is on the order of 100. The speed of response of the selector is one to two orders of magnitude greater than that of resonance devices with similar selectivity. It is feasible to employ additional input signal processing devices for the purpose of improving the noise immunity [28].



APPROVED FOR RELEASE: 2007/02/09: CIA-RDP82-00850R000500020034-7

APPROVED FOR RELEASE: 2007/02/09: CIA-RDP82-00850R000500020034-7



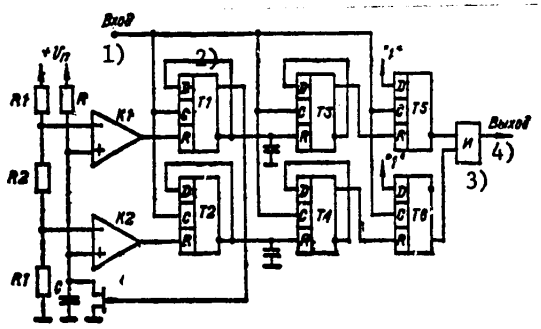


Figure 13. Diagram of Narrowband SChIS

Key:
1. Input
2. Flip-flop No 1
3. AND gate
4. Output

Bibliography

1. Mashbits, L.M. "Tsifrovaya obrabotka signalov v radiotelegrafnoy svyazi" [Digital Processing of Signals in Radio Telegraph Communications], Moscow, Svyaz', 1974, pp 56-80.

2. Mashbits, L.M., Yanshina, G.F. and Chernomortseva, V.P. "Production of Frequency Markers in Swept-Signal Sources for Observing Frequency Response of Receivers," VESTNIK SVYAZI. No 3, 1968, pp 13-15.

3. Timakhov, O.N. and Lyubchenko, V.K. "Selektory impul'sov" [Pulse Selectors], Moscow, Sovetskoye radio, 1966, p 33.

4. Mashbits, L.M. "Analytical Relationships in Discriminating a Period of Predetermined Duration in Voltage Varying in Terms of Frequency," RADIOTEKHNIKA, Vol 24, No 6, 1969, pp 70-75.

5. McKinley, R.I. "Versatile Digital Circuit Filters Highs, Lows or Bands," ELECTRONICS, Vol 44, No 13, 1971, p 66.

6. USSR Patent No 387493. "Device for Comparing Frequencies," I.T. Zimin, published in B.I. [BYULLETEN' IZOBRETENIY], No 27, 1973, p 168.

7. USSR Patent No 721909. "Frequency-Type Pulse Selector," V.I. Korchun and V.V. Lebed', published in B.I., No 10, 1980, p 210.

8. USSR Patent No 738137. "Pulse Selector," V.I. Korchun and V.V. Lebed', published in B.I., No 20, 1980, p 311.



APPROVED FOR RELEASE: 2007/02/09: CIA-RDP82-00850R000500020034-7

APPROVED FOR RELEASE: 2007/02/09: CIA-RDP82-00850R000500020034-7



9. Itskhoki, Ya.S. and Ovchinnikov, N.I. "Impul'snyye i tsifrovyye ustroystva" [Pulse-Driven and Digital Devices], Moscow, Sovetskoye radio, 1973, pp 552-553.

10. Maksimov, M.V. "Zashchita ot radiopomekh" [Protection from Radio Interference], Moscow, Sovetskoye radio, 1976, p 341.

11. USA Patent No 3732563. "Pulse Train Decoder-Degarbler," G.P. Nelson, published 8 May 1973.

12. USSR Patent No 660223. "Repetition Rate Pulse Selector," V.N. Zaytsev, L.M. Zhavoronkov et al., published in B.I., No 16, 1979, pp 276-277.

13. USSR Patent No 660222. "Repetition Rate Pulse Selector," S.V. Popov, published in B.I., No 16, 1979, p 276.

14. Dubitskiy, L.A., Tafel', V.M. and Shvetskiy, B.I. "New Structures for High-Speed Decimal Counters," IZMERENIYA, KONTROL', AVTOMATIZATSIYA, Moscow, TsNIITEIpriborostroyeniya, No 3 (11), 1977, pp 48-52.

15. USSR Patent No 699665. "Pulse Selector," A.I. Balandin, Ye.P. Larichev and Ye.N. Okeanov, published in B.I., No 43, 1979, p 236.

16. USSR Patent No 681549. "Pulse Train Selector," Yu.N. Yerofeyev and V.V. Zaverin, published in B.I., No 31, 1979, p 210.

17. USSR Patent No 681550. "Frequency-Type Pulse Selector," E.Ye. Nesterov, published in B.I., No 31, 1979, p 210.

18. Alfke, P. "Frequency Discriminator Uses One-Shot and Flip-Flop," ELECTRONICS, Vol 46, No 18, 1973, p 92.

19. Yen, T.T. "CMOS Flip-Flop Can Do More than Logic Tasks," ELECTRONICS, Vol 48, No 6, 1975, pp 123-126.

20. Pearson, E.E. "One-Shot/Flip-Flop Pairs Detect Frequency Bands," ELECTRONICS, Vol 45, No 9, 1972, p 104.

21. Volk, A.M. "Two-IC Digital Filter Varies Passband Easily," ELECTRONICS, Vol 46, No 4, 1973, p 106.

22. Shah, M.I. "Programmable Monostable Is Immune to Supply Drift," ELECTRONICS, Vol 46, No 3, 1973, pp 98-99.

23. USSR Patent No 677087. "Device for Comparing Frequencies of Two Pulse Trains," L.N. Mel'nikov, A.V. Margelov et al., published in B.I., No 28, 1979, p 202.

24. USA Patent No 3500069. "Pulse Repetition Frequency Discriminator," R.R. Iohns, published 10 Mar 1970.



APPROVED FOR RELEASE: 2007/02/09: CIA-RDP82-00850R000500020034-7

APPROVED FOR RELEASE: 2007/02/09: CIA-RDP82-00850R000500020034-7



25. USSR Patent No 661761. "Frequency Threshold Device," A.A. Samus', published in B.I., No 17, 1979, p 263.

26. Andreyev, M.I. "Digital Frequency Discriminator Employing Microcircuits," PRIBORY I TEKHNIKA EKSPERIMENTA, No 1, 1979, pp 116-118.

27. Newman, S. "Tone Detector Sharpens Digital Filter's Response," ELECTRONICS, Vol 52, No 24, 1979, pp 118, 119, 121.

28. Glinchenko, A.S. and Chmykh, M.K. "Digital Device for Eliminating Erroneous Crossing of a Signal Through Zero," PRIBORY I TEKHNIKA EKSPERIMENTA, No 2, 1979, pp 112-116.

COPYRIGHT: Tsentral'nyy nauchno-issledovatel'skiy institut informatsii i tekhniko-ekonomicheskikh issledovaniy priborostroyeniya, sredstv avtomatizatsii i sistem upravleniya (TsNIITEIpriborostroyeniya), 1981

8831
CSO: 1860/59



APPROVED FOR RELEASE: 2007/02/09: CIA-RDP82-00850R000500020034-7

APPROVED FOR RELEASE: 2007/02/09: CIA-RDP82-00850R000500020034-7



UDC 621.872 (088.8)

DEVICE FOR ADDITION OF POWERS

Moscow OPISANIYE OZOBRETENIYA 733081 in Russian 7 May 80

[Description of USSR Patent No 733081 by I.V. Lebedev, V.G. Alybin, D.Ya. Ashkenazi and V.P. Belyayev, filed 8 Aug 77, published 7 May 80, class H 03 B 7/14 H 01 P 1/15]

[Text] This invention is in the area of radio engineering, and can be used in various microwave devices.

There exists a device for addition of powers which contains a waveguide segment in the cross-sectional plane of which is located an exciter array in the form of metal rods running parallel to the wide sides of the waveguide segment; diodes placed on the narrow walls of the waveguide segment are connected to the ends of the metal rods; furthermore, the middle of the rods are joined by posts which are perpendicular to them and are connected to the voltage feed elements [1].

However, this device has low operating power and a narrow operating bandwidth. This is because the diodes in the exciter array are not identical.

The purpose of the present invention is to increase the power and expand the operating bandwidth.

In order to achieve this, the device for addition of powers, which contains a waveguide segment with an exciter array mounted in its cross section consisting of metal rods running parallel to the wide sides of the waveguide segment with diodes fastened to the narrow walls of the waveguide segment connected to the ends of the rods; furthermore, the middle of the rods are joined by posts which are perpendicular to them and which are connected to the voltage feed elements, and each post and rod of the exciter array separated by an additional dielectric layer which is located in the planes of the longitudinal sections of the waveguide segment passing through the axis of symmetry of the power feed elements.

The drawing shows a cross-sectional view of the construction of the proposed device.

An excited array is contained in the cross-sectional plane of waveguide segment 1 comprised of metal rods 2 which are parallel to its wide walls. Connected to the ends of the rods are diodes 3, which are fastened to the narrow sides of the waveguide segment; furthermore, the middle of the rods are joined by posts 4 which



APPROVED FOR RELEASE: 2007/02/09: CIA-RDP82-00850R000500020034-7

APPROVED FOR RELEASE: 2007/02/09: CIA-RDP82-00850R000500020034-7



are perpendicular to the rods and which are connected to voltage feed elements 5. Each post 4 and rod 2 are separated by dielectric layer 6, which is located in the plane of the longitudinal section of waveguide segment 1, passing through the axis of symmetry of voltage feed elements 5 to terminals 7.

The device operates as follows.

When voltage is applied to terminal 7, direct current passes through diodes 3 and their impedance drops to an extremely low value, providing a condition in the resonant array of total reflection of the microwave power passing through the waveguide segment. When voltage is absent from terminal 7, diodes 3 represent a large capacitive impedance, and conditions are met in the resonant array for unimpeded transmission of incident microwave power through it.

Dielectric layer 6 runs in the same direction as the microwave currents; consequently, it introduces no additional losses in microwave energy, regardless of the high-frequency properties of the dielectric.

The presence of dielectric layer 6 makes it possible to apply voltage separately to each diode 3. This increases reliability and improves the parameters of the devices which are dependent upon the degree of symmetry of the array, for example, the maximum generated or switched power.

## Patent Claims

A device for addition of powers containing a waveguide segment in the cross-sectional plane of which is an exciter array comprised of metal rods running parallel to the wide walls of the waveguide segment with diodes located on the narrow walls of the waveguide segment connected to the ends of the rods; furthermore, the middle of the rods are joined by perpendicular posts which are also connected to the voltage feed elements, distinguished by the fact that in order to increase power and expand the operating frequency range, each post and exciter array rod are separated by an additional dielectric layer running in the planes of the longitudinal sections of the waveguide segment passing through the axes of symmetry of the voltage feed elements.

## Information Sources Used in Evaluation

1. USSR Author's certificate No. 566207, class H 03 B 7/14, 1975 (prototype).



APPROVED FOR RELEASE: 2007/02/09: CIA-RDP82-00850R000500020034-7

APPROVED FOR RELEASE: 2007/02/09: CIA-RDP82-00850R000500020034-7



733081

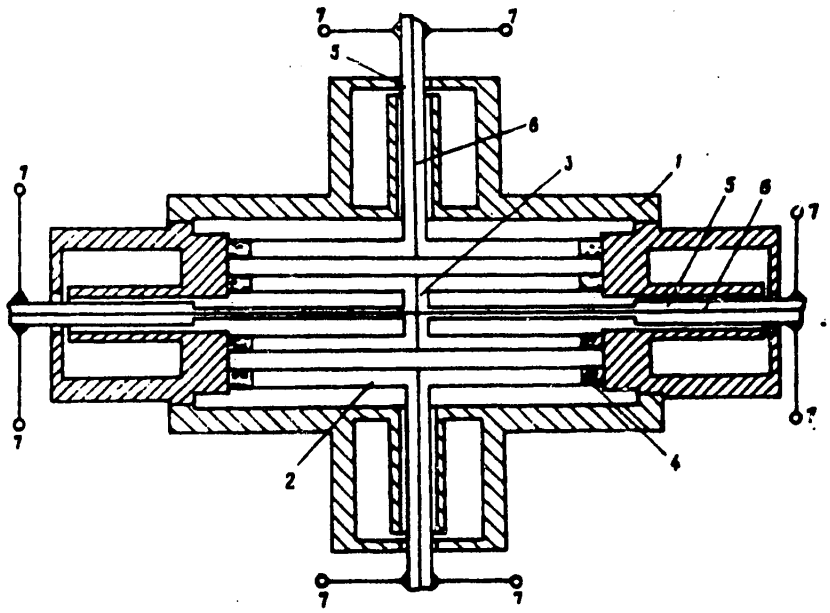


6900
CSO: 8144/0218-B





APPROVED FOR RELEASE: 2007/02/09: CIA-RDP82-00850R000500020034-7

APPROVED FOR RELEASE: 2007/02/09: CIA-RDP82-00850R000500020034-7



RADIO RECEIVER PATENT

Moscow OTKRYTIYA, IZOBRETENIYA, PROMYSHLENNYYE OBRAZTSY, TOVARNYYE ZNAKI in Russian No 29, 1981 (signed to press 10 Jul 81) p 296

[Text] Patent No 11031

Claim No 20095
Class 14-03

Radio Receiver

Authors: I. I. Dezhurnyy, V. M. Kuz'min, V. S. Tsymbalyuk, O. D. Fomin, V. I. Zubkov, Ye. A. Lugovoy and V. I. Gvozdenko

Priority as of 26 July 1979

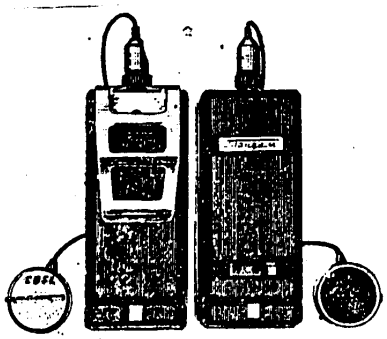

COPYRIGHT: VNIIPI, 1981

CSO: 1860/80-P



APPROVED FOR RELEASE: 2007/02/09: CIA-RDP82-00850R000500020034-7

APPROVED FOR RELEASE: 2007/02/09: CIA-RDP82-00850R000500020034-7



CONVERTERS, INVERTERS, TRANSDUCERS

UDC 621.372.852.27 (088.8)

# WAVEGUIDE REFLECTING PHASE INVERTER

Moscow OPISANIYE IZOBRETENIYA 743084 in Russian 25 Jun 80

[Description of USSR Patent No 743084 by V.G. Vinenko and I.A. Ovechkin, filed 13 Jun 75, published 25 Jun 80, class H 01 P 1/18]

[Text] This invention is in the area of radio engineering and can be used in microwave devices where discrete phase change is required.

There exist waveguide reflector phase inverters which use pin-diodes.

One of the existing phase inverters contains a waveguide transmission line containing a flat diaphragm with two slits, each of which contains a diode structure. A control signal causes the phase inverter to assume four phase states in sequence [1].

Design complexity is a shortcoming of the existing phase inverter, since it requires that the diaphragm be fabricated with great precision.

The technical treatment which is closest to the present invention is a waveguide reflecting phase inverter which contains a waveguide transmission line which is closed at one end, two waveguide stubs placed in series with the waveguide line, and pin-diodes located at the end of the two stubs [2].

Relatively large size is a shortcoming of this phase inverter. The stubs are located at a distance of $\lambda_B/4$ from one another ($\lambda_B$ - wavelength in waveguide), which provides the needed phase shift, and the distance from the short-circuiting switch of the main transmission line to the closest stub is also $\lambda_B/4$. The total length of the phase inverter is thus over $\lambda_B/2$. The lateral dimensions are relatively large because of the extending stubs which are placed at a right angle to the main transmission line. The approximate length of the stubs is $\lambda/4$.

The purpose of the invention is to reduce the size of the device.

This is achieved by placing the stubs, which are an extension of the waveguide, one on top of the other and connecting them to the wide wall, and fastening pin-diodes to the input of each stub.

Figure 1 shows the construction of the waveguide reflecting phase inverter; figure 2 shows view A of figure 1.



APPROVED FOR RELEASE: 2007/02/09: CIA-RDP82-00850R000500020034-7

APPROVED FOR RELEASE: 2007/02/09: CIA-RDP82-00850R000500020034-7



The waveguide reflecting phase inverter consists of waveguide segment 1, waveguide stubs 2, 3, pin-diodes 4, 5, which are fabricated as semiconducting structures, and taps 6 used to apply control current to them.

The conductivity of diodes 4 and 5 which are connected to the beginning of stubs 2 and 3 can take on two values under the influence of control signals. For diode 5, which is connected to stub 2, these values will be $jB'_1$ and $jB''_1$. The conductivity in the plane in which diode 5 is connected is the algebraic sum of the conductivity of diode 5 and the conductivity of shorted stub 2, ($y_m$), which can be written with the help of a familiar relationship as

$$Y_m = jZ_1 \cot \frac{2\pi}{\lambda_B} l_1, \quad (1)$$

where $Z_1$ - characteristic impedance of stub;
$l_1$ - stub length.

Thus, the total conductivity of stub 2 with diode 5 connected to its beginning can be written as

$$Y_1 = jB_1 + jZ_1 \cot \frac{2\pi}{\lambda_B} l_1, \quad (2)$$

where $B_1$ - conductivity of diode, which can take on the two values $B'_1$ and $B''_1$ under the influence of the control signal.

Analogously, the conductivity of stub 3 in plane T with diode 4 connected to its beginning can be written as

$$Y_2 = jB_2 + jZ_2 \cot \frac{2\pi}{\lambda_B} l_2, \quad (3)$$

where $B_2$ - conductivity of diode, which can take on the two values $B'_2$ and $B''_2$ under the influence of the control signal;
$Z_2$ - characteristic impedance of stub 3;
$l_2$ - length of stub 3.

The reflecting impedance in the plane T can be written using the obvious relationship

$$Z_T = \frac{1}{Y_1 Z_0} + \frac{1}{Y_2 Z_0}. \quad (4)$$

Thus, in the proposed construction the value of the reflecting impedance, which determines the phase of the reflected signal, depends upon the impedance of the diodes and the impedance of the loops; consequently, in order to obtain the needed reflecting impedance values, it is possible to vary both the impedance of the diodes, which is inconvenient, as well as the impedance of the stubs, which depends upon their length and characteristic impedances.



APPROVED FOR RELEASE: 2007/02/09: CIA-RDP82-00850R000500020034-7

APPROVED FOR RELEASE: 2007/02/09: CIA-RDP82-00850R000500020034-7



The following formula, which associates the phase shift of the reflected wave ($\phi$) with the value of the reflecting impedance is well known:

$$\tan\frac{\varphi}{2}=\frac{i}{2_r}. \tag{5}$$

Combining equations (2), (3), (4), (5) and keeping in mind the possibility that the control signal may cause the conductivity of the diodes to take on values of $B'_1$, $B''_1$ and $B'_2$, $B''_2$, a system of equations of the following form can be obtained:

$$\begin{aligned}
&\frac{(B'_1+Z_1\cot k\ell_1)(B'_2+Z_2\cot k\ell_2)Z_0}{B_1+B_2+Z_1\cot k\ell_1+Z_2\cot k\ell_2}=\operatorname{tg}\frac{\varphi_0}{2},\\
&\frac{(B'_1+Z_1\cot k\ell_1)(B''_2+Z_2\cot k\ell_2)Z_0}{B_1+B_2+Z_1\cot k\ell_1+Z_2\cot k\ell_2}=\\
&=\tan\left(\frac{\varphi_0+90^\circ}{2}\right),\\
&\frac{(B''_1+Z_1\cot k\ell_1)(B'_2+Z_2\cot k\ell_2)Z_0}{B_1+B_2+Z_1\cot k\ell_1+Z_2\cot k\ell_2}=\operatorname{tg}\left(\frac{\varphi_0+180^\circ}{2}\right),\\
&\frac{(B''_1+Z_1\cot k\ell_1)(B''_2+Z_2\cot k\ell_2)Z_0}{B_1+B_2+Z_1\cot k\ell_1+Z_2\cot k\ell_2}=\\
&=\tan\left(\frac{\varphi_0+270^\circ}{2}\right),
\end{aligned} \tag{6}$$

where $K = 2\pi/\lambda_b$

$\phi_0$ - initial phase.

Given the initial phase $\phi_0$, choice of conductivities $B'_1$, $B''_1$, $B'_2$, $B''_2$, of characteristic stub impedance $Z_1$ and $Z_2$, and of stub lengths $l_1$ and $l_2$, the equations in system (6) can be satisfied.

The values of conductivities $B'_1$, $B''_1$, $B'_2$, $B''_2$ are a function of the parameters of the diodes used and the method by which they are connected to the transmission line. In the construction shown in the drawing, diodes 4 and 5 are soldered between the inductive protrusion in the waveguide.

## Patent Claims

A waveguide reflecting phase inverter containing a waveguide segment and pin diodes located in shorted stubs, distinguished by the fact that in order to reduce size the stubs, which are an extension of the waveguide, are located above one another and connected to the wide wall, and the pin diodes are connected to the input of each stub.



APPROVED FOR RELEASE: 2007/02/09: CIA-RDP82-00850R000500020034-7

APPROVED FOR RELEASE: 2007/02/09: CIA-RDP82-00850R000500020034-7



Information Sources
Used in Evaluation

1. US Patent No 3478284, class 333-98, 1969.

2. UK Patent No 1325381, class H 1 W, 1973.

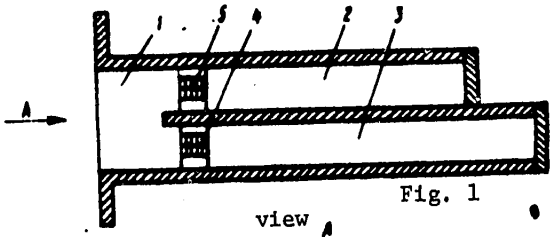


Fig. 1

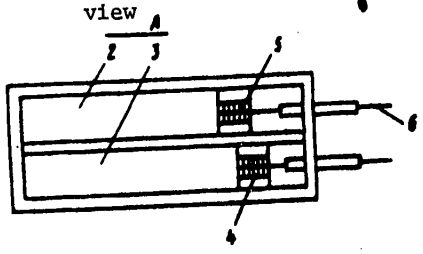


Fig. 2

6900
CSO: 8144/0218-B



APPROVED FOR RELEASE: 2007/02/09: CIA-RDP82-00850R000500020034-7

APPROVED FOR RELEASE: 2007/02/09: CIA-RDP82-00850R000500020034-7



UDC 621.396.677: 621.382 (088.8)

SOLID-STATE PHASE INVERTER CONTROL DEVICE

Moscow OPISANIYE IZOBRETENIYA 750586 in Russian 25 Jul 80

[Description of USSR Patent No 750586 by V.A. Vinogradov and M.L. Slutskiy, filed 26 Dec 77, published 25 Jul 80, class H 01 G 3/26]

[Text] This invention is in the area of radio communication and can be used in antenna array control devices.

There exists a device for controlling solid-state phase inverters which contains forward and backward bias sources, in which the collector of the reverse bias source switching transistor is connected through a resistance which limits current in emergency conditions to the reverse voltage source in order to protect the elements and the reverse bias source switching circuits from short circuiting of the pin-diode or phase inverter coupling line; a powerful current pulse used to dissipate the body charge of the pin-diode at the moment of switching is created by connecting an inductance coil to the collector circuits of this transistor [1].

A shortcoming of this device is the loss of power and impossibility of microminiaturization.

The technical treatment which is closest to the present invention is a device which contains a forward bias source switching transistor, reverse bias source switching transistor with collector connected directly or through a current-limiting resistor to the reverse bias source, and emitter or collector of forward bias source switching transistor connected directly or also through a current-limiting resistor, to the forward bias source [2].

The lack of protection of elements in the reverse bias source switching circuit from line or pin-diode short circuits reduces the reliability of this device.

The purpose of the invention is to improve reliability. The solid-state phase inverter control device, containing forward and reverse bias sources, forward and reverse bias transistors connected to an inverting amplifier, to the forward bias source and to the solid-state phase inverters, achieves this goal by using series-connected pulse shaper and switching transistor, the collector of which is connected through a resistor through the collector of the reverse bias switching transistor, while the emitter is connected to the reverse bias voltage source and, also, through a limiting resistor, to an inverting amplifier and to the base of



APPROVED FOR RELEASE: 2007/02/09: CIA-RDP82-00850R000500020034-7

APPROVED FOR RELEASE: 2007/02/09: CIA-RDP82-00850R000500020034-7



the reverse bias transistor.

The drawing shows the circuit of this device for controlling solid-state phase inverters.

The device contains forward bias source switching transistor 1, reverse bias source switching transistor 2, inverting amplifier transistor 3, current-limiting resistor 4, switching transistor 5 with base connected to switching pulse shaper 6, matching resistors 7 and 8, and pin-diodes 9 and 10 (solid-state phase inverters).

The solid-state phase inverter controlling device is part of a device for controlling a phased antenna array. The control signal applied to one of the control inputs sets the forward or reverse bias mode of pin-diode pair 9 and 10 of one bit of the phase inverter. The number of control inputs is equal to the product of the number of phase inverters and the word length of one phase inverter.

The device operates as follows.

Control signals for pin-diodes 9 and 10 in the form of "high" and "low" voltage levels are applied to the base of forward bias source switching transistor 1 and inverting amplifier transistor 3 from the phase distribution memory register of the antenna array (not shown in drawing). The forward bias condition of pin-diodes 9 and 10 corresponds to the "low" voltage level (diodes 9 and 10 are open, and current from forward bias source $+E_{fb}$ flows through them). The reverse bias condition corresponds to the "high" voltage level at the input (pin-diodes 9 and 10 are closed by voltage from reverse bias source $E_{rb}$).

In the forward bias condition, forward bias source switching transistor 1 is saturated, and reverse bias source switching transistor 2 is cut off; the forward bias source is connected to pin-diodes 9 and 10 through the collector-emitter junction of forward bias source switching transistor 1 and matching resistors 7 and 8.

Regardless of the forward or reverse bias condition of pin-diodes 9 and 10, the collector of reverse bias source switching transistor 2 is connected periodically to the reverse bias source through the collector-emitter junction of switching transistor 5 while switching pulses are applied to its base.

In the reverse bias mode of pin-diodes 9 and 10, forward bias source switching transistor 1 and inverting amplifier transistor 3 are closed; negative potential is established on the base of reverse bias source switching transistor 2 with respect to the emitter and the base-emitter junction is open, and cutoff voltage from the reverse bias source is applied to pin-diodes 9 and 10.

In order to accelerate dispersion of the body charge of pin-diodes 9 and 10 when switching from the forward to the reverse bias condition, the collector of reverse bias source switching transistor 2 is connected to the reverse bias source for a time equal to the length of the switching pulses.



APPROVED FOR RELEASE: 2007/02/09: CIA-RDP82-00850R000500020034-7

APPROVED FOR RELEASE: 2007/02/09: CIA-RDP82-00850R000500020034-7



The switching pulses are formed by switching pulse shaper 6.

If pin-diodes 9 or 10 or the connecting line are short circuited, current with a value close to the maximum dissipating current flows through current-limiting resistor 4, reverse bias source switching transistor 2 and matching resistors 7 and 8 for an amount of time equal to the length of the switching pulse; when there is no switching pulse current flows from the reverse bias source through the collector load of inverting amplifier transistor 3, the base-emitter junction of reverse bias source switching transistor 2, and matching transistors 7 and 8. These currents are small and present no hazard for the circuit components.

This invention improves the reliability of the device.

## Patent Claims

A device for controlling solid-state phase inverters containing forward and reverse bias sources, forward and reverse bias transistors connected to an inverting amplifier, to the forward bias source and to the solid-state inverters, distinguished by the fact that in order to improve reliability additional series-connected pulse shaper and switching transistor are used, with the collector of the switching transistor connected through a resistor to the collector of the reverse bias transistor, the emitter connected to the reverse bias voltage source and to the inverting amplifier and the base of the reverse bias transistor through a limiting resistor.

## Information Sources Used in Evaluation

1. US Patent No 3708697, class 343-854, 1973.

2. Georgopulos, Kh., "Proyektirovaniye modulyatorov dlya upravleniya pin-diodami" [Designing Modulators for Controlling Pin-Diodes], translated from English, 1972, (P-62874), figure 2 (prototype).



APPROVED FOR RELEASE: 2007/02/09: CIA-RDP82-00850R000500020034-7

APPROVED FOR RELEASE: 2007/02/09: CIA-RDP82-00850R000500020034-7



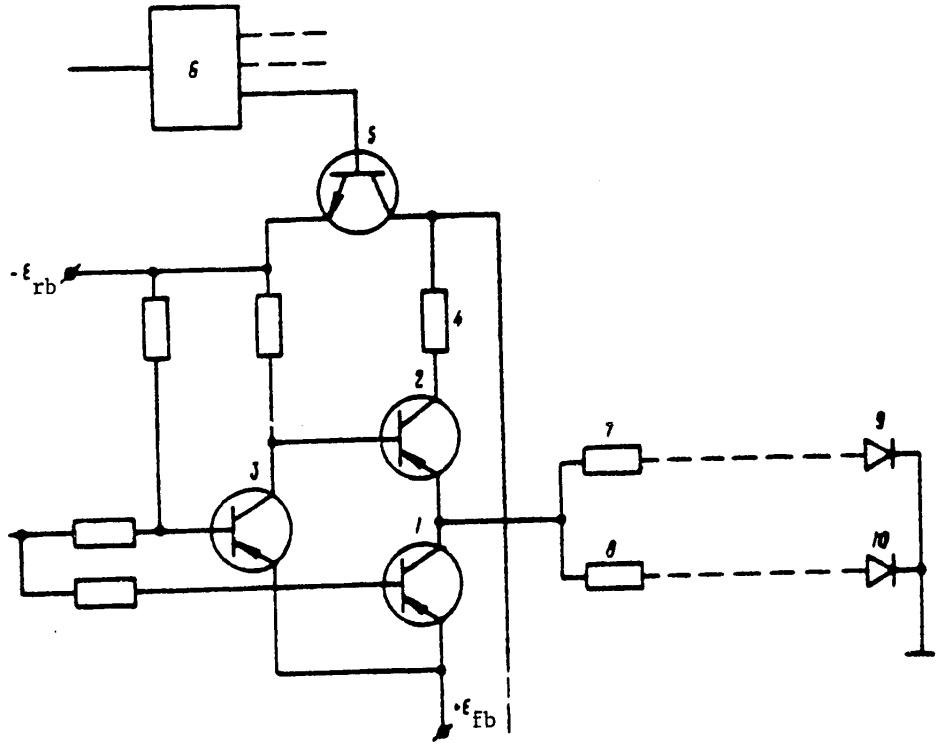


6900
CSO: 8144/0218-B





APPROVED FOR RELEASE: 2007/02/09: CIA-RDP82-00850R000500020034-7

APPROVED FOR RELEASE: 2007/02/09: CIA-RDP82-00850R000500020034-7



INSTRUMENTS, MEASURING DEVICES AND TESTERS, METHODS OF MEASURING, GENERAL EXPERIMENTAL TECHNIQUES

UDC 535.854(088.8)

# PRECISION DIGITAL INFRARED PHASE METER WITH FREQUENCY CONVERSION OF LASER RADIATION

Moscow PRIBORY I TEKHNIKA EKSPERIMENTA in Russian No 4, Jul-Aug 81 (manuscript received 13 Jan 78, after revision 4 Feb 80) pp 203-205

[Paper by V.A. Fedoseyev, V.V. Kalendin, V.I. Kukhtevich and V.Ya. Sup'yan, All-Union Scientific Research Institute of Physical Optics Measurements, Moscow]

[Text] The OTsF-2 precision digital infrared 9 to 11 μm phase meter, designed using a variant of a Mach-Zender interferometer configuration using a homodyne technique with double frequency conversion of laser radiation is described. The phase meter serves for the measurement of constant and slowly changing phase shifts in a range of 0 to 360° with an error of $\leq$ 0.06° and a measurement time of 0.72 sec.

High phase shift measurement precision is achieved in the visible and IR bands when homodyne (with frequency conversion of the optical carrier) or modulation-compensation phase measurement methods are employed [1, 2]. An IR band (9 to 11 μm) compensation phase meter was described in paper [3] for the measurement of constant and slowly changing phase shifts with an error of $\leq$ 1°. The long measurement time (about one minute) and the use of an insufficiently stable mechanical phase compensator are to be numbered among the drawbacks of this phase meter.

The OTsF-2 precision optical digital phase meter, which is intended for the measurement of constant and slowly changing phase shifts in the IR band, is described in this paper. Homodyne conversion of the laser radiation frequency is used in the instrument.

A block diagram of the phase meter is shown in Figure 1. Double frequency conversion of the laser radiation directly in the optical portion of the instrument is used in the phase meter [4]. The optical scheme of the instrument takes the form of a dual beam modified Mach-Zender interferometer, where there are acoustical-optical single band shift modulators, 8 and 13, in the reference and signal channels of the interferometer. The phase object under investigation 3 (for example, an electromagnetic acoustical-optical modulator, optical delay line, etc.) is located in the signal channel. The output of a $CO_2$ laser is fed through the input window 1 of the optical unit to the light splitting plate 2 and routed into the reference and signal channels of the interferometer. The portion of the radiation



APPROVED FOR RELEASE: 2007/02/09: CIA-RDP82-00850R000500020034-7

APPROVED FOR RELEASE: 2007/02/09: CIA-RDP82-00850R000500020034-7



(the reference channel) reflected from plate 2 impinges on mirror 6 and is focused by lens 7 onto the active Ge element of acoustic shift modulator 8 with a $LiNbO_3$ converter. The IR radiation impinges on the acoustical-optical modulator at the Bragg angle ($\simeq 4.5°$) [5]. The acoustical-optical modulator shifts the frequency of the optical carrier by 80 MHz. The high frequency component of this frequency is fed to the modulator from a stabilized crystal oscillator $G_1$ with an output power of about 6 W. The $CO_2$ laser radiation which is shifted in frequency 80 MHz and deflected by twice the Bragg angle ($\simeq 90°$) is shaped by lens 9 into a parallel beam and then goes to the mixer plate 5. The refracted portion of the radiation passes through the phase object being studied 3 (the signal channel, and in being reflected from mirror 4, is directed to the second acoustical-optical single band shift modulator 13 with the focusing 14 and shaping 15 lenses and is then fed to mixer plate 5 where it is combined with the reference beam. Generator $G_2$ with an output power of about 4 watts powers modulator 13 at a frequency of 80,050 MHz. The combined signal and reference beams are directed by reflector 10 and lens 11 to photodetector 12 with a detecting element based on the ternary compound $Cd_xHg_{1-x)}Te$, cooled with liquid nitrogen. Photodetector 15 converts the spatially combined optical signals at frequencies of $w_0$ + 80 MHz and $\omega_0$ + 80,050 MHz (where $\omega_0$ is the optical carrier frequency) to an electrical difference frequency of $\Omega$ = 50 KHz, which is fed to the signal input of a digital display unit (BTsI). A reference signal at the same frequency, 50 KHz, is fed to the second input of the digital display unit, where this frequency is generated in the internal mixer, SM, from the two high frequency voltages at 80,000 and 80,050 MHz incoming from generators $G_1$ and $G_2$. Both generators are stabilized by frequency-phase regulation using an automatic frequency and phase control system (ChFAPCh) [PLL frequency and phase control], which provides for a constant frequency and phase of the intermediate frequency signals at 50 KHz fed to the input of the digital display unit.

The digital display unit, which takes the form of a digital radio frequency phase meter, serves for the measurement of phase difference in a range of 0 to 360° between sinusoidal signals at a frequency of 50 KHz and levels of 300 μV to to 0.4 volts with an error of $\leq$ 0.05°. The phase difference is displayed on the digital panel of the frequency meter. The digital display unit consists of the indicator unit (BI), the quantization pulse generator (GIK), the clock oscillator (VZG) and a Ch3-35 digital frequency meter. The display unit BI generates a train of rectangular pulses, the width of which is proportional to the phase difference in the 50 KHz signals fed to its input. These square wave pulses are filled in with pulses at a frequency of 50 MHz, generated by the quantization pulse generator, and are fed to input A of the Ch3-35 frequency meter. The clock pulses are fed to input B of the frequency meter from the clock oscillator, the VZG. The measurement time is specified by a frequency divider which divides the 5 MHz by 360, which is housed in the clock oscillator unit. The frequency meter operates by measuring the ratio of the frequencies $F_A/F_B$, and the measurement results is displayed in angular degrees on the digital display of the Ch3-35 frequency meter for measurement time of 72 μsec to 0.72 sec with a resolution of $\pm$0.01°.

The analog output of the instrument driving an autorecorder can be used when measuring slowly changing phase shifts. The square wave pulses, the width of which is



APPROVED FOR RELEASE: 2007/02/09: CIA-RDP82-00850R000500020034-7

APPROVED FOR RELEASE: 2007/02/09: CIA-RDP82-00850R000500020034-7



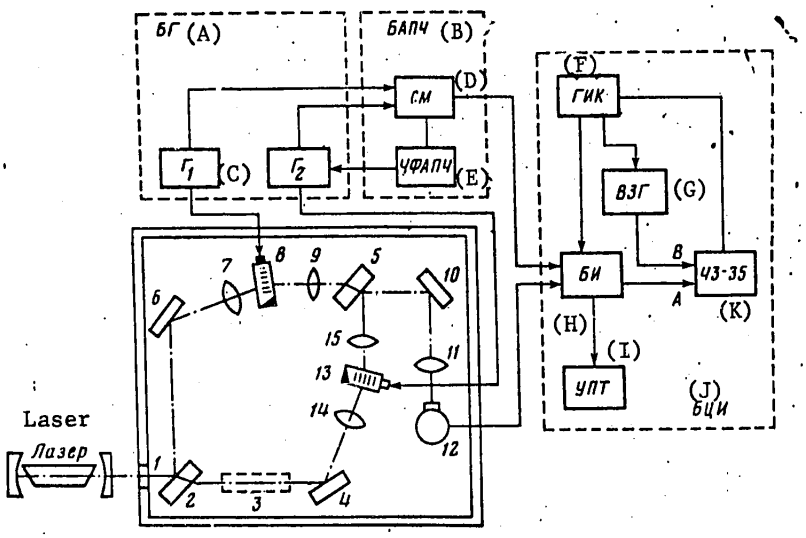


Figure 1. Block diagram of the phase meter.

Key : A. Generator unit;
B. Automatic frequency control unit;
C. Generators 1 and 2;
D. Internal mixer;
E. Automatic frequency and phase control system;
F. Quantization pulse generator;
G. Clock oscillator;
H. Display unit;
I. Direct current amplifier;
J. Digital display unit;
K. Ch3-35 frequency meter.

proportional to the phase shift, are fed through integrating circuits to a DC amplifier (UPT). The DC voltage at the input to the DC amplifier is proportional to the phase shift between the signals in the optical channels of the interferometer.

To improve the sensitivity and stability of the phase shifts being measured, the optical elements of the instrument are rigidly fastened to a massive plate, placed inside a thermostatically controlled multilayer housing. The housing serves to reduce the impact of acoustic interference and to maintain the temperature stability of the phase meter. The absolute error in the radio frequency phase meter measurements was determined by means of comparison with standard phase shift meters at a frequency of 50 KHz [6] and was 0.05° over a measurement time of 0.72 sec.

The OTsF-2 phase meter makes it possible to measure phase shifts in a range of 0 to 360°. The region of instrument insensitivity (the so-called dead zone) when





APPROVED FOR RELEASE: 2007/02/09: CIA-RDP82-00850R000500020034-7

APPROVED FOR RELEASE: 2007/02/09: CIA-RDP82-00850R000500020034-7



measuring shifts close to 0° (or 360°) does not exceed ±2°. There is an input for a supplmental phase shift of 180° to bring the instrument out of the "dead zone". There is an output in the instrument for a digital printer using a binary-decimal 1-2-4-8 code to record the phase values.

To estimate the noise immunity and sensitivity of the OTsF-2 phase meter when measuring slowly changing phase shifts, multiple recordings were made of the drift and fluctuations in the phase difference of $CO_2$ laser radiation (Figure 2). The internal "zero" phase drift of the OTsF-2 phase meter is about 0.01°/sec. The phase shift measurement error is shown below as a function of the measurement time.

| | | | | |
|---|---|---|---|---|
| Measurement time, sec | 0.72 | 0.072 | 0.0072 | 0.00072 |
| Mean square error of ten measurements, degrees | 0.02 | 0.03 | 0.08 | 0.2 |
| Mean square error of a single measurement, degrees | 0.06 | 0.13 | 0.32 | 0.8 |

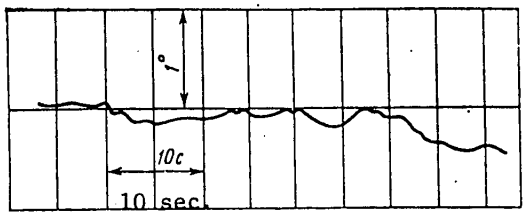


Figure 2. The typical signal drift at the output of the OTsF-2 phase meter.

The use of frequency conversion by means of two acoustical optical modulators [4] in the optical phase meter made it possible to measure phase shifts at the low intermediate frequency 50 KHz, eliminate the impact of high frequency coherent interference and parasitic coupling between the instrument channels as well as reduce phase mismatching in the arms of the interferometer and achieve a high precision in the phase measurements.

The OTsF-2 phase meter measures phase shifts when coherent radiation is fed to its input at a wavelength of 9 to 11 μm having a power of $10^{-2}$ - 10 W, a divergence of $10^{-2}$ - $10^{-4}$ radians and a radiation beam diameter of 1 to 10 mm. It must be underscored that the high precision of the phase shift measurements imposes definite requirements on the parameters on the lasers employed. The radiation source should be single mode, single frequency and frequency stabilized to no worse than $10^{-7}$ and stabilize with respect to power at $\leq$ 1-3 percent over a measurement time of one second.



APPROVED FOR RELEASE: 2007/02/09: CIA-RDP82-00850R000500020034-7

APPROVED FOR RELEASE: 2007/02/09: CIA-RDP82-00850R000500020034-7



The OTsF-2 instrument consists of three units: the optical, electronic-phase metering and the Ch3-35 frequency meter. The dimensions are: optical unit, 500 x 586 x 338 $mm^3$; the electronic phase metering unit, 490 x 170 x 488 $mm^3$; the weight of the instrument is ≈ 40 kg.

BIBLIOGRAPHY

1. Karmashov A.I., Etsin N.Sh, USPEKHI FIZ. NAUK [PROGRESS IN THE PHYSICAL SCIENCES], 1972, Vol 106, No 4, p 689.

2. Kalendin V.V., Kukhtevich V.I., Mukhmarov R.I., "Tr. VNII fiziko-tekhn. i radio-tekhn. izmereniy. Metrologicheskoye obespecheniye izmereniy optiko-fizicheskikh parametrov izlucheniya OKG" ["Proceedings of the All-Union Scientific Research Institute for Applied Physics and Radio Engineering Measurements. Metrological Support for Measurements of the Optical Physics Parameters of Laser Radiation"], Moscow, 1976, p 6.

3. Artemov V.M., Zhelkobayev Zh., Kalendin V.V., et al., PTE [EXPERIMENTAL ENGINEERING AND INSTRUMENTS], 1976, No 2, p 188.

4. Zhelkovayev Zh., Kalendin V.V., Kukhtevich V.I., et al., Patent No. 506755, Published in Bulleting No. 10, 1976, p 97.

5. Mustel' Ye.R., Parygin V.N., "Metody modulyatsii i skanirovaniya sveta" "Light Modulation and Scanning Techniques"], Moscow, Nauka Publishers, 1970.

6. Galakhova O.P., Koltik Ye.D., Kravchenko S.A., "Osnovy fazometrii" ["Fundamentals of Phase Metering"], Leningrad, Energiya Publishers, 1976.

COPYRIGHT: Izdatel'stvo "Nauka", "Pribory i tekhnika eksperimenta", 1981

8225
CSO: 8144/0178



APPROVED FOR RELEASE: 2007/02/09: CIA-RDP82-00850R000500020034-7

APPROVED FOR RELEASE: 2007/02/09: CIA-RDP82-00850R000500020034-7



UDC 621.317.341 (088.8)

# PANORAMIC MEASURING DEVICE FOR COMPLEX PARAMETERS OF MICROWAVE DEVICES

Moscow OPISANIYE IZOBRETENIYA 765755 in Russian 23 Sep 80

[Description of USSR Patent No. 765755 by O.I. Agafoniyeva, A.P. Baklykov, I.K. Bondarenko, Yu.B. Gimpilevich, B.A. Prigoda and A.I. Soboleva, filed 1 Jul 76, class G 01 R 27/28, G 01 R 27/06]

[Text] This invention is in the area of microwave instrumentation and can be used for measuring and monitoring the complex parameters of microwave devices.

There exists a measuring device for complex microwave device parameters which consists of a sweep generator, polarization converter, secondary circular waveguide and detector head, during the rotation of which the complex parameters of microwave devices are measured [1]. The presence of rotating parts, vibration and lag are shortcomings of this device.

There also exists a panoramic device for measuring the complex parameters of microwave devices consisting of a sweep generator, polarization converter, circular waveguide, capacitive probes placed inside a circular waveguide every 45° within the plane of the polarization ellipse, detector heads, each connected to its own probe, and a panoramic display [2]. Shortcomings of this device include the errors caused by the different amplitude-frequency characteristics of the detectors and their temperature and temporal instability, as well as polarization distortions introduced by the probes located on the side wall of the circular waveguide.

The purpose of the invention is to improve measurement accuracy while eliminating polarization distortions.

This is achieved by making the capacitive probes with gaps which contains switching diodes, e.g., pin-diodes which are joined to the control unit and connected to a common detector head which is co-axial with the circular waveguide; furthermore, all of the probes and the connecting rod of the detector head are connected at the center of the circular waveguide.

Figure 1 shows the functional diagram of the proposed instrument; figure 2 shows two views of the microwave section of the instrument in sections A-A and B-B.

The instrument contains sweep generator 1 and polarization converter 2. Four capacitive probes 4-7, connected via switching diodes 8-11 (e.g., pin-diodes) by means of rod 12 to detector head 13, are placed 45° apart in the plane of



APPROVED FOR RELEASE: 2007/02/09: CIA-RDP82-00850R000500020034-7

APPROVED FOR RELEASE: 2007/02/09: CIA-RDP82-00850R000500020034-7



the polarization ellipse inside circular waveguide 3. Switching diodes 8-11 are controlled by control section 14, which is connected between detector head 13 and display 15, which is made up of readout devices 16 and 17 and cathode-ray tube 18; the microwave power passes through polarization converter 2 to load 19, hte parameters of which are being measured.

The instrument operates as follows.

The microwave oscillations pass from sweep generator 1 to polarization converter 2, which converts a type $H_{16}$ waveguide wave or a type TEM coaxial wave to an elliptically polarized $H_{11}$ wave of a generally unmatched load. This wave propagates through circular waveguide 3. Control section 14 sequentially enables probes 4-7 by applying voltage to switching diodes 8-11, which are installed in the gaps of these probes; the activated diode then has current applied, while the disabled diodes have slight negative bias. This makes it possible to achieve transient attenuation of 40 dB. Detector head 13 sequentially outputs voltages defined by the expressions

$$U_4 = K(1 - \rho^2 + 2\rho\cos\psi),$$
$$U_5 = K(1 + \rho^2 - 2\rho\cos\psi),$$
$$U_6 = K(1 + \rho^2 \quad 2\rho\sin\psi),$$
$$U_7 = K(1 - \rho^2 \quad 2\rho\sin\psi),$$

where $U_1$ - $U_4$ are the detector head output voltages obtained from probes 4-7, respectively; K is the coefficient of proportionality, $\rho$ is the absolute value of the coefficient of reflection; $\psi$ is the phase of the coefficient of reflection.

Switching section 14 switches the output of detector head 13 to the inputs of panoramic display 15 in synchronization with the switching of probes 4-7 such that voltages $U_6$ and $U_7$ are applied to the corresponding inputs of readout device 16, and voltages $U_4$ and $U_5$ are applied to the inputs of readout device 17. Voltages

$$U_{16} \quad 4K\rho\sin\psi = K'\rho\sin\psi,$$
$$U_{17} - 4K\rho\cos\psi = K'\rho\cos\psi$$

are output by the readout devices.

These voltages are applied to the vertical and horizontal plates of the cathode-ray tube, which displays the panoramic characteristic of the complex coefficient of reflection.

Because a single detector head is used, the device does not require calibration and is simple to operate. The electronic switching system which connects the probes makes it possible to automate the measurement of complex parameters of microwave devices.

## Patent Claims

A panoramic instrument for measuring complex parameters of microwave devices, containing a sweep generator, polarization converter, circular waveguide containing capacitive probes, detector head and display distinguished by the fact that in order to improve measurement accuracy while eliminating polarization distortions the capacitive probes contain gaps in which switching diodes are



APPROVED FOR RELEASE: 2007/02/09: CIA-RDP82-00850R000500020034-7

APPROVED FOR RELEASE: 2007/02/09: CIA-RDP82-00850R000500020034-7



placed, which are connected with an additional control section; furthermore, these capacitive probes are joined at the center of the circular waveguide and connected to a common detector head which is located coaxially on the circular waveguide.

Information Sources
Used in Evaluation

1. Bondarenko, I.K., Deynega, G.A. and Magrachev, Z.V. "Avtomatizatsiya izmereniy parametrov SVCh-traktov." [Automation of Microwave Circuit Parameter Measurement]. Moscow, Sovetskoye radio, 1969, pp 19-21.

2. US Patent No. 2818546, class 324-58, published 31 Dec 57 (prototype).

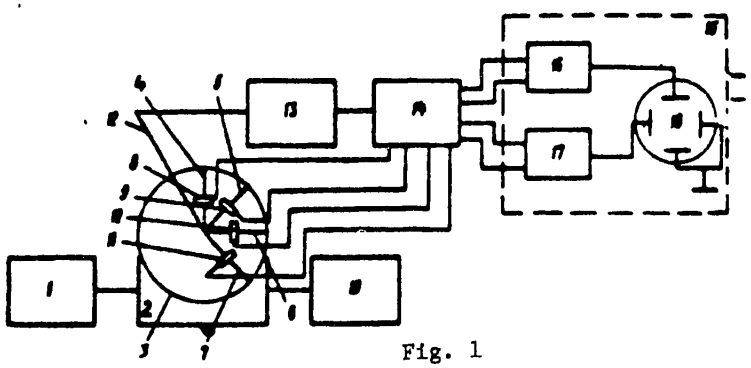

Fig. 1



APPROVED FOR RELEASE: 2007/02/09: CIA-RDP82-00850R000500020034-7

APPROVED FOR RELEASE: 2007/02/09: CIA-RDP82-00850R000500020034-7



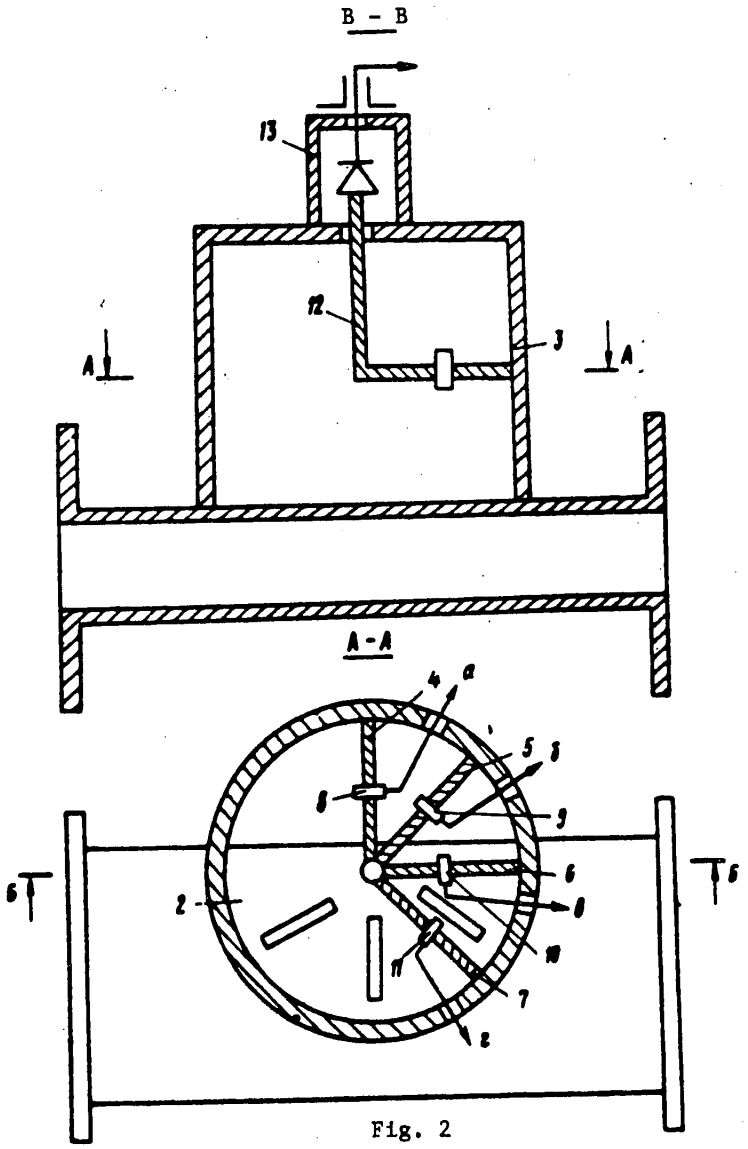


Fig. 2

6900
CSO: 8144/0218-B



APPROVED FOR RELEASE: 2007/02/09: CIA-RDP82-00850R000500020034-7

APPROVED FOR RELEASE: 2007/02/09: CIA-RDP82-00850R000500020034-7



UDC 621.317.382/384:621.375.826

# WIDEBAND INTEGRATED CIRCUIT DIGITAL POWER METER FOR LASER RADIATION

Moscow PRIBORY I TEKHNIKA EKSPERIMENTA in Russian No 4, Jul-Aug 81 (manuscript received 25 Apr 80) pp 197-199

[Paper by A.I. Kirillov, V.I. Kishko and V.F. Morskov]

[Text] A digital integrated circuit laser power meter is described having a measurement range of $10^{-8}$ - $10^{-2}$ W. The analog converter nonlinearity is $\leq$ 5 percent, the digitization error of the digital converter is $\leq$ 2 percent. The spectral sensitivity region is 0.4 to 1.2 micrometers. The temperature instability of the meter in a temperature range of -10 to +40 °C is no more than 6 percent.

Series produced laser power meters have a measurement range of $10^{-6}$ - $10^{-3}$ W [1]. A power meter was described in [2] for an He+Ne laser with a measurement range of $10^{-7}$--$10^{-6}$ W and a threshold sensitivity of $10^{-8}$ (for a signal to noise ratio of 1), which employs a mechanical modulator and a FD-7K silicon photo diode, operating as a detector. The dynamic range of this meter is limited by the fact that the volt-ampere characteristic of the photo diode operating as a detector is nonlinear with a high impedance load [3]. For this reason, it is necessary to have calibrated attenuators for measurements in a range of $10^{-6}$ to $10^{-2}$ W.

The meter considered here operates on the well known principle of autocompensation of the source current (a photo diode in our case) [4] with the subsequent conversion of the autocompensator output voltage to frequency. Operating the photo diode as a rectifier makes it possible to realize a high sensitivity, and automatic compensation of the current, because of the 100 percent negative feedback, assures an almost zero load on the photodiodes, which is defined by the expression [5]:

$$R_{load} \approx R_{fb}/K, \qquad (1)$$

where $R_{fb}$ is the resistance of the feedback resistor; K is the gain of the operational amplifier. In our case, when $R_{fb}$ = 470 Kohm and $K = 5 \cdot 10^4$ (a typical value for a K544UD1A), $R_{load}$ = 10 ohms. With such a load, the volt/ampere characteristic of the photo diode is has good linearity [5]. The dynamic range of the power being measured is extended up to $10^{-2}$ W by reducing the value of the feedback resistor.



APPROVED FOR RELEASE: 2007/02/09: CIA-RDP82-00850R000500020034-7

APPROVED FOR RELEASE: 2007/02/09: CIA-RDP82-00850R000500020034-7



The analog converter (Figure 1) contains an autocompensator for the photo diode current designed around operational amplifier $M_1$ (K544UD1A), the input current of which is $\leq$ 0.1 pA, and a voltage to frequency converter. Switch $B_1$ serves for manually selecting the measurement range in a range of $10^{-4}$ to $10^{-2}$ W. The voltage to frequency converter (v.f.c.), which employs a voltage proportional to the radiation power, is similar to that described in [6] and for the selected nominal values of the components has a conversion factor of 100 Hz/μW in a range of $10^{-8}$ to $10^{-4}$ W, 10 and 1 Hz/μW in a range of $10^{-4}$ to $10^{-3}$ and $10^{-3}$ to $10^{-2}$ respectively; the conversion nonlinearity is $\leq$ 0.02 percent, the temperature coefficient is $\leq$ 0.025 %°C. The meter is zeroed with potentiometer $R_1$.

The output frequency of the v.f.c., which varies from 1 to $10^4$ Hz, is measured by a low frequency digital frequency meter using counters, in which the period is measured, while the value of the frequency is determined as the inverse of the period [7]. The measurement time in this case does not exceed two periods. The frequency meter configuration using counters [7] is simpler than the well-known ones of [8], since it can be designed using standard digital integrated circuits. A functional block diagram of the frequency meter, designed around series K155 integrated circuits, is shown in Figure 2. The frequency being measured, $f_x$, which is proportional to the laser radiation power, is fed to the driver F2 for the period $T_x$ and then to AND gate I3, to the second input of which one of the sample frequencies is fed. The result of measuring the period, $N_T$, is stored by counter Sch2. With the signal for the end of the measurement period, a sample time interval $T_0$ which turns on AND gate I1 for the sample frequency pulses $f_0$ is produced from driver $F_3$ at the output of $F_1$. From the point in time of triggering the driver for $T_0$, the number $N_0$, set by counter Sch1, is compared by means of the code comparator (USr) with the number $N_T$, which is set in counter Sch2. At the moment the codes

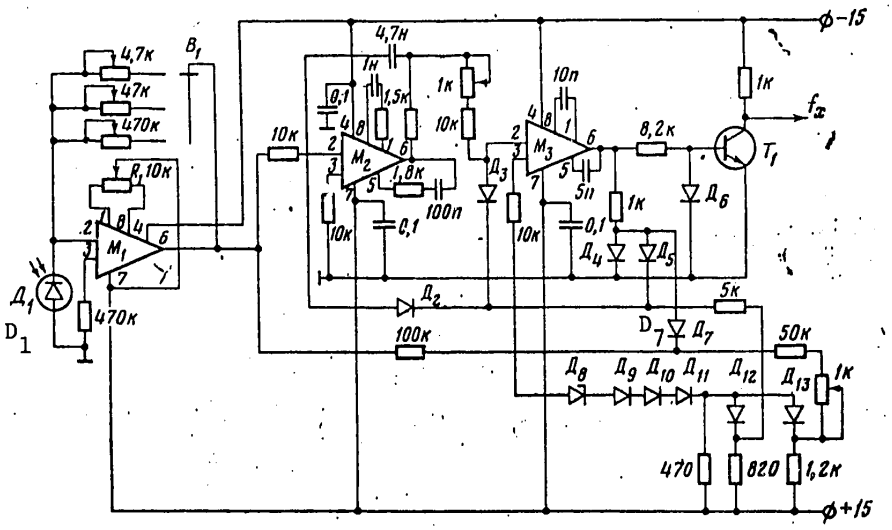


Figure 1. Basic schematic of the analog converter. $M_1$ = K544UD1A; $M_2$, $M_3$ = = K153UD1A; $T_1$KT312B; $D_1$ = FD-7K, $D_2$-$D_7$, $D_9$-$D_{13}$ = KD503B; $D_8$ = D818Ye.



APPROVED FOR RELEASE: 2007/02/09: CIA-RDP82-00850R000500020034-7

APPROVED FOR RELEASE: 2007/02/09: CIA-RDP82-00850R000500020034-7



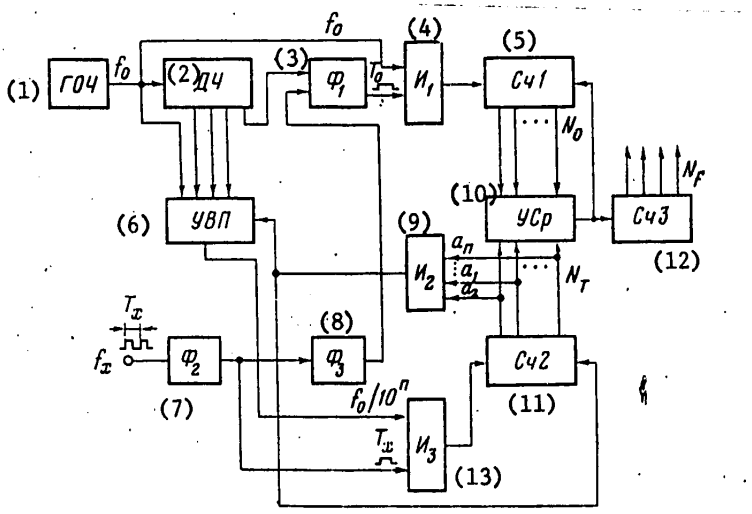


Figure 2. Block diagram of the frequency meter. GOCh is the master reference frequency generator.

Key: 1. GOCh = master frequency generator;
2. DCh = frequency divider;
3. $F_1$ = driver 1;
4. $I_1$ = AND gate 1;
5. Sch1 = counter 1;
6. UVP = measurement range selector;
7. $F_2$ = driver 2;
8. $F_3$ = driver 3;
9. $I_2$ = AND gate 2;
10. USr = code comparator;
11. Sch2 = counter 3;
12. Sch 3 = counter 3.

are equal, a comparison pulse is generated which sets counter Sch1 to zero and feeds the measurement results $N_f$ to the input of counter Sch3. Thus, a number $N_f$ proportional to the frequency being measured $f_x$, will be set in counter Sch3 after a time of $T_0$.

The frequency meter circuitry is supplemented with a measurement range selector (UVP) which connects one of the sample frequencies $f_0/10_n$ (n = 0 -- 3) generated by the frequency divider (DCh) to counter Sch2. With each overflow of counter Sch2, the AND gate $I_2$ generates a pulse which is used at the same time for switching the subband of the measurement range selector and writing the number $N_T/10$ into the counter Sch? [number illegible]. The presence of the measurement selector makes it possible to extend the dynamic range of the frequency meter up to four decades without increasing the number of digits in counters Sch1 and Sch2 or the code comparator.





APPROVED FOR RELEASE: 2007/02/09: CIA-RDP82-00850R000500020034-7

APPROVED FOR RELEASE: 2007/02/09: CIA-RDP82-00850R000500020034-7



A He + Ne LG-76 laser and a standard IMO-2-2 laser power meter were used to calibrate the meter at a wavelength of $\lambda = 0.63$ μ; in this case, the graduation error did not exceed 3 percent. In a measurement range of $10^{-8}$ - $10^{-4}$ W, the meter has a sensitivity of 0.1 V/μW, and in ranges of $10^{-4}$ - $10^{-3}$ and $10^{-3}$ - $10^{-2}$ W, it has a sensitivity of 0.01 and 0.001 V/μW respectively. The temperature instability does not exceed 6 percent in a temperature range of -10 to +40 °C.

BIBLIOGRAPHY

1. Anikina L., Vanyukov G., "Informatsionno-spravochnyy listok" ["Reference Data Sheet"], Moscow, VIMI, 1971, No 001563.

2. Plotnikov V.A., Chastukhina L.N., PTE [EXPERIMENTAL EQUIPMENT AND ENGINEERING], 1971, No 4, p 189.

3. Soboleva N.A., Melamid A.Ye., "Fotoelektronnyye pribory" ["Photoelectronic Devices"], Moscow, Vysshaya shkola publishers, 1974.

4. Aleksandrov V.S., Pryanishnikov V.A., "Pribory dlya izmereniy malykh napryazheniy i tokov" ["Instruments for Measuring Low Voltages and Currents"], Leningrad, Energiya Publishers, 1971.

5. Vendlend, ELEKTRONIKA, 1971, No 11, p 30.

6. Tychino K.K., "Preobrazovateli napryazheniya v chastotu" ["Voltage to Frequency Converters"], Moscow, Energiya Publishers, 1972.

7. Yermolov R.S., "Tsifrovyye chastotomery" ["Digital Frequency Meters"], Leningrad, Energiya Publishers, 1973.

8. Inozemtsev Ye.K., Babayeva O.S., PTE, 1979, No 5, p 156.

COPYRIGHT: Izdatel'stvo "Nauka", "Pribory i tekhnika eksperimenta", 1981

8225
CSO: 8144/0178



APPROVED FOR RELEASE: 2007/02/09: CIA-RDP82-00850R000500020034-7

APPROVED FOR RELEASE: 2007/02/09: CIA-RDP82-00850R000500020034-7



UDC 621.373.826:621.317

# SUBNANOSECOND PYROELECTRIC INFRARED RADIATION DETECTOR

Moscow PRIBORY I TEKHNIKA EKSPERIMENTA in Russian No 4, Jul-Aug 81 (manuscript received 10 Dec 79) pp 205-207

[Paper by V.P. Kuleshov and D.D. Malyuta]

[Text] Results of testing a lithium metaniobate $LiNbO_3$ pyroelectric detector are given for the recording of short $CO_2$ laser pulses. The response lag of the detector is less than 1 nanosecond and the sensitivity is about 0.15 V/MW.

Detectors which have a high operational speed, wide dynamic range and which are not destroyed by irradiation are needed for recording the radiation power of pulsed $CO_2$ lasers. The sensitivity of the detectors can be comparatively low because of the high radiation power. At the present time, detectors are used for these purposes which are based on the effect of entrainment of free charge carriers in the conductors [1], as well as detectors using μ-conductivity semiconductors [2], cooled semiconductor photoresistors [3] and pyroelectric detectors [4, 5].

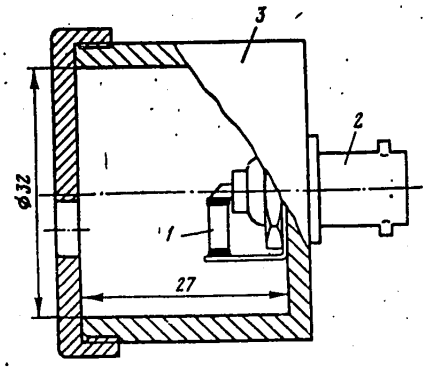


Figure 1. Structural design of a detector with edge electrodes.

Key: 1. Pyroelectric crystal;
2. SR-50-73F high frequency connector;
3. Brass housing with cap.

Pyroelectric detectors receive radiation in a range from the microwave to the ultraviolet wavelength, have a time resolution of < 0.1 nsec and a wide dynamic



APPROVED FOR RELEASE: 2007/02/09: CIA-RDP82-00850R000500020034-7

APPROVED FOR RELEASE: 2007/02/09: CIA-RDP82-00850R000500020034-7



range. Pyroelectric detectors operate at room temperature and are easy to fabricate and operate. Ferroelectric crystals with good pyroelectric properties are usually employed as the material for such detectors: TGS, SBN, $LiTaO_3$, $LiNbO_3$, etc.

When pyroelectrics in the form of rectangular parallelepipeds are used with the electrodes placed on the opposing end faces, two ways of orienting them are possible: the electrodes arranged in planes perpendicular to the beam (a frontal detector) or parallel to it (a detector with edge electrodes). In the absence of thermal losses to radiation and heat transfer, the volt-watt sensitivity of detectors with frontal and edge electrodes is defined by the following expressions:

$$S_1 = \tau\alpha\gamma/\varepsilon C_v;\ S_2 = bS_1/a;\ \tau > RC$$

where C is the detector capacitance; $\tau$ is the time resolution; $\alpha$ is the coefficient or radiation absorption by the detector material; $\gamma$ is the pyroelectric coefficient; $\varepsilon$ is the dielectric permittivity and $C_v$ is the bulk thermal capacity of the pyroelectric material; a and b are the dimensions of the crystal along and transverse to the beam; R is the detector load resistance.

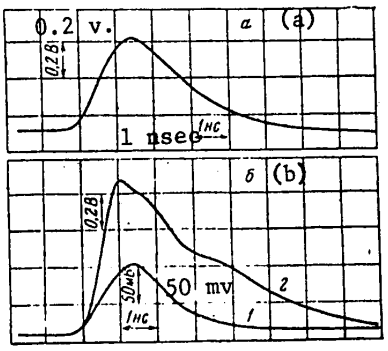


Figure 2. (a) The FP-1 detector signal; (b) $LiNbO_3$ pyroelectric detector signals.

Key: 1. Master laser stage;
2. Following the amplifier.

The condition $\tau > RC$ can be rewritten as follows for the two cases under consideration here: $A_1/a_1 < \tau/\varepsilon R$; $A_2/a_2 < (\tau/\varepsilon R)\cdot(b_2/a_2)^2$ (A is the detector area). It can be seen that the condition in the second case is substantially less stringent than in the first.

The structural design of the detector with edge electrodes which we used is depicted in Figure 1. The $LiNbO_3$ detector crystal had dimensions of 5 x 3 x 1.5 $mm^3$ and an inherent capacitance of about 2 pFd. The electrodes were applied by means of conducting glue based on silver. The electrical contact between the detector and the high frequency connector was made using this same glue. The long cable which connects the detector to the oscilloscope was loaded into a resistance equal to the characteristic impedance (50 ohms). For this reason, the electrical time constant of the detector did not exceed 0.1 nsec.

The waveform of the radiation signal of a master laser stage obtained with the detector using the entrainment effect of a FP-1 is shown in Figure 2, while the signals from the master stage as well as after the amplifier, obtained with the pyroelectric detector, are shown in Figure 2b. They were recorded with an oscilloscope having a bandwidth of 500 MHz. It can be seen that the waveform of the laser master stage radiation signals, obtained by different detectors, is practically the same. As was to be expected, the signal waveform changed following amplification: the slope of the leading edge and the decay time increased.





APPROVED FOR RELEASE: 2007/02/09: CIA-RDP82-00850R000500020034-7

APPROVED FOR RELEASE: 2007/02/09: CIA-RDP82-00850R000500020034-7



Tests of a $LiTaO_3$ detector with frontal electrodes (without a substrate) 30 μm thick and an electrode area of about 3 $mm^2$ and a capacitance of 20 pFd showed (Figure 3) that it is sensitive to ultrasonic oscillations (which circulate between the faces of the crystal), the direction of propagation of which coincides with the spontaneous polarization vector [6].

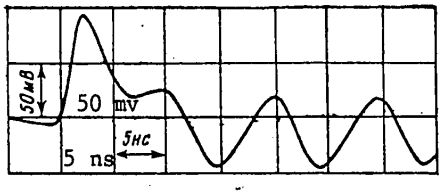


Figure 3. Signal from a $LiTaO_3$ detector with frontal electrodes.

A detector with edge electrodes made of industrial TsTS-19 ceramic (5 x 7 x 0.8 $mm^3$; C = 10 pFd) had a high sensitivity, but unfortunately, the pulse decay was markedly protracted.

The signal rise time for all of the pyroelectric detectors we tested was governed by the electrical time constant of the detector and the oscilloscope bandwidth. The minimum rise time of about 0.7 nsec was obtained when $LiNbO_3$ was employed. This time corresponds to the oscilloscope passband and is evidence of the high speed of the detector and the short leading edge of the radiation pulse at the output of the laser amplifier.

The comparatively high signal voltage (about 7 volts for a $LiNbO_3$ detector) makes it possible to use a "Lotos" oscilloscope with a bandwidth of up to 7 GHz for the recording.

BIBLIOGRAPHY

1. Agafonov V.G., Volkov P.M., Ryvkin B.S., Yaroshetskiy I.D., FIZ. I TEKHN. POLUPROVODNIKOV [SEMICONDUCTOR PHYSICS AND ENGINEERING], 1973, Vol 7, No 12, p 2316.

2. Beregulin Ye.V., Valov P.M., Ryvkin S.M., et al., KVANTOVAYA ELEKTRONIKA [QUANTUM ELECTRONICS], 1978, Vol 5, No 6, p 1386.

3. Butkevich V.G., Trishenkov M.A., Collected Papers, "Spravochnik po lazeram" ["Laser Handbook"], Edited by Prokhorov A.M., Moscow, Sovetskoye Radio Publishers, 1979.

4. Novik V.K., Gavrilova N.D., Fel'dman N.B., "Piroelektricheskiye preobrazovateli" ["Pyroelectric Transducers"], Moscow, Sovetskoye Radio Publishers, 1979.



APPROVED FOR RELEASE: 2007/02/09: CIA-RDP82-00850R000500020034-7

APPROVED FOR RELEASE: 2007/02/09: CIA-RDP82-00850R000500020034-7



5. Voronov V.V., Karlov N.V., Kuz'min G.P., et al., KVANTOVAYA ELEKTRONIKA, 1977, Vol. 4, No. 9, p 1903.

6. Roundy S.V., Byer R.L., APPL. PHYS. LETT., 1972, Vol. 21, No. 10, p 512.

COPYRIGHT: Izdatel'stvo "Nauka", "Pribory i tekhnika eksperimenta", 1981

8225
CSO: 8144/0178



APPROVED FOR RELEASE: 2007/02/09: CIA-RDP82-00850R000500020034-7

APPROVED FOR RELEASE: 2007/02/09: CIA-RDP82-00850R000500020034-7



UDC[621.382: 546.28]: 537.32

# INTEGRATED TEMPERATURE SENSOR USING SILICON DIODE MATRICES

Moscow PRIBORY I SISTEMY UPRAVLENIYA in Russian No 9, Sep 81 pp 29-30

[Article by engineers N. D. Gadzhiyev, R. A. Gadzhiyev and Yu. B. Leshchinskiy]

[Text] In semiconductor thermometry, when designing diode sensors, the temperature relationship between the forward voltage drop $U_{tr}$ across the pn junction of the semiconductor at a constant value of forward current, $I_f$ is usually used. The basic shortcoming of such sensors -- the small value of the temperature coefficient of voltage (TKN) and the large spread of the sensor parameters from sample to sample -- may be eliminated by using integrated technology. The value of TKN for silicon pn junctions is about 2 millivolts/°C, but when they are used as sensors, their TKN may be increased by series connection of several diodes, i.e., using integrated diode matrices. Because of the use of special technological methods in manufacturing integrated diode matrices, a considerable reduction in the spread of forward voltage drops between the diode assemblies within one lot became possible and greatly improves the reproducibility characteristics.

It was established experimentally that the greater the TKN, the smaller the value of forward current $I_f$ which may be seen from Fig. 1. In thermometry, it is essestial that the TKN be practically independent of the temperature, i.e., the slopes of the forward $U_f=f(T)$ at all current values are constant in the entire temperature range. It is precisely this fact that makes it valuable to use the diodes as temperature sensors.

The manufactured matrice represents a diode assembly consisting of 6 to 12 series connected diodes. The base material here has an epitaxial structure

$$\frac{\text{10 KEF-(0.3 to 0.5)}}{\text{300 KDB-10}}$$

in which the pn junction region was created by diffusing a boron impurity in accordance with a planar-diffusion technology. The size of the sensor crystal is $0.7 \times 0.7$ mm$^2$. According to Fig. 1, to obtain the maximum temperature sensitivity and reduce the effect of self-heating on the sensor parameters, a region of small currents, such as $I_f$=100 to 200 microamperes, was selected as the working region. In this case, the output analog signal at room temperature is several volts (depending upon the number of connected diodes).



APPROVED FOR RELEASE: 2007/02/09: CIA-RDP82-00850R000500020034-7

APPROVED FOR RELEASE: 2007/02/09: CIA-RDP82-00850R000500020034-7



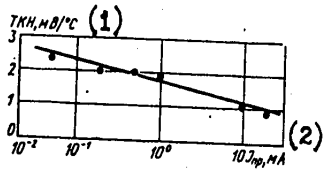


Fig. 1. Relationship between the TKN of a silicon pn junction and the passed current.
1. TKN, millivolts/°C 2. $I_f$, milliamperes

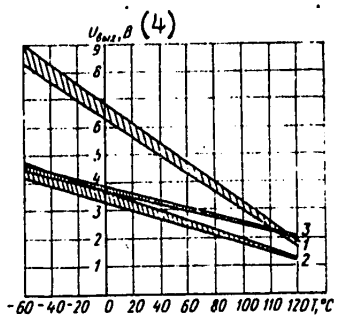


Fig. 2. Output characteristics of the temperature sensor (shaded region of spread within one production lot).
4. $U_{output}$, volts.

Fig. 2 shows the curves of the relationships betwen the value of $U_f$ ($U_{output}$) and the temperature for matrices consisting of six (curves 1) and twelve (curves 2) diodes. The observed spread of values from sample to sample applies to 50 matrices taken from one production lot. The curves substantiate the presence of a linear relationship in the entire temperature range (from -60 to + 120°C). The sensors represent silicon crystals with diode assemblies mounted on the base of the TO5 body.

Special measures [1] were taken to reduce the $\Delta U_f$ spread between diodes in assembling which made it possible to improve the reproducibility of the sensor characteristics. In Fig. 2 (curves 3) are shown characteristics of 50 diode assemblies manufactured on chips, rejected due to the microscopic nonuniformity of the





APPROVED FOR RELEASE: 2007/02/09: CIA-RDP82-00850R000500020034-7

APPROVED FOR RELEASE: 2007/02/09: CIA-RDP82-00850R000500020034-7



specific resistance and which were subjected to preliminary annealing to equalize the nonuniformities with respect to the concentration of impurities in the initial material. It may be seen from the Figure that the spread zone for these assemblies is considerably smaller: it does not exceed ± 0.12 volts at $I_f$=100 microamperes, which is confirmed by histograms.

The advantages of the developed sensors are their high reproducibility of characteristics, fairly high values of the output signal and small size.

Basic sensor specifications

| | |
|---|---|
| Number of diodes | 12 |
| Sensitivity in millivolts/°C | 20-25 |
| Time constant in seconds | 20-30 |
| Dimension in mm | diameter 1.5, l=2 |
| Nonlinearity in % | 0.1 |
| Range of measured temperatures in °C | -60 to 120 |

The sensors passed tests in industrial equipment and were recommended for series production.

The six-diode sensor in particular was used for the accurate measurement of the temperature of the surface of the human body under clinical conditions. To reduce the time constant of the sensor the matrix is mounted directly on the end of a shielded cable 1 mm in diameter, is soldered to its lead-outs and is protected by an epoxy tar with a quartz sand filler. Its time constant was 20-30 seconds. The sensor, fed from a current oscillator with $I_f$=100 microamperes, was connected through a scaling type 701ML19 operational amplifier to the input of a VK7-16 digital voltmeter so that 0-1 volt voltmeter scale corresponded to a temperature of 0-100°C. The calibration was made at two points (0 and 100°C).

The subsequent check of intermediate temperature values on the TS-16 ultrathermostat indicated that the sensor makes it possible to measure temperature in this range to an accuracy not worse that 0.1°C.

COPYRIGHT: Izdatel'stvo "Mashinostroyeniye", "Pribory i sistemy upravleniya", 1981

2291
CSO: 1860/75



APPROVED FOR RELEASE: 2007/02/09: CIA-RDP82-00850R000500020034-7

APPROVED FOR RELEASE: 2007/02/09: CIA-RDP82-00850R000500020034-7



MICROELECTRONICS

UDC 621.382

# PROSPECTS OF USING MEDIA WITH HIGHER DIELECTRIC CONSTANT IN MICROWAVE GIS TECHNOLOGY

Moscow MIKROELEKTRONIKA in Russian Vol 10, No 5, Sep-Oct 81 (manuscript received 13 Mar 80) pp 433-439

[Article by Yu. A. Lifshits and R. P. Seysyan]

[Text] At the present time, microstrip microwave GIS [hybrid integrated circuits] are usually made on substrates with a dielectric constant (DP) of $\varepsilon \approx 10$. This value of DP is satisfactory in many respects [1]: it is possible to produce microstrip lines (MPL) with wave impedances in the range of $20 \div 200$ ohms; the quality factor of microstrip (MP) resonators is sufficient for many applications in circuit engineering, radiation from MPL into the substrate and the surrounding space is not high. However, the relatively small value of the wavelength shortening factor $\sqrt{\varepsilon_e} \approx 2{,}5$ ($\varepsilon_e$ -- effective DP [2]) is responsible for the considerable (on the microelectronic scale) dimensions of the elements of microwave GIS (quarter-wave stub in the 10-centimeter range has a length of about 10 mm). As a result of this, one or, less frequently, several identical circuits are arranged on the substrate. The "piece-by-piece" fabrication of microwave MP GIS plates which is done by performing technological operations characteristic for thin-film microelectronics (vacuum application of conducting and resistive layers, precision photolithography, galvanostegy) contradicts the group-integration principles of microelectronics. This work examines the possibilities of overcoming this contradiction by using substrates with $\varepsilon > 10$.

A substantial characteristic of microelectronic technology is its group-integration nature which provides for successive performance of all operations of the process of the fabrication of a microcircuit plate over the substrate divided upon the completion of the cycle into N identical plates. Realization of this principle ensures the technical and economic effect of microelectronics. The greater the number n of usable plates is obtained from one substrate, the greater is the effect. The yield factor of usable $\eta = n/N$ is determined by the concentration and distribution by the dimensions of critical defects and by topological patterns of the circuit. The value of $\eta$ is a composite function of the topological dimensions and, in some instances, can even grow with the growth of N, particularly for this case of a relatively large-scale topological pattern.

The cost (C) of an IS [integrated circuit] plate (without external elements) is almost proportional to the MP area of the circuit $S_{МП}$, practically does not depend on the complexity of the circuit [3] and can be determined from the relation



APPROVED FOR RELEASE: 2007/02/09: CIA-RDP82-00850R000500020034-7

APPROVED FOR RELEASE: 2007/02/09: CIA-RDP82-00850R000500020034-7



$$C=\frac{\sum_{k=1}^{M} C_k + C_0}{\eta N}=\frac{S_{\text{мп}}}{S_0}\left(\sum_{k=1}^{M} C_k + C_0\right)\eta^{-1}, \quad (1)$$

where $S_0$ -- substrate area, $C_k$ -- expenses on conducting the k-th of the total number M of technological operations of manufacturing a "passive" plate, $C_0$ -- the cost of the substrate.

It follows from (1) that, at a fixed level of technology ( $\eta$ = const), the expenses can be reduced by increasing the value of N, which is achieved by reducing the dimensions of the circuit.

The geometrical length $l$ of MPL sections forming the MP circuit is determined by the necessary electrical length $\vartheta$, while $l=\lambda\vartheta/2\pi\sqrt{\varepsilon_e}$, where $\lambda$ is the wavelength in the free space.

Consequently, when the DP of the substrate changes, the geometric length $l$ changes in proportion to $1/\sqrt{\varepsilon_e}$. If the circuit is a cascade connection of MPL sections oriented along one of the sides of the substrate, then the second dimension of the plate is determined by the considerations of reducing the parasitic connections between paralell MPL and it depends weakly on DP. The decrease of the $S_{\text{МП}}$ area with the increase of DP is approximately proportional to $1/\sqrt{\varepsilon}$.

Table 1

Radioceramic Materials with High DP for the Microwave Range

| (1) Марка | | $\varepsilon$ | $\operatorname{tg}\delta\cdot10^4$ при $f=10$ ГГц, (2) не более | ТКЕ·10⁶, град⁻¹ (3) |
|---|---|---|---|---|
| TL | ТЛ/0 | 35 | 5 | 0±30 |
| | ТЛ/–75 | 50 | 4 | –75±30 |
| TBNS | ТБНС | 80 | 8 | 0±30 |
| TTs | ТЦ/–750 | 100 | 3 | $-(750^{+100}_{-150})$ |
| T | Т-150 | 150 | 10 | $-(1500^{+200}_{-300})$ |
| | Т-250 | 250 | 20 | –3300±1000 |

Key: 1. Trademark
2. f = 10 GHz, not over
3. TKE [temperature coefficient of capacitance] $\cdot 10^6$, degrees$^{-1}$

If the circuit contains parallel stubs or circular (for example, bridge) elements, i.e., if it is oriented by two coordinates of the substrate, then the area of the plate $S_{\text{МП}}$ changes approximately as $1/\varepsilon$.

In real circuits, both configuration cases occur, and the area of the plate is connected with the relative DP by the relation of the following type:

$$S_{\text{мп}}=a/\varepsilon^{\alpha}, \quad (2)$$





APPROVED FOR RELEASE: 2007/02/09: CIA-RDP82-00850R000500020034-7

APPROVED FOR RELEASE: 2007/02/09: CIA-RDP82-00850R000500020034-7



where a is the area of the circuit at $\varepsilon = 1$, $1/2 \leqslant \alpha \leqslant 1$. Then the number of the circuits on the substrate is $N = S_0 \varepsilon^{\alpha}/a$.

It follows from (1) and (2) that when substrates with DP $\varepsilon_1$ and $\varepsilon_2$ are used, the equality $C_1/C_2 = (\varepsilon_2/\varepsilon_1)^{\alpha}$ is fulfilled for the cost of the plates.

With regard to the costs of the substrates $C_{01}$ and $C_{02}$, as well as the coefficients of the yield of suitable $\eta_1$ and $\eta_2$, it is assumed that: $C_{01} = C_{02}$, $\eta_1 = \eta_2$; indexes 1 and 2 refer to the substrates with DP $\varepsilon_1$ and $\varepsilon_2$, respectively.

Thus, an increase in DP, for example, from 10 to 50 ensures a two five-fold decrease in the cost of the GIS plate. Moreover, along with the lowering the production costs, it is possible to ensure the improvement of the weight and the dimensional characteristics of microwave GIS, as well to shift the boundary of the application of the devices with distributed parameters into the area of lower frequencies.

At the present time, ceramic materials have been developed [4-7] which are relatively "transparent" for microwaves ($\operatorname{tg}\delta \leqslant 20 \cdot 10^{-4}$ on frequencies $f \leqslant 10$ GHz) with DP $\leqslant$ 250 (see Table 1) and are suitable for manufacturing microwave GIS substrates.

It should be taken into consideration that materials with DP $\geqslant 100$ are characterized by high values of TKYe [temperature coefficient of capacitance] (TKYe $\leqslant -750 \cdot 10^{-6}$ degrees$^{-1}$). Nevertheless, the possibility of achieving a noticeable technical and economic effect makes their study in this aspect justifiable, particularly in connection with the fact that the active semiconductor part of the circuit quite frequently requires effective heat removal or thermostatic control.

Let us evaluate the MPL parameters on substrates made of ceramic materials with a high DP. Figure 1 gives the necessary designations and shows the dependence of the wavelength shortening factor $\sqrt{\varepsilon_e}$ and the wave impedance Z on the width of the MPL conductor w/h normalized to the height of the substrate which was obtained for three values of DP (10, 50 and 100) in accordance with the relations [2]:

$$\varepsilon_e = (\varepsilon+1)/2 + [(\varepsilon-1)/2]\,[1+10/(\omega/h)]^{-1/2}, \quad (3)$$

$$Z\sqrt{\varepsilon_e} = 59{,}952 \ln (8/(w/h) + (w/h)/4), \quad w/h \leqslant 1, \quad (4a)$$

$$Z\sqrt{\varepsilon_e} = 119{,}904\pi/[(w/h) + 2{,}42 - 0{,}44(h/w) + (1-h/w)^6], \quad w/h \geqslant 1, \quad (4б)$$

assuming that there is no dispersion in MPL: $d\varepsilon_e/d\omega = 0$.

It follows from Figure 1 that the increase of DP from 10 to 100 reduces the length of MP elements to one third. At the same time, the range of the "accessible" wave impedances decreases, which can sometimes limit the circuit engineering possibilities and serves as a source of metrological difficulties. However, the limitation of the values of wave impedances of the channel is not an obstacle for creating the majority of the devices, and in a number of cases the possibility of realizing low-resistance MPL could be an advantage of the substrates in question.

The relations (3), (4a), (4b) make it possible to find maximum relative errors in the shortening factor and the wave impedance due to errors of $\Delta\varepsilon/\varepsilon$, $\Delta h/h$ and $\Delta w/w$:





APPROVED FOR RELEASE: 2007/02/09: CIA-RDP82-00850R000500020034-7

APPROVED FOR RELEASE: 2007/02/09: CIA-RDP82-00850R000500020034-7



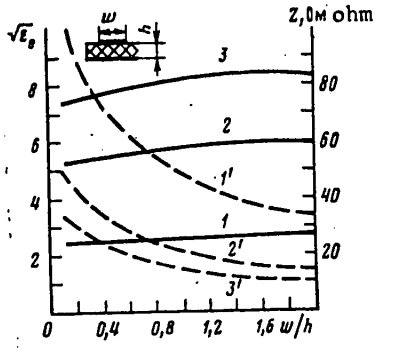


Рис. 1

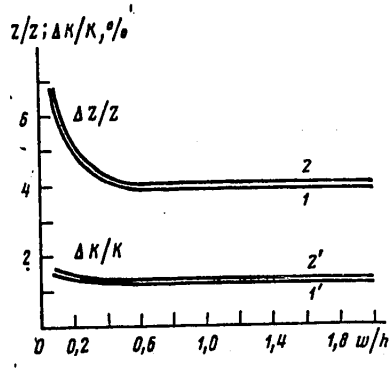


Рис. 2

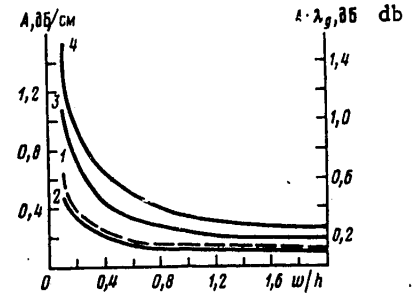


Рис. 3

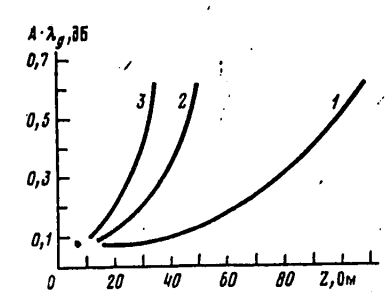


Рис. 4

Figure 1. Dependence of the wavelength shortening factor (solid line) and wave impedance (interrupted lines) of MPL on the normalized width of the conductor at $\mathcal{E}$ =10 (1,1'), 50 (2,2'), 100 (3,3').

Figure 2. Dependence of relative errors in the shortening factor and the wave impedance of MPL on the normalized width of the conductor; $\mathcal{E}$ = 10 (1,1') 50 (2,2'), 100 (1',2'); $\Delta w$ = 10 μm, h = 0.5 mm, $\Delta\mathcal{E}/\mathcal{E}$ = 2%, $\Delta h/h$ = 4%.

Figure 3. Dependence of attenuation in MPL on the normalized width of the conductor (1 -- attenuation computed for the wavelength: 2, 3, 4 -- linear attenuation) at $\mathcal{E}$ = 10 (2), 50 (3), 100 (4); f = 10 GHz, h = 0.5 mm, $\rho = 2.5 \cdot 10^{-6}$ ohm·cm.

Figure 4. Dependence of attenuation calculated for the wavelength on the wave impedance of MPL at $\mathcal{E}$ = 10 (1), 50 (2), 100 (3).

$$(\Delta k/k)_{\text{макс}} = (\Delta\sqrt{\varepsilon_e}/\sqrt{\varepsilon_e})_{\text{макс}} = (1/2)\{[|\Delta\varepsilon|/\varepsilon]/[1+(1/\varepsilon)[(A-1)/(A+1)]]+ +5(|\Delta h|/h+|\Delta w|/w)/((w/h)+10)[[(\varepsilon+1)/(\varepsilon-1)]A+1]\} \quad (5)$$





APPROVED FOR RELEASE: 2007/02/09: CIA-RDP82-00850R000500020034-7

APPROVED FOR RELEASE: 2007/02/09: CIA-RDP82-00850R000500020034-7



Here $A=\sqrt{1+10/(w/h)}$.

$$(\Delta Z/Z)_{\text{макс}}=(\Delta\sqrt{\varepsilon_e}/\varepsilon_e)_{\text{макс}}+F(w/h)\,(|\Delta h|/h+|\Delta w|/w), \qquad (6)$$

$$F(w/h)=\begin{cases}\left|\dfrac{1}{\ln[32+(w/h)^2]/4(w/h)}\,\dfrac{(w/h)^2-32}{(w/h)^2+32}\right|, & w/h\leqslant 1,\\ \dfrac{(w/h)+(h/w)\,(0{,}44+6\,(1-(h/w))^5)}{(w/h)+2{,}42-0{,}44\,(h/w)+(1-(h/w))^6}, & w/h\geqslant 1.\end{cases}$$

It follows from the examination of these relations (Figure 2) that the increase of the DP of the substrates does not make it necessary to increase accuracy requirements for preserving the values of relative errors.

It is assumed in calculations by (5) and (6) that the sources of errors are identical for all values of DP and are: $|\Delta w|$ = 10 μm, $|\Delta\varepsilon|/\varepsilon$ = 2%, $\Delta h/h$=4% at h=0.5 mm and t=10 μm, where t is the thickness of MPL conductors.

The linear attenuation in MPL conductors (Figure 3) computed by the simplified formula

$$A=545{,}4\frac{\sqrt{f\rho}}{Zw}\ \frac{\text{дБ}}{\text{м}}, \qquad (7)$$

where f -- frequency (GHz), ρ -- specific resistance of MPL conductors (Ohm·m) increases with the growth of DP, and attentuation calculated for the wavelength in MPL $\lambda_g$, $A\lambda_g=A\lambda\sqrt{\varepsilon_e}$ does not depend on DP. The values of $A\lambda_g$ found for the values of DP under consideration at a given value of Z are shown in Figure 4.

Figure 4 indicates the necessity of lowering Z in order to preserve a constant value of $A\lambda_g$ as the DP of the substrate increases without changing its thickness.

The intrinsic quality factor $Q_0$ of an MP resonator is defined by the $A\lambda_g$ product:

$$Q_0=27{,}3/A\lambda_g, \qquad (8)$$

therefore, $Q_0$ depends only on the value of the parameter w/h.

Attenuation in the MPL caused by dielectric losses in the substrate calculated for the wavelength in the MPL

$$A_d\lambda_g\approx 27{,}3\sqrt{\varepsilon/\varepsilon_e}\,\operatorname{tg}\delta\approx 40\operatorname{tg}\delta\ \text{дБ} \qquad (9)$$

practically does not depend on DP and w/h. The relation $A_d/A$ (Figure 5) does not exceed 25% in the entire range of changes of w/h being examined: the "dielectric" losses in the MPL are small for real values of $\operatorname{tg}\delta$.

Nonuniformities in MP devices (an open end of MPL, a gap in the conductor, a bend, T-coupling, etc) could excite surface waves in the substrate causing spurious couplings in the circuit. The cutoff frequency of the lowest mode of the H-wave



APPROVED FOR RELEASE: 2007/02/09: CIA-RDP82-00850R000500020034-7

APPROVED FOR RELEASE: 2007/02/09: CIA-RDP82-00850R000500020034-7



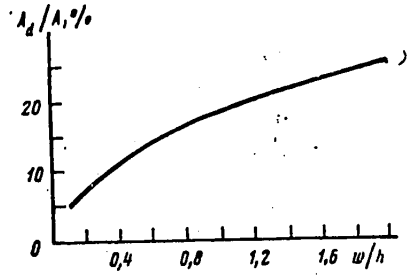


Рис. 5

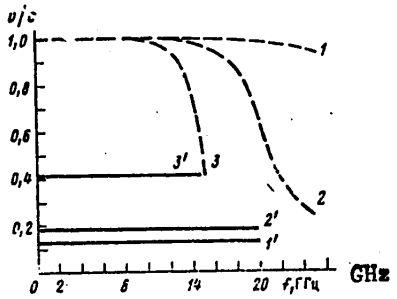


Рис. 6

Figure 5. Dependence of the ratio of dielectric losses to ohmic losses on the normalized width of the MPL conductor: f = 10 GHz, $\rho = 2.5 \cdot 10^{-6}$ Ohm·cm, $\operatorname{tg}\delta = 5 \cdot 10^{-4}$.

Figure 6. Dependence of phase velocity on frequency (1, 2, 3 -- lowest surface E-wave, 1', 2', 3' -- quasi-T-wave in MPL) at $\varepsilon = 10$ (1,1') 50 (2, 2'), 100 (3,3'); w/h = 0.1.

$$f_н = 75/h_{мм}\sqrt{\varepsilon - 1},\ \text{ГГц}, \tag{10}$$

is shown in Table 2 for the case of h = 0.5 mm.

Table 2
Cutoff Frequency of Surface H-Waves

| $\varepsilon$ | 10 | 50 | 100 |
|---|---|---|---|
| $f_н$ (ГГц) GHz | 50 | 21,4 | 15,1 |

The lowest mode of the E-wave has the cutoff frequency $f_E = 0$. The conditions of the excitation of a surface wave by the field of a quasi-T-wave of MPL become more favorable as the velocities of the surface and quasi-T-wave come closer together. Figure 6 shows the dependence of phase velocity normalized to the speed of light v/c of the lowest E-wave on the frequency (curves 1-3) found by solving the appropriate dispersion equation [8].

In the case of a quasi-T-wave propagating without dispersion in MPL, the normalized phase velocity is determined by the value of $\varepsilon_e$

$$v_{мпл}/c = 1/\sqrt{\varepsilon_e} \tag{11}$$

(curves 1', 2', and 3' in Figure 6). It can be seen from Figure 6 that the phase velocity of the surface E-wave is close to $v_{MPL}$ on frequencies above $f_H$ (Table 2). This determines the upper operating frequency of MPL.





APPROVED FOR RELEASE: 2007/02/09: CIA-RDP82-00850R000500020034-7

APPROVED FOR RELEASE: 2007/02/09: CIA-RDP82-00850R000500020034-7



Studies of the MPL parameters on substrates with $\varepsilon = 35 \div 90$ showed, for example, that the extrapolation of the measured values of $\varepsilon_e$ to the value of $\varepsilon_e(f=0)$ yields a result which differs from the result calculated by (3) by not more than 1%. Changes of the value of $\sqrt{\varepsilon_e}$ in a frequency range of $0.001 \div 10$ GHz constitute $\sim 5\%$. Attenuation in MPL coincides qualitatively with that calculated by (7). It can be asserted that a quasi-T-wave propagates in MPL in the above DP and frequency interval, which facilitates the creation of a broad class of MP devices.

Along with studies on the MPL parameters, plates of individual functional MP assemblies were designed and manufactured on substrates with a high DP, including cells of a three-discharge phase shifter, balanced mixer, Gunn-effect oscillator, detector, and others (Figure 7, not included in the translation). Studies of MP assemblies showed the possibility of obtaining parameters which are at least not any worse than those achieved at the present time for GIS on substrates with $\varepsilon \approx 10$, but with smaller dimensions and the use of integrated group methods of production.

Separation of the plate of a complex GIS into simpler ones ensures the possibility of functional control and sufficiently high values of $N = 40 \div 100$ without preventing the creation of complex GIS, because the joining of individual plates does not cause any substantial difficulties and the joints do not serve as sources of any noticeable nonuniformities.

Along with MPL, other types of transmission lines (LP) find applications in creating GIS of the microwave range, for example, slotted lines, coplanar waveguides, and others. Conductors in these LP are arranged in one plane, due to which the influence of the scattering fields increases. The use of substrates with a high DP makes it possible to increase the field concentration in the dielectric substrates. Just as in the case of MPL, the selection of DP must be dictated by the compromise between the values of the shortening factor and the wave impedance.

Increasing the DP of substrates is promising also in creating a "microwaveguide" which is an MPL in which an $H_{10}$-type wave is excited instead of a quasi-T-wave.

Conclusions

1. By increasing the DP of substrates, it is possible to reduce the dimensions of MP elements, which opens up the way for using integrated group methods of technology, as well as makes it possible to create GIS with distributed parameters in the low-frequency part of the range where circuits on substrates with $\varepsilon \approx 10$ are not realizable.

2. Reduction of the dimensions of the plates of microwave GIS by increasing the DP can, as a rule, be ensured with preserving the parameters achieved in the designs of MP devices on substrates with $\varepsilon \approx 10$. In this case it is necessary to use circuit engineering solutions which take into consideration the specific characteristics of MPL on the substrates used.

3. It has been established experimentally that a quasi-T-wave propagates in MPL on substrates with $\varepsilon = 35\text{-}90$ at $0.1 \leqslant (w/h) \leqslant 2$ and $f \leqslant 10$ GHz. MPL parameters can be determined with a sufficient degree of accuracy by the methods developed for the case of $\varepsilon \approx 10$.



APPROVED FOR RELEASE: 2007/02/09: CIA-RDP82-00850R000500020034-7

APPROVED FOR RELEASE: 2007/02/09: CIA-RDP82-00850R000500020034-7



Bibliography

1. Maloratskiy, L. G. "Mikrominiatyurizatsiya elementov i ustroystv SVCh" [Microminiaturization of Microwave Elements and Devices], Moscow, Sovetskoye radio, 1976, 94 pages.

2. Ganston, M. A. R. "Sprovochnik po volnovym soprotivleniyam fidernykh liniy SVCh" [Handbook on Wave Impedances of Microwave Feeder Lines], Moscow, Svyaz', 1976.

3. Gus'kov, G. Ya., Yegorov, Ye. N., and Salgus, K. K. ELEKTRONNAYA TEKHNIKA [Electronic Engineering], Series 10, Microelectronic Devices, 1977, No 6, p 25.

4. "Materialy keramicheskiye radiotekhnicheskiye GOST 5458-75" [Radio Engineering Ceramic Materials GOST 5458-75], Moscow, Izd standartov, 1978.

5. Isayev, V. F., Lifshits, Yu. A., Fridberg, I. D., and Cherkudinov, A. S. "Vysokotemperaturnaya khimiya silikatov i okislov" [High-Temperature Chemistry of Silicates and Oxides], Leningrad, Nauka, 1972, p 112.

6. Varfolomeyev, I. N., Dmitriyev, S. D., and Panin, V. F. ELEKTRONNAYA TEKHNIKA, Series 10, Microelectronic Devices, 1977, No 5, p 46.

7. Narytnik, T. N., Voytenko, A. G., Rotenberg, B. A., Mudrolyubova, L. P. and Lisker, K. Ye. ELEKTRONNAYA TEKHNIKA, Series 1, Microwave Electronics, 1978, No 10, p 102.

8. Vol'man, V. I., and Pimenov, Yu. V. "Tekhnicheskaya elektrodinamika" [Technical Electrodynamics], Moscow, Svyaz', 1971, p 284.

COPYRIGHT: Izdatel'stvo "Nauka", "Mikroelektronika", 1981

10,233
CSO: 1860/63



APPROVED FOR RELEASE: 2007/02/09: CIA-RDP82-00850R000500020034-7

APPROVED FOR RELEASE: 2007/02/09: CIA-RDP82-00850R000500020034-7



UDC 621.382.001.2

# PROBLEMS OF MODELING ELEMENTS OF LARGE-SCALE INTEGRATED CIRCUITS WITH SUBMICRONIC DIMENSIONS

Moscow MIKROELEKTRONIKA in Russian Vol 10, No 5, Sep-Oct 81 (manuscript received 17 Jan 80) pp 387-406

[Article by K. O. Petrosyants and L. S. Khodosh]

[Text] The latest achievements in semiconductor technology connected primarily with the improvement of the methods of alloying, lithography and etching [1-4] will make it possible in the next five years to assimilate and develop mass production of large-scale and superlarge-scale integrated circuits (BIS and superBIS) containing hundreds of thousands of elements with micronic and submicronic dimensions. First such circuits have already been developed. They are for example dynamic ZU [master devices] with random access and with a capacity of 64 kilobits and a static capacity of 16 kilobits [5]. Analysis of the present level and tendencies in the development of semiconductor technology indicates that in a few years the active and passive elements of BIS and superBIS will have the following minimum geometrical parameters: topological dimensions of individual areas of the structure -- up to 1 μm, thickness and depth of diffused and ion-implanted layers -- up to 0.05 ... 0.1 μm, thickness of dielectric, metal and polysilicon films -- up to 0.025...0.05 μm. BIS and superBIS will, evidently, work at lower supply and signal voltages -- of the order of 1... 3 V. These parameters are close to those limit minimum values at which subminiature semiconductor devices and circuits using them can still operate normally [6-9].

The role of automated (machine) designing as a whole and the modeling of BIS and superBIS elements, both of bipolar and MDP [metal-insulator-semiconductor] devices in particular, becomes extremely important at all stages of the designing of these supercomplex circuits [1, 3]. This work examines the modern state of studies in the area of modeling subminiature elements of modern BIS and superBIS, evaluates the potentialities of the existing models and analyzes the problems and ways of further development and improvement of the system of modeling the elements of bipolar and MDP BIS and superBIS.

## Bipolar Elements

Substantial reduction of the dimentions of BIS elements and the use of functionally integrated elements make it necessary to give up the methodology of the analysis of elements as devices with lumped parameters and to examine whole ensembles of elements as a system with distributed constants. This requires solution of fundamental equations of the physics of semiconductors in the form of a system of partial differential equations, which is the basis of physicotechnological modeling [10, 11].



APPROVED FOR RELEASE: 2007/02/09: CIA-RDP82-00850R000500020034-7

APPROVED FOR RELEASE: 2007/02/09: CIA-RDP82-00850R000500020034-7



The following physical effects are determining for BIS and superBIS elements: two-dimensional, in some instances three-dimensional, nature of the processes of current flow and distribution of potentials; distributed nature of the instrument's structure; joint effect of electrical and thermal fields; possibility of the appearance of a disruptive discharge due to the puncturing of the base and through depletion; the effect of the natural delay of the transistor switching in the nanosecond and picosecond ranges; recombination of the carriers on the $Si-SiO_2$ interface on the boundaries with highly allayed regions of the $n^+$ and $p^+$ types, in passive areas of the instrument; influence of spurious effects and coupling.

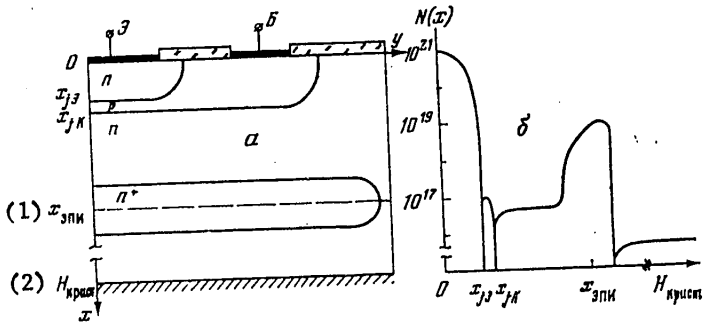


Figure 1. Cross section -- a and the resulting impurity profile -- b of an n-p-n-transistor.

Key: 1. $x_{epi}$
2. $H_{crystal}$

For elements with submicronic dimensions, all these effects are of the same importance and are manifested jointly. As a result of this, it is necessary to consider them in an integrated way, which greatly complicates their modeling.

The elements of bipolar BIS and superBIS are multidopant semiconductor structures which are described mathematically by a three-dimensional system of current transport, continuity, and Poisson equations. It is impossible to solve a three-dimensional problem in the general form due to the limited speed and memory resources of modern computers. As a rule, it is possible to simplify the problem correctly using either a two-dimensional or a quasi-three-dimensional approximation taking into consideration physical effects which are important for the BIS elements. This does not at all exclude the use of models based on a one-dimensional approximation in calculating BIS elements. For example, programs of unidimensional calculation of diffused distribution of impurities [13, 14] and static, transient, frequency characteristics of transistor structures are used effectively [15-17].

Work [18] is an example of correct use of a unidimensional system in application to the analysis of elements with small dimensions.

Two-dimensional models examine the instrument in the cross section plane (Figure 1) and make it possible to take into consideration the distributed nature of the structure and the natural inertness of the instrument at high frequencies, current



APPROVED FOR RELEASE: 2007/02/09: CIA-RDP82-00850R000500020034-7

APPROVED FOR RELEASE: 2007/02/09: CIA-RDP82-00850R000500020034-7



displacement toward the boundaries of the emitter, lateral injection of p-n-junctions, and the effect of passive regions of the base and the collector.

The fundamental system of equations describing a nonsteady-state distribution of the concentrations of n(x, y, t), p(x, y, t) and the electrostatic potential $\varphi(x,y,t)$ in a semiconductor structure is a system of partial differential equation

$$\nabla^2\varphi=-(q/\varepsilon)[p-n+N_Д-N_A], \quad (1)$$

$$\nabla I_p-q(G-R)=-q\partial p/\partial t, \quad (2)$$

$$\nabla I_n+q(G-R)=q\partial n/\partial t \quad (3)$$

and auxiliary equations

$$I_p=q\mu_p p(-\nabla\varphi+\nabla DEV/q)-qD_p\nabla p, \quad (4)$$

$$I_n=q\mu_n n(-\nabla\varphi-\nabla DEC/q)+qD_n\nabla n, \quad (5)$$

$$I_{см}=-\varepsilon\partial(\nabla\varphi)/\partial t, \quad (6)$$

$$R=(pn-n_{ie}^2)/[\tau_n(p+n_{ie})+\tau_p(n+n_{ie})]+(p/\tau_{Ap}+n/\tau_{An}), \quad (7)$$

$$G=-n\mu_n\alpha_n\nabla\varphi-p\mu_p\alpha_p\nabla\varphi, \quad (8)$$

$$n_{ie}^2=n_i^2\exp(\Delta E_g/kT). \quad (9)$$

Equations (4)-(6) describe the phenomena of current transport under the effect of drift, diffusion and electric displacement. Displacement current must be taken into consideration in modeling superfast devices working in the ps range.

The electric field intensity in these equations includes the classical electrostatic component $\nabla\varphi$ and an additional (quasi-electric) component DEV (DEC)/q which appears due to the dependence of the width of the forbidden zone $E_g$ on the space coordinates in a highly alloyed material [19, 20]. Specifically, in the neutral regions of a semiconductor under the condition of a low level of injection $(1/q)DEV(DEC)\approx\approx kT/q\cdot\nabla n_{ie}^2/n_{ie}$, where $n_{ie}$ is the effective intrinsic carrier concentration.

The decrease of $E_g$ depending on the impurity concentration is described by the empirical formula [20-22]

$$\Delta E_g=9\cdot10^{-3}\{\ln(N/10^{17}\ \text{см}^{-3})+([\ln(N/10^{17}\ \text{см}^{-3})]^2+0{,}5)^{1/2}\}\ \text{эВ}, \quad (10)$$

where $N = N_A$ for p-type silicon and $N = N_Д$ for the n-type.

Expression (7) describes the recombination of the carriers under the effect of the Shockley-Read-Hall and Auger mechanisms. The lifetime of the minority carriers depends on the impurity concentration [22]



APPROVED FOR RELEASE: 2007/02/09: CIA-RDP82-00850R000500020034-7

APPROVED FOR RELEASE: 2007/02/09: CIA-RDP82-00850R000500020034-7



$$\tau_p(N_Д)=\tau_{po}/(1+N_Д/7{,}1\cdot10^{15}\ \text{см}^{-3}),\ \tau_n=\tau_{no}/(1+N_A/7{,}1\cdot10^{15}\ \text{см}^{-3}) \quad (11)$$

$$\tau_{Ap}(N_Д)=1/C_{Ap}N_Д^2,\ \tau_{An}(N_A)=1/C_{An}N_A^2, \quad (12)$$

where $C_{Ap}$, $C_{An}$ are the Auger coefficients [23].

In highly alloyed regions, for example, emitters and hidden $n^+$-layers of transistors, $\tau_{Ap}$ could be smaller than $\tau_p$, i.e., the Auger recombination mechanism will prevail [24].

In small-dimension structures, the high-alloyage effect plays an important role, causing degradation of practically all parameters of the device: current transmission coefficient, frequency $f_T$, emitter p-n-junction capacitance, and temperature dependence. Numerical evaluations of this effect confirmed experimentally on transistors with a base thickness of 0.04-0.2 μm show that its inclusion in the model reduces the value of the coefficient $\beta_0$ by one-two orders and the limit frequency $f_T$ by 50-400% [25].

Expression (8) describes the generation of carriers under the effect of avalanche multiplication in a strong electric field. The ionization coefficients for holes and electrons are the functions of the intensity of the electric field $E = -\nabla\varphi$ [26]

$$\alpha_n=3{,}8\cdot10^6\exp(-1{,}75\cdot10^6/|E|),$$
$$\alpha_p=2{,}25\cdot10^7\exp(-3{,}2\cdot10^6/|E|). \quad (13)$$

The boundary conditions for modeling the structure of Figure 1 are described in detail in [12]. On the contacts, we have neutrality of the charge ($p-n+N_Д-N_A=0$) and thermodynamic equilibrium ($pn=n_i^2$). However, the last formula, for devices with small dimensions operating at high levels of injection, should be used somewhat carefully. With consideration for the "splitting" of the Fermi quasi-levels for holes and electrons and the Fermi-Dirac statistics, the condition of the thermodynamic equilibrium on the contact assumes the following form [27]:

$$pn=(n_i^2F_{1/2}(Z)/\exp(Z))\exp[(E_{fn}-E_{fp})/kT],$$

where $|E_{fn}-E_{fp}|$ is the difference in the position of the Fermi quasi-levels for electrons and holes; $F_{1/2}(Z)$ is the Fermi integral of the order of 1/2; $Z=(E_{fn}-E_c)/k_T$, $E_c$ is the energy of the bottom of the conductivity zone; $\gamma=F_{1/2}(Z)/\exp(Z)$ is the degeneration factor which indicates how many times the concentration of the electrons differs from its value calculated by the Maxwell-Boltzmann law. For silicon at room temperature, $\gamma\approx1$ with accuracy of $\leq$ 2%, if $n\leqslant1.5\cdot10^{18}$ $\text{cm}^{-3}$, $p\leqslant5.5\cdot10^{17}$ $\text{cm}^{-3}$.

The initial conditions for the currents and voltages on the contacts are given, as a rule, as zeros.

In the structures of modern fast BIS, metal-semiconductor planar rectifying contacts (Schottky barrier) are used widely. The formulation of the boundary conditions for contacts of this type is examined in [28, 29].





APPROVED FOR RELEASE: 2007/02/09: CIA-RDP82-00850R000500020034-7

APPROVED FOR RELEASE: 2007/02/09: CIA-RDP82-00850R000500020034-7



On surfaces covered with a layer of $SiO_2$ oxide, the normal components of current densities are determined by the speed of surface recombination, and the normal component of the electric field is determined by the density of the surface charge $Q_{ss}$.

The above equations and boundary conditions are true for semiconductor devices with dimensions of their diffusion regions not less than 0.03-0.05 μm, gradients of the concentrations of alloying impurities not over $10^{24}$ $cm^{-4}$, current densities of not over $10^6$ $A/cm^2$, electrical fields not over $10^6$ V/cm, and on frequencies not exceeding $10^{12}$ Hz [18, 30, 31]. Therefore, equations (1)-(9) can be used as a basis for calculating the elements of BIS and superBIS with minimal topological dimensions to 1 μm, though with inclusion of necessary modifications in highly alloyed regions and the Fermi statistics in degenerated regions (20).

Equations (1)-(9) with appropriate boundary and initial conditions are represented in the finite-difference form and then are solved by numerical methods on a computer [32, 33]. As a result of the solution, functions $p(x,y,t)$, $n(x,y,t)$, $\varphi(x,y,t)$ are determined and used for computing currents or voltages on the contacts, p-n junction capacitance, amplification cutoff frequencies, and other parameters.

The construction of two-dimensional models even on a very fast computer is very time-consuming, and takes minutes or even hours [34,35]. Therefore, the development of effective algorithms for solving the fundamental system of equations (1)-(9) is a very urgent problem [36-38].

With the aid of two-dimensional models, it is possible to study the characteristics of devices with a concrete structure without resorting to the manufacturing and experimental studies of experimental prototypes. Let us give a few examples in application to small-size devices. In [39], a model was used successfully to establish the necessary connections between the parameters of the physical structure and the electrical characteristics of an element of the injection-field logic (Figure 2) -- a new promising direction in the creation of superBIS with a superlow consumption. An analogous problem was solved for field-effect transistors with the Schottky barrier gate which are used widely in the solid-state integrated microwave electronics [40]. The work [31] is of great interest. It gives prognoses of critical electrical characteristics of bipolar transistors in which the thicknesses of the emitter and base regions were reduced from 0.4 μm to 0.03 μm. Calculations showed that for a transistor with the dimensions of the emitter 1X1 $\mu m^2$, emitter thickness of 0.03 μm, base thickness of 0.03 μm, the critical frequency of single amplification is $f_T$ = 89 GHz and the current transmission coefficient is $\beta_N$ = 105 at $I_k$ = 0.73 mA, puncture voltage is $U_{BK} < 2$ V; the corresponding parameters for a device with an emitter of 1X1 $\mu m^2$, thicknesses of the emitter and the base of 0.1 μm each have the following values: $f_T$ = 16.8 GHz and $\beta_N$ = 53 at $I_k$ = 0.38 mA, $U_{BK} > 2$ V.

It can be seen from the above examples that programs constructing two-dimensional models are beginning to be used effectively by designers for calculating BIS elements. However, all programs have discrepancies between the accurate models of electrical modes of instruments and greatly simplified mode of two-dimensional impurity profiles which are used as initial information for these programs.

As the level of the integration of circuits grows steadily, such parameters, which are derivatives of the impurtiy profile, as the thickness of the oxide, width of



APPROVED FOR RELEASE: 2007/02/09: CIA-RDP82-00850R000500020034-7

APPROVED FOR RELEASE: 2007/02/09: CIA-RDP82-00850R000500020034-7



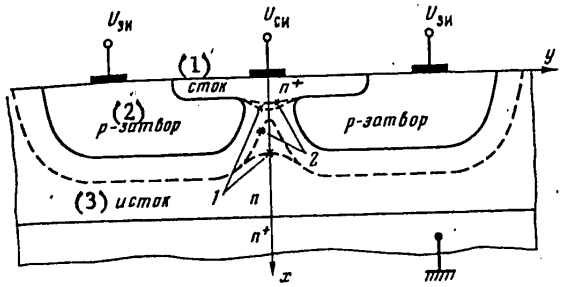


Figure 2. Distribution of the space charge layer (interrupted line) in a field-effect transistor of the element of injection-field logic with parameters $N_{epi} = 2 \cdot 10^{14}$ cm$^{-3}$; $N_{sp} = 5 \cdot 10^{18}$ cm$^{-3}$; $N_{sn^+} = 5 \cdot 10^{20}$ cm$^{-3}$ and applied voltages $U_{зи} = 0.1$ V; $U_{си} = 0$ V -- 1 and 0.9 V -- 2 [27].

Key: 1. Drain
2. p-gate
3. Source

depleted regions and lateral dimensions of p-n-junction, are becoming increasingly important factors determining both the electrical modes of devices, and their maximum permissible geometrical dimensions. It is necessary to develop programs modeling two-dimensional distributions of the impurity concentration of a multistage technological process which includes the operations of ion implantation, diffusion, oxidation, epitaxy, and etching [41-45]. Moreover, it is necessary to take into consideration the concentration relations of the diffusion coefficients of various impurities, the effect of the oxidizing medium, orientation of the substrate, interaction of several impurities during their simultaneous diffusion, and a number of other important effects [46-48]. For micronic and submicronic structures, programs modeling impurity distribution profiles are integral parts of the mathematical means for predicting and computing their electrical characteristics.

Let us examine a number of still unsolved problems of modeling BIS and superBIS elements and map out the ways of their solution.

1. "Instrument self-heating" at high current densities, in essence, limits the increase of the degree of integration of the elements on the crystal [49]. The steady-state temperature distribution T(x,y) in a two-dimensional structure of Figure 1 can be determined by solving the following equation of thermal conduction jointly with equations (1)-(9) with a zero right part in (2), (3) and (6);

$$\nabla(\lambda \nabla T) + P = 0, \qquad (14)$$

where $\lambda(x,y,T)$ -- thermal conduction coefficient; $P(x, y, T) = (j_p + j_n)\nabla\varphi$ -- density of power released in the structure.

The boundary condition for equation (14) are established on the assumption that the heat transfer from the surface of the crystal into the surrounding medium is absent, and the temperature on the lower surface of the substrate is equal to the prescribed temperature.





APPROVED FOR RELEASE: 2007/02/09: CIA-RDP82-00850R000500020034-7

APPROVED FOR RELEASE: 2007/02/09: CIA-RDP82-00850R000500020034-7



The expanded system of equations (1)-(9) and (14) with corresponding boundary conditions is rendered discrete on a two-dimensional difference network and is solved with the aid of the same numerical methods which were used for solving a usual two-dimensional problem [26, 50].

Let us evaluate the influence of thermal effects on an example of a transistor with the dimensions of the emitter of 1X1 $\mu m^2$, thicknesses of the meter and base regions of 0.03 μm working in an active mode with displacements of $U_{БЭ} = 0.9$ V and $U_{КБ} = 2$ V. The work [31] gives calculation for such a structure: collector current $I_k = 2.3$ mA, field intensities in the emitter and collector junctions are approximately the same and are equal to $E \simeq 10^5$ V/cm, the dimensions of the depleted regions are $\Delta X_{j\,э} = 0.03$ μm and $\Delta X_{jk} = 0.3$ μm. Assuming that temperature changes under the effect of power dissipation occur chiefly in the depleted layers of p-n-junctions, we shall obtain from the solutions of the thermal conduction equation (14) at a normal temperature on the substrate that the temperature in this structure increases by $\sim 8^{\circ}C$, and the maximum value of the temperature gradient in p-n-junctions is equal to $\sim 5 \cdot 10^5$ degrees/cm. There occur electron and hole currents in the semiconductor due to this gradient

$$j_{p_{\text{терм}}} = -k(2+\ln p/n_i)\nabla T p \mu_p, \quad (15)$$

(1)

$$j_{n_{\text{терм}}} = k(2+\ln n/n_i)\nabla T n \mu_n. \quad (16)$$

Key: 1. Thermal

Therefore, strictly speaking, (4) and (5) are incomplete [51]. Let us evaluate the contribution which can be made by the component $j_{p\text{therm}}$ and $j_{n\text{therm}}$ to the density of currents of the holes (4) and electrons (5). For the temperature gradient $5 \cdot 10^5$ degrees/cm and concentrations of free electrons $10^{17}$-$10^{20}$ $cm^{-3}$, the maximum value of $j_{n\text{therm}}$ is $\sim 10\%$ of the value of $j_{n\Sigma}$. The contribution of $j_{p\text{therm}}$ is considerably smaller. Thus, for instruments with topological dimensions $> 1$ μm, thicknesses of the regions of the emitter and base $> 0.03$ μm, it is possible to disregard thermal currents of the holes and electrons and to consider only the release of the Joule heat described by equation (14).

2. Electric breakdown is a fundamental reason limiting the minimum dimensions of the device at a prescribed supply voltage. The width of the depletion region of the p-n-junction corresponding to the value of the voltage $U_{\text{breakdown}}$, at which avalanche breakdown occurs determines the minimum values of all remaining dimensions of the device. The value of $U_{\text{breakdown}}$ depends on the level of alloying and the profile shape of the impurity of the p-n-junction, particularly its lateral regions, as well as on the value of the local charge $Q_{ss}$ on the $Si$-$SiO_2$ interface. Approximate models of the breakdown mechanism using spherical or cylindrical approximation of the lateral part of the p-n-junction under the oxide are not suitable for elements with submicronic dimensions. Quantitative evaluation of $U_{\text{breakdown}}$ must be done by using a two-dimensional model with the impurity profile exactly prescribed [41-44].

Let us write the conditions of avalanche breakdown for electrons and holes



APPROVED FOR RELEASE: 2007/02/09: CIA-RDP82-00850R000500020034-7

APPROVED FOR RELEASE: 2007/02/09: CIA-RDP82-00850R000500020034-7



$$\int_{L_1}^{L_2} \alpha_n \exp\left[-\int_{L}^{L_3} (\alpha_n - \alpha_p)\, dl\right] dL = 1,$$
$$\int_{L_1}^{L_2} \alpha_p \exp\left[-\int_{L_2}^{L} (\alpha_n - \alpha_p)\, dl\right] dL = 1, \qquad (17$$

where $\alpha_n(E)$, $\alpha_p(E)$ -- ionization coefficients depending on the field intensity by formulas (13).

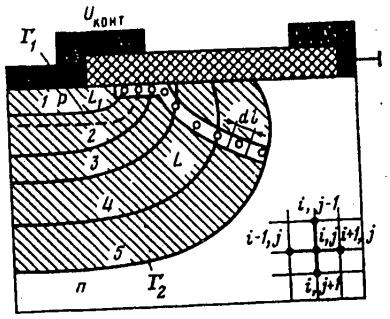


Figure 3. Formation of the avalanche breakdown in a two-dimensional structure of a back-biased planar p-n-junction.

The problem is solved in the following sequence. Various values of the voltage on the p-n-junction being given, we solve the Poisson equation (1) on the assumption that the charge of the mobile carriers is equal to zero. As a result of its solution, we determine the distribution of the potential $\varphi(x,y)$ and gradient $E(x,y)$. Taking this into consideration, we establish the boundaries of the depleted region of the p-n-junction $\Gamma_1$ and $\Gamma_2$. We select the points with the maximum values of the electric field from the two-dimensional block $E(x_i, y_i)$. These points form the path of the maximum multiplication of the carriers L (see Figure 3) along which the avalanche breakdown develops. We calculate the multiplication integrals (17) along the curve L and check the fulfillment of the breakdown conditions. The voltage at which these conditions are fulfilled will be $U_{breakdown}$.

Studies have shown that, for structures with base thicknesses of 0.03-0.15 μm and impurity concentrations in the base of $10^{17}$-$10^{18}$ $cm^{-3}$, avalanche breakdown occurs at field intensities in the collector p-n-junction of $E_{breakdown} \approx 10^5$-$10^6$ V/cm; this corresponds to a back bias of 1.5-2.0 V [8, 31].

The main application area of two-dimensional models is the analysis of the effects of impurity profiles, electrophysical parameters of the semiconductor and the surface, effects of lateral injection of p-n-junctions on the electrical characteristics of instruments.



APPROVED FOR RELEASE: 2007/02/09: CIA-RDP82-00850R000500020034-7

APPROVED FOR RELEASE: 2007/02/09: CIA-RDP82-00850R000500020034-7



The drawback of the examined two-dimensional models is their weak connection with the topology of the instrument.

Quasi-three-dimensional models examine the instrument in the plane of the crystal and make it possible to take into consideration not only the process of the transfer of the carriers deep into the crystal, but also the real topography of the instrument, which is extremely important in designing BIS.

The main assumption on which quasi-three-dimensional models are constructed is that, for modern bipolar instruments manufactured by the methods of planar technology, the dimensions in the topology plane $l_y$, $l_z$ are much greater than the dimensions along the depth of the structure $l_x$. According to the principle of proportional miniaturization, approximately the same relations will continue to be maintained between the dimensions of the instruments. For example, for transistors with the dimensions of the emitter window 1X1 $\mu m^2$, the thicknesses of the regions of the emitter and the base will be 0.05-0.1 $\mu m$.

The model uses the discription of the processes of current spreading of the majority carriers in diffusion regions of the base and the collector

$$\nabla[\sigma_B \nabla U_B] = j_B(U_B, U_K) + \partial q_B/\partial t, \quad (18)$$

$$\nabla[\sigma_K \nabla U_K] = j_K(U_B, U_K) + \partial q_K/\partial t, \quad (19)$$

where $\nabla = \partial\vec{i}/\partial y + \partial\vec{j}/\partial z$, $U_B(y, z, t)$, $U_K(y, z, t)$ and $\sigma_B(y, z)$, $\sigma_K(y, z)$ -- potentials and conductances of the base and collector regions; $j_B(U_B, U_K, t)$, $j_K(U_B, U_K, t)$ and $q_B(U_B, U_K, t)$ and $q_K(U_B, U_K, t)$ -- densities of currents and charges in the base and collector regions.

The densities of the current and the charge include several components which account for various physical mechanisms of recombination and accumulation of the carriers (see Figure 4) in the volume of the neutral region of the base, in the emitter and the collector, on the epitaxial film -- $n^+$-hidden layer interface, in the space-charge layers of the emitter and the collector, on the Si-$SiO_2$ interface, on the ohmic contact, leakage through the lateral surface of the base.

In the general case, the densities of these currents and charges are determined from the solution of a fundamental system of equations of the semiconductor physics one-dimensional along the axis x [52, 53]. Simpler, but at the same time acceptably accurate, expressions connecting the components of the base and collector currents and charges with the voltages on the p-n-junctions, parameters of the impurity profile and electrophysical constants can be obtained by dividing the structure along the coordinate x into space-charge regions of p-n-junctions and quasi-neutral regions of the emitter, the base, and the collector [54-56].

The Debye concept of length $L_D = (\varphi_T \varepsilon/qn_i)^{1/2}$ characterizing the penetration of the field into the depth of the semiconductor is used as a criterion of the validity of the division of the transistor structure into such regions. At a normal temperature,



APPROVED FOR RELEASE: 2007/02/09: CIA-RDP82-00850R000500020034-7

APPROVED FOR RELEASE: 2007/02/09: CIA-RDP82-00850R000500020034-7



$L_D \approx 0.005$ μm. If the width of the transistor base is much greater than $L_D$, then the base can be considered as a quasi-neutral region, since the electric field caused by charges concentrated in the regions of the junctions decreases substantially at a distance of (1-2) $L_D$ from the boundaries of the p-n-junctions. Thus, the principle of the division of the instrument structure into space-charge and quasi-neutral regions remains true also for instruments with submicronic dimensions and a thin base of the order of 0.1 μm.

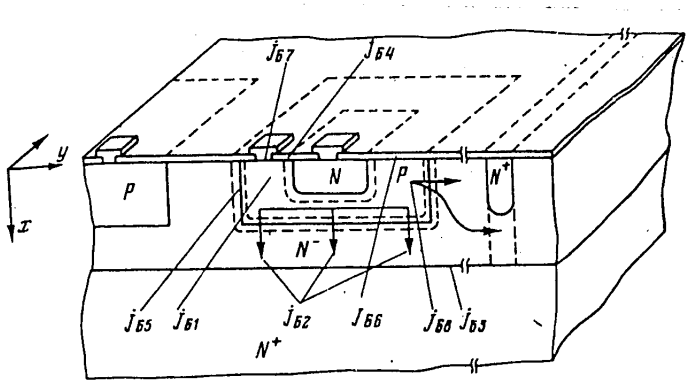


Figure 4. Components of the base current in the structure of an integrated transistor.

The boundary and initial conditions for the system of equations (18), (19) are discussed in detail in [12]. The following is an effective numerical method for solving equations (18)-(19) with the aid of a computer. Having defined the operator $\nabla$ discretely by the spatial variables y and z, the system (18)-(19) can be represented in the following form

$$C(U)dU/dt=F^y(U)+F^z(U)+I(U, t), \qquad (20)$$

where $U=\begin{pmatrix} U_Б \\ U_К \end{pmatrix}$, $C=dq/dU$, $I=-\begin{pmatrix} j_Б \\ j_К \end{pmatrix}$ $F^y(U), F^z(U)$ -- discretely represented parts of the operator $\nabla$ corresponding to the coordinates y and z. The system (20) is solved by the method of generalized splitting [57]. At each subsequent moment of time $t_{n+1}$, the value of the vector U is calculated by the formula

$$U^{n+1}=U^n+h[C^n-0{,}5h(\partial F^y/\partial U+0{,}5\partial I/\partial U)]^{-1}C^n[C^n-0{,}5h(\partial F^z/\partial U+ +0{,}5\partial I/\partial U)]^{-1}[F^y(U)+F^z(U)+I(U, t)] \qquad (21)$$

where k is the step of integration by time. The volume of computations by formula (21) and the memory expenditures at each time step are directly proportional to the number of points of the difference network, which ensures the maximum economy of computation expenditures.

To date, many programs using the quasi-three-dimensional approach in the static mode have been developed and experience has been accumulated in using these programs for solving the problem of designing the topology of various IS and BIS elements [58-60].



APPROVED FOR RELEASE: 2007/02/09: CIA-RDP82-00850R000500020034-7

APPROVED FOR RELEASE: 2007/02/09: CIA-RDP82-00850R000500020034-7



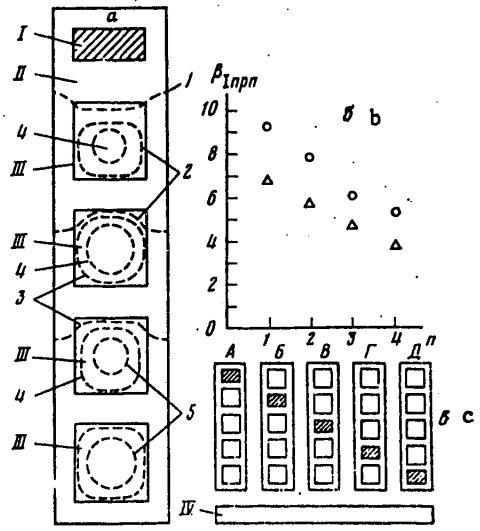


Figure 5. a -- Distribution of electric potentials in the base region of a 4-collector $I^2L$-gate with the parameters $W_{epi}$=6 μm; $N_{epi}=6\cdot10^{15}$ cm$^{-3}$; $n_{s\sigma} = 2.5\cdot10^{18}$ cm$^{-3}$; $n_{sk} = 4\cdot10^{20}$ cm$^{-3}$; $W_{\sigma}$ = 0.65 μm. I -- base contact, II -- base, III -- collectors (n -- number of collectors), IV -- injector. 1 -- 625 mV; 2 -- 623 mV; 3 -- 622 mV; 4 -- 621 mV; 5 -- 618 mV; b -- current transmission coefficients of individual collectors of the transistor with topology A; c -- topological variants of $I^2L$-gate.

Table 1

Amplification Coefficients of Various Collectors for Topological Variants of Figure 5c with Specific Resistance of the Base Layers $\zeta Б_{act}$ = 30 kOhm/□, $\zeta Б_{pas}$ = 170 Ohms/□ (calculations were done at $I_Б$ = 30 μA and $I_И$ = μA)

| (3) Вариант топологии рис. 5, в | $\beta_{I_i}=I_{K_i}/I_Б$ | | | | (1) $\frac{\lvert\beta_{I_{макс}}-\beta_{I_{мин}}\rvert}{\beta_{I_{макс}}}\cdot100\%$ (2) |
|---|---|---|---|---|---|
| | К1 | К2 | К3 | К4 | |
| А | 10 | 7,6 | 7 | 7,8 | 30 |
| Б | 9,5 | 8,7 | 7,9 | 8,7 | 17 |
| В | 7,1 | 8,7 | 9,4 | 9,7 | 27 |
| Г | 5,7 | 6,2 | 8,8 | 11,7 | 53 |
| Д | 4,7 | 5,4 | 6,9 | 11 | 57. |

Key: 1. Maximum
2. Minimum
3. Variant of topology of Figure 5 c

As an example, let us examine the result of the calculation of a typical cell of an $I^2L$ BIS obtained with the program described in [60]. Figure 5a shows the distribution





APPROVED FOR RELEASE: 2007/02/09: CIA-RDP82-00850R000500020034-7

APPROVED FOR RELEASE: 2007/02/09: CIA-RDP82-00850R000500020034-7



of electric potentials in the base area of a four-collector n-p-n-$n^+$-transistor. Figure 5b shows the results of the modeling (circles) of the effect of the decrease of the current transmission coefficient of individual collectors as they get farther away from the base contact in the structure of Figure 5a, which is important for $I^2L$-transistors; the triangles designate the experimental data. Comparison of various topological variants of the $I^2L$-gate of Figure 5c is given in Table 1. It can be seen that preference should be given to variants А, Б , В, in which the base contact and the injector are spaced, and the injector compensates the spurious incidence of voltage on the resistance of the base layer. In topologies Г and Д , the positive effect of the injector is "screened" by the base contact. Such evaluations acquire especially important significance in further reduction of the geometry and changeover to micronic dimensions, since the spurious effect of the resistivity of the regions is one of the main factors limiting the improvement of the characteristics of bipolar instruments.

Let us examine two urgent problems of the modeling of BIS elements which fit well into the limits of the quasi-three-dimensional approach.

The problem of combined modeling of electrical and thermal fields in BIS elements has not yet been solved. Let us formulate it with the following correct prerequisites: -- heat transfer is accomplished only due to thermal conduction, while radiation and convection are disregarded; -- heat sources are located in a narrow layer with thickness $X_{jk} \ll H_{crystal}$ near the surface of the crystal (see Figure 1a); -- the upper surface of the crystal is adiabatic, i.e., $\partial T/\partial n = 0$, and the lower surface is isothermal $T(y,z) = T_A$.

Then the following thermal conduction equation must be solved jointly with equations (18) and (19):

$$\nabla[\lambda(T)\nabla T(y, z)] = Q(y, z, T) - \lambda(T)(T - T_A)/H^2_{\text{крист}}, \quad (22)$$

(1)

Key: 1. Crystal

where $Q(y, z, T) = (1/H_{\text{крист}})[j_э(y, z, T)U_{БЭ}(y, z, T) + j_к(y, z, T)U_{БК}(y, z, T)]$ -- density of the power released by p-n-junctions in a layer with thickness $X_{jk}$.

In expressions (18) and (19), it is necessary to introduce the dependence of the conductions and densities of currents on the temperature.

In order to solve equations (18), (19) and (22), it is expedient to use the method of finite differences in combination with the procedure of quasi-linearization and the PVR block method.

Modeling of BIS Fragments. Let us extend the examined three-dimensional approach to the case of modeling electrical characteristics of whole BIS fragments containing vertical and horizontal transistor p-n-p-structures combined on the crystal. The elements interact with one another through a common epitaxial layer of the n-type and through lateral injection of the p-regions.



APPROVED FOR RELEASE: 2007/02/09: CIA-RDP82-00850R000500020034-7

APPROVED FOR RELEASE: 2007/02/09: CIA-RDP82-00850R000500020034-7



The electrical coupling of the elements through the common epitaxial n-layer is described by equation (19). Equation (18) is solved for each of the p-regions with consideration for the interaction of neighboring p-regions with it.

For the boundary points of each i, j-pair of neighboring p-regions (see Figure 6), it is necessary to solve the following system of equations:

$$\nabla[\sigma_i \nabla \psi_i] = j_i(\psi_i, \psi_j), \quad \nabla[\sigma_j \nabla \psi_j] = j_j(\psi_i, \psi_j), \tag{23}$$

with the conditions $$\sigma_i \partial\psi_i/\partial n = I_{i_{\text{кол}}}(\psi_j) - I_{i_{\text{инж}}}(\psi_i), \quad \sigma_j \partial\psi_j/\partial n = I_{j_{\text{кол}}}(\psi_i) - I_{j_{\text{инж}}}(\psi_j), \tag{24}$$

where $j_i(\psi_i, \psi_j)$, $j_j(\psi_i, \psi_j)$ -- current densities in the boundary points of $p_i$-region and $p_j$-region, respectively; $I_{i_{\text{инж}}}(\psi_i)$, $I_{j_{\text{инж}}}(\psi_j)$ -- linear densities of currents injected by $p_i$ and $p_j$-regions into the n-regions; $I_{i_{\text{кол}}}(\psi_j)$ $I_{j_{\text{кол}}}(\psi_i)$ -- linear densities of currents collected by the $p_i$-region from $p_j$-region and vice versa (see Figure 6).

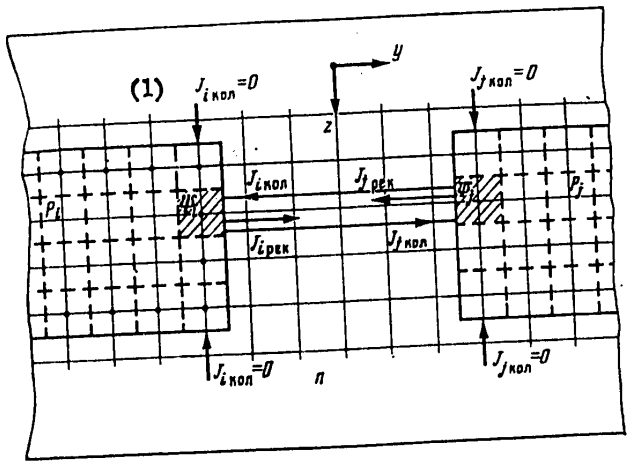


Figure 6. Boundary conditions for describing electric interaction of two p-regions.
Key: 1. collector

Expressions connecting the densities of the currents in (23) and (24) with the potentials $\psi_i$ and $\psi_j$, parameters of the impurity profile, and electrical characteristics of the semiconductor are shown in [61].

The system (23) is solved by the same method as the system (18)-(19), only the potentials $\psi_i$ and $\psi_j$ appear as unknown.



APPROVED FOR RELEASE: 2007/02/09: CIA-RDP82-00850R000500020034-7

APPROVED FOR RELEASE: 2007/02/09: CIA-RDP82-00850R000500020034-7



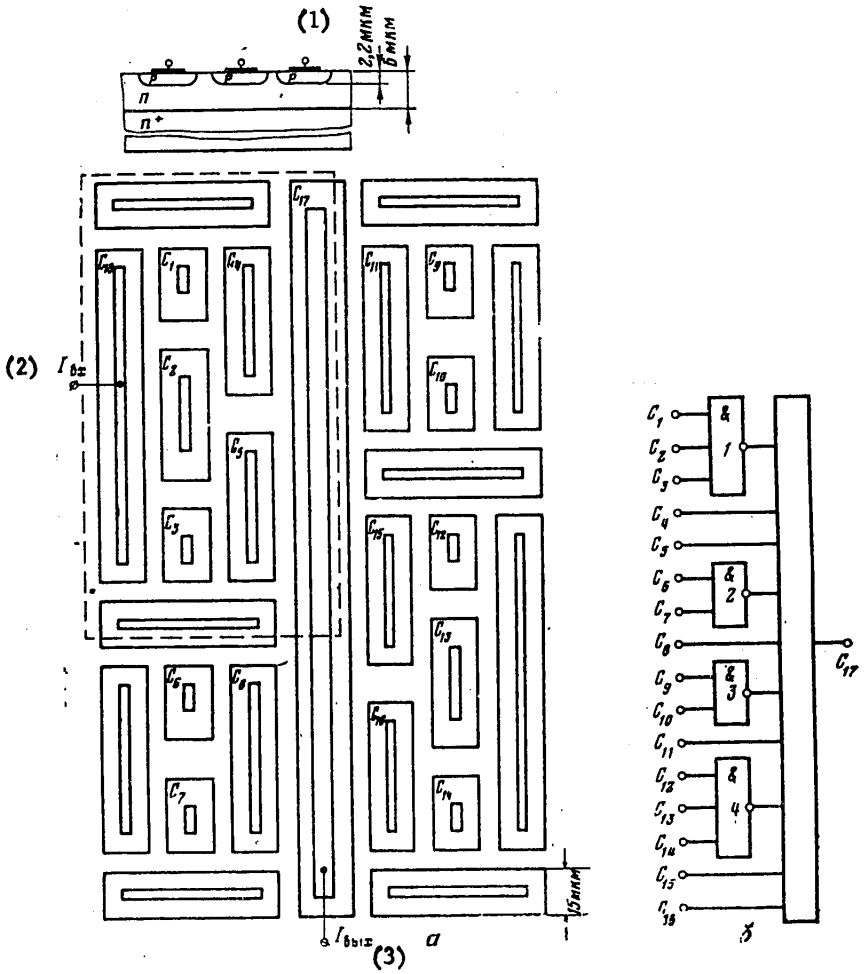


Figure 7. Structure, topology -- a and logical circuit -- b of a BIS fragment using elements with current interception ($N_{epi} = 6 \cdot 10^{15}$ cm$^{-3}$, $N_{sp} = 5 \cdot 10^{18}$ cm$^{-3}$).

Key: 1. μm
2. $I_{input}$
3. $I_{output}$

On the basis of the proposed approach, a program was constructed whose potentialities are illustrated on an example of the modeling of a fragment of integrated logic with current interception. The calculation of the fragment of Figure 7a consisting of 27 p-regions on a network of 80X50 points took 16 minutes on an YeS-1022 computer. The results of the current computation for one of the logical states of gate 1 are shown in Table 2.





APPROVED FOR RELEASE: 2007/02/09: CIA-RDP82-00850R000500020034-7

APPROVED FOR RELEASE: 2007/02/09: CIA-RDP82-00850R000500020034-7



Table 2

Illustration of the Effectiveness of Current Transmission in a PTL-Element

| $C_1$ | $C_2$ | $C_3$ | $C_4$ | $C_5$ | $I_{вх}$, мкА ($C_{10}$) (1) | $I_{вых}$, мкА ($C_{11}$) (2) | $K_I$ |
|---|---|---|---|---|---|---|---|
| 0 | 1 | 0 | 0 | 1 | 233 | 13 | 0,05 |

Key: 1. $I_{input}$, μA
2. $I_{output}$, μA

According to our evaluations, the calculation of a BIS fragment containing one hundred p-regions on a computer with an immediate-access memory of 256-512 Kbytes and effective speed of $4 \cdot 10^5$ op/s will take $\sim$ 30 minutes.

Consideration of the real topology of elements and the possibility of modeling functionally integrated fragments containing dozens of transistors make quasi-three-dimensional models very promising in designing BIS and superBIS.

Evaluating the prospects of using two-dimensional and quasi-three-dimensional physicotopological models for describing instruments with dimensions less than 1 μm, it is possible to conclude the following. Down to the minimum topological dimensions of active elements of the order of 0.25 μm, the fundamental equations (1)-(9) and/or (18)-(19) will be acceptable for their modeling, however, as this limit is approached, it will be necessary to make substantial modifications in these equations connected with the consideration of the quantum-dimensional effects [8, 62]. Beyond this limit, both the operating principles and the structure of active elements, as well as the fundamental equations necessary for their modeling, must be fundamentally different. Moreover, the problem of the possibility of creating practical instruments with such small dimensions remains to be open [63].

MDP-Elements

Just as for bipolar transistors, the best results from the viewpoint of accuracy of description and the range of applications are yielded by using two-dimensional numerical models of MDP-transistors based on direct solution of the fundamental system of Poisson equations of continuity and transfer for the longitudinal section of the instrument [33]. These models make it possible to take into account the exact dependence of mobility on the field, impurity concentration and temperature and practically any distribution of impurities in the substrate (which is particularly important for modern structures with ionic-alloyed channels). With the aid of such models, it is possible to "predict" accurately the volt-ampere characteristics of the instruments being developed and their most important electrical parameters (threshold voltage, specific transconductance, through-depletion voltage) as a function of the physicotopological parameters, to develop and correct "working" models for machine calculation of electrical circuits of BIS and superBIS, and to solve many other problems.

At the present time, in connection with the development of the production of superBIS with microminiature active and passive elements, the importance of two-dimensional models as a means for calculating MDP-instruments has increased greatly. This is



APPROVED FOR RELEASE: 2007/02/09: CIA-RDP82-00850R000500020034-7

APPROVED FOR RELEASE: 2007/02/09: CIA-RDP82-00850R000500020034-7



connected with the growth of the "two-dimensionality" of the behavior of MDP-instruments as their geometrical dimensions decrease and with the ever increasing complexity and length of experimental studies and adjustment of new technology.

Theoretical studies [62, 63] show that two-dimensionsl models of the type described in [33] will be generally applicable for describing and studying planar MDP-transistors down to the minimum channel length of about 0.25 μm, i.e., for three or four more generations of integrated circuits. This indicates the necessity of further improvement of such models both with respect to a more accurate description of the physical relations used in them, and with respect to increasing the effectiveness of the algorithms of numerical solutions of the equations of models.

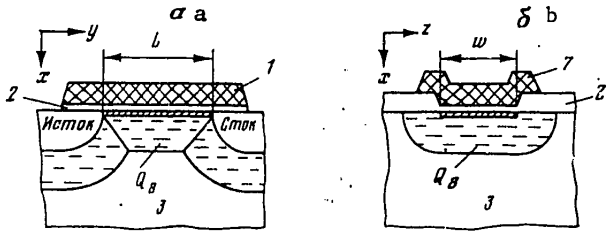


Figure 8. Illustration of the effects of a short -- a and a narrow -- b channel and the appropriate geometrical approximations used for calculating the effective charge of the substrate $Q_B$: 1 -- gate; 2 -- oxide; 3 -- substrate.

The model constructed in the MINIMOS program [64] can serve as an example of a modern numerical two-dimensional model of an MDP-transistor. This program performs a numerical solution of the fundamental system for majority carriers with the use of more accurate models of mobility. Provisions are made in it for several methods of describing the impurity profile of the substrate, including the use of the results of calculations of the impurity profile with the aid of the program for modeling technological processes SUPREM [42], which makes this model essentially physicotechnological. This model was used successfully for analyzing MDP-transistors with the length of the gate electrode of 1 μm and with various impurity profiles of the channel obtained with the aid of ion implantation.

In practice, at the present time, simpler quasi-two-dimensional models of MDP-elements based on a smooth approximation of the Shockley channel are used more widely [12, 65-68, and others]. This is explained by the high complexity of two-dimensional models and the corresponding mathematical means, by high expenditures of the machine time, as well as by the relative (in comparison with bipolar elements) simplicity of the operating principle of the planar MDP-transistor. Quasi-two-dimensional models ensure a very adequate accuracy of the modeling of MDP-transistors in the programs of circuit analysis and in many instances are suitable for calculating and optimization of the instruments themselves down to the minimum topological dimensions of the order of 1.5...2 μm [69].



APPROVED FOR RELEASE: 2007/02/09: CIA-RDP82-00850R000500020034-7

APPROVED FOR RELEASE: 2007/02/09: CIA-RDP82-00850R000500020034-7



In quasi-two-dimensional models, the channel is characterized by the specific surface charge of mobile carriers $Q_n$ (for the sake of definiteness, we shall be examining an n-channel transistor everywhere), defined unambiguously for any cross section of the channel by the one-dimensional Gauss equation. For this reason, the charge $Q_n$ depends only on the gate-substrate voltage $U_3$ and the channel-substrate voltage $U_k$, i.e.,

$$Q_n=Q_n(U_3, U_k). \tag{25}$$

In turn, the channel current for the steep region of the characteristics of the instrument is found from the solution of an ordinary differential equation with separable variables of the following type [76]:

$$I=W\mu_n[Q_n dU_k/dy+\varphi_T dQ_n/dy]=W\mu_n[Q_n+\varphi_T dQ_n/dy]dU_k/dy, \tag{26}$$

where $\mu_n$ -- mobility of the carriers depending on the longitudinal $E_y$ and transverse $E_x$ electric field, temperature, and impurity concentration, W -- channel width, $\varphi_T$ -- temperature potential. The adopted system of coordinates is shown in Figure 8.

Practically all the existing quasi-two-dimensional models differ from one another in the steep region of the characteristics in the approximations of the relations $Q_n = Q_n(U_3, U_k)$ and $\mu_n = \mu_n(E_x, E_y)$ and by the inclusion or noninclusion of the diffusion component of the current (second addend in equation (26)), and in the flat region of the characteristics (when smooth approximation of the channel is partially disturbed) -- in the mathematical description of the channel region near the drain.

The physical sense of smooth approximation of the channel is that, for an ordinary planar MDP- transistor, the following inequalities are fulfilled along the major part of the channel length L:

$$E_x \gg E_y, \quad dE_x/d_x \gg dE_y/d_y, \tag{27}$$

and, therefore, the distribution of charges in any section of the channel is defined very precisely by the one-dimensional Gauss equation, and the boundaries and charges of depleted regions -- by one-dimensional Poisson equation.

The condition of the applicability of smooth approximation of the channel for planar MDP-transistors has the following form [67]:

$$L/x_g \geqslant 30, \tag{28}$$

where $x_g$ is the thickness of the gate oxide.

For the MDP-elements of modern series-produced BIS, $L \geqslant 3$ μm and $x_g \leqslant 0.1$ μm, therefore, the condition (28) for them is fulfilled, and quasi-two-dimensional models operate normally. The changeover to MDP-elements with channel lengths $< 3$ μm is done in accordance with the principle of proportional miniaturization [70] which provides for simultaneous proportional reduction of all geometrical dimensions of the structure, including the oxide thickness. As a result of this, the principle of proportional miniaturization, which guarantees the preservation of the working ability of MDP-elements of small dimensions, at the same time ensures the fulfillment of the condition (28), which makes it possible to use modernized quasi-two-dimensional models of the type described in [65-68] with a channel length of at least up to 1 μm.



APPROVED FOR RELEASE: 2007/02/09: CIA-RDP82-00850R000500020034-7

APPROVED FOR RELEASE: 2007/02/09: CIA-RDP82-00850R000500020034-7



Theoretical analysis and experimental data indicate that the influence of all effects determining the behavior of MDP-instruments with moderately small (L $\gtrsim$ 3 μm) channel lengths is fully preserved in subminiature MDP-instruments. These effects include [12]: influence of the substrate charge; mobility modulation of the carriers by the transverse and the longitudinal (drift velocity saturation effect) fields and its dependence on the impurity concentration and temperature; finite drain conduction in saturation (in the flat region of the characteristics); self-capacitance nonlinearity of the MDP-instrument (gate-drain, gate-source, gate-substrate)and capacitance nonlinearity of drain-substrate and source-substrate.

All these effects are taken into consideration in the majority of the models of subminiature MDP-transistors developed to date [65-68 and others]. It should be mentioned that, down to the channel dimensions L, W $\approx$ 1 μm, fully acceptable and accurate results are achieved by using a simple semiempirical description of mobility of the type

$$\mu_n=\mu_{no}(1+E_x/E_{kx})^{-1}(1+\mu_{no}E_y/V_{lim})^{-1}, \quad (29)$$

where $\mu_{no}$ -- surface mobility at $E_x$, $E_y \to 0$ determined by the average impurity concentration and temperature, $E_{kx}$ -- characteristic transverse field, $V_{lim}$ -- limit drift velocity of the carriers. By using the relation (29) in the integration of the current equation (26), it is possible, as a rule, to obtain equations of the volt-ampere characteristics in quasi-two-dimensional models in the form of explicit analytical expressions.

However, for MDP-instruments with small (L, w $\lesssim$ 3 μm) dimensions, a number of additional physical effects are added, which substantially modifies their behavior.

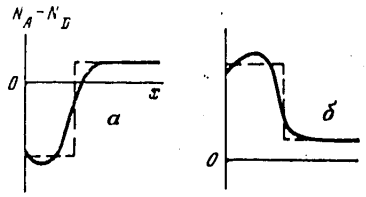


Figure 9. Schematic impurity distribution in the transverse section of the channel for two types of ionic-alloyed MDP-transistors: depleted with a builtin channel -- a and enriched with an "alloyed" channel -- b.

Firstly, even if the principle of porportional miniaturization is observed, the dimensions of the depleted drain-substrate, source-substrate and channel-substrate regions decrease considerably slower than the goemetrical dimensions of the instruments, due to which there form regions at the edges of the channel in which the one-dimensional nature of the distribution of charges is greatly disturbed (effects of a short [71, 72] and a narrow [72-73] channel, see Figure 8).

On the basis of the geometrical approximation shown in Figure 8, the correcting factors k is calculated for the effective charge of the substrate $Q_B$, which appears in



APPROVED FOR RELEASE: 2007/02/09: CIA-RDP82-00850R000500020034-7

APPROVED FOR RELEASE: 2007/02/09: CIA-RDP82-00850R000500020034-7



equations (25), (26). This factor allows for the changes in the effective charge of the substrate under the effect of the edge effects (for the effect of a short channel $k < 1$, for the effect of a narrow channel $k > 1$). Experimental checking of the appropriate models showed that, if the condition (28) is observed, they ensure a sufficient degree of accuracy in the range L, $w \geqslant 1$ μm [74]. If necessary, the modeling of these effects can be done with the aid of two-dimensional models with subsequent approximation of the obtained relations for quasi-two-dimensional "electrical" models [75, 76].

Secondly, with the miniaturization of the MDP-elements, their working voltages will be decreasing simultaneously, and will be 1.5...3 V for digital MDP-circuits at L, $W \simeq 1$ μm. Moreover, it will be required to have an accurate modeling of the behavior of MDP-elements (particularly for dynamic BIS) in the near-threshold region (in the mode of "weak inversion"), which is $\sim \alpha \varphi_f$ V in terms of the voltage on the gate. Here, $1 < \alpha < 1.2$, $\varphi_f = 0.25...0.35$ V is the Fermi level in the substrate. Quasi-two-dimensionsl models for describing the current of an MDP-transistor in the mode of weak inversion exist already [77, 78 and others], however, they are not coupled with quasi-two-dimensional models for the active mode (mode of "strong inversion" and require relatively high computation expenditures.

Thirdly, digital MDP of BIS and superBIS use widely MDP-elements with ionic-alloyed (IL) channels -- depleted MDP-transistors with builtin channels (alloyed with an opposite type of impurity) and enriched with an induced channel (alloyed with the same type of impurity), Figure 9. The modeling of the volt-ampere characteristics of such instruments, even with the quasi-two-dimensional approach, requires, in the general case, to consider the nonlinear real distribution of the impurity, i.e., to perform a numerical calculation of the relation $Q_n(U_3, U_k)$ from the one-dimensional Poisson equation with subsequent numerical integration of the current equation (26) [79]. Such quasi-two-dimensional numerical models approach the models of the type described in [33] with respect to their complexity and computation expenditures and can be used only for calculating the MDP-elements as such.

For these reasons, models of MDP-transistors with IL-channels intended for circuit designing, and even for calculating transistors themselves, are constructed more frequently on the basis of step-by-step approximation of the impurity profile of the channel (interrupted line in Figure 9). These approximations make it possible, in both cases, to obtain the function $Q_n(U_3, U_k)$ in the form of an integrable expression and, due to this, to obtain explicit analytical solutions of the equation (26) for the current of the channel [79-81]. It is also possible to consider the effect of the length and width of the channel on the threshold voltage by relatively simple methods [82].

Both for instruments with ionic-alloyed channels, and for instruments with reduced geometrical dimensions of the channels, an important role is played by mathematical models of threshold voltage as such [68, 71, 73-76, 79-82]. These models, both numerical and simpler analytical, are used more and more widely at the present time in the computation and optimization of the technological design parameters of MDP-elements [69, 83]. They are constructed by finding the voltage on the gate $V_3$ which reduces the specific density of the charge $Q_n(U_3, U_k)$ to zero.



APPROVED FOR RELEASE: 2007/02/09: CIA-RDP82-00850R000500020034-7

APPROVED FOR RELEASE: 2007/02/09: CIA-RDP82-00850R000500020034-7



The basic characteristics of the modeling of MDP-elements on sapphire (insulating) substrates include the consideration for the floating mode of the substrate and avalanche multiplication in the drain junction and a specific mode of operation of n-channel instrument (deep depletion mode) [84-86].

When developing any quasi-two-dimensional models of MDP-elements for technical circuit computations, special attention must be given to the reduction of computation expenditures and smoothness of all functions describing the model [87]. In all possible cases, it is necessary to avoid the use of transcendental functions and internal iterative processes, replacing them by simple approximating expressions (see, for example, [67, 75, 88]). In subsystems of technical circuit designing of MDP of BIS, it is necessary to have a complete set of models -- from the most accurate of the type described in [65-68] to the simplest -- and units of automatic coupling of simpler models with more complicated models [88]. An analogous approach (automatic coupling of simple electrical models with complex physicotopological models) will also be necessary in constructing and using macromodels of MDP-gates and fragments of BIS [89].

Conclusions

1. The modern system of multidimensional modeling of bipolar and MDP-transistors will make it possible to solve successfully the basic problems of modeling and computation of the elements and functionally integrated fragments of BIS and superBIS with minimal topological dimensions up to 0.25...0.3 μm and minimal thicknesses of the layers of structures to 0.01...0.02 um if the numerical methods of solving fundamental equations of the physics of semiconductors are improved further and the descriptions of physical effects used in the models are refined.

2. For solving the problems of modeling and calculation of the elements of BIS and superBIS with submicronic dimensions, it will be necessary to develop effective algorithms and programs for modeling multidimensional distribution of impurities for multistage technological processes including a set of operations of ion implantation, thermal diffusion, oxidation, and epitaxy.

3. When developing both multidimensional and simpler quasi-multidimensional and one-dimensional models, it is necessary to take all possible measures for reducing computation expenditures -- to use various approximations and effective initial approximations in iterations and other computation methods.

4. Precise modeling of subminiature bipolar and MDP-elements of BIS and superBIS in programs of technical circuit designing will require a considerable modernization of the existing models: for example, for bipolar instruments, it will be necessary to consider natural inertness of the transistors and the specific characteristics of functionally integrated n-p-n and p-n-p-structures; and for MDP-instruments -- the effects of a short and a narrow channel, the mode of weak inversion, and nonlinear distribution of the impurity along the depth of the channel.

5. Systems of the parameters of models of bipolar and MDP-elements for technical circuit designing must include not only the parameters defined or refined with the aid of electrical measurements, but also the basic physicotopological parameters characterizing the structure of the elements.



APPROVED FOR RELEASE: 2007/02/09: CIA-RDP82-00850R000500020034-7

APPROVED FOR RELEASE: 2007/02/09: CIA-RDP82-00850R000500020034-7



Bibliography

1. Keypis. ELEKTRONIKA, 1978, Vol 51, No 24, p 29.

2. Laymen. ELEKTRONIKA, 1979, Vol 52, No 8, p 26.

3. Yau, H. N. et al. IEEE Trans on Ed, 1979, v ED-26, No 4, p 318.

4. Laymen. ELEKTRONIKA, 1980, Vol 53, No 14, p 26.

5. Posa, D., and Allen, R. ELEKTRONIKA, 1980, Vol 53, No 4, p 42.

6. Hoeneisen, B,m Mead, C. A. SOL-ST ELECTR, 1972, v 15, No 7, p 819.

7. Hoeneisen, B., Mead, C. A. SOL-ST ELECTR, 1972, v 15, No 8, p 891.

8. Kiiz. TIIER, 1975, Vol 63, No 5, p 5.

9. "Technology", in the book: Elektronika: proshloye, nastoyashcheye, budushcheye" [Electronics: Past, Present and Future], Moscow, Mir, 1980, p 248.

10. Vasenkov, A. A. ELEKTRONNYA TEKHNIKA, Series 3, Microelectronics, 1978, No 6 (78),p 3.

11. Valiyev, K. A., et al. In the book: "Mikroelektronika i poluprovodnikovyye pribory" [Microelectronics and Semiconductor Devices], edited by A. A. Vasenkov and Ya. A. Fedotov, No 1, Moscow, Sov Radio, 1976, p 6.

12. Nosov, Yu. R., Petrosyants, K. O., and Shilin, V. A. "Matimaticheskiye modeli elementov integral'noy elektroniki" [Mathematical Models of Integrated Electronics], Moscow, Sovetskoye radio, 1976.

13. Chebotayev, Ye. V., Rudenko, A. A., and Kokina, G. Ye. In the book: "Mikroelektronika [Microelectronics], edited by A. A. Vasenkov, No 9, Moscow, Sovetskoye radio, 1976, p 47.

14. Ovanov, N. M., and Novikov, V. I. In the book: "Matematicheskoye modelirovaniye" [Mathematical Modeling], Riga, LGU, 1978, p 92.

15. Khetchel, Dzhoy, and Kuli. In the book: "Avtomatizatsiya v proyektirovanii" [Automation in Designing], edited by D. Kalakhan et al, Moscow, Mir, 1972.

16. Petrosyants, K. O. ELEKTRONNAYA TEKHNIKA, Series 2, Semiconductor Devices, 1975, No 1(93), p 43.

17. Petrosyants, K. O. ELEKTRONNAYA TEKHNIKA, Series 2, Semiconductor Devices, 1976, No 3(105), p 11.

18. Hart P., Van't Hof T., Klaassen F. IEEE JOURN SOL-ST CIRCUITS, 1979, v SC-14, No 2, p 343.



APPROVED FOR RELEASE: 2007/02/09: CIA-RDP82-00850R000500020034-7

APPROVED FOR RELEASE: 2007/02/09: CIA-RDP82-00850R000500020034-7



19. Van Overstraeten, R., De Man, H., Mertens, R. IEEE TRANS ON ED, 1973, v ED-20, No 3, p 290.

20. Lundstrom, M., Schwartz, R., Gray, J. SOL-ST ELECTR, 1981, v 24, No 3, p 195.

21. Layou, H., Tuft, R. IEEE TRANS ON ED, 1979, v ED-26, No 7, p 1014.

22. Ching Yuau Wu. SOL-ST ELECTR, 1980, v 23, No 12, p 1215.

23. Dziewior, J., Schmid, M. APPL PHYS LETT, 1977, v 31, p 346.

24. Shibib, M., Lindholm, F., Fossum, J. IEEE TRANS ON ED, 1979, v ED-26, No 7, p 1104.

25. Tang, D. IEEE TRANS ON ED, 1980, v ED-27, No 3, p 563.

26. Gaur, S. IBM JOUR RES DEVELOP, 1977, v 21, No 2, p 306.

27. Marshak, A., Van Vliet, K. SOL-ST ELECTR, 1980, v 23, No 12, p 1223.

28. Mikhaylov, G. S., and Rudenko, A. A. ELEKTRONNAYA TEKHNIKA, Series 3, Microelectronics, 1979, No 4(82), p 88.

29. Valiyev, K. A.; Pashintsev, Yu. I.; and Petrov, G. V. "Primeneniye kontakta metal-poluprovodnik v elektronike" [Applications of Metal-Semiconductor Contacts in Electronics], Moscow, Radio i svyaz', 1981.

30. Gavrilov, O. T., and Tikhodeyev, Yu. S. ELEKTRONNAYA TEKHNIKA, Series 2, Semiconductor Devices, 1973, No 1(73), p 3.

31. Gaur, S. IEEE JOUR SOL-ST CIRCUITS, 1979, v SC-14, No 2, p 337.

32. Yeliseyev, V. S.; Mirgorodskiy, Yu. N.; and Rudenko, A. A. In the book: "Mikroelektronika" edited by A. A. Vasenko, No 8, Moscow, Sovetskoye radio, 1975, p 352.

33. Afontsev, S. A., et al. ZARUBEZHNAYA RADIOELEKTRONIKA, 1975, No 8, p 64.

34. Pol'skiy, B. S., and Pokhvalina, L. S. IZV AN LATVIYSKOY SSR, Series of Physical and Technical Sciences, 1977, No 4, p 59.

35. Rudenko, A. A. ELEKTRONNAYA TEKHNIKA, Series 3. Microelectronics, 1978, No 6(78) p 32.

36. Adachi, T., Yoshii, A., Sudo, T. IEEE TRANS ON ED, 1979, v ED-26, No 7, p 1026.

37. Buturla, E., Cottrell, P. SOL-ST ELECTR, 1980, v 23, No 4, p 331.

38. Adler, M. SOL-ST ELECTR, 1980, v 23, No 8, p 845.

39. Batalov, B. V.; Kremlev, V. Ya.; and D'yakonov, V. M. MIKROELEKTRONIKA, 1979, Vol 8, No 1, p 34.



APPROVED FOR RELEASE: 2007/02/09: CIA-RDP82-00850R000500020034-7

APPROVED FOR RELEASE: 2007/02/09: CIA-RDP82-00850R000500020034-7



40. Afontsev, S. A., et al. MIKROELEKTRONIKA, 1977, Vol 6, No 2, p 179.

41. Rudenko, A. A., and Chebotayev, Ye. V. ELEKTRONNAYA PROMYSHLENNOST', 1979, No 4(76), p 23.

42. Antoniadis, D., Dutton, R. IEEE TRANS ON ED, 1979, v ED-26, No 4, p 490.

43. Warner, D., Wilson, C. BSTJ, 1980, v 59, No 1, p 1.

44. Tielert, R. IEEE TRANS ON ED, 1980, v ED-27, No 8, p 1479.

45. Russel, H., Haberger, K., Hoffman, K., Prinke, G., Dümcker, R., Sachs, A. IEEE TRANS ON ED, 1980, v ED-27, No 8, p 1484.

46. Antoniadis, D., Rodoni, M., Dutton R. J ELECTR SOC SOL-ST SCI AND TECHNOL, 1979, v 126, No 11, p 1939.

47. Lee, H., Dutton, R., Antoniadis, D. J ELECTR SOC SOL-ST SCI AND TECHNOL, 1979, v 126, No 11, p 2001.

48. Antoniadis, D., Gonzales, A., Dutton, R. J ELECTR SOC SOL-ST SCI AND TECHNOL, 1978, v 125, No 5, p 813.

49. Fayzulayev, B. N., and Pervov, A. C. In the book: "Mikroelektronika i poluprovodnikovyye pribory", edited by A. A. Vasenkov and Yu. A. Fedotov, Moscow, Sov Radio, 1979, No 4, p 149.

50. Gaur, S., Navon, D. IEEE TRANS ON ED, 1976, v ED-23, No 1, p 50.

51. Chryssafis, A., Love, W. SOL-ST ELECTR, 1979, v 22, No 3, p 249.

52. Nosov, Yu. R., and Petrosyants, K. O. In the book: "Poluprovodnikovyye pribory i ikh primeneniye" [Semiconductor Instruments and Their Applications], edited by Ya. A. Fedotov, No 28, Moscow, Sov radio, 1975.

53. Petrosyants, K. O. ELEKTRONNAYA TEKHNIKA, Ser 3, Microelectronics, 1975, No 2 (56).

54. Rofail, S., Elmasry, M., Heasell, E. IEEE TRANS ON ED, 1977, v ED-24, No 3, p 234.

55. Hendrickson, T., Huang, J. IEEE JOURN SOL-ST CIRCUITS, 1977, v sc-12, No 2, p 171.

56. Petrosyants, K. O. Proc SUMMER SYMPOSIUM ON CIRCUIT THEORY. SHORT CONTRIBUTIONS. Prague, Czechoslovakia, Sept 1977, p 477.

57. Mishin, A. A. Reports of the All-Union Seminar: "Sensitivity of Electronics and Electromechanical Devices and Systems, Moscow, 1979.



APPROVED FOR RELEASE: 2007/02/09: CIA-RDP82-00850R000500020034-7

APPROVED FOR RELEASE: 2007/02/09: CIA-RDP82-00850R000500020034-7



58. Kazenkov, G. G., Mayorov, S. A., and Rudenko, A. A. ELEKTRONNAYA TEKHNIKA, Ser 3, Microelectronics, 1978, No 6(78), p 17.

59. Avdeyev, Ye. U., and Zverev, S. A. ELEKTRONNAYA TEKHNIKA, Ser 3, Microelectronics, 1978, No 6(78), p 23.

60. Petrosyants, K. O., and Ryabov, N. N. IZV VUZOV SSSR. RADIOELEKTRONIKA, 1980, Vol 13, No 6, p 50.

61. Berger, H., Dreckmann, U. IEEE TRANS ON ED, 1979, v ED-26, No 7, p 1038.

62. Barker, J. R., Ferry, D. K. SOL-ST ELECTR, 1980, v 23, No 6, p 519.

63. Barker, J. R., Ferry, D. K. SOL-ST ELECTR,1980, v 23, No 6, p 531.

64. Selberherr, S., Schütz, A., Pötzl, H. W. IEEE TRANS ON ED, 1980, v ED-27, No 8, p 1540.

65. Compeers, J., De Man, H. G., Sansen, W. M. C. IEEE TRANS ON ED, 1977, v ED-24, No 6, p 739.

66. Hoeffinger, B., Sibbert, H., Zimmer, G. IEEE TRANS ON ED, 1979, v ED-26, No 4, p 513.

67. Dang, L. M. IEEE TRANS ON ED, 1979, v ED-26, No 4, p 436.

68. Taylor, G. W. SOL-ST ELECTR, 1979, v 22, No 8, p 701.

69. Molta, R. F. et al IEEE TRANS ON ED, 1980, v ED-27, No 8, p 1559.

70. Dennard, R. H. et al. IEEE JOURN SOL-ST CIRCUITS, 1974, v SC-9, No 5, p 256.

71. Yau, L. D. SOL-ST ELECTR, 1974, v 17, No 10, p 1059.

72. Wang, P. P. IEEE TRANS ON ED, 1978, v ED-25, No 7, p 779.

73. Jeppsön, K. O. ELECTR LETTERS, 1975, v 11, No 14, p 297.

74. Merckel, G. SOL-ST ELECTR, 1980, v 23, No 12, p 1207.

75. Toyabe, T., Asai, S. IEEE TRANS ON ED, 1979, v ED-26, No 4, p 453.

76. Kroell, K. E., Ackermann, G. K. SOL-ST ELECTR, 1976, v 19, No 1, p 77.

77. Nashuhara, T., Etoh J., Nagata, M. IEEE TRANS ON ED, 1974, v ED-21, No 6, p 363.

78. Scott, D. B., Chamberlain S. G. IEEE JOURN SOL-ST CIRCUITS, 1979, v SC-14, No 3, p 633.



APPROVED FOR RELEASE: 2007/02/09: CIA-RDP82-00850R000500020034-7

APPROVED FOR RELEASE: 2007/02/09: CIA-RDP82-00850R000500020034-7



79. Blyumkin, L. M., Lyakhov, M. N., Khodosh, L. S., and Simonov, V. A. ELEKTRONNAYA PROMYSHLENNOST', 1974, no 12, p 23.

80. Nosov, Yu. R., and Khodosh, L. S. MIKROELEKTRONIKA, 1973, Vol 2, No 5, p 395.

81. Wang, P. P. IEEE TRANS ON ED, 1977, v ED-24, No 3, p 196.

82. Kodosh, L. S. ELEKTRONNAYA TEKHNIKA, Ser 2, Semiconductor Instruments, 1980, No 7(42), p 71.

83. Yokoyama, K., Yoshi, A., Horiguchi, S. IEEE TRANS ON ED, 1980, v ED-27, No 8, p 1509.

84. Eaton, S. S., Lavelic, B. IEEE TRANS ON ED, 1978, v ED-25, No 8, p 907.

85. Jerdonek, R. T., Bandy, W. R. IEEE TRANS ON ED, 1978, v ED-25, No 8, p 899.

86. Jerdonek, R. T., Bandy, W. R., Birnbaum, J. IEEE TRANS ON ED, 1980, v ED-27, No 8, p 1566.

87. Fraser, D. L., Director, S. W. ELECTRONIC CIRCUITS AND SYSTEMS, 1978, v 2, No 2, p 39.

88. Khodosh, L. S., and Shilin, V. A. In the book: "Avtomatizatsiya proektirovaniya v elektronike" [Automation of Designing in Electronics], Kiev, Tekhnika, 1972, No 6.

89. Rabbat, N. B., Ryan, W. D., Hossain, S. IEEE TRANS ON ED, 1975, v ED-22, No 8, p 523.

COPYRIGHT: Izdatel'stvo "Nauka", "Mikroelektronika", 1981

10,233
CSO: 1860/63



APPROVED FOR RELEASE: 2007/02/09: CIA-RDP82-00850R000500020034-7

APPROVED FOR RELEASE: 2007/02/09: CIA-RDP82-00850R000500020034-7



SELECTED ABSTRACTS OF ARTICLES FROM JOURNAL 'MICROELECTRONICS', SEPTEMBER-OCTOBER 1981

Moscow MIKROELEKTRONIKA in Russian Vol 10, No 5, Sep-Oct 81 pp 478-480

UDC 539.2

STATIONARY AND TRAVELING DISSIPATIVE STRUCTURES IN ACTIVE KINETIC MEDIA

[Abstract of article by Kerner, B. S. and Osipov, V. V.]

[Text] The authors studied the properties of homogeneous active distributed media which are promising for creating fundamentally new functional microelectronic devices. On the basis of the theory of such media developed earlier by the authors, they analyzed in detail the simplest one, two, and three-dimensional spatially inhomogeneous states in the form of a single strata, a spot, or a drop which can be written in some stability regions of a homogeneous state of the medium. They analyzed the type of more complex stable spatially inhomogeneous states. Analysis of stable inhomogeneous states traveling without attenuation is given in order to reveal the possibility of reading inhomogeneous structures recorded earlier. Some other functional possibilities of the media in question are discussed. Figures -- 8, bibliography -- 35 items.

UDC 621.382

A DEVICE WITH CHARGE COUPLING AND AN OUTPUT UNIT BASED ON AN AVALANCHE DIODE

[Abstract of article by Trishenkov, M. A. and Eskin, Yu. M.]

[Text] The authors examine the possibilities of using the avalanche multiplication effect in the output assembly of a charge-coupled device. It is shown that this effect can increase the ability of such a device to register weak information charges. Examples of the designs of such output assembly are given. Figures -- 3, bibliography -- 10 items.

UDC 539.2

DISPERSION OF SURFACE MAGNETOSTATIC WAVES IN THE PRESENCE OF A TRAVELING WAVE OF ELASTIC DEFORMATION

[Abstract of article by Popkov, A. F.]

[Text] On the basis of magnetostatics equations and equations of motion of the magnetic moment and with consideration for magnetostriction, the author studied the



APPROVED FOR RELEASE: 2007/02/09: CIA-RDP82-00850R000500020034-7

APPROVED FOR RELEASE: 2007/02/09: CIA-RDP82-00850R000500020034-7



characteristics of the propagation of surface magnetostatic waves (PMV) in the presence of a traveling acoustic wave in the area of stable interaction. Using the method of the theory of singular perturbations, he derived equations describing the interaction of forward and backward magnetostatic waves moving parallel to the acoustic wave. The value is found of the frequency splitting of the dispersive branch of PMV under the conditions of its nonelastic Bragg scattering on a wave of elastic deformation. Evaluations indicate that a surface acoustic wave of 1 mW creates a nontransmission band in the first Brillouin zone $\Delta\omega/\omega \sim 10^{-3}$ in an ytterium ferrite -- garnet plate 10 μm thick located on a 0.5 cm wide substrate unlimited with respect to thickness. In the first order of the theory of perturbation, it is shown that, due to the nonlinearity of the dispersion relation $\omega(k)$ of PMV, it is possible to have the interaction of two forward waves having a shift with respect to the wave number and frequency along with the interaction of forward and backward waves. Figures -- 3, bibliography -- 25 items.

UDC 535.8:535.241.13

DYNAMICS OF OPTICAL RECORDING OF INFORMATION IN MDPDM-STRUCTURES

[Abstract of article by Klimova, N. V.]

[Text] Numerical methods are used to study unsteady processes in MDPDM [metal-dielectric-semiconductor-dielectric-metal] structures during optical recording of information with consideration for a self-consistent field. The drift and diffusion of the carriers are considered, as well as their capture on the surface states of the semiconductor-dielectric interfaces and volume traps. It is shown that the distribution of the electric field intensity is essentially nonuniform over the thickness of the specimen. When there is a great difference in the mobility of the carriers, the sign of the full space charge corresponds to the sign of less mobile carriers. It is shown that the presence of recombination traps increases somewhat the recording time, but improves the conditions of storing the recorded information, preventing its erasing. Figures -- 3, bibliography -- 5 items.

UDC 535.8:535.241.13

BISTABLE PROPERTIES OF A SPACE MODULATOR WITH INTERNAL FEEDBACK

[Abstract of article by Kompanets, I. N., Parfenov, A. V. and Popov, Yu. M.]

[Text] The authors studied a nonlinear optical device whose bistable properties are ensured by internal photoelectric feedback between the light-modulating and a photosensitive layers. The light-modulating medium was a liquid crystal alloyed with a dye which changes its absorption when an electrical field is applied. The switching light energy is $\sim 10^{13}$ J/element at a density of the resolvable image elements of $10^4$ cm-2. The cycle time is 100 ms and can be improved by two orders. Figures -- 2, bibliography -- 6 items.



APPROVED FOR RELEASE: 2007/02/09: CIA-RDP82-00850R000500020034-7

APPROVED FOR RELEASE: 2007/02/09: CIA-RDP82-00850R000500020034-7



UDC 535.8:535.241.13

ELECTRIC ABSORPTION IN SMOOTH HETEROJUNCTIONS Al-$SiO_2$-nGaAs-$n^+GaAs_xP_{1-x}$-$n^+$GaP

[Abstract of article by Morozov, S. F., Blagodarov, A. N., Vigdorovich, Ye. N., Gorshkov, Yu. A., Kunin, V. Ya. and Sveshnikov, Yu. N.]

[Text] The authors examined the characteristics of electric absorption in MDP [metal-dielectric-semiconductor]-heterostructures Al-$SiO_2$-nGaAs-$n^+GaAs_xP_{1-x}$-$n^+$GaP with a transitional layer $GaAs_xP_{1-x}$ of a variable composition matching GaP and GaAs lattices. They analyzed the kinetics of electric absorption under the effect of voltage pulses of various polarities and lengths; optical memory was revealed in recording by an enriching pulse due to electron capture on the $SiO_2$-GaAs interface. They measured spectral and field dependence of the absorption coefficient $\alpha$ GaAs; an empirical relation was obtained for $\alpha$ as a function of the energy of light quanta and the intensity of the electric field. It was concluded that it is promising to use smooth heterojunctions GaAs-$GaAs_xP_{1-x}$-GaP in optical electronics. Figures --2, bibliography -- 6 items.

UDC 621.382.3

SPECIAL CHARACTERISTICS OF PHOTOEMISSION IN MDP-STRUCTURES WITH CONSIDERATION FOR A CHARGE LOCALIZED IN THE DIELECTRIC

[Abstract of article by Sakharov, B. N., Smirnova, O. N. and Gol'dfarb, V. A.]

[Text] The authors studied the effects of a charge localized in a dielectric on the nature of the changes in the boundary potential barriers during changes in the applied voltage with consideration for the intensity of the mirror image. They examined the dependence of this effect on the values, the sign and the forms of distribution of the charge. It is shown that a positive charge in a dielectric in the vicinity of the emitting boundary reduces the degree of the lowering of the height of the potential barrier as the external shift for the injected electrons increases, and increases it for the holes. This makes it possible to determine the emitting boundary of the photoemission current. In this case, the form of the charge distribution shows itself substantially only in the case of the fields of external displacement and charge directed in the opposite direction in dielectrics. Figures -- 3, bibliography -- 7 items.

UDC 621.382

MEASUREMENT OF THE BULK LIFETIME OF MINORITY CARRIERS FROM THE ANALYSIS OF THEIR RECOMBINATION IN A SUBSTRATE OF MDP-STRUCTURES

[Abstract of article by Kats, Ya. L., Klyaus, Kh. I., Li, I. I. and Cherepov, Ye. I.]

[Text] This is a theoretical and experimental examination of the process consisting of the injection and recollection of minority carriers of the charge in the inversion layer of the MDP volume. It is shown that the time characteristics of this process depend weakly on the length of the injecting pulse, the type of the conductivity, the degree of alloying, the amplitude of the applied voltage and the capacitance



APPROVED FOR RELEASE: 2007/02/09: CIA-RDP82-00850R000500020034-7

APPROVED FOR RELEASE: 2007/02/09: CIA-RDP82-00850R000500020034-7



of the dielectric layer of the MDP structure. This method makes it possible to determine the lifetime of the minority carriers of the charge from the analysis of the time characteristics of the process. Figures -- 2, bibliography -- 7 items.

UDC 621.315.592

CREATION OF LOW-RESISTANCE REGIONS ON THE SURFACE OF GERMANIUM BY THE METHOD OF IONIC ALLOYING

[Abstract of article by Godakov, S. S., Klyukvin, A. B. and Mikhaylutsa, Ye. V.]

[Text] The authors studied the possibility of creating low-resistance regions on the surface of Ge by irradiating it with ions of phosphorus with an energy of E=40 keV. They showed the practicality of using short pulses of laser radiation for annealing the forming radiation defects. By measuring the depth distribution profiles of phosphorus in unannealed specimens by the method of mass spectrometry of secondary ions, it was shown that there occurs redistribution of the impurity even in the process of ion irradiation due to the formation of a large amount of radiation defects. It was found that the acceleration of diffusion is observed both in the region where the formation of defects occurs and beyond its limits. Figures -- 2, bibliography -- 5 items.

UDC 539.217.1

AN OBJECTIVE QUANTITATIVE CRITERION OF POROSITY OF THIN FILMS

[Abstract of article by Aranovich, G. L. and Kuznetov, G. D.]

[Text] The authors proposed a new quantitative criterion of porosity of thin layers which does not depend on the pore registration mode. It makes it possible to compare the results of monitoring porosity (continuity) performed by various methods for various films. The obtained results can be used as a basis in standardizing the requirements for the porosity of thin films. Figures -- 1, table -- 1, bibliography -- 2 items.

COPYRIGHT: Izdatel'stvo "Nauka", "Mikroelektronika", 1981

10,233
CSO: 1860/63



APPROVED FOR RELEASE: 2007/02/09: CIA-RDP82-00850R000500020034-7

APPROVED FOR RELEASE: 2007/02/09: CIA-RDP82-00850R000500020034-7



OSCILLATORS, MODULATORS, GENERATORS

UDC 621.317.765

# TECHNOLOGICAL AMTs 1550 CRYSTAL OSCILLATOR

Moscow PRIBORY I SISTEMY UPRAVLENIYA in Russian No 9, Sep 81 p 32

[Article by A. A. Mel'nikov, candidate of technical sciences, N. A. Yermolayev, I. A. Yerasov, and A. N. Shesternin, engineers]

[Text] The AMTs1550 oscillator is designed for the excitation of watch crystal resonators (KR) at the frequency of sequential resonance and for measuring the dynamic impedance of resonators with a normalized (taking into account the capacitance of the winding) capacitance of the load, as well as without it. In a set with a type ChZ-34 frequency meter, it measures frequency or the oscillation period of the oscillator. A possibility is provided in the device for regulating the excitation level of the monitored KR, as well as for measuring the voltage amplitude on the resonator in digital form. The oscillator makes it possible to determine the dynamic inductance, capacitance, the Q-factor and the capacitive coefficient of the KR.

Specifications

| | |
|---|---|
| Range of reproduced frequencies (period) in Hz (microseconds) | 32,500-33,000 (30,303-30,769) |
| Reproducibility of the resonance frequency (period) at a Q-factor $Q \geq 5000$ | $\pm (1.40, Q+0.5 \times 10^{-6})$ |
| Lead capacitance in picofarads | 5; 12.5; 25 |
| Error in setting load capacitance in % | $\pm 2$ |
| Measurement range of dynamic resistance $R_K$ in kohms | 1-150 |
| Error in measuring resistance $R_K$ in %<br>at $R_K < 10$ kohms<br>at $R_K \geq 10$ kohms | <br>$\pm [5+3(10/R_K-1)]$<br>$\pm (5+5 R_K/150)$ |
| Range of voltage amplitude change on KR in millivolts | 30-200 |





APPROVED FOR RELEASE: 2007/02/09: CIA-RDP82-00850R000500020034-7

APPROVED FOR RELEASE: 2007/02/09: CIA-RDP82-00850R000500020034-7



| | |
|---|---|
| Error in measuring voltage amplitude on KR in %, not greater than | $\pm 10$ |
| Power dissipated in the KR in watts, not greater than | $5 \times 10^{-6}$ |
| Oscillator productivity in resonators in hours, not less than | 600-720 |

The basis of the device is the self-excited oscillator method for measuring the equivalent electrical parameters of the KR by inserting the tested resonator in the corresponding circuit.

Structurally the oscillator consists of a measuring and controlling unit with a four-character digital indicator and a self-excited oscillator proper with a contacting device in which is installed the KR being monitored.

The oscillator is made of series K140, K153, K155 and K284 microcircuits. The power is supplied from a 220-volt, 80 Hz AC network; power consumed is 25 volt-amperes. The dimensions are: self-excited oscillator -- 80x120x90 mm; measuring and controlling unit -- 185x240x310 mm.

The equipment was developed by the Penza affiliate of the VNIITI pribor [All-Union Scientific Research Technological Institute of Instrument Making].

COPYRIGHT: Izdatel'stvo "Mashinostroyeniye", "Pribory i sistemy upravleniya", 1981

2291
CSO: 1860/75



APPROVED FOR RELEASE: 2007/02/09: CIA-RDP82-00850R000500020034-7

APPROVED FOR RELEASE: 2007/02/09: CIA-RDP82-00850R000500020034-7



PUBLICATIONS, INCLUDING
COLLECTIONS OF ABSTRACTS

ABSTRACTS FROM JOURNAL 'METROLOGY', SEPTEMBER 1981

Moscow METROLOGIYA (YEZHEMESYACHNOYE PRILOZHENIYE K NAUCHNO-TEKHNICHESKOMY ZHURNALU "IZMERITEL'NAYA TEKHNIKA") in Russian No 9, Sep 81 pp 62-64

UDC 621.396.96 : 621.391.833

SELECTION OF PULSE-PHASE DISCRIMINATOR PARAMETERS

[Abstract of article by Mitsenko, I.D., and Galun, V.B., published in METROLOGIYA, No 9, 1981, p 3]

[Text] The influence of the parameters of a pulse-phase discriminator on the accuracy with which the time position of a pulse is registered is examined. An optimal estimate of its parameters, responding to the requirement of minimal error under given signal detection conditions, is given. 2 illustrations, 6 bibliographic references.

UDC 681.3.004.14:519.2

REAL-TIME PROCEDURE FOR PROCESSING MEASUREMENT INFORMATION

[Abstract of article by Krivotsyuk, V.I., Kreshuk, V.V. and Matveyev, A.A. published in METROLOGIYA, No 9, 1981, p 10]

[Text] A procedure is proposed for real-time processing of measurement information. An example is given and comparability in terms of computational costs is estimated. 8 bibliographic references.

UDC 681.3: 621.317.7

LINGUISTIC APPROACH IN MODELING COMPLEX INFORMATION-MEASURING SYSTEMS

[Abstract of article by Fedotov, B.G., published in METROLOGIYA, No 9, 1981, p 161

[Text] An approach is proposed for modeling complex information measuring systems based on fuzzy set theory. 3 illustrations, 3 bibliographic references.



APPROVED FOR RELEASE: 2007/02/09: CIA-RDP82-00850R000500020034-7

APPROVED FOR RELEASE: 2007/02/09: CIA-RDP82-00850R000500020034-7



UDC 621.833.002.56: 006.354.065

MONITORING MOVING GEAR WHEELS IN MULTISECTIONAL GEARED TRANSMISSIONS

[Abstract of article by Idelvich, A.Ya., published in METROLOGIYA, No 9, 1981, p 22]

[Text] Methods and devices for monitoring moving gear wheels in geared transmissions are described. 2 illustrations, six bibliographic references.

UDC 621.375.826

MEASUREMENT OF SPATIAL INTENSITY DISTRIBUTION IN IR-BAND BEAMS OF POWERFUL QUASI-CONTINUOUS LASERS

[Abstract of article by Vavilov, V.P., Morozov, P.A., Tanaseychuk, S.Yu., Morozova, S.P., and Malysheva, T.P., published in METROLOGIYA, No. 9, 1981, p 27]

[Text] Numerical estimates are obtained for the correspondence between the spatial distribution of the power density of laser radiation and the temperature field on a metal target. 4 illustrations, 4 bibliographic references.

UDC 634.8-6/.8

MEASUREMENT OF SPATIALLY MUTUAL SPECTRUM OF TURBULENT PRESSURE PULSATIONS AGAINST BACKGROUND OF ACOUSTIC NOISE

[Abstract of article by Kazimorov, Yu.A., and Markin, V.I., published in METROLOGIYA, No 9, 1981, p 31]

[Text] A method is described for determining the spatially mutual spectrum of turbulent pressure pulsations against the background of acoustic noise based on measurements of turbulent pressure pulsations at three points. 1 illustration, 4 bibliographic references.

UDC 531.768.068.9

INFLUENCE OF VIBRATION ON PRECISION OF ACCELEROMETER WITH VOLTAGE-DIGITAL CODE CONVERTER

[Abstract of article by Konovalov, S.F., published in METROLOGIYA, No 9, 1981, p 36]

[Text] The influence of harmonic and random vibration on the accuracy of digital accelerometers with various types of voltage-digital code converters is examined. 2 illustrations, 4 bibliographic references.

UDC 621.316.925.44

ANALYSIS OF DEAD ZONES OF LIQUID-FILLED MANOMETRIC TEMPERATURE SENSOR-RELAYS

[Abstract of article by Khludeyev, A.F., published in METROLOGIYA, no 9, 1981, p 36]



APPROVED FOR RELEASE: 2007/02/09: CIA-RDP82-00850R000500020034-7

APPROVED FOR RELEASE: 2007/02/09: CIA-RDP82-00850R000500020034-7



[Text] A method for analyzing the dead zone of liquid-filled manometric temperature sensor-relays is given. An evaluation of the analysis formula is presented. 1 bibliographic reference.

UDC 621.316.99

DEFINITION OF ISOLATION PARAMETERS OF INDIVIDUAL PHASES WITH RESPECT TO GROUND IN NETWORK WITH ISOLATED NEUTRAL

[Abstract of article by Tsapenko, Ye.F. and Sluchevskiy, Yu.N., published in METROLOGIYA, No 9, 1981, p 44]

[Text] A familiar method of determining the isolation resistances and equal-valued capacitances of individual phases with respect to ground in a network with isolated neutral is characterized briefly, and a method is proposed which allows for unequal capacitances. An example of analysis is given. 1 illustration, 1 bibliographic reference.

UDC 621.376.23

RESOLUTION OF DIODE METERS FOR LOW-INDEX AMPLITUDE MODULATION

[Article by Nevolin, V.V., published in METROLOGIYA, No 9, 1981, p 50]

[Text] A method is proposed for defining the internal noise diode detectors used to determine the resolution of low-index modulation meters. 1 illustration, 4 bibliographic references.

UDC 531.733: 532.539.5

DESIGN AND ANALYSIS OF CHARACTERISTICS OF HIGH-FREQUENCY RESONANT PRIMARY TRANSDUCERS OF GAS CONTENT OF NONPOLAR MEDIA

[Abstract of article by Mayorov, V.A., and Kupriyanov, A.S., published in METROLOGIYA, No 9, 1981, p 55]

[Text] Formulas are derived for calculating the nominal statistical characteristics of high-frequency resonant primary transducers for gas content of non-polar media for pipelines with inside diameters between 20 and 124 mm. 1 table, 1 illustration, 3 bibliographic references.

COPYRIGHT: IZDATEL'STVO STANDARTOV, 1981

6900
CSO: 1860/62



APPROVED FOR RELEASE: 2007/02/09: CIA-RDP82-00850R000500020034-7

APPROVED FOR RELEASE: 2007/02/09: CIA-RDP82-00850R000500020034-7



UDC 531.719.2.082.4

ACOUSTICAL DISTANCE MEASUREMENT AND CONTROL METHODS

Moscow AKUSTICHESKIYE METODY IZMERENIYA RASSTOYANIY I UPRAVLENIYA in Russian 1981 (signed to press 8 Apr 81) pp 2-5, 206-207

[Annotation, foreword and table of contents from book "Acoustical Distance Measurement and Control Methods", by Aleksey Alekseyevich Gorbatov and German Yevgen'yevich Rudashevskiy, Energoizdat, 5000 copies, 208 pages]

[Text]

## Annotation

In contrast to the first edition published in 1973, the present book contains a more complete and systematized exposition of new methods and means of remote contactless measurement of distances in a gaseous (air) medium which have been put to industrial use. The physical foundations of measurements using elastic waves, methods of modulating and converting signals, and devices for remote control of the operation of electrical devices are examined.

The book is intended for engineering-technical and scientific workers in the area of automation and monitoring-instrumentation technology.

[The book was reviewed by A. V. Furduyev.]

## Foreword

The present book, which was written five years after the first edition [1] was published, was conceived as a systematized exposition of the theoretical and experimental foundations of echo ranging and acoustical control, which now comprise a division of technical acoustics. The authors' task was to produce a work which would be identically suitable for studying the theoretical and experimental foundations of echo ranging and acoustical control, and for developing corresponding devices having a wide range of capabilities. Because of its limited size, this book was not able to touch upon a number of important methodical questions of the optimal circuit design for echo ranging devices, and did not have a section on acoustical control. In addition, new structural and circuit treatments have recently appeared, electroacoustic converters have been developed with improved characteristics for operation in gaseous media, and the area of application of echo ranging meters has expanded.



APPROVED FOR RELEASE: 2007/02/09: CIA-RDP82-00850R000500020034-7

APPROVED FOR RELEASE: 2007/02/09: CIA-RDP82-00850R000500020034-7



The rapid development of echo ranging technology has resulted from the increased demands of many branches of the economy for new means of measuring the relative spatial position of machine components, the dimensions of production output, liquid levels in bunkers, monitoring the surface profile of a deformed construction, etc., as well as the significantly improved capabilities of electronics which have made it possible to create compact, reliable and economical signal conversion and processing devices.

The need for rapid, precise echo ranging in the 0.1-10 meter range is dictated by a number of practical tasks. Even though they can be solved using radar and optical methods (including television), acoustic echo ranging, based on using acoustic waves primarily in the ultrasonic frequency range, has a number of advantages. These include relative simplicity of emission and reception of oscillations, compactness of transceiving elements in equipment, high resistance to chemical and optical pollution of the environment, capability of operating in aggressive media under high pressures, capability of remoting the secondary equipment far from the site of the measurements, long service life, lack of moving parts, simplicity of servicing, relatively low cost, practically instantaneous readiness to operate when power is turned on, insensitivity to electromagnetic interference, high reliability and many others.

Nontheless, the perceptible relationship between the propagation velocity of elastic oscillations in gaseous media and temperature, humidity, as well as the possible influence of external acoustic interference, require that correcting and stabilizing modules be used in these devices. For these reasons, modern precision sound ranging equipment represents devices with highly developed electronics. It is appropriate to mention the fact here that the first laboratory models of sound ranging devices did not appear until after the war, although the principle of measuring distances by the propagation time of artificial radiation has been known for a long time, and was first expressed in the scientific literature by the Russian scientist academician Zakharov in 1804 after his balloon flights.

As a means for transmitting information for wireless remote control, ultrasound began to attract the attention of developers in the late 1960s. Acoustic remote control is based on transmitting instructions in the form of directional ultrasonic waves, with a distinguishing feature--the oscillation frequency--corresponding to each instruction. The advantage of such devices is primarily the lack of radio emission; they are compact, simple, and relatively inexpensive. Acoustic control devices are now used in industrial and domestic automation for transmitting instructions over distances of up to 30 meters.

We should remind the reader of yet another important advantage of ultrasound in automatic fire hazard warning systems, and in systems for detecting foreign moving bodies in closed spaces. These systems are based on the occurrence of Doppler frequency shift in the sonic field when local regions of the medium (for example, heated air currents) or other sound-reflecting objects move in it. Although these systems are somewhat complex, they have a number of undisputable advantages: high sensitivity (they are triggered long before the appearance of an open flame and at low movement velocities of foreign bodies), require no



APPROVED FOR RELEASE: 2007/02/09: CIA-RDP82-00850R000500020034-7

APPROVED FOR RELEASE: 2007/02/09: CIA-RDP82-00850R000500020034-7



illumination, are insensitive to acoustic interference, and permit monitoring of the situation even when the geometry of the internal space is complex.

These examples provide clear evidence that short-wave aeroacoustics is now being used in various areas of the economy. As this technology is assimilated and put into industrial production, its range of utilization will undoubtedly expand.

One particular specific point in planning echo ranging and acoustical control devices should be pointed out. The group of problems facing the developers of such equipment is quite varied. These include primarily problems of constructing a common structure for an electroacoustic device or system, allowing for the required meteorological and operating characteristics, estimating the possibilities of practical implementation, choosing the type of transceiving elements and the method for modulating the oscillations, the circuit design in consideration of the available hardware base, formation and display of the set of measured parameters, plus many others. Success in solving each of these problems leaves its imprint on the meteorological and operating qualities of a future system and, in the final analysis, determine the success of the development as a whole. The present book touches upon all of the aforementioned problems to some degree, and systematizes the basic scientific-technical treatments which are now known in this area.

It is the authors' pleasant duty to express their gratitude to N. I. Brazhnikov for his thorough analysis of the manuscript and his advice on improving individual chapters of the book.

Table of Contents

Foreword 3

Chapter 1. Introduction 6

1.1. The nature of ultrasound. Problems of echo-ranging and acoustical control 6
1.2. Development of echo ranging methods and devices 11
1.3. Structures for echo ranging devices, threshold recorders and remote control instruments 15

Chapter 2. Elastic wave propagation in gaseous medium 21

2.1. Properties of elastic medium. Plane sonic wave. Parameters of sonic field 21
2.2. Directional wave emission 31
2.3. Sound absorption in gases 39

Chapter 3. Modulation of emitted oscillations 44

3.1. Classification of echo locators by type of emission 45
3.2. Pulsed emission without carrier frequency 49
3.3. Pulsed emission at carrier frequency 54



APPROVED FOR RELEASE: 2007/02/09: CIA-RDP82-00850R000500020034-7

APPROVED FOR RELEASE: 2007/02/09: CIA-RDP82-00850R000500020034-7



3.4. Continuous emission with frequency modulation 58
3.5. Continuous emission with amplitude modulation 62
3.6. Influence of frequency dependence of absorption on signal transmission 64

Chapter 4. Power relationships in echo location 66

4.1. Sound reflection from obstacles 68
4.2. Reception and detection of oscillations 79
4.3. Power relationships 96

Chapter 5. Error sources 96

5.1. Methodical error factors 96
5.2. Speed of sound in gases 99
5.3. Influence of movement of medium on measurement accuracy 101

Chapter 6. Methods for improving accuracy 104

6.1. General evaluation of task 104
6.2. Thermal compensation 108
6.3. Autocorrection 114

Chapter 7. Interference and interference control 122

7.1. Reverberation. Influence of nonuniformity of medium 123
7.2. Electrical and mechanical interference 137
7.3. Repeated sound reflection 141
7.4. Industrial acoustic noise 141

Chapter 8. Electroacoustic converters 142

8.1. Acoustic and electrical parameters of converters 143
8.2. Elements of ultrasonic oscillating systems 153
8.3. Electrodynamic converters 159
8.4. Magnetostriction converters 162
8.5. Piezoceramic converters 166
8.6. Condensor (capacitive) converters 174

Chapter 9. Dynamic properties of echo location circuits 175

9.1. Spectrum of pulse-width modulated signal and dynamic error 178
9.2. Interpolation 180
9.3. Reduction of dynamic error, expansion of bandwidth 184
9.4. Speed and error during echo ranging in the air 186



APPROVED FOR RELEASE: 2007/02/09: CIA-RDP82-00850R000500020034-7

APPROVED FOR RELEASE: 2007/02/09: CIA-RDP82-00850R000500020034-7



Chapter 10. Ultrasonic remote control and warning 187

10.1. Remote control devices 188
10.2. Warning devices 196

Appendix 198

Bibliography 202

COPYRIGHT: Energoizdat, 1981

6900
CSO: 1860/48



APPROVED FOR RELEASE: 2007/02/09: CIA-RDP82-00850R000500020034-7

APPROVED FOR RELEASE: 2007/02/09: CIA-RDP82-00850R000500020034-7



UDC 621.314.6:621.384.65

CASCADE GENERATORS

Moscow KASKADNYYE GENERATORY in Russian 1980 (signed to press 15 Jul 80) pp 2-3, 196-197

[Annotation, foreword and table of contents from book "Cascade Generators", by Boris Iosifovich Al'bertinskiy and Mikhail Pavlovich Svin'in, Atomizdat, 1550 copies, 197 pages]

[Text]

## Annotation

This book is devoted to the theory, development and design of cascade generators, which are now one of the most widely used high- and superhigh- direct voltage sources. The developmental trends of cascade generators implemented using traditional capacitor-gate schemes, as well as inductive coupling schemes which have recently come into use, are examined. Engineering calculation methods are cited and information is given on existing domestic and foreign installations of various types, as well as their components, construction materials and supply systems.

The book is intended for engineering-technical workers at scientific-research institutes, design bureaus and industrial enterprises involved in the development and operation of cascade generators and devices based on same. The book may also be useful to senior students specializing in high voltage technology and electrical physics.

One hundred and thirty-nine figures, 10 tables, 73 bibliographic references.

## Foreword

This book explains questions of the theory, development and design of cascade generators, which are now one of the most widely used types of high and superhigh direct voltage sources.

The traditional area of application of cascade generators is in electrophysical equipment, primarily high-voltage accelerators of various types intended for applications and basic research which are distinguished by compactness and a



APPROVED FOR RELEASE: 2007/02/09: CIA-RDP82-00850R000500020034-7

APPROVED FOR RELEASE: 2007/02/09: CIA-RDP82-00850R000500020034-7



high average power level, providing accelerating voltage instability of up to $10^{-5}$ - $10^{-6}$ relative units with significant beam currents. Cascade generators are also used successfully for powering other electrophysical and electrotechnical devices: electrostatic lenses, deflectors, energy analyzers, X-ray equipment, electrostatic painting installations, for testing high voltage dc equipment, etc.

The recent expansion of the area of application of cascade generators has raised interest in questions of their calculation, design and operation, many of which up to the present have been touched upon only in the periodic literature. The book uses materials from domestic and foreign monographs, publications in the periodic literature and original work of the authors, which provide a fairly complete picture of the status of this subject.

Sections 1.3-1.5, 2.4, 3.1, 3.3, 3.4, 3.7, 4.1 and 4.2 were written by B. I. Al'bertinskiy, while M. P. Svin'in wrote the Introduction, sections 1.1, 1.2, 1.6, 2.1-2.3, 3.2, 3.5, 3.6, and 4.3-4.6, chapter 5 and the Conclusion. The authors express their gratitude to V. V. Akulov, A. S. Ivanov, G. I. Razin, M. T. Fedotov and V. I. Chuyko for their helpful discussions and assistance in selecting material and preparing the manuscript.

Table of Contents

Foreword 3

Introduction 4

Chapter 1. Theory of circuits with series cascade feed 14

1.1. Basic processes in cascade generator scheme with capacitive cascade coupling 14
1.2. Cascade generator with capacitive coupling in free-running mode 18
1.3. Cascade generator with capacitive coupling in stationary load mode 22
1.4. Design calculation of capacitively coupled cascade generators 30
1.5. Emergency modes in capacitively coupled cascade generators 33
1.6. Cascade generators with inductively coupled cascades 44

Chapter 2. Theory of circuits with parallel cascade feed 53

2.1. Some formulas for single-phase rectifier circuits with capacitive filter 53
2.2. Cascade generators with capacitive cascade coupling 62
2.3. Cascade generators with inductive cascade coupling 68
2.4. Features of emergency modes of inductively coupled cascade generators 70

Chapter 3. Construction elements of cascade generators and calculation of nonstandard elements 73

3.1. Characteristics of basic construction materials and insulating media 73



APPROVED FOR RELEASE: 2007/02/09: CIA-RDP82-00850R000500020034-7

APPROVED FOR RELEASE: 2007/02/09: CIA-RDP82-00850R000500020034-7



3.2. Characteristics of standard cascade generator circuit elements 87
3.3. High voltage valves 105
3.4. Condenser columns and protective resistances 109
3.5. Cores 111
3.6. Windings of inductive elements 120
3.7. Electrostatic fields in primary insulating intervals 122

Chapter 4. Calculation and design of cascade generators. Calculation examples 130

4.1. Half-wave generator with capacitive cascade coupling 130
4.2. Balanced generator with capacitive cascade coupling 132
4.3. Capacitively coupled generators with parallel cascade feed 140
4.4. Cascade connection of isolation transformers 144
4.5. Cascade generators with sectioned core 148
4.6. Cascade generators with closed core 150

Chapter 5. Cascade generator voltage supply and stabilization systems 163

5.1. Singularities of some regulators 164
5.2. Rectifiers 168
5.3. Frequency converters 169
5.4. Matching transformers and compensating reactive elements 174
5.5. Measuring dividers and sensors in feedback devices 176
5.6. Feedback devices 178
5.7. Voltage supply in stabilization systems of some cascade generators 179

Conclusion 189

COPYRIGHT: Atomizdat, 1980

6900
CSO: 1860/57



APPROVED FOR RELEASE: 2007/02/09: CIA-RDP82-00850R000500020034-7

APPROVED FOR RELEASE: 2007/02/09: CIA-RDP82-00850R000500020034-7



UDC 621.382.233.011.222.072

CLASSIFICATION OF THYRISTORS

Moscow ELEMENTY RADIOELEKTRONNOY APPARATURY, VYPUSK 40: TIRISTORY in Russian 1980 (signed to press 3 Oct 80) pp 2-3, 65

[Annotation, introduction and table of contents of book "Radio Electronics Equipment Parts: Thyristors", by Vladimir Yakovlevich Zamyatin and Boris Vladimirovich Kondrat'yev, Izdatel'stvo "Sovetskoye radio", 40,000 copies, 65 pages]

[Text] A classification of thyristors is given with respect to the principles of control, form of the volt-ampere characteristic, average current and basic function. Their design, basic parameters, most important characteristics and their dependence on operating mode and temperature are examined. Examples of the design of several thyristor circuits employed in radio engineering, converter techniques and electronics. Basic rules for the operation and selection of thyristors are formulated.

For a broad circle of readers connected with the operation and repair of electronics and radio engineering equipment.

4 tables, 68 illus., biblio. of 23 titles.

Reviewed by Doctor of Technical Sciences Yu. I. Konev and Candidate of Technical Sciences A. N. Dumanevich.

The creation of a wide range of functional assemblies and devices for the varied types of electronics and radio engineering equipment would currently be unthinkable without thyristors. The growing demand for thyristors is explained by the advantages which are inherent in these items from the semiconductor instrument building sector, namely: small dimensions and weight (per unit of power), extremely high allowable voltages and currents, high efficiency, long service life, instantaneous readiness for operation, high mechanical strength, etc. Thyristors are advantageously distinguished from transistors by significantly greater allowable voltages and currents and the smaller power required for control, because a control current is only required to switch on a thyristor. They compete successfully with several types of gas discharge and electric vacuum devices.





APPROVED FOR RELEASE: 2007/02/09: CIA-RDP82-00850R000500020034-7

APPROVED FOR RELEASE: 2007/02/09: CIA-RDP82-00850R000500020034-7



Thyristors are semiconductor devices based on a multilayered p-n-p-n structure. They are used as the active elements in many electronics equipment circuits, and they have found broad application. A large number of forms and types of thyristors for various purposes are currently produced. Devices have been created with currents of from 1 to hundreds of amperes and voltages of from 10s to several kilovolts.

Silicon is the basic material for creating thyristors. In the last 2-3 years, both here and abroad, research has been underway on the possibility of creating thyristors based on other semiconductor materials: gallium arsenide, silicon carbide, etc. The experimental results make it possible to assume a significant improvement in the characteristics of such thyristors as compared with the silicon ones.

The process of thyristor development is still far from complete. A further increase is expected in the level of power (current and voltage) and switching (current and voltage build-up rates) characteristics.

CONTENTS


| | | |
|---|---|---|
| Introduction | | 3 |
| I. | Operating principles and classification of thyristors | 4 |
| | Operating principles of thyristors | 4 |
| | Methods of switching thyristors on and controlling them | 10 |
| | Typical thyristor circuit and control diagrams | 13 |
| | Methods for tripping thyristors | 14 |
| | Typical thyristor tripping circuits | 16 |
| | Thyristor classification | 17 |
| II. | Basic thyristor parameters | 19 |
| | Parameters of the device | 20 |
| | Maximally allowable parameters of the operating mode | 24 |
| III. | Thyristor design | 30 |
| IV. | Modern thyristor nomenclature | 33 |
| V. | Thyristor reliability | 40 |
| | Reliability indicators | 40 |
| | Basic types of failure | 41 |
| | Ways to increase reliability | 43 |
| VI. | Main areas of thyristor application | 45 |
| | Static two-way a.c. and d.c. switches | 46 |
| | Circuits with phase control | 49 |




APPROVED FOR RELEASE: 2007/02/09: CIA-RDP82-00850R000500020034-7

APPROVED FOR RELEASE: 2007/02/09: CIA-RDP82-00850R000500020034-7



Inverters 50
Frequency converters (cycloinverters) 53
Pulse modulators 54
Automation circuitry 54

VII. Recommendations on the selection and application of thyristors 56

VIII. Testing the electrical modes of thyristors in equipment 59

Measurement of basic circuit parameters 60
Measurement of control circuit parameters 61

List of Literature 63

COPYRIGHT: Izdatel'stvo "Sovetskoye radio", 1980

9194
CSO: 1860/9



APPROVED FOR RELEASE: 2007/02/09: CIA-RDP82-00850R000500020034-7

APPROVED FOR RELEASE: 2007/02/09: CIA-RDP82-00850R000500020034-7



UDC 621.314.27-51

CONTROL SYSTEMS FOR THYRISTOR FREQUENCY CONVERTERS

Moscow SISTEMY UPRAVLENIYA TIRISTORNYMI PREOBRAZOVATELYAMI CHASTOTY in Russian 1981 (signed to press 2 Mar 81) pp 2-3, 144

[Annotation, foreword and table of contents from book "Control Systems for Thyristor Frequency Converters", by Valeriy Aleksandrovich Bizikov, Vladimir Nikolayevich Mironov, Stanislav Grigor'yevich Obukhov and Ravil' Nazimovich Shamgunov, Energoizdat, 10,000 copies, 144 pages]

[Text]

## Annotation

Problems of the development of modules and construction of systems for controlling valve-type frequency converters are examined, as are problems of converter control of autonomous and slave networks, methods of voltage formation and voltage parameter regulation. Examples are given of circuits for controlling autonomous voltage inverters and directly coupled frequency converters. The development of logic circuits is presented using the simulation apparatus of finite automata.

The book is intended for engineers working in the area of converter technology, as well as graduate students in the industrial electronics specialty.

[This book was reviewed by G. G. Zhemerov.]

## Foreword

The technical improvement of valve-type frequency converters is moving in two basic directions: optimization of the converter power circuit and optimization of switching element control. The capabilities in the first direction have been discovered, and are utilized fairly fully, while only the first steps have so far been taken in the second direction. Improvement of the hardware base was a prerequisite for control optimization. The use of power thyristors with high dynamic indicators, two-operation thyristors, power transistors in the power section of a converting system and integrated microcircuits in the information part of the system makes it possible, by improving the control algorithms, to achieve better quality indicators of the energy before and after conversion. Work in this direction has recently appeared frequently in the Soviet and foreign press.



APPROVED FOR RELEASE: 2007/02/09: CIA-RDP82-00850R000500020034-7

APPROVED FOR RELEASE: 2007/02/09: CIA-RDP82-00850R000500020034-7



The authors have attempted, on the basis of classifying algorithms for controlling valves and valve groups, to compile general functional diagrams, isolate common information units and provide a methodology for the development. The book presents a large number of circuits for pulsed generators with adjustable frequency, adjustable delay circuits, and sinusoidal voltage generators with adjustable frequency in amplitude. The logic units in the control systems have been synthesized on the basis of standard integrated logic microcircuits. In order to use the calculation relationships, the brief theoretical considerations which are the prerequisite for synthesiing the logic units are sufficient. In addition, the book contains a large number of practical circuits with recommendations for their application.

The authors express their gratitude to reviewer G. G. Zhemerov and editor Ye. Ye. Chaplygin, who helped to improve the quality of the book.

Table of Contents

Foreword 3

Chapter 1. Valve-type converter control 4

1.1. Voltage formation methods using thyristor frequency converters 4
1.2. Controlling autonomous voltage inverters 8
1.3. Regulation of autonomous inverter output voltage 17
1.4. Singularities of controlling thyristor autonomous voltage inverters with forced switching modules 23
1.5. Controlling network-driven converters 25
1.6. Functional diagrams of control systems 29

Chapter 2. Modulators and master oscillators 32

2.1. Adjustable timing oscillators 32
2.2. Delay and pulse shaping modules 41
2.3. Choice of lead signal shape 48
2.4. Circuits of oscillators with step signal formation 55
2.5. Modulators 64
2.6. Phase reversal 74

Chapter 3. Control system logic modules 78

3.1. Logical functions of control systems 78
3.2. Typical control system logic modules 79
3.3. Synthesis of control system logic modules 92
3.4. Examples of logic modules 103
3.5. Ways of improving noise tolerance of frequency converter control systems 117



APPROVED FOR RELEASE: 2007/02/09: CIA-RDP82-00850R000500020034-7

APPROVED FOR RELEASE: 2007/02/09: CIA-RDP82-00850R000500020034-7



Chapter 4. Output units of control systems 128

4.1. Requirements for output units of control systems 128
4.2. Circuits of output units 134
4.3. Use of photon-coupled pairs in output units 137

Bibliography 140

COPYRIGHT: Energoizdat, 1981

6900
CSO: 1860/46



APPROVED FOR RELEASE: 2007/02/09: CIA-RDP82-00850R000500020034-7

APPROVED FOR RELEASE: 2007/02/09: CIA-RDP82-00850R000500020034-7



UDC 621.397.2

DIGITAL ENCODING OF TELEVISION IMAGES

Moscow TSIFROVOYE KODIROVANIYE TELEVIZIONNYKH IZOBRAZHENIY in Russian 1981 (signed to press 13 Jan 81) pp 2-3, 238-239

[Annotation, foreword and table of contents from book "Digital Encoding of Television Images", by Il'ya Ioannovich Tsukkerman, Boris Moiseyevich Kats, Dmitriy Savel'yevich Lebedev, et al., Izdatel'stvo "Radio i svyaz'", 8000 copies, 240 pages]

[Text]

## Annotation

The principles, problems and prospects for application of digital image coding methods in television are examined. In addition to a theoretical analysis of image coding, examples of computer modeling and experimental findings from existing devices are given. Methods for effective image coding are analyzed on the basis of data on the statistics of images and their psychophysiological redundancy.

The book is intended for engineering and technical workers specializing in the area of television.

[This book was reviewed by M. I. Krivosheyev, Yu. M. Braude-Zolotarev and L. S. Vilenchik.]

## Foreword

Modern television technology primarily uses analog methods for representing and transmitting images. There are few examples of applied television systems using digital image conversion. Broadcast television, in spite of the appearance of individual digital devices, remains essentially analog.

The capabilities of analog methods in television have apparently nearly reached their limit. In order to improve picture quality further, reduce losses during repeated rerecording and transmission over long-distance communication links, as well as to improve the reliability of television equipment and to prefect and automate broadcast technology, digital television must be used. The coding of television images occupies a central place in this multifaceted problem.



APPROVED FOR RELEASE: 2007/02/09: CIA-RDP82-00850R000500020034-7

APPROVED FOR RELEASE: 2007/02/09: CIA-RDP82-00850R000500020034-7



Questions of digital image coding are thoroughly represented in the scientific-technical literature. Computer-based image conversion operations are studied in particular detail.

A new scientific area has arisen which is called digital image processing in English (which translates [to Russian] approximately as tsifrovaya obrabotka izobrazheniy), or more briefly, iconics [ikonika in Russian]. Digital image processing methods are becoming increasingly important for solving problems of data analysis in medicine, biology, high-energy physics, astronomy, material science, geology and soil science, in studying natural resources, in automatic control of technological processes, and in many other areas of science and technology. Several monographs have recently been published which touch upon these matters to some extent (for example, cf. [88, 92, 104, 147, 241, 253]). However, none of these books discusses thoroughly enough the problem of real-time image coding, which is characteristic for digital television. The monograph Televideniye i teoriya informatsii (Television and Information Theory) [61], published in 1965, was written as a theoretical introduction to this problem; however, at that time the necessary technical methods and facilities for practical implementation of such coding did not exist. Digital coding is considered briefly in the recently published item [131] and the popular scientific brochure [137], both of which touch upon many other problems of digital television.

The purpose of the present book is to expand upon the current status of work on digital coding in television on the basis of studying image statistics and the properties of visual perception. Together with materials in the scientific-technical literature, the book explains to a significant degree research work done by the authors in the area of digital television. Image coding algorithms were verified by simulation on computers equipped with image input-output devices and with the help of television devices operating in real time. When we speak of digital coding of television images, we mean primarily the problems of developing professional devices for digital television broadcasts. Successful solution of these problems is also very important for the introduction of digital methods to applications television, including the creation of digital systems for automatic image analysis and recognition of visual patterns. The introduction and chapter 1 and 2 were written by I. I. Tsukkerman, chapter 3 by I. I. Tsukkerman and N. N. Shotatskiy, chapter 4 by B. M. Kats and S. V. Sardyko, chapter 5 by all four authors jointly, chapter 6 by S. V. Sardyko and I. I. Tsukkerman, chapter 7 by D. S. Lebedev, chapter 8 by Ye. Z. Sorokaya and V. A. Khleborodov, chapter 9 by V. G. Makoveyev (V. V. Bykov participated in writing §9.1 and 9.2). The bibliography was assembled by B. M. Kats.

The authors' collective expresses their deep thanks to Professor M. I. Krivosheyev and Professor S. V. Novakovskiy for their helpful counsel and remarks during duscussions of the material in the book.



APPROVED FOR RELEASE: 2007/02/09: CIA-RDP82-00850R000500020034-7

APPROVED FOR RELEASE: 2007/02/09: CIA-RDP82-00850R000500020034-7



Table of Contents


| | |
|---|---|
| Foreword | 3 |
| Introduction | 4 |
| Chapter 1. Statistics of television images | 10 |
| 1.1. Statistical characteristics of images | 10 |
| 1.2. Spatial frequency spectrum | 16 |
| 1.3. Typical configurations | 19 |
| 1.4. Color statistics | 22 |
| Chapter 2. Singularities of visual perception and coding of television images | 25 |
| 2.1. Visual thresholds and image quantization | 26 |
| 2.2. Linear approximation to image filtering in the visual system | 28 |
| 2.3. Group image coding in the visual system | 34 |
| 2.4. Limitations of color vision | 36 |
| 2.5. Subjective evaluation of image quality in color television | 41 |
| Chapter 3. Image digitization during digital coding | 42 |
| 3.1. Some concepts of the theory of digitization of multidimensional messages | 43 |
| 3.2. Orthogonal digitization structure in interlaced scanning | 53 |
| 3.3. Checkerboard structure of sample arrangements in frame | 63 |
| 3.4. Checkerboard structure of sample arrangement in field | 75 |
| 3.5. Diagonal structure of sample arrangement in frame | 84 |
| 3.6. Time digitization of images | 88 |
| Chapter 4. Analog-digital and digital-analog conversion | 89 |
| 4.1. Structures of television analog-digital converters | 90 |
| 4.2. Digital-analog converters | 103 |
| 4.3. Precision characteristics of analog-digital and digital-analog conversion | 107 |
| Chapter 5. Predictive coding of television images | 116 |
| 5.1. Linear prediction in television | 117 |
| 5.2. Quantization of prediction error signals | 120 |
| 5.3. Linear-prediction image coding algorithms | 123 |
| 5.4. Noise tolerance of dual PCM systems | 130 |




APPROVED FOR RELEASE: 2007/02/09: CIA-RDP82-00850R000500020034-7

APPROVED FOR RELEASE: 2007/02/09: CIA-RDP82-00850R000500020034-7



Chapter 6. Group coding of television images 136

6.1. Coding with conversion 138
6.2. Adaptive group coding 152

Chapter 7. Digital methods for image correction 160

7.1. Linear filtering of images 161
7.2. Optimal filtering 171
7.3. Drop-out correction 176
7.4. Recovery of distorted images 182

Chapter 8. Coding of complete color television signal 187

8.1. Complete color television signal spectra 188
8.2. Digitization of complete color television signals 199
8.3. Coding of complete color television signals using dual PCM methods 206

Chapter 9. Digital coding of images in television broadcast 216

9.1. The problem of digital video recording 217
9.2. Devices for signal processing in television broadcast based on digital memory 220
9.3. Directions of development of digital broadcast television 223

Bibliography 226

COPYRIGHT: Izdatel'stvo "Radio i svyaz'", 1981.

6900
CSO: 1860/45



APPROVED FOR RELEASE: 2007/02/09: CIA-RDP82-00850R000500020034-7

APPROVED FOR RELEASE: 2007/02/09: CIA-RDP82-00850R000500020034-7



ELECTRICAL AND OPTICAL PROPERTIES OF SEMICONDUCTORS

Makhachkala ELEKTRICHESKIYE I OPTICHESKIYE SVOYSTVA POLUPROVODNIKOV in Russian 1980 pp 2-4

[Annotation and table of contents of book "Electrical and Optical Properties of Semiconductors," edited by Kh. I. Amirkhanov, D. Kh. Amirkhanova, R. I. Bashirov, A. Z. Gadzhiyev, V. I. Martovitskiy and V. A. Yelizarov (responsible secretary), Dagestanskiy filial AN SSSR, Institut fiziki]

[Text] The collection contains the results of research on the equilibrium and non-equilibrium states of the electron gas in the technically most important semiconductors.

Works on optical phenomena in $A_2B_6$ type wide band semiconductors and on certain vitrious systems are also included in the collection.

The works presented in the collection will be of use to specialists in semiconductors semiconductor equipment engineers.

CONTENTS

Kh. I. Amirkhanov, Dzh. Kh. Amirkhanova, P. P. Khokhlachev, R. S. Zubayruyev. On the question of the applicability of the Wideman-Franz law in slitless crystals based on telluride of mercury 5

Kh. I. Amirkhanov, R. I. Bashirov, Sh. G. Suleymanov. Gallium arsenide magnetic diodes 12

Kh. I. Amirkhanov, B. I. Klyukvin, N. M. Anapol'skiy. Cyclotron resonance in the valence zone of germanium given uniaxial tension 18

M. R. Isayev, B. G. Aliyev. Current instability in silicon $p^+$-p-$n^+$ structures in transposed electrical and magnetic fields 25

K. M. Aliyev. Comparative volt-ampere characteristics of short and long germanium double injection p-i-n structures 30



APPROVED FOR RELEASE: 2007/02/09: CIA-RDP82-00850R000500020034-7

APPROVED FOR RELEASE: 2007/02/09: CIA-RDP82-00850R000500020034-7



V. Z. Zhokhov, A. A. Stepurenko, V. I. Pustovoyt, M. M. Mazur. Influence of a magnetic field on current instability in tellurium 35

N. N. Liberman. Accustoelectrical current instability in tellurium along the Z axis 42

M-R. A. Magomedov. S-type volt-ampere characteristics in monocrystalline selenium film 47

R. M. Gadzhiyeva, Dzh. Kh. Amirkhanova. Galvanomagnetic properties of $Cd_xHg_{1-x}Te$ crystals at low temperatures 52

M. I. Daunov, A. B. Magomedov, A. E. Ramazanova. Magnetoresistance in hole (conductivity) $CdSnAs_2$ 58

R. I. Bashirov, V. A. Yelizarov. Tape recorder oscillations of transverse magnetic resistance on heated electrons in indium antimonide 65

A. Yu. Mollayev, S. M. Salikhov. The effect of electron gas heat-up on negative magnetic resistance in n-InP 73

M. A. Aliyev. The effect of dislocation on the specific electrical resistance of plastically deformed germanium 79

T. A. Shakhnazarov. The effect of interzonal screening on electron mobility in $Zn_xHg_{1-x}Te$ 83

G. G. Gadzhiyev, A. A. Kamarzin, B. N. Magdiyev, Yu. N. Malovitskiy. Electrical properties of lanthanium sulfides 87

Ar. A. Abdullayev. On ruptured bonds and the coefficient of overstress in atomic semiconductors 90

R. R. Bashirov. A spin analogy method in semiconductor theory 95

A. Z. Gadzhiyev. IR transmission and reflection spectra of vitrious chalcogenid semiconductors of the $GeSe_nTIy$ system and their structural peculiarities 101

A. A. Babayev. Photoluminescence in vitrious $Ge_2S_3$ and $Ge_2Se_3$ 107

B. M. Atayev, D. A. Shaikhov. Exciton luminescence of epitaxial zinc oxide layers as a function of precipitation conditions and electrical properties 114

A. D. Adukov, R. A. Rabadanov. p-n plasmas and liquid in epitaxial zinc oxide layers 121



APPROVED FOR RELEASE: 2007/02/09: CIA-RDP82-00850R000500020034-7

APPROVED FOR RELEASE: 2007/02/09: CIA-RDP82-00850R000500020034-7



M. A. Rizakhanov, F. S. Gabibov, A. A. Abdullayev. The effect of stationary excitation on the spectral distribution of the effects of an extrinsic photocurrent in CdS < Ag > crystals 129

M. A. Abdullayev, R. P. Seysyan. The levels and series of a dimagnetic exciton in the reciprocal magnetic bearing spectra (OMP) of gallium arsenide 136

A. Kh. Abduyev, A. M. Bagamadova, L. L. Aksenova. Photoelectrical properties of ZnO-ZnS system 143

A. Z. Gadzhiyev, M. M. Gafurov. Temperature-phase changes in the IR absorption spectra of the crystalline and molten nitrates of alkaline metals 148

N. M. Anapol'skiy, B. I. Klyukvin. An 8-mm radiospectrometer for studying cyclotron resonance in monoaxial stressed semiconductors 159

COPYRIGHT: Unknown

9194
CSO: 1860/7



APPROVED FOR RELEASE: 2007/02/09: CIA-RDP82-00850R000500020034-7

APPROVED FOR RELEASE: 2007/02/09: CIA-RDP82-00850R000500020034-7



UDC 621.385.6

ELECTRONIC MICROWAVE DEVICES

Moscow ELEKTRONNYYE SVCh PRIBORY in Russian 1981 (signed to press 6 Feb 81) pp 2-4, 7-14, 270-271

[Annotation, foreword, introduction and table of contents of book "Electronic Microwave Devices" by Sergey Vladimirovich Kukarin, Izdatel'stvo "Radio i svyaz'", 8000 copies, 272 pages]

[Text]

## Annotation

The technical operating specifications and areas of application of modern electronic devices, including triodes and tetrodes, magnetron-type devices, klystrons, traveling- and backward-wave tubes, hybrid devices, semiconductor diodes and transistors, as well as oscillators and amplifiers based on them, are presented.

The book is intended for specialists interested in microwave devices and their areas of application. It may also be helpful to graduate school teachers and students.

[This book was reviewed by Doctor of Technical Sciences Professor V.N. Sretenskiy and Doctor of Technical Sciences V.P. Sazonov.]

## Foreword

This is the second edition of the book published by Izdatel'stvo "Sovetskoye radio" in 1962 under the title "Sovremennoye sostoyaniye i tendentsii razvitiya priborov SVCh (Current Status and Developmental Trends of Microwave Devices)". The contents of the book have been completely revised and expanded, since significant changes have occurred in this dynamically developing area of electronic technology in the intervening years. These changes involve the further development of vacuum-type microwave devices, as well as the appearance and intensive development of a new class of electronic microwave instruments and devices based on the use of semiconductor diodes and transistors.

Microwave electronics has achieved major successes in this country, as is indicated in the reviews by N.D. Devyatkov [1] on vacuum microwave devices, and by A.S. Tager [3] on solid-state devices. Many of the achievements of Soviet scientists and engineers have preceded, and technically exceeded, the best results obtained by foreign firms. This is the case within a broad area of microwave electronics,



APPROVED FOR RELEASE: 2007/02/09: CIA-RDP82-00850R000500020034-7

APPROVED FOR RELEASE: 2007/02/09: CIA-RDP82-00850R000500020034-7



from superminiature vacuum and solid-state devices up to powerful and superpowerful microwave devices [1-25]. The Soviet reader is thoroughly familiar with the technical specifications of domestic microwave devices from the handbooks and brochures in the series "Radio Electronic Equipment Elements" published by Izdatel'stvo "Sovetskoye radio" [26-38]. Questions of the application of these devices are examined in detail in [19,20].

A wide range of microwave devices is also produced by numerous companies in America, Europe and Asia both to satisfy domestic requirements and for sale on the world market.

The status and developmental trends of this area of electronic technology are considered in the present book using primarily examples of foreign microwave devices about which information is of interest for a broad group of readers. The reviews of the status and developmental trends of foreign microwave devices published by the "Elektronika" Central Scientific Research Institute [39 - 65], as well as a great deal of material, handbooks and advertising information published in the foreign literature [67,264] were used in the preparation of the manuscript.

A great deal of assistance in selecting the necessary materials and illustrations, and in discussing individual sections of a manuscript, was provided by V.M. Lomakin, I.P. Bludov, P.R. Kalish, V.I. Mints, V.D. Mel'nikov, V.G. Zaytseva and L.A. Sokolova, to whom the author expresses his gratitude. The author was grateful to receive and make use of the comments of reviewers V.N. Sretenskiy and V.P. Sazonov.

It was difficult to avoid certain shortcomings and inaccuracies in working with such a large amount of material; therefore, any remarks or suggestions of readers, which should be addressed to the publisher, will be gratefully received.

## Introduction

The development of radar, radio-relay and space communications, television, radio navigation, industrial and domestic electronics, radio astronomy, radio spectroscopy, nuclear physics, medicine and many other branches of science and technology is inseparably involved with the extensive utilization of microwave frequencies (0.3-3000 GHz). Depending upon the wavelength of the electromagnetic oscillations, microwave frequencies are divided into the following bands: decimeter (0.3-3 GHz), centimeter (3-30 GHz), millimeter (30-300 GHz) and submillimeter (300-300 GHz) [19].

The decimeter and centimeter wavebands have been assimilated to the greatest degree, and are used extensively in practice. However, there has been increased recent interest in the utilization of millimeter waves in high-resolution radar systems, radio relay communications links, secure spacecraft communications systems, radio astronomy and radio spectroscopy. It has become possible to use the microwave band in these areas thanks to the creation and production of all of the necessary electronic devices which support the generation of oscillation, signal amplification and conversion, and receive-transmit circuit switching in this range [5].



APPROVED FOR RELEASE: 2007/02/09: CIA-RDP82-00850R000500020034-7

APPROVED FOR RELEASE: 2007/02/09: CIA-RDP82-00850R000500020034-7



In connection with the wide variety of functions handled, the varying requirements for technical specifications of devices and the limited working frequency range of each instrument, coverage of the entire microwave band has required a long list of electornic microwave devices. In addition, because of competition between manufacturers and individual directions in microwave electronics, many devices have been created for the same purpose which have parameter values and technical specifications which are close to one another.

In order to systematize examination of the status and analysis of the developmental trends of microwave devices, it is useful to divide the entire field into four groups of instruments which differ in the physical principles used:

--group I - vacuum-type microwave devices based on the phenomena of current transmission through a vacuum;
--group II - solid-state instruments and microwave devices based on utilizing the propties of semiconductor devices and ferrites;
--group III - plasma (gas-discharge) microwave devices based on utilizing the phenomena of current transmission through gases;
--group IV - hybrid microwave devices which combine several physical principles in a single device.

This system of classification reflects the most significant differences between devices, emphasizes specific design features and fabrication techniques, and does not contradict the existing traditional division of instruments into classes, forms and types.

I. Vacuum-type microwave devices represent the largest group, including devices using electrostatic (network) and electrodynamic control.

1. Electrostatically controlled devices include metal-ceramic triodes and tetrodes and devices with brake fields. These devices are used extensively in the microwave range thanks to the creation of special designs which reduce the harmful influence of electron flight time on the operation of the instruments [1, 26]. Regardless of the long history of existence and development of these devices, they continue to be improved in the areas of increased efficiency and operating reliability, increased output power, assimilation of the short-wave portion of the centimeter waveband, and in the area of creating sealed multifunctional modules.

2. Electrodynamically controlled devices include magnetron-type devices, traveling- and backward-wave tubes, klystrons, and cyclotron resonance masers (gyrotrons).

2.1. Magnetron-type devices include auto-oscillators and amplifiers which operate in hybrid electrical and magnetic fields.

Auto-oscillators include ordinary magnetrons, coaxial-cylinder magnetrons, inverted coaxial-cylinder magnetrons, magnetrons with electronic frequency tuning, magnetron-type backward-wave tubes and stabilizer diodes (platinotrons in self-



APPROVED FOR RELEASE: 2007/02/09: CIA-RDP82-00850R000500020034-7

APPROVED FOR RELEASE: 2007/02/09: CIA-RDP82-00850R000500020034-7



excited oscillation mode). These types of devices, in turn, are divided in terms of operating mode into pulsed and continuous, and in terms of power level into superhigh and high power, medium power and low power. Of these, the most widely used are ordinary magnetrons operating in either pulsed or continuous modes. In addition, in the past 10 years a great deal of attention has been devoted to the development of coaxial-cylinder magnetrons, which are being used increasingly instead of ordinary magnetrons.

Magnetron-type amplifiers include amplitrons (platinotrons in amplification mode), direct-wave electron injection devices (magnetron-type traveling-wave tubes, beamatrons) and backward-wave devices (magnetron-type backward-wave tubes), as well as forward-wave devices with open electron flux (dematrons). Magnetron amplifiers, like self-excited oscillators, are divided in terms of operating modes into pulsed and continuous, and in terms of power level into superhigh- and high-power, medium- and low-power.

2.2. O-type traveling-wave tubes (with longitudinal electrical and magnetic fields) also comprise a broad group of electrodynamically controlled vacuum-type microwave devices. This group includes amplifying traveling-wave tubes (TWT) with various output power levels and low-noise amplifier TWT. In terms of output power, amplifier TWTs are divided into super-high and high-power, medium-power and low-power. Super-high and high-power TWT are also divided into pulsed and continuous.

Considerable attention has recently been devoted to the creation of wideband and two-mode TWT, miniature TWT, including those using printed-circuit delay systems for phased antenna arrays and medium-power TWT for spacecraft.

2.3. O-type backward-wave tubes comprise a relatively small class of microwave devices. These devices are used as microwave oscillators with electronic frequency tuning in the range extending from decimeter to submillimeter waves exclusively in the continuous operating mode. In terms of power, these are divided into high-power and low-power backward-wave tubes.

2.4. Klystrons comprise a broad group of microwave devices, and are divided in terms of operating principle into drift-tube klystrons and reflex klystrons. Drift-tube klystrons include amplifying multi-resonator klystrons and oscillator klystrons with a small number of resonators. These devices have been developed for both pulsed and continuous operation. Multi-resonator amplifying klystrons are divided into super-high and high-power. Oscillator klystrons include two- and three-resonator klystrons, as well as distributed interaction klystrons. These klystrons are medium- and low-power devices. Reflex klystrons have been developed for utilization as low-power continuous-mode microwave oscillators.

2.5. Cyclotron resonance masers are a new developing class of microwave devices in which the operating principle is based on relativistic electron flux. Bunches of electrons are obtained in these devices by grouping of electrons, which is done by using the relativistic relationship between cyclotron frequency and electron energy. This principle has been used to create oscillators and amplifiers which



APPROVED FOR RELEASE: 2007/02/09: CIA-RDP82-00850R000500020034-7

APPROVED FOR RELEASE: 2007/02/09: CIA-RDP82-00850R000500020034-7



operate in hybrid electrical and magnetic fields with electrons spinning in a longitudinal magnetic field. In terms of operating mode, these are divided into pulsed and continuous.

2.6. Hybrid microwave devices now comprise a small but successfully developing class of vacuum-type microwave devices. These are based on using different classes of components in a unified construction. A typical example of this type of hybrid device is the twistron, which successfully combines multi-resonator klystrons and broadband TWT elements in a single device.

II. Solid-state devices and microwave devices represent a new broad group of microwave devices whose development has recently received a very great deal of attention. The heightened interest in these instruments and devices is due mainly to their major potential capabilities for sucessfully solving problems involved in the integrated miniaturization of radio electronic equipment.

This group includes active and passive instruments and microwave devices, as well as hybrid integrated microwave circuits.

1. Solid-state active instruments and microwave devices include oscillators and amplifiers using semi-conductor microwave diodes and transistors. These devices have the same function as low-power vacuum-type microwave devices, and have been developed to replace the latter.

1.1. Solid-state microwave oscillators are based on tunnel and transit-time avalanche diodes, Gunn diodes and field-effect and bipolar transistors. These oscillators provide both pulsed and continuous microwave oscillation, and are divided into low- and high-power. Further development of solid-state microwave oscillators involves their use as the basis for integrated devices including an oscillator, frequency control circuit, power supply, etc.

1.2. Solid-state microwave amplifiers are based on tunnel, varactor and transit-time avalanche diodes, Gunn diodes, bipolar and field-effect transistors. These are divided into low-noise amplifiers and power amplifiers. Solid-state microwave amplifiers, like oscillators, are often produced together with power supplies.

2. Passive microwave devices consist of various microwave elements which detect, convert and multiply frequency, change the phase of microwave oscillations, decouple and switch channels, and limit microwave output power. These devices include detectors and mixers, frequency multipliers and phase inverters, power switches and limiters, gates and circulators. They are based on the use of semiconductor microwave diodes (detector, mixer, tunnel, multiplier and switching) and ferrites. Passive microwave devices are used and produced as individual discrete devices, or as component parts of integrated microwave devices.

3. Hybrid integrated microwave circuits represent a new and rapidly developing class of microwave devices based on the use of microminiaturized active and passive solid-state microwave devices and microelectronic technology.



APPROVED FOR RELEASE: 2007/02/09: CIA-RDP82-00850R000500020034-7

APPROVED FOR RELEASE: 2007/02/09: CIA-RDP82-00850R000500020034-7



In addition to single-function oscillator, amplifier and other circuits, these devices also include integrated multifunctional circuits used in transmitting, receiving and transceiving sections of radioelectronic equipment, including phased antenna arrays.

III. Plasma (gas-discharge) microwave devices include both active and passive devices.

1. Passive gas-discharge microwave devices include gas-filled switching tubes which use gas-discharge under the influence of high-power microwave pulses to turn off the microwave section while the pulses are present. In terms of function, these are divided into preliminary spark-gap, spark-gap transmit-receive tubes and spark-gap anti-transmit-receive tubes [12].

2. Active plasma microwave devices have not been developed or studied thoroughly enough as yet. Individual experimental models of plasma microwave oscillators have recently appeared which differ from vacuum devices in that the electron beam passes through a plasma in which the electron density is higher than that of the beam. Since the maximum currents of the beams propagating in the plasma significantly exceed the maximum currents in vacuum devices, it becomes possible to achieve high output power.

IV. Hybrid microwave devices represent a new developing group of microwave devices. This group includes devices with various purposes, including vacuum-semiconductor amplifiers, hybrid spark-gap devices, indicating instruments, etc. [58, 59]. Vacuum-semiconductor microwave amplifiers are based on the interaction between an electron beam and a semiconductor target, while hybrid spark-gap devices represent a gas-filled switching tube together with a solid-state power limiter. These examples do not exhaust all of the possibilities of hybrid devices which may appear in the near future.

The above groups and classes of microwave devices are characterized by differing levels of development. Industrial production of vacuum-type and solid-state microwave devices has been mastered to the greatest degree. The data in the table below [not included -- Tr] provide evidence of the level of industrial production of these devices. The table does not include information on all groups and classes of devices. For example, there is no information about the sales volume of microwave triodes and tetrodes, which is difficult to isolate from the overall sales of electrostatically controlled devices. Neither is there any information about gas-discharge and hybrid microwave devices. As the table shows, the world market for microwave devices continues to increase. Vacuum-type devices hold the lead in the overall sales of microwave devices (70% in 1976 and 65% in 1980). The production and sales of high-power vacuum-type microwave instruments which have no solid-state competitors continue to increase.

In addition, the sales of O-type backward-wave tubes and reflex klystrons, which are gradually being replaced by solid-state microwave oscillators, are dropping off. Low-power and low-noise traveling-wave tubes are also being replaced successfully by solid-state amplifiers using semiconductor diodes and transistors. It



APPROVED FOR RELEASE: 2007/02/09: CIA-RDP82-00850R000500020034-7

APPROVED FOR RELEASE: 2007/02/09: CIA-RDP82-00850R000500020034-7



is also apparent from the table that the sales of solid-state microwave devices increased by a factor of 1.5 between 1976 and 1980, while the sales of vacuum-type devices increased by only a factor of 1.27.

The status and developmental trends of all basic groups and classes of microwave devices are examined in the present book on the basis of analyzing and generalizing the voluminous periodic domestic and foreign technical literature. Presented as illustrations are generalized data on the level of characteristics achieved for instruments, tables of the basic parameters of the best or typical industrial models, and figures which characterize the design and appearance of the microwave devices in question.

While not exhaustive, the author feels that the data presented can be used to achieve a sufficiently thorough presentation of the current level of development of electronic microwave devices. Because of its limited size, the book omits certain classes of instruments, including brake-field devices, cyclotron-resonance maser oscillators and amplifiers, masers, plasma devices, gas-filled switching tubes, semiconductor and ferrite passive devices, and acoustoelectronic devices: analysis of the status and developmental trends of these can be the subject of special work.

Table of Contents


| | Page |
|---|---|
| Foreword | 3 |
| Conventional notation | 5 |
| Introduction | 7 |
| Part 1. Microwave Vacuum Devices | |
| Chapter 1. Electrostatically controlled devices | 15 |
| 1.1. Triodes | 16 |
| 1.2. Tetrodes | 22 |
| 1.3. Triode and tetrode modules | 24 |
| Chapter 2. Magnetron-type devices | 26 |
| 2.1. Ordinary pulsed magnetrons | 25 |
| 2.2. Coaxial-cylinder magnetrons | 35 |
| 2.3. Continuous magnetrons | 41 |
| 2.4. Voltage-tunable magnetrons | 46 |
| 2.5. M-type backward-wave tubes | 51 |
| 2.6. Magnetron type amplifiers | 54 |
| Chapter 3. Traveling-wave tubes | 64 |
| 3.1. Pulsed TWT | 67 |
| 3.2. High-power continuous TWT | 76 |
| 3.3. Two-mode TWT | 80 |
| 3.4. Spacecraft TWT | 84 |




APPROVED FOR RELEASE: 2007/02/09: CIA-RDP82-00850R000500020034-7

APPROVED FOR RELEASE: 2007/02/09: CIA-RDP82-00850R000500020034-7



3.5. Mini-TWT 90
3.6. Printed-circuit TWT 94
3.7. Low-noise and low-power TWT 97
3.8. TWT modules 100

Chapter 4. Clystrons 102

4.1. Pulsed amplifier klystrons 107
4.2. Continuous amplifier klystrons 114
4.3. Oscillator klystrons 127
4.4. Reflex klystrons 132

Chapter 5. O-type backward-wave tubes 138

Chapter 6. Hybrid microwave devices 146

6.1. Twistrons 147
6.2. Electron-semiconductor devices 148
6.3. Hybrid spark-gap devices 152

Part 2. Solid-State Microwave Devices

Chapter 7. Semiconductor microwave diodes and transistors 155

7.1. Detector diodes 158
7.2. Mixer diodes 160
7.3. Tunnel diodes 164
7.4. Avalanche transit-time diodes 169
7.5. Gunn diodes 175
7.6. Microwave transistors 182
7.7. Microwave field-effect tetrodes 189

Chapter 8. Solid-state microwave oscillators 191

8.1. Oscillators using avalanche transit time diodes 195
8.2. Oscillators using Gunn diodes 203
8.3. Transistored oscillators 208

Chapter 9. Solid-state microwave amplifiers 213

9.1. Tunnel-diode amplifiers 217
9.2. Avalanche transit-time diode amplifiers 220
9.3. Gunn-diode amplifiers 224
9.4. Parametric amplifiers 229
9.5. Transistorized amplifiers 237

Conclusion 246

Bibliography 260

Subject index 268

COPYRIGHT: Izdatel'stvo "Radio i svyaz'", 1981

6900
CSO: 1860/64



APPROVED FOR RELEASE: 2007/02/09: CIA-RDP82-00850R000500020034-7

APPROVED FOR RELEASE: 2007/02/09: CIA-RDP82-00850R000500020034-7



UDC: 568.28

INDUSTRIAL TELEPHONE COMMUNICATION, ELECTRICAL SIGNALING AND INSTALLATION OF ELECTRIC CLOCKS

Moscow PROIZVODSTVENNAYA TELEFONNAYA SVYAZ', ELEKTRICHESKAYA SIGNALIZATSIYA I ELEKTROCHASOFIKATSIYA in Russian 1981 (signed to press 23 Dec 80) pp 2, 231-232

[Annotation and table of contents from book "Industrial Telephone Communication, Electrical Signaling and Installation of Electric Clocks" by Aleksandr Nikolayevich Volotskoy, Izdatel'stvo "Radio i svyaz'", 20,000 copies, 232 pages]

[Text]

Annotation

The principles of organizing industrial telephone communication--dispatcher, director, operational and public-address--are explained. Basic types of equipment used, their operating principle and operating features are described. Information is given about electrical signaling devices (security and fire), as well as the installation of electric clocks.

The book is intended for technical school students in the specialty "Automatic Electrical Communication".

[This book was reviewed by S. V. Koshelev and V. N. Nazarov.]

Table of Contents

Foreword 3

Chapter 1. Singularities of industrial communication 4

1.1. Modern industrial enterprises and methods for controlling them 4
1.2. Industrial communication and its importance in the production control process 6
1.3. Types of industrial communication, their singularities and areas of application 7



APPROVED FOR RELEASE: 2007/02/09: CIA-RDP82-00850R000500020034-7

APPROVED FOR RELEASE: 2007/02/09: CIA-RDP82-00850R000500020034-7



Chapter 2. Operational communication 8

2.1. Basic requirements for operational communication 8
2.2. Singularities of operational communication 9
General information 9
Singularities of public-address communication 10
Singularities of circular communication 19
2.3. Construction of operational telephone communication 25
2.4. Operational communication facilities 28
General information 28
Conversation devices 28
Amplifiers 30
Switches 30
Communication panels 39
Conversation documentation devices 40
Specialized automatic telephone exchanges 41

Chapter 3. Operational communication devices 41

3.1. Operational communication switches 41
General information 41
Type KD switches 43
"Kristall" type device 44
Type SOS-30M device 63
3.2. Mobile operational telephone communication equipment 71
Selective communication 71
Conference communication 79
[Railroad] switch communication switchboards 83
3.3. Type EDTS-66 operational power system communication equipment 87

Chapter 4. Public-address communication 90

4.1. Singularities and types of public-address communication 90
4.2. PGS circular and selective systems 94
PGS-71 equipment 94
"Radius" PGS equipment 100
4.3. RPS administrative-locator communication 101
4.4. Loudspeaker coverage of areas at production enterprises 104
4.5. Communication with mobile facilities 107

Chapter 5. Administrative-management telephone communication 116

5.1. Singularities of administrative-management telephone communication 116
5.2. Construction of administrative-management telephone communication network 119
5.3. Type UPATS-100/400 telephone exchanges 120
5.4. Automatic ATS K-100/2000 telephone exchanges 156
5.5. Automatic ATS K-50/200M telephone exchanges 163
5.6. Type UATS-49 automatic telephone exchanges 172



APPROVED FOR RELEASE: 2007/02/09: CIA-RDP82-00850R000500020034-7

APPROVED FOR RELEASE: 2007/02/09: CIA-RDP82-00850R000500020034-7



5.7. Quasi-electronic automatic telephone exchanges 184
5.8. Special-purpose telephone devices 187

Chapter 6. Electrical signaling 194

6.1. Purpose of electrical signaling 194
6.2. Types of electrical signaling and their basic requirements 195
6.3. Security alarms 196
6.4. Reception of signals from alarms 199
6.5. Type TOL-10/100 fire signaling installation 201

Chapter 7. Installation of electric clocks 214

7.1. Purpose of installation of electric clocks and concept of unified time system 214
7.2. Master electric clocks 215
7.3. Slave electric clocks 224
7.4. Electric clock installations and boards 225

List of abbreviations 228

Bibliography 230

COPYRIGHT: Izdatel'stvo "Radio i svyaz'", 1981

6900
CSO: 1860/40



APPROVED FOR RELEASE: 2007/02/09: CIA-RDP82-00850R000500020034-7

APPROVED FOR RELEASE: 2007/02/09: CIA-RDP82-00850R000500020034-7



UDC 621.311:681.586

MEASUREMENT ELEMENTS IN POWER SYSTEM EMERGENCY AUTOMATIC EQUIPMENT

Moscow IZMERITEL'NYYE ORGANY PROTIVOAVARIYNOY AVTOMATIKI ENERGOSISTEM in Russian 1981 (signed to press 24 Mar 81) pp 2-4, 158-159

[Annotation, foreword and table of contents from book "Measurement Elements in Power System Emergency Automatic Equipment", by Feliks Mikhaylovich Rozenblyum, Energoizdat, 9000 copies, 160 pages]

[Text]

## Annotation

This book examines new principles for making transducers for active power, frequency, phase difference, rate of frequency variation and slip ratio. The design of active power relays, relays for phase angle, frequency, derivatives of these quantities, as well as combination relays which respond simultaneously to the absolute values of quantities and their derivatives are given. The circuits used in panels containing automatic equipment measurement elements are examined, as are questions of improving operating reliability of the equipment and utilizing continuous and periodic testing devices.

The book is intended for engineers involved in designing and operating power system emergency automation equipment, and also may be useful for graduate students in the corresponding specialties.

## Foreword

The automated dispatcher control and emergency automatic equipment system play a major role in solving problems of the development of inter-system connections which support reliable, stable operation of the power systems in the USSR Unified Power System. The basic devices in the emergency automation system are measurement elements, the accuracy and reliability of which determine the high operating efficiency of the entire emergency automation system. Meeting the requirements of high precision of automation measuring elements makes it possible to utilize the throughput capacity of power transmission lines fully. A great deal of work has been devoted to analyzing the operation of emergency automation devices, requirements for measurement elements and problems of analyzing actuation parameters. However, previously published work fails to encompass a large number of high-precision measurement elements which have developed in recent years.



APPROVED FOR RELEASE: 2007/02/09: CIA-RDP82-00850R000500020034-7

APPROVED FOR RELEASE: 2007/02/09: CIA-RDP82-00850R000500020034-7



In the present book the author attempted, in a systematic fashion, to examine various principles of executing measurement elements for recording the values and rate of change of active power, frequency, and phase difference of voltages in different parts of a power system, as well as their slip ratio. The appearance of a new component base - integrated microcircuits - has made it possible to create reliable measurement elements using digital and digital-analog principles which provide high accuracy in measuring the mode parameters of the power system being monitored.

The book examines problems of increasing the reliability of measurement elements using devices for continuous and periodic testing, and describes a number of devices intended for adjusting the actuation parameters of elements which measure rate of frequency change.

The methodology given for adjusting the required actuation parameters of various combined measuring elements and of elements which react to a single power system mode parameter is needed for correct design and operation of these devices in power systems. A systematized exposition of these questions, with application to devices used in power system emergency automation equipment, is given first.

The author is grateful to high co-workers at the VNIIR [expansion unknown] who worked with him in developing and testing a number of measurement elements built on the basis of new principles. The author is also deeply grateful to B.I. Iof'yev for his helpful advice and remarks made while editing the manuscript, and to G.L. Brukhis for his extensive editing work.

Table of Contents

Foreword 3

Chapter 1. Active-Power Measurement Elements 5

1. Basic types and function of active-power measurement elements 5
2. Principles of implementing active-power relays 6
3. Comparative analysis of principles of implementing power transducers 9
4. Analysis of square-law generator power transducer circuits 14
5. Accounting for influence of transient processes on operation of power transducers with filters 23
6. Analysis of influence of saturation of intermediate current transformer during short-circuiting on output signal of power transducer 33
7. Measurement elements of current and previous active power 37
8. Principles of implementing elements for measuring discharge (surge) and rate of variation of active power 39
9. Analysis of dynamic characteristics of elements for measuring power discharge 52
10. Recommendations for adjustment of characteristics of elements for measuring power discharge 59



APPROVED FOR RELEASE: 2007/02/09: CIA-RDP82-00850R000500020034-7

APPROVED FOR RELEASE: 2007/02/09: CIA-RDP82-00850R000500020034-7



Chapter 2. Frequency and Rate-of-Change Measurement Elements 61

11. Function of elements which record frequency variation 61
12. Principles of implementing frequency elements 62
13. Principles of implementing frequency rate-of-change elements 86
14. Combined frequency and rate-of-change elements 89
15. Digital frequency transducer 94
16. Rate-of-frequency-change sensor 101
17. Principles of implementing test devices for assigning rate of frequency change 108

Chapter 3. Elements for Measuring Phase Difference and Slip Ratio 118

18. Function of phase difference and slip measurement elements 118
19. Modeling voltage vector of opposite end of power transmission line 119
20. Principles of implementing phase difference sensors 127
21. Measurement elements for slip 140
22. Combined phase difference and slip measurement elements 143
23. Panel of phase difference and slip measurement elements 147

Bibliography 155

COPYRIGHT: Energoizdat, 1981

6900
CSO: 1860/106



APPROVED FOR RELEASE: 2007/02/09: CIA-RDP82-00850R000500020034-7

APPROVED FOR RELEASE: 2007/02/09: CIA-RDP82-00850R000500020034-7



UDC 621.315.1.027.8.001.2

MECHANICAL SECTION DESIGN FOR OVERHEAD SUPERHIGH VOLTAGE LINES

Moscow PROYEKTIROVANIYE MEKHANICHESKOY CHASTI VOZDUSHNYKH LINIY SVERKHVYSOKOGO NAPRYAZHENIYE in Russian 1981 (signed to press 26 Mar 81) pp 2-4, 335-336

[Annotation, foreword and table of contents from book "Mechanical Design Section for Overhead Superhigh Voltage Lines", by Abram Simkhovich Zelichenko and Boris Ivanovich Smirnov, Energoizdat, 5000 copies, 336 pages]

[Text]

## Annotation

Singularities of designing overhead superhigh voltage power transmission lines are examined. Practical methods are given for solving problems involving the selection and justification of all elements of overhead lines, as well as methods for estimating their operating reliability. Technical-economic efficiency indicators are given for superhigh voltage line structures. This book has been prepared by leading specialists of Energoset'proyekt [All-Union State Planning, Surveying and Scientific Research Institute of Power Systems and Electric Power Networks], who have many years of experience in planning and operating power transmission lines.

The book is intended for engineers and technicians involved in planning, installing and operating power transmission lines.

[This book was reviewed by G. A. Illarionov.]

## Foreword

The present development of electrical power engineering is characterized by an increase of up to 46 million kW and more in thermo-electric, hydraulic and nuclear power plants. Work continues on the creation of the USSR Unified Power System. Work is simultaneously underway on the creation of the International Combined Power System, which includes power organizations in the USSR and in the European member countries of the CEMA.

The expanded construction of superhigh voltage lines of 330 kW and greater is playing the main role in creating combined power systems.



APPROVED FOR RELEASE: 2007/02/09: CIA-RDP82-00850R000500020034-7

APPROVED FOR RELEASE: 2007/02/09: CIA-RDP82-00850R000500020034-7



The world's first 500 kV ac transmission line (1959) and 800 (± 400) kV dc transmission line (1962) were constructed and put into operation in the USSR. The USSR has now accumulated a great deal of experience in planning, constructing and operating 330-750 kV power transmission lines; the planning and construction is underway for the first 1150 kV ac Siberia-Kazakhstan-Ural and 1500 kV dc Ekibastuz-Center lines.

Major achievements have been reached in the USSR in the area of creating long-distance superhigh voltage transmission as a result of the joint work of leading scientific-research, planning, construction and operating organizations. On the basis of extensive theoretical and experimental research, planning and design developments, as well as experience in constructing, adjusting and operation, these organizations have solved all of the basic problems involved in creating superhigh voltage power transmission lines.

The purpose of the present book is to acquaint the reader with the main problems of planning overhead superhigh voltage power transmission lines. The second edition of M. A. Mel'nikov, S. S. Rokotyan and A. N. Sheremtsis' book Proyektirovaniye Elektricheskoy Chasti Vozdushnykh Liniy Elektroperedachi 330-500 kV (Planning of Electrical Part of 330-500 kV Overhead Power Transmission Lines), which presents problems of electrical calculations for superhigh voltage lines, was published in 1974. In the present book, the authors have made the first attempt to systematize problems of planning primarily the mechanical part of superhigh voltage lines. Electrical parameters are considered only to the extent needed to provide a foundation and understanding of the design approaches used for individual line elements.

A special place in the book is devoted to the influence of overhead superhigh voltage lines on the environment and to original designs of individual elements of superhigh voltage lines.

The authors have attempted to omit all questions of designing the mechanical part of overhead lines which are not specific to superhigh voltage lines, and have made only the necessary references to unavailable publications.

The authors are deeply grateful to reviewer Candidate of Technical Sciences G. A. Illarionov for his valuable advice and remarks which were taken into consideration in the manuscript.

Table of Contents

Foreword 3

Chapter 1. Development of superhigh voltage lines 5

1.1. General information 5
1.2. Experimental bases 11

Chapter 2. General requirements and norms for planning 17

2.1. General normative positions 17



APPROVED FOR RELEASE: 2007/02/09: CIA-RDP82-00850R000500020034-7

APPROVED FOR RELEASE: 2007/02/09: CIA-RDP82-00850R000500020034-7



2.2. Superhigh voltage overhead lines passing through populated and unpopulated areas 18
2.3. Intersections and convergence with power transmission lines 23
2.4. Intersections and convergence with railroads 26
2.5. Intersections and convergence with highways 28
2.6. Lines laid along dikes and dams 30
2.7. Intersections and convergence with pipelines and tramways 30
2.8. Normative requirements for individual elements of superhigh voltage lines 33
2.9. Order of planning 34

Chapter 3. Path selection and determination of climatic conditions 37

3.1. Path selection 37
3.2. Climatic conditions 41

Chapter 4. Selection of construction of split phase and ground-wire cables 52

4.1. Selection of split-phase versions and methods of technical-economic comparison of versions 52
4.2. Singularities of selection of pole construction versions for dc lines 75
4.3. Problems of selecting rational design of conductors and mechanical design of split-phase conductors 78
4.4. Span fastening of split-phase conductors, distance bars and their construction 80
4.5. Choice of type and cross-section of ground-wire cables 85
4.6. Features of choosing type and construction of conductors and large connector adapters 92
4.7. Dyammics of conductors and cables 93

Chapter 5. Choice of insulator string and cable fasteners 104

5.1. Selection of insulator type and construction 104
5.2. Justification of choice of support clamp type 118
5.3. Configuration and construction of support and tension insulator strings 121
5.4. Construction of cable fasteners and insulator inserts in spans for joining cables 144
5.5. Protective intervals on supporting and tension insulator strings and on insulated cable fastenings 148

Chapter 6. Determination of external loads on supports and support dimensions 150

6.1. Calculation conditions for various types of supports 150
6.2. Technical-economic calculations for selecting economical height and construction of supports 153
6.3. Determining wind and ice load on conductors, cables and support elements 157



APPROVED FOR RELEASE: 2007/02/09: CIA-RDP82-00850R000500020034-7

APPROVED FOR RELEASE: 2007/02/09: CIA-RDP82-00850R000500020034-7



6.4. Deviations of conductors, cables and insulator strings for calculating support dimensions 170
6.5. Loop bypass schemes on anchor and transposition supports 179

Chapter 7. Support and foundation constructions 191

7.1. Types of supports and foundations used for superhigh voltage overhead lines and their singularities 191
7.2. Construction of long-span supports and their foundations 207
7.3. Area of application of various types of supports (free-standing, guyed) 211

Chapter 8. Lightning protection and ground devices 214

8.1. Lightning overvoltage protection devices. Optimal angles of cable lightning protection angles 214
8.2. Cable gounding schemes and selection of spark gaps 222
8.3. Constructions and selection of support grounding 233

Chapter 9. Some problems of power transmission line operating reliability 249

9.1. Problem of superhigh voltage overhead line reliability 249
9.2. Generalization of operating experience 251
9.3. Line operating reliability under ice and wind loads 260
9.4. Line strength under longitudinal loads 263
9.5. Estimation of line reliability 274

Chapter 10. Influence on environment 279

10.1. General assumptions 279
10.2. Land allocation 280
10.3. Aesthetic effect of lines 283
10.4. Effect of electrical field 291
10.5. Acoustic noise and radio interference 310
10.6. Elimination of ozone and nitrous oxides 316

Chapter 11. Technical-economic indicators 316

11.1. Basic specific indicators 316
11.2. Consumption of materials and equipment 321
11.3. Construction cost 327

References 332

COPYRIGHT: Energoizdat, 1981

6900
CSO: 1860/44



APPROVED FOR RELEASE: 2007/02/09: CIA-RDP82-00850R000500020034-7

APPROVED FOR RELEASE: 2007/02/09: CIA-RDP82-00850R000500020034-7



UDC 621.396.001.4/.57

MODELING AND TESTING OF RADIO EQUIPMENT

Leningrad MODELIROVANIYE I ISPYTANIYA RADIOOBORUDOVANIYA in Russian 1981 (signed to press 5 Feb 81) pp 2, 5-6, 303-304

[Annotation, foreword and table of contents from book "Modeling and Testing of Radio Equipment" by Pavel Pavlovich Beskid, Yevgeniy Mikhaylovich Vinogradov, Viktor Ivanovich Vinokurov, Yevgeniy Germanovich Pashchenko, Aleksandr Valdimirovich Smol'yaninov and Igor' Pavlovich Kharchenko, Izdatel'stvo "Sudostroyeniye", 1900 copies, 304 pages]

[Text] Annotation

This book touches upon a broad group of problems involving the modeling and testing of radio electronic systems at various stages of their development and operation. General principles are explained for the construction of models and their application to problems of estimating the effective scattering area of complex targets, antenna directivity patterns, complex-structure fields within the area of a ship or other object, the electromagnetic compatibility of various systems (radar, communication, etc.) and the construction of simulators and trainers. Methods are considered for experiment planning during modeling and full-scale trials, as well as the methodology for processing the findings. One chapter is devoted to the automation of computer modeling.

The book is of interest for specialists involved with developing, producing and operating radioelectronic systems of various types, as well as technical school students specializing in the area of radio electronics.

[This book was reviewed by Doctor of Technical Sciences G. I. Novikov and Candidate of Technical Sciences Ye. A. Shtager. The scientific editor was Doctor of Technical Sciences V. I. Vinokurov.]

Simulation has been used for many years in engineering practice during the development of systems and devices. Successes in cybernetics and computer technology have led to significant achievements in the area of simulation, as a result of which it has become one of the main methods used in investigating complex processes and systems.



APPROVED FOR RELEASE: 2007/02/09: CIA-RDP82-00850R000500020034-7

APPROVED FOR RELEASE: 2007/02/09: CIA-RDP82-00850R000500020034-7



The present book covers problems of the application of simulation (mathematical and physical) in creating various types of radioelectronic systems and the radioelectronic equipment used with complex objects (ships, aircraft, etc.).

Research on the following is of the greatest interest for this category of problems:

--processes occurring in devices and systems;

--the operation of a group of systems for the purpose of ensuring their coordinated functioning (integration) and electromagnetic compatibility;

--the influence of propagation paths, scattering singularities and wave radiation on system characteristics;

--the influence of the environment (including superstructures and construction components of the carrier) on the characteristics of equipment and systems operating in various wavebands;

--determination of the intensity and distortions of the field created in the vicinity of the platform (ship, aircraft) by various types of radio technical fccilities;

--reliability and efficiency characteristics;

--methods of planning tests which provide needed information about the object under investigation.

Most of these questions are considered in the present book.

This book does not touch upon such important problems as system simulation, reliability and efficiency analysis and certain others. In the author's opinion, these have been treated sufficiently in the literature. There are also certain aspects which are of a controversial nature.

The book is intended for a broad group of engineering-technical and scientific workers involved in developing, producing and operating various types of radioelectronic systems, as well as graduate students.

Participants in the preparation of this book included Candidate of Technical Sciences Yu. A. Gustov (section 6.5), V. N. Chekin (section 2.3) and G. I. Semenov (section 5.4). Chapter 3 makes use of work carried out by Ye. G. Pashchenko in conjunction with V. V. Dobryanskiy and V. P. Kozlovskiy.

Table of Contents

List of abbreviations and notation 3

Foreword 5



APPROVED FOR RELEASE: 2007/02/09: CIA-RDP82-00850R000500020034-7

APPROVED FOR RELEASE: 2007/02/09: CIA-RDP82-00850R000500020034-7



Chapter 1. Principles of model construction 7

1.1. Methods and singularities of simulation 7
1.2. Stages of construction and implementation of model 9
1.3. Elements of the theory of dimensionality and similarity 16
1.4. Physical simulation 25
1.5. Features of mathematical modeling 29

Chapter 2. Simulation of high frequency fields 54

2.1. Tasks and features of simulation 54
2.2. Mathematical computer modeling of effective scattering area pattern of complex bodies 63
2.3. Simulation of directivity characteristics of radiator array using analog computer 82
2.4. Optical modeling of high-frequency fields 86

Chapter 3. Simulation of low-frequency electromagnetic fields and fields with complex structure 102

3.1. Tasks and features of simulation 102
3.2. Method for simulating field on ground 106
3.3. Simulating reradiation from metal structures in local electromagnetic field 116
3.4. Construction of benches for simulating low-frequency fields and fields with complex structure 126
3.5. Investigating characteristics of radioelectronic devices in field of local structure 132

Chapter 4. Models of combined operation of a group of radioelectronic devices 142

4.1. Tasks and features of simulation 142
4.2. Physical modeling of electromagnetic compatibility 144
4.3. Mathematical modeling 148

Chapter 5. Computer automation of mathematical modeling 158

5.1. Tasks and means of automation using digital computers 158
5.2. Methods for automatic digital computer model construction 168
5.3. System for automating simulation of radio circuits in order to investigate noise tolerance and electromagnetic compatibility 174
5.4. TRAKT--source language of simulation system 187

Chapter 6. Simulators and trainers 197

6.1. Principles of constructing simulators and training equipment 197
6.2. Simulators of radar echos from objects at sea 199



APPROVED FOR RELEASE: 2007/02/09: CIA-RDP82-00850R000500020034-7

APPROVED FOR RELEASE: 2007/02/09: CIA-RDP82-00850R000500020034-7



6.3. Simulators of echo signals from ocean surface and shore 207
6.4. Analog-digital modules in simulators and trainers 212
6.5. Construction principles of spin-echo simulators 216
6.6. Application of echo signal trainers and simulators 226

Chapter 7. Experimental design in simulation and testing stages 229

7.1. Classification of tests and their organization 229
7.2. Models of extremal experiments 239
7.3. Clarification of mathematical model using test results 254
7.4. Special types of experimental design 260

Chapter 8. Processing testing and simulation results 266

8.1. Tasks and stages of processing 266
8.2. Estimation of parameters 273
8.3. Hypothesis verification 278
8.4. Construction and analysis of empirical models 284
8.5. Discovery of regular components 293

Bibliography 299

COPYRIGHT: Izdatel'stvo "Sudostroyeniye", 1981

6900
CSO: 1860/47



APPROVED FOR RELEASE: 2007/02/09: CIA-RDP82-00850R000500020034-7

APPROVED FOR RELEASE: 2007/02/09: CIA-RDP82-00850R000500020034-7



UDC 62.52:621.397.621

MODERN METHODS AND DEVICES FOR DATA DISPLAY

Moscow SOVREMENNYYE METODY I USTROYSTVA OTOBRAZHENIYA INFORMATSII in Russian
1981 (signed to press 23 Apr 81) pp 2-4, 214-216

[Annotation, foreword and table of contents from book "Modern Methods and Devices for Data Display", edited by M. I. Krivosheyev and A. Ya. Breytbart, Izdatel'stvo "Radio i svyaz'", 20,000 copies, 216 pages]

[Text]

## Annotation

The design fundamentals and construction methods of modern data display systems are given. The construction features of displays and display systems, as well as achievements in the development of the hardware base and of devices for information display systems are presented. The use of data display facilities in the national economy is examined.

The book is intended for specialists involved in developing, engineering and operating modern data display facilities; it may also be useful for automatic control system design specialists and graduate students in corresponding specialties.

[This book was reviewed by A. Ya. Breytbart.]

## Foreword

The appearance of more sophisticated electronic computers makes it possible to apply automated control systems (ACS) in widely varying areas of science, technology and the national economy, for example, in radar, in controlling space flights, in rail and air transport, nuclear power plants, aviation training equipment, in centralized control of industrial enterprises, in the surface and submarine fleet, in centralized goods delivery and warehouse accounting systems, in telephone and telegraph communication systems, in medicine, and in systems for modeling and processing scientific-research findings.

Data display facilities (DDF), which act as the communication link in man-machine systems, form one of the basic branches of automated control systems.



APPROVED FOR RELEASE: 2007/02/09: CIA-RDP82-00850R000500020034-7

APPROVED FOR RELEASE: 2007/02/09: CIA-RDP82-00850R000500020034-7



The DDF used in early automated control systems were cathode-ray television tubes. However, the increasingly complex requirements set for automated control systems, and particularly for display facilities, have required the development of other effective means for solving this problem.

The development of microelectronics has made it possible to develop such discrete display devices as electroluminescent and liquid crystal matrix indicators, gas-discharge displays, and various projection devices having the required parameters. The present book describes display devices which are now in use. A great deal of attention is devoted to the principles and methods by which they are designed and constructed, as well as their application.

The book is divided into six chapters.

Chapter 1 examines the fundamentals and problems of designing DDF, methods for calculating the characteristics of readout devices and methods for optimizing the selection of DDF type and parameters.

Chapter 2 is devoted to methods and principles of designing DDF, as well as questions of improving their efficiency and reliability.

Chapter 3 describes displays and display systems. Particular attention is devoted to color display systems.

Chapter 4 contains a description of DDF components and devices, including cathode-ray devices, character synthesizing displays, gas-discharge displays, liquid-crystal displays, and various types of electroluminescent indicators.

Chapter 5 describes special-purpose television devices for displaying information. Methods of constructing graphic and three-dimensional images are examined.

Chapter 6 is devoted to the application of methods and devices for displaying information in the national economy, including use in automated dispatcher control systems, in the monitoring the diagnostic systems of communication equipment, in telephony and telegraphy. A brief description of television video games is given.

This book was written by a broad group of specialists involved in DDF development. It is intended for engineering and technical workers involved in developing, designing and operating modern data display facilities, and may also be useful for specialists involved in automated control system planning as well as graduate students in corresponding specialties.

The book chapters were edited as follows: chapters 1 and 2 by I. I. Litvak and V. K. Samsonov; chapter 3 by N. A. Oshchepkov and I. Ye. Soloveychik; chapter 4 by I. I. Litvik; chapter 5 by I. N. Gulin; and chapter 6 by A. Ya. Breytbart. Overall editing of the book was done by M. I. Krivosheyev and A. Ya. Breytbart.



APPROVED FOR RELEASE: 2007/02/09: CIA-RDP82-00850R000500020034-7

APPROVED FOR RELEASE: 2007/02/09: CIA-RDP82-00850R000500020034-7



Table of Contents

Foreword 3

Chapter 1. Design fundamentals of modern data display systems

Litvak, I. I.
1.1. Problems of development of general method for designing data display systems 5

Lazarev, Ye. M., Pokrovskaya, M. Ye.
1.2. Method for calculating characteristics of readout devices during design and evaluation of data display apparatus 12

Gavrich, A. V.
1.3. Allowance for relationship between characteristics of data display facilities during their classification and evaluation 16

Litvak, I. I., Pokrovskaya, M. Ye.
1.4. Method for optimizing selection of type and parameters of data display systems 18

Chapter 2. Methods and principles of constructing data display systems

Ageykin, D. I., Knopov, Yu. T. [deceased], Yemal'yanov, V. S.
2.1. Operator data display in sporadic monitoring systems 23

Smolyarov, A. M.
2.2. Effectiveness of matrix readout 28

Litvak, I. I., Severinovskiy, N. S.
2.3. Toward the possibility of improving flexibility of character-synthesis display apparatus 31

Ivanov, Ye. L., Litvak, I. I., Melikov, G. G., Surkov, A. V.
2.4. Analysis of data conversion in dynamically controlled display devices 35

Melikov, G. G.
2.5. Influence of input data stream on regeneration in display device 42

Gustyakov, M. D., Lazarev, Ye. M., Molotova, A. Yu.
2.6. Possibilities for improving efficiency of utilization of digital character-synthesis indicators 45

Smolyarov, A. M., Shesterkin, A. N.
2.7. Methods for improving reliability of data reproduction on gas-discharge displays 48



APPROVED FOR RELEASE: 2007/02/09: CIA-RDP82-00850R000500020034-7

APPROVED FOR RELEASE: 2007/02/09: CIA-RDP82-00850R000500020034-7



Chapter 3. Displays and display systems

Grishin, V. G., Starodubtsev, V. F.
3.1. Multi-gradation readout of large data files on color relief display 51

Valikhmetov, B. A., Nikolayev, Yu. N., Pilipchatin, Ye. N., Postevka, D. P.
3.2. Color graphics terminal 55

Repinskiy, A. M., Soloveychik, I. Ye.
3.3. CRT-based graphics display with color coding of data 60

Gurvich, G. A., Lenchuk, V. S., Pogrebinskiy, S. B.
3.4. Control of peripheral equipment systems in color-coded display systems 64

Todoroy, D. N., Peretyatkov, S. M.
3.5. Color-coded graphics display software 67

Artamonov, A. G., Bolotnikov, V. N., D'yachkova, G. P., Churakova, V. G.
3.6. Microprocessor applications in display systems 70

Gurvich, G. A., Lenchuk, V. S., Pogrebinskiy, S. B.
3.7. Data documentation in color-coded display systems 72

Maydel'man, I. N., Mironov, V. A., Oshchepkov, N. A., Revenko, A. N.
3.8. Toward the problem of creating intelligent displays 77

Chapter 4. Elements and devices in data display systems

Vinevich, S. V. [deceased]
4.1. Cathode-ray devices for data display and their prospects for development 82

Gorfinkel', B. I., Abalduyev, B. V., Korovkin, A. I., Medvedev, R. S., Mikhaylov, A. N.
4.2. Character-synthesizing indicators based on low-voltage cathode luminescence effect 89

Barenboym, A. M., Molotova, A. Yu.
4.3. Alternating-current gas-discharge display with planar electrode positioning 98

Voroncheva, V. R., Gel'shteyn, M. I.
4.4. Digital gas-discharge display with low-voltage grid control 100

Murtazina, N. V., Petrenko, Z. G., Sukhenko, Ye. P.
4.5. Liquid-crystal light modulators and color-beam polarization modulators 104



APPROVED FOR RELEASE: 2007/02/09: CIA-RDP82-00850R000500020034-7

APPROVED FOR RELEASE: 2007/02/09: CIA-RDP82-00850R000500020034-7



Bobylev, Yu. P., Peterimov, S. V., Shoshin, V. M.
4.6. Multiplexed control of liquid crystal displays 109

Avetisova, M. G., Lyamichev, I. Ya.
4.7. Electroluminescent mimic panels and areas of application 117

Antipov, B. L., Kul'kov, V. P., Markov, P. A., Savel'yev, G. A.
4.8. Matrix-controlled dot-matrix electroluminescent storage screen 121

Ivanov, Ye. L., Il'inskiy, V. I., Melikov, G. G., Nefedov, B. M.
4.9. Modules for constructing common-user electroluminescent character displays 124

Ovchinnikov, V. I.
4.10. Capability of automating design and fabrication of electroluminescent mimic panels 126

Avramenko, F. F., Inozemtseva, Yu. I., Lazarev, Ye. M., Lyubarskaya, M. G.
4.11. High-contrast electroluminescent indicators in data display devices 128

Il'inskiy, V. I., Ovchinnikov, V. I., Shvartsberg, V. R., Shipilova, N. Ya., Shuvalov, N. N.
4.12. Microassembly-type control circuit for electroluminescent indicators 130

Shvartsberg, V. R.
4.13. Vacuum-luminescent, light-diode and gas-discharge indicator micro-assemblies for data display devices 133

Morozov, B. S., Pribytkov, V. Ya.
4.14. Device for measuring operating parameters of character-synthesis indicators 136

Bogdanov, B. A., Boguslavskiy, R. Ye., Severinovskiy, N. S.
4.15. 5760-element electroluminescent dot-matrix screen 138

Chapter 5. Television methods and devices for data display

Guglin, I. N.
5.1. Television-screen data display 141

Konov, K. I., Vasileva, Ts. Ts. (Bulgaria)
5.2. Use of read-only memory in television character generators 144

Yegorova, S. D., Zapalatovskiy, A. V., Kolesnik, V. A., Sidorov, V. I.
5.3. Fragment coding method in automating graphic image input to TV displays 147



APPROVED FOR RELEASE: 2007/02/09: CIA-RDP82-00850R000500020034-7

APPROVED FOR RELEASE: 2007/02/09: CIA-RDP82-00850R000500020034-7



Kosnikov, Yu. N., Sergeyev, N. P.
5.4. Application of binary multiplier in basic image formation devices 149

Avgustov, Ye. F.
5.5. Formation of image of three-dimensional object on TV screen illuminating invisible lines 155

Ul'yanov, V. N.
5.6. Formation of characters on TV screen using Walsh functions 158

Chapter 6. Application of data display methods and devices in the national economy

Gribanov, L. M., Razin, A. I., Samsonov, V. K.
6.1. Color television data display system 162

Gribanov, L. M., Makiyevskiy, V. A., Khodak, V. A.
6.2. Television data display system for transmitting graphic and printed materials 166

Guglin, I. N., Mayzul's, R. A.
6.3. Special-purpose data display devices 171

Ovlasyuk, I. Ya.
6.4. Television-type display equipment for load-dispatching centers 177

Gol'dbaum, I. Ya., Loginov, V. A., Samokish, M. A.
6.5. Utilization of TV displays in automatic channel switching systems 183

Filimonov, A. A., Shlyapoberskiy, V. I.
6.6. Use of "AGAT-2000M" display in communication equipment monitoring and diagnostic system 187

Zhuravlev, V. A., Shcherbakov, V. G.
6.7. Features of application of display facilities in data systems based on "AGAT-2000" display system 190

Vasil'yev, S. N., Soloveychik, I. Ye., Churakova, V. G.
6.8. Utilization of liquid-crystal indicators in telephony 194

Gavrish, A. V., Sevumyan, Yu. R.
6.9. "Rubin" display modules and their industrial application 197



APPROVED FOR RELEASE: 2007/02/09: CIA-RDP82-00850R000500020034-7

APPROVED FOR RELEASE: 2007/02/09: CIA-RDP82-00850R000500020034-7



Volotnikov, V. N., Kenigfest, L. A., Repinskiy, A. M., Yarmarkin, K. K.
6.10. Display-type telegraph terminal 199

Guglin, I. N.
6.11. Features of data display in television video games 202

List of abbreviations 207

Bibliography 208

COPYRIGHT: Izdatel'stvo "Radio i svyaz'", 1981

6900
CSO: 1860/56



APPROVED FOR RELEASE: 2007/02/09: CIA-RDP82-00850R000500020034-7

APPROVED FOR RELEASE: 2007/02/09: CIA-RDP82-00850R000500020034-7



UDC 621.374

PULSE RADAR CIRCUITS

Moscow IMPUL'SNYYE SKHEMY RLS in Russian 1981 (signed to press 26 Mar 81)
pp 2-3, 222-223

[Annotation, foreword and table of contents from book "Pulsed Radar Circuits", by Vladilen Grigor'yevich Grigor'yants, Voyenizdat, 17,000 copies, 224 pages]

[Text]

## Annotation

This book examines the physical processes in pulse circuits of modern radards, and describes the properties and characteristic features of widely used circuits and the action of basic adjustments. A special chapter is devoted to modular microcircuits.

The book is intended for engineering and technical staffs which operate radars, students and auditors at military academies, as well as a wide group of readers interested in problems of pulsed technology.

## Foreword

The present book is intended for engineering and technical personnel exploiting radar equipment. The purpose of the book is to help the reader who is familiar with the fundamentals of radio technology and radar to clarify the design and functioning principles of pulse radar devices, thus preparing him for independent reading (analysis) of the schematic diagrams of such devices. The latter is necessary for high quality preventive maintenance, and rapid detection and repair of malfunctions. The main attention in the book is devoted to examining physical processes in typical pulse circuits which are widely used in operational radar equipment, the characteristic features and properties of such circuits, the different versions which are in practical use, and the influence of basic parameters and adjustments. Modern trends in the construction of pulse devices were taken into consideration in preparing the material. Because the schematic diagrams used in existing radars were generally executed according to earlier GOSTs, the author considered it advisable to use some of the same graphic notations in the diagrams and alphanumeric designations for elements as were used in the first



APPROVED FOR RELEASE: 2007/02/09: CIA-RDP82-00850R000500020034-7

APPROVED FOR RELEASE: 2007/02/09: CIA-RDP82-00850R000500020034-7



edition of the book. The new graphic designations used in the diagrams are given in GOST 2.730-73, 2.755-74, etc., and the alphanumeric designations can be found in GOST 2.710-75.

Some of the material was written by A. V. Kuznetsov (§3, Chapter II; §5, 6, Chapter III; Chapter IV; §3, Chapter IV) and I. Ye. Golubev (Chapter VII).

Table of Contents


| | |
|---|---|
| Foreword | 3 |
| Chapter 1. Simple shaping circuits | 4 |
| §1. Basic types of RC and RL circuits | - |
| 1. Effect of square pulse on RC circuit. Basic types of RC circuits | - |
| 2. Effects of square pulse on RL circuit. Basic types of RL circuits | 7 |
| §2. Practical application of integrating RC circuits | 8 |
| 1. Obtaining linearly varying voltage | - |
| 2. Stretching pulse edges | 9 |
| 3. Obtaining time delay | 11 |
| 4. Converting pulse width modulation to pulse amplitude modulation | 14 |
| 5. Smoothing filters. Extraction of constant component | - |
| 6. Integrating-differentiating filter | 17 |
| 7. Influence of parasitic parameters | 18 |
| §3. Practical application of differentiating RC circuits | 19 |
| 1. Shortening (sharpening) of pulses | - |
| 2. Influence of parasitic parameters | 20 |
| 3. High frequency correction of voltage divider | 22 |
| §4. RC crossover circuits | 24 |
| 1. Pulse transmission through RC crossover circuit | - |
| 2. Level hold circuits. Recovery of constant component | 29 |
| §5. Shock-excitation tuned circuit | 32 |
| §6. Frequency correction elements in pulse amplifiers | 37 |
| Chapter 2. Pulse limiters | 46 |
| §1. Diode limiters | - |
| 1. General information about limiters | - |
| 2. Serial diode limiters | 47 |
| 3. Parallel diode limiters | 50 |
| 4. Influence of parasitic parameters | 53 |
| §2. Limiters using multielectrode tubes | 56 |
| 1. Grid limiters | - |
| 2. Anode limiters with bottom anode current cutoff | 59 |
| 3. Anode limiters with top anode current cutoff | 60 |
| 4. Two-way limiters using multielectrode tubes | 61 |




APPROVED FOR RELEASE: 2007/02/09: CIA-RDP82-00850R000500020034-7

APPROVED FOR RELEASE: 2007/02/09: CIA-RDP82-00850R000500020034-7



§3. Transistors in limiter and switching circuits 65
1. Transistorized limiters -
2. Transient processes in transistor switching circuit 67

Chapter 3. Two-stage square pulse generators 72

§1. General information -
§2. Electron-tube flip-flops 76
1. Balanced flip-flops -
2. Flip-flop resolution time 80
3. Balanced flip-flop triggering circuits 86
4. Cathode-coupled flip-flop 92
§3. Electron-tube one-shot multivibrators 95
1. Cathode-coupled one-shot multivibrator -
2. Cathode-coupled positive-grid one-shot multivibrator 100
3. Triggering and forced interruption of one-shot multivibrators 103
§4. Multivibrators using electron tubes in self-excited oscillation mode 106
1. Basic multivibrator circuit -
2. Improved versions of basic multivibrator circuit 112
§5. Transistorized flip-flop 114
1. External-bias flip-flop -
2. Automatic bias flip-flop 120
3. Emitter-coupled flip-flop 121
§6. Transistorized multivibrators 122
1. Multivibrator using transistors in self-excited oscillation mode -
2. Transistorized one-shot multivibrators 126

Chapter 4. Blocking oscillators 133

§1. General characteristics of blocking oscillators -
§2. Physical processes in electron-tube blocking oscillator 134
1. Basic and equivalent circuits of blocking oscillators in triggered mode -
2. Pulse triggering and edge shaping 135
3. Pulse top shaping 138
4. Pulse cutoff shaping and resetting circuit to initial state 139
§3. Alternate tube-type circuits for blocking oscillators 140
1. Blocking oscillator operating in self-excited oscillation mode -
2. Blocking oscillator with tuned circuit in grid circuit 142
3. Blocking oscillator with delay line in grid circuit 143
§4. Transistorized blocking oscillator 144



APPROVED FOR RELEASE: 2007/02/09: CIA-RDP82-00850R000500020034-7

APPROVED FOR RELEASE: 2007/02/09: CIA-RDP82-00850R000500020034-7



Chapter 5. Synchronization of pulse generators. Pulsed frequency dividers 149

§1. Principles of synchronization and frequency division -
§2. Synchronization of blocking oscillators and multivibrators 151
§3. Frequency division using triggered blocking oscillators in multivibrators 154
§4. Frequency division and pulse counting using flip-flops 154
§5. Some complex frequency divider circuits 161
1. Feedback dividers -
2. Dividers with reference pulse train gating 164

Chapter 6. Sawtooth voltage generators 166

§1. Parameters and principles of obtaining sawtooth voltages -
§2. Electron-tube sawtooth voltage generators 171
1. Exponential voltage generators with integrating RC-circuit -
2. Sawtooth voltage generators with current-stabilizing one-port network 173
3. Sawtooth voltage generators with compensating positive voltage feedback 176
4. Sawtooth voltage generators with compensating negative voltage feedback. Phantastrons. 183
§3. Transistorized sawtooth voltage generators 206
1. Exponential voltage generator with integrating RC circuit -
2. Sawtooth voltage generator with positive voltage feedback 208

Chapter 7. Integrated circuits for pulsed devices 212

§1. General information on integrated microcircuits. Functioning principles, notation system and operating characteristics of integrated logic microcircuits. -
§2. Potential-type integrated logic microcircuits 215
1. Single-stage logic integrated logic circuits 216
2. Two-stage logic integrated logic circuits 217
3. Integrated-circuit flip-flops 219

Bibliography 224

COPYRIGHT: Voyenizdat, 1981 s izmeneniyami

6900
CSO: 1860/43



APPROVED FOR RELEASE: 2007/02/09: CIA-RDP82-00850R000500020034-7

APPROVED FOR RELEASE: 2007/02/09: CIA-RDP82-00850R000500020034-7



UDC 658.58:62-5

PROBLEMS OF OPTIMAL DETECTION AND LOCALIZATION OF MALFUNCTIONS IN RADIOELECTRONIC EQUIPMENT

Moscow ZADACHI OPTIMAL'NOGO OBNARUZHENIYA I POISKA OTKAZOV V REA in Russian 1981 (signed to press 27 Mar 81) pp 2, 279-280

[Annotation and table of contents from book "Problems of Optimal Detection and Localization of Malfunctions in Radioelectronic Equipment", by Gennadiy Sergeyevich Pashkovskiy, Izdatel'stvo "Radio i svyaz'", 8000 copies, 280 pages]

[Text]

Annotation

Mathematical models of problems of optimal detection and location of malfunctions in radioelectronic equipment are examined. Algorithms are given for writing optimal programs for various optimality criteria. For the first time, solutions to these problems are reduced to engineering design methodologies which are convenient for manual computation as well as machine implementation.

The book is intended for specialists involved in designing and operating radioelectronic equipment. It is also useful for mathematicians interested in problems of combinatory optimization.

[This book was reviewed by Candidates of Technical Sciences V.D. Kudritskiy and M.V. Zhukov.]

Table of Contents

Editor's foreword 3

Chapter 1. Mathematical Models and Methods for Optimizing Malfunction Detection and Localization 8

1.1. Mathematical models of tested devices and malfunction search processes 8
1.2. Statistical optimization of sequential testing programs of high-reliability systems 16
1.3. Statistical optimization of sequential test programs of systems with arbitrary element reliability 24
1.4. Monitoring operability and diagnosis with minimax criteria 32



APPROVED FOR RELEASE: 2007/02/09: CIA-RDP82-00850R000500020034-7

APPROVED FOR RELEASE: 2007/02/09: CIA-RDP82-00850R000500020034-7



1.5. Models and methods of optimizing combination search 36
1.6. Decision-making regarding recovery of object of control using incomplete data 41
1.7. Problems of combinatory optimization and characterization of solution methods 44
1.8. Informal description of recursive method 46

Chapter 2. Optimal Methods of Testing and Diagnosing High Reliability Systems 50

2.1. Statement of the problem 50
2.2. Substantive description of solution method 51
2.3. Optimal diagnostic algorithm 56
2.4. Approximate diagnostic algorithms 69
2.5. Monitoring operability of high reliability systems 78

Chapter 3. Optimal Methods of Testing Systems With Arbitrary Element Reliability 85

3.1. Optimal algorithm for finding malfunctions and effecting repair 85
3.2. Approximate search algorithms with subsequent repair 103
3.3. Special cases of malfunction location problems followed by repair 112
3.4. Optimal algorithm for identifying status 118
3.5. Construction of quasi-optimal identification programs 129
3.6. Testing operability of systems with arbitrary element reliability 133

Chapter 4. Optimization of Test Programs Without Reliability Information 141

4.1. Algorithms for writing optimal diagnostic programs using minimax criterion 141
4.2. Approximate algorithms for diagnosing systems with single malfunction 149
4.3. Programs for finding malfunctions with subsequent repair using minimax criterion 155
4.4. Algorithms for writing quasi-optimal programs for finding malfunctions with subsequent repair 164
4.5. Monitoring operability of systems without reliability information 171
4.6. Minimax repair strategies 176

Chapter 5. Methods of Synthesizing Optimal ASK Structures 180

5.1. Combination search model 180
5.2. Optimal synthesis of ASK for diagnosing systems with single malfunction 182
5.3. Approximate algorithms for synthesizing ASK for systems with single malfunction 200
5.4. Synthesis of optimal structures for ASK for finding malfunctions and replacing faulty elements 212



APPROVED FOR RELEASE: 2007/02/09: CIA-RDP82-00850R000500020034-7

APPROVED FOR RELEASE: 2007/02/09: CIA-RDP82-00850R000500020034-7



5.5. Approximate algorithsm for synthesizing test systems for finding malfunctions and repairing test objects 225
5.6. Optimal synthesis of structures of ASK for testing operability 230

Chapter 6. Choosing Among Decisions Under Ambiguous Conditions and Optimal Test Planning 237

6.1. Model of test planning and decision-making under ambiguous conditions 237
6.2. Locally optimal plans in terms of minimum average total expenditure criterion 239
6.3. Statistically optimal planning of testing and decision-making 250
6.4. Locally optimal minimax plans 261
6.5. Globally optimal minimax plans 270

Bibliography 274

COPYRIGHT: Izdatel'stvo "Radio i svyaz'", 1981

6900
CSO: 1860/68



APPROVED FOR RELEASE: 2007/02/09: CIA-RDP82-00850R000500020034-7

APPROVED FOR RELEASE: 2007/02/09: CIA-RDP82-00850R000500020034-7



UDC 621.311.001(57+24):681.142

METHODS OF OPTIMIZATION IN CONTROLLING ELECTRICAL POWER SYSTEMS

Novosibirsk METODY OPTIMIZATSII PRI UPRAVLENII ELEKTROENERGETICHESKIMI SISTEMAMI in Russian 1981 (signed to press 24 Oct 80) pp 2, 256-257

[Annotation and table of contents from book "Methods of Optimization in Controlling Electrical Power Systems", by Lembit Arsen'yevich Krumm, Izdatel'stvo "Nauka", 1250 copies, 257 pages]

[Text]

Annotation

This monograph systematizes and generalizes the basic methodological principles and ideas of optimization in controlling steady-state modes of complex electrical power systems (CEPS). An analysis is given from a historical stance, primarily from the viewpoint of allowing for electrical system limitations. Both classical and integrated approaches, as well as various combinations thereof, are examined. The prospects of development of optimization methods in controlling CEPS are shown.

The book is of interest for workers at scientific and research, design and operating organizations involved with problems of developing and utilizing automated control system software in power engineering, as well as for graduate students.

Table of Contents

Note from the author 3

Introduction 4

Chapter I. Development of Methods for Optimizing Instantaneous Mode of CEPS 9

Preliminary remarks -

§1. Classical optimization methods (1919-1957) 10
§2. Appearance of integrated optimization methods (1957-1960) 26
§3. Development of integrated optimization methods since 1960 33
§4. Combination of optimization methods in classical approach (beginning in 1960) 44



APPROVED FOR RELEASE: 2007/02/09: CIA-RDP82-00850R000500020034-7

APPROVED FOR RELEASE: 2007/02/09: CIA-RDP82-00850R000500020034-7



1. Classical conditions of mode optimality and methods of defining various dependent mode parameters 45
2. Methods of allowing for limitations during optimization of generator active power 52
3. Methods of allowing for limitations during optimization of generator reactive power 64
Conclusions 73

Chapter II. Development of Methods of Realizing Implicit Functions in Controlling Steady-State SES Modes 80

Preliminary remarks -

§1. Methods for defining steady-state SES modes (linear approach) prior to 1932 84
§2. Interative methods for defining steady-state SES modes (nonlinear approach) (1932-1957) 87
§3. Methods for realizing theory of implicit functions defined by equations for self-adjusting SES modes (1932-1957) 91
§4. Methods of allowing for topological features of equations of steady-state SES modes (1932-1957) in phase II 116
§5. Development of methods under conditions of integrated optimization (beginning in 1957) 120
§6. Investigation of self-adjusting SES modes (beginning in 1957) 140
Conclusions 149

Chapter III. Development of Methods for Optimizing Mode and Complement of Operating Equipment in Cycles of Short-Term and On-Line Control 158

Preliminary remarks -

§1. Classical optimization methods (1940-1961) -
§2. Switch from classical methods to integrated optimization methods (1958-1961) 165
§3. Features of development of various methods (1961-1965) 168
§4. SEI [Siberian Power Institute] and All-Union Scientific Research Institute of Electric Power Engineering methodologies (beginning in 1965) 172
§5. Characterization of other research (beginning in 1965) 185
Conclusions 195

Chapter IV. Development of Methods for Optimizing Processes in Electric Power Systems Considering Incomplete Initial Information, and Its Prospects 204

Preliminary remarks -

§1. Methods of allowing for incomplete initial information in optimizing instantaneous and short-term modes in EPS under normal operating conditions during 1964-1974 209



APPROVED FOR RELEASE: 2007/02/09: CIA-RDP82-00850R000500020034-7

APPROVED FOR RELEASE: 2007/02/09: CIA-RDP82-00850R000500020034-7



2. General conception of development of methods for integrated optimization of processes in EPS (beginning in 1974) 227
3. Methods of optimizing modes allowing for incomplete initial information (beginning in 1974) 241
Conclusions 246

Conclusion 248

List of abbreviations 253

Bibliography 255

COPYRIGHT: Izdatel'stvo "Nauka", 1981 .

6900
CSO: 1860/71



APPROVED FOR RELEASE: 2007/02/09: CIA-RDP82-00850R000500020034-7

APPROVED FOR RELEASE: 2007/02/09: CIA-RDP82-00850R000500020034-7



UDC 621.3:629.12"313"

PROSPECTS FOR DEVELOPMENT FOR MARITIME ELECTRICAL ENGINEERING

Leningrad PERSPEKTIVY RAZVITIYA SUDOVOY ELEKTROTEKHNIKI in Russian 1981 (signed to press 27 Nov 80) pp 4-8, 187

[Annotation, foreword and table of contents from book "Prospects for Development for Maritime Electrical Engineering", by Georgiy Ivanovich Kitayenko, Yuriy Pavlovich Kos'kin, Yuriy Alekseyevich Svetlikov (deceased) and Veniamin Frantsevich Samoseyko, Izdatel'stvo "Sudostroyeniye", 1970 copies, 188 pages]

[Text]

## Annotation

Based on analysis of the status of maritime electrical engineering, the book predicts the development of parameters of electric power systems, protective devices, drives, start-control equipment, power converters, etc. A great deal of attention is devoted to questions of creating new types of power sources, deep-water electrical engineering, electromagnetic hydroreactive motors, cryogenic technology and superconducting equipment.

The book is intended for engineering-technical and scientific workers involved in research and designing maritime electrical equipment. It may also be of interest for teachers and students of senior courses at technical institutions of higher learning.

[This book was reviewed by A.Ye. Vorontsov.]

## Foreword

During this period of accelerated scientific-technical progress, in which science has become a determining factor in the economic and social development of society, it has become extremely important to make the correct choice of directions of development of science and technology so as to permit concentrating the efforts of the country's engineering-technical personnel on solving problems with the greatest long-range significance. It is now difficult to find technical solutions which can provide a noticeable immediate economic effect. Further advancement requires substantial long-range programs designed for large collectives at scientific research institutes. We know that scientific research represents an extremely profitable area of investment which promises the greatest profit; however, increasing expenditures are required for implementing programs of research.



APPROVED FOR RELEASE: 2007/02/09: CIA-RDP82-00850R000500020034-7

APPROVED FOR RELEASE: 2007/02/09: CIA-RDP82-00850R000500020034-7



For precisely this reason, attempts have recently been made here and abroad to predict the development of branches of the national economy and of individual types of technology.

A great number of articles and books have been devoted to predicting the development of ship building and maritime transport. Item [16] contains a quite complete bibliography on this matter (cf. bibliography to chapter 1).

The amount of electric power equipment installed aboard vessels depends to a significant degree upon the capacity of the power installations $N_e$, which is influenced by the vessel cargo capacity, speed, automation and signaling. We can track the increase in the values of $N_e$ using the example containerships. In 1975 the worldwide fleet included 45 such vessels with speeds of 25-30 knots and power plant capacity of over 50,000 h.p. Of these, 29 had $N_e > 80,000$ h.p.; and in 8 US vessels $N_e = 120,000$ h.p. Plans are now being developed for container vessels with $N_e = 200,000$ h.p. and more. A plan is being drawn up for a ship in England capable of carrying 5,000 containers at a speed of 30 knots with $N_e =$ 210,000 h.p. In Japan, a 3500-container vessel will have a speed of 35 knots and $N_e = 250,000$ h.p. According to predictions of US specialists, the international fleet will have 140 vessels with power exceeding 100,000 h.p. in 1980, and 500 such vessels in 1990. Similar prospects are foreseen for other types of vessels as well (Chapter 1 [16]).

The power plant is the most complicated system aboard a vessel; its development is determined to a significant extent by changes in the basic parameters of the vessel. On the other hand, new achievements in electrical engineering, electrical equipment development and power engineering make it possible to create vessels based on new technical principles, e.g., ships using electromagnetic hydroreactive engines. The prediction of the development of maritime electrical engineering must allow for achievement in shipbuilding and the electrical engineering industry (chapter 1 [27]).

The book develops two approaches to predicting the development of maritime electrical engineering. One of them involves developing methods and models of prediction, while the other is a descriptive method involving expertise. Both of these approaches complement one another. Prediction methods and models provide an apparatus for quantitative estimation of the future development of maritime electrical engineering. The methodology involved, especially the analytical algorithms, can be used in studying a broad class of problems in the area of maritime electrical engineering, both those which are being solved at present as well as those which may arise in the future.

In contrast to the first approach, with which it is now impossible, for the reasons indicated below, to make specific numerical calculations for all tasks involved in predicting the development of maritime electrical engineering, an attempt is made using the descriptive-expert panel approach to answer all basic problems which arise during the practical solution of prediction problems.

Here are two facts which are involved in using the first prediction approach: first of all, the extrapolation models which are most widely used in prediction theory require as initial information a precise and rather full retrospective



APPROVED FOR RELEASE: 2007/02/09: CIA-RDP82-00850R000500020034-7

APPROVED FOR RELEASE: 2007/02/09: CIA-RDP82-00850R000500020034-7



series of values which characterize the predicted process. A special information service must be created to obtain this information, which forms a data bank in support of the methodology in question. The organization of such a service will make it possible, over time, to have sufficiently complete and valid information for solving practical prediction problems. Secondly, many important problems (in particular, prediction of the appearance of new types of maritime electrical equipment) does not involve the examination of extrapolation models. No effective or workable models have yet been developed for such problems. We may hope that objective quantitative methods of evaluating the future status of maritime electrical engineering will be used increasingly as the problem of insufficient information is overcome by gradually accumulating source data and creating new prediction methods.

When predicting the development of technology, authors generally make note of the risk involved in solving the type of problem involved. The predictions made in the present work can be considered as an expert estimate of the prospects of development of maritime electrical engineering provided by the authors of the book. It is not impossible that another group of experts would have a different opinion from that presented in this book. In making their predictions, the authors take a conservative approach when necessary. For example, the section on expert panel-descriptive prediction is given without allowing for the time factor of the development of individual areas of maritime electrical engineering. This prediction is necessary in order to form the goals of development of the branch of technology. In those cases in which the authors have sufficient source information, prediction is done on the basis of developed models.

The book makes use of works published by the authors, domestic and foreign monographs and articles, as well as reviews on maritime electrical engineering contained in the collections "Sudostroyeniye za rubezhom" (Shipbuilding Abroad). Chapter 1 was written by Doctor of Technical Sciences Yu.A. Svetlikov and Candidate of Technical Sciences V.F. Samoseyko, chapter 2 by Doctor of Technical Sciences G.I. Kitayenko and Doctor of Technical Sciences Yu.P. Kos'kin.

A number of the positions put forth in the book were discussed with specialists of the shipbuilding and electrical engineering industries. The authors are deeply grateful to all comrades who participated in discussing the materials in the book, especially I.I. Adrianov, D.A. Gidaspov, A.N. Kaganovich and P.G. Meshcheryakov.

The authors express their gratitude to N.V. Belousova, R.I. Gladkikh and L.S. Kos'kina for their great assistance in making calculations, as well as selecting and processing the literature.

All critical remarks and suggestions should be addressed to 191065, Leningrad, ul. Gogolya, 8, Izdatel'stvo "Sudostroyeniye".

Table of Contents

Foreword 5



APPROVED FOR RELEASE: 2007/02/09: CIA-RDP82-00850R000500020034-7

APPROVED FOR RELEASE: 2007/02/09: CIA-RDP82-00850R000500020034-7



Chapter 1. Methods of Investigating Regularities in the Development of Maritime Electrical Engineering 9

1.1. Methodological principles -
1.2. Information support for research models 18
1.3. Investigation of developmental trends of determining parameters of maritime electric power systems 37
1.4. Methods of measuring maritime electric power systems as function of parameters of future vessels 60
1.5. Analysis of structured problems of development of maritime electrical engineering 81
References to chapter 1 103

Chapter 2. Problems of Development of Maritime Electrical Engineering 105

2.1. Modern maritime electrical engineering and its problems -
2.2. Electric energy parameters 113
2.3. Deep-water electrical engineering 125
2.4. New electric power sources 133
2.5. Electromagnetic hydroreactive engines 147
2.6. Cryogenic technology and superconducting electrical equipment 150
2.7. Trends of development of maritime electrical engineering 174
References to chapter 2 182

Conclusion 185

COPYRIGHT: Izdatel'stvo "Sudostroyeniye", 1981

6900
CSO: 1860/105



APPROVED FOR RELEASE: 2007/02/09: CIA-RDP82-00850R000500020034-7

APPROVED FOR RELEASE: 2007/02/09: CIA-RDP82-00850R000500020034-7



UDC 621.396.96.001(07)

RADAR DATA PROCESSING AGAINST INTERFERENCE BACKGROUND

Moscow TEORIYA I TEKHNIKA OBRABOTKI RADIOLOKATSIONNOY INFORMATSII NA FONE POMEKH in Russian 1981 (signed to press 20 Apr 81) pp 2-3, 410-416

[Annotation, foreword and table of contents from book "Theory and Practice of Radar Data Processing Against an Interference Background", by Yakov Davidovich Shirman and Vladimir Nikolayevich Manzhos, reviewed by doctors of the engineering sciences and professors V.Ye. Dulevich and M.B. Sverdlik, Izdatel'stvo "Radio i svyaz'", 10,000 copies, 416 pages]

[Text] Questions of optimizing multichannel and single channel detection systems as well as radar signal measurement and resolution are generalized.

Primary attention is devoted to design principles and questions of the engineering realization of various analog and digital detectors and signal parameter meters for signals against a background of correlated nonsteady-state interference as well as questions of adaptation to conditions of apriori ambiguity, etc. A large number of illustrative examples is cited.

The book is intended for specialists engaged with the theory, design and operation of radio electronic hardware and systems.

Foreword

The rapid development of radio electronics, and radar processing engineering theory in particular, makes it difficult to generalize the multifarious publications in this field. Nonetheless, there is the insistent need for generalizing publications which encompass the state of the art of the theory and the prospects for implementing its conclusions.

An urgent but difficult task is therefore the theoretical generalization of new questions and "those which have arisen" concerning radar processing against a background of interference from unified, sufficiently general procedural standpoints. For example, the refinement of the component base has expanded the possibility for multichannel reception. Signals and interference are described by a set of time functions or by time and coordinate functions in this case. The object of the optimization becomes the space-time processing of the signals against a background of interference, which provides for effective interference suppression in many situations (not just in radar). The generalization of the new problems of the indicated processing comprises a weighty portion of the problem posed above.



APPROVED FOR RELEASE: 2007/02/09: CIA-RDP82-00850R000500020034-7

APPROVED FOR RELEASE: 2007/02/09: CIA-RDP82-00850R000500020034-7



This book is an attempt to solve this problem to some extent. The courses of lectures on radar theory are taken as its basis: for engineers completing their training; for graduate students and degree candidates preparing to meet the candidata minimum. Special attention has been devoted to questions which are not always accessible or fully treated in the literature: the theory of primary space-time processing of radar data against a background of correlated interference, which provides not only for the accumulation of the useful signals, but also for the cancellation of interfering ones; the theory of measurements of timewise constant and changing signal parameters against a background of interference during primary and secondary processing; adaptation theory; adaptive antennas and moving target indication systems; new techniques of coherent processing of simple and complex space-time signals: digital, optical and spin methods.

Serious attention has been devoted to the compactness, generality and accessibility of the presentation of the comparatively complex theoretical material. Many years of teaching experience and personal research in the field treated here are reflected in the book. A large number of examples is given. The book can prove useful not only to engineers and graduate students, but also to students in the higher educational institutes. That which yesterday was the prerogative of a narrow group of researchers is today becoming public property.

The authors would like to express their gratitude for the useful comments of V.Ye. Dulevich, D.I. Lekhovitskiy and M.B. Sverdlik.

Table of Contents

Foreword 3

1. General Information on Radar Data and its Processing

I. Fundamentals of Multichannel Radar Signal Detection Theory

2. The Formulation of Optimization Problems for Signal Detection and Techniques of Solving Them

2.1. The formulation of problems of signal detection optimization 7
2.2. The main indicators for two and three alternative detection efficiency 9
2.3. Detection optimality criteria 10
2.4. Optimizing solutions in the case of two alternative detection 11
2.5. Optimizing solutions in the case of three alternative detection 14

3. Optimal Detection of a Time Digitized Signal with Known Parameters Against a Background of Correlated Gaussian Interference

3.1. The formulation of the problem. Signal and interference models 17
3.2. Optimal detection algorithms for a time digitized signal with known parameters 21
3.3. The quality indicators and parameter of two alternative detection of a digitized signal sample 24
3.4. Accumulation, compensation and interelement normalization with respect to the interference level as component parts of optimal weighted processing (the example of a two element sample) 25



APPROVED FOR RELEASE: 2007/02/09: CIA-RDP82-00850R000500020034-7

APPROVED FOR RELEASE: 2007/02/09: CIA-RDP82-00850R000500020034-7



4. Optimal Multichannel Detection of a CW Signal with Known Parameters Against a Background of Correlated Gaussian Interference

4.1. The transition from digitized realizations to continuous ones 27
4.2. The integral matrix equation of a weighting vector 29
4.3. The major results of multichannel detection theory for CW signals and examples of its application 30
4.4. Brief information from the theory of linear filters for CW signals with constant parameters 36
4.5. Matched filtration as a detection operation against a background of steady-state white noise 38
4.6. Optimal filtration as a detection operation against a background of steady-state nonwhite noise 41

5. Specific features of the Multichannel Detection of High Frequency Signals

5.1. The complex notation for narrow band high-frequency oscillations 42
5.2. The approximation of integrals from the products of narrow band high frequencies 43
5.3. The calculation of cross-correlation functions of random narrow band high-frequency oscillations, M[a(t)b(s)], in linear systems with constant parameters 44
5.4. Complex notation for received oscillations, the useful signal oscillation and the interference oscillations. The complex correlation matrix of interference 45
5.5. Complex notation for the main relationships of the detection theory for CW signals with known parameters 46
5.6. A model of white noise for the narrow band description of high frequencies 49
5.7. Examples of multichannel detector synthesis using complex notation of high-frequency oscillations 50
5.8. Complex notation of filtration equations of high-frequency oscillations 53

6. Specific Features of Multichannel Detection of Coherent Signals with Random Noninformational Parameters

6.1. A procedure to account for noninformational signal parameters and its application to detection against a background of gaussian interference 54
6.2. The likelihood ratio and optimal detection algorithm for a signal with a random initial phase 56
6.3. The likelihood ratio and optimal detection algorithm for a signal with random initial phases and amplitudes 57
6.4. Structural configurations of detectors for signals with a random initial phase and a with a random amplitude and initial phase 61
6.5. Quality indicators for a two alternative optimal detector of coherent signals with random parameters 62

7. Optimal Detection of the Simplest Incoherent Signals in Gaussian Interference in the Case of Multichannel Reception

7.1. General information on incoherent signals 65



APPROVED FOR RELEASE: 2007/02/09: CIA-RDP82-00850R000500020034-7

APPROVED FOR RELEASE: 2007/02/09: CIA-RDP82-00850R000500020034-7



7.2. Optimal incoherent signal detection algorithms for the simplest incoherency models 66
7.3. Methods of calculating the efficiency of post detector incoherent signal storage 70
7.4. Examples of calculating the statistical characteristics of the output voltages and efficiency indicators for post detector storage devices 73
7.5. Incoherent signal detection quality indicators in the case of a fixed sample volume 76
7.6. Incoherent signal sequential detection quality indicators 78
7.7. Quasi-optimal procedures of binary and multilevel digital incoherent storage 81

8. Specific Design Features of Detectors of Random Gaussian Signals against a Background of Gaussian Interference

8.1. The general problem of detecting a discrete gaussian random process against a background of discrete gaussian interference 83
8.2. Auxiliary mathematical propositions 84
8.3. Expressions for the logarithm of the likelihood ratio for digitized and CW signals 87
8.4. Example of synthesis of optimal detectors for coherent gaussian signals 89
8.5. Example of synthesis of optimal detectors for incoherent gaussian signals 91
8.6. Example of synthesis of optimal detectors for partially coherent gaussian signals 97

II. Radar Signals and Modern Techniques of Processing Them

9. Mismatch and Resolution Functions of Coherent Space-Time Signals. Signals without Intrapulse Modulation and Methods of Processing Them.

9.1. General relationships for coherent signal mismatch functions 103
9.2. Spatial (angular) mismatch functions 104
9.3. Time-frequency mismatch functions 105
9.4 Mismatch functions and the ambiguity solid for single radar pulses without intrapulse modulation 108
9.5. Processing techniques for single radar pulses without intrapulse modulation 111
9.6. Mismatch functions and processing techniques for coherent radar pulse trains 112
9.7. Principles of correlation filter processing and specific features of its use in the case of quasi-continuous signals 117
9.8. Specific features of matched and optimal resolution 119
9.9. Weighted processing of coherent radar pulse trains 122

10. Frequency Modulated Signals and Methods of Processing Them

10.1. Mismatch functions for linearly frequency modulated radar pulses 123
10.2. Compression of LFM radar pulses in matched filters 127
10.3. Correlation filter processing with generalized heterodyning 131



APPROVED FOR RELEASE: 2007/02/09: CIA-RDP82-00850R000500020034-7

APPROVED FOR RELEASE: 2007/02/09: CIA-RDP82-00850R000500020034-7



11. Phase Keyed Signals and Methods of Processing Them

11.1. Signals based on Barker codes and multiphase codes 135
11.2. Signals based on linear recurrent digital sequences 138
11.3. Continuous 0, π signals, keyed M-sequences 142
11.4. Continuous 0, ϕ signals, keyed M-sequences 144
11.5. Pulsed 0, π signals, keyed M-sequences 145

12. New Digital and Analog Coherent Processing Techniques

12.1. Specific features of digital coherent processing 146
12.2. Discrete (digital) processing in the time domain 149
12.3. Digital filtering in the frequency domain 152
12.4. The fast Fourier transform 156
12.5. The realization and utilization of a fast Fourier transform 159
12.6. The Walsh transform as a possible digital processing technique 160
12.7. Numerical transformations as a possible digital processing technique 164
12.8. New analog processing techniques. The dual pulse processing method using spin echo 166
12.9. A three pulse processing method using spin echo 171
12.10. The possibilities of using spin waves 173
12.11. Optical processing methods 175
12.12. Matched coherent optical processing in side-looking synthesized aperture radars 180

III. Fundamentals of Multichannel Radar Measurement Theory

13. The Formulation and Procedure in the Solution of the Optimal Measurement of Radar Signal Parameters. Basic Laws Governing a Regular Measurement

13.1. The formulation of optimal measurement problems 183
13.2. The post-test probability density in Bayes estimation theory 185
13.3. Optimizing estimates based on a minimum average risk criterion. Estimates of the post-test probability density maximum and the greatest likelihood 186
13.4. The post-test probability density and correlation matrix of vector parameter regular measurement errors in the absence of apriori data 190
13.5. The multidimensional error ellipsoid for a regular measurement in the absence of apriori data 192
13.6. Very simple examples of point and interval regular Bayes estimation 193
13.7. The post-test probability density and correlation matrix for vector parameter regular measurement errors where apriori data are present 195
13.8. Discriminator methods of optimal measurement 197

14. Specific Features of the Optimal Measurement of Timewise Constant Parameters of Coherent Signals against a Background of White Noise

14.1. The varieties of measurable parameters and the initial relationships 200
14.2. Likelihood equations and inverse regular measurement error correlation matrices for the nonpower parameters of coherent signals where their initial phase is random and apriori data are lacking 201



APPROVED FOR RELEASE: 2007/02/09: CIA-RDP82-00850R000500020034-7

APPROVED FOR RELEASE: 2007/02/09: CIA-RDP82-00850R000500020034-7



14.3. Equations of generalized discriminators of nonpower parameters of coherent signals where their initial phase is random 203
14.4. Examples of optimal nontracking delay time and frequency meters 203
14.5. The potential accuracy of the separate measurement of delay time and frequency 205
14.6. The potential accuracy of the combined measurement of delay time and frequency 207
14.7. Time discriminators 209
14.8. Frequency and time-frequency discriminators 212
14.9. The potential accuracy of angular coordinate measurement 214
14.10. Examples of dual channel phase angle meters 216
14.11. An example of a multichannel phase angle meter designed around a receiving antenna array 220
14.12. An example of an amplitude angle meter 221
14.13. Specific features of coherent signal power parameter measurements 223

15. Specific Features of the Optimal Measurement of Timewise Constant Parameters of Incoherent Signals against a Background of White Noise

15.1. General features of the measurement of timewise constant nonpower parameters of incoherent signals 225
15.2. Specific features of the utilization of a model for a rapidly fluctuating incoherent signal in measurement theory 227
15.3. A calculation procedure for the potential precision of the regular measurement of nonpower scalar parameters of incoherent signals against a background of white noise 230
15.4. Calculation of the potential precision of delay time and frequency measurements of rapidly fluctuating signals 233
15.5. Specific features of time and frequency measurements using incoherent signals 237
15.6. An example of an angle of arrival meter for spatially incoherent oscillations 239
15.7. An example of an angle of arrival meter for timewise incoherent oscillations 241
15.8. An example of a noise signal delay time difference meter 243
15.9. An example of an angular velocity meter for the motion of a rapidly fluctuating signal source 247

16. Optimal Measurement of Parameters which Vary Discretely with Time. Specific Features of Indirect Measurement

16.1. Models of the timewise change in signal parameters 248
16.2. A Gaussian-Markov model for a discrete change in a parameter 249
16.3. Possibilities of accounting for the time interrelationship of the random elements of a real time maneuver 250
16.4. Examples of modeling changes in parameters 251
16.5. A variant of a model for a discrete change in a parameter as applied to the case of indirect measurement. The concepts of filtration, prediction and smoothing estimates 253
16.6. Linearized equations and structural configurations for the filtration of discrete estimates in the case of direct measurement 255
16.7. Linearized equations and structural configurations for the filtration of discrete estimates in the case of indirect measurement 257



APPROVED FOR RELEASE: 2007/02/09: CIA-RDP82-00850R000500020034-7

APPROVED FOR RELEASE: 2007/02/09: CIA-RDP82-00850R000500020034-7



16.8. Examples of the synthesis and analysis of meters for discretely timewise changing parameters 260
16.9. Cumulative optimal smoothing of estimates of a discretely changing parameter 269
16.10. The general case of optimal measurement of a discretely changing markov parameter 271

17. Optimal Measurement of Parameters which Change Continuously with Time

17.1. A model of a continuous change in a parameter 273
17.2. The characteristics of a model of a continuous change in a parameter 275
17.3. Equations and structural configurations for filtration in the case of continuous estimation 276
17.4. Examples of the synthesis and analysis of meters for continuously timewise changing parameters 279
17.5. Cumulative optimal smoothing and interpolation of estimates of a continuously changing parameter 288
17.6. The inadequacy of models and the divergence of estimates of measured parameters 289

IV. Detection-Measurement, Adaptation and Related Questions

18. Detection-Measurements and Its Anomalies

18.1. General considerations regarding detection-measurement 293
18.2. Detection-measurement during secondary processing of information 295
18.3. Detection-measurement when combining information from several different sources. The principle of equality. 297
18.4. Detection-measurement and measurement anomalies 299
18.5. Anomalies in estimating the dispersion and espectation value for samples from a normal set with a small number of elements in the samples 301

19. Various Ways of Taking Noninformational Parameters of Signal and Interference into Account. Adaptation. Nonparametric Detection.

19.1. Various ways of taking noninformational parameters into account under apriori unknown conditions 304
19.2. Introducing and accounting for noninformational parameters under conditions of apriori ambiguity 308
19.3. Examples of accounting for noninformational parameters 309
19.4. Adaptation 313
19.5. The synthesis of automatic noise gain control 315
19.6. The simplest ways of taking the nongaussian nature of interference into account 317
19.7. Nonparametric sign detectors 320
19.8. Nonparametric rank detectors 322
19.9. The nature of nonlinear transformations when using ranking algorithms 324



APPROVED FOR RELEASE: 2007/02/09: CIA-RDP82-00850R000500020034-7

APPROVED FOR RELEASE: 2007/02/09: CIA-RDP82-00850R000500020034-7



20. Specific Features of Parametric Signal Detection and Measurement against a Background of Interference with Known and Unknown Spatial Correlations

20.1. Models of signals and interference. The formulation of the problem 327
20.2. The inversion of a special kind of correlation matrices with large dimensions 328
20.3. The inversion of any kind of correlation matrices with large dimensions 330
20.4. Variants of space-time coherent processing against a background of correlated interference with known correlation matrices 332
20.5. Weighting vectors and directionality characteristics 336
20.6. Gain and energy utilization factors 340
20.7. Specific features of space-time processing in broadband systems 342
20.8. Principles of estimating complex correlation matrices for spatially correlated interference 344
20.9. Discrete estimation of a correlation matrix for interference which changes with time 345
20.10. Continuous estimation of a correlation matrix for interference which changes with time 348
20.11. Estimation of a changing inverse correlation interference matrix 350
20.12. Estimation of a weighting vector. The use of correlation feedback in processors. 352
20.13. Analog processors with correlation feedback loops 356
20.14. Transient processes during adaptation 360
20.15. Adaptation in the case of a high intensity useful signal 363
20.16. Specific features of optimal measurement of signal parameters against a background of correlated interference 365
20.17. Examples of optimal measurement against a background of correlated interference 366

21. Specific Features of the Detection and Measurement of Signal Parameters against a Background of Interference with Known and Unknown Time Correlations

21.1. Models of interference with a known correlation. The formulation of the problem 368
21.2. Variants of models of passive interference with known parameters 370
21.3. Specific features of the utilization of a model for steady-state nonwhite noise in velocity gating designs 376
21.4. The possibilities for using a steady-state nonwhite noise model in spatial gating 379
21.5. Specific features of gating in the case of unmodulated CW and quasicontinuous transmissions 381
21.6. Velocity gating in pulsed radars with unambiguous range measurement in each pulse train period 381
21.7. Design examples of the simplest compensation devices applied to various models of passive interference for the case of unique range measurement 384
21.8. The velocity characteristics of the compensation circuitry for moving target indication 387
21.9. The coefficients of energy utilization, gain and subnoise visibility of coherent signals against a background of time correlated interference 388



APPROVED FOR RELEASE: 2007/02/09: CIA-RDP82-00850R000500020034-7

APPROVED FOR RELEASE: 2007/02/09: CIA-RDP82-00850R000500020034-7



21.10. The simplest methods of adapting MTI to individual unknown interference characteristics 390
21.11. The possibilities of designing adaptive MTI circuits with the estimation of the direct and inverse correlation matrices or the optimal weighting vector 392

Appendices 395
Main Symbols Used 398
Bibliography 400
Subject Index 406

COPYRIGHT: Izdatel'stvo "Radio i svyaz'", 1981

8225
CSO: 1860/8



APPROVED FOR RELEASE: 2007/02/09: CIA-RDP82-00850R000500020034-7

APPROVED FOR RELEASE: 2007/02/09: CIA-RDP82-00850R000500020034-7



UDC 621.396.664(024)

RADIO MEASUREMENTS

Moscow RADIOIZMERENIYA in Russian 1980 (signed to press 18 Nov 80) pp 2, 238-240

[Annotation and table of contents from book "Radio Measurements" by Aleksandr Nikolayevich Pashkov, Nikolay Vasil'yevich Avenirov, Aleksandr Vasil'yevich Kisilev and Valentin Ivanovich Akimov, Voyenizdat, 16,000 copies, 240 pages]

[Text] Annotation

The increase in the number and types of radio measurement instruments makes it necessary to use a variety of methods to test them. This book describes the design principles of radio measurement instruments, rules for testing various groups of instruments, techniques and singularities of use, as well as the methodology for selecting test devices.

The book is intended for a broad group of readers interested in metrology, and can be used to train and update specialists at testing organizations.

Table of Contents

Introduction 3

Chapter 1. General Information on Radiotechnical Measurement Devices 5

1.1. Classification of radiotechnical measurement devices 5
1.2. Metrological characteristics of radiotechnical measurement devices 18

Chapter 2. General Problems of Testing Radio Measurement Instruments 22

2.1. Basic concepts and definitions 22
2.2. Testing conditions 25
2.3. Documents regulating measurement device testing 25
2.4. Selection of standard measurement devices for making tests 26
2.5. How to prepare and conduct testing of a radio measurement instrument 28

Chapter 3. Instrumentation Oscillators and Their Testing 31

3.1. Design principles of instrumentation oscillators 31



APPROVED FOR RELEASE: 2007/02/09: CIA-RDP82-00850R000500020034-7

APPROVED FOR RELEASE: 2007/02/09: CIA-RDP82-00850R000500020034-7




1. Function and classification 31
2. Functional elements of instrumentation oscillators 33
3. Technique of application of instrumentation oscillators 35

3.2. Low frequency instrumentation oscillators 37
1. General information 37
2. Features of functional sections of low-frequency instrumentation oscillators 39
3. Metrological characteristics of low-frequency oscillators and basic testing rules 45

3.3. High-frequency instrumentation oscillators 47
1. General information 47
2. Features of functional sections of high-frequency oscillators 53
3. Metrological characteristics of high-frequency oscillators and basic testing rules 58

3.4. Pulse generators 66
1. General information 66
2. Features of functional sections of pulse generators 68
3. Metrological characteristics of pulse generators and basic testing rules 75

Chapter 4. Instruments for Measuring Voltage and Current and Their Testing 79

4.1. General information 79
4.2. Functional diagrams of voltmeters. Measurement of alternating voltage 81
4.3. Digital voltmeters 87
4.4. Voltage measurement technique 91
4.5. Metrological characteristics of voltmeters and basic testing information 92
4.6. Ammeter design principles 94

Chapter 5. Instruments for Power Measurement and Their Testing 96

5.1. Design principles of low- and high-frequency power meters 96
5.2. Features of microwave power meters 98
5.3. Absorption-type watt meters 100
1. Calorimetric method of power measurement 100
2. Thermoresistor method of power measurement 102
5.4. Measurement of transmitted power 107
5.5. Measurement of pulsed power 109
5.6. Metrological characteristics of power meters and basic testing information 110

Chapter 6. Instruments for Measuring Intensity of Electrical and Magnetic Fields and Their Testing 112

6.1. Design principles of radio wave field intensity meters 112
6.2. Field intensity meter antennas 119




APPROVED FOR RELEASE: 2007/02/09: CIA-RDP82-00850R000500020034-7

APPROVED FOR RELEASE: 2007/02/09: CIA-RDP82-00850R000500020034-7



6.3. Instrumentation receivers 121
6.4. Metrological characteristics of field intensity meters and basic testing information 123

Chapter 7. Instruments for Investigating Wave Form and Their Testing 124

7.1. Design principles of electronic oscillographs 124
7.2. Features of functional sections of vertical beam deflection channel 126
7.3. Horizontal beam deflection channel. Types of scan and scan voltages 127
7.4. Oscillograph measuring instruments 131
7.5. Oscillographic measurement technique 132
7.6. Methodological characteristics of electronic oscillographs and besic testing information 134

Chapter 8. Instruments for Measuring Frequency and Time Intervals and Their Testing 136

8.1. Design principles of instruments for measuring frequency and time intervals 136
8.2. Resonant frequency meters 138
8.3. Heterodyne frequency meters 138
8.4. Counting electronic frequency and time interval meters 141
8.5. Standard-frequency reproduction devices 147
8.6. Metrological characteristics of frequency and time interval meters and basic testing rules 149

Chapter 9. Instruments for Measuring Phase Shift and Their Testing 155

9.1. Design principles of phase shift meters 155
9.2. Functional diagrams of needle and digital phase meters 158
9.3. Metrological characteristics of phase meters and basic testing information 166

Chapter 10. Instruments for Measuring Signal Spectrum Parameters and Their Testing 169

10.1. Design principles of instruments for spectrum analysis and evaluation of spectral composition of oscillations 169
10.2. Spectrum analyzers 175
10.3. Nonlinear distortion meters 179
10.4. Amplitude modulation percentage meters 181
10.5. Frequency deviation meters 183
10.6. Metrological characteristics of spectrum analyzer and basic testing rules 184
10.7. Metrological characteristics of nonlinear distortion meters and basic testing information 188
10.8. Metrological characteristics of amplitude modulation percentage characteristics and basic testing rules 189
10.9. Metrological characteristics of frequency deviation meters and basic testing information 192



APPROVED FOR RELEASE: 2007/02/09: CIA-RDP82-00850R000500020034-7

APPROVED FOR RELEASE: 2007/02/09: CIA-RDP82-00850R000500020034-7



Chapter 11. Devices for Measuring Passive Circuit Parameters and Their Testing 193

11.1. Measurement of lumped-constant circuit parameters 193
1. Design principles of instruments for measuring parameters of circuits with lumped constants 193
2. Instruments using voltmeter-ammeter principle 195
3. Bridge-type instruments 196
4. Resonant instruments. Q-meters 198
5. Metrological characteristics of instruments for measuring parameters of lumped-constant circuits and basic testing information 203

11.2. Measuring parameters of distributed-constant circuits 203
1. Design principles of instruments for measuring parameters of circuits with distributed constants 203
2. Instrumentation lines and their testing 205
3. Impedance meters and their testing 217
4. Automation of measurement of parameters of circuits with distributed constants 222

11.3. Measurement of Absolute Value of Gain (Attenuation). Attenuators 227
1. Attenuator design principles 227
2. Methods for measuring absolute value of gain (attenuation) 231
3. Devices for attenuation measurement 233
4. Metrological characteristics of attenuators and basic testing information 235

Bibliography 237

COPYRIGHT: Voyenizdat, 1980

6900
CSO: 1860/99



APPROVED FOR RELEASE: 2007/02/09: CIA-RDP82-00850R000500020034-7

APPROVED FOR RELEASE: 2007/02/09: CIA-RDP82-00850R000500020034-7



UDC 537.312.62:621.372.834

SUPERCONDUCTING ACCELERATING MICROWAVE STRUCTURES

Moscow SVERKHPROVODYASHCHIYE USKORYAYUSHCHIYE SVCh-STRUKTURY in Russian 1981 (signed to press 3 Feb 81) pp 2-4, 208

[Annotation, foreword and table of contents from book "Superconducting Accelerating Microwave Structures", by Andrey Nikolayevich Didenko, Larisa Mikhaylovna Sevryukova and Al'bert Aleksandrovich Yatis, Energoizdat, 1150 copies, 208 pages]

[Text]

## Annotation

Superconducting microwave strucures are now used extensively in linear and cyclic accelerators, as well as high-energy particle separators.

The goal of this book is to provide a presentation of the current status of the problem of utilizing superconducting microwave structures in accelerator technology and nuclear physics. Problems of developing methods for obtaining super-pure metals and alloys for fabricating microwave structures are illuminated, and modern methods for technological processing of the working surface of accelerating structures are described in detail. A great deal of attention is devoted to atomic and nuclear-physical analysis methods and their utilization in superconductor technology.

Results obtained by the authors, as well as the achievements of Soviet and foreign scientists in the area of microwave structure theory, technology and application, are presented.

The book is intended for scientific workers and graduate students working in the area of accelerated technology and applied superconductivity, and for students in senior physics courses.

37 tables, 90 illustrations, 423 bibliographic references.

## Foreword

Superconductivity is one of the most interesting physical phenomena. Superconducting magnets are in extensive use. However, superconducting microwave structures are used to a significantly smaller degree, even though they are of great interest for many branches of science and technology, primarily accelerator technology and nuclear physics. This is mainly because the tremendous capabilities which such systems have are poorly understood. To a certain degree, this is explained by



APPROVED FOR RELEASE: 2007/02/09: CIA-RDP82-00850R000500020034-7

APPROVED FOR RELEASE: 2007/02/09: CIA-RDP82-00850R000500020034-7



the scattered nature of available publications and the lack of sufficient books on this topic. Only two books have been published to present. A.N. Didenko's monograph "Sverkhprovodyashchiye volnovody i rezonatory" (Superconducting Waveguides and Resonators) (Moscow, Izdatel'stvo Sovetskoye radio, 1973), is devoted to superconducting waveguides and resonators in general. F.F. Mende, I.N. Bondarenko, and A.V. Trubitsin's book "Sverkhprovodyatsiye i okhlazhdayemye rezonansnye sistemy" (Superconducting and Cooled Resonant Systems) (Kiev, Izdatel'stvo Naukova Dumka 1976) examines low-power microwave systems, for example, high-stability microwave oscillators, gravimeters, etc.

The goal of the present book is to provide a presentation of the current status of the utilization of superconducting microwave structures in accelerator technology.

Chapter 1 studies the fundamentals of hf superconductivity. Types of losses of electrical energy in microwave structures which cause the occurrence of residual resistance are examined. Technological and design methods for reducing losses are explained in detail.

Chapter 2 describes electrophysical and thermo-physical characteristics of suprconducting low- and high-power microwave structures. Problems occurring in the creation of microwave structures for accelerator technology (thermal instability, secondary electron effect, electron mechanical instability) are considered, as is the relationship between the surface impedance of resonant systems, as well as Q-factor, and the level of microwave power input. Special attention is devoted to eliminating the multiplicatory effect in microwave structures. General requirements for the stagblity of parameters of superconducting microwave systems and instrumentation are given.

Chapter 3 presents methods of volumetric and surface analysis as applied to superconducting niobium and niobium-alloy materials. Methods of neutron and charged-particle activation analysis are studied. The most complete presentation is that of the method for instantaneous analysis of near-surface layers of superconducting materials based on Coulomb ion scattering, the use of nuclear reactions, flourescent analysis spectroscopy, Auger electrons, secondary ion spectroscopy, etc.

Chapter 4 examines methods for obtaining super-pure metals and alloys for making superconducting sections of linear and cyclic accelerators. The possibility of preparing superconducting resonators and waveguides of monocrystals, as well as the prospects for utilizing such new materials as nitrides and carbides, are discussed. Electrical instability in an electrochemical system is examined for the first time with application to the electromechanical processing of ac and dc microwave structures. A description is given of equipment for high temperature annealing in ultrahigh vacuum and for electromechanical processing of superconducting structures.

Problems of removing heavy element impurities electrochemically from near-surface layers of niobium and niobium-based alloys and of applying protective coatings



APPROVED FOR RELEASE: 2007/02/09: CIA-RDP82-00850R000500020034-7

APPROVED FOR RELEASE: 2007/02/09: CIA-RDP82-00850R000500020034-7



with good electrophysical properties on the surface of structures are examined. Information is given on the condition of the surface of superconducting materials during different stages of surface processing: this information was obtained by Soviet and foreign scientists using methods of nuclear-physical analysis of elementary composition.

Chapter 5 analyzes the application of superconducting microwave structures in accelerator technology and nuclear physics. Questions of using hf-superconducting devices in linear electron, proton and heavy ion accelerators and in superconducting cyclic accelerators, as well as the possibility of using superconducting microwave systems as the basis for creating electron microscopes, are discussed. A great deal of attention is devoted to the use of superconducting microwave structures in high-energy particle separators.

Materials from foreign and Soviet scientists which were discussed at conferences and meetings on applied superconductivity and charged-particle accelerators over the past five years which were published in the proceedings from these conferences and various journals were used in writing the book, as were original findings obtained at the Scientific Research Institute for Nuclear Physics at the Tomsk Polytechnical Institute.

Chapters 1 and 2 were written jointly by A.N. Didenko and L.M. Sevryukova, chapter 3 by A.A. Yatis, chapter 4 by L.M. Sevryukova, and chapter 5 by A.N. Didenko.

Table of Contents

Foreword 3

Chapter 1. Fundamentals of High-Frequency Superconductivity 5

1.1. Surface resistance of superconducting materials at microwave frequencies
1.2. Losses of microwave energy caused by impurities and defects in crystal structure 12
1.3. Dielectric losses in films and impurities 17
1.4. Energy losses caused by generation of sound waves by incident electromagnetic radiation 21
1.5. Additional losses in superconducting microwave structures under influence of magnetic fields 28

Chapter 2. Electrophysical Characteristics of Superconducting Microwave Structures 35

2.1. Electrophysical parameters of superconducting waveguides and resonators 35
2.2. Critical magnetic hf fields. Basic thermophysical characteristics of superconducting microwave structures 45



APPROVED FOR RELEASE: 2007/02/09: CIA-RDP82-00850R000500020034-7

APPROVED FOR RELEASE: 2007/02/09: CIA-RDP82-00850R000500020034-7



2.3. Emission effect in superconducting microwave structures and electrical field gradients 53
2.4. General requirements for stability of parameters of superconducting microwave systems 62

Chapter 3. Methods of Analyzing Superconducting Materials 76

3.1. Basic information 70
3.2. Volumetric activation analysis 73
3.3. Instantaneous nuclear analysis methods 83
3.4. Mass-spectrometric analysis 95
3.5. Low-energy electron spectroscopy 99
3.6. X-ray analysis methods 104
3.7. Comparative characterization 109

Chapter 4. Superconducting Materials and Technology of Superconducting Microwave Structures 116

4.1. Fabrication of superconducting microwave structures from lead and niobium 116
4.2. Electrochemical polishing of working surface of superconducting resonators and structures 124
4.3. High temperature annealing of niobium superconducting resonators and waveguides in high vacuum 134
4.4. Anode oxidation and its use for protecting and cleaning surface layer 144
4.5. Technology for obtaining superconducting alloy-based microwave structure coating 156
4.6. Prospects for utilization of monocrystals, nitrides and carbides for fabricating microwave structures 172

Chapter 5. Application of Superconducting Microwave Structures in Accelerator Technology and Nuclear Physics 176

5.1. Superconducting linear accelerators 176
5.2. Utilization of superconducting accelerating systems in cyclic accelerators 181
5.3. Superconducting separators for high-energy charged particles 188
5.4. Creation of electron microscopes based on superconducting accelerating systems 192

Conclusion 196

Bibliography 197

COPYRIGHT: Energoizdat, 1981

6900
CSO: 1860/104

- END -



APPROVED FOR RELEASE: 2007/02/09: CIA-RDP82-00850R000500020034-7